A UNITED STATES DEPARTMENT OF COMMERCE PUBLICATION

SECTION A

# JOURNAL OF RESEARCH

## of the NATIONAL BUREAU OF STANDARDS

JNBAAR 76A (3) 165-319, May-June 1972

# Physics and Chemistry

U.S. DEPARTMENT OF COMMERCE
National Bureau of Standards

**Journal of Research**

**of the**

**National Bureau of Standards**

A. Physics and Chemistry

May–June • 1972

VOLUME • 76A

NUMBER • 3

Editor: C. W. Beckett

Associate Editor: D. D. Wagman

Publication dates:
Feb. 1, Apr. 1, June 1, Aug. 1, Oct. 1, Dec. 1, 1972

J. Res. Nat. Bur. Stand. (U.S.), A

**JOURNAL OF RESEARCH**

The National Bureau of Standards Journal of Research reports research and development in the fields of activity shown at right. Also included from time to time are survey articles on topics closely related to the Bureau's scientific and technical program.

The Journal is published in three separate sections as follows:

**A. Physics and Chemistry**

Contains papers of interest primarily to scientists working in these fields. Issued six times a year. Annual subscription: domestic, $9.50; foreign, $11.75. Single copy, varies.

**B. Mathematical Sciences**

Presents studies and compilations designed mainly for the mathematician and the theoretical physicist. Issued quarterly. Annual subscription: domestic, $5.00; foreign, $6.25. Single copy, $1.25.

The National Bureau of Standards[1] was established by an act of Congress March 3, 1901. The Bureau's overall goal is to strengthen and advance the Nation's science and technology and facilitate their effective application for public benefit. To this end, the Bureau conducts research and provides: (1) a basis for the Nation's physical measurement system, (2) scientific and technological services for industry and government, (3) a technical basis for equity in trade, and (4) technical services to promote public safety. The Bureau consists of the Institute for Basic Standards, the Institute for Materials Research, the Institute for Applied Technology, the Center for Computer Sciences and Technology, and the Office for Information Programs.

**THE INSTITUTE FOR BASIC STANDARDS** provides the central basis within the United States of a complete and consistent system of physical measurement; coordinates that system with measurement systems of other nations; and furnishes essential services leading to accurate and uniform physical measurements throughout the Nation's scientific community, industry, and commerce. The Institute consists of a Center for Radiation Research, an Office of Measurement Services and the following divisions:

Applied Mathematics—Electricity—Heat—Mechanics—Optical Physics—Linac Radiation[2]—Nuclear Radiation[2]—Applied Radiation[2]—Quantum Electronics[3]—Electromagnetics[3]—Time and Frequency[3]—Laboratory Astrophysics[3]—Cryogenics[3].

**THE INSTITUTE FOR MATERIALS RESEARCH** conducts materials research leading to improved methods of measurement, standards, and data on the properties of well-characterized materials needed by industry, commerce, educational institutions, and Government; provides advisory and research services to other Government agencies; and develops, produces, and distributes standard reference materials. The Institute consists of the Office of Standard Reference Materials and the following divisions:

Analytical Chemistry—Polymers—Metallurgy—Inorganic Materials—Reactor Radiation—Physical Chemistry.

**THE INSTITUTE FOR APPLIED TECHNOLOGY** provides technical services to promote the use of available technology and to facilitate technological innovation in industry and Government; cooperates with public and private organizations leading to the development of technological standards (including mandatory safety standards), codes and methods of test; and provides technical advice and services to Government agencies upon request. The Institute also monitors NBS engineering standards activities and provides liaison between NBS and national and international engineering standards bodies. The Institute consists of the following technical divisions and offices:

Engineering Standards Services—Weights and Measures—Flammable Fabrics—Invention and Innovation—Vehicle Systems Research—Product Evaluation Technology—Building Research—Electronic Technology—Technical Analysis—Measurement Engineering.

**THE CENTER FOR COMPUTER SCIENCES AND TECHNOLOGY** conducts research and provides technical services designed to aid Government agencies in improving cost effectiveness in the conduct of their programs through the selection, acquisition, and effective utilization of automatic data processing equipment; and serves as the principal focus within the executive branch for the development of Federal standards for automatic data processing equipment, techniques, and computer languages. The Center consists of the following offices and divisions:

Information Processing Standards—Computer Information—Computer Services—Systems Development—Information Processing Technology.

**THE OFFICE FOR INFORMATION PROGRAMS** promotes optimum dissemination and accessibility of scientific information generated within NBS and other agencies of the Federal Government; promotes the development of the National Standard Reference Data System and a system of information analysis centers dealing with the broader aspects of the National Measurement System; provides appropriate services to ensure that the NBS staff has optimum accessibility to the scientific information of the world, and directs the public information activities of the Bureau. The Office consists of the following organizational units:

Office of Standard Reference Data—Office of Technical Information and Publications—Library—Office of International Relations.

[1] Headquarters and Laboratories at Gaithersburg, Maryland, unless otherwise noted; mailing address Washington, D.C. 20234.
[2] Part of the Center for Radiation Research.
[3] Located at Boulder, Colorado 80302.

U.S. DEPARTMENT OF COMMERCE
Peter G. Peterson, Secretary
Lawrence M. Kushner, Acting Director
NATIONAL BUREAU OF STANDARDS

Order all publications from the Superintendent of Documents
U.S. Government Printing Office, Washington, D.C. 20402

Use of funds for printing this publication approved by the Director of the Bureau of the Budget (June 22, 1966).

JOURNAL OF RESEARCH of the National Bureau of Standards—A. Physics and Chemistry
Vol. 76A, No. 3, May–June 1972

# Thermodynamics of Standard Cells of the Saturated Cadmium Sulfate Type

**Walter J. Hamer**

**Institute for Basic Standards, National Bureau of Standards, Washington, D.C. 20234**

**(December 21, 1971)**

This paper gives data on the thermodynamic functions of standard cells of the saturated cadmium sulfate type, as obtained from calorimetric and equilibrium data at 25 °C or from the electromotive forces (emfs) and emf-temperature coefficients of the cell for the temperature range of 0 to 43.6 °C. The functions considered are the changes in Gibbs energy, enthalpy, entropy, and heat capacity for the cell reaction. The electromotive forces are expressed on the $V_{69}$ volt and the $t_{68}$ temperature scale. Results are expressed on the SI and for comparisons with literature data in terms of the defined thermochemical calorie. The effect of expressing the emf-temperature coefficient as a function of temperature in different ways on the values for the changes in entropy and heat capacity for the cell reaction is discussed. Finally, the observed emf of the standard cell at 25 °C is compared with emfs calculated from various values reported for the standard potentials of the cadmium-amalgam and mercury-mercurous sulfate electrodes and the activity coefficient of cadmium sulfate in saturated aqueous solution.

Key words: Emf-temperature coefficients of standard cells; emfs of standard cells; standard potential of standard cells; thermodynamics of standard cells.

## 1. Introduction

It is the purpose of this paper to present data on the thermodynamic functions of standard cells of the saturated cadmium sulfate type,[1] as obtained from calorimetric and chemical equilibrium data, and to compare these data with those obtained from the electromotive force (emf) and emf-temperature coefficient of the cell. The thermodynamic functions considered are the changes in Gibbs energy (free energy), $\Delta G$; enthalpy (heat content), $\Delta H$; entropy, $\Delta S$; and heat capacity at constant pressure, $\Delta C_p$, where the changes are equal to the differences between the thermodynamic quantities of the products and the reactants of the cell reaction. Thermodynamically, these are given or are related by:

$$\Delta G = \Delta H - T\Delta S = \Delta H + T[d(\Delta G)/dT]_p \quad (1)$$

$$\Delta S = \int_0^T \Delta C_p d \ln T \quad (2)$$

and

$$\Delta C_p = [d(\Delta H)/dT]_p \quad (3)$$

where $T$ is the Kelvin temperature (defined in the thermodynamic scale by assigning 273.16 K to the triple point of water; freezing point of water, 273.15 K [1][2]).

The thermodynamic functions for a galvanic cell (or standard cell) may be obtained from its emf, $E$, and its emf-temperature coefficient, $dE/dT$, and are given by:

$$\Delta G = -nEF \quad (4)$$

$$\Delta H = -nEF + nFT(dE/dT) \quad (5)$$

$$\Delta S = nF(dE/dT) \quad (6)$$

and

$$\Delta C_p = nFT(d^2E/dT^2) \quad (7)$$

where $n$ is the number of equivalents involved in the cell reaction (in the present case $n$ is 2) and $F$ is the Faraday. $F$ has a value of 96487 coulombs per gram-equivalent [1, 2, 3, 4] or 23060.9 calories per volt per gram-equivalent.[3] Accordingly, a comparison may be made between the thermodynamics of the overall reaction of a standard cell as determined from calorimetric and chemical equilibrium data or from emf data.

[1] Also referred to as the Weston cell after Edward Weston who invented the cell in 1892.

[2] Figures in brackets indicate the literature references at the end of this paper.

[3] Based on the relation 1 thermochemical calorie (defined) = 4.1840 J [1].

## 2. The Standard Cell (saturated $CdSO_4$ type)

The conventional standard cell of the saturated cadmium sulfate type,[4] considered here, may be represented by:

$$(-)\mathrm{Cd,Hg}(2p)\left|\mathrm{CdSO_4}\cdot\frac{8}{3}\mathrm{H_2O(s)}\right|\mathrm{CdSO_4(ss)}\left|\mathrm{CdSO_4}\right.$$
$$\left.\cdot\frac{8}{3}\mathrm{H_2O(s)}\right|\mathrm{Hg_2SO_4(s)}\left|\mathrm{Hg(l)}\right.(+)$$

where the vertical lines indicate the interface between two distinct phases (the amalgam consists of 2 phases, one solid and one liquid, but for simplicity vertical lines are not used in designating it), $2p=2$ phases, ss = saturated solution, s = solid (or paste), and l = liquid. The cell reaction is [5]:

$$x\mathrm{Cd},y\mathrm{Hg}(2p)+\mathrm{Hg_2SO_4(s)}+\frac{8/3}{m-8/3}\mathrm{CdSO_4}$$
$$\cdot m\mathrm{H_2O(ss)}\rightarrow\frac{m}{m-8/3}\mathrm{CdSO_4} \qquad (8)$$
$$\cdot\frac{8}{3}\mathrm{H_2O(s)}+2\mathrm{Hg(l)}+(x-1)\mathrm{Cd},y\mathrm{Hg}(2p)$$

where $x$ moles of Cd are associated with $y$ moles of Hg in the amalgam and $m$ is the number of moles of water associated with 1 mole of $CdSO_4$ in the saturated solution. Ten percent amalgams are now generally used, although there is now a trend to a return to the use of 12½-percent amalgams as they are more suitable for portable (or shippable) cells. At 25 °C $m$ has a value of 15.089 [6].

The overall reaction for the cell may be considered as the sum of five reactions, namely:

$$\text{(a)}\quad \mathrm{Cd(s)}+\mathrm{Hg_2SO_4(s)}\rightarrow\mathrm{CdSO_4(s)}+2\mathrm{Hg(l)} \qquad (9)$$

$$\text{(b)}\quad \mathrm{CdSO_4(s)}+\mathrm{H_2O(l)}\rightarrow\mathrm{CdSO_4\cdot H_2O(s)} \qquad (10)$$

$$\text{(c)}\quad \mathrm{CdSO_4\cdot H_2O(s)}+\frac{5}{3}\mathrm{H_2O(l)}\rightarrow\mathrm{CdSO_4}\cdot\frac{8}{3}\mathrm{H_2O(s)} \qquad (11)$$

$$\text{(d)}\quad \frac{8/3}{m-8/3}\mathrm{CdSO_4}\cdot m\mathrm{H_2O(ss)}\rightarrow\frac{8}{3}\mathrm{H_2O(l)}$$
$$+\frac{8/3}{m-8/3}\mathrm{CdSO_4}\cdot\frac{8}{3}\mathrm{H_2O(s)} \qquad (12)$$

and

$$\text{(e)}\quad \mathrm{Cd(10\%\ amalgam)}\rightarrow\mathrm{Cd(s)} \qquad (13)$$

for which, reaction (e) excepted, calorimetric or thermal data are available.

## 3. Calorimetric and Chemical Equilibrium Data

### Reaction (a)

For reaction (a) Cohen, Helderman, and Moesveld [7] obtained −45,346 cal mol$^{-1}$ at 18 °C for the difference between the heats of formation of $CdSO_4$ and $Hg_2SO_4$; this difference is also equivalent to the heat of reaction (a) since the heats of formation of the elements, Cd and Hg, in their standard states are zero.[5] However, Cohen et al. arrived at their value for the heat of reaction (a) from combined calorimetric and emf data. They obtained their value by combining the value for the heat of solution of $CdSO_4$ in water at 18 °C to give a solution 2.559 percent in $CdSO_4$ with the value for the heat of reaction of an unsaturated standard cell (2.559% in $CdSO_4$) which they obtained from the observed emf of the cell at 18 °C and the measured emf-temperature coefficient of the cell at 18 °C.

For our purpose, however, we need to obtain the heat of reaction (a) directly from calorimetric data. This heat value may be obtained from the heats of reaction of Cd and $CdSO_4$ with other substances and of Hg and $Hg_2SO_4$ with other substances, as outlined by the following equations (unfortunately, most of the data were obtained many years ago). In these equations, the numbers in parentheses indicate, according to convention, the number of moles of water in which the substance is dissolved. Although, according to convention, the moles of water involved in dilution or solution [eqs (a4) and (a5) under Cd and $CdSO_4$, for example] are not included in representing the reaction they are included here so that the equations balance, but are shown in parentheses with an asterisk to indicate that the heat of formation of water is not used in determining the heat of dilution or solution. Likewise, when the water contains KI or KI + $I_2$, it is also shown in parentheses with a superscript to indicate that the heat of formation of this water, containing KI or KI + $I_2$, is not used in determining the heat of dilution or solution (in the summation of the following reactions this quantity cancels). Also, in each case the values reported in calories were first converted to international joules using the factor used by the individual authors; these were then converted to absolute joules using the factor 1.000167 and these in turn were then converted (for comparison purposes) to calories using the presently accepted thermochemical definition of the calorie (see footnote 3) and are designated by the symbol *cf* meaning conversion factor. Also in the equations that follow, s = solid, l = liquid, and g = gas. The numbers in parentheses after each value for $\Delta H$ denote the ± uncertainty, discussed later.

[4] This is the type of standard cell presently used in the maintenance of the unit of emf in National Laboratories.

[5] Calorie is retained for the unit of energy when the literature is cited. More is given on this point including the use of SI later in this paper. The thermochemical calorie is presently defined in terms of the joule by the relation given in footnote 3.

**Cd and $CdSO_4$**

(a1) $Cd(s) + 2\ HCl(200) \rightarrow CdCl_2(400) + H_2(g)$

$\Delta H_1(20\ ^\circ C) = -17{,}230(70)$ cal $mol^{-1} = -72{,}033(293)$ J $mol^{-1}$ [8]
$\Delta H_1(18\ ^\circ C) = -17{,}290(90)$ cal $mol^{-1} = -72{,}284(377)$ J $mol^{-1}$ [8]
$\Delta H_1(18\ ^\circ C)^{cf} = -17{,}276(90)$ cal $mol^{-1} = -72{,}284(377)$ J $mol^{-1}$

(a2) $CdCl_2(400) + BaSO_4(s) \rightarrow CdSO_4(200) + BaCl_2(200)$

$\Delta H_2(19\ ^\circ C) = 5{,}683(55)$ cal $mol^{-1} = 23{,}742(230)$ J $mol^{-1}$ [9]
$\Delta H_2(18\ ^\circ C) = 5{,}793(60)$ cal $mol^{-1} = 24{,}201(251)$ J $mol^{-1}$ [10, 11]
$\Delta H_2(18\ ^\circ C)^{cf} = 5{,}784(60)$ cal $mol^{-1} = 24{,}201(251)$ J $mol^{-1}$

(a3) $BaCl_2(400) + H_2SO_4(400) \rightarrow BaSO_4(s) + 2\ HCl(400)$

$\Delta H_3(19\ ^\circ C) = -9{,}152(55)$ cal $mol^{-1} = -38{,}234(230)$ J $mol^{-1}$ [9]
$\Delta H_3(18\ ^\circ C) = -9{,}262(60)$ cal $mol^{-1} = -38{,}694(251)$ J $mol^{-1}$ [10, 11]
$\Delta H_3(18\ ^\circ C)^{cf} = -9{,}248(60)$ cal $mol^{-1} = -38{,}694(251)$ J $mol^{-1}$

(a4) $BaCl_2(200) + (200\ H_2O)^* \rightarrow BaCl_2(400)$

$\Delta H_4(18\ ^\circ C) = -50(1)$ cal $mol^{-1} = -209(4)$ J $mol^{-1}$ [12]
$\Delta H_4(18\ ^\circ C)^{cf} = -50(1)$ cal $mol^{-1} = -209(4)$ J $mol^{-1}$

(a5) $2\ HCl(400) \rightarrow 2\ HCl(200) + (400\ H_2O)^*$

$\Delta H_5(18\ ^\circ C) = 120(2)$ cal $mol^{-1} = 502(8)$ J $mol^{-1}$ [12]
$\Delta H_5(18\ ^\circ C)^{cf} = 120(2)$ cal $mol^{-1} = 502(8)$ J $mol^{-1}$

(a6) $H_2SO_4(222) + (178\ H_2O)^* \rightarrow H_2SO_4(400)$

$\Delta H_6(18\ ^\circ C) = -303(3)$ cal $mol^{-1} = -1{,}268(12)$ J $mol^{-1}$ [12]
$\Delta H_6(18\ ^\circ C)^{cf} = -303(3)$ cal $mol^{-1} = -1{,}268(12)$ J $mol^{-1}$

(a7) $CdSO_4(400) \rightarrow CdSO_4(s) + (400\ H_2O)^*$

$\Delta H_7(18\ ^\circ C) = 10{,}690(25)$ cal $mol^{-1} = 44{,}756(105)$ J $mol^{-1}$ [7]
$\Delta H_7(18\ ^\circ C)^{cf} = 10{,}697(25)$ cal $mol^{-1} = 44{,}756(105)$ J $mol^{-1}$

(a8) $CdSO_4(200) + (200\ H_2O)^* \rightarrow CdSO_4(400)$

$\Delta H_8(18\ ^\circ C) = -206(2)$ cal $mol^{-1} = -862(8)$ J $mol^{-1}$ [12]
$\Delta H_8(18\ ^\circ C)^{cf} = -206(2)$ cal $mol^{-1} = -862(8)$ J $mol^{-1}$

sum: $Cd(s) + H_2SO_4(222) \rightarrow CdSO_4(s) + H_2(g) + (222\ H_2O)^*$

$\Delta H_{1-8}(18\ ^\circ C)^{cf} = -10{,}482(69)$ cal $mol^{-1} = -43{,}858(289)$ J $mol^{-1}$

**Hg and $Hg_2SO_4$**

(a9) $Hg_2SO_4(s) + 2\ KI(694)^\# \rightarrow Hg(l) + HgI_2(694)^\# + K_2SO_4(694)^\#$

$^\#$ – contains 5.25 moles of KI

$\Delta H_9(14\ ^\circ C) = -44{,}100(560)$ cal $mol^{-1} = -184{,}236(2339)$ J $mol^{-1}$ [13]

(a10) $HgI_2(858)^\phi \rightarrow Hg(l) + I_2(858)^\phi$

$\phi$ – contains 6.5 moles of KI and 1.0 mole of $I_2$

$\Delta H_{10}(14\ ^\circ C) = 31{,}300(400)$ cal $mol^{-1} = 130{,}762(1671)$ J $mol^{-1}$ [13]

(a11) $I_2(858)^{\phi} \rightarrow I_2(s) + (858\ H_2O)^{\phi *}$

$^{\phi}$ – contains 6.5 moles of KI and 1.0 mole of $I_2$

$\Delta H_{11}(14\ ^{\circ}C) = -200(2)$ cal $mol^{-1} = -835(8)$ J $mol^{-1}$ [13]

sum of (a9), (a10), and (a11): $Hg_2SO_4(s) + 2\ KI(694)^{\#} + HgI_2(858) \rightarrow$
$2\ Hg(l) + HgI_2(1123)^{\alpha} + K_2SO_4(1123)^{\alpha} + I_2(s)$

$\alpha$ – contains 8.5 moles of KI and 0.5 mole of $I_2$

$\Delta H_{9-11}(14\ ^{\circ}C) = -13{,}000(162)$ cal $mol^{-1} = -54{,}309(676)$ J $mol^{-1}$
$\Delta H_{9-11}(18\ ^{\circ}C) = -12{,}844(172)$ cal $mol^{-1} = -53{,}658(718)$ J $mol^{-1}$ [10, 11, 14, 15]
$\Delta H_{9-11}(18\ ^{\circ}C)^{cf} = -12{,}825(172)$ cal $mol^{-1} = -53{,}658(720)$ J $mol^{-1}$

(a12) $HgI_2(1123)^{\alpha} \rightarrow HgI_2(858)^{\phi} + (265\ H_2O)^{\beta *}$

$\beta$ – contains 2 moles of KI

$\Delta H_{12}(18\ ^{\circ}C) = -2(0.1)$ cal $mol^{-1} = -8(0.4)$ J $mol^{-1}$ [12]
$\Delta H_{12}(18\ ^{\circ}C)^{cf} = -2(0.1)$ cal $mol^{-1} = -8(0.4)$ J $mol^{-1}$

(a13) $Cl_2(g) + H_2(g) \rightarrow 2\ HCl(g)$

$\Delta H_{13}(18\ ^{\circ}C) = -44.120(24)$ cal $mol^{-1} = -184.644(100)$ J $mol^{-1}$ [16]
$\Delta H_{13}(18\ ^{\circ}C)^{cf} = -44{,}131(24)$ cal $mol^{-1} = -184{,}644(100)$ J $mol^{-1}$

(a14) $I_2(s) + 2\ HCl(g) \rightarrow 2\ HI(g) + Cl_2(g)$

$\Delta H_{14}(22\ ^{\circ}C) = 55.933(100)$ cal $mol^{-1} = 233{,}985(418)$ J $mol^{-1}$ [17]
$\Delta H_{14}(18\ ^{\circ}C) = 55{,}949(110)$ cal $mol^{-1} = 234{,}053(460)$ J $mol^{-1}$ [10, 18]
$\Delta H_{14}(18\ ^{\circ}C)^{cf} = 55{,}940(110)$ cal $mol^{-1} = 234{,}053(460)$ J $mol^{-1}$

(a15) $2\ HI(g) + (222\ H_2O)^{*} \rightarrow 2\ HI(111)$

$\Delta H_{15}(18\ ^{\circ}C) = -38{,}344(50)$ cal $mol^{-1} = -160{,}431(209)$ J $mol^{-1}$ [12]
$\Delta H_{15}(18\ ^{\circ}C)^{cf} = -38{,}344(50)$ cal $mol^{-1} = -160{,}431(209)$ J $mol^{-1}$

(a16) $2\ HI(100) + 2\ KOH(100) \rightarrow 2\ KI(200) + 2\ H_2O(l)$

$\Delta H_{16}(20\ ^{\circ}C) = -27{,}830(20)$ cal $mol^{-1} = -116{,}349(84)$ J $mol^{-1}$ [19]
$\Delta H_{16}(18\ ^{\circ}C) = -28{,}034(29)$ cal $mol^{-1} = -117{,}202(121)$ J $mol^{-1}$ [19]
$\Delta H_{16}(18\ ^{\circ}C)^{cf} = -28{,}012(29)$ cal $mol^{-1} = -117{,}202(121)$ J $mol^{-1}$

(a17) $2\ KOH(111) + 2\ HI(111) + 2\ KI(200) \rightarrow 2\ KOH(100) + 2\ HI(100) + 2\ KI(222)$

$\Delta H_{17}(18\ ^{\circ}C) = 16(1)$ cal $mol^{-1} = 67(4)$ J $mol^{-1}$ [12]
$\Delta H_{17}(18\ ^{\circ}C)^{cf} = 16(1)$ cal $mol^{-1} = 67(4)$ J $mol^{-1}$

(a18) $2\ KI(222) + (944\ H_2O)^{\gamma *} \rightarrow 2\ KI(694)^{\#}$

$\gamma$ – contains 10.5 moles of KI

$\Delta H_{18}(18\ ^{\circ}C) = 115(1)$ cal $mol^{-1} = 481(4)$ J $mol^{-1}$ [12]
$\Delta H_{18}(18\ ^{\circ}C)^{cf} = 115(1)$ cal $mol^{-1} = 481(4)$ J $mol^{-1}$

(a19) $K_2SO_4(277.5) + 2\ H_2O(l) \rightarrow H_2SO_4(55.5) + 2\ KOH(111)$

$\Delta H_{19}(17\ ^{\circ}C) = 32{,}966(300)$ cal $mol^{-1} = 137{,}930(1255)$ J $mol^{-1}$ [20]
$\Delta H_{19}(18\ ^{\circ}C) = 32{,}907(310)$ cal $mol^{-1} = 137{,}683(1297)$ J $mol^{-1}$ [10, 14, 15]
$\Delta H_{19}(18\ ^{\circ}C)^{cf} = 32{,}907(310)$ cal $mol^{-1} = 137{,}683(1297)$ J $mol^{-1}$

(a20) $H_2SO_4(55.5) + (166.5\ H_2O)^* \rightarrow H_2SO_4(222)$

$\Delta H_{20}(18\ °C) = -390(10)$ cal mol$^{-1}$ $= -1{,}632(42)$ J mol$^{-1}$ [12]
$\Delta H_{20}(18\ °C)^{cf} = -390(10)$ cal mol$^{-1}$ $= -1{,}632(42)$ J mol$^{-1}$

(a21) $K_2SO_4(1123) \rightarrow K_2SO_4(277.5) + (845.5\ H_2O)^{\delta *}$

$\delta$ – contains 8.5 moles of KI

$\Delta H_{21}(18\ °C) = -195(2)$ cal mol$^{-1}$ $= -816(8)$ J mol$^{-1}$ [12]
$\Delta H_{21}(18\ °C)^{cf} = -195(2)$ cal mol$^{-1}$ $= -816(8)$ J mol$^{-1}$

sum: $Hg_2SO_4(s) + H_2(g) + (222\ H_2O)^* \rightarrow 2\ Hg(l) + H_2SO_4(222)$

$\Delta H_{9-21}(18\ °C)^{cf} = -34{,}921(135)$ cal mol$^{-1}$ $= -146{,}109(565)$ J mol$^{-1}$

**Cd, $CdSO_4$ – $Hg_2SO_4$, Hg**

sum: $Cd(s) + Hg_2SO_4(s) \rightarrow CdSO_4(s) + 2\ Hg(l)$

$\Delta H_{1-21}(18\ °C)^{cf} = -45{,}403(66)$ cal mol$^{-1}$ $= -189{,}967(276)$ J mol$^{-1}$
$= -45{,}403(397)$ cal mol$^{-1}$ $= -189{,}967(1661)$ J mol$^{-1}$

It should be noted here that two uncertainties are given; these are discussed later under overall uncertainties. This value for $\Delta H_{1-21}(18\ °C)^{cf}$ may be converted to a value at 25 °C by using known values of the heat capacities of Cd(s) [10], $Hg_2SO_4(s)$ [14], $CdSO_4(s)$ [21, 22] and Hg(l) [14], as a function of temperature, namely[6]:

$$C_p[Cd(s)] = (5.333 + 0.00294\,T) \text{ cal mol}^{-1} \quad (14)$$

$$C_p[Hg_2SO_4(s)] = (13.8 + 0.060\,T) \text{ cal mol}^{-1} \quad (15)$$

$$C_p[CdSO_4(s)] = (10.771 + 0.0437\,T) \text{ cal mol}^{-1} \quad (16)$$

$$C_p[Hg(l)] = (7.368 - 0.0023\,T) \text{ cal mol}^{-1} \quad (17)$$

$$\Delta C_p[\text{reaction (a)}] = (6.374 - 0.02384\,T) \text{ cal mol}^{-1} \quad (18)$$

all of which may be expressed in J mol$^{-1}$ using the relation given in footnote 3. The heat of reaction (a) at 25 °C is then found to be $-45{,}407$ cal mol$^{-1}$ or $-189{,}983$ J mol$^{-1}$. Incidentally, the data of Bichowsky and Rossini [12] for the overall reaction lead to $-45{,}720$ cal mol$^{-1}$ at 18 °C or $-45.716$ cal mol$^{-1}$ at 25 °C (on the presently accepted definition of the calorie) for $\Delta H$ for reaction (a); NBS Circular 500 [23] gives $-44{,}021$ cal mol$^{-1}$ at 25 °C while revised NBS Circular [24] gives $-45{,}450$ cal mol$^{-1}$; this last value agrees within 43 cal mol$^{-1}$ of the overall sum given above. These latter values [12, 23, 24] are combinations of heat and emf data.

Notes on some of the above reactions should be given here. Richards and Tamaru [8] found that the temperature coefficient of the heat of solution of cadmium in concentrated HCl was $-71$ cal/°C and believed that even for dilute acid it amounted to as much as $-30$ cal/°C. Since reaction (a1) is for dilute acid $-30$ cal/°C is taken for the temperature coefficient; owing to the estimation made by Richards and Tamaru a large uncertainty of $\pm 10$ cal/°C is attributed to this value.

Thomsen [9] stated that the temperature of his observations for reactions (a2) and (a3) was 18–20 °C. A mean temperature of 19 °C is taken here, and Thomsen's values were corrected to 18 °C using the known heat capacity of $BaSO_4(s)$ [10] as a function of temperature and the heat capacities of the $Ba^{++}$ and $SO_4^=$ ions at 25 °C given by Pitzer and Brewer [11] (these latter values were assumed to be temperature and concentration independent). Since the difference of (a2) and (a3) is taken in arriving at the value for the overall reaction, an error in this temperature correction is negligible.

The temperature correction for the sum of the reactions (a9), (a10), and (a11) was obtained from the known heat capacities of $Hg_2SO_4(s)$ [14], Hg(l) [14], and $I_2(s)$ [10] as functions of temperature and of KI, $HgI_2$, and $K_2SO_4$ as functions of concentration and temperature as follows. The heat capacity of $HgI_2$ was taken equal to that of KI (since it was dissolved in KI solutions) and that of $K_2SO_4$ as equal to 0.917 times twice the heat capacity of KOH (the temperature coefficient for $K_2SO_4$ was taken equal to that for KOH). The factor 0.917 is the ratio of the heat capacity of 2KOH and $K_2SO_4$ at infinite dilution; the value for $SO_4^=$ was taken from the compilation of Pitzer and Brewer [11]. The heat capacities of aqueous solutions of KI and KOH at 25 °C, as a function of concentration, were taken from the compilation of Parker [15]. The temperature coefficient for HCl was used for the temperature coefficient of KI and the temperature coefficient of NaOH was used for the temperature coefficient for KOH [15]. These values lead to:

$$\Delta C_p[\text{sum of reactions (a9), (a10), (a11)}] = -579.9 + 2.14\,T \quad (19)$$

[6] Each equation was altered slightly to make it conform with the values in reference [24] at 25 °C.

for the change in heat capacity for the sum of reactions (a9), (a10), and (a11). The estimated uncertainty for equation (19) is ± 10 cal/°C.

The temperature correction for reaction (a14) was obtained using the known heat capacities of $I_2$(s) [10], HCl(g) [18], HI(g) [18], and $Cl_2$(g) [10] as functions of temperature, or:

$$\Delta C_p\,[\text{reaction (a14)}] = -0.84 - 0.0101\,T - 76000/T^2 \quad (20)$$

An uncertainty of ±10 cal/°C is assigned to this temperature correction.

Richards and Rowe [19] found an average of −50.9 cal/°C for the temperature coefficient for the neutralization of HCl(100) and of $HNO_3$(100) with LiOH(100), NaOH(100), and KOH(100). This average temperature coefficient is assumed here to also apply to the neutralization of KOH(100) with HI(100) with an uncertainty of ±9 cal/°C, the spread found between the values found for the neutralization of HCl(100) and of $HNO_3$ (100) with KOH(100).

Müller [20] measured the neutralization of $H_2SO_4$ (55.5) with potassium hydroxide of various dilutions (one mole of KOH in 13.508, 27.420, and 51.626 liters of water) at 17 °C. A value for the heat of neutralization of $H_2SO_4$(55.5) with one mole of KOH in 2 liters of water was obtained by extrapolation of $\Delta H$ (neutralization) against $\sqrt{\text{volume}}$; $\Delta H$ (neutralization) versus $\sqrt{\text{volume}}$ is a straight line over the range of observations made by Müller. An uncertainty of ± 150 cal/°C per mole of KOH(111) is assigned to this heat of reaction owing to the spread in the three values obtained by Müller. This neutralization value is much higher than the older values of Thomsen [9] and Berthelot [25]. The older values were probably low because of the presence of carbonate in the alkali as has been shown for similar cases by Keyes, Gillespie, and Mitsukuri [26]. The value was corrected to 18 °C, with an estimated additional uncertainty of ±10 cal/°C using the known heat capacity of water [14][7] as a function of temperature and of $H_2SO_4$. KOH, and $K_2SO_4$ as functions of concentration and temperature using the procedure discussed above in obtaining the temperature coefficient for the sum of the reactions (a9), (a10), and (a11). These values lead to

$$\Delta C_p\,[(\text{reaction (a19)}] = 574.17 - 1.772\,T \quad (21)$$

for the change in heat capacity for reaction (a19).

For the reactions (a13) and (a14) the uncertainties given in the parentheses are the ± uncertainties given by the experimenters. In the other cases the experimenters were not explicit on their experimental uncertainties. For (a1), Richards and Tamaru [8] stated that the maximum uncertainty if all errors were additive, which would be highly unlikely, would be 70 cal mol$^{-1}$, and that the probable error was undoubtedly much less. Their maximum uncertainty is retained here and an additional uncertainty of ±10 cal/°C is assigned to the temperature coefficient. The uncertainties assigned to (a2) and (a3) were deduced from the temperature correction, i.e., were taken as one half the correction. For (a7), Cohen, Helderman and Moesveld [7] made eight determinations of the heat evolved; the standard deviation of their mean value is 7 cal mol$^{-1}$. The average spread in their values is taken, however, as the overall uncertainty. For (a10) Varet gave a general value which differs from that given above for (a10) by 400 cal mol$^{-1}$; this is taken as the uncertainty and the same percentage uncertainty is assigned to (a9), a reaction also studied by Varet. For (a16) Richards and Rowe stated that the maximum uncertainty in their value was 0.07 percent, and is used here. The estimated uncertainty for (a19) was discussed above. The uncertainties for the other reactions, which are mostly ones for solution or dilution, are estimated ones.

The overall uncertainty value is obtained from the sum of the uncertainties for each reaction taking care of sign. An overall uncertainty may also be taken as the root sum square value of the uncertainties of the 21 reactions, namely 397 cal mol$^{-1}$ or 1661 J mol$^{-1}$ and is the second uncertainty given above. The actual uncertainty probably lies between these two estimates. A root mean square value of the uncertainty is 88 cal mol$^{-1}$ or 368 J mol$^{-1}$; this value of the uncertainty is close to the first one listed above.

Values for the entropy of Cd(s), $Hg_2SO_4$(s), $CdSO_4$(s), and Hg(l) at 25 °C are 12.37 [27], 47.96 [24], 29.41 [21], and 18.19 [27] cal K$^{-1}$ mol$^{-1}$, or 51.75, 200.66, 123.05, and 76.02 J K$^{-1}$ mol$^{-1}$, respectively. Therefore, $\Delta S_a$ for reaction (a) is 5.42 cal K$^{-1}$ mol$^{-1}$ or 22.68 J K$^{-1}$ mol$^{-1}$. This value combined with the value of $\Delta H_a$, given above, gives according to eq (1) −47.023 cal mol$^{-1}$ or −196,745 J mol$^{-1}$ for the Gibbs energy (free energy) change, $\Delta G_a$, for reaction (a). Since $\Delta G = -nEF$ [see eq (4)] $E$ would be 1.0195396 V at 25 °C for the standard cell of the saturated cadmium sulfate type, if the cell reaction were as depicted by reaction (a). Also, since $\Delta S = nF(dE/dT)$ [see eq (6)], $dE/dT$ for the cell at 25 °C would be 0.00011751 V/°C, if the cell reaction were as depicted by reaction (a). Since these values do not agree with the observed ones (see later) it follows that the cell reaction does not correspond to reaction (a).

The heat capacities at 25 °C of Cd(s), $Hg_2SO_4$(s), $CdSO_4$(s), and Hg(l) are, respectively, 6.21 [24], 31.54 [24], 23.806 [24], and 6.688 [24] cal K$^{-1}$ mol$^{-1}$ or 25.90, 132.00, 99.62, and 27.82 J K$^{-1}$ mol$^{-1}$; $\Delta C_p$ is therefore, −0.580 cal K$^{-1}$ mol$^{-1}$ or −2.427 J K$^{-1}$ mol$^{-1}$. Stull and Sinke [27] give 6.19 cal K$^{-1}$ mol$^{-1}$ for Cd(s). Papadopoulos and Giauque [21] give 23.806 cal K$^{-1}$ mol$^{-1}$ for $CdSO_4$(s), and Giauque, Barieau and Kunzler [14] give 31.689 and 6.702 cal K$^{-1}$ mol$^{-1}$ for $Hg_2SO_4$(s) and Hg(l), respectively. These values yield −0.669 cal K$^{-1}$ mol$^{-1}$ or −2.799 J K$^{-1}$ mol$^{-1}$ for $\Delta C_p$(a).

### Reaction (b)

The Gibbs energy change for reaction (b) is given by:

[7] Equation given in reference [14] was altered slightly to make equation consistent with the 25 °C value given in reference [22].

$$\Delta G_b = RT \ln \frac{p^*}{p^0} = RT \ln \frac{0.62}{23.7667}$$

$$= -2160 \text{ cal mol}^{-1} = -9037 \text{ J mol}^{-1} \quad (22)$$

where $p^0$ is the vapor pressure of water at 25 °C [28], $p^*$ the vapor pressure of the system $CdSO_4 \cdot H_2O - H_2O$, $T$ the Kelvin temperature, and $R$ the gas constant (1.98717 cal $K^{-1}$ $mol^{-1}$ or 8.3143 J $K^{-1}$ $mol^{-1}$ [1]). Ishikawa and Murooka [29] obtained 0.62 mm Hg for $p^*$. The values in mm Hg may be converted to pascals by the relation 1 mm Hg (0 °C) = 1.333224 $\times 10^2$ pascals.

The entropies for $CdSO_4$(s), $H_2O$(l), and $CdSO_4 \cdot H_2O$(s) at 25 °C are, respectively, 29.41 [21], 16.71 [24], and 36.82 [21] cal $K^{-1}$ $mol^{-1}$ or 123.05, 69.91, 154.05 J $K^{-1}$ $mol^{-1}$; therefore, $\Delta S_b$ for reaction (b) is −9.30 cal $K^{-1}$ $mol^{-1}$ or −38.91 J $K^{-1}$ $mol^{-1}$. This value combined with the value for $\Delta G_b$ above gives by eq (1) −4,933 cal $mol^{-1}$ or −20,640 J $mol^{-1}$ for $\Delta H_b$, the heat of reaction for reaction (b). Papadopoulos and Giauque [21] measured the heats of solution of $CdSO_4$(s) and $CdSO_4 \cdot H_2O$(s) in 400 moles of water at 25 °C for which they obtained −10,977 and −6095 cal $mol^{-1}$ or −45,928 and −25,501 J $mol^{-1}$, respectively. These yield −4,882 cal $mol^{-1}$ or −20,426 J $mol^{-1}$ for $\Delta H_b$ which differs by 51 cal $mol^{-1}$ or 214 J $mol^{-1}$ from that calculated above.

The heat capacities of $CdSO_4$(s), $H_2O$(l), and $CdSO_4 \cdot H_2O$(s) at 25 °C are, respectively, 23.806 [21], 17.995 [30], and 32.157 [21] cal $K^{-1}$ $mol^{-1}$ or 99.58, 75.29, and 134.544 J $K^{-1}$ $mol^{-1}$; therefore, $\Delta C_{p(b)}$ for reaction (b) is −9.644 cal $K^{-1}$ $mol^{-1}$ or −40.350 J $K^{-1}$ $mol^{-1}$.

**Reaction (c)**

The Gibbs energy change for reaction (c) is given by:

$$\Delta G_c = \frac{5}{3} RT \ln \frac{p^{**}}{p^0} = \frac{5}{3} RT \ln \frac{17.4}{23.7667}$$

$$= -308 \text{ cal} = -1289 \text{ J} \quad (23)$$

where $p^{**}$ is the vapor pressure of the system $CdSO_4 \cdot \frac{8}{3} H_2O - CdSO_4 \cdot H_2O$ and $p^0$, $T$, and $R$ have the same significance as given above. The average of the results of Ishikawa and Murooka [29] and of Carpenter and Jette [31] gives 17.4 mm Hg for $p^{**}$. Conversion to pascals may be done as stated above.

The entropies for $CdSO_4 \cdot H_2O$(s) and $H_2O$(l) have been given above. The entropy of $CdSO_4 \cdot \frac{8}{3} H_2O$(s) is 54.89[21] cal $K^{-1}$ $mol^{-1}$ or 229.66 J $K^{-1}$ $mol^{-1}$. $\Delta S_c$ is, therefore, −9.78 cal $K^{-1}$ $mol^{-1}$ or −40.92 J $K^{-1}$ $mol^{-1}$. This value combined with the value for $\Delta G_c$ given above gives by eq (1) −3,224 cal or −13,489 J for $\Delta H_c$, the heat of reaction for reaction (c). Papadopoulos and Giauque [21] measured the heats of solution of $CdSO_4 \cdot H_2O$(s) and $CdSO_4 \cdot \frac{8}{3} H_2O$(s) in 400 moles of water at 25 °C for which they obtained −6,095 and −2,899 cal $mol^{-1}$ or −25,502 and −12,129 J $mol^{-1}$, respectively. These yield −3,196 cal $mol^{-1}$ or −13,372 J $mol^{-1}$ for $\Delta H_c$ which differs by 28 cal $mol^{-1}$ or 117 J $mol^{-1}$ from that calculated above.

The heat capacities of $CdSO_4 \cdot H_2O$(s) and $H_2O$(l) have been given above. The heat capacity of $CdSO_4 \cdot \frac{8}{3} H_2O$(s) at 25 °C is 50.972 cal $K^{-1}$ $mol^{-1}$ [21] or 213.26 J $K^{-1}$ $mol^{-1}$. Therefore, $\Delta C_{p(c)}$ for reaction (c) is −11.177 cal or −46.765 J.

**Reaction (d)**

The Gibbs energy change for reaction (d) is given by:

$$\Delta G_d = \frac{8}{3} RT \ln \frac{p^0}{p^s} = \frac{8}{3} RT \ln \frac{23.7667}{21.17} = 184 \text{ cal} = 770 \text{ J} \quad (24)$$

where $p^s$ is the vapor pressure of a saturated solution of $CdSO_4 \cdot \frac{8}{3} H_2O$ and $p^0$, $T$, and $R$ have the significance given above. Ishikawa and Murooka [29] obtained 21.17 mm Hg for the vapor pressure of the saturated solution at 25 °C; this value may be converted to pascals as described above. Holsboer [32] found that 1,044 calories or 4,368 joules of heat were evolved when one mole of $CdSO_4 \cdot \frac{8}{3} H_2O$(s) was dissolved in enough water to form the saturated solution at 25 °C; for (8/3)/($m$−8/3) mole of salt the heat evolved would be 224 cal or 938 J since $m$ = 15.089 [5, 6] at 25 °C and (8/3)/($m$ − 8/3) = 0.2147. Combining these values for $\Delta G_d$ and $\Delta H_d$ gives 0.13 cal $K^{-1}$ or 0.544 J $K^{-1}$ for $\Delta S_d$, the entropy change for reaction (d).

Cohen and Moesveld [33] obtained 0.5836 cal $g^{-1}$ or 2.4414 J $g^{-1}$ for the specific heat of a saturated solution of $CdSO_4 \cdot \frac{8}{3} H_2O$ at 19 °C which becomes 0.5823 cal $g^{-1}$ or 2.4359 J $g^{-1}$ at 25 °C based on the higher concentration of the saturated solution at 25 °C and the ratio of the specific heat of water at 25 and 19 °C. Accordingly (8/3)/($m$−8/3) mole of a saturated solution of $CdSO_4 \cdot \frac{8}{3} H_2O$ has a heat capacity of 59.93 cal $K^{-1}$ or 250.705 J $K^{-1}$ at 25 °C; on the present thermochemical calorie the value is 59.92 cal $K^{-1}$ or 250.706 J $K^{-1}$. Combining this value with the heat capacity of $H_2O$(l) and $CdSO_4 \cdot \frac{8}{3} H_2O$(s), given above, gives −0.999 cal $K^{-1}$ or −4.180 J $K^{-1}$ for $\Delta C_{p(d)}$ for reaction (d).

The above values are summarized in tables 1 and 2; data are given in SI units in the first section of each table and in defined calories in the second section. Table 1 is based on experimental values for the Gibbs energy changes for reactions (b), (c), and (d) and the enthalpy changes for reactions (a) and (d). Table 2 is based on experimental values for the Gibbs energy change of reaction (d) and the enthalpy changes of reactions (a), (b), (c), and (d). The addition of these values for reactions (a), (b), (c), and (d) gives sum 1 or the values for the reaction in a standard cell of the

TABLE 1. *Thermodynamic data for the reaction in standard cells of the saturated cadmium sulfate type at 25 °C—based on experimental Gibbs energies for reactions (b), (c), and (d) and experimental enthalpies for reactions (a) and (d)*

| Reaction | Gibbs energy change $\Delta G$ J mol$^{-1}$ | Enthalpy change $\Delta H$ J mol$^{-1}$ | Entropy change $\Delta S$ J K$^{-1}$ mol$^{-1}$ | Heat-capacity change $\Delta C_p$ J K$^{-1}$ mol$^{-1}$ |
|---|---|---|---|---|
| (a) | #(−196,745) | −189,983 | 22.68 | [φ]−2.427 |
| (b) | −9,037 | (−20,640) | −38.91 | −40.350 |
| (c) | −1,289 | (−13,489) | −40.92 | −46.765 |
| (d) | 770 | 937 | (0.544) | −4.180 |
| sum 1 | −206,301 | −223,175 | −56.606 | −93.722 |
| (e)* | 9,743 | 23,764 | 47.03 | 0 |
| sum 2[p] | −196,558 | −199,411 | −9.576 | −93.722 |
| (e)** | 9,738 | 21,240 | 38.58 | 204.26 |
| sum 3[q] | −196,563 | −201,935 | −18.026 | 110.538 |
| | (cal mol$^{-1}$)[j] | cal mol$^{-1}$ | cal K$^{-1}$ mol$^{-1}$ | cal K$^{-1}$ mol$^{-1}$ |
| (a) | (−47,023) | −45,407 | 5.42 | [φ]−0.580 |
| (b) | −2,160 | (−4,933) | −9.30 | −9.644 |
| (c) | −308 | (−3,224) | −9.78 | −11.177 |
| (d) | 184 | 224 | (0.13) | −0.999 |
| sum 1 | −49,307 | −53,340 | −13.53 | −22.400 |
| (e)* | 2,328.6 | 5,679.8 | 11.24 | 0 |
| sum 2[p] | −46,978.4 | −47,660.2 | −2.29 | −22.400 |
| (e)** | 2,327.5 | 5,076.4 | 9.22 | 48.82 |
| sum 3[q] | −46,979.5 | −48,263.6 | −4.31 | 26.420 |

# Values in parentheses were calculated from the relation $\Delta G = \Delta H - T\Delta S$.
[φ] See text for alternate value of −2.799 J K$^{-1}$ mol$^{-1}$ or −0.669 cal K$^{-1}$ mol$^{-1}$.
* Based on data of Hulett [34] and Getman [35].
[p] Sum 1 + (e)*.
** Based on data of Parks and LaMer [39].
[q] Sum 1 + (e)**.
[j] 1 Thermochemical calorie (defined) = 4.184 J [1].

TABLE 2. *Thermodynamic data for the reaction in standard cells of the saturated cadmium sulfate type at 25 °C—based on experimental enthalpies for reactions (a), (b), (c), and (d) and experimental Gibbs energy for reaction (d)*

| Reaction | Gibbs energy change $\Delta G$ J mol$^{-1}$ | Enthalpy change $\Delta H$ J mol$^{-1}$ | Entropy change $\Delta S$ J K$^{-1}$ mol$^{-1}$ | Heat-capacity change $\Delta C_p$ J K$^{-1}$ mol$^{-1}$ |
|---|---|---|---|---|
| (a) | #(−196,745) | −189,983 | 22.68 | [φ]−2.402 |
| (b) | (−8,824) | −20,426 | −38.91 | −40.350 |
| (c) | (−1,171) | −13,372 | −40.92 | −46.765 |
| (d) | 770 | 937 | (0.544) | −4.180 |
| sum 1 | −205,970 | −222,844 | −56.606 | −93.722 |
| (e)* | 9,743 | 23,764 | 47.03 | 0 |
| sum 2[p] | −196,227 | −199,080 | −9.576 | −93.722 |
| (e)** | 9,738 | 21,240 | 38.58 | 204.26 |
| sum 3[q] | −196,232 | −201,604 | −18.026 | 110.538 |
| | (cal mol$^{-1}$)[j] | cal mol$^{-1}$ | cal K$^{-1}$ mol$^{-1}$ | cal K$^{-1}$ mol$^{-1}$ |
| (a) | (−47,023) | −45,407 | 5.42 | [φ]−0.580 |
| (b) | (−2,109) | −4,882 | −9.30 | −9.644 |
| (c) | −280 | −3,196 | −9.78 | −11.177 |
| (d) | 184 | 224 | (0.13) | −0.999 |
| sum 1 | −49,228 | −53,261 | −13.53 | −22.400 |
| (e)* | 2,328.6 | 5,679.8 | 11.24 | 0 |
| sum 2[p] | −46,899.4 | −47,581.2 | −2.29 | −22.400 |
| (e)** | 2,327.5 | 5,076.4 | 9.22 | 48.82 |
| sum 3[q] | −46,900.5 | −48,184.6 | −4.31 | 26.420 |

# Values in parentheses were calculated from the relation $\Delta G = \Delta H - T\Delta S$.
[φ] See text for alternate value of −2.799 J K$^{-1}$ mol$^{-1}$ or −0.669 cal K$^{-1}$ mol$^{-1}$.
* Based on data of Hulett [34] and Getman [35].
[p] Sum 1 + (e)*.
** Based on data of Parks and LaMer [39].
[q] Sum 1 + (e)**.
[j] 1 Thermochemical calorie (defined) = 4.184 J [1].

saturated cadmium sulfate type at 25 °C if the anode were made of cadmium metal rather than cadmium amalgam.

**Reaction (e)**

Calorimetric and chemical equilibrium measurements on reaction (e) have not been made. It is necessary, therefore, to rely on electrochemical measurements for information on reaction (e). Hulett [34] and Getman [35] measured the emf of the cell:

$$(-)\mathrm{Cd(metal)}\,|\,\mathrm{CdSO_4(sol)}\,|\,\mathrm{Cd\ amalgam\,(8\text{–}10\%)(+)} \quad \text{(A)}$$

at a series of temperatures and obtained:

$$E\ (\text{in volts}) = 0.050487 - 0.0002437\,(t - 25\ ^\circ\mathrm{C}) \quad (25)$$

for the emf as a function of temperature. In cell (A) sol denotes an aqueous solution. Sir Frank Smith [36] showed that 8-percent and 10-percent amalgams have the same electrical potential. Hulett and Getman's emfs, expressed in international volts were converted to absolute volts here using the relation: 1 international volt (USA) = 1.0003384 absolute volts [37, 38]. Their results give 2,328.6 cal mol$^{-1}$, 5,679.8 cal mol$^{-1}$, 11.24 cal K$^{-1}$ mol$^{-1}$, and 0 cal K$^{-1}$ mol$^{-1}$ or 9,742.9 J mol$^{-1}$, 23,764.2 J mol$^{-1}$, 47.03 J K$^{-1}$ mol$^{-1}$, and 0 J K$^{-1}$ mol$^{-1}$ for $\Delta G_e$, $\Delta H_e$, $\Delta S_e$, and $\Delta C_{p(e)}$, respectively, for reaction (e). (Note that reaction (e) is for the reverse reaction of the above cell.) These values are added to sum 1 in tables 1 and 2 to give sum 2 for the thermodynamic data for the reaction at 25 °C in standard cells of the saturated cadmium sulfate type.

Parks and LaMer [39] also measured the emf of the above cell (A) over the temperature range of 0 to 40 °C. They expressed their results by the equation:

$$E\ (\text{in volts}) = 0.055399 - 0.000148\,t - 0.00000385\,t^2 + 0.000000075\,t^3. \quad (26)$$

Their emfs, given in international volts were converted

here to absolute volts using the relation given directly above. Their results lead to 2,327.5 cal $mol^{-1}$, 5.076.4 cal $mol^{-1}$, 9,22 cal $K^{-1}$ $mol^{-1}$, and 48.82 cal $K^{-1}$ $mol^{-1}$ or 9,738.3 J $mol^{-1}$, 21,239.6 J mol, 38.58 J $K^{-1}$ $mol^{-1}$, and 204.26 J $K^{-1}$ $mol^{-1}$ for $\Delta G_e$, $\Delta H_e$, $\Delta S_e$, and $\Delta C_{p(e)}$, respectively, for reaction (e) at 25 °C. The value for $\Delta G_e$ agrees well with that obtained from Hulett and Getman's data but the values for the other thermodynamic functions do not. These differences are discussed in more detail later. These values are added to sum 1 in tables 1 and 2 give sum 3 for alternate thermodynamic data for the reaction at 25 °C in standard cells of the saturated cadmium sulfate type.

## 4. Electromotive Force and Emf-temperature Coefficient

The electromotive force of the so-called "neutral" or Normal standard cell was initially determined at 20 °C in terms of the international ohm and the international ampere by an International Committee on Electrical Units and Standards which met at the National Bureau of Standards in 1910.[8] As a result of numerous experiments they arrived at a value of 1.0183 V for the emf of the cell at 20 °C; values derived from this were later assumed to be significant to the fifth, sixth, or seventh decimal as a basis of measurement [5] and subsequent "absolute" measurements of the ohm and ampere confirmed the validity of this process. Somewhat earlier [42, 43, 44] Wolff investigated extensively the emf-temperature coefficient of the "neutral" type of standard cell made with 12½-percent cadmium amalgams. Wolff based his emf-temperature formula (or equation) on the results obtained from 0 to 40 °C, inclusive, on 137 cells, made in various ways, after rejecting the results on 63 cells for a variety of reasons, including cell leakage, abnormal initial emfs, excessive emf-temperature hysteresis, erratic behavior, or chemical instability. Wolff [42] first arrived at the approximate emf-temperature formula:

$$E_t = E_{20\,°C} - 0.0000406(t-20) - 0.000000939(t-20)^2 + 0.000000009(t-20)^3 \quad (27)$$

by the method of least squares on the means of all observations on ten cells selected on the basis of their fast attainment of equilibrium after temperature changes. Using this approximate equation he then determined the residuals for all of the 137 cells at each temperature and calculated the corrections needed for the coefficients in eq (27) above. In this way he arrived at the emf-temperature formula:

$$E_t = E_{20\,°C} - 0.00004064(t-20) - 0.000000942(t-20)^2 + 0.0000000096(t-20)^3 \quad (28)$$

The 137 cells used to obtain eq (28) consisted of seven different groups of cells, namely, (1) 11 cells made with electrolytic mercurous sulfate prepared at low current densities [45], (2) 53 cells made with electrolytic mercurous sulfate prepared at higher current densities [46], (3) 22 cells made with mercurous sulfate prepared chemically in different ways, (4) 19 cells made with various samples of commercial mercurous sulfate, (5) 13 cells made with exchange (gift) samples of electrolytic mercurous sulfate, (6) nine exchange cells (foreign and domestic), and (7) 10 cells made with high current-density electrolytic mercurous sulfate but with different samples of cadmium sulfate synthesized or treated in various ways. Except for group (7) the cadmium sulfate was commercial grade which was recrystallized several times from distilled water.

Wolff [43] later gave a different formula wherein the first, second, and third coefficients in eq (27) or (28) were, respectively, 0.00004075, −0.000000944, and 0.0000000098 (these were uncorrected for residuals, compare data in references [42] and [43]).

The International Conference on Electrical Units and Standards meeting in London in 1908 adopted the formula (since known as the International formula) [47]:

$$E_t = E_{20\,°C} - 0.0000406(t-20) - 0.00000095(t-20)^2 + 0.00000001(t-20)^3 \quad (29)$$

giving weight to Wolff's original (provisional) emf-temperature formula, eq (27) above. It should be noted that practically the same result follows if the data obtained on groups (4) and (6), for which the cells were not well characterized, and on those cells for which the emf-temperature coefficient at 20 °C exceeds one microvolt are eliminated; these eliminations leave 99 cells for evaluation. Using these 99 cells gives:

$$E_t = E_{20\,°C} - 0.00004049(t-20) - 0.000000951(t-20)^2 + 0.00000000962(t-20)^3 \quad (30)$$

Equation (29), the International Temperature Formula, has been confirmed within the experimental uncertainty many times in succeeding years [48–53] for temperatures from 15 to 40 °C. The limits of uncertainty in the equation are discussed later.

Equations (29) and (30) may be given in the alternate forms:

$$E = E_{0\,°C} + 0.0000094\,t - 0.00000155\,t^2 + 0.00000001\,t^3 \quad (31)$$

$$E = E_{0\,°C} + 0.000009094\,t - 0.0000015282\,t^2 + 0.00000000962\,t^3. \quad (32)$$

Vigoureux and Watts [54], Obata and Ishibashi [55], and Ishibashi and Ishizaki [50] also measured the emf-temperature coefficient of standard cells of the saturated cadmium sulfate type. However, their cells were of the "acid" type. i.e., sulfuric acid was added to the cell in small amounts (0.1 *N* for ref. [54] and various amounts for ref. [55] and ref. [50]) and will, therefore, not be considered here. Furthermore, Vigoureux and Watts gave emphasis to measurements below 0 °C.

[8] Some measurements on the emf of standard cells were made earlier (see references [5, 40], and [41]) but these were not standardized internationally in terms of the mechanical units. The term "neutral" cell refers to one in which sulfuric acid, in low concentrations, is not intentionally added to the cell; actually, cadmium sulfate hydrolyzes to give sulfuric acid of 0.00092 *N* [5].

Obata and Ishibashi made measurements only from 15.6 to 29.6 °C, and Ishibashi and Ishizaki from 15 to 30 °C.

The results of Wolff were expressed in international volts and on the temperature scale based on the constant-volume hydrogen gas thermometer, defined in terms of melting ice (0 °C) and boiling water (100 °C), the hydrogen being taken at an initial manometric pressure of one meter of mercury; realization of the temperature scale was effected through mercurial thermometers calibrated in terms of the gas thermometer [56]. This temperature scale was the same as that adopted as the International Temperature Scale of 1927 [57].

On January 1, 1948 the international volt was replaced by the absolute volt; the change [37] for the United States was 1 international volt (USA)=1.000330 absolute volts. Then on January 1, 1969 another change [38] was made; the factor was: 1 USA $volt_{48}$=1.0000084 USA $volt_{69}$. Accordingly, the total change in going from the old international volt (USA) to the modern absolute volt is: 1 international volt (USA)= 1.0003384 absolute USA $volt_{69}$. In 1948 the International Temperature Scale was revised [57] but differed from the 1927 scale only at temperatures above 630 °C and, therefore, out of the range of work done on standard cells by Wolff. However, in 1968 another revision of the International Temperature Scale was made [58] which did affect the precise value of the emf-temperature coefficient of standard cells; for example, $t_{68}-t_{48}$ is −0.004 °C at 10 °C, −0.007 °C at 20 °C, −0.009 °C at 30 °C and zero at the melting point of ice and the boiling point of water.

In view of the above changes in the basis of reference for the volt and in the International Temperature Scale, changes in the voltage standard and in the results obtained by Wolff on the emf-temperature coefficient become necessary. With these changes eq (29) and the alternate form, eq (31) become, respectively:

$$E = E_{20\,°C} - 0.000004064(t-20) - 0.00000095006(t-20)^2 + 0.000000010034(t-20)^3 \quad (33)$$

and

$$E = E_{0\,°C} + 0.0000094019\,t - 0.0000015521\,t^2 + 0.000000010034\,t^3 \quad (34)$$

In table 3 the thermodynamic data for standard cells of the saturated cadmium sulfate type are given for temperatures from 0 to 43.6 °C [the transition temperature, $CdSO_4 \cdot \frac{8}{3}\ H_2O(s) = CdSO_4 \cdot H_2O(s)$], inclusive, as calculated from emf data and eq (33) or eq (34). In this table the changes in emf from international to absolute (1948), to absolute (1969), and for the different temperature scales are given. The thermodynamic data given herein are calculated from the most recent values of the emf, i.e., on $V_{69}$ and $t_{68}$. The emf at 20 °C in column 2 is that recommended by the International Committee on Electrical Units and Standards; it was based on the emf of cells prepared with mercurous sulfate made chemically or by dc electrolysis. Numerous investigations have indicated that mercurous sulfates prepared in different ways, providing they do not contain basic mercurous sulfate or mercuric ions, yield cells of the same emf. However, recent studies to be discussed in a subsequent paper, show that mercurous sulfate prepared by dc electrolysis gives cells with an emf exceeding those in column 5 of table 3 by 16.8 μV. This difference is small and amounts to only 3.24 J $mol^{-1}$ (0.77 cal $mol^{-1}$) in $\Delta G$ and $\Delta H$, see footnote to tables 3, 4, and 10.

The uncertainties listed, 1σ, are mean standard deviations obtained from the data on the 99 cells measured by Wolff, and includes an uncertainty of 5.4 μV[9] arising from the combined uncertainties in the absolute measurement of the ampere and the ohm.

## 5. Comparisons of Calorimetric and Equilibrium Data With Electrochemical (or Electrical) Data at 25 °C

Comparisons of calorimetric and equilibrium data with electrochemical data are given in table 4 for 25 °C. Insufficient data are available for direct comparisons at other temperatures. Six facts are evident from inspection of the data, namely:

(1) Remarkable agreement is obtained for $\Delta G$, $\Delta H$, and $\Delta S$ between the calorimetric and equilibrium data (sum 2) and electrochemical data in Part I if the emf data for cell (A) obtained by Hulett [34] and Getman [35] are used for reaction (e). This agreement may be coincidental in view of the uncertainties in the older heat data or results from a cancellation of errors, but even so it adds weight to the reliability of the postulated chemical reactions for standard cells of the saturated cadmium sulfate type. For example, Harned and Owen [62] state "It should be emphasized . . . that the nature of the chemical reactions, corresponding to a particular electrode, or cell, cannot be determined by electromotive force measurements alone. Cells reactions, no matter how simple and obvious, must be treated as hypothetical until it can be shown that thermodynamic quantities calculated from the electromotive force, $\Delta F$[$\Delta G$], $\Delta H$, equilibrium constants, etc. have been checked by other evidence."

(2) The difference of 1.722 J $K^{-1}$ $mol^{-1}$ (0.410 cal $K^{-1}$ $mol^{-1}$) between the $\Delta C_p$ values (sum 2 and electrochemical) may well be accounted for by the data for cell (A) for which $\Delta C_p$ is zero. More careful measurements on cell (A) may well show that the emf of this cell as a function of temperature is second- or third-order rather than a linear function.

(3) The data show that the results of Parks and LaMer [39] for cell (A), although they give good agreement with calorimetric data for $\Delta G$, yield

[9] This is a root sum square value. Recently, John Clarke [59] gave the uncertainty as ±2.6 ppm (or μV); this is about one half the root sum square uncertainty in published values for the absolute ampere [60] and the absolute ohm [61].

TABLE 3. *Electromotive forces and thermodynamic data for standard cells of the saturated cadmium sulfate type*

| Temperature | | Electromotive force, V | | | | Gibbs energy change, $\Delta G$ | |
|---|---|---|---|---|---|---|---|
| °C | Int | $Abs_{48}$ & $t_{48}$ | $Abs_{69}$ & $t_{48}$ | $Abs_{69}$ & $t_{68}$ [b] | $\sigma_m(\mu V)$ | (J $mol^{-1}$) [c] | (cal $mol^{-1}$) [d] |
| 0 | 1.0186520 | 1.0189881 | 1.0189968 | 1.0189967 | 8.14 | −196,639.9(4.8) | −46,998.0(1.1) |
| 3 | 1.0186665 | 1.0190026 | 1.0190112 | 1.0190112 | 8.12 | −196,642.7(4.8) | −46,998.6(1.1) |
| 5 | 1.0186615 | 1.0189976 | 1.0190061 | 1.0190062 | 8.10 | −196,641.7(4.8) | −46,998.4(1.1) |
| 10 | 1.0186010 | 1.0189371 | 1.0189456 | 1.0189455 | 8.08 | −196,630.0(4.8) | −46,995.6(1.1) |
| 15 | 1.0184780 | 1.0188141 | 1.0188226 | 1.0188224 | 8.07 | −196,606.2(4.8) | −46,989.9(1.1) |
| 18 | 1.0183773 | 1.0187133 | 1.0187219 | 1.0187216 | 8.06 | −196,586.8(4.8) | −46,985.3(1.1) |
| 20 | 1.0183000 | 1.0186360 | 1.0186445 | 1.0186442 | 8.06 | −196,571.8(4.8) | −46,981.7(1.1) |
| 25 | 1.0180745 | 1.0184105 | 1.0184190 | 1.0184185 | 8.07 | −196,528.3(4.8) | −46,971.3(1.1) |
| 28 | 1.0179195 | 1.0182554 | 1.0182639 | 1.0182634 | 8.08 | −196,498.4(4.8) | −46,964.1(1.1) |
| 30 | 1.0178090 | 1.0181448 | 1.0181533 | 1.0181528 | 8.08 | −196,477.0(4.8) | −46,959.0(1.1) |
| 35 | 1.0175110 | 1.0178467 | 1.0178552 | 1.0178547 | 8.09 | −196,419.5(4.8) | −46,945.3(1.1) |
| 40 | 1.0171880 | 1.0175236 | 1.0175323 | 1.0175317 | 8.10 | −196,357.2(4.8) | −46,930.4(1.1) |
| 43.6 [a] | 1.0169446 | 1.0172797 | 1.0172886 | 1.0172878 | 8.11 | −196,310.1(4.8) | −46,919.2(1.1) |

| Emf-temperature coefficient, $\mu V\ K^{-1}$ | | | | | | Entropy change, $\Delta S$ | | Enthalpy change, $\Delta H$ | |
|---|---|---|---|---|---|---|---|---|---|
| °C | Int | $Abs_{48}$ & $t_{48}$ | $Abs_{69}$ & $t_{48}$ | $Abs_{69}$ & $t_{68}$ | $\sigma_m(\mu V)$ | J $K^{-1}$ $mol^{-1}$ | cal $K^{-1}$ $mol^{-1}$ | (J $mol^{-1}$) [c] | (cal $mol^{-1}$) [d] |
| 0 | 9.40 | 9.40 | 9.40 | 9.40 | 0.14 | 1.814(.027) | 0.433(.006) | −196,147.4(11.8) | −46,880.3(2.8) |
| 3 | 0.37 | 0.37 | 0.37 | 0.36 | .11 | 0.069(.022) | .017(.005) | −196,624.8(10.4) | −46,994.5(2.5) |
| 5 | −5.35 | −5.35 | −5.36 | −5.37 | .10 | −1.036(.020) | −0.248(.004) | −196,930.1(9.9) | −47,067.4(2.2) |
| 10 | −18.60 | −18.61 | −18.61 | −18.63 | .06 | −3.595(.012) | −0.859(.003) | −197,647.1(7.7) | −47,238.8(2.0) |
| 15 | −30.35 | −30.36 | −30.36 | −30.39 | .04 | −5.864(.008) | −1.402(.002) | −198,295.0(6.6) | −47,393.6(1.7) |
| 18 | −36.68 | −36.70 | −36.70 | −36.72 | .04 | −7.086(.008) | −1.694(.001) | −198,649.3(6.6) | −47,478.2(1.3) |
| 20 | −40.60 | −40.62 | −40.61 | −40.64 | .04 | −7.843(.008) | −1.874(.002) | −198,870.4(6.6) | −47,531.1(1.5) |
| 25 | −49.35 | −49.37 | −49.36 | −49.39 | .04 | −9.531(.008) | −2.278(.002) | −199,370.3(6.6) | −47,650.5(1.6) |
| 28 | −53.88 | −53.90 | −53.89 | −53.92 | .04 | −10.404(.008) | −2.487(.002) | −199,632.2(6.6) | −47,713.1(1.7) |
| 30 | −56.60 | −56.62 | −56.61 | −56.63 | .04 | −10.929(.008) | −2.612(.002) | −199,790.7(6.7) | −47,750.8(1.7) |
| 35 | −62.35 | −62.37 | −62.35 | −62.37 | .06 | −12.036(.012) | −2.877(.002) | −200,128.4(8.0) | −47,831.8(1.8) |
| 40 | −66.60 | −66.62 | −66.59 | −66.60 | .09 | −12.853(.018) | −3.072(.004) | −200,380.6(10.0) | −47,692.1(2.3) |
| 43.6 [a] | −68.73 | −68.76 | −68.71 | −68.72 | .13 | −13.261(.025) | −3.169(.007) | −200,506.4(12.3) | −47,927.0(3.3) |

TABLE 3. *Electromotive etc.*—Continued

| Second derivative, $d^2E/dT^2$, $\mu V\ K^{-1}\ K^{-1}$ | | | | | | Heat-capacity change, $\Delta C_p$ | |
|---|---|---|---|---|---|---|---|
| °C | Int | $Abs_{48}$ & $t_{48}$ | $Abs_{69}$ & $t_{48}$ | $Abs_{69}$ & $t_{68}$ | $\sigma_m(\mu V)$ | J $K^{-1}$ $mol^{-1}$ | cal $K^{-1}$ $mol^{-1}$ |
| 0..... | −3.100 | −3.101 | −3.102 | −3.104 | 0.010 | −163.62(.53) | −39.11(.13) |
| 3..... | −2.920 | −2.921 | −2.921 | −2.924 | .008 | −155.80(.43) | −37.24(.10) |
| 5..... | −2.800 | −2.801 | −2.801 | −2.803 | .008 | −150.46(.43) | −35.96(.10) |
| 10 ..... | −2.500 | −2.501 | −2.501 | −2.502 | .006 | −136.72(.33) | −32.68(.08) |
| 15 ..... | −2.200 | −2.201 | −2.200 | −2.201 | .003 | −122.40(.17) | −29.25(.04) |
| 18 ..... | −2.020 | −2.021 | −2.020 | −2.021 | .001 | −113.52(.06) | −27.13(.01) |
| 20 ..... | −1.900 | −1.901 | −1.900 | −1.900 | .001 | −107.49(.06) | −25.69(.01) |
| 25 ..... | −1.600 | −1.601 | −1.599 | −1.599 | .001 | −92.00(.06) | −21.99(.01) |
| 28 ..... | −1.420 | −1.420 | −1.419 | −1.418 | .002 | −82.43(.11) | −19.70(.02) |
| 30 ..... | −1.300 | −1.300 | −1.299 | −1.298 | .003 | −75.94(.18) | −18.14(.04) |
| 35 ..... | −1.000 | −1.000 | −0.998 | −0.997 | .006 | −59.29(.35) | −14.17(.09) |
| 40 ..... | −0.700 | −0.700 | −0.698 | −0.696 | .008 | −42.06(.48) | −10.05(.12) |
| 43.6 [a]... | −0.484 | −0.484 | −0.481 | −0.479 | .009 | −29.30(.55) | −7.00(.13) |

[a] All values at 43.6 °C are extrapolated values.
[b] Based on combined results obtained with chemically-prepared and dc-electrolytic mercurous sulfate: the values are 18.6 $\mu$V higher for dc-electrolytic mercurous sulfate alone.
[c] Higher by 3.24 J $mol^{-1}$ for dc-electrolytic mercurous sulfate alone.
[d] Higher by 0.77 cal $mol^{-1}$ for dc-electrolytic mercurous sulfate alone.

results for $\Delta H$, $\Delta S$, and especially $\Delta C_p$ (actually of opposite sign) that differ widely from the electrochemical data on standard cells of the saturated cadmium sulfate type. Actually, Parks and LaMer gave too much weight to an apparent curvature in the variation of the emf of cell (A) with temperature.

(4) The enthalpy data of Papadopoulos and Giauque [21] lead to values for $\Delta G$ and $\Delta H$ that are lower than the electrochemical values by 301.3 J $mol^{-1}$ (71.9 cal $mol^{-1}$) and 290.0 J $mol^{-1}$ (69.3 cal $mol^{-1}$), respectively. These differences which amount, respectively, to only 0.16 percent and 0.15 percent, are beyond the uncertainties estimated by Papadopoulos and Giauque. Sometimes cadmium sulfate contains occluded sulfuric acid (especially if digested in sulfuric acid during the purification) which would cause a decrease in $\Delta G$ and $\Delta H$ for the cell reaction (see conclusions to this paper). Such occlusions could not explain the above differences in $\Delta G$ and $\Delta H$ between the calorimetric and electromotive force data since the occlusions would have to amount to about 1 molal $H_2SO_4$ (see conclusions to this paper) which is entirely out of the range of possibility.

(5) If the alternate heat capacity data for reaction (a), discussed above, are used they yield a value for sum 2 which differs more from the electrochemical value than the value given in table 4 (actually, the alternate heat capacity data for reaction (a) yield −94.231 J $K^{-1}$ $mol^{-1}$ (−22.474 cal $K^{-1}$ $mol^{-1}$) for sum 2 rather than the value shown).

(6) The enthalpy data of Papadoupolos and Giauque [21], if used with the enthalpy data of Bichowsky and Rossini [12], corrected to 25 °C, or the enthalpy data of Circular 500 [23] or the enthalpy data of revised NBS Circular [24, 30] still do not agree with the electrochemical data.

TABLE 4. *Comparison of calorimetric and equilibrium data with electromotive force data*

*Part 1*—Based on table 1: experimental values of $\Delta G$ for reactions (b), (c), and (d) and of $\Delta H$ for reactions (a) and (b)

| Calorimetric and equilibrium data | $\Delta G$ J $mol^{-1}$ | $\Delta H$ J $mol^{-1}$ | $\Delta S$ J $K^{-1}$ $mol^{-1}$ | $\Delta C_p$ J $K^{-1}$ $mol^{-1}$ |
|---|---|---|---|---|
| sum 2..... | −196,558 | −199,411 | −9.576 | [d] −93.722 |
| sum 3..... | −196,563 | −201,935 | −18.026 | 110.538 |
| Electrochemical data..... | [a] −196,528.3 | [a] −199,370.0 | −9.531 | −92.00 |
| **Calorimetric and equilibrium data** | **cal $mol^{-1}$** | **cal $mol^{-1}$** | **cal $K^{-1}$ $mol^{-1}$** | **cal $K^{-1}$ $mol^{-1}$** |
| sum 2..... | −46,978.4 | −47,660.2 | −2.29 | −22.400 |
| sum 3..... | −46.979.5 | −48,263.6 | −4.31 | 26.420 |
| Electrochemical data..... | [b] −46,971.3 | [b] −47,650.5 | −2.278 | −21.99 |

TABLE 4. *Comparison etc.*—Continued

*Part II*—Based on table 2: experimental values of $\Delta G$ for reaction (d) and of $\Delta H$ for reactions (a), (b), (c), and (d)

| Calorimetric and equilibrium data | $\Delta G$ J mol$^{-1}$ | $\Delta H$ J mol$^{-1}$ | $\Delta S$ J K$^{-1}$ mol$^{-1}$ | $\Delta C_p$ J K$^{-1}$ mol$^{-1}$ |
|---|---|---|---|---|
| sum 2 | −196,227 | −199,080 | −9.576 | [φ] −93.722 |
| sum 3 | −196,232 | −201,604 | −18.026 | 110.538 |
| Electrochemical data | [a] −196,528.3 | [a] −199,370.0 | −9.531 | −92.00 |
| **Calorimetric and equilibrium data** | **cal mol$^{-1}$** | **cal mol$^{-1}$** | **cal K$^{-1}$ mol$^{-1}$** | **cal K$^{-1}$ mol$^{-1}$** |
| sum 2 | −46,899.4 | −47,581.2 | −2.29 | −22.400 |
| sum 3 | −46,900.5 | −48,184.6 | −4.31 | 26.420 |
| Electrochemical data | [b] −46,971.3 | [b] −47,650.5 | −2.278 | −21.99 |

[φ] See tables 1 and 2 for a note on an alternate value.
[a] Higher by 3.24 J mol$^{-1}$ for dc-electrolytic mercurous sulfate.
[b] Higher by 0.77 cal mol$^{-1}$ for dc-electrolytic mercurous sulfate.

## 6. Range of Precision in Emf Results

In table 3 it is evident that the uncertainties in the data are greater at the two ends of the temperature range. For the emf, these reside in the experimental measurements but for the derived quantities, $\Delta H$, $\Delta S$, and $\Delta C_p$, they may be dependent in addition on the emf-temperature function used to represent the data. Since the emf data available on the standard cell of the saturated cadmium sulfate type are known with high precision they may be used to illustrate the effect an emf-temperature function has on the derived thermodynamic data. Accordingly, the emf data of table 3 were fitted (method of least squares) to second-, third-, and fourth-order equations in the temperature of the form (fourth order shown):

$$E = E_{0\,°C} + \alpha t + \beta t^2 + \gamma t^3 + \delta t^4. \qquad (35)$$

Also, since the literature [11, 62–65] is filled with results on the measurements of the emfs of galvanic cells to only 0.01 mV or 10 $\mu$V, and over a range of temperatures, the emf data of table 3 were rounded to 0.01 mV and then fitted (method of least squares) to second-, third-, and fourth-order equations in the temperature of the form of eq (35). The coefficients of the form equations for the several procedures are given in table 5.

Results are given in tables 6, 7, 8, and 9. In table 6 the emfs are given as obtained for fourth-, third-, and second-order equations and for emfs either known to 0.01 $\mu$V or rounded to 0.01 mV. Inspection shows that either third- or fourth-order equations may be used to represent the emfs.[10] Inspection also shows that the differences in $\Delta G$ are practically negligible between the fourth- and third-order fits. If the precision of the observations is lowered to 0.01 mV (table 7) the errors in $\Delta G$ are still practically negligible between the fourth- and third-order fits (see footnote 10). As expected, however, second-order equations are inadequate to represent $E$ and $\Delta G$ with either resolutions of 0.1 $\mu$V or 0.01 mV in $E$.

For $\Delta S$ and $\Delta C_p$ the situation is quite different, see tables 8 and 9. Values of $\Delta S$ as given by fourth and third order equations are practically the same, except above 40 °C or at 0 °C for a resolution of 0.1$\mu$V in $E$ but differ from 0.013 to 0.179 J K$^{-1}$ mol$^{-1}$ (0.007 to 0.043 cal K$^{-1}$ mol$^{-1}$) for a resolution of 0.01 mV in $E$. Particular attention should be given to a comparison, say at 25 °C, between a fourth (or third) order fit to 0.1 $\mu$V in $E$ and a *second* order fit to 0.01 mV in $E$ (most common procedure reported in the literature); a difference of 0.607 (0.606) J K$^{-1}$ mol$^{-1}$ (0.145 cal K$^{-1}$ mol$^{-1}$) is obtained. This difference is large and has mistakenly lead some observers [66–69], under similar cases, to conclude that the emf measurements

TABLE 5. *Coefficients in the equation:* $E = E_{0°} + \alpha t + \beta t^2 + \gamma t^3 + \delta t^4$

(On $V_{69}$ and $t_{68}$ scales)

(to 0.1 $\mu$V)

| Order | $E_{0°}$ | $\alpha \times 10^6$ | $\beta \times 10^6$ | $\gamma \times 10^9$ | $\delta \times 10^{11}$ |
|---|---|---|---|---|---|
| 4th | 1.0189968 | 9.3415 | −1.5454 | 9.7894 | 0.27990 |
| 3d | 1.0189967 | 9.4019 | −1.5521 | 10.034 | ..... |
| 2d | 1.0190260 | −1.5507 | −0.89411 | ..... | ..... |

(to 0.01 mV or 10 $\mu$V)

| | | | | | |
|---|---|---|---|---|---|
| 4th | 1.01900 | 9.9747 | −1.6498 | 13.828 | −4.2920 |
| 3d | 1.01900 | 9.0481 | −1.5469 | 10.082 | ..... |
| 2d | 1.01903 | −1.9569 | −0.88584 | ..... | ..... |

[10] Since the values in table 3 were generated from a third-order equation [see eqs (33) or (34)], the fit of a fourth-order equation would be no better than that of a third-order. However, derived quantities, especially $\Delta C_p$, may be slightly different; actually the difference gives an estimate of the uncertainty in the derived quantity.

TABLE 6. *Results from fourth, third, and second order equations for the emf of standard cells of the saturated cadmium sulfate type as a function of temperature (to 0.1 μV)*

| Temperature, °C | Electromotive force, V | | | Δ *in* Δ*G*, | | | | Δ in Δ*G*, | |
|---|---|---|---|---|---|---|---|---|---|
| | | | | Δ*E*, μV | | J mol$^{-1}$ | | cal mol$^{-1}$ | |
| | 4th order | 3d order | 2d order | 4–3 | 4–2 | 4–3 | 4–2 | 4–3 | 4–3 |
| 0 | 1.0189968 | 1.0189967 | 1.0190260 | 0.1 | −29.2 | 0.02 | −5.63 | 0.005 | −1.35 |
| 3 | 1.0190112 | 1.0190112 | 1.0190133 | 0 | −2.1 | 0 | −0.41 | 0 | −0.10 |
| 5 | 1.0190061 | 1.0190062 | 1.0189959 | −0.1 | 10.2 | −0.02 | 1.97 | −0.005 | 0.47 |
| 10 | 1.0189455 | 1.0189455 | 1.0189211 | 0 | 24.4 | 0 | 4.71 | 0 | 1.13 |
| 15 | 1.0188224 | 1.0188224 | 1.0188012 | 0 | 21.2 | 0 | 4.09 | 0 | 0.98 |
| 18 | 1.0187217 | 1.0187216 | 1.0187084 | 0.1 | 13.3 | 0.02 | 2.57 | 0.005 | 0.61 |
| 20 | 1.0186443 | 1.0186442 | 1.0186373 | 0.1 | 7.0 | .02 | 1.35 | .005 | .32 |
| 25 | 1.0184186 | 1.0184185 | 1.0184284 | 0.1 | −9.8 | .02 | −1.89 | .005 | −0.45 |
| 28 | 1.0182635 | 1.0182634 | 1.0182816 | 0.1 | −18.1 | .02 | −3.49 | .005 | −0.83 |
| 30 | 1.0181529 | 1.0181528 | 1.0181748 | 0.1 | −21.9 | .02 | −4.23 | .005 | −1.01 |
| 35 | 1.0178547 | 1.0178547 | 1.0178764 | 0 | −21.7 | .02 | −4.19 | .005 | −1.00 |
| 40 | 1.0175317 | 1.0175316 | 1.0175334 | 0.1 | −1.7 | .02 | −0.33 | .005 | −0.08 |
| 43.6 [a] | 1.0172880 | 1.0172878 | 1.0172587 | 0.2 | 29.3 | .04 | 5.65 | .01 | 1.35 |

[a] Extrapolated values.

TABLE 7. *Results from fourth, third, and second order equations for the emf of standard cells of the saturated cadmium sulfate type as a function of temperature (to 0.01 mV or 10 μV)*

| Temperature, °C | Electromotive force, V | | | Δ in Δ*G*, | | | | Δ in Δ*G*, | |
|---|---|---|---|---|---|---|---|---|---|
| | | | | Δ*E*, mV | | J mol$^{-1}$ | | cal mol$^{-1}$ | |
| | 4th order | 3d order | 2d order | 4–3 | 4–2 | 4.3 | 4–2 | 4–3 | 4–2 |
| 0 | 1.01900 | 1.01900 | 1.01903 | 0 | −0.03 | 0 | −5.79 | 0 | −1.38 |
| 3 | 1.01902 | 1.01901 | 1.01902 | 0.01 | 0 | 1.93 | 0 | 0.46 | 0 |
| 5 | 1.01901 | 1.01901 | 1.01900 | 0 | 0.01 | 0 | 1.93 | 0 | 0.46 |
| 10 | 1.01895 | 1.01895 | 1.01892 | 0 | .03 | 0 | 5.79 | 0 | 1.38 |
| 15 | 1.01882 | 1.01882 | 1.01880 | 0 | .02 | 0 | 3.86 | 0 | 0.92 |
| 18 | 1.01872 | 1.01872 | 1.01871 | 0 | .01 | 0 | 1.93 | 0 | .46 |
| 20 | 1.01864 | 1.01864 | 1.01864 | 0 | 0 | 0 | 0 | 0 | 0 |
| 25 | 1.01842 | 1.01842 | 1.01843 | 0 | −0.01 | 0 | −1.93 | 0 | −0.46 |
| 28 | 1.01826 | 1.01826 | 1.01828 | 0 | −0.02 | 0 | −3.86 | 0 | −0.92 |
| 30 | 1.01815 | 1.01815 | 1.01817 | 0 | −0.02 | 0 | −3.86 | 0 | −0.92 |
| 35 | 1.01786 | 1.01785 | 1.01788 | 0.01 | −0.02 | 1.93 | −3.86 | 0.46 | −0.92 |
| 40 | 1.01753 | 1.01753 | 1.01753 | 0 | 0 | 0 | 0 | 0 | 0 |
| 43.6 [a] | 1.01729 | 1.01729 | 1.01726 | 0 | 0.03 | 0 | 5.79 | 0 | 1.38 |

[a] Extrapolated values.

are in error whereas, in fact, the differences arise from a lack of resolution or in imprecision of the instruments employed. For $\Delta C_p$, this situation is even more marked, see table 9. Values of $\Delta C_p$, as given by fourth and third order equations are nearly the same, although the fourth-order results are probably preferable, if the resolution in $E$ is 0.1 μV. However, for a resolution of only 0.01 mV in $E$, large differences are found between fourth and third order fits, but the third-order fits agree more closely with the fourth and third order fits on 0.1 μV resolution in $E$; *third-order fits are, therefore, selected as final representations*, in line with eqs (29) and (31) given above. As above for $\Delta S$, particular attention should be given to a comparison, say at 25 °C, between a third-order fit to 0.1 μV in $E$ and a *second* order fit to 0.01 mV in $E$ (most common procedure reported in the literature); a difference of 9.93 J K$^{-1}$ mol$^{-1}$ (2.37 cal K$^{-1}$ mol$^{-1}$) is obtained. This value is again large and has mistakenly lead some observers [66–69], under similar cases, to conclude that the emf measurements are in error by as much as 1 mV whereas, in fact, the differences rest with the degree of resolution in the measuring equipment.

The situation in regard to both $\Delta S$ and $\Delta C_p$ is more serious at the extremes of temperature. This is shown in figures 1 and 2. It is obvious from these figures that $\Delta S$ and $\Delta C_p$, as determined from emfs of different resolutions and equations of different order differ at the extremes of temperature and that in order to determine them, especially $\Delta C_p$, at 0 °C and 40 °C

TABLE 8. *Entropy changes for reactions in standard cells of the saturated cadmium sulfate type as calculated by different functions*

| | (to 0.1 μV in $E$) | | | (to 0.01 mV or 10 μV in $E$) | | | (to 0.1 μV in $E$) | | | (to 0.01 mV or 10 μV in $E$) | | |
|---|---|---|---|---|---|---|---|---|---|---|---|---|
| | J $K^{-1}$ $mol^{-1}$ | | | | | | cal $K^{-1}$ $mol^{-1}$ | | | | | |
| Temperature, °C | 4th order | 3d order | 2d order | 4th order | 3d order | 2d order | 4th order | 3d order | 2d order | 4th order | 3d order | 2d order |
| 0 | 1.803 | 1.814 | −0.299 | 1.925 | 1.746 | −0.378 | 0.431 | 0.433 | −0.072 | 0.460 | 0.417 | −0.090 |
| 3 | 0.065 | 0.069 | −1.334 | 0.086 | 0.008 | −1.403 | 0.015 | 0.017 | −0.319 | 0.021 | .002 | −0.335 |
| 5 | −1.037 | −1.036 | −2.025 | −1.063 | −1.093 | −2.087 | −0.248 | −0.248 | −0.484 | −0.254 | −0.261 | −0.499 |
| 10 | −3.592 | −3.595 | −3.750 | −3.675 | −3.640 | −3.797 | −0.859 | −0.859 | −0.896 | −0.878 | −0.870 | −0.907 |
| 15 | −5.861 | −5.864 | −5.475 | −5.937 | −5.896 | −5.506 | −1.401 | −1.402 | −1.309 | −1.419 | −1.409 | −1.316 |
| 18 | −7.084 | −7.086 | −6.511 | −7.136 | −7.109 | −6.532 | −1.693 | −1.694 | −1.556 | −1.706 | −1.699 | −1.561 |
| 20 | −7.841 | −7.843 | −7.201 | −7.873 | −7.860 | −7.215 | −1.874 | −1.874 | −1.721 | −1.882 | −1.879 | −1.725 |
| 25 | −9.532 | −9.531 | −8.926 | −9.508 | −9.532 | −8.925 | −2.278 | −2.278 | −2.133 | −2.272 | −2.278 | −2.133 |
| 28 | −10.406 | −10.404 | −9.961 | −10.355 | −10.395 | −9.950 | −2.487 | −2.487 | −2.381 | −2.475 | −2.484 | −2.378 |
| 30 | −10.931 | −10.929 | −10.652 | −10.867 | −10.912 | −10.634 | −2.612 | −2.612 | −2.546 | −2.597 | −2.608 | −2.542 |
| 35 | −12.036 | −12.036 | −12.377 | −11.975 | −12.000 | −12.344 | −2.877 | −2.877 | −2.958 | −2.862 | −2.868 | −2.950 |
| 40 | −12.849 | −12.853 | −14.102 | −12.856 | −12.796 | −14.053 | −3.071 | −3.072 | −3.371 | −3.073 | −3.058 | −3.359 |
| 43.6 [a] | −13.248 | −13.261 | −15.345 | −13.365 | −13.189 | −15.284 | −3.166 | −3.169 | −3.667 | −3.194 | −3.152 | −3.653 |

[a] Extrapolated values.



TABLE 9. *Heat capacity changes for the reaction in standard cells of the saturated cadmium sulfate type as calculated by different functions*

| | (to 0.1 μV in $E$) | | | (to 0.01 mV or 10 μV in $E$) | | | (to 0.1 μV in $E$) | | | (to 0.01 mV or 10 μV in $E$) | | |
|---|---|---|---|---|---|---|---|---|---|---|---|---|
| | J $K^{-1}$ $mol^{-1}$ | | | | | | cal $K^{-1}$ $mol^{-1}$ | | | | | |
| Temperature, °C | 4th order | 3d order | 2d order | 4th order | 3d order | 2d order | 4th order | 3d order | 2d order | 4th order | 3d order | 2d order |
| 0 | −162.91 | −163.62 | −94.26 | −173.92 | −162.96 | −93.39 | −38.94 | −39.11 | −22.53 | −41.57 | −38.95 | −22.32 |
| 3 | −155.29 | −155.80 | −95.29 | −162.82 | −155.08 | −94.41 | −37.12 | −37.24 | −22.78 | −38.91 | −37.07 | −22.57 |
| 5 | −150.08 | −150.46 | −95.98 | −155.53 | −149.71 | −95.10 | −35.87 | −35.96 | −22.94 | −37.17 | −35.78 | −22.73 |
| 10 | −136.59 | −136.72 | −97.71 | −137.77 | −135.87 | −96.81 | −32.65 | −32.68 | −23.35 | −32.93 | −32.48 | −23.14 |
| 15 | −122.44 | −122.40 | −99.43 | −120.72 | −121.45 | −98.51 | −29.26 | −29.25 | −23.77 | −28.85 | −29.03 | −23.55 |
| 18 | −113.63 | −113.52 | −100.47 | −110.85 | −112.52 | −99.54 | −27.16 | −27.13 | −24.01 | −26.50 | −26.89 | −23.79 |
| 20 | −107.62 | −107.49 | −101.16 | −104.44 | −106.45 | −100.22 | −25.72 | −25.69 | −24.18 | −24.96 | −25.44 | −23.95 |
| 25 | −92.12 | −92.00 | −102.89 | −89.02 | −90.87 | −101.93 | −22.02 | −21.99 | −24.59 | −21.28 | −21.72 | −24.36 |
| 28 | −82.50 | −82.43 | −103.92 | −80.21 | −81.23 | −102.96 | −19.72 | −19.70 | −24.84 | −19.17 | −19.42 | −24.61 |
| 30 | −75.95 | −75.94 | −104.61 | −74.53 | −74.69 | −103.64 | −18.15 | −18.14 | −25.00 | −17.81 | −17.85 | −24.77 |
| 35 | −59.09 | −59.29 | −106.34 | −61.05 | −57.94 | −105.35 | −14.12 | −14.17 | −25.41 | −14.59 | −13.85 | −25.18 |
| 40 | −41.54 | −42.06 | −108.06 | −48.64 | −40.60 | −107.06 | −9.93 | −10.05 | −25.83 | −11.63 | −9.71 | −25.59 |
| 43.6 [a] | −28.47 | −29.30 | −109.30 | −40.42 | −27.76 | −108.29 | −6.81 | −7.00 | −26.12 | −9.66 | −6.64 | −25.88 |

[a] Extrapolated values.

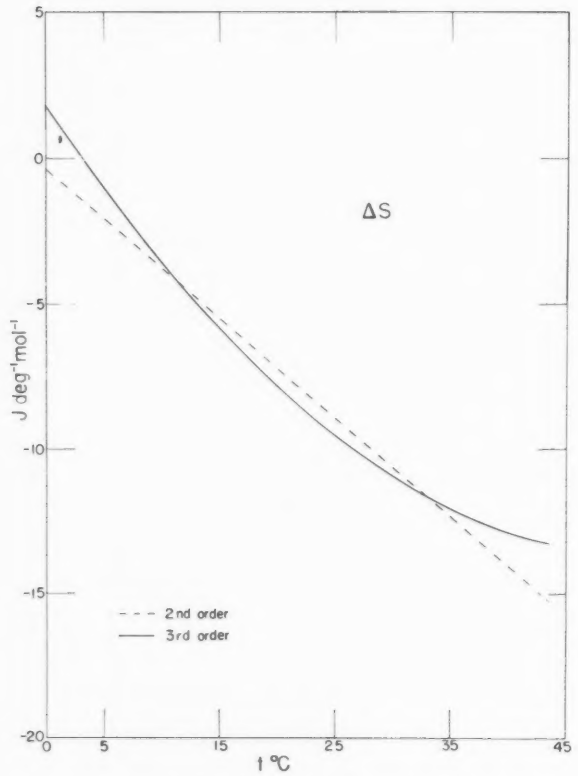


FIGURE 1. *Temperature variations in entropy change for the reaction in standard cells of the saturated cadmium sulfate type, as determined by different functions.*

(Fourth-order function gives nearly the same results as the third-order function and is, therefore, not shown)

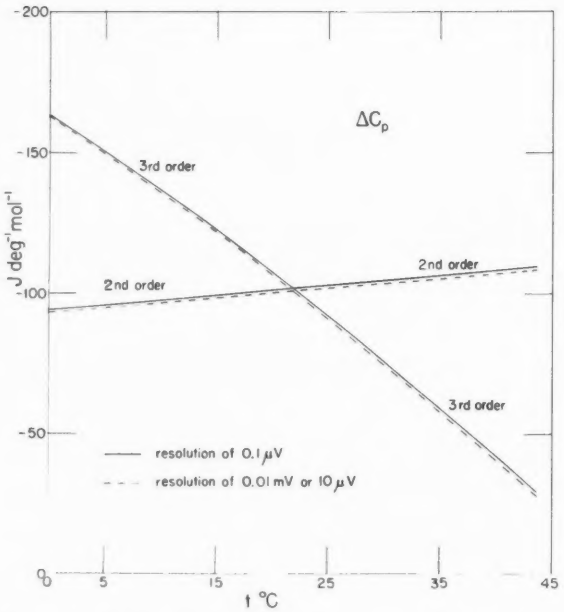


FIGURE 2. *Temperature variations in heat-capacity change for the reaction in standard cells of the saturated cadmium sulfate type, as determined by different functions.*

(Fourth-order function gives slightly different values than the third-order function, see text, table 9, for values).

with the certainty shown at 25 °C, higher resolution in emf and studies over a broader temperature range,[11] if possible, are necessary.

## 7. Alternate Emf Studies

In the foregoing sections calorimetric and equilibrium data relating to standard cells of the saturated cadmium sulfate type were compared with emf data of such cells. In this section emf data on various cells, which in combination, yield a saturated cadmium sulfate cell, will be compared with the emf of the saturated cadmium sulfate cell. Comparisons are limited to 25 °C where sufficient data are on hand.

Harned and Hamer [70] obtained 0.96495 V (converted to the $V_{69}$ scale) at 25 °C for the emf of the cell:

$$(-)\ \text{Pb-Hg}(2p)\ |\ \text{PbSO}_4(s)|\text{Na}_2\text{SO}_4(sol)|\ \text{Hg}_2\text{SO}_4(s)\ |\ \text{Hg(l)}\ (+) \qquad \text{(B)}$$

LaMer and Parks [71] obtained 0.0013 V for the standard emf, $E^0$, of the cell:

$$(+)\ \text{Pb-Hg}(2p)\ |\ \text{PbSO}_4(s)\ |\ \text{CdSO}_4(a=1)\ |\ \text{Cd-Hg (11\%)}\ (-) \qquad \text{(C)}$$

using the Gronwall, LaMer, and Sandved [72] treatment of interionic attraction to obtain $E^0$. Here $a$ denotes activity of the solute. On converting to absolute volts and using recent values of the physical constants [1] and the dielectric constant of water [73], it was found that the Gronwall, LaMer, and Sandved treatment did not lead to constant values of $E^0$ for the emf data of LaMer and Parks at the various concentrations of $CdSO_4$. However, a straight-line extrapolation to $m=0$ to obtain $E^0$ follows by taking $CdSO_4$ as incompletely dissociated with a dissociation constant of 0.0059 mol kg$^{-1}$ at 25 °C (an ion size of 3 Å was used in the extrapolation). Extrapolations to $m=0$ gives 0.00184 V instead of 0.0013 V, given by LaMer and Parks.[12]

[11] It would appear, at first glance, that Vigoureux and Watts [54] met this criterion, since they carried their measurements to −20 °C thus making possible a good evaluation of $\Delta C_p$ at 0 °C. However, the emf goes through a maximum at 3 °C, thus limiting the effectiveness of a second-order equation to a narrow range of 3 °C to −20 °C, thereby not providing sufficient resolution for $\Delta C_p$ at 0 °C. In cases where a maximum or minimum in emf did not occur extension of measurements to −20 °C or lower would enhance the evaluation of $\Delta C_p$ by a second-order equation. However, higher order equations should be used.

[12] In their 1931 paper LaMer and Parks gave results at 0 and 25 °C. In their 1933 paper (stated to give better results) they gave results of measurments at 0, 10, 20, and 30 °C, but not for 25 °C. Using the above treatment, i.e., taking $CdSO_4$ as incompletely dissociated, $E^0$ was calculated at these four temperatures which were then fitted to a third-order equation using least squares to give: $E^0$ (in volts) = 0.01698 − 0.0003588 $t$ − 0.000012949 $t^2$ + 0.00000012328 $t^3$. At 25 °C this equation yields 0.00184 V, the value given above for $E^0$; also interpolation of the data for the dissociation constants for these temperatures gives 0.0059 mol kg$^{-1}$ for the dissociation constant for 25 °C.

Combining cells (B) and (C) gives 0.96679 V for the cell:

$$(-)\ \text{Cd-Hg(11\%)} \mid \text{CdSO}_4(a=1) \mid \text{Hg}_2\text{SO}_4(\text{s}) \mid \text{Hg(l)}\ (+) \qquad \text{(D)}$$

which is the cadmium sulfate standard cell but for a $CdSO_4$ solution having an activity of one rather than for a saturated solution of $CdSO_4$. This emf may be converted to that for a saturated solution of $CdSO_4$ using the Nernst equation:

$$E_{\text{standard cell}} = E^0_{\text{standard cell}} - \frac{RT}{F} \ln m_{\text{CdSO}_4}\gamma_{\text{CdSO}_4} \qquad (36)$$

where

$E^0_{\text{standard cell}} = 0.96679$ V, given above, $m$ is the molality of a saturated solution of $CdSO_4$, 3.6789 [6], $\gamma$ is the mean stoichiometric activity coefficient of $CdSO_4$, and $R$, $T$, and $F$ have the significance given previously in this paper. Harned and Owen [74] and Robinson and Stokes [75] list values of $\gamma$ from 0.1 to 3.5 molal. Fitting averages of their values above 2 $m$ ($\gamma$ goes through a minimum at 2.5 $m$) to an equation of the form:

$$\log \gamma = \frac{-4A\sqrt{I}}{1+1.5\sqrt{I}} + aI + bI^2 + cI^3 \qquad (37)$$

where $A = 0.5108$ [76] and $I$ = ionic strength, gives:

$$\log \gamma = \frac{-2.0432\sqrt{I}}{1+1.5\sqrt{I}} - 0.10780\,I + 0.0091117\,I^2 - 0.00020852\,I^3 \qquad (38)$$

where coefficients $a$, $b$, and $c$ were obtained by the method of least squares. This equation yields 0.03646 for $\gamma$ for a saturated solution of $CdSO_4$ at 25 °C. Substituting this value in eq (36) together with the above values for $m$ and $E^0$ leads to 1.01840 $V$ for a "neutral" standard cell of the saturated cadmium sulfate type at 25 °C which agrees remarkably well with the observed value, 1.0184185 $V$, see table 3. This agreement is remarkable since the emfs used in obtaining $E^0$ were measured to only 0.01 mV.

Another approach to the emf of the standard cell of the saturated cadmium sulfate type may be made using a combination of the three cells:

$$(-)\ \text{Cd-Hg(11\%)} \mid \text{CdCl}_2(\text{sol}) \mid \text{AgCl(s)} \mid \text{Ag(s)}\ (+) \qquad \text{(E)}$$

$$(+)\ \text{Ag(s)} \mid \text{AgCl(s)} \mid \text{HCl(sol)} \mid \text{H}_2(\text{g}),\ \text{Pt}\ (-) \qquad \text{(F)}$$

$$(-)\ \text{Pt, H}_2(\text{g}) \mid \text{H}_2\text{SO}_4(\text{sol}) \mid \text{Hg}_2\text{SO}_4(\text{s}) \mid \text{Hg(l)}\ (+) \qquad \text{(G)}$$

where $g$ = gas and the other symbols have the significance given above. The emfs of these cells were measured for a series of concentrations and temperatures by Harned and Fitzgerald [77], Harned and Ehlers [78], and Harned and Hamer [79], respectively. For the first two cells, the authors obtained the standard potential, $E^0$, of the cells directly by standard extrapolations using the Debye-Hückel [80] theory of interionic attraction. For the third cell, however, owing to the very high solubility of $Hg_2SO_4$ in dilute solutions of sulfuric acid, the authors calculated $E^0$ using values of the activity coefficients of $H_2SO_4$ obtained from emf measurements of the cell [81]:

$$(-)\ \text{Pt, H}_2(\text{g}) \mid \text{H}_2\text{SO}_4(\text{sol}) \mid \text{PbSO}_4(\text{s}) \mid \text{PbO}_2(\text{s}),\ \text{Pt}\ (+) \qquad \text{(H)}$$

The authors measured the emfs of cells (E), (F), (G), and (H) in international volts and for extrapolations to $m=0$ to obtain $E^0$, used the values of the physical constants then in use [82]; their results were converted here to absolute volts using the factor given above, and the presently recommended values for the physical constants [1] were used in the extrapolations to $m=0$ to obtain values of $E^0$. For 25 °C, the $E^0$ values of cells (E), (F), and (G) thus obtained are 0.57399 V,[13] 0.22247 V, and 0.61536 V, respectively. These lead to 0.96688 V for cell (D) whereas the first method using cells (B) and (C) leads to 0.96679 V; this is not a bad agreement considering that the second method involves three different cells, one of which contains an incompletely dissociated electrolyte, $CdCl_2$, and another involves indirect calculations using a combination of results on two cells, cells (G) and (H). This latter value gives 1.01849 V for the emf of the standard cell of the saturated cadmium sulfate type at 25 °C. The agreement here with the observed emf is not as good as in the first case, but is still within the probable error of the measurements; more is given later on this agreement.

The emfs of cells (E), (F), (G), and (H) have been measured by others. Horsch [84], Lucasse [85], Quintin [86], and Treumann and Ferris [87] measured the emfs of cell (E) at a series of concentrations, except that Horsch used a 4.6-percent amalgam and Lucasse, one of unstated percentage. When Horsch's emfs are corrected from 4.6 percent to 11 percent amalgam by adding 0.00293 V, derivable from Smith's [36] measurements, his results agree closely on the average with the results of Harned and Fitzgerald, except below 0.00025 molal where Horsch stated that his results deviated from a smooth curve. Lucasse's amalgams

[13] Harned and Fitzgerald [77] gave 0.57390 international volt for $E^0$ (a typographical error listed this as 0.57300 international volt) based on a dissociation constant of 0.011 mol kg$^{-1}$ for the equilibrium: $CdCl^+ \rightleftharpoons Cd^{++} + Cl^-$ and 5 Å for the ion-size parameter in treating interionic attraction; they assumed that the dissociation: $CdCl_2 \rightarrow CdCl^+ + Cl^-$ was complete. Their $E^0$ value becomes 0.57409 absolute volts using the factor between international and absolute volts given above. They stated their experimental accuracy to be of the order of 0.1 mV. Using more recent values for the physical constants [1] and $T$ [1] and the dielectric constant of water [73] it was found that a better fit to their data was obtained using 0.010 mol kg$^{-1}$ for the dissociation constant and 7 Å for the ion-size parameter; these lead to 0.57399 absolute volt for $E^0$. Incidentally, Reghellato and Davies [83] obtained 0.0101 mol l$^{-1}$ for the dissociation constant from electrolytic conductivity measurements.



459-033 OL - 72 - 2

apparently were 1½ percent in cadmium since, if the difference in the potentials between 1½- and 11-percent amalgams is added to Lucasse's emfs they then agree excellently with those of Harned and Fitzgerald at all concentrations above 0.01 *m*; however, Lucasse's measurements were not made to sufficiently low concentrations to afford an evaluation of $E^0$. Quintin's emfs agree closely with those of Harned and Fitzgerald; her emfs yield 0.57395 V for $E^0$ for cell (E), or 0.04 mV lower than the value obtained from the measurements of Harned and Fitzgerald. Quintin's value for $E^0$ gives 0.96683 V for cell (D) which yields with the $E^0$ values for cells (F) and (G) a value of 1.01844 V for the standard cell of the saturated cadmium sulfate type. This value agrees better with the observed emf of a standard cell than the data of Harned and Fitzgerald. However, the standard deviation of the mean of Quintin's measurements is $0.12_8$ mV as compared with $0.03_4$ mV for Harned and Fitzgerald's results.

The emf of cell (F) has been measured by others in addition to the one cited above. For $E^0$ at 25 °C Prentiss and Scatchard [88] arrived at a value of 0.22250 V from the earlier measurements excluding those of Harned and Ehlers [78]. MacInnes [89] gave 0.22258 V, Hamer [90] 0.22239 V, Harned and Paxton [91] 0.22239 V, and Bates and Bower [92] 0.22234 V; where necessary these were converted to absolute volts using the factor between international and absolute volts given above. The differences in these values are generally attributed to the differences in the methods of preparation of the silver-silver chloride electrodes or methods of extrapolation to $m=0$ [88]. The average of these values, namely, 0.22244 V agrees within 0.03 mV of the value of Harned and Ehlers, used above. Since Harned and Fitzgerald for cell (E) and Harned and Ehlers for cell (F) used silver-silver chloride electrodes prepared in the same way, the characteristics of the silver-silver chloride electrode should be eliminated if we use their $E^0$ values in arriving at $E^0$ for cell (D) since we take the difference of cells (E) and (F) in arriving at $E^0$ for cell (D).

The emfs of cell (G) have been measured by many in addition to those cited above [79]. Results are listed in table 10. Those marked with a superscript *b* were calculated here; the authors did not give values for $E^0$. The value of Harned and Hamer when combined with the $E^0$ value for the cadmium-amalgam electrode and the *m* and γ of saturated $CdSO_4$ yields an emf for the standard cell of the saturated cadmium sulfate type that agrees well with the observed emf. The average of the values of Harned and Sturges [98], Randall and Stone [101], Trimble and Ebert [102], Müller and Reuther [104], and Beck et al., namely, 0.61555 V (or 0.61551 V, see footnote e of table 10) agrees within 0.19 (or 0.15) mV of the value of Harned and Hamer.

The recent values for $E^0$ for cell (G) of Beck, Dobson, and Wynne-Jones [105] and of Covington, Dobson, and Wynne-Jones [69] are not in good agreement, differing by 0.31 mV; the first [105] agrees fairly closely with earlier value of Harned and Hamer [79] whereas the latter [69] agrees fairly well with the very early value of Lewis and Lacey [95]. However, when combined with the $E^0$ value of the cadmium-amalgam electrode and the *m* and γ of saturated cadmium sulfate, the $E^0$ value of Covington et al. for the mercury-mercurous sulfate electrode yields a value for the emf of the standard cell of the saturated cadmium sulfate type which is at great variance (−3.3 mV) from the observed value. There can be little doubt that their $E^0$ value for the mercury-mercurous sulfate electrode is in error. The value of Beck et al. for $E^0$ of the mercury-mercurous sulfate electrode leads to a better value for the emf of the standard cell of the saturated cadmium sulfate type than does that of Covington et al., but even so yields a value that is about 0.45 mV above the observed value.

These additional $E^0$ values for cells (E), (F), and (G) show that the original selection of data [77–79] for these three cells is justified. The slight difference of 0.09 mV in the calculated value of the emf of the

TABLE 10. *Values of the standard potential of the mercury-mercurous sulfate electrode and of the standard cell* (a=1) *and the corresponding electromotive force of the saturated standard cell at 25 °C*

(all values on $V_{69}$ scale)

| Date | Experimenters | Hg, $Hg_2SO_4$ | Standard cell | |
|---|---|---|---|---|
| | | $E^0$ | $E^0$ | $E$(sat.) |
| | | *Volt* | *Volt* | *Volts* |
| 1910 | Brønsted [93] | [a,b]0.6170 | 0.96843 | 1.02004 |
| 1914 | Lewis and Lacey [95] | .6129 | .96433 | 1.01594 |
| 1918 | Randall and Cushman [94] | [c].6215 | .97293 | 1.02454 |
| 1921 | Ferguson and France [97] | [b].6199 | .97133 | 1.02294 |
| 1925 | Harned and Sturges [98] | [b].61534 | .96677 | 1.01838 |
| 1926 | Åkerlöf [99] | [b].6168 | .96823 | 1.01984 |
| 1927 | Randall and Langford [100] | [d].6245 | .97593 | 1.02754 |
| 1929 | Randall and Stone [101] | [b].61550 | .96693 | 1.01854 |
| 1933 | Trimble and Ebert [102] | [b].6156 | .96703 | 1.01864 |
| 1933 | MacDougall and Blumer [103] | .6294 | .98083 | 1.03244 |
| 1935 | Harned and Hamer [79] | .61536 | .96679 | 1.01840 |
| 1942 | Müller and Reuther [104] | .6155 | .96693 | 1.01854 |
| 1960 | Beck, Dobson, and Wynne-Jones [105] | [e].61582 | .96725 | 1.01886 |
| 1965 | Covington, Dobson, and Wynne-Jones [69] | .61251 | .96394 | 1.01555 |
| 1969 | Gardiner, Mitchell, and Cobble [67] | [f].61251 | .96394 | 1.01555 |
| 1970 | Sharma and Prasad [107] | .6135 | .96493 | 1.01564 |

Observed emf of standard cell [g] = 1.0184186

[a] See Randall and Cushman [94]; these authors reported necessary corrections for Brønsted's data and reported some earlier results of Arthur Edgar who, however, measured his emfs only to 1 mV.

[b] Calculated here from emfs for 0.05 to 0.21 *m* using activity coefficients of sulfuric acid given in reference [79].

[c] Given in Lewis and Randall [96].

[d] Stated to be a provisional value.

[e] Ives and Smith [106] listed this value as 0.61560 V—becomes 0.61561 V on $V_{69}$ scale; reason for discrepancy is unknown.

[f] Selected by these authors in a recalculation of the activity coefficients of sulfuric acid, i.e., the 1965 value.

[g] For dc-electrolytic mercurous sulfate exclusively 1.0184354 V.

standard cell of the saturated cadmium sulfate type as given by cells (B) and (C) on the one hand and by cells (E), (F), and (G) on the other hand can be attributed largely to uncertainties in extrapolations to obtain $E^0$ values, especially for cell (E) wherein cadmium chloride may show more complex dissociation [108] than assumed by Harned and Fitzgerald. The total uncertainty of 0.09 mV is, therefore, attributed entirely to cell (E), which is within the uncertainty stated by the authors.

The $E^0$ for the positive electrode of the standard cell is obtained directly from cell (G),[14] while the $E^0$ for the negative electrode of the standard cell is obtained from the $E^0$'s of cells (B), (C), and (G), or $E_B + E_C - E_G$. These give:

| | $E^0$, V |
|---|---|
| Positive electrode | 0.61536 |
| Negative electrode | −0.35143 |
| Complete cell | 0.96679 |

which give for a saturated solution of cadmium sulfate (assuming that $\gamma_{Cd^{++}} = \gamma_{SO_4} = \gamma_{CdSO_4}$):

| | $E$, V | |
|---|---|---|
| Positive electrode | 0.64117 | 0.6411743 |
| Negative electrode | −0.37724 | −0.3772443 |
| Complete cell | 1.01841 | 1.0184186 |
| Observed value | | 1.0184186 |

As a basis for measurement, the difference of 8.6 $\mu$V between the calculated and observed value for the complete cell may be divided between the values for the two electrodes to give the values in the last column.

## 8. Reproducibility

The good check between calorimetric and equilibrium data and emf data of standard cells of the saturated cadmium sulfate type on the one hand and between emf data on galvanic cells related to the standard cell and the emf of the standard cell itself on the other hand, given above, does not imply that standard cells having the emfs given above to 0.1 $\mu$V (see table 3), can be made easily and readily without great care. Cells can be made, however, without extreme care that will agree in emf to 0.01 mV as illustrated by data in table 3.

Various reasons have been advanced why standard cells cannot be made that agree in emf to 0.1 $\mu$V. The main reasons are: (1) differences in acidity of the solution, (2) differences in acidity between the two distinct electrodes of the cell, (3) differences in extent of reactions between the solution and the cell container (glass), (4) differences in the size of crystals of both cadmium and mercurous sulfates, (5) undersaturation or oversaturation with cadmium sulfate at either one or both of the electrodes, (6) undersaturation of the solution with mercurous sulfate at the positive electrode, (7) presence of mercuric ions at the positive electrode, (8) amalgam composition, (9) impurities, and (10) cell construction. Of these the ones relating to acidity are the most important; amalgam composition, saturation of the solution with cadmium sulfate at both electrodes and with mercurous sulfate at the positive electrode, crystal size, and amount of mercuric ions can be readily controlled. Also by purification, impurities can be reduced to a minimum; impurities with higher electrical potential than hydrogen must be eliminated. Soluble trace impurities, although they may have no effect on the stability of the cell, may alter the initial emf slightly through a solvent effect affecting the value of the activity coefficient of cadmium sulfate. Thermodynamically, the emf and emf-temperature coefficient are independent of cell construction; however, the rate of attainment of equilibrium after a temperature change can be affected by cell design. The H-form of cell used here and in modern cells permits attainment of temperature equilibrium in relatively short times.

The acidity of the solution and the distribution of the acid throughout the cell affect the emf. Increases in acidity in the cell as a whole decrease the emf of the cell [5, 50, 55, 109, 110]. Increase in acidity at the negative electrode alone increases the emf of the cell while more acid at the positive electrode alone decreases the emf of the cell [36]; these arise from changes in the potential of the acidified electrode and a liquid-junction potential at the interface of the neutral and acid compartments of the cell. If the acid is confined to the region of the mercury-mercurous sulfate paste the liquid-junction potential will differ from that produced if the acid extends to a region above the paste.

Low concentrations of $H_2SO_4$ (less than 0.1 $N$) affect only slightly the emf-temperature coefficient of the cell [4, 49, 54, 55]. The relation between the emf-temperature coefficient and the acidity appears to be irregular; more on this will be given in a subsequent paper. Addition of sulfuric acid, through a common-ion effect, decreases the solubility of cadmium sulfate but the total sulfate concentration ($SO_4^=$ ion from $CdSO_4$ + $SO_4^=$ ion from $H_2SO_4$) exceeds that of $CdSO_4$ alone. However, the activity coefficient of $CdSO_4$ is decreased by the addition of $H_2SO_4$, so that the activity of $CdSO_4$ in water or in water-sulfuric acid mixtures is nearly constant. High concentrations of $H_2SO_4$, of the order of 1 $N$ (or 0.5 M) increase the emf-temperature coefficient of the cell [49, 50]. However, concentrations of $H_2SO_4$ this high cause excessive gassing at the cadmium-amalgam electrode and are not used for precision cells.

Even though acid affects the initial emf of standard cells, the long-range stability of the cells is affected only slightly. This is evident from the long-range stability exhibited by standard cells of different acidity maintained at the National Bureau of Standards [5, 111] and from international comparisons of cells of various acidities [112]. In the ultimate, stability in emf is the important criterion in the maintenance of the unit of emf, rather than the actual value of the emf. Thermodynamically, however, the value of the emf is all important, in that it gives a measure of the Gibbs energy change or maximum available energy of the cell, and an

[14] As stated earlier, data from cell (H) are required to get $E^0$ for cell (G).

insight into whether the assigned value is consistent with related thermodynamic quantities.

---

The author is indebted to Bruce F. Field for writing the computer programs for the emf-temperature equations, to Anna Skapars for making recent checks on the emf-temperature coefficients of standard cells of the saturated cadmium sulfate type, and to Georges Leclerc of the Bureau International des Poids et Mesures for information on the acidity of standard cells submitted to the International Bureau by the various National Laboratories for international comparisons.

## 9. References

[1] New values for the physical constants—recommended by NAS–NRC, Nat. Bur. Stand. (U.S.), Tech. News Bull. **47,** No. 10. 195 (1963); Consistent set of physical constants proposed. Chem. and Eng. News **41,** No. 46. 43 (Nov. 18. 1963).
[2] Craig. D. N., Hoffman. J. I., Law. C. A., and Hamer. W. J., J. Res. Nat. Bur. Stand. **64A** (Phys. and Chem.), No. 5. 381–402 (Sept.-Oct. 1960).
[3] Hamer. W. J., and Craig. D. N., J. Electrochem. Soc. **111,** 1434 (1964).
[4] Hamer. W. J., J. Res. Nat. Bur. Stand. (U.S.), **72A** (Phys. and Chem.), No. 4. 435–439 (July-Aug. 1968).
[5] Hamer. W. J., Standard cells. their construction. maintenance. and characteristics. Nat. Bur. Stand. (U.S.), Monogr. 84. 40 pages (1965).
[6] Brickwedde. L. H., J. Res. Nat. Bur. Stand. (U.S.), **36,** 377–388 (1946) RP1707.
[7] Cohen. E., Helderman. V. D., and Moesveld. A. L. Th., Z. physik. Chem. **96,** 259 (1920).
[8] Richards. T. W., and Tamaru. S., J. Am. Chem. Soc. **44,** 1060 (1922).
[9] Thomsen. H. P. J. J., Thermochemische unter suchungen. Vo. I–IV, Barth. Leipzig (1882–86).
[10] Kelley. K. K., Contributions to the data on theoretical metallurgy. XIII. High-temperature heat-content. heat-capacity. and entropy data for the elements and inorganic compounds. Bull. 584. Bur. Mines. 1960.
[11] Pitzer. K. S., and Brewer. L., Lewis and Randall Thermodynamics (McGraw-Hill Book Comp., Inc., New York. N.Y., 1961).
[12] Bichowsky. F. R., and Rossini. F. D., The thermochemistry of the chemical substances (Reinhold Publishing Corp., New York. N.Y., 1936).
[13] Varet. R., Ann. chim. phys. (3) **8,** 79 (1896).
[14] Giauque. W. F., Barieau. R. E., and Kunzler. J. E., J. Am. Chem. Soc. **72,** 5685 (1950).
[15] Parker. V. B., Thermal properties of aqueous uni-univalent electrolytes. Nat. Stand. Ref. Data Ser. Nat. Bur. Stand. (U.S.), **2,** 69 pages (Apr. 1965).
[16] Rossini. F. D., J. Res. Nat. Bur. Stand. (U.S.), **9,** 679–702 (1932) RP499.
[17] Günther. P., and Wekua. K., Z. physik. Chem. **A154,** 193 (1931).
[18] Kelley. K. K., Contributions to the data on theoretical metallurgy. X. High-temperature heat-content. heat-capacity. and entropy data for the elements and inorganic compounds. Bull. 476. Bur. Mines. 1949.
[19] Richards. T. W., and Rowe. A. W., J. Am. Chem. Soc. **44,** 684 (1922).
[20] Müller. J. A., Bull. soc. chim. (4) **23,** 8 (1918).
[21] Papadopoulos, W. N., and Giauque, W. F., J. Am. Chem. Soc. **77,** 2740 (1955).
[22] Personal calculation using data of reference [21].
[23] Rossini. F. D., Wagman. D. D., Evans. W. H., Levine. S., and Jaffe. I., Selected values of chemical thermodynamic properties. Nat. Bur. Stand. (U.S.), Circ. 500 (1952).
[24] Wagman. D. D., Evans. W. H., Parker. V. B., Halow. I., Bailey. S. M., and Schumm. R. H., (a) Selected values of chemical thermodynamic properties, tables for first thirty-four elements in the standard order of arrangement, Nat. Bur. Stand. (U.S.), Tech Note 270–3, 266 pages (Jan. 1968); (b) Selected values of chemical thermodynamic properties, tables for elements 35 through 53 in the standard order of arrangement, Nat. Bur. Stand. (U.S.), Tech. Note 270–4. 151 pages (1965).
[25] Berthelot. P. E. M., Ann. chim. phys. (4) **29,** 433 (1873).
[26] Keyes. F. G., Gillespie. L. J., and Mitsukuri. S., J. Am. Chem. Soc. **44,** 707 (1922).
[27] Stull. D. R., and Sinke. G. C., Thermodynamic properties of the elements. Am. Chem. Soc., Washington. D.C. (1956).
[28] Wexler. A., and Greenspan. L., J. J. Res. Nat. Bur. Stand. (U.S.), **75A** (Phys. and Chem.), No. 3, 312–230 (May–June 1971).
[29] Ishikawa. F., and Murooka. H., Bull. Inst. Phys. Chem. Res. (Tokyo) **9,** 781 (1933).
[30] Wagman. D. D., Evans. W. H., Halow. I., Parker. V. B., Bailey. S. M., and Schumm. R. H., Selected values of chemical thermodynamic properties. Part 1. Tables for the first twenty-three elements in the standard order of arrangement. Nat. Bur. Stand. (U.S.), Tech. Note 270–1. 127 pages Oct. 1965).
[31] Carpenter. C. D., and Jette. E. R., J. Am. Chem. Soc. **45,** 578 (1923).
[32] Holsboer. H. B., Z. physik. Chem. **39,** 691 (1902).
[33] Cohen. E., and Moesveld. A. L. Th., Z. physik Chem. **95,** 305 (1920).
[34] Hulett. G. A., Trans. Am. Electrochem. Soc. **7,** 333 (1905); **15,** 435 (1909).
[35] Getman. F. H., J. Am. Chem. Soc. **39,** 1806 (1917).
[36] Smith. F. E. (Sir Frank), Proc. Phys. Soc. (London) **22,** 11 (1910); Phil. Mag. **19,** 250 (1910); Natl. Phys. Lab. Coll. Res. **6,** 137 (1910).
[37] Announcement of a change in electrical and photometric units, NBS Circ. 459, 1947.
[38] Nat. Bur. Stand. (U.S.), Tech. News Bull. **52,** 204 (1968); **53,** 13 (1969).
[39] Parks. W. G., and LaMer. V. K., J. Am. Chem. Soc. **56,** 90 (1934).
[40] Hamer. W. J., Inst. Soc. Am., M2–1–Mestind–67, 1967; Proc. Conf. ISA, **22,** Part 1, 1 (1967).
[41] Hamer. W. J., Standard cells. Ch. 12. The primary battery. Ed. G. W. Heise and N. C. Cahoon (John Wiley & Sons. New York. N.Y., 1971).
[42] Wolff. F. A., Trans. Am. Electrochem. Soc. **13,** 187 (1908).
[43] Wolff. F. A., Bull. BS **5,** 309 (1908).
[44] Wolff. F. A., and Waters. C. E., BS Circ. No. 29 (1910).
[45] Wolff. F. A., Trans. Am. Electrochem. Soc. **5,** 49 (1904).
[46] Wolff. F. A., and Waters. C. E., Bull. BS **4,** 70 (1907).
[47] International conference on electrical units and standards, Appendix to the report: Notes to the specifications as to the methods adopted in various standardizing laboratories to realize the international ohm and the international ampere, and to prepare the Weston Normal Cell (Darling & Sons, Ltd., London, 1908).
[48] Vosburgh. W. C., and Eppley. M., J. Am. Chem. Soc. **45,** 2268 (1923).
[49] Vosburgh. W. C., J. Optical Soc. Am. & Rev. Sci. Instr. **12,** 511 (1926).
[50] Ishibashi. Y., and Ishizahi. T., Res. Electrotech. Lab. (Tokyo), No. 318 (1931).
[51] Froehlich. M., Z. Instr. **74,** 216 (1966); private communication, 1969.
[52] Vincent. G. D., IRE Trans. Instr. **I-7,** No. 3 and 4, 221 (1958).
[53] Law. C. A., and Skapars. A., results NBS. 1955–70, unpublished.
[54] Vigoureux. P., and Watts. S., Proc. Phys. Soc. (London) **45,** 172 (1933).
[55] Obata. J., and Ishibashi. Y., Researches Electrotech. Lab. No. 11, 7 (1921).
[56] Waider. C. W., and Dickinson. H. C., Bull. BS **3,** 663 (1907).
[57] NBS Tech. News Bull. **33,** No. 3, 28 (1949).
[58] NBS Tech. News Bull. **53,** 12 (1969).
[59] Clarke. J., Phys. Today **24,** No. 8, 30 (1971).
[60] Driscoll. R. L., and Cutkosky. R. D., J. Res. Nat. Bur. Stand. (U.S.), **60,** 297–305 (1958) RP2846.
[61] Cutkosky. R. D., J. Res. Nat. Bur. Stand. (U.S.), **65A** (Phys. and Chem.), No. 3, 147–158 (May-June 1961).

[62] Harned, H. S., and Owen, B. B., The Physical Chemistry of Electrolytic Solutions, 3rd ed., ACS Monograph Series No. 137 (Reinhold Book Corp., New York, N.Y., 1958) p. 428.
[63] Latimer, W. M., The Oxidation States of the Elements and Their Properties in Aqueous Solutions, 2nd ed. (Prentice-Hall, Inc., Englewood Cliffs, N.J., 1952).
[64] MacInnes, D. A., The Principles of Electrochemistry (Reinhold Publ. Corp., New York, N.Y., 1939).
[65] Ives, D. J. G., and Janz, G. J., Eds., Reference Electrodes, Theory and Practice (Academic Press, New York, N.Y., 1961).
[66] Brackett, T. E., Hornung, E. W., and Hopkins, T. E., J. Am. Chem. Soc. **82,** 4155 (1960).
[67] Gardner, W. L., Mitchell, R. E., and Cobble, J. W., J. Phys. Chem. **73,** 2017 (1969).
[68] Beck, W. H., Singh, K. P., and Wynne-Jones, W. F. K., Trans. Faraday Soc. **55,** 331 (1959).
[69] Covington, A. K., Dobson, J. V., and Wynne-Jones, W. F. K., Trans. Faraday Soc. **61,** 2050 (1965).
[70] Harned, H. S., and Hamer, W. J., J. Am. Chem. Soc. **57,** 33 (1935).
[71] LaMer, V. K., and Parks, W. G., J. Am. Chem. Soc. **53,** 2040 (1931); **55,** 4343 (1933).
[72] Gronwall, T. H., LaMer, V. K., and Sandved, K., Physik. Z. **29,** 358 (1928).
[73] Malmberg, C. G., and Maryott, A. A., J. Res. Nat. Bur. Stand. (U.S.), **56,** 1–8 (1956) RP2641.
[74] Reference [62], p. 565.
[75] Robinson, R. A., and Stokes, R. H., Electrolyte solutions, 2nd ed. (Butterworths Sci. Publ., London, 1959) p. 502.
[76] Hamer, W. J., Nat. Stand. Ref. Data Ser. Nat. Bur. Stand. (U.S.), **24,** 274 pages (Dec. 1968).
[77] Harned, H. S., and Fitzgerald, M. E., J. Am. Chem. Soc. **58,** 2624 (1936).
[78] Harned, H. S., and Ehlers, R. E., J. Am. Chem. Soc. **54,** 1350 (1932); **55,** 652, 2179 (1933).
[79] Harned, H. S., and Hamer, W. J., J. Am. Chem. Soc. **57,** 27 (1935).
[80] Debye, P., and Hückel, E., Physik. Z. **24,** 185, 305 (1923).
[81] Hamer, W. J., J. Am. Chem. Soc. **57,** 9 (1935).
[82] Reference [62], 1st ed., Ch. (5), 1943.
[83] Righellato, E. C., and Davies, C. W., Trans. Faraday Soc. **26,** 592 (1930).
[84] Horsch, W. G., J. Am. Chem. Soc. **41,** 1787 (1919).
[85] Lucasse, W. W., J. Am. Chem. Soc. **51,** 2597 (1929).
[86] Quintin, Mlle M., Compt. Rendus **200,** 1579 (1935).
[87] Treumann, W. B., and Ferris, L. M., J. Am. Chem. Soc. **80,** 5048 (1958).
[88] Prentiss, S. S., and Scatchard, G., Chem. Rev. **13,** 139 (1933).
[89] Reference [64], p. 187, table I.
[90] Hamer, W. J., Ph.D. Dissertation, Yale University, New Haven, Conn., 1932.
[91] Harned, H. S., and Paxton, T. R., J. Phys. Chem. **57,** 531 (1953).
[92] Bates, R. G., and Bower, V. E., J. Res. Nat. Bur. Stand. (U.S.), **53,** 283–290 (1954) RP2546.
[93] Brønsted, J. N., Z. physik. Chem. **68,** 693 (1910).
[94] Randall, M., and Cushman, O. E., J. Am. Chem. Soc. **40,** 393 (1918).
[95] Lewis, G. N., and Lacey, W. N., J. Am. Chem. Soc. **36,** 804 (1914).
[96] Lewis, G. N., and Randall, M., Thermodynamics and the Free Energy of Chemical Substances (McGraw-Hill Book Co., Inc., New York, N.Y., 1923) p. 407.
[97] Ferguson, A. L., and France, W. G., J. Am. Chem. Soc. **43,** 2150 (1921).
[98] Harned, H. S., and Sturgis, R. D., J. Am. Chem. Soc. **47,** 945 (1925).
[99] Åkerlöf, G. C., J. Am. Chem. Soc. **48,** 1160 (1926).
[100] Randall, M., and Langford, C. T., J. Am. Chem. Soc. **49,** 1445 (1927).
[101] Randall, M., and Stone, H. A., J. Am. Chem. Soc. **51,** 1752 (1929).
[102] Trimble, H. M., and Ebert, P. F., J. Am. Chem. Soc. **55,** 958 (1933).
[103] MacDougall, F. H., and Blumer, D. R., J. Am. Chem. Soc. **55,** 2236 (1933).
[104] Müller, F., and Reuther, H., Z. Electrochem. **48,** 220 (1942).
[105] Beck, W. H., Dobson, J. V., and Wynne-Jones, W. F. K., Trans. Faraday Soc. **56,** 1172 (1960).
[106] Reference [65], p. 405.
[107] Sharma, L., and Prasad, B., J. Indian Chem. Soc. **47,** 379 (1970).
[108] Sahn, G., and Prasad, B., J. Indian Chem. Soc. **46,** 233 (1969).
[109] Vosburgh, W. C. J. Am. Chem. Soc. **47,** 1265 (1925).
[110] Smith, F. E. (Sir Frank), Natl. Phys. Lab. Report 60, 1920; Dic. App. Phys. **2,** 268 (1920).
[111] Hamer, W. J., Brickwedde, L. H., and Robb, P. R., Electrochemical Constants, NBS Circ. 524, ch. 12, 1953.
[112] Leclerc, Georges, private communications, 1971.

(Paper 76A3–716)

JOURNAL OF RESEARCH of the National Bureau of Standards—A. Physics and Chemistry
Vol. 76A, No. 3, May–June 1972

# An Improved State Equation in the Vicinity of the Critical Point

**Olav B. Verbeke***

**Institute for Basic Standards, National Bureau of Standards, Boulder, Colo. 80302**

**(December 21, 1971)**

An improved state equation for the vicinity of the critical point is proposed. An analysis of the experimental data on helium and xenon has been carried out in order to investigate the influence of the number of constants in the equation and the $P\rho T$ range on the critical constants $T_c$ and $\rho_c$ and on the critical exponents $\alpha$, $\beta$, $\gamma$, and $\delta$. No such influence has been detected. The model for the critical point, recently proposed by Widom, has been checked regarding its consequences for the rectilinear diameter. No definite confirmation but indications for its correctness have been found.

Key words: Compressibility; critical point; equation of state; fluid; low temperature; methane; scaling law; specific heat; helium; xenon.

## 1. Introduction

Recently an equation of state for the vicinity of the critical point has been proposed by Verbeke et al. [1].[1] This equation was applied to the data for xenon of Habgood and Schneider [3]. In a subsequent paper the equation was applied to data for methane of Jansoone et al. [2]. It is the purpose of this paper to report improvements in the equation which have been made since then.

## 2. Formulation of the Modified State Equation

Several questions concerning the original equation remained to be answered.

The temperature derivative, $\frac{d^2P_s}{dT^2}$, where $P_s$ is the vapor pressure and $T$ is the temperature, is believed to diverge as

$$\frac{d^2P_s}{dT^2} \sim (T_c - T)^{-\alpha_2} \tag{1}$$

close to the critical point. The value of $\alpha_2$ must, according to the weak inequality of Griffiths which is based on thermodynamics, be less than or equal to $\alpha+\beta$, where $\beta$ is the exponent of the power law for the difference of the coexisting densities and $\alpha$ is the exponent of the power law for $C_v$. It has been proved [7] for an equation of state of the type proposed by M. S. Green et al. [4], that $\alpha$ must be equal to $\alpha_2$. The present equation can also, but must not necessarily, imply the latter equality.

The divergence of $\frac{d\rho_m}{dT}$, where $\rho_m$ is the rectilinear diameter, is a consequence of a model for the critical state, which has recently been proposed by Widom and Rowlinson [5]. This divergence is given by another power law,

$$\frac{d\rho_m}{dT} \sim (T_c - T)^{-\alpha_1}$$

with $\alpha_1 = \alpha$ (as derived by Widom). The same model yields a similar divergence of $\frac{d\rho_l}{dT}$, where $\rho_l$ is the line of symmetry in the $C_v(P, T)$ surface where $C_v$ is the specific heat at constant volume. A divergence of $\frac{d\rho_l}{dT}$ was incorporated in our original eq (1) in order to provide a similar divergence in all terms of that equation: since $\lambda$ in that equation was not necessarily equal to 1, the corresponding $\alpha_1$ was restricted to

$$\alpha_1 = 1 - \beta.$$

It was found, however, that a value of $\lambda$ different from 1 does introduce a discontinuity across the critical isochore.

In order to test the conjectures on $\alpha_1$ and $\alpha_2$ made by M. S. Green et al. and Widom respectively, our original equation [1] was modified as follows:

$$P = P_s + B(\rho)(T - T_s) + A\rho(\rho - \rho_l)[(T + T_c - 2T_s)^{1+\mu} - (T_c - T_s)^{1+\mu}] \tag{2}$$

with

$$P_s = P_{s0} + P_{s1}T_s + P_{s2}(T_c - T_s)^{2-\alpha_2}, \tag{3}$$

*On detail to the National Bureau of Standards, Contract CST 8109, from the Katholieke Universiteit of Leuven, Heverlee, Belgium.

[1] Figures in brackets indicate the literature references at the end of this paper.

$$B(\rho) = P_{s1} + B_1(\rho - \rho_m)|\rho - \rho_m|^{\mu/\beta} + B_2 \ldots, \quad (4)$$

$$\rho_m = \rho_c + \rho_{m1}(T_c - T_s)^{1-\alpha_1}, \quad (5)$$

$$T_s = T_c - [C|\rho - \rho_m|]^{1/\beta} \quad (6)$$

and

$$\rho_l = \rho_c + \rho_{l0}(T - T_s)^{1-\alpha_1}. \quad (7)$$

It can be shown from eq (2) that the exponent, $\alpha$, of the power law for $C_v$ can be expressed in terms of $\mu$ and $\beta$ as follows:

$$\alpha = 1 - (2\beta + \mu).$$

Several questions can now be formulated.

1. Is $\alpha = \alpha_1 = \alpha_2$?
2. Is $\rho_{m1}$ equal to $-\rho_{l0}$?
3. Is there any $P\rho T$ range-dependence for the exponents $\beta$, $\gamma$, $\delta$ for the following power laws $\rho_e - \rho_g \sim (Y_c - T)^\beta$ (the indices $l$ and $g$ refer to liquid and gas),
$$\frac{1}{\rho}\left(\frac{\partial \rho}{\partial p}\right)_T \sim |T_c - T|^{-\gamma}$$
(at saturation or at the critical isochore),
$$|\rho - \rho_c|_{T = T_c} \sim |P - P_c|_\delta.$$
4. How many terms are relevant in equation (6)?

Answers to these questions have been obtained by applying eq (2) to two substances for which excellent data is available, i.e., the data on helium by Roach [6] and the data on xenon by Habgood and Schneider [3]. As far as the latter data are concerned, a rather large difference was detected previously between the measurements on isochores and on isotherms [1]. The error (for version 2) with the isotherm data included amounted to 0.00311 atmospheres versus 0.00227 without. In the subsequent analysis only measurements on isochores have been considered.

## 3. Analysis and Results

Before estimating the $P\rho T$ range dependence of the critical point parameters, the ranges have to be defined. The choice of the ranges will always be more or less arbitrary. In this case the ranges are defined by confining the variables density, temperature and pressure within a selected percentage around the cirtical point parameters. The method of defining the various ranges is illustrated in figure 1. The actual ranges indicated by the cross hatching in figure 1 are given in table 1. A single significant parameter, $N$, the number of data points in the range, results from this limiting procedure; $N$ will be taken as a quantitative measure of the range. In table 1 the boundaries are defined for each range and for each substance, and the corresponding number of data points in the range is given. Range No. 1 for helium extends farther than any other range, and for this range the number of coefficients, $B$, in eq (6) was varied in order to investigate their relevance.

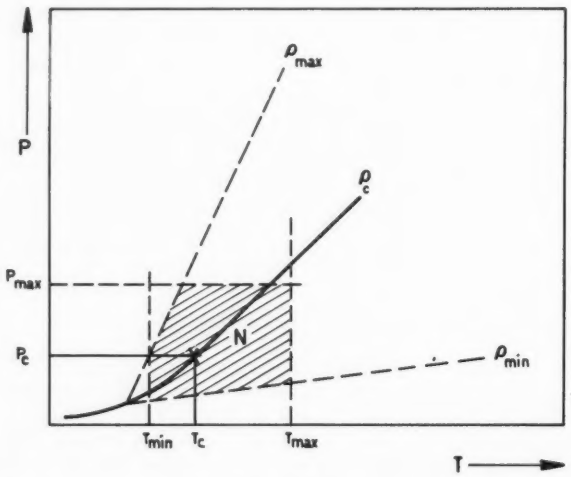


FIGURE 1. *Schematic* P–T *diagram showing boundaries of a "range" around the critical point.*

The variation of the error and the apparent values of the scaling exponents $\alpha$, $\beta$, $\gamma$, and $\delta$ as a function of the number of coefficients in eq (6) is shown in figure 2. $B_0$ and $B_1$ were found to provide a satisfactory description for data of the given accuracy within the given range. Beyond these two constants, no dependence on the number of $B$'s was found for $\alpha$ and $\gamma$ and only a slight dependence for $\beta$ and $\delta$. Consequently in further calculations all other $B$-s have been assumed to be zero. Equation (2) can be applied on the data in two alternative versions; version 1 where $\alpha_1$, $\alpha_2$, $\rho_{m1}$ and $\rho_{l0}$ are independent adjustable

TABLE 1. *Boundaries of the different* P$\rho$T *ranges for xenon and helium and the number of data points left in each range*

| No. of range | $\left(\frac{\lvert\rho_{max} - \rho_c\rvert}{\rho_c}\right)$ | $\left(\frac{\lvert T_{max} - T_c\rvert}{T_c}\right)$ | $\left(\frac{\lvert P_{max} - P_c\rvert}{P_c}\right)$ | Number of data points, $N$ | |
|---|---|---|---|---|---|
| | | | | Xenon | Helium |
| 1..... | 0.50 | 0.05 | 0.08 | 173 | 414 |
| 2..... | .35 | .035 | .05 | | 295 |
| 3..... | .30 | .03 | .05 | 142 | |
| 4..... | .10 | .01 | .02 | 114 | |

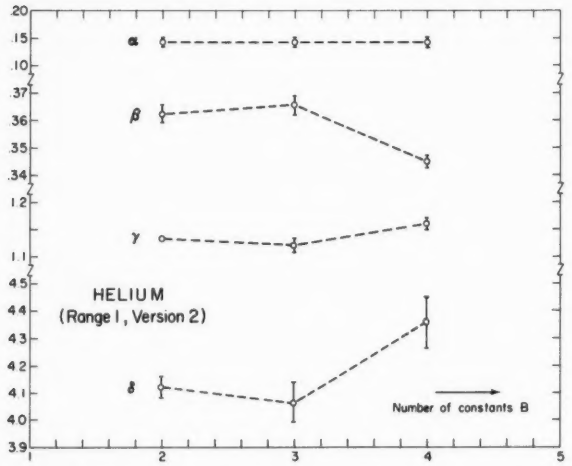


FIGURE 2. *α. β. γ and δ and their dependence on the number of* B's *in eq (2).*

parameters and version 2, where $\alpha_1 = \alpha_2 = 1 - (2\beta + \mu)$ and $\rho_{m1} = -\rho_{r0}$. The two versions are compared for helium and for xenon in table 2. The difference in the quality of fit between the two versions is not substantial, and therefore further speculations on the range dependence of the critical parameters have been carried out with version 2. The dependence of the critical exponents $\alpha$, $\delta$, $\gamma$ and $\beta$ on the range is illustrated in figure 3. The constants for range 1 and for version 2 of equation (2) are given for helium in table 3, and for xenon in table 4.

The estimation of the parameters has been carried out through an iterative procedure. Initial constants have been chosen and the equation has been linearized with respect to the deviations of the constants. These deviations were then calculated by the well known least-squares methods for the linear case.

The error analysis is carried out on the basis of the correlation matrix for the linear case. There may be some doubt whether this is entirely justified in the case of a nonlinear equation.

TABLE 2. *Comparison of the relevant parameters for the two versions of eq (2) and for helium and xenon*

| Range No. | Parameter | Helium | | Xenon | |
|---|---|---|---|---|---|
| | | Version 1 | Version 2 | Version 1 | Version 2 |
| 1 | $\delta$ | 4.28 ±0.09 | 4.16 ±0.06 | 4.45 ±0.14 | 4.39 ±0.101 |
| | $\gamma$ | 1.128 ± .004 | 1.119 ± .003 | 1.232 ± .012 | 1.191 ± .006 |
| | $\beta$ | .343 ± .003 | .353 ± .002 | .356 ± .005 | .351 ± .005 |
| | $\alpha$ | .184 ± .008 | .173 ± .006 | .054 ± .020 | .108 ± .014 |
| | $\alpha_1$ | .270 ± .045 | .173 ± .006 | .287 ± .116 | .108 ± .014 |
| | $\alpha_2$ | .400 ± .026 | .173 ± .006 | .470 ± .045 | .108 ± .014 |
| | $\rho_{r0}$ | −.00100 ± .00015 | −.00132 ± .00015 | −.0000417 ± .0000131 | −.0000145 ± .000004 |
| | $\rho_{m1}$ | +.00208 ± .00022 | $-\rho_{r0}$ | +.0000453 ± .0000186 | $-\rho_{r0}$ |
| | $\sqrt{\frac{\Sigma \Delta P_i}{N-NC}}^*$ atm | 0.00072 | 0.00074 | 0.00224 | 0.00227 |
| 2(He) and 3(Xe) | $\delta$ | 4.24 ±0.24 | 4.13 ±0.08 | 3.73 ±0.76 | 4.72 ±0.39 |
| | $\gamma$ | 1.137 ± .012 | 1.138 ± .009 | 1.178 ± .016 | 1.208 ± .012 |
| | $\beta$ | .351 ± .009 | .363 ± .006 | .430 ± .052 | .324 ± .012 |
| | $\alpha$ | .161 ± .023 | .135 ± .015 | −.039 ± .106 | .142 ± .033 |
| | $\alpha_1$ | .277 ± .286 | .135 ± .015 | −.149 ± .389 | .142 ± .033 |
| | $\alpha_2$ | .338 ± .124 | .135 ± .015 | .060 ±1.591 | .142 ± .033 |
| | $\rho_{r0}$ | −.000314 ± .000439 | +.00013 ± .0004 | −.0000105 ± .0000070 | −.0000251 ± .0000059 |
| | $\rho_{m_1}$ | +.00168 ± .00107 | $-\rho_{r0}$ | +.000228 ± .000057 | $-\rho_{r0}$ |
| | $\sqrt{\frac{\Sigma \Delta P_i}{N-NC}}^*$ | 0.00059 | 0.00059 | 0.00198 | 0.00203 |
| 4 | $\delta$ | | | | 5.73 ±8.19 |
| | $\gamma$ | | | | 1.284 ± .074 |
| | $\beta$ | | | | .271 ± .129 |
| | $\alpha$ | | | | .172 ± .283 |
| | $\alpha_1$ | | | | .172 ± .283 |
| | $\alpha_2$ | | | | .172 ± .283 |
| | $\rho_{r0}$ | | | | +.0000171 ± .0000425 |
| | $\rho_{m1}$ | | | | $-\rho_{r0}$ |
| | $\sqrt{\frac{\Sigma \Delta P_i}{N-NC}}^*$ | | | | 0.00209 |

*$N$ is the number of data points; $NC$ is the number of constants.

TABLE 3. *Constants for eq (2) applied to helium data* [6][a]

| Constants of the equation | | | |
|---|---|---|---|
| Constant | Value | Error | The standard deviation is 0.00074 |
| $A$ | 0.32043251E 04 | 0.10131254E 03 | |
| $P_{s1}$ | .17091894E 01 | .19034584E−02 | |
| $B_1$ | .33758179E 03 | .12381564 02 | |
| $P_{s2}$ | .72719432E 00 | .34948345E−01 | Maximum error in pressure is −0.0025 atm. |
| $P_{s0}$ | −.66253524E 01 | .98947437E 02 | At $T=5.26370$ and |
| $\rho_{t0}$ | −.13174329E−02 | .15183463E−03 | $P=2.40487$ atm. |
| $2-\alpha_2$ | $=1+2\beta+\mu$ | | |
| $C$ | 0.74227144E 02 | .45068578E 00 | |
| $\rho_c$ | .17232286E−01 | .52370344E−05 | |
| $\rho_{m1}$ | $-\rho_{t0}$ | | |
| $T_c$ | .51909878E 01 | .27286947E−03 | |
| $\beta$ | .35366522E 00 | .23593233E−02 | |
| $\mu$ | .11915742E 00 | .33542782E−02 | |
| $1-\alpha_1$ | $=2\beta+\mu$ | | |
| Derived Constants | | | |
| Constant | Value | Error | |
| $\alpha$ | 0.17351214E 00 | 0.60508733E−02 | |
| $\gamma$ | .11191574E 01 | .33542782E−02 | |
| $\delta$ | .41644543E 01 | .62999387E−01 | |

[a] The density range is 50, the temperature range is 5 and the pressure range is 8 percent around the critical point. The number of data points is 414.

TABLE 4. *Constants for eq (2) applied to xenon data* [3][a]

| Constants of the equation | | | |
|---|---|---|---|
| Constant | Value | Error | The standard deviation is 0.00227. |
| $A$ | 0.94959356E 04 | 0.21903837E 03 | |
| $P_{s1}$ | .11860651E 01 | .83952672E−03 | |
| $B_1$ | .13935997E 04 | .53686691E 02 | |
| $P_{s2}$ | .15611421E−01 | .23977382E−02 | Maximum error in pressure is 0.0067 atm. |
| $P_{s0}$ | −.28601355E 03 | .24339522E 00 | At $T=289.13990$ K and |
| $\rho_{t0}$ | −.14547437E−04 | .39990010E−05 | $P=56.3430$ atm. |
| $2-\alpha_2$ | $=1+2\beta+\mu$ | | |
| $C$ | 0.47872048E 03 | .12869899E 01 | |
| $\rho_c$ | .84971537E−02 | .39913666E−05 | |
| $\rho_{m1}$ | $-\rho_{t0}$ | | |
| $T_c$ | .28976481E 03 | .31386983E−02 | |
| $\beta$ | .350500350 00 | .46079306E−02 | |
| $\mu$ | .19110181E 00 | .63731809E−02 | |
| $1-\alpha_1$ | $=2\beta+\mu$ | | |
| Derived Constants | | | |
| Constant | Value | Error | |
| $\alpha$ | 0.10789750E 00 | 0.13966633E−01 | |
| $\gamma$ | .11911018E 01 | .63731809E−02 | |
| $\delta$ | .43982899E 01 | .10541327E 00 | |

[a] The density range is 50, the temperature range is 5 and the pressure range is 8 percent around the critical point, the number of data points is 165.

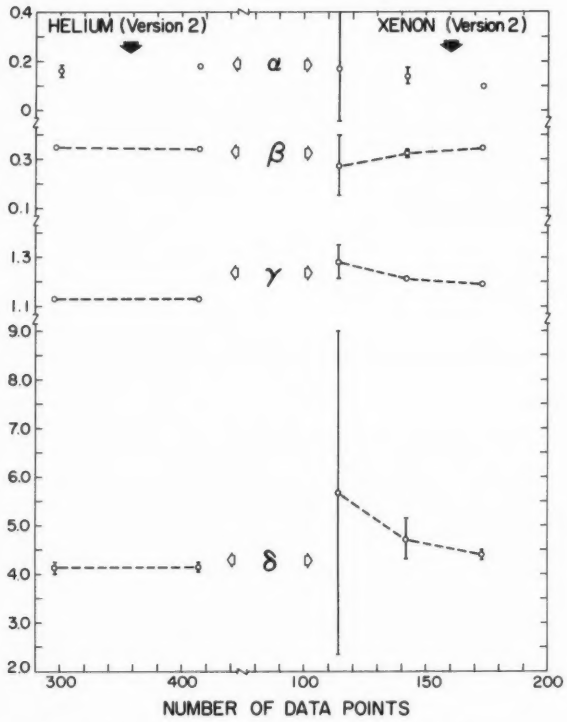


FIGURE 3. *α, β, γ and δ for helium and xenon and their dependence on the number of data points (error bars are indicated by the cross-hatched strips).*

## 4. Conclusions

Only qualitative conclusions can be drawn from table 2. The values obtained for $\alpha_1$ and $\alpha_2$, indeed, are consistent with the divergences as claimed by Widom and by Green et al. The values obtained, however, are larger than $\alpha$. Furthermore the equality $\rho_{m1} = -\rho_{f0}$ seems to check out qualitatively. It should be emphasized however that the accuracy of the data, although being within the limits of the present state of the art, does not allow definite conclusions. The small differences obtained for $\alpha$, $\beta$, $\gamma$, and $\delta$ in versions 1 and 2 and by other authors [7] could be explained by the fact that equations of this type can be very suggestive with respect to these values.

It should also be noted that the value for $\alpha$ obtained for helium is much higher than the values obtained in the past by other authors [7].

In a more recent analysis, however, higher values have been obtained [8]; other recent experiments on helium also suggest higher values for $\alpha$ (e.g., $\alpha = 0.14$ [9]).

It can be seen from the error bars in figure 3 that helium is the more likely candidate for interpretation of the resulting exponents:

The agreement between the exponents for the different ranges and for the different versions of the state equation for helium is almost within the error bars.

Noteworthy is the fact that $\alpha_1$ tends to be higher ($\sim 0.3 \pm 0.1$) than $\alpha$ and that $\alpha_2$ seems to be even higher ($\sim 0.45$) for version 1 and for both helium and xenon.

We do not exclude the possibility that these values are suggested by version 1 but it is noteworthy that an $\alpha_2$ equal to 0.45 is still lower than $\alpha + \beta$ ($0.15 + 0.355$). This value ($\alpha_2 = 0.45$) however, would imply a thermodynamic potential divergent at the critical point, a possibility which is doubted by many.

A weak point in eq (2) is the nonanalyticity introduced by the second term on the right side of eq (6) resulting in a divergent $\left(\frac{\partial^2 P}{\partial \rho^2}\right)_T$ for $\rho$ equal to $\rho_m$. This nonanalyticity can be avoided but we doubt that its influence on the critical parameters is important.

More difficult to avoid is the nonanalyticity introduced by the third term of eq (2). This nonanalyticity disappears when $\gamma/\beta$ is an integer, say $\gamma/\beta \equiv 3$, for instance. This effect may have had the odd result of producing rather high values for $\alpha$.

---

We are indebted to J. M. H. Levelt Sengers for stimulating discussions on this subject, and to V. Jansoone who suggested the error analysis. Most of of the calculations were performed on the CDC3800 computer, the use of which was granted by the Cryogenics Division of the National Bureau of Standards, Boulder, Colorado 80302. We are also indebted to the "Rekencentrum" of the University of Leuven, Belgium where part of the computations were performed.

## 5. References

[1] Verbeke, O. B., Jansoone, V., Gielen, R., J. DeBoelpaep, Journal of Physical Chemistry **73,** 4076 (1969).
[2] Jansoone, V., Gielen, H., J. DeBoelpaep, O. B. Verbeke, Physica **46,** 213 (1970).
[3] Habgood, H. W., Schneider, W. G., Can. J. Chem. **32,** 98 (1954).
[4] Green, M. S., Vicentini-Missoni, M., Levelt Sengers, J. M. H., Phys. Rev. Letters **18,** 1113 (1967).
[5] Widom, B., Rowlinson, J. S., J. Chem. Phys. **52,** 1670 (1970).
[6] Roach, P. R., Physical Rev. **170,** 213 (1968).
[7] Vincentini-Missoni, M., Levelt Sengers, J. M. H., Green, M. S., J. Res. Nat. Bur. Stand. (U.S.), **73A** (Phys. and Chem.), No. 6, 563–583 (Nov.–Dec. 1969).
[8] Green, M. S., Cooper, M. J., Levelt Sengers, J. M. H., Phys. Rev. Letters **26,** 492 (1971).
[9] Moldover, M. R., Phys. Rev. **182,** 342 (1969).

(Paper 76A3–717)

JOURNAL OF RESEARCH of the National Bureau of Standards—A. Physics and Chemistry
Vol. 76A, No. 3, May–June 1972

# Dilute Solution Theory of Polymer Crystal Growth: Fractionation Effects

**Isaac C. Sanchez* and Edmund A. DiMarzio**

**Institute for Materials Research, National Bureau of Standards, Washington, D.C. 20234**

**(February 4, 1972)**

A nonequilibrium (kinetic) theory of polymer molecular weight (MW) fractionation is formulated and applied to binary and multicomponent polyethylenes crystallized from unstirred xylene solutions. High MW components crystallize more readily than do low MW components. This fractionation effect is enhanced as the crystallization temperature is raised. At low crystallization temperatures (high undercoolings) the polymer tends to fractionate according to the volume fraction distribution of its MW components and thus, the number average MW of the crystal that is formed is approximately equal to the weight average MW of the polymer in solution. It is shown that MW fractionation does not depend on the details of nucleation, but rather on the rates for post-nucleation crystal growth. The effects of MW polydispersity on crystalline properties is considered and in particular it is shown that polydispersity tends to mask the intrinsic dependence of crystal thickness on MW. The variables which govern and influence fractionation are also discussed.

Key words: Cilia; dissolution temperature; fractionation; rate constant; undercooling.

## 1. Introduction

There is a growing body of experimental evidence that indicates that when a polymer polydispersed in molecular weight (MW) begins crystallizing, the high MW components preferentially crystallize first. This phenomena has been observed in both stirred [1–3][1] and unstirred [1, 4, 5] solutions of polyethylene and xylene. It is also thought to occur during crystallization from the melt and would appear to affect the resulting crystalline morphology. Fractionation has been invoked to explain spherulitic growth habits [6, 7] and is believed to accompany the formation of extended-chain crystals [8–12]. For monomeric materials, crystallization from solution or from the melt (zone refining) is a standard procedure for achieving high purity and one wonders what the limitations are for polymeric materials.

Polymer MW fractionation during crystal growth is also of interest for other reasons; an important one is the fact that all polymers are polydisperse in MW to some degree. For example, in crystallization studies one sometimes tries to follow the variation of a crystal property with MW (average) by working with sharp MW fractions. A knowledge of the amount of fractionation that is occurring gives one a better idea of whether the distribution is sharp enough for the experiment in question; i.e., in crystallization experiments the very notion of a "sharp" MW fraction is intimately tied up with the amount of fractionation that occurs.

Moreover, MW fractionation implies that the central regions of a cyrstallite can have a MW composition that is different than the peripheral regions since the solution becomes depleted of high MW components as the crystal grows in lateral size. Thus, there is a composition heterogeneity in the crystal and a concomitant spatial variation in all those properties that are a function of composition. It has been suggested that isothermal thickening of polymer crystals is caused by this variation in crystal composition [13, 14].

Heretofore, theoretical studies of MW fractionation have essentially been equilibrium theories [4, 5, 15, 16]. However, equilibrium treatments of fractionation have a limited range of applicability [15] since polymer crystals are formed under nonequilibrium conditions. The undercooling is typically 20 to 30 °C and as will be demonstrated, fractionation is a sensitive function of undercooling.

In a previous publication [17], hereafter referred to as paper I, we developed a kinetic theory of polymer crystal growth from dilute solution for a monodisperse polymer. In a second paper [18], paper II, we applied the theory to polyethylene (PE) crystallized from xylene solutions. These works provide a foundation on which we can build a nonequilibrium theory of fractionation in unstirred solutions. This is done in section 2. In section 3 we apply the theory to the PE-xylene system and in section 4 the conclusions of the study are discussed.

*NRC–NAS Postdoctoral Research Associate, 1969–71. Present address: Xerox Corporation, Rochester, N.Y. 14603.

[1] Figures in brackets indicate the literature references at the end of this paper.

## 2. Theory

### 2.1. Relation to Papers I and II

It is perhaps best to begin by recalling the experimental situation on which our model is based. In dilute solution, thin (ca. 100 Å) plate-like lamellar crystals grow to large lateral size by accretion of the polymer molecules to the outer edges of the crystal. The polymer molecules composing the crystals are oriented with their molecular axes perpendicular to the basal plane of the lamella [19, 20]. Since the contour length of the molecule is larger than the lamellar thickness the molecules must fold. Cleavage experiments show that the molecules tend to fold parallel to the growing edge [21] and crystallographic properties indicate more or less tight folds on the surface of the crystal [20]. The molecules can thus be viewed as lying down in parallel growth strips (fold planes). The growth rate is of the order of strips per second [22]. The smoothness of the growing edge is a measure of the rate of nucleating a strip compared to the rate of filling in the nucleated strip. Smooth surfaces correspond to rare nucleation events, but one cannot make a quantitative statement without recourse to theory.

In papers I and II we described and calculated the growth rates of such crystals from a monodisperse polymer solution. One of the interesting aspects of this treatment is that the rate of nucleation $S^*$ of a strip is a rare event compared to the rate of filling in of the strip, $S'$, under most growth conditions. This means that the overwhelming number of molecules that comprise the grown strip, and therefore the crystal, are non-nucleating molecules. Under these conditions one can write the growth rate $G$ for the change of a lateral dimension with time as [17]

$$G=G(S^*,S',N) \tag{2.1}$$

where $N$ is the number of nucleation sites. In the more general case $G$ is a function of the forward and backward rate constants for nucleation as well as the forward and backward rate constants for filling in.

This formula remains valid even if we have a polydisperse system, the $S^*$ and $S'$ merely need be interpreted as total growth rates:

$$S^*=\sum S_i^* \tag{2.2}$$

$$S'=\sum S_i' \tag{2.3}$$

$S_i'$ is the net rate at which molecules of type $i$ are being added to an already nucleated strip. Since most molecules of a growth strip are of the fill-in type the fraction of species $i$ incorporated into the crystal is given by

$$f_i=S_i' \Big/ \sum S_i'. \tag{2.4}$$

Nucleation must be viewed as the compound event of attaching a molecule (or cilium) to the crystal edge followed by the subsequent stabilization of this molecule by other molecules. $S_i^*$ is the rate at which molecules of type $i$ initiate the growth of a strip. The fraction of growth strips whose initial molecule is type $i$ is a calculable quantity but it is uninteresting.

In paper I we pointed out that the functional form of eq (2.1) for the growth rate $G$ is unknown, except in two limiting cases. We argued that for polymer crystallization the following limiting case

$$G \sim S^* \tag{2.5}$$

is valid when $S^* \ll S'$. We wish to point out that the composition of the crystal does not depend on the functional form of $G$ and the prescription for calculating the composition remains valid even if $S^*$ is sufficiently close to $S'$ so that eq (2.5) is no longer a useful approximation. Hillig has given an alternate expression for $G$ which might be a useful approximation in some regions of growth [23]. His method can be easily adapted to our two dimensional growth problem. The result is

$$G \sim (S^*S')^{1/2}. \tag{2.6}$$

Equation (2.5) is expected to hold when the number of nuclei per $N$ sites is the order of one or less (i.e., $S'/S^*N > 1$) and results in a smooth edge, while eq (2.6) holds when $S'/S^*N$ is small and results in a rough (highly reentrant growth) edge. As was pointed out in the appendix of paper I the effective value of $N$ may be considerably smaller than the number of sites on an edge due to defects of various types which destroy the continuity of the crystal along the edge.

### 2.2. LDP Kinetic Theory

Lauritzen, DiMarzio, and Passaglia (LDP) have formulated a theory to describe the steady state rate of growth and composition of a chain growing in a multicomponent system [24]. A chain in the system grows by the sequential addition of any of the $n$ components (species) of the system to one end of the chain. Only nearest neighbor interactions are considered; the rate constants $\alpha^{ij}$ for adding species $j$ to a chain ending in species $i$ and $\beta^{ij}$ for removing species $j$ from a chain ending in $(i,j)$ are assumed to be independent of chain length (this restriction can be relaxed, [25] but it is not necessary to do so in the present application of the theory). Initiation of a new chain by species $j$ is governed by the unique rate constant pair $(\alpha_0^j, \beta_1^j)$.

If $S_\nu^j$ is the current or rate at which chains $\nu$ units long ending with species $j$ are produced, $S_\nu^{ij}$ the current for chains $\nu$ units long ending with the pair $(i,j)$ etc., then LDP showed that

$$\lim_{\nu\to\infty} S_\nu^j/N_\nu^j = S_\nu^{ij}/N_\nu^{ij} = \ldots = \lambda^j \tag{2.7}$$

where $N_\nu^j$ is the number of chains (occupation number) $\nu$ units long that end with species $j$ in the ensemble of chains and $N_\nu^{ij}$ and higher order occupation numbers are similarly defined. The ratios of currents to their corresponding occupation number in the limit of large chain lengths become a function of the terminal

species only. Also the currents and occupation numbers become independent of $\nu$ for large $\nu$. The quantities $\lambda^j$ are defined by a set of nonlinear equations:

$$\lambda^j = \sum_{i=1}^{n} \frac{\alpha^{ji}\lambda^i}{\beta^{ji} + \lambda^i} \tag{2.8}$$

where $n$ is the total number of components in the system. The net rate at which chains are initiated is given by

$$S_T = \sum S^j = \sum_j \lambda^j N^j = \sum_j \frac{\alpha_0^j \lambda^j N_0}{\beta_1^j + \lambda^j} \tag{2.9}$$

where $N_0$ is the number of sites where chain initiation can occur. The fraction $f_j$ of component $j$ in the chain is given by

$$f_j = \lambda^j N^j / \Sigma_j \lambda^j N^j \tag{2.10}$$

where the occupation numbers $N^j$ are obtained from the recursion relation

$$N_\nu^i = \sum_j \frac{\alpha^{ji} N_{\nu-1}^j}{\beta^{ji} + \lambda^i} \tag{2.11}$$

where $N_1^i = \alpha_0^i N_0/(\beta_1^i + \lambda^i)$. For large $\nu$ eq (2.11) becomes

$$N^i = \sum_j \frac{\alpha^{ji} N^j}{\beta^{ji} + \lambda^i}. \tag{2.12}$$

In the present application of the LDP theory, the components of the system are the various molecular weight species present in a polymer heterogeneous in molecular weight and the "chain" referred to above is a growth strip on a crystal face. As we pointed out in section 2.1, polymer single crystal growth is two-dimensional (2–D) in character; however, because of the relative rates of nucleation and growth the crystal grows essentially by the sequential addition of 1–D growth strips (fold planes). This crystal growth feature allows one to employ a 1–D theory like the LDP theory to describe the formation and composition of these growth strips.

In paper I we showed that when the crystal growth strip was composed only of polymer molecules of degree of polymerization $P_j$ which added one crystal stem at a time, then there emerges *effective* rate constants for adding the molecule as a unit. These forward and backward rate constants for the whole molecule were denoted as $A_0, B_1$ for the nucleation step and as $A_1, B_2$ for post-nucleation growth. Thus, in a system containing molecules of various lengths we can assign forward and backward rate constants $(A_0^j, B_1^j)$ and $(A_1^j, B_2^j)$ to each size molecule and evaluate these rate constants as was done in paper I and paper II. This assumes that adding a molecule of length $j$ to the crystal is independent of the molecules already in the crystal, i.e.,

$$\begin{aligned} \alpha^{1j} &= \alpha^{2j} = \ldots = \alpha^{nj} = A_1^j \\ \beta^{1j} &= \beta^{2j} = \ldots = \beta^{nj} = B_2^j. \end{aligned} \tag{2.13}$$

The identification $\alpha_0^j = A_0^j$ and $\beta_1^j = B_1^j$ completes the specification of the rate constants. This set of rate constants leads to a simplification of the LDP theory equations:

$$\lambda^1 = \lambda^2 = \ldots = \lambda^n \equiv \lambda$$

and

$$\lambda = \sum_j^n \frac{A_1^j \lambda}{B_2^j + \lambda} \tag{2.14}$$

Moreover,

$$S_T = \sum_j^n \frac{A_0^j \lambda N_0}{B_1^j + \lambda}. \tag{2.15}$$

At this point we should identify the nucleation rate $S^*$ and the post-nucleation rate $S'$ of section 2.1 with the LDP equations so that the full physical significance of these quantities become apparent:

$$S_j^* = \frac{A_0^j \lambda}{B_1^j + \lambda}, \quad S^* = \Sigma_j S_j^* = S_T/N_0 \tag{2.16}$$

and

$$S_j' = \frac{A_1^j \lambda}{B_2^j + \lambda}, \quad S' = \Sigma_j S_j' = \lambda. \tag{2.17}$$

Thus, from eq (2.4) the fraction of species $j$ that is incorporated is given by

$$f_j = \frac{A_1^j}{B_2^j + \lambda}. \tag{2.18}$$

Since $\lambda$ is only a function of the post-nucleation rate constants $(A_1^j, B_2^j)$, $f_j$ is independent of the nucleation rate constants $(A_0^j, B_1^j)$. Also note that eq (2.18) can be derived directly from eqs (2.10) and (2.12).

### 2.3. Energetics and Thermodynamics

#### a. General Considerations

The LDP kinetic theory does not require a determination of the free energy of mixing of the components in the crystalline phase as is required by equilibrium theories of the fractionation phenomena [5, 16]. From LDP theory, we have

$$\alpha^{ij}/\beta^{ij} = \exp\left[(\mu_j - \epsilon_{ij})/kT\right] \tag{2.19}$$

where $\mu_j$ is the chemical potential of species $j$ in solution and $\epsilon_{ij}$ is the interaction energy associated with adding species $j$ to a chain ending in species $i$. The free energy change $(\mu_j - \epsilon_{ij})$ that is required to evaluate the rate constants does not require or presume a knowledge of the free energy change associated with the mixing of species in the chain. In fact, the net change in chemical potentials caused by the mixing is calculable from the theory. For example, in a $n$ component system where the components are similar in size and the $\epsilon_{ij}$ are not too dissimilar, the total mixing entropy would be given to an excellent approximation by

$$\Delta S_{\text{mix}} = -k\Sigma_j^n N_j \ln (N_j/\Sigma_i N_i) \tag{2.20a}$$

or

$$\Delta S_{\text{mix}}/\Sigma_i N_i = -k\Sigma_j f_j \ln f_j \tag{2.20b}$$

where $N_j$ is the number of elements in the chain of species $j$ and $f_j$ is the mole fraction of species $j$ in the chain. If the components vary in size, then $\ln f_j$ would be replaced by $\ln v_j$ where $v_j$ is the volume fraction of species $j$ in the chain. Now the change in chemical potential $\Delta\mu_i$ caused by mixing is given by

$$\Delta\mu_j = \frac{\partial}{\partial N_j}(-T\Delta S_{\text{mix}}) \tag{2.21}$$

$$\Delta\mu_j = kT \ln f_j$$

where the mole fractions $f_j$ can be determined from eq (2.18).

In general, when the interaction energies $\epsilon_{ij}$ cannot be ignored then [26]

$$\Delta S_{\text{mix}}/\Sigma N_i = -k\,\Sigma_{i,j} f_{ij} \ln (f_{ij}/f_i) \tag{2.22}$$

where $f_{ij}$ is the fraction of $(i, j)$ pairs in the chain and from LDP theory is given by

$$f_{ij} = \alpha^{ij}\lambda^j N^i/(\beta^{ij} + \lambda^j) S_T. \tag{2.23}$$

In the special case where there is no correlation between components, as in the present application, then $f_{ij} = f_i f_j$ and eq (2.22) reduces to eq (2.20b).

#### b. Evaluation of $\mu_j - \epsilon_{ij}$

If the free energy change $\mu_j - \epsilon_{ij}$ required in eq (2.19) refers to the crystallization of the entire molecule, then (ignoring for the moment surface effects)

$$\mu_j - \epsilon_{ij} = \mu_j^0 - \mu_j^c + RT \ln a_j \tag{2.24}$$

where $\mu_j^0$ is the chemical potential of *pure* species $j$ in a melt at temperature $T$ (the standard state); $\mu_j^c$ in the chemical potential of species $j$ in a *homogeneous* crystal of species $j$ and $a_j$ is the activity of species $j$ in solution.

The term $RT \ln a_j$ is the difference in chemical potential between a pure melt of species $j$ and a polymer solution containing all species; it is given by [27]

$$\ln a_j = \ln v_2^j - (x_j - 1) + v_2 x_j (1 - 1/\bar{x}_\eta) + x_j \chi (1 - v_2)^2 \tag{2.25}$$

where $v_2^j$ is the volume fraction of species $j$ in solution; $v_2 = \Sigma_j^n v_2^j$ is the total volume fraction of polymer; $x_j$ in the ratio of the molar volume of species $j$ to that of the solvent; $\bar{x}_\eta$ is the number average of $x_j$ is the solution phase and $\chi$ is the polymer-solvent interaction parameter which in general is a function of the molecular weight of species $j$.

The term $\mu_j^c - \mu_j^0$ is the difference in chemical potential between a homogeneous melt and a homogeneous crystal of species $j$ and is given by

$$\mu_j^0 - \mu_j^c = P_j \Delta G_u^0(T, j) \tag{2.26}$$

where $P_j$ is the degree of polymerization of species $j$ and $\Delta G_u^0(T, j)$ is the difference in free energy between a monomer unit (belonging to species $j$) in a melt and one embedded in a crystal. Different approximations can be employed for $\Delta G_u^0$; however, for polyethylene (PE) the following approximation is best: [18]

$$\Delta G_u^0(T, j) = \Delta H_u (T_m^0 - T)(1 + T/T_m^0)/2T_m^0 \tag{2.27}$$

where $\Delta H_u$ is the enthalpy of fusion per mole of monomer at the equilibrium melting point $T_m^0$. Of course, $T_m^0$ is a function of molecular weight, $T_m^0 \equiv T_m^0(j)$.

It is convenient to define a "psuedo" equilibrium dissolution temperature $T_j^0$ for species $j$ by setting eq (2.24) equal to zero. Using eqs (2.26) and (2.27) yields.

$$T_j^0 = T_m^0(j)[r + (1 + r^2)^{1/2}] \tag{2.28}$$

where

$$r = RT_m^0 \ln a_j/\Delta H_u P_j. \tag{2.29}$$

In Paper II it was shown that if the partial molar heat of mixing molten polymer with solvent was small compared to the molar heat of fusion, then eq (2.24) can be expressed as

$$\mu_j - \epsilon_{ij} = P_j\left[\Delta G_u^0(T, j) - \frac{T}{T_j^0}\Delta G_u^0(T_j^0, j)\right] \tag{2.30a}$$

and from eq (2.27), we have

$$\mu_j - \epsilon_{ij} = P_j[\Delta H_u (T_j^0 - T)(1 + TT_j^0/T_m^{0^2})/2T_j^0]. \tag{2.30b}$$

In summary eq (2.30) represents the change in free energy associated with removing species $j$ from a

solution containing all species and placing it in a crystal containing only species $j$. Of course, if the polymer molecule is in a chain-folded configuration, surface free energies must be added.

If the solution consisted only of solvent and species $j$, then $T_j^0$ becomes the equilibrium dissolution temperature $T_d^0$ for the monodisperse polymer-solvent system. The "psuedo" equilibrium dissolution temperature $T_j^0$ differs from $T_d^0$ in that it includes in its definition (through ln $a_j$) the entropy of mixing of the various molecular weight species in solution; however, as one might expect there is very little difference (usually less than 1°) in the two temperatures.

#### c. High Undercooling Limit

In eq (2.25) the volume fraction $v_2^j$ of species $j$ is required. From the definition of volume fraction it can be readily shown that

$$v_2^j = (M_j p_j / M_n) v_2 \tag{2.31}$$

where $p_j$ is the probability or mole fraction of species $j$ in solution, $M_j$ is its molecular weight (MW) and $M_n = \Sigma_j\, p_j M_j$ is the number average MW. Note that $v_2^j \neq p_j v_2$ and that the volume fraction is a weight average property ($M_w$):

$$M_w = \Sigma_j\, M_j v_2^j / v_2. \tag{2.32}$$

In the limit of high undercoolings $B_2^j \to 0$ so that

$$\lambda \to \Sigma_j\, A_1^j \tag{2.33}$$

$$f_j \to A_1^j / \Sigma_j A_1^j. \tag{2.34}$$

Now the forward rate constants chosen in accordance with paper II (c.f. sec. IIIa) give in the high undercooling limit.

$$A_j^j \to v_2^j / \sqrt{x_j} \tag{2.35}$$

thus

$$f_j = v_2^j / \sqrt{x_j} / (\Sigma_j\, v_2^j / \sqrt{x_j}). \tag{2.36}$$

The factor $\sqrt{x_j}$ arises from the reduction of polymer conformations near a crystal surface. More generally the 1/2 power of $x_j$ is replaced by $2\delta$ where $\delta$ has the limits of zero and 1/2 ($0 < \delta < 1/2$).[17] Our best estimate of $\delta$ in the equilibrium limit was $\delta = 1/4$, however in the high undercooling limit a smaller value for $\delta$ may be more appropriate. In any event, in the absence of a surface $\delta = 0$ and we obtain

$$f_j \to v_2^j / v_2. \tag{2.37}$$

This result is consistent with physical intuition because the probability of finding a polymer molecule at a particular place in the solution is equal to $v_2^j / v_2$. Therefore, in the absence of energetic and surface effects (all polymeric species which come in contact with the crystal niche are incorporated) fractionation will occur according to volume fraction. This is a significant conclusion because as mentioned previously volume fraction is closely related to the weight average properties of the polymer and thus to a first approximation, the number average MW of the crystal will equal the weight average MW of the polymer in solution. Of course, we are treating the case where the composition of the solution does not change substantially during the course of crystallization. In the usual experimental range of undercoolings energetics play an important role in fractionation as will be demonstrated in section 3.

In the above considerations we have ignored preexponential (diffusion) factors. The rate determining step is presumed to be not diffusion to the crystal surface, but rather incorporation into the growth niche. This opinion has been expressed elsewhere for dilute solution crystallization [22]. The present theory can easily accommodate diffusional factors when they exist. In the simplest approximation the diffusion constant of a polymer molecule is inversely proportional to MW and, therefore, the exponent of $x_j$ in eqs (2.35) and (2.36) or wherever it occurs in rate constants would change from 1/2 to 3/2.

## 3. Results

### 3.1. Constants and Parameters

The constants and parameters used in this study are identical to those listed in table III of paper II for polyethylene in xylene which serves as a model system. As in paper II we will employ a semi-empirical relation for the equilibrium dissolution temperature $T_j^0$;

$$T_j^0 = \{T_m^0(j)\,[1 + r + (1 + r^2)^{1/2}] - 29\}/2 \tag{3.1}$$

where $r$ is defined by eq (2.29), Flory-Vrij values are used for $T_m^0(j)$ and the $\chi$ interaction parameter for a species of molecular weight $M_j$ is the Pennings' relation

$$\chi = 0.372 - 25.2/\sqrt{M_j}. \tag{3.2}$$

The evaluation of the rate constants ($A_0^j$, $B_1^j$) and ($A_1^j$, $B_2^j$) differ from our previous evaluation of these rate constants in paper II in two ways: (1) the localization free energy $F_L$ now becomes equal to

$$F_L(j) = kT \ln (v_2^j / \sqrt{x_j}) \tag{3.3}$$

for each species $j$ and (2) $T_j^0$ replaces $T_d^0$. The replacement of $T_d^0$ by $T_j^0$ reflects the fact that the free energy associated with the mixing of the $n$ components in solution has been taken into account.

In the special case where the extended or contour length of the polymer molecule is less than the crystal thickness, $A_0$ and $A_1$ can be set equal to zero, or the extended length rather than the crystal thickness can



459-033 OL - 72 - 3

be used in evaluating the rate constants with or without a correction for chain end incorporation in the crystal. Regardless of the approximation employed the result is essentially the same—negligible amounts of these short molecules are incorporated.

### 3.2. Two Component System

#### a. Solution of λ Equation

A case of particular interest is the two component system, i.e., a system of solvent and two polymeric species. In this case eq (2.14) can be solved analytically with the result

$$\lambda = \{\gamma_1 + \gamma_2 + [(\gamma_1 + \gamma_2)^2 + 4\,(A_1^1 B_2^2 + B_2^1 \gamma_2)]^{1/2}\}/2 \quad (3.4)$$

where $\gamma_1 = A_1^1 - B_2^1$ and $\gamma_2 = A_1^2 - B_2^2$. Experimentally, one can hope to make measurements on blends of two very sharp MW fractions. The results should approximate those for two perfectly sharp MW fractions for which eq (3.4) obtains.

#### b. Method of Calculation

The calculational procedure for the two component system is outlined below:

(a) The mole fraction of each component in solution is fixed, as well as other parameters such as temperature and total volume fraction.

(b) A crystal thickness value is chosen and the rate constants ($A_0^j$, $B_1^j$) and ($A_1^j$, $B_2^j$) which are given by eqs (3.3) through (3.6) in paper II are calculated.

(c) Lambda, which is the post-nucleated growth rate of the strip, is evaluated from eq (3.4), the crystal compositions $f_j$ are determined from eq (2.18) and the total nucleation rate $S_T$ is calculated from eq (2.15). Now there are two possible types of nuclei—solution molecules or cilia. Both nucleation rates are calculated. However, each term $A_0^j\lambda/(B_1^j+\lambda)$ for cilia nucleation must be multiplied by the weighting factor $f_j/<j>$ because the probability that a cilium belonging to molecule $j$ is available for nucleation is proportional to the fraction of $j$ molecules being incorporated into the crystal and the density of cilia along the growth strip which in turn is inversely proportional to the average spacing $<j>$ between cilia.

(d) The growth rate $S_T$ passes through a maximum as a function of lamella thickness. To obtain $S_T(l)$, the lamella thickness $l$ is incremented in 2.5 Å intervals and the above procedure (a to c) is repeated at each $l$. A natural lower bound on $l$ occurs because crystal thicknesses less than a certain value $l_c$ are not possible since they correspond to thermodynamically unstable crystals ($\lambda = 0$ at $l_c$). For large lamella thicknesses the calculation is carried on until the nucleation rate is at least two orders of magnitude less than the maximum nucleation rate.

#### c. Method of Averaging

The most important quantity to be calculated is the composition of the crystallites that are formed. Although the $f_j$ are uniquely determined for a given crystal thickness and are independent of nucleation rate constants, theory predicts that a distribution of crystallite thicknesses may evolve. If $S_T(l_i)$ is the nucleation rate for crystallites of thickness $l_i$, we can define the average composition $<f_j>$ (or any other property of the crystals) in the following way:

$$<f_j> = \Sigma_i f_j(l_i) S_T(l_i) / \Sigma_i S_T(l_i). \quad (3.5)$$

On physical grounds weighting $f_j$ by $S_T$ is not strictly correct because material conservation has not been taken into account. For example, if the lateral dimensions of a crystal are proportional to $S_T$, then the volume or mass of the lamellar crystal is proportional to $S_T^2 l$ which is the proper weighting function. However, average properties calculated with either weighting function yield similar results. Alternatively one could calculate the $f_j$ at the maximum value of $S_T$ but this procedure is not always adequate for two component systems because $S_T$ occasionally is slightly binodal and tends to be broad.

Either the solution molecule or cilia nucleation rates can be used to calculate average properties. In general, utilization of the cilia nucleation rate leads to better fractionation, i.e., more of the high MW component is incorporated. Since it is still unknown at this time how much each of the two nucleation rates contribute to the total nucleation rate, we have arbitrarily presented results in figures 1 thru 6 based on the solution molecule nucleation rate.

#### d. Kinetic Phase Diagrams

Figures 1 to 3 give some results for binary systems of polyethylene. They are kinetic phase diagrams although they differ from the usual temperature-composition phase diagram representations. Since the crystallization temperature is an experimentally controllable variable we have chosen to present the results for isothermal crystallization conditions.

The effect of crystallization temperature on fractionation is illustrated in figure 1. One sees that even at 84 °C one is near the high undercooling limit given by eq (2.37). Rejection of the low MW component is enhanced as the crystallization temperature is increased. The high temperature limit which is equilibrium crystallization is of little interest since in this region the growth rates are so small that no crystals will be observed in experiments of laboratory time scale.

One sees by means of figure 1 that successive recrystallization can be used to purify a binary system. This is achieved by taking the crystals that form initially in the solution and after dissolving them in solvent, recrystallizing them and so on. A measure of the efficiency of the process is given by the initial slope of the curve. For 88° the slope is about 1/10 and therefore one would obtain 10 times more purity with each recrystallization. Thus, provided one is willing to spend the effort one can prepare polyethylene of arbitrary purity.

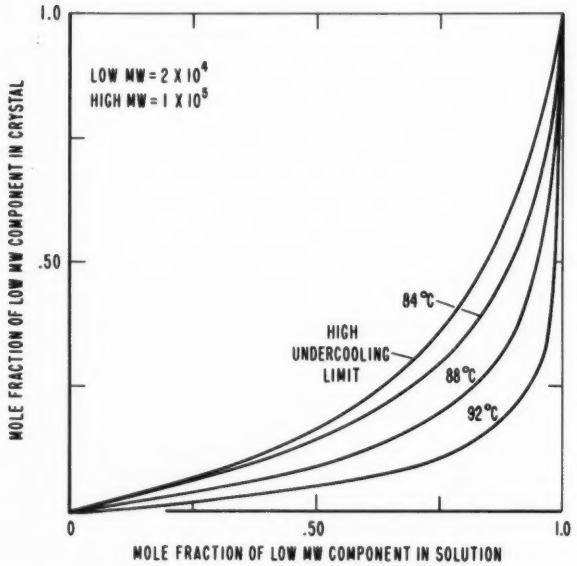


FIGURE 1. *Crystal composition versus polymer solution composition for a binary PE at various crystallization temperatures.*

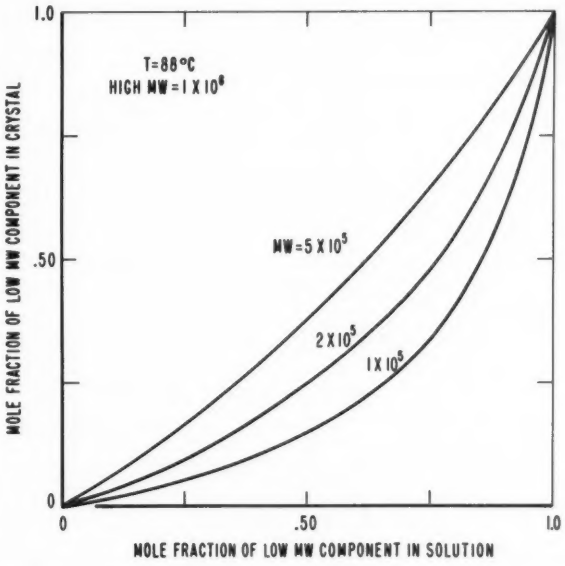


FIGURE 3. *Crystal composition versus polymer solution composition for several binary PEs at a crystallization temperature of 88 °C.*

The high MW component is 1 x $10^6$ in all cases. *(cf. fig. 2).*

From figure 2 one sees that the fractionation process is more efficient the larger the difference in molecular weights, and from figure 3 one sees that the process is less efficient at high molecular weights.

A general feature of all three sets of curves is that the crystal is always of higher average molecular weight than the solution from which it was crystallized. One wonders whether this is always the case. For polyethylene the use of eq (3.1) for the dissolution temperature guarantees that this is so. However, if for some reason a polymer system had dissolution temperatures that were constant or varied weakly with molecular weight, the question would need to be reexamined.

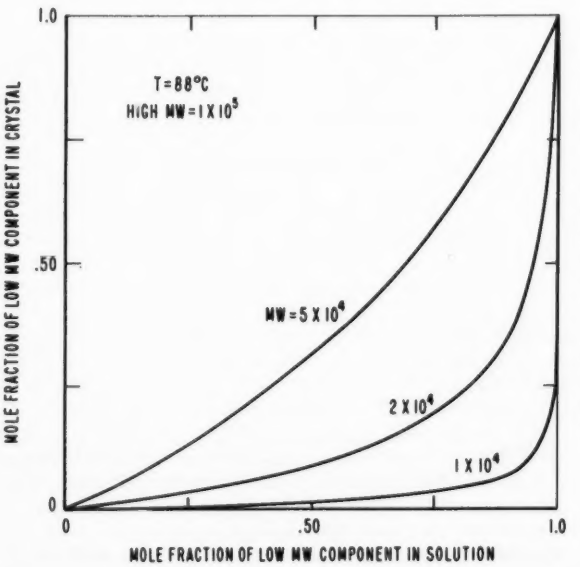


FIGURE 2. *Crystal composition versus polymer solution composition for several binary PEs at a crystallization temperature of 88 °C.*

The high MW component is 1 x $10^5$ in all cases.

#### e. Effects of Secondary Ciliation

Another important aspect of the two component system is that it enables one to check an assumption of the present theory. Secondary ciliation has been ignored in the present theory, i.e., we have assumed that once a molecule begins folding into a growth niche it is not interrupted by another molecule. One can always go to solutions dilute enough so that this situation obtains. A theory exists for a two component system which allows for all degrees of molecular interruption during growth [25]. This theory is complicated because it involves solving a large number of nonlinear simultaneous equations. Solution of these equations for a multicomponent system is very difficult, but a binary system is reasonably amenable to analysis. In the appendix it is shown that the same fractionation is predicted from both theories at small undercoolings which suggests that neglect of secondary ciliation effects is valid also for the multicomponent system.

### 3.3. Multicomponent Systems

#### a. Molecular Weight Distribution

The MW distributions of commercially available linear polyethylenes are usually very broad. Weight average to number average molecular weights ($M_w/M_n$) in the range 5 to 10 are not uncommon and log-normal

distribution functions are often used to characterize these MW distributions [28]:

$$P(\log M)d(\log M) = (2\pi\sigma^2)^{-1/2} \exp\left[-\frac{(\log M - \mu)^2}{2\sigma^2}\right] d(\log M) \quad (3.6)$$

If $\log M$ (common logarithm) follows a normal or Gaussian law, then $M$ is distributed according to a log-normal law:

$$P(M)dM = [P(\log M)/M \ln 10]dM \quad (3.7)$$

with

$$< M > \equiv M_n = 10^{\mu + \sigma^2 \ln 10/2} \quad (3.8)$$

$$< M^2 > / < M >^2 \equiv M_w/M_n = 10^{\sigma^2 \ln 10}. \quad (3.9)$$

A continuous distribution function can often be accurately represented by a discrete distribution function and vice versa. In the present case it was found that a broad normal distribution can be well represented by a discrete distribution containing $k$ points disposed at equal intervals on the $\log M$ scale if $k$ is greater than about 25. A good representation of the continuous distribution means that the calculated $M_n$ and $M_w$ values that are obtained from the discrete distribution are close to the exact values given in eqs (3.8) and (3.9). Each interval $\Delta$ is set equal to $8\sigma/(k-1)$ where $\sigma$ is the mean square deviation of the Gaussian distribution function (3.6). The points or intervals are distributed so that 3/8 of them lie on the low MW side of the mean $\mu$ and 5/8 of them lie on the high MW side of $\mu$. In the calculations presented here $k$ was set equal to 33, i.e., fractionation is being examined in a system containing 33 different MW species of polymer. The mole fraction of species $k$ in solution is equal to $P(M \quad (M_{k+1} - M_{k-1})$ when properly normalized.

#### b. Method of Calculation

The calculation procedure employed for the multicomponent system is similar to that described in section 3.2b for the two component system. The mole fractions of each MW species are now determined by the log-normal distribution as discussed above. The differences in the calculations are briefly outlined below:

(a) The $\lambda$ equation, eq (2.14), is solved numerically by successive iteration beginning with the trial solution

$$\lambda = \Sigma_j A_j^i. \quad (3.10)$$

Usually 4 or 5 iterations, except very near the critical thickness $l_c$, secures convergence with an error of 1 part in $10^4$ or better.

(b) The $f_j$ and other properties are calculated at the maximum value of the nucleation rate rather than averaging over all nucleation rates. The nucleation rate $S_T$, although broad, is unimodal and average properties will not significantly differ from those computed near the maximum value of $S_T$.

#### c. Crystal Composition

Figure 4 is a representative example of the kind of information obtainable from theory. Curve 1 is the distribution in histogram form of the 33 different molecular weight species in solution. On the scale of the graph, 8 of the highest MW species cannot be shown because their mole fraction concentrations are so small. At high undercoolings and in the absence of energetic and diffusional effects the polymer would fractionate according to volume fraction; the volume fractions are shown in curve 2. At a crystallization temperature of 90 °C energetics are important and fractionation is enhanced. Curve 3 is the predicted distribution of MWs for a crystal formed in a solution where the distribution of MWs is given by curve 1 at a crystallization temperature of 90 °C. The $M_n$ and $M_w/M_n$ for the polymer in solution are $1 \times 10^4$ and 9.0, respectively. The $M_n$ and $M_w/M_n$ for the crystal, however, are $1.5 \times 10^5$ and 2.9. Will dissolution of the crystal followed by recrystallization enhance the fractionation even more? The answer is yes, but the enhancement is undramatic. Curve 4 is the result of recrystallizing from a solution where the MW distribution is given by curve 3. The $M_n$ increases to about $3 \times 10^5$, but $M_w/M_n$ remains near 2.9.

Figure 5 summarizes the results of many calculations. The $M_n$ of each MW distribution was fixed at $1 \times 10^4$ and the width of the distribution as measured by the $M_w/M_n$ ratio was allowed to vary. Calculations were carried out at 3 crystallization temperatures to illustrate the effect of temperature on the fractionation. As in the two component system, fractionation is enhanced as the crystallization temperature is raised.

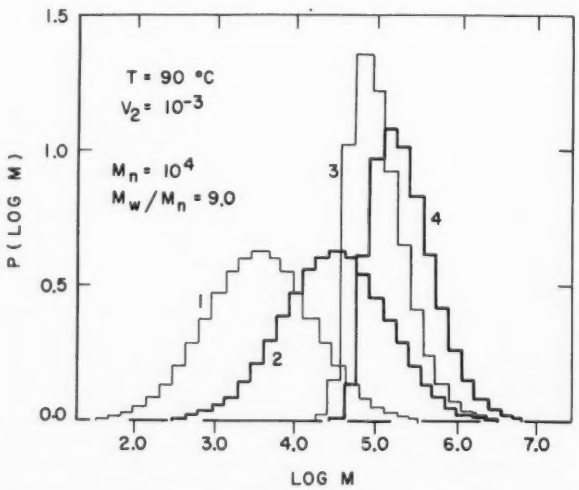


FIGURE 4. *Fractionation histograms for a multicomponent (33) PE.*

Curve 1 is a log-normal distribution of the PE in solution. Curve 2 is the volume fraction distribution of the polymer; in the high undercooling limit the MW distribution of the crystal that is formed would be given by curve 2. Curve 3 is the resulting crystal MW distribution that obtains from curve 1 at a crystallization temperature of 90 °C. Curve 4 is the resulting crystal MW distribution that obtains from curve 3 (recrystallization).

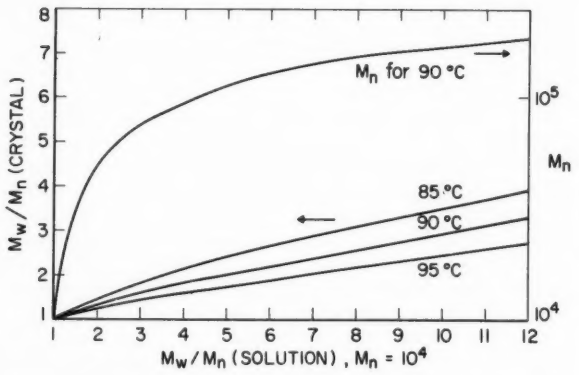


FIGURE 5. *Molecular weight distribution* ($M_w/M_n$) *in the resulting crystal versus MW distribution of polymer in solution.*

The $M_n$ of the polymer in solution is $1\times10^4$ in all cases; the $M_n$ of the crystal resulting from the 90 °C crystallization is also shown.

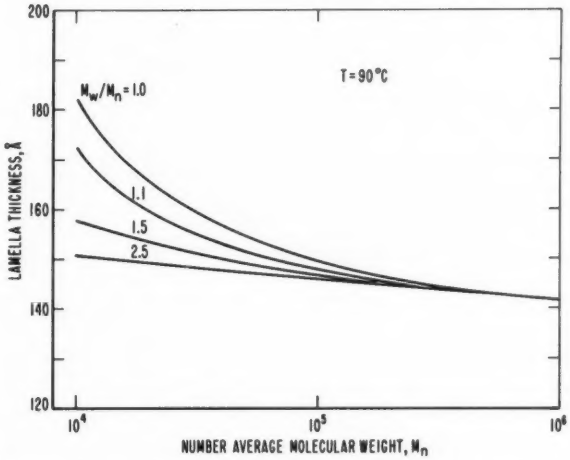


FIGURE 6. *The effects of MW polydispersity on crystal thickness is shown.*

At crystallization temperatures lower then 90 °C the variations in crystal thickness with MW are even smaller.

#### d. Polydispersity Effects

Molecular weight polydispersity can significantly affect crystal properties, especially those properties which should depend on the average MW of the polymer. In paper II we calculated the variation of crystal thickness with MW for monodisperse polymer and found that at a crystallization temperature of 90 °C a variation of crystal thickness of about 40 Å occurs over a MW range of $10^4$ to $10^6$. Smaller variations are predicted for lower crystallization temperatures. Experimental attempts to observe such a variation in crystal thickness have been unsuccessful [29]. In figure 6 we have compared calculated values of lamella thickness at 90 °C for polyethylenes with various degrees of MW polydispersity. A $M_w/M_n$ ratio of 1.5 which corresponds to a relatively good fraction of PE reduces the variation of lamella thickness to about 20 Å. Fractionation during crystallization tends to mask the intrinsic dependence of crystal thickness on MW.

In general, the dependence of any crystal property on MW will be diminished by the effects of polydispersity. This includes the dependence of crystal growth rates on MW. In paper II it was shown that if cilia are the primary nucleating species in polymer crystal growth, then the dependence of crystal growth rates of polymer concentration are relatively weak. Moreover, this concentration dependence should weaken even more and eventually disappear as the MW of the polymer increases. Under normal experimental conditions the MW composition of the polymer in solution is continuously changing with time. Since the high MW components are selectively removed from the solution early in the crystallization, the $M_n$ of the polymer remaining in solution continually decreases. Initially the growth rate may be very weakly dependent or independent of concentration, but in later stages of growth the dependence on concentration should increase. The effect that is measured is an average over the entire range of growth which, of course, could be quite concentration dependent.

It should be noted that a similar type argument cannot be put forth to justify that lamella thickness should increase as the polymer solution becomes depleted in high MW components. If, in fact, the thickness is initially established by high MW species then a persistence of that thickness over the entire range of crystal growth is to be expected. An energetically unfavorable increase in total lateral surface free energy would accompany an increase in crystal thickness (caused by the mismatch of adjacent growth strips), and although there is a favorable increase in bulk free energy associated with the increase in crystal thickness, the unfavorable increase in lateral surface free energy will be larger in the usual range of undercoolings. The net result should be that some persistence of the crystal thickness should obtain. Indeed, if this is true, then Kawai's theory [13, 14] of thickening of polymer crystals is no longer valid.

## 4. Discussion

### 4.1. Conclusions

A nonequilibrium theory of polymer MW fractionation has been formulated and applied to binary and multicomponent PEs crystallized from unstirred xylene solutions. We have treated the case where the composition of the polymer in solution is presumed not to vary during the course of the crystallization. From this theoretical study the following conclusions have been drawn:

(1) high MW components are selectively incorporated into the crystal;

(2) fractionation is inhanced as the crystallization temperature is raised (see figs. 1 and 5);

(3) fractionation is independent of the total polymer concentration $v_2$;

(4) fractionation is relatively insensitive to choices

of the lateral and end surface free energies $\sigma$ and $\sigma_e$;

(5) at high undercoolings the $M_n$ of the crystal will be approximately equal to the $M_w$ of the polymer in solution from which it was formed;

(6) in binary PEs fractionation not only depends on the ratio of the MWs, but also on the absolute magnitudes of the MWs (see figs. 2 and 3);

(7) fractionation tends to mask the intrinsic dependence of crystal thickness on MW (see fig. 6);

(8) fractionation is not determined by the MW species involved in nucleation, it only depends on the rates ($A_1^j$, $B_2^j$) for post-nucleation crystal growth.

The important variables that govern polymer MW fractionation are (1) the pseudo equilibrium dissolution temperatures $T_j^0$, (2) the volume fractions $v_2^j$, (3) the prefactors $1/\sqrt{x_j}$ that arise due to the loss of conformational entropy of a flexible polymer near a crystal-solution interface, (4) the "dilution factor," which is to be discussed below, and (5) diffusion constants which were not explicitly considered in the present study. The variables $T_j^0$ and $v_2^j$ favor the incorporation of high MW components whereas the remaining variables favor incorporation of low MW components.

The pseudo equilibrium dissolution temperature increases with MW because it is a function of the equilibrium melting temperature $T_m^0$ which increases with MW and because the $\chi$ interaction parameter which is a measure of the solubility of the MW species also varies with MW. Thus, at a fixed crystallization temperature those MW components with the highest dissolution temperatures have the greatest energetic driving forces for crystallization. However, there is another energetic effect which favors the incorporation of low MW components which was alluded to in section 3.2d. Incorporation of low MW polymer produces more cilia on the crystal surface; energetically a cilium contributes much less to the surface free energy than a chain fold. Therefore, dilution of the number of chain folds on the crystal surface by cilia, the "dilution factor," is energetically favorable. For PE in xylene the variation of the dissolution temperature with MW is sufficiently strong so that this dilution effect is overwhelmed and high MW species are favored; nonetheless, it seems possible that a polymer solvent might exist where the variation in the dissolution temperature with MW is sufficiently weak so that the dilution effect might dominate.

Although fractionation depends on the volume fraction distribution ($A_1^j \sim v_2^j$ of the MW components in solution (conclusion 5), it does not depend on the total volume fraction $v_2$ of the polymer in solution (conclusion 3). The reason for the latter is that for dilute polymer solutions, dissolution temperatures are only weakly dependent on $v_2$, both theoretically [1] and experimentally [1, 2].

A qualifying note needs to be added to conclusion 8. The fraction of a MW species that is incorporated into the crystal is only a function of the post-nucleation rate constants ($A_1^j$, $B_2^j$) and the thickness of the crystal ($l$). Since a distribution of crystal thicknesses is theoretically possible, a distribution of compositions are also possible and the *average* composition of the crystals formed will depend in a weak and indirect way on the nucleation rates for crystals of various thicknesses (see section 3.2b). This explains why fractionation is only weakly dependent on the value of the lateral surface free energy $\sigma$ (conclusion 4) since it only appears in nucleation rate constants.

Fractionation is also relatively independent of $\sigma_e$, but for different reasons. The value of $\sigma_e$ establishes a lower bound $l_c$ for the range of thermodynamically stable crystal thicknesses. The energetics which govern fractionation do not depend very much on the magnitude of $l_c$ or $l$, but rather on the thermodynamic stability of the crystal as measured by the difference $l - l_c$. Thus, the magnitude of $\sigma_e$ which largely determines $l_c$ does not play an important role in MW fractionation.

### 4.2. Extensions

Mention should be made on how the theory can be extended and improved. The first obvious extension is that nonequilibrium MW fractionation needs to be considered from stirred solutions. The situation is complicated from a theoretical point of view by virtue of the fact that the crystalline morphology is highly complex [30]. Some progress along theoretical lines has been made [2], but much work remains.

A second possible extension is that MW fractionation during crystallization from the melt needs to be considered as well as the effect of pressure on the fractionation phenomena. Although it appears reasonable to ignore diffusional and crystal thickening effects in solution crystallization, they probably play important role in melt crystallization.

In the present study we have assumed that the MW composition of the solution did not vary during the course of the crystallization. This restriction needs to be relaxed and can probably be easily accomplished by use of an adiabatic approximation.

Finally, there is a need to develop a molecular theory which will predict how the $\chi$ interaction parameter varies with MW. Fractionation is very sensitive to the variation of the dissolution temperature with MW and as was mentioned previously, the dissolution temperature depends on $\chi$. The dependence of $\chi$ on MW is probably closely associated with long range intramolecular interactions (excluded volume effects) which implies that developing a theory for $\chi$ may be as difficult as solving the excluded volume problem.

## 5. Appendix: Comparison of Fractionation Effects With or Without Secondary Ciliation

From eq (2.18) and the expressions for ($A_1^j$, $B_2^j$) we obtain for the equilibrium limit ($\lambda \to 0$)

$$f_j = (\alpha_0^1/\beta_1^1)_j (\alpha/\beta)^{v_j - 1} \qquad j = 1, 2 \qquad \text{(A.1)}$$

where $\nu_j$ is the total number of folds for molecules of type $j$. The corresponding equation that obtains when secondary ciliation is allowed is given by eq (123) of reference [25]:

$$f_j = \frac{(\alpha_0^1/\beta_1^1)_j[1-(\alpha/\beta)_j^{\nu_j}]}{1-(\alpha/\beta)_j}. \qquad \text{(A.2)}$$

These expressions reduce to each other in the infinite dilute solution limit. One has $(\alpha_0^1/\beta_1^1)_j \to 0$ and $(\alpha/\beta)_j \gg 1$. In the usual experimental range $(\alpha/\beta)_j > 1$ and the expressions will still be nearly identical for large $\nu_j$, but not necessarily for small $\nu_j$.

The equivalence of eqs (A.1) and (A.2) does not mean that there is no secondary ciliation. It means rather that even the approximate treatment which ignores secondary ciliation gives the correct results for fractionation (and growth rates) even though ciliation may occur.

An estimate of the amount of ciliation can be obtained by realizing (eq 120 of ref. [25]) that for a given MW species, the fraction of it incorporated into the crystal with $k$ and only $k$ folds is proportional to $(\alpha/\beta)^k = B^k$. Thus one obtains for the expected number of folds in a polymer of length $\nu_j$ (maximum of $\nu_j$ folds) the expression

$$<\nu_j> = B\frac{\partial}{\partial B}\ln\left[\Sigma_{k=1}^{\nu_j} B^k\right]$$

$$= \frac{(\nu_j+1)B^{\nu_j+1}}{B^{\nu_j+1}-1} - \frac{B}{B-1}. \qquad \text{(A.3)}$$

In the infinite dilute solution limit $B \gg 1$ and $<\nu_j> \to \nu_j$. In the usual concentration ranges $B > 1$ and $<\nu_j> < \nu_j$.

## 6. References


[1] Pennings, A. J., in Characterization of Macromolecular Structure. Publication No. 1573 of the National Academy of Science. Washington. D.C., 1968. p. 214.
[2] Pennings, A. J., J. Polym. Sci. Part C. **No. 16,** 1799 (1967).
[3] Kawai, T., Matsumoto, T., Kato, M., and Maeda, H., Kolloid Z.Z. Polym. **222,** 1 (1968).
[4] Koningsveld, R., and Pennings, A. J., Recl. Trav. Chim. Pays-Bas **83,** 552 (1964).
[5] Sadler, D. M., J. Polym. Sci. Part A-2, **9,** 779 (1971).
[6] Keith, H. D., and Padden, F. J., Jr., J. Appl. Phys. **34,** 2409 (1963).
[7] Keith, H. D., and Padden, F. J., J. Appl. Phys. **35,** 1270 (1964).
[8] Anderson, F. R., J. Appl. Phys. **35,** 64 (1964).
[9] Kawai, T., Makromol. Chem. **84,** 294 (1965).
[10] Prime, R. B., and Wunderlich, B., J. Polym. Sci. A-2, **7,** 2061 (1969).
[11] Prime, R. B., and Wunderlich, B., J. Polym. Sci. A-2, **7,** 2073 (1969).
[12] Rees, D. V., and Bassett, D. C., J. Polym. Sci. A-2, **9,** 385 (1971).
[13] Kawai, T., Makromol. Chem. **84,** 290 (1965).
[14] Kawai, T., Kolloid Z.Z. Polym. **229,** 116 (1969).
[15] Kawai, T., J. Polym. Sci. B **3,** 83 (1965).
[16] Kawai, T., Makromol. Chem. **102,** 125 (1967).
[17] Sanchez, I. C., and DiMarzio, E. A., J. Chem. Phys. **55,** 893 (1971).
[18] Sanchez, I. C., and DiMarzio, E. A., Macromolecules **4,** 677 (1971).
[19] Keller, A., Phil. Mag. **2,** 1171 (1957).
[20] Keller A., Rept. Progr. Phys. **31,** 623 (1968).
[21] Lindenmeyer, P. H., J. Polym. Sci. C **1,** 5 (1963).
[22] Blundell, D. J., and Keller, A., J. Polym. Sci. B **6,** 433 (1968).
[23] Hillig, W. B., Acta Met. **14,** 1868 (1966).
[24] Lauritzen, J. I., Jr., DiMarzio, E. A., and Passaglia, E., J. Chem. Phys. **45,** 4444 (1966).
[25] DiMarzio, E. A., J. Chem. Phys. **47,** 3451 (1967).
[26] Mullins, W. W., Phys. Rev. **114,** 389 (1959).
[27] Flory, P. J., Principles of Polymer Chemistry (Cornell Univ. Press. Ithaca. N.Y., 1953). p. 513.
[28] Blundell, D. J., and Keller, A., J. Macromol. Sci. Phys. **2,** 337 (1968).
[29] Bair, H. E., and Salovey, R., J. Macromol. Sci. Phys. **3,** 3 (1969).
[30] Pennings, A. J., Van der Mark, J. M. A. A., and Kiel, A. M., Kolloid Z. Z. Kolloid Polym. **237,** 336 (1970).


(Paper 76A3-718)

JOURNAL OF RESEARCH of the National Bureau of Standards—A. Physics and Chemistry
Vol. 76A, No. 3, May–June 1972

# The Formation of Curved Polymer Crystals: Poly(4-methylpentene-1)

**F. Khoury and J. D. Barnes**

**Institute for Materials Research, National Bureau of Standards, Washington, D.C. 20234**

(February 4, 1972)

An optical and electron microscopical study is described of the habits exhibited by poly(4-methylpentent-1) crystals (Modification I tetragonal unit cell) grown at temperatures between 50 and 90 °C from 0.1 percent solutions of the polymer in equivolume mixtures of xylene and amyl acetate. A distinct trend in the effect of crystallization temperature (supercooling) on the habits of the crystals is illustrated and discussed. The lamellar crystals formed in that temperature range are all the more pronouncedly curved the lower the crystallization temperature. To indicate but the extremes in this trend, the crystals varied from essentially planar ones whose constitutent square shaped chain-folded lamellae (bounded laterally by {100} faces and up to 20 $\mu$m on a side) are four-sectored and only very slightly buckled as previously indicated by Bassett et al., to distinctly curved four-fold symmetrical hollow bowl shaped ones having a radius of curvature of about 2.5 $\mu$m and in which the surface of the curved multilayered wall of which they are constituted changes in orientation through 180° from the base (pole) to the periphery. In contrast with the four-sectored character of the lamellae in the aforementioned essentially planar crystals, the constituent lamellae in all the distinctly dished and bowl-like crystals formed in the temperature range 50 to 90 °C are multisectored, their lateral development being characterized by the formation at their periphery during growth of successive arrays of {100} microfaceted sectored outgrowths. The reasons why the lamellar crystals of poly (4-methylpentene-1) are all the more pronouncedly curved the lower the crystallization temperature are explored and discussed. Conjectures concerning the origins of this phenomena are advanced in the form of a working 'model.'

Key words: Chain-folded; crystal, curved; electron microscopy; lamellar; optical microscopy; poly-(4-methylpentene-1); polymer; solution-grown.

## 1. Introduction

Investigations of the crystal habits exhibited by poly(4-methylpentene-1) (P4MP), polychlorotrifluoroethylene, and polyoxymethylene when these polymers are crystallized from dilute solutions have led us to the observation that, broadly speaking, whereas at high crystallization temperatures the solutions yield lamellar crystals which are planar or nearly planar in character, at lower crystallization temperatures multilayered lamellar crystals are formed which exhibit distinctly curved shapes and which are all the more pronouncedly curved, i.e., they have a smaller radius of curvature, the lower the crystallization temperature [1].[1] Indeed, at high supercoolings the polymer solutions yield hollow bowl-shaped crystals. This paper, which consists of two parts, concerns the formation of curved crystals of P4MP. First, a description will be presented of the formation, habits, and fine structural characteristics of curved crystals of P4MP grown from 0.1 percent solutions of the polymer in equi-volume mixtures of xylene and amyl acetate at temperatures between 90 and 50 °C. Second, considerations based on the observations derived from this study regarding the origins of the curved habits exhibited by these crystals and why they are all the more pronouncedly curved the lower the crystallization temperature will be advanced and discussed.

As background to the study of P4MP reported herein, previously published investigations on the structure and crystallization habits of this polymer are summarized below.

The crystal structure of P4MP was reported several years ago by Frank, Keller and O'Connor [2] who determined, on the basis of an x-ray and electron diffraction study of solution grown crystals of P4MP which had been formed by slowly cooling hot polymer solutions to room temperature, that the unit cell is tetragonal, the cell parameters being $a = b = 18.66$ Å, $c = 13.80$ Å. Four chains, each in a 7/2 helical conformation, pass through the unit cell which contains twenty-eight monomer units. The axes of the helices are parallel

[1] Figures in brackets indicate the literature references at the end of this paper.

to the $c$ axis of the cell. According to Frank et al. [2], and later Bassi et al. [3], the space group is probably P4̄. This unit cell structure which is that most commonly exhibited by crystalline P4MP has since been referred to as Modification I in view of subsequent reports of the existence of two other less stable crystalline modifications of P4MP [4–8]. The habits of P4MP crystals grown from solution were first described by Frank, Keller, and O'Connor [2]. These were crystals from the same preparations used in the determination of the unit cell structure of P4MP (Mod I) mentioned above. The simplest crystals observed by Frank et al. [2] were thin square-shaped lamellae of P4MP which are bounded laterally by {100} faces at which growth occurs through the accretion of the chain molecules along correspondingly parallel {200} planes. These lamellae are composed of four sectors (fold domains)[2] which are distinguished by the {200} planes along which the molecules are folded as shown schematically in figure 1. Electron diffraction patterns obtained from these crystals indicated that the chain molecules are oriented normal to the plane of these seemingly flat lamellae. Bassett [9] and Bassett et al. [10] have more recently reported that the otherwise ideally tetragonal unit cell is slightly distorted in the constituent sectors of such four-sectored lamellae. Evidence of the distortion of the unit cell was derived from an analysis of Moiré patterns exhibited in the electron microscope by bilayered crystals (in which each of the two superimposed chain-folded lamellae or layers is four-sectored) which indicated that the spacing of the {200} planes in each of the four constituent sectors in individual layers differs by $\sim 0.1$ percent according to whether or not they are fold planes [9]. This asymmetric distortion of the unit cell in each sector has been attributed to the bulkiness of the chain folds. Furthermore, the dark field {200} diffraction contrast characteristics exhibited by these bilayered crystals in the electron microscope indicated that their constituent lamellae, as grown, are not perfectly planar but suggested instead that they possess a very slight "conicalness" [9, 10]. According to Bassett et al. [9, 10], this latter feature (which escapes detection under the optical microscope [10]), is associated with the distortion of the unit cell in the constituent sectors of the chain-folded lamellae. On the basis of the magnitude of the unit cell distortion and assuming to a first approximation that the lamellae are conical, their angle of inclination was estimated to be $\sim 2°$.

In addition to the simple four-sectored lamellae referred to above, Frank et al. [2] observed in the same preparations numerous tetragonal crystals (all of Modification I) which exhibited under the electron microscope ample evidence of having undergone substantial pleating and folding over when they sedimented upon the carbon substrate. Indeed, the majority of the crystals in their preparations exhibited such features. In many instances the corners of the basal

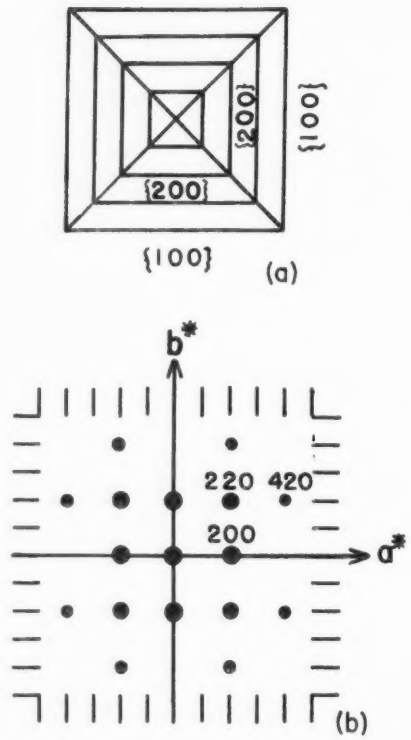


FIGURE 1. *(a) Schematic representation of a four-sectored chain-folded lamella of P4MP bounded laterally by {100} faces. The chain molecules are folded along {200} planes which are parallel to these faces. (b) $a^*b^*(a^*=b^*)$ plane of the reciprocal lattice of the modification 1 unit cell of P4MP. The strongest spots observed in diffraction patterns obtained from lamellar crystals of this modification with the electron beam perpendicular to the lamellae are indicated. They are the reflections from the {200}, {220}, and {420} sets of planes.*

lamella were observed to have folded over onto the interior of the crystal. Similar crystals have been observed by Woodward [11] who suggested that such crystals are hollow pyramidal in character, having steep sides and "deformed square bases." Further insight into the growth habits and fine structures of crystals of P4MP which exhibit evident collapse features such as those mentioned above when they sediment upon a flat substrate is provided by the combined optical and electron microscope investigation reported herein of the crystallization of P4MP.

## 2. Experimental Details

### 2.1. Materials and Preparative Methods

Poly(4-methylpentene-1) in powder form and having an intrinsic viscosity $\eta = 4.6$ dl/g [12] was used throughout this study. According to Hoffman, Fries and Condit [13] the relationship between $\eta$ and the number average molecular weight ($M_n$) of P4MP is

$$\eta = 1.94 \times 10^{-4} (M_n)^{0.81}$$

[2] The terms sector and fold-domain will be used synonymously throughout this paper.

which gives $M_n = 252{,}000$ for the above polymer.

The poly(4-methylpentene-1) was crystallized from solution in equivolume mixtures of xylene (good solvent) and amyl acetate (poor solvent). Both solvents were distilled independently prior to use. Solutions with a concentration of 0.1 percent (*w/v*) of the polymer in the mixed solvent system (50 ml) were prepared by heating appropriate quantities of P4MP mixed with solvent at 140 °C for half an hour. The resulting solutions were then transferred to baths held isothermally, within ± 0.1 °C, at temperatures in the range 50 and 90 °C (i.e., 50, 70, 80, and 90 °C) for from 1 to 3 days, during which periods the polymer crystallized in the form of crystals in suspension in solvent. In order to prevent further crystallization of polymer still in solution when the preparations are finally cooled from the crystallization temperature to room temperature, the mother liquor was in all instances isothermally exchanged, prior to cooling, with fresh equivolume mixtures of xylene and amyl acetate preheated to the temperature of each preparation. The following procedure was followed in each instance: Each preparation was rapidly transferred from the crystallization bath and poured into an isothermally controlled filtration vessel maintained at a temperature corresponding to that of the crystallization bath. The type of filtration vessel used was essentially similar in design to a filtering apparatus previously described by Bassett et al. [14]. Uncrystallized polymer was eliminated by alternate filtration and addition of fresh preheated (to the temperature of the preparation) solvent mixture to the suspension of crystals, care being taken to ensure that the crystals were continuously immersed in liquid and not allowed to dry between successive additions of fresh solvent mixture to the suspension. Two to three exchanges of the solvent medium were carried out in each instance. After a final addition of a fresh preheated solvent mixture to the suspension of crystals, the filtration vessel containing the latter suspension was allowed to cool to room temperature.

In a few experiments which will be mentioned later in the paper (sec. 3.5) a self-nucleating procedure analogous in principle to that used by Blundell, Keller and Kovacs [15] in the case of polyethylene was adopted to crystallize P4MP from 0.1 percent solutions of the polymer in equivolume mixtures of xylene and amyl acetate. The thermal histories of the self-nucleated solutions were as follows: 140 °C (1/2 hr) → 70 °C (1 hr) → 130 °C (1/2 hr) → T °C, where T °C = 50 °C and 90 °C were the chosen crystallization temperatures after redissolving at 130 °C. Following crystallization at T °C the preparations were subjected to isothermal filtering and washing in the manner described above.

## 2.2. Microscopy

### a. General

Both optical and the electron microscopy were necessary in order fully to characterize the shapes as well as the fine structural details of the curved crystals discussed in ensuing sections. These crystals collapse and flatten very readily when they are sedimented and allowed to dry on a flat carbon substrate as required for electron-microscopic observations. Although some information regarding the as-grown shapes of the crystals could be derived from the nature of the collapse features they exhibit under the electron microscope, detailed characterization of their as-grown shapes could only be derived by observing them under the optical microscope while in suspension in liquid.

### b. Optical Microscopy

The as-grown shapes of the crystals were determined by examining them as they tumbled or were induced to tumble slowly while in suspension in solvent at room temperature under a microscope using phase contrast optics. Glass slides having a shallow central well in which droplets containing crystals in suspension were deposited and subsequently covered with a thin coverglass were used for this purpose. Examination of the crystals was facilitated by diluting the solvent medium with a liquid having a refractive index sufficiently different from that of the crystals which is ~ 1.46 in order to enhance contrast. Dilution with a Cargille[3] liquid of refractive index 1.70, which did not affect the crystals, was found most convenient particularly for recording and exhibiting the salient features of the crystals photographically.

### c. Electron Microscopy

For transmission electron microscopy, droplets of each preparation containing crystals in suspension were deposited on electron microscope grids covered with a film of carbon. The solvents were allowed to evaporate at room temperature, after which the dried crystals were shadowed in vacuo with a platinum-palladium alloy (80% Pt/20% Pd). In instances in which crystals were too thick to allow their fine structure to be observed in transmission (e.g., see sec. 3.4) shadow transfer replicas of the crystals were prepared. In such instances drops of the preparation containing crystals in suspension were deposited on a microscope slide; the crystals were allowed to dry at room temperature, after which they were shadowed with metal (Pt/Pd). A backing layer of carbon was then evaporated onto the shadowed crystals. The composite carbon-metal "film" was then floated off the slide on distilled water. The crystals were found to adhere to the "film," portions of which were picked up on electron microscope grids and allowed to dry in air. The crystals were then dissolved by immersing the grids supporting the replicas in xylene for two hours at 139 to 140 °C.

The electron microscope used in most of this study was a JEM 6a[3] which was operated at 80 kV using the double condenser system.

[3] Trade name used only for the purpose of identification and in no way implies endorsement or recommendation by NBS.

## 3. Observations on the Morphologies of Poly(4-methylpentene-1) Crystals

### 3.1. General

A description is presented in succeeding subsections (3.2–3.4) of the morphologies exhibited by P4MP crystals which are formed when 0.1 percent solutions of the polymer initially maintained at 140 °C are subsequently transferred to baths held at temperatures between and including 90 and 50 °C within which range crystallization occurs. In anticipation of what follows it may be noted at this stage that electron diffraction patterns obtained from selected areas of individual crystals formed within that range of temperatures as well as x-ray powder patterns obtained from samples from each preparation were consistent with the Modification I tetragonal unit cell structure proposed by Frank et al. [2]. A typical x-ray powder pattern is shown in figure 2 in which the 200; the 220; the composite 311, 212; the 321; the 411; and the composite 331, 420, 322, 203; rings may be discerned. The corresponding measured spacings are $9.3_1$, $6.6_0$, $5.2_9$, $4.8_3$, $4.3_0$, $4.1_4$ Å. This particular pattern was obtained from a sample of crystals from a 50 °C preparation.

### 3.2. Crystals Formed at 90 °C

The onset of faint cloudiness in the solutions, indicating the occurrence of crystallization, was observed 30 to 40 min after transfer to the 90 °C bath. The developing crystals are initially well dispersed in the mother liquor which exhibits uniform cloudiness. In time, however, they tended to agglomerate in random clusters consisting of several crystals which tended to adhere to one another due to some intergrowing which occurs between vicinal crystals within each cluster.

A mixed population of lamellar cystals differing in both size and shape are formed at this temperature. Interestingly a correlation was observed between the relative sizes of the crystals and their respective habits and fine structures. Before proceeding with more detailed descriptions of the morphological characteristics of the various crystals, it may be pointed out from the outset that whereas the smaller crystals among the entire population were essentially planar in character, the larger crystals had detectably curved overall shapes which, however, as will be seen later, were less pronouncedly curved than crystals formed at lower temperatures.

The smaller crystals formed at 90 °C were mono- or multilayered, their habit being identical to that of the simplest very nearly planar four-sectored chain-folded lamellae previously observed by other workers [2, 8–11]. An example of such a crystal is shown in figure 3. The morphological characteristics of this species of crystal as seen under the optical and electron microscopes bear to be recapitulated here since they provide a useful basis of reference with respect to which the morphologies of the larger and more complex crystals formed at 90 °C, as well as the crystals formed at lower temperatures, may be compared. The constituent lamellae in these smaller crystals are square-shaped and are bounded laterally by {100} faces. Furthermore superimposed layers frequently develop in a spiral-like fashion through the agency of screw dislocations in the basal lamella, as may be seen in figure 3. The essentially planar character of these crystals is readily revealed when they are viewed edge-on while in suspension in liquid under the optical microscope using phase contrast. An edge-on perspective of such a crystal is shown in figure 4 in which it may be seen to exhibit an essentially linear profile. It is not possible unequivocally to resolve under the optical microscope the very slight "conicalness" which it has been suggested [9, 10] these crystals possess. Nevertheless, morphological evidence which is consistent with Bassett et al.'s [9, 10] interpretation of dark field electron images which indicate that these crystals are

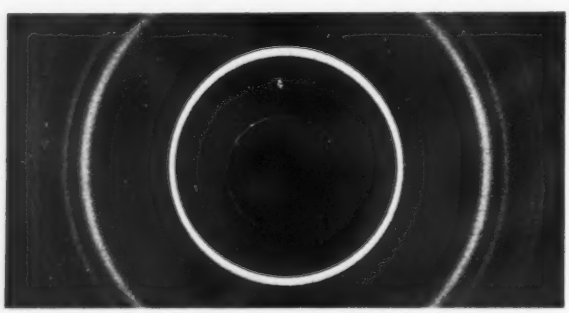

FIGURE 2. *A modification I x-ray pattern typical of those obtained with a powder camera from samples of crystals formed at temperatures between 90 and 50 °C.*

This particular pattern was obtained from a sample of crystals from a 50 °C preparation. Proceeding from the center outwards the rings which may be readily discerned are the 200; the 220; the composite 311, 212; the 321; the 411; and the composite 331, 420, 322, 203.

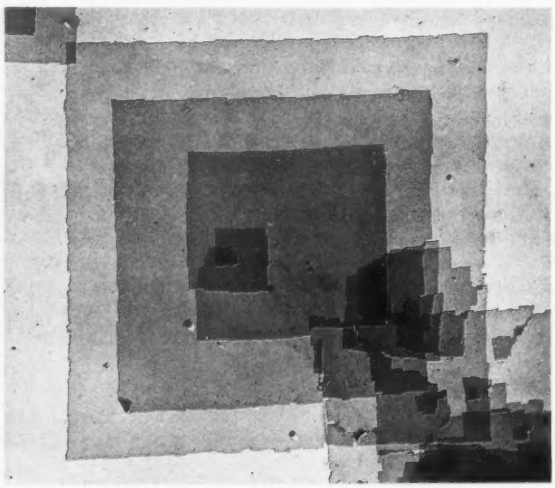

FIGURE 3. *Electron micrograph showing an example of one of the smaller essentially planar lamellar crystals of P4MP formed at 90 °C, Pt/Pd shadowed, × 3500.*

FIGURE 4. *Edge-on view under the optical microscope of one of the smaller essentially planar (compare with subsequent optical micrographs) lamellar crystals of P4MP formed at 90 °C. The crystal (center of micrograph) is in suspension in liquid. Phase contrast,* × *1300.*

not perfectly planar and that they collapse on drying on a substrate is provided by an examination of shadowed crystals under the electron microscope. Shadowing characteristically reveals faintly discernible ridges which may be traced along the diagonals of each square-shaped lamella as may be seen in figure 5. These ridges correspond to the boundaries between the four constituent sectors or fold domains in each lamella. Figure 5a represents a region near the bottom left-hand corner of the basal lamella in the crystal shown in figure 3 viewed at higher magnification. Figure 5b represents a region further upfield in the same crystal where three lamellae overlap and the three arrows point to the sector delineating ridge in each lamella. Such sector delineating ridges which have been previously observed by Woodward [11] suggest that the lamellae undergo slight localized pleating at the sector boundaries as the crystals collapse upon the substrate. For the purpose of later comparison (e.g., see figs. 9–10 onwards) the essentially smooth character of the edges of the lamellae in this crystal may also be noted in figure 5.

It has been pointed out above that the crystals formed at 90 °C tended to cluster and intergrow while in suspension in the solvent at the crystallization temperature. The species of crystals described in the previous paragraph, which represent the smaller fraction of the total crystal population, were generally observed to be situated at the periphery of clusters consisting of other larger and more complex crystals. This latter observation coupled with the fact that they are the smallest among the entire population of crys-

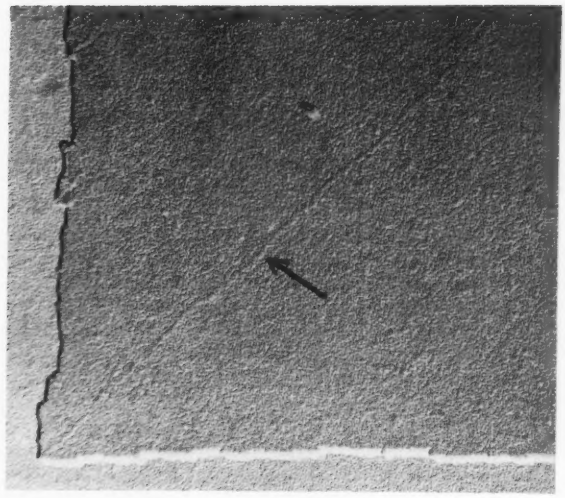

(a)

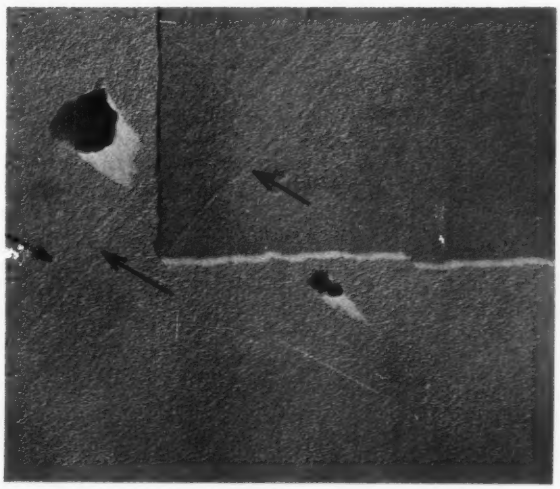

(b)

FIGURE 5. *(a) A view at high magnification of the bottom left hand corner of the basal lamella in the crystal shown in figure 3. The arrow points to a faint ridge which runs from the corner of the lamella inwards along a path corresponding to the diagonal. Pt/Pd shadowed* × *32000. (b) A region further upfield along the same diagonal direction in the crystal. The arrows point to the diagonal ridges in the three superimposed lamellae situated in that region. Pt/Pd shadowed,* × *29,000.*

tals, their edges being about 20 $\mu$m or less in length, indicates that they developed during the more advanced stages of the depletion of polymer from solution.

We turn now to a consideration of the morphological characteristics of the larger and more complex crystals formed at 90 °C. These larger crystals are multilayered, the sides of their basal lamella being up to 45 $\mu$m or so long; furthermore, these crystals are distinctly curved. This latter feature is readily perceived when they are

examined edge-on while in suspension in liquid. When viewed in this latter perspective they characteristically exhibit a crescent-like profile, as shown in figure 6 in which such crystals oriented edge-on with respect to the field of view may be seen. It should also be pointed out that some large multilayered crystals were observed which consisted of two families of lamellae which were curved in opposite directions.

An example of a large curved crystal as observed in the electron microscope at low magnification is shown in figure 7 in which its multilayered character may be clearly seen (notwithstanding the fact that there is another overlapping crystal in the upper left hand part of the micrograph). In addition, the incidence of appreciable pleating which results from the collapse of these nonplanar crystals when they sediment upon the substrate may be seen in figure 7.

An electron diffraction pattern which was obtained from a crystal similar to those in figures 6 and 7 is shown in figure 8a, and the corresponding selected area near the periphery of the crystal is shown in figure 8b (note the pleats). The diffraction pattern in figure 8a corresponds to the zero layer (i.e., the $a^*b^*$ plane where $a^* = b^*$ in P4MP) of the reciprocal lattice net of P4MP, the innermost and most intense spots being 200 and the next most intense are 220 and 420 in accordance with Frank et al. [2]. It is evident from the disposition of the 200 reflections along directions normal to the edges of the lamellae that the chain folded layers in these larger crystals are also bound laterally by {100} growth faces as is the case in the smaller crystals discussed in previous paragraphs. However, examination under the electron microscope of the periphery of the curved lamellae in these crystals reveals a profusion of pronounced step-like reentrances. This feature may be readily seen in figures 9 and 10 depicting portions along the sides of the basal lamella in two such crystals in which well developed orthogonally reentrant facets are evident. This is in contrast with the relatively smooth character of the lateral edges of the smaller four-sectored crystals (figs. 5a, 5b). In short the {100} sides of

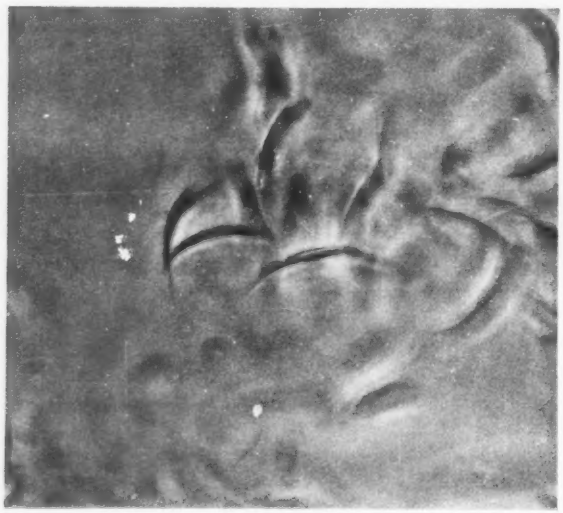

FIGURE 6. *Edge-on view under the optical microscope of some larger species of crystals (center of micrograph) formed at 90 °C.*

The crystals are in suspension in liquid and exhibit a crescent-like profile when viewed in this orientation. Phase contrast, × 490.

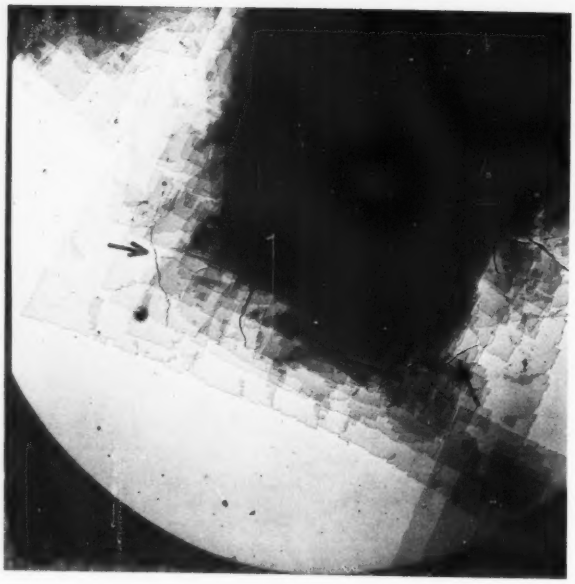

FIGURE 7. *Electron micrograph showing an example of the larger perceptibly curved crystals of P4MP formed at 90 °C.*

Arrows point to pleats resulting from the collapse of these crystals upon sedimentation and drying on the substrate. Pt/Pd shadowed, × 1700.

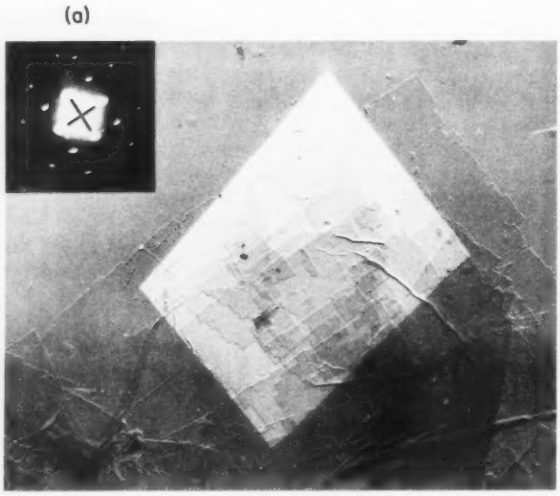


FIGURE 8. *(a) Inset. Electron diffraction pattern obtained from a region of one of the larger perceptibly curved crystals of P4MP formed at 90 °C. The arms of the cross drawn in the center of the pattern point to the 200 spots. (b) Selected area from which the diffraction pattern was obtained. Gold shadowed, × 4000.*

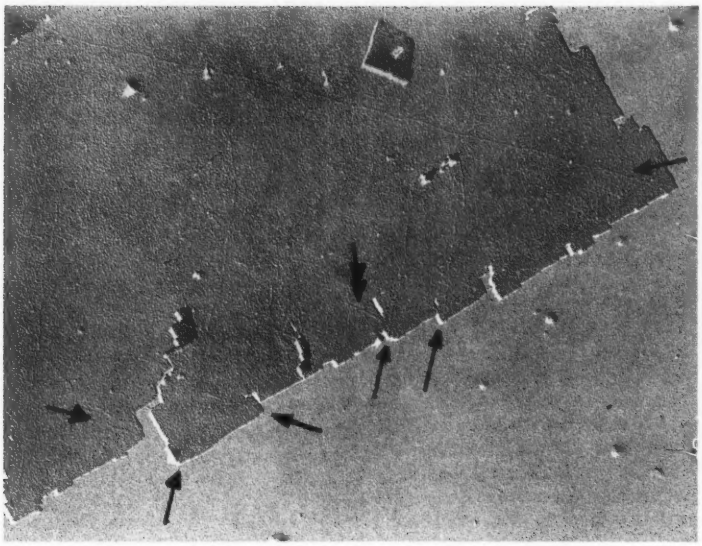

FIGURE 9. *Electron micrograph of a portion of the periphery of the basal lamella in one of the larger perceptibly curved crystals of P4MP formed at 90 °C showing well developed reentrant {100} microfacets and faint sector delineating ridges which can be traced from leading microcorners inwards along paths often at ~ 45° to the sides of the lamella. Unbarbed arrows point to some of these ridges. Barbed arrow points to a ridge deviating appreciably from 45° orientation. Pt/Pd shadowed, × 12,500.*

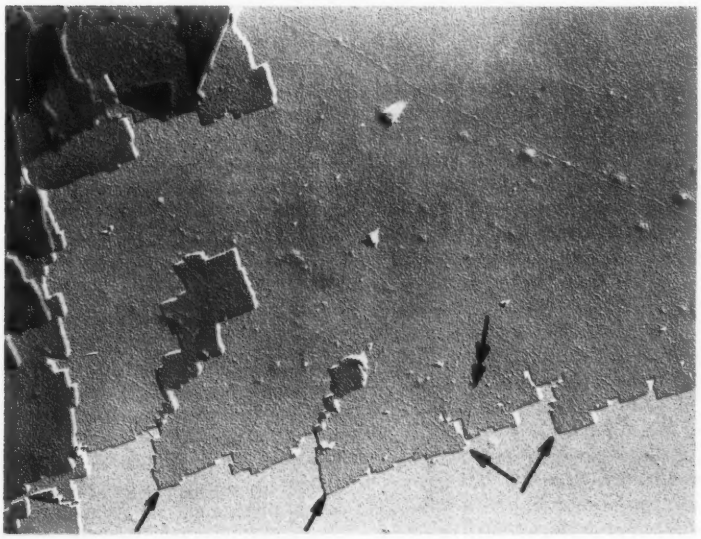

FIGURE 10. *Electron micrograph of a portion of the periphery the basal lamella in another of the larger perceptibly curved crystals of P4MP formed at 90 °C showing well developed reentrant {100} microfacets and faint sector delineating ridges which can be traced from leading microcorners inwards along paths at ~ 45° to the side of the lamella. Unbarbed arrows point to some such ridges. Barbed arrow points to a sector delineating ridge whose orientation deviates appreciably from the 45° angle. Pt/Pd shadowed, × 12,500.*

the lamellae in the larger crystals are distinctly microfaceted: the microfacets are {100}. The existence of well developed reentrant {100} microfacets suggests in itself that the lamellae in these crystals are multisectored, i.e., that they consist of a mosaic of fold domains, neighboring domains being subtended at the edges of the lamellae during the process of growth by adjacent {100} microfacets which are orthogonal to one another and along both of which chain-folding occurs. The multisectored (as distinct from four-sectored) character of the lamellae in these larger curved crystals is further substantiated by the fact that when they are shadowed with metal and examined under the electron microscope, a network of faintly discernible domain delineating ridges is revealed on their upper surface. Such ridges are pointed to in figures 9–10. These ridges can usually be traced from leading microcorners, formed by adjacent {100} microfacets at the periphery of the lamellae, inwards often along paths oriented at ~ 45° to the sides of the lamellae, although this angle does vary from 45° (barbed arrows in figure 9 and figure 10 point to such cases) as a result of situations which arise at the periphery where new chain folded planes are formed more rapidly along a {100} microfacet facing the surrounding medium than along an adjacent reentrant {100} microfacet. As has been advanced earlier in the case of four-sectored lamellae, these ridges presumably result from the occurrence of slight localized pleating along the fold domain boundaries when the lamellae collapse on drying in addition to the much more pronounced pleating and overfolding which these larger curve lamellae undergo as pointed out earlier with reference to figure 7.

We shall in due course consider further the nature of the as-grown character of the larger curved crystals formed at 90 °C in the light of observations derived from crystals grown at lower temperatures. This will be done in section 4 in which inter alia the matter of the differences between the larger and smaller crystals formed at 90 °C will also be broached. It will suffice at this stage to point out that the observations derived from the combination of optical and electron microscopic observations on the population of crystals formed at 90 °C which are described above are suggestive in themselves of a phenomenological correlation between the fine (domain) structure and the as-grown conformation of the constituent lamellae in the crystals. It is of interest to note that the lamellae in the larger crystals are multisectored and that these lamellae are perceptibly curved, whereas the smaller crystals whose constituent lamellae are four-sectored are essentially planar and correspondingly they do not exhibit any pronounced collapse features upon sedimentation as is the case with the larger curved crystals. As will be seen in subsequent subsections, crystallization at lower temperatures leads exclusively to the formation of crystals whose constituent lamellae are multisectored as well as curved.

Finally it may be noted that the thickness of the lamellae in the crystals formed at 90 °C as determined from a low angle x-ray diffraction pattern obtained from a mat of such crystals (using a Rigaku-Denki low angle camera with pinhole collimation) with the plane of the mat parallel to the x-ray beam was found to be 139 Å.

### 3.3. Crystals Formed from Solutions Cooled at 80 °C

Crystallization occurs rapidly when solutions initially held at 140 °C are transferred to a bath at 80 °C. The lapse of time corresponding to the onset of cloudiness coincides closely to the time taken (~ 10 min) by the solution to cool from 140 to 80 °C. Under these conditions an essentially uniform population of lamellar crystals is yielded. Considerably less *in situ* clustering of the crystals occurred in these preparations than was the case at 90 °C. When they are viewed edge-on under the optical microscope, while they are in suspension in liquid, the crystals exhibit crescent-like profiles as shown in figure 11, in short, these crystals are curved. A representative crystal in suspension in liquid is also shown in figure 12, in which it is depicted as seen in two different perspectives. Figure 12a represents the crystal as viewed edge-on; its crescent shaped profile may be readily discerned. In figure 12b the same crystal is shown after it had rotated through 90° about an axis oriented at ~ 30° with respect to the vertical in the field of view (see arrow). In this latter perspective, in which the crystal is viewed along a direction very nearly parallel to its central axis, it may be seen to exhibit an essentially square-shaped peripheral profile which is, however, rounded at the corners. Furthermore, it can be noted that the crystal also exhibits more pronounced contrast or scatter of light in the vicinity of its apparently rounded corners than is evident elsewhere along its periphery. These two features are characteristic of all the crystals formed at 80 °C when they are viewed along their central axis. They bear revealingly on the nature of the as-grown curved shape of these crystals. In order to discuss their significance in this respect more comprehensibly however, it is necessary first to consider the morphology of the crystals as observed under the electron microscope.

Electron micrographs of two representative crystals formed on cooling the polymer solutions to 80 °C are shown in figures 13–14. As may be seen in these two figures the crystals formed under these conditions are characteristically multilayered, the sides of their basal lamella being about 20 $\mu$m to 25 $\mu$m. A selected area electron diffraction pattern obtained from a portion of such a crystal is shown in figure 15a, the corresponding selected region in the crystal is shown in figure 15b. The disposition in electron diffraction patterns obtained from such crystals of the 200 reflections relative to the crystals clearly indicates that the lamellae are bounded laterally by {100} growth 'faces'; however, as is the case in the larger curved crystals formed at 90 °C, these faces are pronouncedly microfaceted as may be discerned in figures 13–14, and in more detail at higher magnification in figure 16 in which pronounced reentrant steps are evident at the edges of the basal lamella in such a crystal; in short the microfacets are {100}. In addition, shadowing the crystals

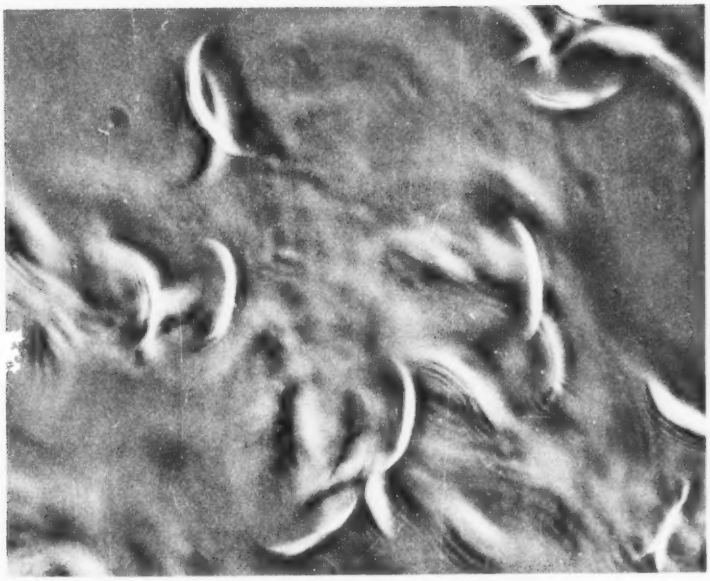

FIGURE 11. *Several P4MP crystals formed at 80 °C viewed edge-on in suspension in liquid under the optical microscope.*

Note their crescent-like profiles. Phase contrast, ×900.

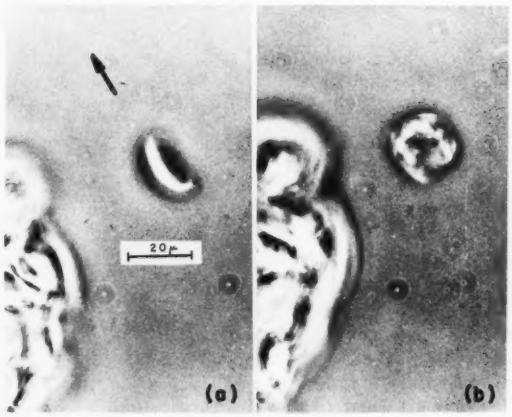


FIGURE 12. *Two views under the optical microscope of a P4MP crystal formed at 80 °C. The crystal is in suspension in liquid. (a) Edge-on view of crystal. (b) The same crystal after it had rotated through ~90° about an axis (arrow) oriented at ~30° with respect to the vertical in the field of view.*

Phase contrast, ×450.

with metal reveals, as was the case in the large curved crystals formed at 90 °C, faintly discernible ridges at the surface of the lamellae. Although some such ridges can be traced from leading corners formed by adjacent {100} microfacets at the periphery of the lamellae, inwards along paths at 45° to the lamella edges, they are very often discontinuous, badly defined and cannot be traced to a particular peripheral corner, in addition to the fact that they often deviate from the 45° orientation relative to the sides of the lamellae (some more evident ridges are pointed out in figure 16). There is no question however from the distinctly microfaceted character of the periphery of the lamellae in these crystals that their constituent curved lamellae are multisectored.

These curved crystals undergo deformations of a pronounced character when they collapse upon drying on a substrate. Thus, cracks are frequently observed in the peripheral regions of the basal lamella in collapsed crystals, as may be seen in figures 13–14. These cracks generally extend from the periphery inwards roughly at right angles to the sides of the basal lamella; furthermore, as would be expected from this manner of deformation which involves "cleaving" across some



459-033 OL - 72 - 4

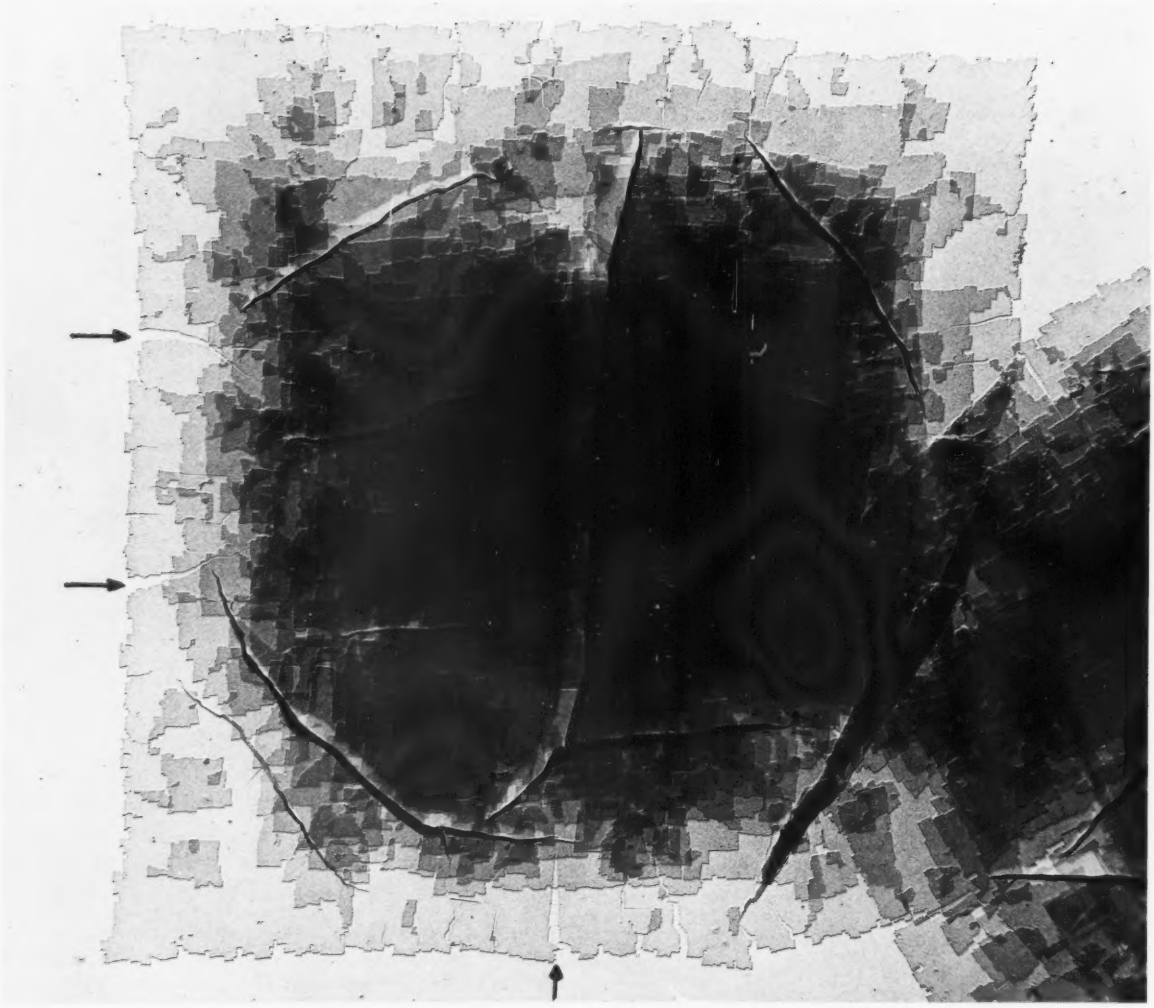

FIGURE 13. *Electron micrograph of a typical P4MP crystal formed at 80 °C.*

Arrows point to cracks incurred in the basal lamella upon sedimentation and drying on the substrate. It can also be seen that the crystal has undergone pronounced pleating and buckling upon sedimentation. Pt/Pd shadowed, × 5900.

fold-domains in the lamella in which the chain molecules are folded along planes at right angles to the cleavage direction, the cracks are characteristically traversed by fine fibrils which extend between the adjoining undeformed portions of the lamella. This latter feature is readily discernible at high magnifications as shown in figure 17. The cracks and associated fibrillation which occur upon sedimentation in the evidently non-planar basal lamella are no doubt a consequence of its tendency to spread out upon the substrate as it collapses during drying. The crystals also undergo pronounced pleating and folding when they collapse upon the substrate. The pronouncedly pleated and folded portions of the crystals shown in figures 13–14 may be clearly discerned as somewhat narrow extended regions which exhibit substantial opacity to the incident electron beam. While the disposition of such pleating and folding varied somewhat from one crystal to another, particularly in the central portions of the crystals, opaque regions corresponding to such deformations were always observed which "subtended" the four apices of the basal lamella. Such regions, oriented at $\sim 45°$ to the sides of the basal lamella are evident in the crystals shown in figures 13–14.

In addition to undergoing the deformations described in the previous paragraph, several sedimented crystals were observed which exhibited yet another type of deformation in that the apical (corner) portions of the

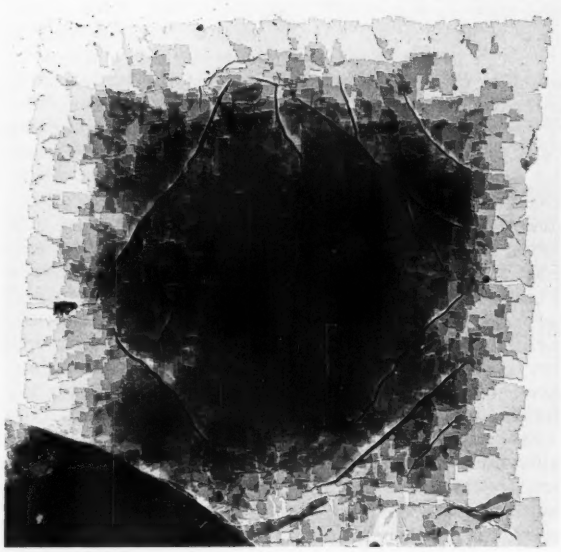

FIGURE 14. *Electron micrograph of typical P4MP crystal formed at 80 °C.*

Pt/Pd shadowed, × 3500.

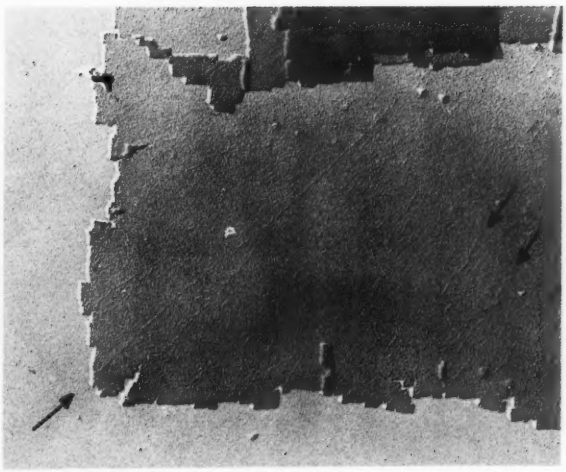

FIGURE 16. *Portion of the basal lamella in a P4MP crystal formed at 80 °C.*

Arrows point to faint ridges on the surface of the lamella. Pt/Pd shadowed, × 13900.

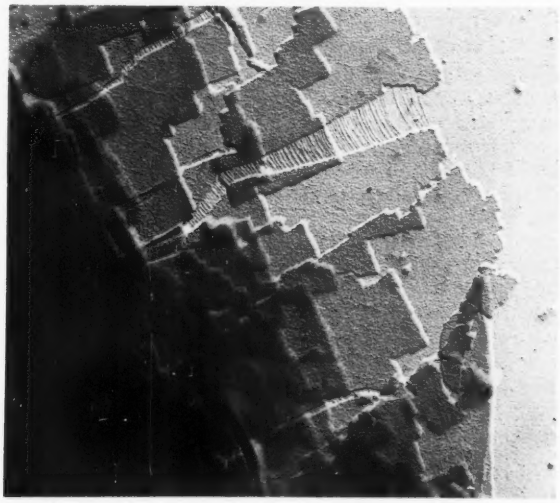

FIGURE 17. *A portion near the periphery of the basal lamella in a P4MP crystal formed at 80 °C showing a large crack traversed by fibrils.*

Pt/Pd shadowed, × 16500.

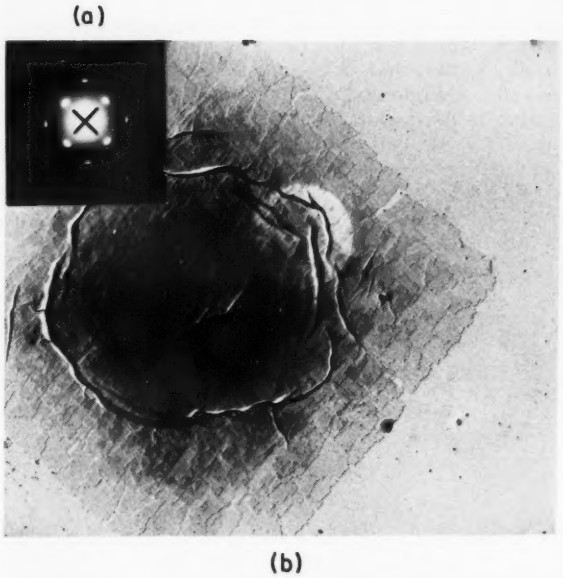


FIGURE 15. *(a) Inset. Selected area electron diffraction pattern obtained from a P4MP crystal formed at 80 °C. The arms of the cross at the center of the pattern point to the 200 spots. (b) Electron micrograph showing area (lighter circular region) from which diffraction pattern was obtained. Heavy gold shadowing, × 3400.*

basal lamella were doubled back onto (or tucked under) the collapsed interior of the crystals, as may be seen at (A), (B), and (C) in the crystal shown in figure 18, in which three of the corners of the basal lamella have folded back inwards and collapsed part way towards the central axis. The fourth corner (D), whose right angled character is evident, did not fold back completely in this instance; that it tended to do so is

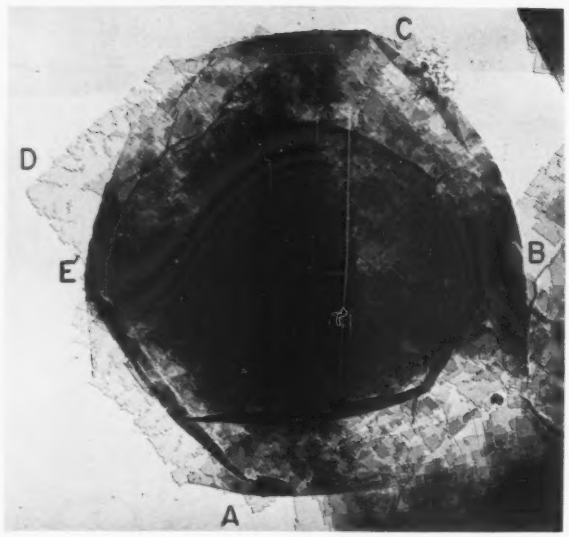


FIGURE 18. *A crystal of P4MP formed at 80 °C in which the corners of the basal lamella have folded or tended to fold back towards the interior of the crystal upon sedimentation and drying, see text.*

Pt/Pd shadowing, ×3400.

evidenced however by the manner in which the crystal is pleated back and forth at (E). It is of interest to note that those portions of the outline of this collapsed crystal, which subtend the folded apical regions of the basal lamella, i.e., at (A), (B), and (C) are rounded in character. This latter feature which is clearly consistent with the fact that the crystal, as grown, has a curved conformation, was characteristically observed in all instances in which the corners of the basal lamella had folded backwards during the process of sedimentation and drying. The very fact that the corners of the basal lamella do occasionally fold over also has a bearing on the conformation of these curved crystals. Its relevance in this latter respect is examined, in conjunction with other features described in the foregoing paragraphs, in the ensuing further discussion of the conformational characteristics of the crystals.

Having established that the crystals are curved, that they are multilayered, and that their constituent chain-folded lamellae, which are bounded laterally by {100} growth faces, are multisectored and collapse readily when the crystals are sedimented upon a substrate, we turn at this stage to the consideration of an aspect of the shape of the crystals which has not been specifically discussed so far, namely, the nature of the as-grown conformation of the periphery of their leading basal lamella whose lateral edges define the rim of these distinctly dished objects. It has been clearly shown that the basal lamella is bounded laterally by {100} faces and that the four apices (corners) of that lamella are right-angled and not rounded, as may be seen for example in figures 13–14 and figure 16. It has also been pointed out previously, however, with reference to figure 12b, that when one views one of these crystals in the uncollapsed state along its central axis, it exhibits a *profile* corresponding to a square which is rounded at the corners. On the basis of this latter feature, and since it is evident that the periphery of the basal lamella is not rounded at the corners, it can be readily concluded with reference to figure 19, that the apical portions of the basal lamella in the crystals as-grown must be appreciably upturned as shown schematically in figure 19c, and that, as is also illustrated in the same diagram, the sides of that lamella must be bowed with respect to the plane of reference (FG) (see fig. 19a) which is tangential to the surface of the crystal at its 'pole' (H). In other words, both the inclination of the basal lamella and hence the vertical displacement of its periphery with respect to the plane of reference FG are maximal at the four corners of the lamella and least pronounced at the midpoints along its lateral edges. The model shown in figure 19c is further substantiated by yet another feature which has also been pointed out earlier with reference to the phase contrast optical micrograph shown in figure 12b, namely, that in addition to appearing rounded at the corners, the crystals, when viewed in the uncollapsed state along their central axis, exhibit more pronounced contrast, and hence greater effective thickness with respect to the direction of observation, in the vicinity of their apparently rounded corners than elsewhere along their four-fold symmetrical *outline*. Such an effect is implicit in the model shown in figure 19c on the basis of which one would also anticipate that the apical portions of the basal lamella would exhibit a tendency to fold backwards when the crystal is sedimented and dried. The occasional folding of the basal lamella in the latter manner has been pointed out above, and while this feature, which has also been previously observed by Frank, Keller, and O'Connor [2] and Woodward [11] in some sedimented crystals of P4MP, is not conclusive in itself, it is, to say the least, consistent with the model shown in figure 19c.

Further substantiation that the apical portions of the crystals which are yielded on cooling the polymer solutions to 80 °C are preferentially 'curled,' in accordance

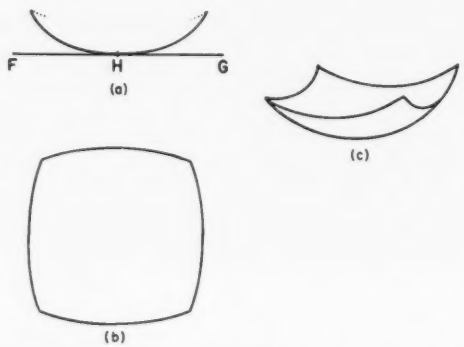


FIGURE 19. *Schematic representation of P4MP crystal formed at 80 °C. (a) Edge-on view; (F G) is a plane of reference which is tangential to the surface of the crystal at its pole (H). (b) Flat-on view. (c) Three dimensional perspective.*

with figure 19c, and 'head' the remainder of the crystal in its propagation in a curved fashion relative to the plane of reference (FG) (fig. 19a), is provided by the manifestation of this feature in an unequivocally detectable and more dramatic fashion in crystals formed at lower temperatures, as will be seen in the ensuing section.

It may finally be noted that the thickness of the lamellae in the crystals formed at 80 °C as determined from a low angle x-ray diffraction pattern obtained from a mat of such crystals with the plane of the mat parallel to the x-ray beam was found to be 124 Å.

### 3.4. Crystals Formed at Temperatures Below 80 °C

The species of crystals described in this subsection were formed when polymer solutions initially held at 140 °C were subsequently transferred to baths maintained at 70 and 50 °C. Crystallization is extremely rapid at these temperatures, the onset of cloudiness was observed to occur (at ~ 70–75 °C) before thermal equilibrium was attained. It may be pointed out from the outset that the crystals yielded in these preparations exhibited shapes which were similar to one another but that their sizes differed depending on thermal history. Thus, the solutions cooled to 70 °C yielded the largest, and those cooled to 50° yielded the smallest crystals.

An example is shown in figure 20 of several randomly oriented crystals formed on cooling a solution to 70 °C. This phase contrast micrograph depicts the crystals as seen while in suspension in liquid. They are hollow fishbowl-like objects which collapse very readily when they are allowed to sediment and dry on a substrate. When they are examined (in the collapsed state) in transmission in the electron microscope, they exhibit, due to the thickness of their wall, an overall opacity to the electron beam which frustrates the examination of their fine structure directly. Replicas of collapsed crystals prepared by the shadow transfer technique described earlier (section 2.2c) revealed, not unexpectedly, that they possess a lamellar morphology, their curved wall being constituted of numerous superimposed chain-folded lamellae. A replica of a collapsed crystal is shown in figure 21 in which the layered (lamellar) morphology of the crystal can be seen. Such replicas also reveal that the sides of the constituent lamellae in these crystals are profusely microfaceted, indicating that the lamellae are multisectored. No sector delineating ridges are observed however. As may also be seen in figure 21, adjacent microfacets are orthogonal to one another, in short it may be readily surmised that these lateral growth facets are {100} as is the case in the crystals formed at higher temperatures. Bearing in mind the lamellar texture of these crystals we now turn to a more detailed description and analysis of their overall shape.

Three differently oriented crystals which are representative of the type formed on cooling the polymer solutions to 70 °C are shown in figure 22. Figure 22a represents the characteristic appearance exhibited by these bowl-like objects when they are viewed, while in suspension in liquid, flat-on, i.e., along their central axis (in this instance the central axis of the crystal is actually slightly inclined to the direction of observation).

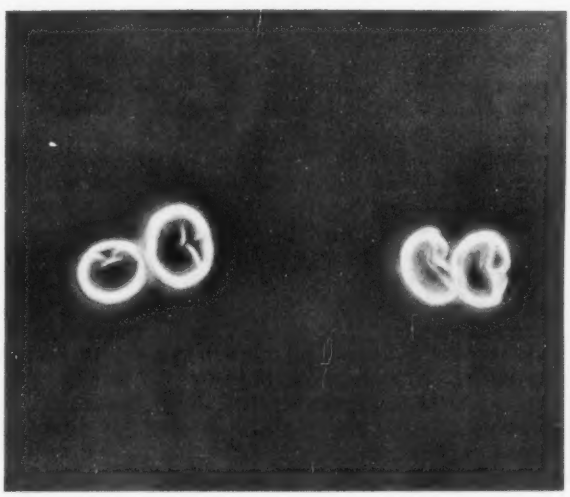

FIGURE 20. *Optical micrograph showing four hollow bowl-shaped crystals of P4MP typical of those formed on cooling the solutions to 70 °C.*

The crystals are in suspension in liquid. Phase contrast, × 830.

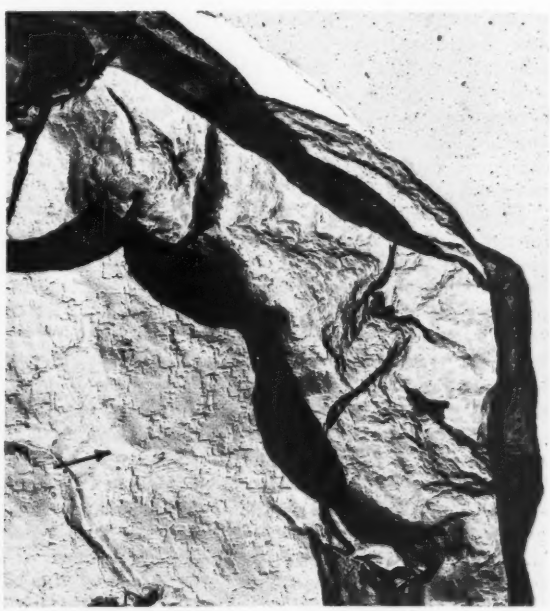

FIGURE 21. *Electron micrograph of replica of a portion of the surface of a collapsed hollow bowl-shaped type of P4MP crystals formed on cooling the polymer solution to 70 °C.*

Arrow points to region in which the lamellar character of the wall is evident as is the microfaceted character of the edges of the lamellae, × 11,000.

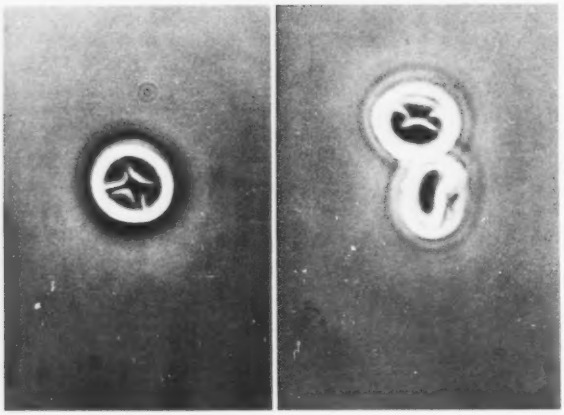


FIGURE 22. *Optical micrographs showing three perspectives of hollow bowl-shaped type of P4MP crystals formed on cooling the polymer solutions to 70 °C. The crystals are in suspension in liquid. (a) Flat-on view, i.e., view along the central axis of the crystal. (b) Lower crystal is oriented edge-on with respect to the direction of observation. The orientation of upper crystal lies between the flat-on and edge-on perspectives.*

Phase contrast, × 830.

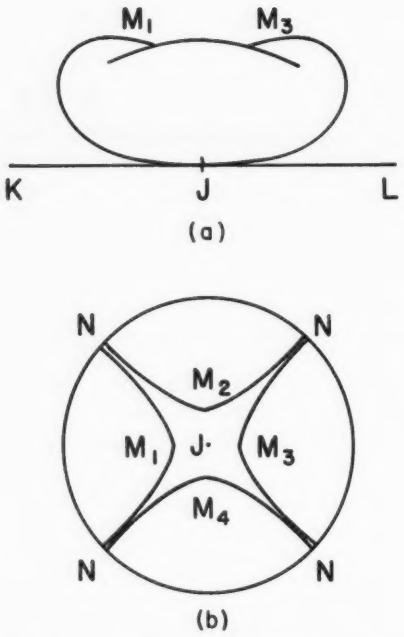


FIGURE 23. *Schematic representation of (a) Edge-on view and (b) flat-on view of hollow bowl-shaped crystals formed on cooling solutions to 70 °C.*

(KL) is a plane tangential to the outer surface of the crystal at its pole (J). ($M_{1-4}$) are the four symmetrically disposed leading extremities of the curved lamellar wall. (N) denotes positions along the rim of the crystal which are intermediate between the leading extremities (M).

In this perspective the crystals exhibit a circular outline whose diameter is 12 $\mu$m to 15 $\mu$m. One may also readily detect within the outline of the crystal shown in figure 22a the characteristic tetracuspid profile exhibited by its rim (i.e., the open end of the bowl) in this perspective. This feature indicates quite clearly that these crystals develop in a coherent four-fold symmetrical fashion about their central axis. A side (edge-on) view of a crystal similar to that shown in figure 22a may be seen in the lower part of figure 22b, and a crystal whose orientation with respect to the direction of viewing lies between the flat-on and edge-on extremes may be seen in the upper part of figure 22b.

For the sake of clarity in discussing further the conformational characteristics of these bowl-like crystals and attempting to characterize their habit in crystallographic terms, the edge-on and flat-on perspectives of these hollow bowl-shaped crystals are reproduced schematically in figure 23a and figure 23b, respectively, in which (J) represents the pole of the crystal, (KL) is a plane of reference which is tangential to the surface of the crystal at (J), and ($M_{1-4}$) denote the symmetrically disposed leading extremities of the rim of the crystal which lie along four equispaced "longitudes" of preferential development ($JM_{1-4}$). Consideration of the crystals shown in figure 22 and schematically in figure 23 indicates that on progressing from J along the surface of the crystal to any of the extremities M, the orientation of the surface of the lamellar envelope of which these objects are constituted changes progressively through 180° or more with respect to the plane (KL), whereas at intermediate "longitudes" (JN) along which growth is seemingly slowest, the change in orientation tapers to about 90°.

This four-fold symmetrical disparity in the growth and curling of the lamellar envelope along the (JM) relative to the (JN) longitudes provides a basis for characterizing the habit of these crystals more specifically, namely, in terms of the orientation of the unit cell at their pole (J) relative to the disposition of the (JM) and (JN) longitudes. This relationship may be deduced from a consideration of the conformational characteristics of the crystals formed at 80 °C coupled with the reasonable expectation that under the conditions of higher undercooling which govern the development of crystals from solutions cooled at 70°C, growth will tend to occur (in dendritic fashion) preferentially at the corners of an initially formed lamellar precursor crystal bounded laterally by {100} faces. Briefly, it may be readily surmised, as shown schematically in figure 24 (and with reference to figure 23), that at the pole (J) the (JM) longitudes coincide with ⟨110⟩ whereas the (JN) longitudes coincide with ⟨100⟩ and that [001] (i.e. the c axis of the unit cell) is normal to the surface of the crystal throughout as shown in figure 24a. The orientation of the tetragonal unit cell at the pole (J) relative to the crystal as it is viewed along its central axis of four-fold symmetry is outlined in figure 24b.

Confirmation of the crystallographic assignment depicted in figure 24 from which it is evident that growth along each of the (JM) longitudes involves an 180° (or more) change in orientation of the stems of the folded molecules (c axis) in the lamellar envelope relative to the plane (KL), was obtained from crystals

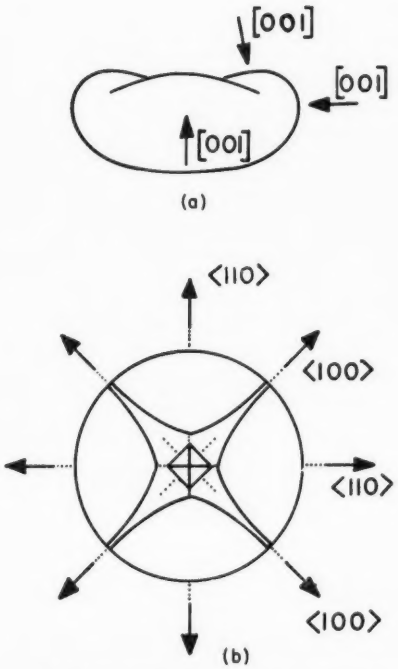


FIGURE 24. *Schematic representation of (a) edge-on view and (b) flat-on view of hollow-bowl-shaped crystals formed on cooling solutions to 70 °C, showing relationship between the orientation of the unit cell at the pole of the crystal relative to the crystal as a whole, as well as the 180+° change in c axis orientation on proceeding from the pole, along the surface of the crystal, to its leading extremities (i.e., along the (JM) longitudes, see fig. 23).*

grown on cooling polymer solutions to 50 °C. As pointed out earlier, these crystals were smaller than those formed on cooling to 70 °C but possessed similar shapes and, more pertinently, had a wall consisting of fewer superimposed lamellae thus permitting their direct examination in transmission in the electron microscope.

A general view including numerous randomly oriented crystals (suspended in liquid) which were formed on transferring a 0.1 percent solution initially held at 140 °C to a bath at 50 °C is shown in figure 25 in which the variation in the sizes of the crystal formed is evident. Their diameter when viewed along their central axis of four-fold symmetry was between 5 $\mu$m − 10 $\mu$m. Figure 26 is an electron micrograph showing several such crystals after they had collapsed on a carbon substrate. The similarity in shape between these smaller and thinner walled crystals and those formed on cooling the solutions to 70 °C is revealed in the crystals (P), (Q), and (R) which evidently initially impinged upon the substrate with their central axis of four-fold symmetry oriented by chance at right angles to the carbon film and subsequently collapsed upon the film on drying in an essentially uniform fashion corresponding to a mere flattening about their central axis. The circular outline of these collapsed crystals may be clearly seen in figure 26, as can the inner essentially tetracuspid-shaped boundary between the less transparent outer portions (where the lamellar

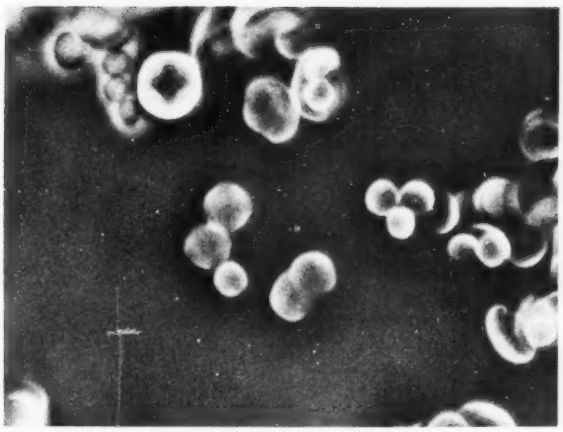

FIGURE 25. *Optical micrograph showing several P4MP bowl-shaped crystals formed on cooling a polymer solution to 50 °C.*

The crystals are in suspension in liquid. Phase contrast, ×1000.

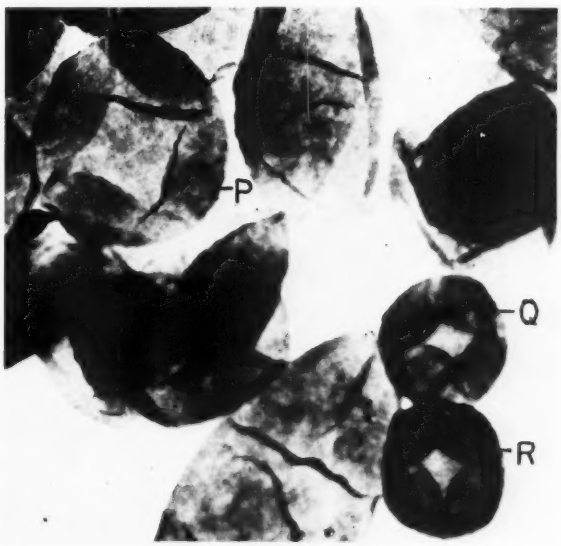


FIGURE 26. *Electron micrograph showing several collapsed bowl-shaped crystals of P4MP formed on cooling a polymer solution to 50 °C.*

(P), (Q) and (R) denote crystals which have collapsed relatively uniformly about their central axis upon drying. Unshadowed, ×3900.

envelope is doubled on itself) and the more transparent central (polar) portion of the flattened lamellar envelope. This boundary delineates in effect the projected outline of the rim of these crystals upon the substrate prior to collapse, allowance being made for some distortion about the central axis as the crystal flattens. The similarity between these crystals and those yielded by the 70° preparation is further demonstrated in figure 27 in which a large and a smaller crystal (suspended in liquid) from the 50 °C preparation, are shown which are respectively oriented with their central axis normal and parallel to the field of view. The

tetracuspid profile of the rim of the appropriately oriented former crystal is discernible, but faintly so due to the relatively thinner nature of the wall of the crystal, as compared to those formed on cooling to 70 °C.

Having demonstrated the similarity in the shape of the crystals formed on cooling the polymer solutions to 70 and 50 °C, we turn to a consideration of the electron diffraction characteristics exhibited by crystals yielded in the latter instance when these crystals have collapsed about their central axis in the essentially uniform fashion exhibited by crystals (P), (Q), and (R) in figure 26. Such a crystal is shown in figure 28b, the corresponding diffraction pattern (electron beam normal to the field of view) is shown in figure 28a. The disposition of the 200 and the 220 reflections in figure 28a relative to the tetracuspid profile formed by the folded over portions in the flattened crystal clearly confirms the relationship indicated in figure 24 between the lattice orientation at the pole of these bowl-like objects relative to their overall four-fold symmetrical shape. In addition, the diffraction pattern is consistent with the observed preferred orientation of the {100} microfacets in the lamellar terraces in the central protion of the crystal, as indicated by the cross in the right-hand side of figure 28b.

FIGURE 27. *Optical micrographs of two bowl-shaped crystals of P4MP formed on cooling a polymer solution to 50 °C.*

The crystals are in suspension in liquid. The larger one is seen in flat-on perspective and the smaller one in edge-on perspective. Phase contrast, ×1400.

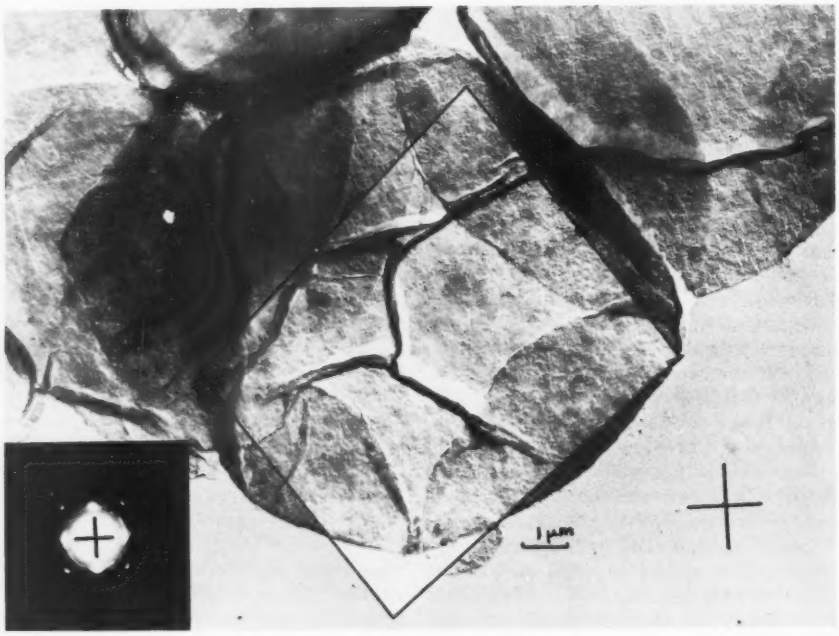


FIGURE 28. *(a) Inset. Electron diffraction pattern obtained from the central region of a collapsed bowl-shaped crystal of P4MP formed on cooling polymer solution to 50 °C. The arms of the cross drawn at the center of the pattern point to the strong 200 reflections. (b) Selected region from which the diffraction pattern was obtained. The arms of the cross drawn at the right hand side of the micrograph indicate the preferred orientation of the {100} microfacets in the terraces situated in the central portion of the crystal. Gold shadowed, × 7500.*

The {100} microfaceted (and hence multisectored) character of the constituent lamellae in the crystals formed at 50 °C can be seen in the crystal shown in figure 29 which tended to tear outwards upon collapsing thus revealing (see arrow) a portion of its periphery (rim). No sector delineating ridges were observed even at high magnifications in the constituent terraces of the crystals grown in the 50 °C preparations.

Finally, it may be noted that the thickness of the lamellae in the crystals formed on cooling the polymer solutions to 50 °C as determined from a low angle x-ray diffraction pattern obtained from a mat of such crystals with the x-ray beam parallel to the plane of the mat was found to be 121 Å.

### 3.5. Further Comments on, and Summary of, the Main Characteristics of the P4MP Crystals Described in Sections 3.2 to 3.4

The purpose of this section is to summarize the main features of the experimental observations reported in sections 3.2 to 3.4 as a preliminary to the considerations and conjectures pertaining to the origins and "mechanism of development" of curved crystals of P4MP which are discussed in section 4. In addition we shall comment further herein on the formation of both planar four-sectored and perceptibly curved multisectored lamellar crystals at 90 °C.

In considering the influence of crystallization conditions on the habits of P4MP crystals, it may be noted from the outset that, with the exception of those smaller crystals formed at 90 °C whose constituent lamellae are essentially planar and four-sectored, the larger crystals formed at 90 °C (e.g. figures 6–10) as well as those formed at lower temperatures exhibit under the optical microscope distinctly detectable curved shapes; furthermore, the constituent lamellae in these distinctly curved crystals are multisectored.

A consideration of sections 3.2 to 3.4 also reveals that the lower the crystallization temperature the more pronouncedly curved are the crystals yielded in suspension in solvent. It is also evident that all the distinctly curved multisectored lamellar crystals are multilayered (i.e., they consist of two or more superimposed chain folded layers) and exhibit four-fold symmetrical shapes which are specifically related to one another. Thus, for example, the hollow bowl-shaped crystals formed on cooling the polymer solutions to 50 °C (figs. 25–29) are simply miniature versions (with respect to overall shape) of those formed on cooling the polymer solutions to 70 °C (figs. 20–22). The radius of these bowls as measured at right angles to their central axis of four-fold symmetry provides a rough measure of the curvature of their lamellar wall. The radii of the hollow bowls formed on cooling the polymer solutions to 50 and 70 °C were found to be between 2.5 $\mu$m and 5 $\mu$m, and between 6 $\mu$m to 7.5 $\mu$m, respectively.[4] In considering the lamellar crystals formed at temperatures above 70 °C, it may be readily visualized that had the curved crystals formed at 80 °C

[4] That lower crystallization temperatures lead to the formation of more pronouncedly curved lamellar crystals is also reflected by the character of the individual bowl-shaped crystals grown in the preparations cooled to 70 °C. Thus, it has been pointed out in section 3.4 that crystallization is extremely rapid at 70 °C and that consequently the onset of crystal growth occurs before temperature equilibrium is attained at 70 °C, when the solutions are cooled to that temperature. Accordingly, as may be seen for example from the edge on profile of the bowl-shaped crystals (e.g., fig. 22b) the initially formed polar regions of the bowls which develop at higher ambient temperature during the cooling of the solutions to 70 °C are less pronouncedly curved than the peripheral regions which develop at a more advanced stage of thermal equilibrium.

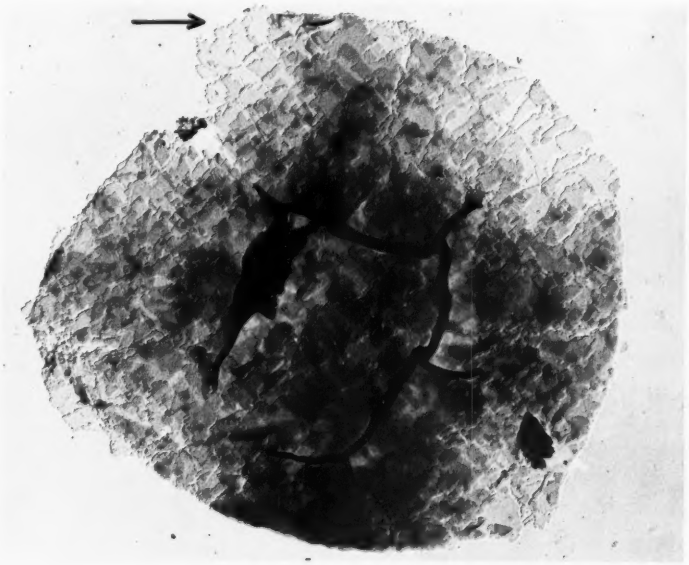

FIGURE 29. *Electron micrograph of a crystal formed on cooling a polymer solution to 50 °C.*

The crystal tended to tear outwards upon collapsing on the substrate revealing a portion of its periphery (see arrow). Pt/Pd shadowed, × 10000.

(figs. 11–19) and the large (multisectored) species of curved crystals formed at 90 °C (figs. 6–10) not stopped growing due to the depletion of polymer from the mother liquor, they would have developed further and would have eventually curled back toward their central axis of four-fold symmetry with the corners of the basal lamella leading the way, so to speak, as shown in figure 19 (it may be reasonably assumed that this latter feature is also manifested in the large curved crystals formed at 90 °C but is not readily detectable due to the less pronounced curvature of these crystals). It may be roughly estimated from their respective edge-on profiles, that if the curved multisectored lamellar crystals formed at 80 and 90 °C had indeed continued to grow as envisaged above the radius of the resulting bowl-shaped objects measured at right angles to their central axis of four-fold symmetry would be about 15 $\mu$m and about 30–40 $\mu$m, respectively.

While it is evident from the foregoing that lower crystallization temperatures, which favor more rapid lateral growth of chain folded polymer lamellae, lead to the formation of more pronouncedly curved crystals of P4MP, it should be noted that crystallization at 90 °C yielded a mixed population of crystals among which two types were readily distinguishable, namely, the smaller essentially planar crystals whose constituent lamellae are four-sectored, and the largest perceptibly curved ones whose constituent lamellae are multisectored. While both these types of crystals are less pronouncedly curved than those formed at lower temperatures, and thus conform with the overall trend to more pronounced curvature the lower the crystallization temperature, the formation of these differing crystals in the same preparation at 90 °C prompts further comment. Noting that these preparations were filtered at the temperature of crystallization (see section 2.1) it is significant that it is the smallest crystals (basal lamella up to about 20 $\mu$m on a side), and hence those formed during the more advanced stages of depletion of polymer from the mother liquor, which are essentially planar and whose constituent lamellae are four-sectored, whereas the largest members of the population (basal lamella ~ 40 $\mu$m to 45 $\mu$m on a side) whose constituent lamellae are multisectored are perceptibly curved. The difference between the fine structures of the smaller crystals (four-sectored) and the larger crystals (multisectored) may be attributed to a combination of two factors, namely, the continuous depletion of polymer from the mother liquor as well as to fractionation [16], the latter factor leading progressively to a continuing decrease in the molecular weight of the polymer still in solution during the process of crystallization. Both of these factors would be expected to lead to a progressive decrease in the rate of lateral propagation of developing chain folded lamellae over the duration of their growth. In short, the average rate of lateral growth of the initially formed multisectored basal lamella in the largest perceptibly curved crystals formed at 90 °C would be expected to be greater than that of the four-sectored lamellae in the smaller essentially planar crystals. This is substantiated by the nature of the respective fine structures of the lamellae in the larger and smaller crystals. It is common experience that conditions which favor more rapid lateral growth rates in chain-folded polymer lamellae lead to multisectoring. That this is the case is certainly born out by the fact that the constituent lamellae in the P4MP crystals formed at lower temperatures than 90 °C are all multisectored. While one may thus reasonably attribute the fact that the constituent lamellae in the smallest crystals formed at 90 °C are four-sectored to their propagation laterally at slower overall growth rates as compared to the larger crystals, it is evident that the continuously changing rate of lateral growth of both the large and small crystals must be the same and diminish coincidentally in both types during the period corresponding to the development of the smaller crystals which propagate in a four-sectored fashion. Since it is evident that the outer regions of the basal lamella in the larger crystals are multisectored, we must conclude that notwithstanding the slower growth conditions under which these regions must have developed, the ambient conditions were not sufficient to lead progressively to a total "smoothing out" of their {100} growth faces and thus to overcoming of the earlier multisectored manner of propagation of these lamellae.

After the work described in sections 3.1 to 3.4 had been completed Blundell Keller and Kovacs [15] have described a "self-seeding" technique for growing polyethylene crystals from solution which yielded crystals of uniform size. Using a similar technique we were able to obtain a uniform population of four-sectored lamellar crystals of P4MP at 90 °C. The preparation details are given in section 2.1 we shall therefore only mention here that the final step in the procedure involved taking a 0.1 percent solution of P4MP held at 130 °C and immersing it in a bath at 90 °C. Four-sectored chain-folded monolayers as well as crystals consisting of more than one four-sectored chain-folded layer were formed. The monolayers and the basal lamella in the multilayered crystals were similar in size (~ 10 $\mu$m on a side). Evidently all the crystals had started to grow simultaneously from predetermined nuclei, presumably residual crystal nuclei which had not been dissolved at 130 °C. A corner portion of a crystal formed under these conditions is shown in figure 30 in which a diagonally oriented domain delineating ridge and the essentially smooth character of the lateral edges of the lamella can be seen. An electron micrograph depicting a distinct crack near the periphery of a crystal formed in this preparation is shown in figure 31. As would be expected from the four-sectored character of the crystal, that portion (unbarbed arrow) of the crack which runs parallel to the crystal edge is not traversed by fibrils, whereas fibrils can be seen in the short portion of the crack which runs at an angle to the edge (barbed arrow). The crystals formed in this self-seeded preparation exhibited, not unexpectedly, no detectable curvature when viewed edge-on in suspension in liquid in the optical microscope. The fact that by the time crystallization was essentially completed the crystals formed at 90 °C in this self-seeded preparation

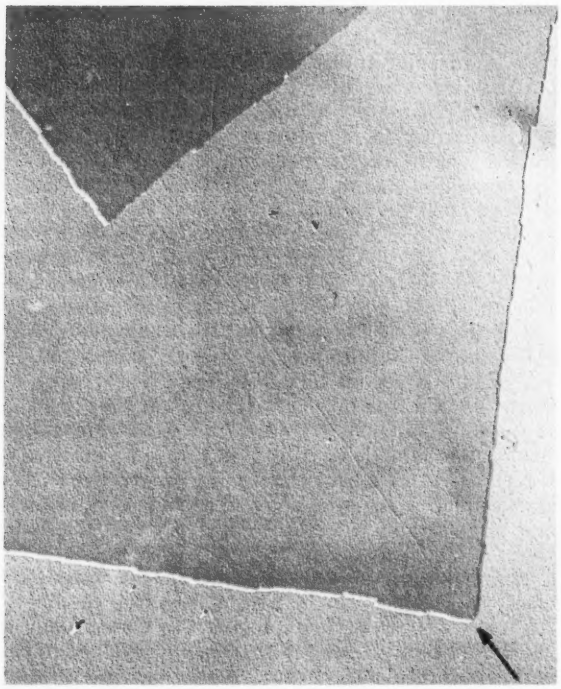

FIGURE 30. *Electron micrograph of a corner of a four-sectored P4MP crystal grown at 90 °C using self-seeding procedure.*

Arrow points to diagonal ridge which delineates domain boundary. Pt/Pd shadowed. × 12000.

were considerably smaller than those formed in the unseeded preparation at the same temperature may be attributed to the large number of heterogeneous nuclei available for growth, the net effect of which nuclei is to lead to a more rapid rate of depletion of the polymer in solution and hence to a slower average rate of lateral propagation of the crystals under these circumstances as compared to that which prevails during the earlier stages of propagation of the considerably larger multisectored crystals formed in the unseeded preparation at the same temperature. This would account for the fact that all the crystals yielded in the self-seeded preparation are four-sectored. We have not pursued this matter further. It suffices for our present purposes to note that our accounting earlier of the presence of both four-sectored and multisectored crystals in unseeded preparations crystallized at 90 °C in terms of different rates of lateral propagation prevailing during their formation is plausible in the light of the differences we have observed between unseeded and seeded preparations. As a further check of the observation derived from the unseeded preparations crystallized between 90 and 50 °C that lower crystallization temperatures lead to the formation of curved P4MP crystals from solution, a self-seeded 0.1 percent solution (see sec. 2.1) was prepared using the same procedure as that used in the self-seeded preparation crystallized at 90 °C which was mentioned above, it was however transferred from a bath at 130 °C to one held at 50 °C. Under those conditions the population of crystals was indistinguishable from that obtained on cooling unseeded solutions to 50 °C and consisted of hollow bowl-like crystals whose constituent lamellae

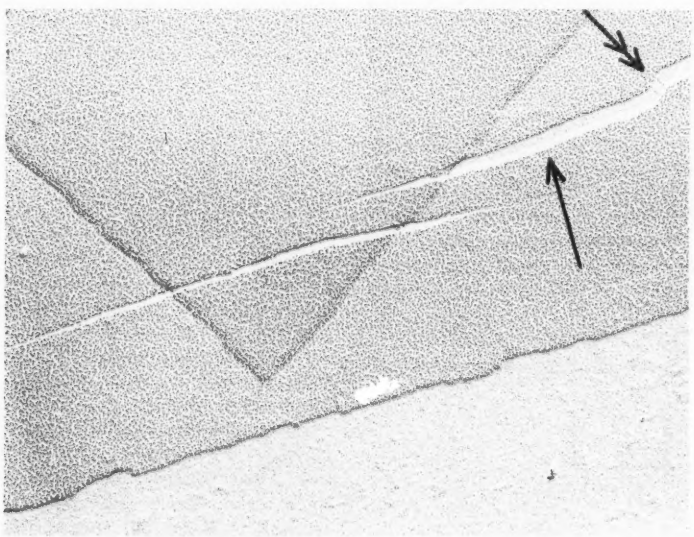

FIGURE 31. *Region near the edge of a four-sectored lamella showing cracks.*

Unbarbed arrow points to a portion of a crack which runs parallel to the edge of the crystal. No fibrils traverse this portion of the crack. Barbed arrow points to fibrils in the portion of the crack which is not parallel to the edge of the crystal. Gold decorated. × 31000.

were multisectored. The radius of individual bowls as measured at right angles to their central axis of four-fold symmetry was in the range 2.5 $\mu$m to 5 $\mu$m.

## 4. On the Origins and Mechanism of Formation of Curved Crystals of P4MP

### 4.1. Summary of, and Comments on, Previous Observations on Four-Sectored Lamellar Crystals of P4MP

Before attempting to discuss why it is as has been illustrated in sections 3.2–3.5 that lamellar crystals of P4MP formed between 90 and 50 °C from 0.1 percent solutions of the polymer in an equivolume mixture of xylene and amyl acetate are all the more pronouncedly curved the lower the temperature at which they are formed, it is relevant to first dwell on the nature of the as-grown shape of four-sectored lamellar crystals of P4MP which in our experience are formed from solution at low supercooling, i.e., under conditions which favor slower lateral propagation of the lamellae. As

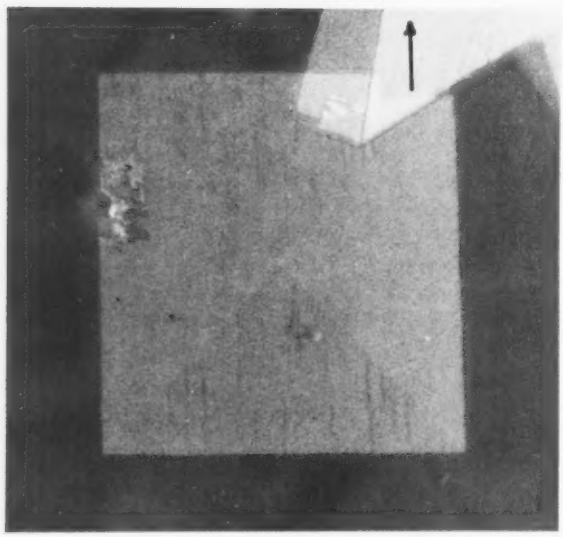

(a)

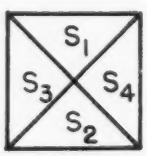


(b)

FIGURE 32. *(a) 200 dark field electron micrograph of a four-sectored crystal formed at 90 °C using self-seeding procedure. This image was formed using the diffraction spot from the {200} planes in the crystal which are parallel to the arrow in the picture. Unshadowed, ×5000. (b) Schematic representation of the four-sectored crystal with sectors identified, see text.*

pointed out in section 3.2, these crystals exhibit an essentially linear profile when they are viewed edge-on while in suspension in liquid; it bears reiterating here that they are however not perfectly flat, as has been previously pointed out by Bassett et al. [9, 10], although their departure from planarity is relatively minimal and escapes detection under the optical microscope. The deduction due to Bassett et al. [9, 10], that four-sectored lamellae are not perfectly planar stems from the diffraction contrast characteristics exhibited by these crystals in dark-field electron micrographs formed by imaging the {200} planes. A dark-field electron micrograph of a four-sectored monolayer crystal formed at 90 °C (this particular crystal was grown in the self-seeded preparation mentioned in section 3.5) is shown in figure 32a. For the sake of clarity a schematic representation of such a crystal is shown in figure 32b in which the four constituent sectors are identified. The {200} planes which are imaged in the dark-field electron micrograph shown in figure 32a are those which run vertically in the field of view as indicated by the arrow in the top right-hand corner of the micrograph. The four-sectored character of the crystal is clearly revealed in this dark-field image, in which it may be readily seen that the upper and lower sectors or fold-domains ($S_1$, $S_2$ fig. 32b) in which the {200} planes which are being imaged are not fold planes are darker than the other two sectors ($S_3$, $S_4$ fig. 32b) in which the {200} planes which are being imaged are fold planes. In addition, darker non-diffracting streaks which traverse sectors ($S_1$, $S_2$) at right angles to the corresponding outer edges which subtend these sectors may be readily seen. This systematic difference in contrast between those sectors in which the {200} planes which are being imaged are not fold planes, and those sectors in which the corresponding planes are fold planes is a characteristic feature exhibited by four-sectored lamellae which was first observed by Bassett et al. [9, 10]. If the {200} planes which run horizontally in figure 32a had been imaged, sectors ($S_3$, $S_4$) would have appeared darker than sectors ($S_1$, $S_2$) and furthermore non-diffracting streaks would have been observed in ($S_3$, $S_4$), these streaks being oriented at right angles to the outer edges of the crystal which subtend the $S_3$ and $S_4$ sectors. Clearly, if these four-sectored lamellae were perfectly flat as-grown, the molecular stems in their four-constituent domains would be expected to be parallel to one another throughout the lamellae and oriented at right angles to the plane of the lamellae, consequently no difference in contrast between the constituent sectors should be observed in dark field images and the appearance (contrast) of the lamellae in {200} dark-field images should be uniform throughout. The observed diffraction contrast characteristics described above however indicate, according to Bassett et al. [9, 10], that in the four-sectored crystals, sedimented upon a flat substrate, the molecular stems in the crystals are not perfectly parallel to one another throughout but rather that the stems in each sector are slightly tilted about an axis normal to the corresponding {100} face which subtends that sector, i.e., about an

axis which is parallel to the {200} planes which are not fold planes in each sector. The extent of this tilt within each sector in the sedimented crystal is not uniform as evidenced by the darker non-diffracting streaks observed in dark-field images in the darker sectors ($S_1$, $S_2$ fig. 32a) in which the {200} planes which are imaged are not fold planes.

The evidence summarized above has been interpreted by Bassett el al. [9, 10], as indicating that the crystals as grown are not perfectly planar, the tilt of the molecules in each sector about an axis perpendicular to the corresponding {100} growth face suggesting that the lamellae as grown possess a slight "conicalness." Before dwelling on this latter aspect further it is necessary first to consider another feature of four-sectored lamellae which bears on the possible origin of their nonplanar character. An analysis due to Bassett [9] of dark field Moiré patterns exhibited by bilayer crystals of P4MP in which the two superimposed chain-folded layers are four-sectored and slightly rotated relative to one another about an axis normal to the plane of the lamellae has indicated that there is a very small fractional difference of $\sim 10^{-3}$ in the spacing between those {200} planes in each sector which are fold planes and those which are not. For the sake of brevity in what ensues these planes will henceforth be referred to as $\{200\}_f$ and $\{200\}_{nf}$ planes respectively (f = fold, nf = non-fold). In short, the idealized tetragonal subcell in each sector is slightly distorted. This feature has been attributed to the asymmetric bulkiness of the chain folds by Bassett et al. [9, 10], who have suggested that the nonplanar character of four-sectored lamellae of P4MP is due to buckling consequent to the inherent distortion of the subcell in their constituent domains resulting from the bulkiness of the chain folds. It is not unreasonable to presume that stresses which arise within the lattice, particularly at the sector boundaries where the mismatch in spacing between the $\{200\}_f$ planes in one sector and the $\{200\}_{nf}$ planes in adjoining ones must be accommodated, as well as stresses at the fold surfaces [17], cause an overall slight buckling of the lamella. If one proceeds on the assumption that $d_{\{200\}f} > d_{\{200\}nf}$ then on the basis of the magnitude of the difference of $\sim$ 0.1 percent between the spacings it may be roughly estimated, geometrically, that the buckled lamella, as grown, is slightly conical in character and has an angle of elevation which is probably not greater than $\sim 2°$. This estimate is arrived at as follows: Imagine an idealized flat four-sectored crystal in which $d_{\{200\}f} = d_{\{200\}nf}$ as shown in figure 33. It may be readily calculated that if a fractional difference of $\sim 10^{-3}$ is applied to each sector such that $d_{\{200\}f} > d_{\{200\}nf}$ then this would lead to an angular deficit of $\sim 3'$ between adjacent sectors and hence to a total angular deficit of 12′ on circumnavigating the lamella [9, 10], as shown in exaggerated form in figure 33 (full lines). A reconstruction of the lamella from these distorted sectors such that there be continuity between sectors at the center 0 as well as across sector boundaries, may be accomplished by simultaneously lifting the sectors out of the plane of the diagram at (0) where they are initially in contact. However, if the elevated sectors are kept flat, there would result in view of their thickness a V-shaped groove along the boundaries between the sectors. This feature may be overcome by bending or buckling the individual sectors so that contact between adjacent sectors is made throughout their thickness, hence the conicalness of the lamella. By the same token it may be visualized that the lamella is rounded at the apex (0) so that continuity is maintained between the sectors at (0) as shown in figure 34 which represents schematically a central cross-sectional view of two opposite sectors in the lamella. The angle of inclination $\theta°$ of such a quasi-conical lamella may be estimated to be $\sim 2°$ [12, 13]. It is envisaged that the molecular stems are oriented normal to the surface of the lamella throughout. Upon sedimentation and drying on a substrate such a crystal would tend to flatten and spread on the substrate and it is in that state that it exhibits the faint diagonal fold-domain boundary delineating ridges mentioned previously and the {200} dark field diffraction contrast characteristics which have been pointed out above with reference to figure 32.

The considerations which have been advanced above concerning the nonplanar character of four-

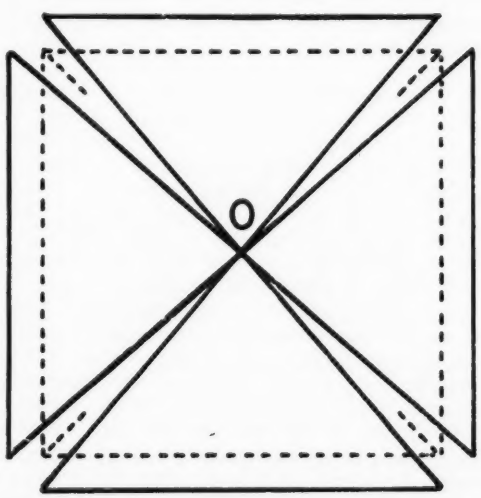


FIGURE 33. *Schematic representation of an idealized four-sectored crystal in which* $d_{\{200\}f} = d_{\{200\}nf}$ *in each sector* (– – –), *and distorted sectors in which* $d_{\{200\}f} > d_{\{200\}nf}$ (——).

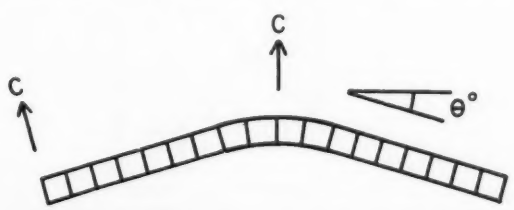


FIGURE 34. *Schematic representation of central cross-sectional view of two opposite sectors in a slightly conical four-sectored lamella.*

sectored lamellae are based on the assumption that in each sector $d_{\{200\}f} > d_{\{200\}nf}$. One cannot however distinguish from Moiré patterns which of these spacings is the larger. In short the possibility cannot be discounted that $d_{\{200\}} < d_{\{200\}nf}$. If the latter were indeed the case, then it can be seen that the application of a corresponding fractional difference of $\sim 10^{-3}$ between these spacings to an idealized four-sectored lamella ($d_{\{200\}f} = d_{\{200\}nf}$) results in a total angular *excess* of 12′ between sectors in which case on the basis of admittedly simplified model building (from paper sectors) it can be envisaged that the lamella would be buckled, but rather than being quasi-conical it could conceivably adopt a four-fold symmetrical wavy or corrugated conformation such as shown in perspective in figure 35 in which the molecular stems are also envisaged as being normal to the surface of the lamella throughout. Alternatively, the lamella could adopt a somewhat distorted but yet essentially conical shape.

In short, then, while there is no question that four-sectored lamellae are not perfectly planar but are instead slightly buckled there is some uncertainty about their exact as-grown shape. The fact that one observes sector boundary delineating ridges in sedimented crystals can be accounted for as resulting from a tendency of each sector to spread in a direction parallel to the corresponding growth face when the crystal collapses as shown by the arrows in figure 36.

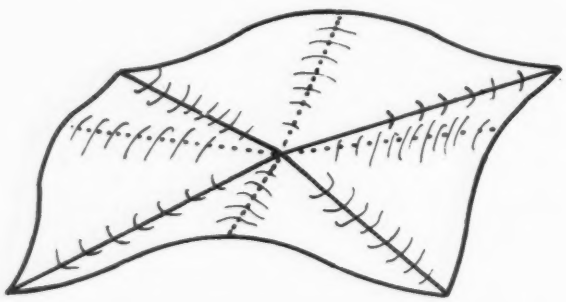

FIGURE 35. *Three dimensional perspective of a possible four-sectored lamella having a four-fold symmetrical wavy conformation resulting from* $d_{\{200\}f} < d_{\{200\}nf}$ *in each sector.*

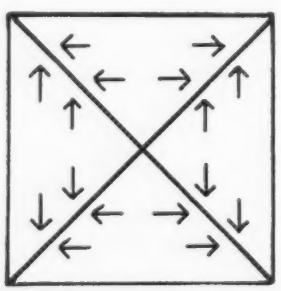

FIGURE 36. *Schematic representation of the possible origin of the ridges which delineate sector boundaries in collapsed four-sectored crystals, see text.*

This can be expected to occur both whether the crystal has a slight conicalness or whether it has a four-fold symmetrical wavy conformation such as shown in figure 35. The question then is: can one differentiate between the two cases on the basis of the dark field diffraction contrast images? These clearly indicate that whereas in the collapsed state the $\{200\}_f$ planes in each sector satisfy most closely the Bragg condition for diffraction the $\{200\}_{nf}$ planes in each sector deviate from that condition and are tilted relative to that condition about an axis perpendicular to the corresponding {100} edges. While the extent of this tilting is not uniform it is significant as may be noted in figure 32 that all regions in sectors $S_1$ and $S_2$ in which the {200} planes which contribute to the image are not fold planes are consistently darker than sectors $S_3S_4$. This feature can be viewed as favoring conicalness in the crystals as grown, as opposed to the model shown in figure 35, the argument being that in the latter case one would expect to see some strongly diffracting streaks in sectors $S_1$ and $S_2$ comparable in intensity to that of sectors $S_3$ and $S_4$. The absence of such streaks while favoring conicalness is not unequivocal proof of this feature as opposed to the model shown in figure 35 nor can it be taken as definitely establishing that $d_{\{200\}f} > d_{\{200\}nf}$ since the possibility cannot be ruled out that the lamella could also adopt a conical-like shape if $d_{\{200\}f} < d_{\{200\}nf}$.

Having pointed out that some uncertainty exists concerning the exact as-grown shape of four-sectored lamellae which are no doubt buckled we shall nonetheless proceed in what follows with a discussion of the variation of the curvature of multisectored lamellar crystals of P4MP with crystallization temperature based on the assumption that four-sectored lamellae possess a very slight conicalness.

### 4.2. Preliminary Considerations and Outline of Discussion on the Origins of the Dependence of the Curvature of P4MP Crystals on Temperature of Crystallization

The factors summarized above concerning four-sectored crystals provide a basis, or at any rate a starting point, for considerations pertaining to why it is, as has been described in sections 3.2–3.5, that P4MP crystals are all the more pronouncedly curved the lower the temperature at which they are formed. Interestingly, the constituent lamellae in all the P4MP crystals which are distinctly curved, such as the larger crystals formed at 90 °C (unseeded preparation, figs. 6–10), as well as all those crystals formed at lower temperatures, are not four-sectored but are multisectored. The multisectored lamellae in these crystals have one feature in particular in common with four-sectored lamellae, namely, the chain molecules in their constituent sectors or fold domains are also folded along {200} planes. It is consequently not unreasonable to consider, *first*, that as is apparently the case in four-sectored lamellae, interfold interactions leading to a distortion ($d_{\{200\}f} \neq d_{\{200\}nf}$) of the subcell in each fold domain also occur in the multisectored lamellae in

the curved crystals formed in the range 90 to 50 °C,[5] and *second*, that this feature induces each component domain in these lamellae to buckle under the influence of stresses resulting from the accommodation across domain boundaries of the respective subcell distortions in adjoining domains, as well as due to stresses at the fold surfaces. On the basis of these two premises, a multisectored lamella may be visualized as a mosaic structure whose building blocks, i.e., its constituent fold domains, are inherently slightly curved or buckled due to the bulkiness of the chain folds, and contribute *incrementally* to the overall curvature of the lamella. Accepting in principle that the overall curvature of a multisectored lamella is a cumulative consequence of the inherent nonplanar character of its constituent fold domains, one is still left with the problem of explaining the fact that the lower the crystallization temperature the more pronouncedly curved are the multisectored lamellar crystals of P4MP formed in suspension in solvent. We shall advance in what ensues a simple working hypothesis or model on the basis of which the observed trend in the dependence of the curvature of the P4MP crystals on supercooling is explained qualitatively in terms of the combined influence of two factors. These factors are: the inherent buckling of fold domains caused by the bulkiness of the chain folds, and the average lateral size of the fold domains in the multisectored lamellae which is governed by the supercooling dependent development of new fold domains at the periphery of a developing lamella throughout its growth. For the sake of simplicity in the exposition of the conjectures upon which this hypothesis is based we will initially discuss the development of a curved multisectored monolayer and proceed from there to the case of curved crystals which consist of two or more superimposed multisectored chain-folded terraces. We will assume that $d_{\{200\}f} > d_{\{200\}nf}$ in the constituent fold domains of the multisectored lamellae and that the fractional difference between these interplanar spacings is the same ($\sim 10^{-3}$) as that found by Bassett [9] in four-sectored lamellae irrespective of the crystallization conditions. This hypothesis and its limitations will then be discussed.

[5] The direct determination of the existence, or otherwise, of a subcell distortion in multisectored lamellae using Moiré techniques is frustrated by many factors including the deformation of the curved crystals when they collapse, as well as by the small sizes of their constituent domains which does not lend itself to the use of these techniques whose success depends on the ability of obtaining extensive Moiré patterns in which the separation and orientation of Moiré lines can be readily related to the domain boundaries in superimposed terraces.

### 4.3. Hypothetical Model Pertaining to the Origins of Curvature and Its Variation in P4MP Crystals

In keeping with the outline given above we shall first consider the propagation of a single multisectored lamella developing from a four-sectored precursor crystal assuming that $d_{\{200\}f} > d_{\{200\}nf}$ and that the fractional difference between these spacings, $10^{-3}$ [9], is the same in both the precursor and the multisectored lamella which evolves therefrom. It is also envisaged as indicated in the earlier discussion of Bassett's observations that the four-sectored precursor possesses a slight conicalness and has an angle of inclination $\theta \sim 2°$, that it is rounded at the pole, and that the molecular stems are oriented at right angles to the surface throughout this (conically shaped) lamellar precursor. A plan view representing such a precursor crystal is shown schematically in figure 37a (efgh) and a side view depicting the cross-section of the crystal corresponding to a cut along one of its diagonals (fOh in figure 37a) is shown in figure 37b in which (O′O) is the normal to the surface of the lamella at its pole. (O′O) coincides with the axis of four-fold symmetry of the lamella and is also normal to the plane of reference (kk) (figure 37b): The normals to the surface of the lamella at (f) and (h) are (f′f) and (h′h), respectively.

In accordance with the visualization indicated above that the four-sectored precursor is rounded at the pole,

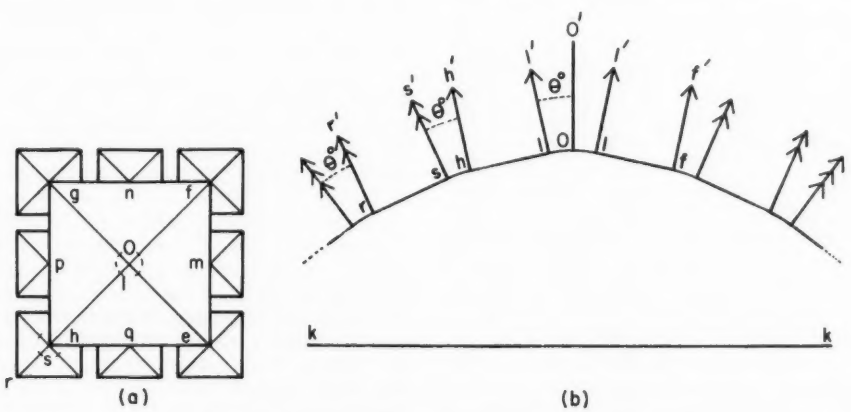


FIGURE 37. *(a) Plan view representing sectored outgrowths developing at the periphery of a four-sectored precursor. (b) Edge-on view of a diagonal cross-section of the developing multisectored crystal depicted in (a), showing suggested incremental contribution of sectored outgrowths to the overall curvature of the lamella, see text.*

it is assumed as shown in figure 37b, that on proceeding from its pole (O) to its periphery following radial paths outwards along the surface, e.g., along the diagonal path (Oh) there occurs within a small distance (O1) where (O1) $<<$ (Oh), a gradual inclination of $\theta°$ of the lamella relative to the plane kk and that beyond (1) the inclination of the lamella with respect to (kk) remains essentially constant. In other words, it is assumed that the angle between the surface normals at (O) and (h) is equal to the angle of inclination $\theta°$ referred to earlier, and that the normals to the surface of the lamella at (1) and (h) are parallel to one another. The molecular stems are considered to be normal to the lamellar surface throughout.

Bearing the above features attributed to a four-sectored lamella in mind, the formation is imagined (as a consequence of multiple nucleation) of sectored outgrowths centered about the corners (efgh) as well as the midpoints (mnpq) along the sides of such a precursor lamella, as shown in figure 37a. In essence then figure 37a is intended to represent an early stage in the evolution of a multisectored lamella from a four-sectored precursor crystal. As pointed out earlier, we will assume in what follows that $d_{\{200\}f} > d_{\{200\}nf}$ and that the fractional difference ($\sim 10^{-3}$) between these interplanar spacings is independent of the crystallization conditions and is the same both in the fold domains of the precursor four-sectored crystal as well as in the constituent fold domains of the sectored outgrowths which develop therefrom. Accordingly, each tri- or tetra-sectored outgrowth shown in figure 37a may be considered to have a slight "conicalness" akin to that of the central four-sectored precursor. This conicalness is not centered however about the normal to the lamella at the pole (O) but, rather, about the corresponding surface normals at e, f, g, h, and m, n, p, q about which the outgrowths develop. As shown cross-sectionally in figure 37b this latter feature is envisaged to lead to a corresponding increase in the inclination of the peripheral regions of the developing lamella relative to the plane (kk) by an additional increment of $\theta°$ (this increment could be as large as $2\theta$ as is the case between opposite sectors in the four-sectored precursor). By analogy with the four-sectored precursor, this additional inclination is depicted in figure 37b as occurring close to the center of initiation of each outgrowth e.g., between (h) and (s) where (hs) is much smaller than (hr). Thus, the total inclination of the developing multisectored lamella relative to the reference plane (kk) on proceeding outwards from (O) to (r) along the surface of the crystal is envisaged in the model depicted in figure 37b to be $2\theta°$, i.e., an increase of $\theta°$ in the inclination of the growing lamella relative to the plane (kk) over that of the four-sectored precursor has resulted from the nucleation and development of the inherently nonplanar sectored outgrowth centered about the precursor's periphery at (h). The same argument applies to the other sectored outgrowths shown in figure 37a. It may be visualized that the nucleation and development of a new set of sectored outgrowths centered about the corners and sides of the previous ones shown in figure 37a will lead to a further inclination $\theta°$ of the lamella relative to the plane (kk) and hence, cumulatively, to a total inclination of $3\theta°$ of the surface of the lamella (and hence the orientation of the molecular stems) relative to the plane (kk) on proceeding from the pole (O) to the periphery of the newest sectored outgrowth, and so forth.

The thrust of this hypothetical representation of the development of a curved multisectored lamella of P4MP given above is that the evolving lamella grows in a curved fashion as a cumulative consequence of the combined effects of two factors namely, the intrinsic conicalness of about $\theta°$ (due to the asymmetric bulkiness of chain folds) of new sectored outgrowths which are generated intermittently at the periphery of the lamella during growth, and the frequency per unit path length from pole to periphery at which the new sectored outgrowths are formed. This latter feature determines according to the model depicted in figure 37b the number of small quasi-discreet inclinations of $\theta°$ which occur per unit path length along longitudinal paths traced from the pole of the monolayer to its periphery and thus governs the radius of curvature of the lamella. Conceptually then, for a constant conicalness of $\theta°$ in sectored outgrowths one would expect that the smaller the lateral dimensions which sectored outgrowths attain before new outgrowths develop therefrom in a multisectored lamella, the larger will be the number of inclinations of $\theta°$ per unit path length from pole to periphery, consequently the average radius of curvature of the lamella will be correspondingly smaller. We shall discuss, qualitatively the matter of sectored outgrowth sizes in curved crystals of P4MP formed at the different temperatures in relation to the curvature of the crystals in due course. Before doing so however it is pertinent to dwell first on two aspects of the multisectored mode of propagation of P4MP lamellae which have been omitted in the exposition of the model given above pertaining to why such lamellae are curved. These aspects have a bearing on this latter feature, and although their influence on the curvature of the lamellae is indeterminate their existence and possible roles in this connection must be raised in association with the hypothetical considerations which were advanced above.

First, it should be borne in mind that the growth of the lamellae in a multisectored fashion involving the intermittent development of new sectored outgrowths at its periphery entails the occurrence of distinct reentrant corners as depicted schematically in figure 38 (this feature is evident in the electron micrographs of the periphery of such lamellae shown in sections 3.2–3.4), as well as the accretion of chain molecules in folded conformation along the {100} facets which subtend such corners. This results in the generation of diagonal fold domain or sector boundaries which terminate at these corners. Such boundaries are depicted in figure 38 (arrows ↑). One would expect that the same disparity in spacing between the $\{200\}_f$ and the $\{200\}_{nf}$ planes due to the asymmetric bulkiness of the chain folds will occur across such boundaries as has been indicated earlier occurs across the fold domain boundaries which terminate at leading

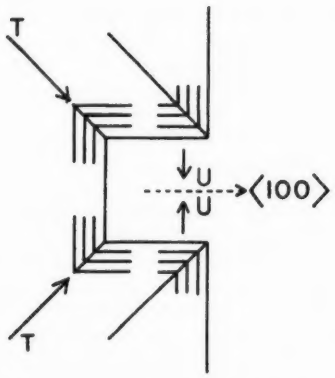


FIGURE 38. *Schematic representation of the generation of sector boundaries (T) which terminate at reentrant corners in a developing multisectored lamellae, as well as the generation of ⟨100⟩ sector boundaries (U) between impinging sectored outgrowths.*

corners in sectored outgrowths. The effect of the accommodation of the disparity in spacing between the $\{200\}_f$ and $\{200\}_{nf}$ planes along fold domain boundaries terminating at reentrant corners on the conicalness (angle $\theta°$) which it has been suggested sectored outgrowths intrinsically tend to adopt, remains indeterminate.

Second we have omitted in the preceding discussion to take into consideration the influence which the lateral impingement of adjoining sectored outgrowths may have on the manner of propagation of a multisectored lamella possessed, according to the conjectures advanced above, of an intrinsic tendency to develop in a cumulatively curved fashion due to the innate conicalness of the sectored outgrowths. In addition to imparting, cumulatively, curvature in a multisectored lamella, it may be envisaged that the intrinsic conicalness of sectored outgrowths causes imperfections in registry (see below) to occur between adjoining sectored outgrowths when they impinge as they propagate laterally, thus giving rise to the question of how these additional imperfections influence in turn the mode of propagation of the lamella. We shall consider and discuss this matter below following a brief indication of the nature of these imperfections.

The impingement of neighboring sectored outgrowths as they propagate laterally at the periphery of a developing multisectored lamella gives rise to the occurrence of ⟨100⟩ boundaries between impinging domains in the lamella as indicated schematically in figure 38 (boundary denoted U). Because of the inherent conicalness of the sectored outgrowths as well as the resulting cumulatively curved character which this feature imparts to the developing lamella it can be expected that impinging fold-domains belonging to adjoining sectored outgrowths will not always be in crystallographic registry and that slight misorientations, as well as disinclinations of the impinging {100} facets relative to one another, will occur. We shall, henceforth, refer to such imperfections as "imperfections in crystallographic registry." Another likely type of situation which also can be expected to arise is the occurrence, in association with the aforementioned imperfections in crystallographic registry, of differences in height between neighboring sectored outgrowths relative to one another along a direction normal to the surface of the crystal. The consequence of such relative displacements is that when the sectored outgrowths impinge, steps are created at the upper and lower surfaces of the lamella. We shall henceforth refer to such situations which simulate a shearing of the lamella at right angles to its surface corresponding in effect to the generation of a screw-dislocation, as "imperfections in height registry" between impinging domains, with the understanding that such imperfections in height registry also involve imperfect crystallographic registry between the impinging {100} facets involved.

The following considerations may be raised concerning the possible influence of the aforementioned imperfections in registry at ⟨100⟩ boundaries between impinging sectored outgrowths upon the curvature of a multi-sectored lamella. It may be envisaged that the accommodation of imperfections in crystallographic registry at the periphery of a developing multisectored lamella gives rise to localized internal stresses which could possibly entail a modification of the innately buckled character of the constituent fold domains in adjoining sectored outgrowths when these outgrowths impinge as they propagate laterally. The gist of this consideration is that imperfections in crystallographic registry, of the type indicated above, could have a modifying influence on the innate conicalness of sectored outgrowths thus leading effectively to either increases or decreases in their angle of inclination $\theta$ by say $d\theta$. The resulting "radius of curvature" of a particular multisectored lamella would accordingly be expected to be: (a) smaller, (b) larger, or (c) essentially unaffected, relative to what the radius would be in the absence of any modifying influence due to outgrowth impingement, depending respectively on whether this latter feature always leads (a) to an effective average increase to $(\theta+d\theta)$, or (b) to an effective average decrease to $(\theta-d\theta)$, in the angle of inclination of sectored outgrowths relative to their innate angle $\theta$, or (c) to the occurrence with equal probability of increases and decreases in angle of inclination relative to $\theta$ in which case $d\theta$ would be effectively zero. The same considerations also apply to imperfections in height registry.

Whether the curvature of multisectored lamellae is influenced to any appreciable extent, if at all, by the two types of imperfections indicated above, namely imperfections in crystallographic and height registry at ⟨100⟩ boundaries between impinging sectored outgrowths, is an open question.

In summary then, the main features of the discussion presented so far on the origins of the curature of P4MP crystals are: Conjectures were first advanced to the effect that: (i) a multisectored lamella develops in a curved fashion as a consequence of the cumulative influence of one type of imperfection, namely the intrinsically slightly conical nature (due to the bulkiness of chain folds which lead to a disparity in spacing



459-033 OL - 72 - 5

between $\{200\}_f$ and $\{200\}_{nf}$ planes) of sectored outgrowths which develop in successive arrays at its periphery during growth, and (ii) that the curvature of the lamella will vary depending on the frequency per unit path length, from its pole to its periphery, of the development of new sectored outgrowths each of which contributes incrementally to its overall curvature. An indication was then given of some additional imperfections which can be envisioned to arise in the multisectored lamella during the process of growth. The possible modifying influence which these additional imperfections might have on the curvature which the lamella derives in the first instance from the intrinsic conicalness of sectored outgrowths were indicated but are indeterminate.

Before discussing the observed variation of the curvature of multisectored lamellar crystals of P4MP with crystallization temperature in the light of the synthesis embodied in the hypothetical model represented schematically in figure 37, it is appropriate to digress at this juncture and to dwell briefly on a feature which all the perceptibly curved multisectored crystals of P4MP exhibit in common, namely they are all multilayered, i.e., they all consist of two or more superposed chain-folded layers. On the basis of the aforementioned model this latter feature may be attributed in the first instance to the incidence of imperfections in height registry between impinging sectored outgrowths at the periphery of their leading multisectored lamella throughout growth [18]. The likelihood of the occurence at the periphery of a growing curved multisectored lamella of such imperfections which simulate in effect screw dislocations has been pointed out above. In short, the steps which are envisioned to be generated at the upper and lower surfaces of such a multisectored lamella at its periphery during growth act as sources for the development of additional chain-folded multisectored layers.

A consideration of the electron micrographs of the large curved multisectored lamellar crystals formed at 90 °C and the crystals formed at 80 °C clearly reveals that new chain-folded terraces are generated at the periphery of the leading (basal) lamella throughout its growth (see for example figs. 7, 13, 14). In addition examination of the periphery of such crystals (see for example the higher magnification electron micrographs shown in fig. 10 and fig. 16) shows that, as is common in polymer crystal growth, the propagation of new chain-folded layers or terraces from the leading lamella involves a relative displacement during growth of adjoining peripheral portions of that lamella relative to one another at right angles to the surface of the lamella through a distance equal to the thickness of the lamella. These additional terraces in such crystals of P4MP do not exhibit a propensity for continuing to grow in a spiral-like fashion resulting in the development of several superimposed layers centered about the screw dislocation-like imperfection. It appears rather, judging from the electron micrographs, that the formation of the numerous superimposed terraces in these crystals is contributed to in large measure by the generation of new curved terraces at the periphery of each additional curved multisectored terrace which develops during the growth of the crystal, due to the incidence of imperfections in height registry between impinging sectored outgrowths at the periphery of each terrace as is the case in the leading (basal) lamella. Furthermore, similar terrace initiating imperfections in height registry probably occur as a result of imperfect height registry between neighboring terraces when they impinge laterally.

In addition to the aspects of the multilayered character of the 90 °C and 80 °C curved crystals discussed above, it should be pointed out that healing, i.e., a return in height registry between overlapping terraces (as would result from two dislocation-like defects of opposite hand [18a]), also occurs at the periphery of these crystals. Whether such healing is a consequence of internal stress buildup resulting from the initial imperfections in height registry, which give rise to the generation of the additional terraces or whether it is primarily a statistical feature associated with the formation of successive arrays of new sectored outgrowths at the periphery of multisectored lamella, remains an open question.

Although the hollow bowl shaped crystals formed at 70 and 50 °C do not lend themselves to as detailed an examination as the curved crystals formed at 90 and 80 °C insofar as their multilayered character is concerned, available evidence indicates that their development in a multilayered fashion is similar to that of the crystals formed at higher temperatures. The fact that the hollow-bowl shaped crystals formed at 50 °C consist of fewer superimposed chain-folded layers than those formed at 70 °C is most probably an effect of polymer depletion from solution associated with the formation of a relatively larger number of simultaneously growing crystals at 50 than at 70 °C.

Returning to the matter of the variation of the curvature of P4MP crystals with crystallization temperature, we refer back to the hypothetical model depicted in figure 37. The explanation which is embodied in that model of the curvature of a multisectored chain folded monolayer may be readily considered to apply to each constituent multisectored lamellar terrace in a multilayered crystal. Accordingly, on the basis of that model, in which it is assumed that sectored outgrowths possess an intrinsic conicalness $\theta°$, the overall curvature of a multilayered crystal will still depend on the frequency, per unit longitudinal path length, at which new sectored outgrowths are formed at the periphery of its leading lamella during growth. The higher that frequency the larger the number of incremental inclinations of $\theta°$ per unit path length and hence the smaller will be the radius of curvature of the multilayered crystal. Furthermore the higher that frequency the smaller will be the average lateral dimensions attained by sectored outgrowths before new ones develop therefrom, and hence the smaller will be the lateral extent of individual fold domains in the constituent chain-folded layers in the crystal.

Qualitatively, a consideration of the periphery of the basal lamella in the crystals formed at different temperatures indicates that sectored outgrowths tend to be smaller the lower the temperature at which the

crystals are formed. This may be judged, for example, from a comparison of the peripheral regions in the basal lamella in the large curved crystals formed at 90 °C, such as shown in figures 9 and 10, and that portion of the periphery of the basal lamella in the collapsed crystal grown in a 50 °C preparation which is shown in figure 29 (region pointed to by arrow). Taking the sizes of leading {100} microfacets (i.e., microfacets facing outwards as distinct from reentrant microfacets) as a rough indication of the lateral dimensions of sectored outgrowth which develop in successive arrays at the periphery of the lamellae in these crystals, it may be seen that the larger leading {100} microfacets in figures 9 and 10 are ~0.5 $\mu$m to 1 $\mu$m long, whereas the leading {100} microfacets in the peripheral region pointed to in the crystal shown in figure 29 are not larger than 0.2 $\mu$m long.[6] There are, however, substantial uncertainties involved in: (a) attempting to derive—from an examination of the topography of the lateral edges of the multisectored lamellae formed at the different temperatures—a rigorous quantitative measure of the lateral dimensions which sectored outgrowths *attain*[7] on average before new ones develop therefrom and before they impinge laterally with nearest neighbors,[8] and (b) estimating the radii of curvature of the large distinctly dished crystals formed at 90 °C as well as the dished crystals formed at 80 °C from their edge-on profiles. These uncertainties impede a fruitful quantitative analysis of the relationship between the curvature of the crystals formed at different temperatures and the multisectored character of their constituent lamellae. Such an analysis would provide a more rigorous verification of the hypothetical model (depicted in fig. 37) which has been advanced above and used as a basis for explaining the observed increasingly curved character which P4MP crystals exhibit the lower the crystallization temperature. Alternatively, such an analysis could shed some tangible indications of additional factors, not considered so far, which it may be envisaged could possibly contribute to the increased curvature of the crystals the lower the temperature at which they are formed. Some such factors are indicated below.

We have assumed in our discussion so far that the disparity (attributed to the asymmetric bulkiness of chain folds) in spacing between the $\{200\}_f$ planes and the $\{200\}_{nf}$ planes in the sectored outgrowths which develop in successive arrays at the periphery of multisectored lamellae does not vary with crystallization temperature and that the intrinsic conicalness (angle of inclination $\theta°$) which sectored outgrowths adopt is the same at all temperatures. The possibility must be considered that the fractional disparity in spacing between the $\{200\}_f$ and the $\{200\}_{nf}$ planes, which as determined by Bassett [9] is about $10^{-3}$ in four-sectored lamellae, may differ intrinsically from this value depending on the crystallization conditions. Thus, it may be envisaged that at low crystallization temperatures, which lead to the formation of multisectored lamellae and which favor a more rapid folding of the chain molecules along their periphery during growth the lower the temperature, the folds may tend to be less regular and hence have bulkier conformations (giving rise correspondingly to larger differences between $d_{\{200\}f}$ and $d_{\{200\}nf}$) causing the sectored outgrowths to be intrinsically more pronouncedly buckled. In other words, the intrinsic conicalness of the sectored outgrowths could conceivably tend to be larger the lower the crystallization temperature. In short, in terms of the hypothetical model depicted in figure 37, it may be envisaged that multisectored lamellae will be more pronouncedly curved the lower the crystallization temperature not only, as discussed earlier, because of the larger frequency at which new sectored outgrowths are formed and corresponding incremental inclinations of $\theta°$ occur per unit path length from pole to periphery, but also because these incremental inclinations may tend to be intrinsically larger the lower the crystallization temperature. To this consideration must be added the possibility that even for a constant fold conformation the buckling of sectored outgrowths may tend to be enhanced in some degree at lower crystallization temperatures due to the thinner character of the lamellae.

In view of the multiplicity of factors such as those indicated in the previous paragraph as well as those pointed out in the earlier discussion of the hypothetical model depicted in figure 37 (e.g., the occurrence and effect of imperfections in lateral and height registry on the intrinsic conicalness of impinging sectored outgrowths) which it may be envisaged could contribute to the curvature of the multisectored lamellar crystals of P4MP formed at different temperatures but whose roles in this connection are quantitatively indeterminate at present, the simple qualitative explanation of the observed variation of the curvature of P4MP crystals with crystallization temperature which was advanced earlier in this subsection (4.3) with reference to figure 37 remains speculative at this stage as do the assumptions and conjectures on which it is based. To recapitulate briefly, these assumptions and conjectures are: (i) The primary souce of the curvature of a multisectored lamella of P4MP is an intrinsic conicalness (angle of inclination $\theta°$ of the order of 2°) in the sectored outgrowths which develop in successive arrays at its periphery; (ii) the intrinsic conicalness in sectored outgrowths is a consequence of buckling under the influence of the bulkiness of the chain folds which leads to a fractional difference of $10^{-3}$ [9] between $d_{\{200\}f}$ and $d_{\{200\}nf}$ in their constituent folds domains; (iii) the overall curvature of a multisectored lamella is a *cumulative* consequence of the intrinsic conicalness of the sectored outgrowths which develop in successive arrays at its periphery

[6] It may be noted that, taking the roughly estimated radius of curvature of the larger curved crystals formed at 90 °C as being 35 $\mu$m it can be calculated that incremental inclinations, assumed to be $\theta = 2°$, along longitudinal paths from pole to periphery would occur at intervals (representing the lateral dimensions of sectored outgrowths) of about 1.2 $\mu$m, whereas in the case of the crystals formed at 50 °C whose observed radii vary between 2.5 $\mu$m and 5 $\mu$m the corresponding intervals would be about 0.09 $\mu$m and 0.17 $\mu$m, respectively.

[7] As distinct from the dimensions they exhibit in the process of development to full size.

[8] It is evident from a consideration of the electron micrographs, e.g., figures 9, 10, 16, that there are substantial variations in the sizes of both leading and reentrant {100} microfacets at the periphery of the multisectored lamellae.

and is governed by the frequency per unit path length from pole to periphery at which new sectored outgrowths are generated during the growth of the lamella, the higher that frequency the smaller the radius of curvature of the lamella. These assumptions and conjectures serve in themselves to set off the complexities which underlie the quantitative elucidation of the phenomenon described in this paper and provide thereby a foundation for the further study of its origins.

---

The authors wish to express their gratitude to R. K. Eby, E. Passaglia, and D. H. Reneker for their encouragement as well as for the benefit of helpful discussions during the course of this work.

## 5. References and Notes

[1] Barnes. J. D., and Khoury. F., Bull. Am. Phys. Soc. **10,** 366 (1965); HG3. HG4. ibid. **11,** 248 (1966); FA10. FA11. ibid **12,** 385 (1967). GD2.
[2] Frank. F. C., Keller. A., and O'Connor. A., Phil. Mag. **4,** 200 (1959).
[3] Bassi. I. W., Bonsignori. O., Lorenzi. G. P., Pino. P., Corradini. P., and Temussi. P. A., J. Polym. Sci. A2. **9,** 193 (1971).
[4] Tanda. Y., Kawasaki. N., Imada. K., and Takayanagi. M., Rept. Progr. Polymer Phys. Japan **9,** 165 (1966).
[5] Tanda. Y., Imada. K., and Takayanagi. M., Kogyo Kagaku Zasshi **69,** 1971 (1966).
[6] Kawasaki. N., and Takayanagi. M., Rept. Progr. Polymer Phys. Japan **10,** 337 (1967).
[7] Takayanagi. M., and Kawasaki. N., J. Macromol. Sci. **B1,** 741 (1967).
[8] Nakajima. A., Hayashi. S., Taka. T., and Utsumi. N., Kolloid-zschr. Z. Polymere **234,** 1097 (1969).
[9] Bassett. D. C., Phil. Mag. Ser. VIII. **10,** 595 (1964).
[10] Bassett. D. C., Dammont. F. R., and Salovey. R., Polymer Lond. **5,** 579 (1964).
[11] Woodward. A. E., Polymer Lond. **5,** 293 (1964).
[12] Hiltz. A. A., private communication.
[13] Hoffman. A. S., Fries. B. A., and Condit. P. C., J. Polymer Sci. Pt. C., No. 4. 109 (1964).
[14] Bassett. D. C., and Keller. A., Phil. Mag. **7,** 1553 (1962).
[15] Blundell. D. J., Keller. A., and Kovacs. A. J., J. Polymer Sci. **B4,** 481 (1966).
[16] Sadler. D. M., J. Polymer Sci. A2. **9,** 779 (1971).
[17] It should be noted that the occurrence of stresses at the fold surfaces of chain-folded lamellae due to steric interactions between neighboring folds has been previously invoked in a suggested explanation of the incidence of twist in the constituent radiating lamellae in polyethylene spherulites. J. D. Hoffman and J. L. Lauritzen, Jr., J. Res. Nat. Bur. Stand. (U.S.), **65A (Phys. and Chem.),** No. 4, 297–336 (1961).
[18] The generation of new terraces resulting from either built-in or accidental displacements in height registry between adjoining portions at the periphery of multisectored chain-folded lamellae is a common feature in polymer crystal growth e.g., see (a) Reneker. D. H., and Geil. P. H., J. Appl. Phys. **31,** 1916 (1960); (b) Bassett, D. C., and Keller, A., Phil. Mag. **7,** 1553 (1962); (c) Keith. H. D., J. Appl. Phys. **35,** 3115 (1964).

(Paper 76A3–719)

JOURNAL OF RESEARCH of the National Bureau of Standards—A. Physics and Chemistry
Vol. 76A, No. 3, May–June 1972

# Photoionization of Propylene, Cyclopropane, and Ethylene. The Effect of Internal Energy on the Bimolecular Reactions of $C_2H_4^+$ and $C_3H_6^+$*

**L. W. Sieck and P. Ausloos**

**Institute for Materials Research, National Bureau of Standards, Washington, D.C. 20234**

**(October 13, 1971)**

The ion-molecule chemistry occurring in photoionized ethylene, propylene and cyclopropane has been investigated in the NBS high pressure mass spectrometer. Emphasis has been placed on determining the overall effect of internal excitation on the absolute rate coefficients for the various reactions. This was accomplished by comparing the behavior found when ionization was induced by photon absorption at the ionization threshold with that found at higher photon energies. The values for the absolute rate coefficients for the formation of excited compound ions at various photon energies were as follows (units of $10^{-10}$ cm$^3$/molecule · s); $C_2H_4^+$, 9.6 (10.6 eV photons); 8.5 (11.7 eV photons); $C_3H_6^+$, 8.4 (10.0 eV photons); 6.8 (11.7 eV photons); $C_3D_6^+$, 7.8 (10.0 eV photons), 6.1 (11.7 eV photons); *c*-$C_3H_6^+$ and *c*-$C_3D_6^+$, 2.2 (10.0 eV photons); 2.2 (11.7 eV photons). The distributions of product ions obtained from the unimolecular decomposition of the compound ion in each system have also been determined at various photon energies, and considerable variation has been observed. In general, the variations are similar to those found elsewhere when the kinetic energy of the reactant ion is increased. The bimolecular reactions of the $C_6D_{12}^+$ compound ion obtained from $C_3D_6^+$ have been investigated at higher pressures, and separate experiments involving isotopically labeled ethylenes have provided new information concerning the nature of the compound ion in that system. Results obtained from other laboratories are discussed in some detail, and in most cases the differences found for the same system are explicable in terms of the energy content (internal and/or kinetic) of the reactant ion.

Key words: Collisional stabilization; hydrocarbons; ion-molecule reactions; photoionization; rate constants; structures of ions.

## 1. Introduction

Although a great deal of information has been accumulated concerning the effect of ion kinetic energy on the rates and mechanisms of ion-molecule reactions [1],[1] the effects of internal energy remain relatively unexplored. However, several recent investigations [2] of proton transfer reactions occurring in inorganic systems using high resolution photoionization mass spectrometry have demonstrated that the cross sections for certain processes may be extremely sensitive to changes in the vibrational energy content of the reactant ion. This behavior was quantitatively investigated in a recent study from this laboratory [3], which involved a determination of the absolute rate coefficient for the reaction $NH_3^+ + NH_3 \rightarrow NH_4^+ + NH_2$ as a function of internal energy, including $v' = 0$ of $NH_3^+$ as a standard. Investigations of this type have also been extended to a few complex organic systems using variable energy electron impact ionization coupled with Ion Cyclotron Resonance (ICR) mass spectrometry [4], but only relative rate coefficients have been determined. This article describes a mass spectrometric investigation of the ion-molecule reactions occurring in ethylene, propylene, and cyclopropane under conditions of thermal kinetic energy using the photoionization technique to produce primary ions. Although these systems have been subjected to considerable study in other laboratories by electron impact mass spectrometry [4–29], the internal energy content of the reacting ions has always been indeterminate due to the electron energy spread (when low energy electrons were used) and the fact that, in may cases, ionization was induced by 100–200 eV electron bombardment. In the present study ionization was induced by photoabsorption at energies only slightly in excess of the ionization threshold; propylene, I.P. = 9.72 eV (10.0 eV photons); cyclopropane, I.P. = 10.09 eV (hot band ionization with 10.0 eV photons); and ethylene, I.P. = 10.48 (10.6 eV photons) [30]. Analogous experiments were also carried out at using 11.7 eV photons in order to specify the effect of internal excitation. Such absolute rate coefficient determinations are particularly important since they provide the only reasonable basis for standardizing the results

*This research was supported by the U.S. Atomic Energy Commission.

[1] Figures in brackets indicate the literature references at the end of the paper.

obtained in other laboratories for the same systems. Some additional experiments were performed at elevated pressures both in the mass spectrometer and in closed systems in order to elucidate certain aspects of the effect of density on the reaction mechanism and to provide information concerning the structures of certain product ions.

## 2. Experimental Procedure

All experiments were carried out using the NBS high pressure photoionization mass spectrometer described in detail elsewhere [31]. The results presented here involve the interactions of thermal ions with a kinetic energy distribution corresponding to kT at 295 K. The techniques involved in deriving rate coefficients and other kinetic parameters have also been discussed elsewhere [31]. Ionization was induced via photolysis with 123.6 nm (10.0 eV), 116.5 nm (10.6 eV) and 106.7–104.8 nm (average energy of 11.7 eV) photons, henceforth referred to as 10.0, 10.6, and 11.7 eV.

## 3. Results

### 3.1. Propylene

Fragmentation of $C_3H_6^+$ was not observed at either 10.0 or 11.7 eV. The relative probabilities (given as percentages) for production of $C_3H_7^+$, $C_4H_7^+$, $C_4H_8^+$, and $C_5H_9^+$ via the overall process:

$$C_3H_6^+ + C_3H_6 \rightarrow C_6H_{12}^{+*} \rightarrow \text{products other than}^2\ C_3H_6^+ \quad (1)$$

at the two energies are given in table 1. The relative probabilities for production of the various ions were found to be essentially independent of pressure up to approximately 1.5 millitorr, at which point ca. 50 percent of the $C_3H_6^+$ had reacted. The branching ratios could not be precisely determined at higher pressures due to consecutive reactions.

The decay curves found for $C_3D_6^+$ at the two energies are given in figure 1. Absolute rate coefficients for the production of products other than $C_3H_6^+$, have been derived under conditions where nonreactive scattering of ions is negligible (initial slopes) and are given in table 1. Analogous data has been obtained for the $C_3D_6^+$–$C_3D_6$ reaction pair. The observed branching ratios and rate coefficients are given in tables 1 and 2, respectively.

Experiments at 10.0 eV were also carried out at pressures up to approximately 0.1 torr in both $C_3H_6$ and $C_3D_6$. The variation in the product ion mass spectrum for some major ions from $C_3D_6$ is given in figure 2.

TABLE 1. *Percentage yields in the overall reaction*

$C_3H_6^+$ (from propylene) + $C_3H_6$ → products other than $C_3H_6^+$

| Product ion | 10.0 eV [a] | 11.7 eV [a] | Zero field [b] | ICR [c] | Ref. [16] | Ref. [15] | Ref. [12] |
|---|---|---|---|---|---|---|---|
| $C_3H_7^+$ | 12 | 20 | 21 | 19 | 23 | 27 | 29 |
| $C_4H_7^+$ | 7 | 10 | 11 | 12 | 12 | 18 | 26 |
| $C_4H_8^+$ | 46 | 35 | 42 | 42 | 40 | 34 | 22 |
| $C_5H_9^+$ | 35 | 30 | 26 | 27 | 25 | 21 | 15 |
| Σ other | < 3 | < 4 | | | | | |

$C_3D_6^+ + C_3D_6$ → products other than $C_3D_6^+$

| Product ion | 10.0 eV | 11.7 eV | Ref. [9] |
|---|---|---|---|
| $C_3D_7^+$ | 6.5 ± 0.5 | 11.5 | 17.5 |
| $C_4D_7^+$ | < 1.0 | 8.6 | 14.8 |
| $C_4D_8^+$ | 52 | 44 | 43 |
| $C_5D_9^+$ | 35 | 31 | 24.7 |
| $C_6D_{12}^+$ | 5.0 ± 0.5 | 3.2 ± 0.3 | 0 |

[a] Present work.
[b] Reference [17].
[c] Average values taken from references [17] and [7].

TABLE 2. *Rate coefficients* [a] *for disappearance of primary ions*

| Reaction pair | 10.0 eV [b] | 11.7 eV [b] | Flash [c] | Electron impact |
|---|---|---|---|---|
| Ethylene | 9.6 ± 0.2 | 8.5 ± 0.2 | 7.3 | [d] 8.3 |
| Propylene | 8.4 ± 0.4 | 6.8 ± 0.3 | 7.9 | [e] 7.6 |
| Propylene-$d_6$ | 7.8 ± 0.4 | 6.1 ± 0.3 | ..... | [e] 6.3 |
| Cyclopropane | 2.2 ± 0.2 | 2.2 ± 0.2 | 11.4 | [e] 1.5, [f] 2.0, [f] 2.1 |

[a] $cm^3$/molecule · s × $10^{10}$.
[b] This work, estimated accuracy better than 7 percent, ethylene values at 10.6 and 11.7 eV.
[c] Flash photoionization, reference [8].
[d] Reference [19].
[e] Reference [9].
[f] Reference [36].

### 3.2. Cyclpropane

Ion-molecule interactions occurring in cyclopropane were investigated using 10.6 and 11.7 eV photons in both *c*-$C_3H_6$ and *c*-$C_3D_6$. Photoionization of *c*-$C_3H_6$ at 11.7 eV yields 16 percent $C_3H_5^+$, while the extent of fragmentation in *c*-$C_3D_6$ is ~ 2 percent. The decay curves found for *c*-$C_3D_6^+$ at the two energies are given in figure 2, and the associated product ions are given in table 3. Rate coefficients for the overall conversion of $C_3H_6^+$ ($C_3D_6^+$) to products other than $C_3H_6^+$ ($C_3D_6^+$) are given in table 2.

### 3.3. Ethylene

Photolysis of $C_2H_4$, CHD=CHD, $CH_2CD_2$, and $C_2H_4$—$C_2D_4$ mixtures were carried out at both 10.6

[2] The terminology "products other than – – – –" will be used extensively in this article and is intended to denote those chemical products which are distinguishable from the parent ion in the mass spectrometer; i.e., have a different *m/e* (mass to charge ratio). A chemical process in which hydrogens are exchanged, for example, cannot be detected without the use of isotopically labeled molecules since the products will still be $C_3H_6^+$ and $C_3H_6$ in photoionized $C_3H_6$. In addition, charge exchange reactions are not detected in like systems, although they may constitute a major reaction channel. Consequently, the rate coefficients derived for reactions of $C_3H_6^+$, $C_3H_7^+$, etc. in the pure system reflect only the rate of disappearance of the respective parent ions, and do not include contributions to the total reactivity which may be associated with hydrogen exchange or charge transfer.

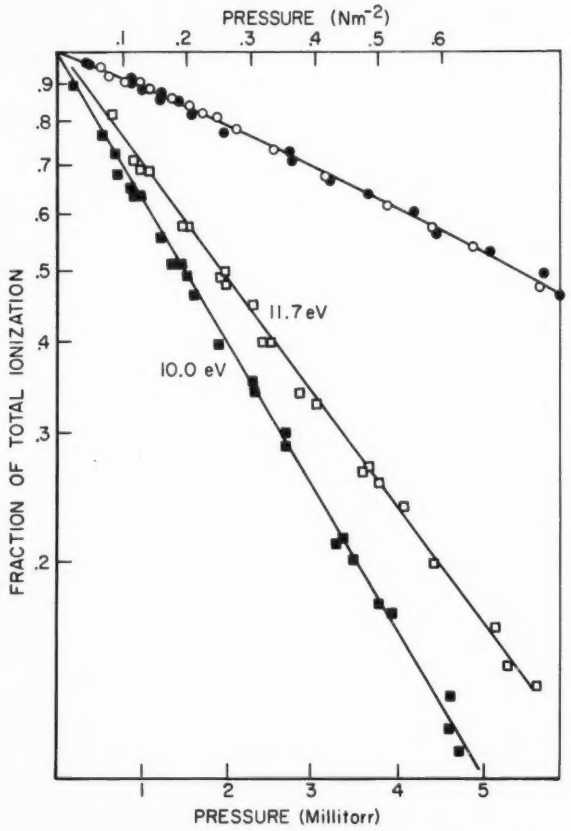


FIGURE 1. *Decay curves for $C_3D_6^+$ from propylene-$d_6$ (□ – 11.7 eV; ■ – 10.0 eV) and c-$C_3D_6$ (○ – 11.7 eV; ● – 10.0 eV) following photoionization at 10.0 and 11.7 eV.*

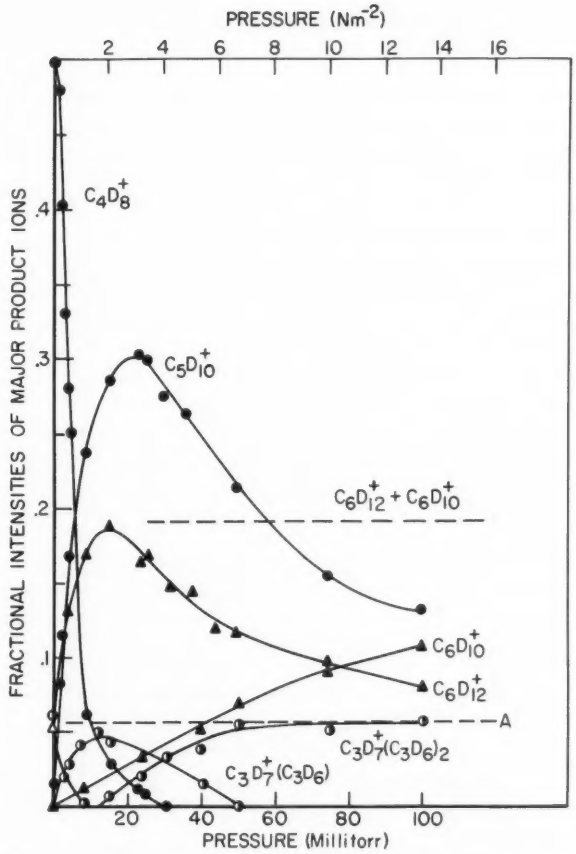


FIGURE 2. *The fractional intensities of some major product ions resulting from the photoionization of $C_3D_6$ at 10.0 eV versus pressure.*

Line A represents $\Sigma\, C_3D_7^+ + C_3D_7^+(C_3D_6) + C_3D_7^+(C_3D_6)_2$.

TABLE 3. *Percentage yields in the overall reaction*

$C_3H_6^+$ (from cyclopropane) + cyclopropane → products other than $C_3H_6^+$

| Product ion | eV [a] | | | ICR [d] | Flash [e] | Zero field [d] | Trapped ion [f] |
|---|---|---|---|---|---|---|---|
| | 10.0 [b] | 10.0 [c] | 11.7 [c] | | | | |
| $C_3H_7^+$ | 4 | 4 | 8 | 7 | 4 | 8 | 12 |
| $C_4H_7^+$ | 9 | 12 | 15 | 17 | 24 | 13 | 13 |
| $C_4H_8^+$ | 75 | 73 | 69 | 68 | 47 | 75 | 66 |
| $C_5H_9^+$ | 12 | 11 | 8 | 9 | 9 | 4 | 5 |
| $C_3H_5^+$ | 0 | 0 | 0 | 0 | 9 | 0 | 4 |
| $C_3H_4^+ + C_3H_3^+$ | 0 | 0 | 0 | 0 | 7 | 0 | 0 |

[a] Present work.
[b] *c*-$C_3H_6$.
[c] *c*-$C_3D_6$.
[d] Reference [17].
[e] Reference [8].
[f] Reference [36].

and 11.7 eV. The decay curves found in photoionized $C_2H_4$ are displayed in figure 3, and the associated rate coefficients for the reaction:

$$C_2H_4^+ + C_2H_4 \rightarrow \text{products other than } C_2H_4^+ \qquad (2)$$

are given in table 2. The secondary ion distribution is given in table 4.

### a. Ethylene-$d_2$

The isotopic composition of the $C_3(H,D)_5^+$ ions from *cis*-1,2 dideuteroethylene (isotopic impurity 5.82% $C_2H_3D$) and 1,1 dideuteroethylene (isotopic impurity 2.46% $C_2H_3D$) were also determined. We found that the observed distribution of the $C_3(H,D)_5^+$ ions from both analogs exhibited subtle changes as a function of chamber pressure, although the respective distributions were essentially invariant at very low pressures where the probability for collision of initially produced $C_3^+$ ions with $C_2H_2D_2$ was negligibly small. The isotopic distributions of the $C_3(H,D)_5^+$

ions obtained from the two analogs under conditions where only 2–5 percent of the parent ions had reacted are given in table 4. Also included for comparison is the distribution obtained with CHD=CHD under conditions where the fractional intensity of $C_2H_2D_2^+$ constituted 10 percent of the composite mass spectrum (90% reacted).

TABLE 4. *Ethylene*

Isotopic composition of $C_3X_5^+$ products from labeled ethylenes [a]

| Molecule | Photon energy | $-CH_3$ | $-CH_2D$ | $-CD_2H$ | $-CD_3$ | *m/e* 41 |
|---|---|---|---|---|---|---|
| *cis*-CHDCHD | 10.6 | 8.34 | 37.78 | 40.57 | 11.97 | 1.35 |
| *cis*-CHDCHD | 11.7 | 8.30 | 39.39 | 39.80 | 11.25 | 1.27 |
| $CH_2CD_2$ | 10.6 | 8.34 | 38.65 | 41.18 | 10.87 | 0.98 |
| $CH_2CD_2$ | 11.7 | 8.67 | 39.43 | 40.87 | 10.12 | 0.91 |
| $CH_2CD_2$ [b] | ($e^-$) | 8.23 | 40.7 | 41.1 | 9.88 | n.d. |
| *cis*-CHDCHD [c] | 11.7 | 8.42 | 39.06 | 38.49 | 12.02 | 2.01 |

Product yields [d] obtained from the overall sequence $C_2H_4^+ + C_2H_4 \rightarrow$ Products Other Than $C_2H_4^+$

| Photon energy | $C_3H_4^+$ | $C_3H_5^+$ | $C_3H_6^+$ | $C_4H_7^+$ | $C_2H_5^+$ |
|---|---|---|---|---|---|
| 10.6 | 5.6 | 80.0 | 0.8 | 13.7 | 0.00 |
| 11.7 | 4.4 | 85.0 | 0.9 | 9.8 | $\leq 0.4$ |

[a] Collected for $C_{13}$ contributions, but includes $C_3X_4^+$ where x = H or D. Values given as percentage yields.

[b] Taken from reference [22].

[c] Yields of 90 percent conversion, this work.

[d] As percent of secondary ion mass spectrum, conversions $\leq 2$ percent.

#### b. $C_2H_4$–$C_2D_4$ Mixtures

Equimolar mixtures of $C_2H_4$ and $C_2D_4$ (5.58% $C_2D_3H$) were investigated at 11.7 eV in order to determine the contribution from exchange reactions such as $C_2D_4^+ + C_2H_4 \rightarrow C_2D_3H^+$, etc. It was found that the total probability for formation of $C_2D_3H^+$, $C_2H_2D_2^+$, and $C_2H_3D^+$ was 1.1 percent of the total probability for production of $C_3^+$ and $C_4^+$ ions. Since only ~ 50 percent of the collisions are between perdeuterated and perprotonated reactants, the total probability for exchange is 0.022 assuming no isotope effects and making no corrections for collision frequency due to differences in the thermal velocities of $C_2H_4^+(C_2H_4)$ and $C_2D_4^+(C_2D_4)$ at 300 K. The isotopic distribution obtained for the exchanged products, after correcting for the $C_2D_3H$ impurity, was as follows; $C_2D_3H^+$, 0.3; $C_2D_2H_2^+$, 0.5; and $C_2H_3D^+$, 0.2. It was not possible to investigate such processes quantitatively at 10.6 eV due to the fact that the total ion signal at this energy was approximately a factor of 20 lower than that associated with the photoionization of ethylene at 11.7 eV.

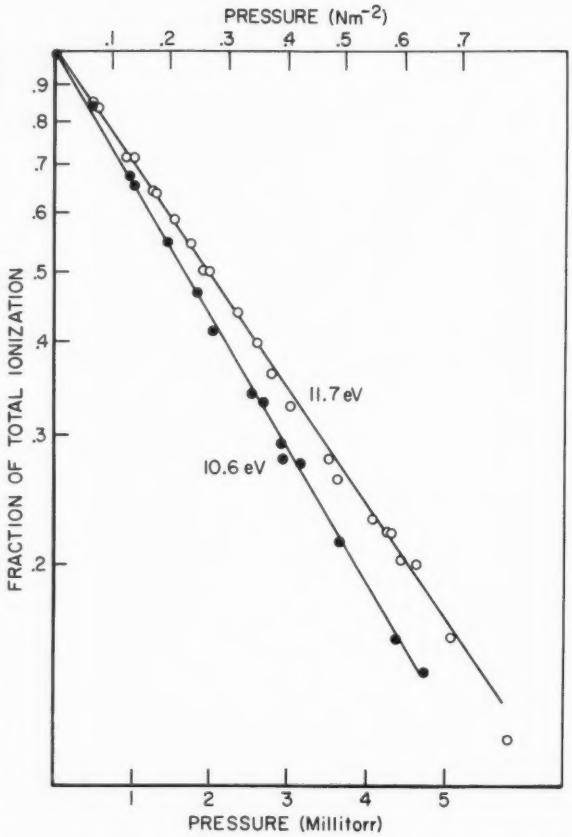


FIGURE 3. *Decay curves for $C_2H_4^+$ following photoionization of $C_2H_4$ at 10.6 and 11.7 eV.*

The relative rate coefficients for reaction of $C_2D_4^+$ and $C_2H_4^+$ in a $C_2H_4$–$C_2D_4$ mixture containing 1 percent $C_2D_4$ were also determined at 11.7 eV. It was found that the reaction:

$$C_2D_4^+ + C_2H_4 \rightarrow \text{products other than } C_2D_4^+ \quad (3)$$

is approximately 7 percent faster than the rate of removal of $C_2H_4^+$ in such mixtures. Analogous experiments with dilute mixtures of $C_2H_4$ and $C_2D_4$ gave a similar result; i.e., the conversion of $C_2H_4^+$ to products other than $C_2H_4^+$ is approximately 8 percent faster in $C_2D_4$ than in $C_2H_4$. The difference in residence times between $C_2H_4^+$ and $C_2D_4^+$ was taken into account in determining these values.

## 4. Discussion

### 4.1. Propylene

The overall reaction of $C_3H_6^+$ with $C_3H_6$ has probably been subjected to more scrutiny by mass spectrometry in various laboratories [4–18] than any

other reaction involving complex olefinic ions. When the collision frequency is sufficiently low to preclude stabilization of $C_6H_{12}^+$ compound ion produced via process (1), there is general agreement that the unimolecular decomposition of the complex leads to the formation of $C_3H_7^+$, $C_4H_7^+$, $C_4H_8^+$, and $C_5H_9^+$ as the major ions. Other studies [15] have provided detailed information concerning the nature of the intermediate ion and the associated unimolecular fragmentation processes. As pointed out in the introduction, the purpose of the present study was to determine the overall mechanistic effect, if any, of changes in the internal energy content of the reactant ions and to search for additional reaction paths for the molecular ion at elevated pressures which may have escaped the attention of previous investigators.

#### a. Effect of Energy

The branching ratios obtained in the present study at the two energies are compared with representative data obtained by electron impact ionization in table 1. The citations for the Zero Field and ICR techniques (ICR citations are average values taken from several laboratories), reflect the interactions of $C_3H_6^+$ ions which are essentially thermal. The other electron impact entries reflect the ratios obtained under conditions where the reactant ion has been accelerated to kinetic energies slightly in excess of $kT$, while the final entry gives results obtained by photoionization at 10.2 eV at a field strength of 10 V/cm. Within experimental error there is good agreement between the ratios obtained at 11.7 eV (2 eV above the ionization potential of $C_3H_6$) and those obtained by electron impact using both the Zero Field and ICR techniques, indicating that the photoionization of $C_3H_6$ at 106.7–104.8 nm gives an internal energy distribution roughly equivalent to that obtained with "low energy" electrons. It is difficult to draw any exact correlations since the electron energies used in other laboratories are usually not specified.

When the photon energy is increased from 10.0 to 11.7 eV the fractional yields of $C_3H_7^+$ and $C_4H_7^+$ increase while $C_4H_8^+$ and $C_5H_9^+$ decrease in relative importance. Consideration of the literature values given in table 1, and the results of systematic studies involving propylene in which kinetic energy has been varied over a wide range [13, 16] confirms that the same trends are observed as the kinetic energy of the reactant ion is increased; i.e., $C_3H_7^+$ and $C_4H_7^+$ increase and $C_4H_8^+$ and $C_5H_9^+$ decrease. This is a clear demonstration that an increase in the internal energy content of a reactant ion gives the same overall effect as an increase in kinetic energy for a relatively complex set of competing unimolecular decomposition processes involving a compound ion. Although the conversion of kinetic into internal energy has been well documented in various laboratories, the mechanism has always proceeded through an otherwise endothermic reaction channel (such as the formation of a dissociative charge exchange product).

A similar variation in the distribution of product ions with photon energy was obtained for the $C_3D_6^+ - C_3D_6$ reaction pair, but in this case the fractional yields of $C_3D_7^+$ and $C_4D_7^+$ are reduced compared to the perprotonated system. This effect is probably related to the fact that the $C_6D_{12}^+$ intermediate ion contains slightly less energy at the time of fragmentation. We have also observed (table 1) stable $C_6D_{12}^+$ ions in $C_3D_6$ at pressures where collisional stabilization of the intermediate ion is negligible (pressures $\leq 0.5$ millitorr). Under the same experimental conditions the yields of $C_6H_{12}^+$ from $C_3H_6^+$ were negligibly small ($< 1\%$). Peers [16] has also observed the bimolecular formation of stable $C_6H_{12}^+$ in propylene, but again with a fractional yield $< 1$ percent. The bimolecular formation of large yields of stable $C_6D_{12}^+$ in $C_3D_6$ may be attributed to the increased dissociative lifetime of the perdeuterated system. A change in the internal energy also affects the relative probability for formation of stable $C_6D_{12}^+$ as evidenced by the fact that the fractional yield decreases substantially ($\sim 40\%$) when the energy is increased from 10.0 to 11.7 eV.

Up to this point we have dealt only with the effect of internal energy on the relative rates of unimolecular decomposition of the compound ion along various competing channels. An equally important effect is the role of internal energy in affecting the overall rate coefficient for conversion of $C_3H_6^+$ into products other than $C_3H_6^+$. Reference to figure 1 and the rate data given in table 2 indicates that an increase in energy from 10.0 to 11.7 eV results in an approximately 20 percent decrease in the rate coefficient. The present values are compared with those available from other laboratories, and the general agreement is quite satisfactory considering the differences in experimental techniques. The reduction in the total rate coefficient with increasing internal energy has been reported for other systems [4], and has been attributed either to a decrease in the lifetime of the compound ion or an increase in the probability for charge exchange. In this context we would like to point out that a clear distinction must be made between the effect on the apparent overall rate coefficient and the effect on the relative probabilities for fragmentation of the compound molecule-ion (once formed) along various competing channels. For example, it is incorrect to discuss the formation of $C_5H_9^+$ from $C_3H_6^+$ in terms of a rate constant or reaction cross section for the *reaction* ($C_3H_6^+ + C_3H_6 \rightarrow C_5H_9^+ + CH_3$). In our view, once the $C_6H_{12}^{+*}$ compound state is formed the reaction of $C_3H_6^+$ with $C_3H_6$ is over. The unimolecular fragmentation patterns, as well as the relative probability (lifetime) for dissociation into $C_5H_9^+ + CH_3$ will certainly depend on the internal energy content of the excited hexene ion, but this is a problem in unimolecular, not bimolecular, reaction kinetics.

An additional point may be made concerning the results contained in tables 1 and 2. Even after taking into account the 20 percent decrease in the overall rate coefficient for removal of $C_3H_6^+$ and $C_3D_6^+$ as the photon energy is increased, one still finds a substantial increase in the absolute rate of production of $C_3H_7^+$ and $C_3D_7^+$. As mentioned earlier, tandem experiments [15] have shown that the production of these ions proceeds through a long range process which is chemically distinct from that (those) responsible for subsequent production of $C_4^+$, $C_5^+$, and $C_6^+$ ions, in which C–C bonds are formed and extensive randomization of hydrogen is observed. The evidence is clear that this long range transfer process is favored both when the reactant ion is produced in high vibrational states and under conditions of high kinetic energy.

#### b. Reactions Occurring at Higher Pressures

In a previous article from this laboratory [32] it was shown that propane was obtained in large yields via an ionic mechanism when propylene was photoionized at 10.0 eV at pressures greater than 2 torr. The mechanism proposed to account for propane formation was as follows:

$$C_3H_6^+ + C_3H_6 \rightarrow C_6H_{12}^+ \quad (4)$$

$$C_6H_{12}^+ + C_3H_6 \rightarrow C_6H_{10}^+ + C_3H_8 \quad (5)$$

Although several laboratories have carried out mass spectrometric experiments at high pressures of propylene (0.1 [8], 0.25 [15], and 0.9 torr [11]) this particular reaction sequence has not been detected. However, large yields of $C_6H_{12}^+$, as well as $C_9H_{18}^+$ were observed directly in a recent flash photoionization study [8]. In order to resolve these apparently contradictory results we have investigated the photoionization of propylene at pressures up to approximately 0.1 torr. We chose the deuterated analog for detailed study due to the fact that $C_3D_6^+$ forms $C_6D_{12}^+$ at 10.0 eV in large yields compared to the perprotonated analog. Typical results are given in figure 2, which reproduces the fractional composition of the product ion mass spectrum for some major ions from $C_3D_6$ at pressures up to approximately 100 millitorr. The successive addition of $C_3D_6$ to $C_3D_7^+$ is clearly indicated, as well as the conversion of $C_4D_8^+$ into $C_5D_{10}^+$, etc. These sequences have been reported previously for the perprotonated system [16]. We have also observed the addition of $C_3D_6$ to $C_4D_8^+$, $C_4D_9^+$, and $C_5D_9^+$ ions, as well as other concurrent reactions, but these processes are not germaine to this discussion and the associated fractional yields of these species have been omitted from the figure. The important experimental observation is the rapid formation of substantial yields of $C_6D_{12}^+$ and its subsequent reaction with $C_3D_6$ to give $C_6D_{10}^+$ via $D_2$ transfer:

$$C_3D_6^+ + C_3D_6 \xrightarrow{M} C_6D_{12}^+ \xrightarrow{C_3D_6} C_6D_{10}^+ + C_3D_8. \quad (6)$$

The sum of the fractional contributions from $C_6D_{12}^+$ and $C_6D_{10}^+$ reaches a value of $0.19 \pm 0.1$ at approximately 10 millitorr and remains constant up to the maximum pressure studied (100 millitorr). Reactions occurring at higher pressures could not be investigated quantitatively due to the complexity of the resulting spectrum. The direct observation of the $D_2$ transfer reaction involving the $C_6D_{12}^+$ ion verifies the mechanism proposed earlier in this laboratory [32] to account for propane formation in photoionized propylene, and the ion-pair yield of 0.19 derived in this study compares well with the value of 0.14 reported for $C_3H_8$ formation in photoionized $C_3H_6$. Recent mass spectrometric experiments from this laboratory [33] have confirmed that the analogous reaction scheme also occurs in $i$-$C_4H_8$ and $i$-$C_4D_8$, although in this case the fractional yield for the $H_2(D_2)$ transfer product is approximately 0.5. We mentioned earlier that other investigators were unable to detect processes (4) and (5) in $C_3H_6$. Although our own experiments with $C_3H_6$ over the pressure range covered in figure 2 did reveal the formation of $C_6H_{12}^+$ and $C_6H_{10}^+$, the sum of the fractional yields of these products was extremely low ($\leq 0.02$) at our highest pressure (100 millitorr). It is likely that the formation of such ions would have been overlooked in previous experiments involving high energy electron impact ionization which would yield a variety of fragments from $C_3H_6^+$ in addition to the molecule-ion. One intriguing feature of the sequences represented by processes (5) and (6) is that they are not quantitative for removal of $C_3H_6^+$ and $C_3D_6^+$ even at pressures up to one atmosphere based on chemical evidence (the ion-pair yields for propane formation reach a constant value $\leq 0.2$). A possible explanation for this effect is that proposed previously; namely, that the $C_6H_{12}^+$ ions which do react via $H_2$ transfer have cyclic structures whereas the majority of the $C_6H_{12}^+$, $C_9H_{18}^+$, etc., ions are acyclic and disappear simply by consecutive olefinic condensation reactions. Other investigators have, on occasion, suggested unique structures for those $C_6H_{12}^{+*}$ compound ions which unimolecularly fragment at low pressures [15]. However, as pointed out by Harrison [13, 17], and as indicated in a recent study in this laboratory [34], the modes of decomposition of a compound ion depend critically on the internal energy of the system. Many different isomeric structures may exist under these conditions, and the dissociation is likely to occur from any or all of these configurations. Therefore, it is not surprising that ten or more $C_6H_{12}$ isomeric products were recovered when the photoionization of propylene was carried out in a closed system in the presence of $(CH_3)_3N$ (I.P. = 7.8 eV), which acts as a charge acceptor in the process:

$$C_6H_{12}^+ + (CH_3)_3N \rightarrow C_6H_{12} + (CH_3)_3N^+. \quad (7)$$

This process was very efficient as evidenced by the fact that the total ion-pair yield of the $C_6$ products resulting from the photoionization of a mixture containing 10 mole percent of $(CH_3)_3N$ in 4 torr of $C_3H_6$

was 0.70. When NO (I.P. = 9.2 eV) is substituted for $(CH_3)_3N$ to yield decreases by approximately a factor of four. This effect can be ascribed to the fact that the ionization potentials of many of the $C_6H_{12}$ isomers are lower than that for NO, rendering the charge transfer process endothermic.

The observation of a large number of isomeric structures does not, however, indicate that the isomerization processes are dictated solely by statistical factors since five of the ten major products account for 80 percent of the yield. It has also been confirmed by Henis [5] that randomization of hydrogen atoms in the compound ion occurs only to a limited extent for the higher olefins. Additional information concerning the $C_6H_{12}^{+*}$ ion has been derived by Wagner [35], who investigated the solid phase radiolysis of propylene under conditions where deactivation of $C_6H_{12}^{+*}$ will essentially freeze the ion in its initial configuration. Although a large number of $C_6H_{12}$ isomers were observed, the major products were 1-hexene and 3-methyl-1-pentene.

### 4.2. Cyclopropane

For the $c\text{-}C_3H_6^+ - c\text{-}C_3H_6$ reaction pair the rate coefficients obtained at 10.6 and 11.7 eV are in excellent agreement with recent values from Harrison's laboratory [36] by the Zero Field Pulse and trapped ion techniques. However, the values of 2.2, 2.1, and $2.0 \times 10^{-10}$ cm$^3$/molecule · s are considerably lower than that ($11.4 \pm 2.4$) derived by Strausz, et al. [8] using the flash photoionization technique. This latter method involves flash photoionization via a continuum lamp (useful energies extending from the ionization threshold for the molecule to approximately 11.7 eV) followed by time-resolved analysis using mass spectrometry. We find no variation in the rate coefficient with increasing photon energy, and are unable to account for the observed difference in reactivity.

The following overall processes were also observed by the flash technique:

$$c\text{-}C_3H_6^+ + c\text{-}C_3H_6$$

$$\rightarrow C_3H_4^+ + C_3H_8 \qquad (\Delta H = -0.12 \text{ eV}) \quad (8)$$

$$\rightarrow C_3H_3^+ + C_3H_8 + H \qquad (\Delta H = 1.1 \text{ eV}). \quad (9)$$

(Heats of reaction assume ground state reactants and the thermodynamically favored structures for products). These products have not been observed in studies involving electron impact ionization of cyclopropane under thermal conditions [9, 13, 17] and were not observed in the present study at any photon energy. This result indicates that even though a fraction of the $C_3H_6^+$ ions resulting from photoionization of cyclopropane at 11.7 eV may be in the second electronic state (11.07 eV) [37] the additional energy is not effective in overcoming the energy barrier for these processes.

The product distribution resulting from the overall sequence:

$$c\text{-}C_3H_6^+ + c\text{-}C_3H_6 \rightarrow \text{products other than } C_3H_6^+ \quad (10)$$

does vary with photon energy (table 3), and the distribution obtained at 11.7 eV agrees very well with the electron impact values. In this context it is important to note that those products which decrease in relative importance as the photon energy is increased ($C_4H_8^+$, $C_5H_9^+$) are also those which decrease in relative importance as the kinetic energy of the reactant ion is increased. Alternatively, the relative rate of formation of $C_3H_7^+$ in cyclopropane increases as both the photon and kinetic energy are increased.

The high relative abundance of the $C_4H_8^+$ produced in the cyclopropane system (table 3) as compared to the propylene system (table 1) is of interest. This is due to the fact that once a C—C bond is broken in the neutral partner of the $c\text{-}C_3H_6^+ - c\text{-}C_3H_6$ collision collision complex, elimination of ethylene from the neutral can occur rapidly without extensive rearrangement. The analogous reaction has been found to occur in a recent study of the $C_4H_8$ isomers. In this case the methylcyclopropane system exhibits an unusually high relative abundance of the $C_5H_{10}^+$ as an overall reaction product compared with the other $C_4H_8$ isomers. As pointed out for cyclopropane, elimination of the neutral molecule (propylene) in methylcyclopropane would also occur without rearrangement once a C—C bond is broken in the neutral reacting partner.

### 4.3. Ethylene

The overall reaction of $C_2H_4^+$ with $C_2H_4$ has been subjected to considerable investigation in both the closed system photolysis [34, 38–39] and radiolysis [34, 39] as well as very extensively by kinetic mass spectrometry [4–5, 8, 18–29]. The evidence favors formation of an excited butene-like reaction intermediate which, at low pressures, decomposes mainly into $C_3H_5^+$ and $C_4H_7^+$

$$C_2H_4^+ + C_2H_4 \rightarrow C_4H_8^{+*} \rightarrow C_3H_5^+ + CH_3 \quad (11)$$

$$\rightarrow C_4H_7^+ + H. \quad (12)$$

At higher densities, where collisional stabilization of $C_4H_8^{+*}$ is effective, the chemical studies in closed systems have provided a great deal of information concerning the various isomerization processes and structures associated with the intermediate ion [34, 38–39]. The present results concern the interactions of ethylene ions produced in the ground electronic state (the maximum photon energy of 11.7 eV is approximately 0.6 eV below the threshold for electronic excitation) [40] under conditions where stabilization of $C_4H_8^{+*}$ is negligible.

#### a. Effect of Internal Energy

The fractional yields of the $C_3^+$ and $C_4^+$ products associated with the $C_2H_4^+ - C_2H_4$ reaction pair exhibit several rather subtle variations with photon energy.

The major effect involves the change in the ratio $C_4H_7^+/C_3H_5^+$, which decreases from 0.17 to 0.11 as the energy is increased from 10.6 to 11.7 eV. Comparison of the breakdown patterns and appearance potential measurements for the various $C_4H_8$ isomers [41] indicates that the energy threshold for the formation of the $C_4H_7^+$ fragment from $C_4H_8^+$ in those systems is consistently lower than that for $C_3H_5^+$. Consequently an increase in the internal energy content of the $C_4H_8^+$* ion produced in the $C_2H_4^+ - C_2H_4$ system would be expected to favor production of $C_3H_5^+$, and this is the trend observed experimentally. In the present study we have not observed the production of $C_2H_5^+$ as a secondary ion (possibly a fractional yield of 0.004 at 11.7 eV) although previous results indicate the formation of this ion in significant yields. Apparently overall formation of $C_2H_5^+$ occurs only for highly excited $C_2H_4^+$ or under conditions of excess kinetic energy.

The decay curves of figure 3 indicate a decrease of approximately 11 percent in the overall rate coefficient for process (2) when the photon energy is increased from 10.6 to 11.7 eV. As was found for the $C_3H_6^+ - C_3H_6$ reaction pair the absolute value of the rate coefficient obtained at 11.7 eV is in excellent agreement with the "low energy" electron impact results and compares well with that obtained by flash photoionization. Gross and Norbeck [4] have recently investigated the effect of internal energy on the cross section for production of $C_3H_5^+$ (process 11) using variable energy electron impact ionization. Their results indicated a decrease of approximately 30 percent in the cross section when the electron energy was increased from threshold to 25 eV. Considering our respective absolute rate coefficients at the two energies (our measurement at 10.64 eV is only slightly in excess of the photoionization threshold of $10.51 \pm .04$ eV) and the respective overall product distributions given in table 4, we calculate a decrease of approximately 7 percent in the rate of production of $C_3H_5^+$ at 11.7 eV when compared to threshold. This change is consistent in magnitude with that observed by Gross and Norbeck, over this limited range, but the vibrational energy distribution in $C_2H_4^+$ is unknown in both cases.

It has been suggested [4] that under those conditions where the rate coefficient for process (2) is substantially reduced from the threshold value one should observe an increase in the yields of isotopically exchanged ethylenes in $C_2H_4 - C_2D_4$ mixtures; i.e., an increase in the probability for return to starting material should favor overall processes such as:

$$C_2H_4^+ + C_2D_4 \rightarrow C_4D_4H_4^+ \rightarrow C_2H_3D^+ + C_2D_3H, \text{ etc.} \quad (13)$$

Some exchange has been observed in $C_2H_4 - C_2D_4$ mixtures in single stage mass spectrometer [19] and when $C_2H_4^+$ is impacted onto $C_2D_4$ in a tandem instrument [20]. We have investigated the exchange processes at 11.7 eV and have found (see Results) that exchanged products account for only 2.2 percent of the sum total of all processes (excluding charge exchange) which may occur at this energy. Furthermore, the tandem results of Tiernan and Futrell [20] indicate a total contribution from exchange processes $< 5$ percent even when ionization is induced with 100 eV electrons. These observations indicate that dissociation of the complex ion into reactants occurs with very little hydrogen exchange. The only alternative overall channel is that which is empirically equivalent to simple charge exchange:

$$C_2H_4^+ + C_2D_4 \rightarrow C_2D_4^+ + C_2H_4, \text{ etc.} \quad (14)$$

Such processes have been observed by ICR [22] in $C_2H_4 - C_2D_4$ mixtures as well as in tandem experiments [20]. We have found (see Results) that the rate coefficient for the process $C_2D_4^+ + C_2H_4 \rightarrow$ products other than $C_2D_4^+$ is approximately 7 percent faster than that for $C_2H_4^+ + C_2H_4 \rightarrow$ products other than $C_2H_4^+$. Charge exchange between $C_2H_4^+$ and $C_2H_4$ would not be detected in our instrument, whereas charge exchange from $C_2D_4^+$ to $C_2H_4$ would be detected as an increase in the apparent rate coefficient for removal of $C_2D_4^+$. Essentially the same result was found for the reaction of $C_2H_4^+$ with $C_2D_4$. Tiernan and Futrell [20] observed substantially more charge exchange in the $C_2H_4^+ - C_2D_4$ reaction pair ($\sim 30\%$), but whether this was due to the fact that the internal energy content of $C_2H_4^+$ was higher (100 eV electrons) or the ions were slightly epithermal ($0 < E < 0.4$ eV) cannot be determined from their data. Finally, Bowers, et al. [22] have concluded that an increase in kinetic energy results in a corresponding increase in the probability for charge exchange in ethylene, but that the total reaction probability (charge exchange plus contributions from process 13) remains constant. In any event, the accumulated data indicates that the separation of the interaction pair into $C_2H_4^+ + C_2H_4$ proceeds without significant hydrogen randomization among the reactants.

#### b. Randomization of Hydrogen in $C_4H_8^+$*

There is general agreement among various workers that the $C_4H_8^+$* compound ion involved in processes (11) and (12) has a relatively long lifetime ($\geq 10^{-8}$ s) with respect to dissociation. Consideration of the isotopic composition of the $C_3X_3^+$ (X = H or D) ions produced in $C_2H_4 - C_2D_4$ mixtures and the partially labeled analog $CH_2 = CD_2$ has also resulted in a consensus opinion that all hydrogens are equivalent in that $C_4H_4D_4^+$* compound ion obtained in such systems. For example, in a recent ICR study by Bowers et al. [22], the distribution of the $C_3X_5^+$ products obtained from the $CH_2 = CD_2^+ - CH_2 = CD_2$ reaction pair was found to be essentially equivalent to that obtained from a $C_2H_4 - C_2D_4$ mixture and complete randomization was concluded. Unfortunately, such agreement is

not proof of complete randomization if a cyclic structure (cyclobutane ion) is assumed to represent the configuration of $C_4H_4D_4^+$*, since in this case the carbon atoms may retain the original H or D atoms and give the same distribution of $C_3X_5^+$ products after dissociation. Complete randomization of hydrogen in the $C_4H_4D_4^+$ ion would be verified, however, irrespective of the assumed structure, if the same distribution were obtained from the $CHD=CHD^+ - CHD=CHD$ and $CH_2CD_2^+ - CH_2CD_2$ reaction pairs, particularly if the relative probabilities for loss of $CH_3$ and $CD_3$ were the same for both analogs. The results of such experiments are given in table 4, and the distribution obtained by Bowers et al. [22], for $CH_2=CD_2$ is included for comparison. Consideration of the data obtained for the two analogs indicates that the effect of increasing photon energy for any particular analog is minimal, and those subtle variations which do occur can probably be ascribed to a decrease in the probability for loss of $CX_4$ (methane) from $C_4H_4D_4^+$ at 11.7 eV (see product distribution from the $C_2H_4^+ - C_2H_4$ reaction pair, table 4). The important feature of the results is the agreement between the distributions obtained from $CHD=CHD$ and $CH_2=CD_2$, which is excellent considering the fact that the isotopic purities of the starting materials are slightly different (see Results). On this basis we conclude that randomization of hydrogen atoms is complete in the compound ion.

The extensive scrambling in $C_4H_4D_4^+$* which does occur is not unreasonable in view of the relatively long dissociative lifetime ($5\times10^{-6}$ s) for $C_4H_8^+$* observed in the 11.7 eV photoionization of $C_2H_4$ [38]. Somewhat lower lifetimes have been estimated as a result of mass spectrometric studies [28], but under conditions where ionization of $C_2H_4$ was induced by high energy electron impact.

Some additional remarks are appropriate concerning the nature of $C_4H_8^+$*. It has been shown that $i$-$C_4H_8^+$ is one of the isomeric structures formed in the photoionization [34, 38–39a] and electron impact ionization of $C_2H_4$ [34]. The fact [34] that the $i$-$C_4H_8^+$ structure increases relative to linear structures as the internal energy of $C_4H_8^+$* increases indicates that methyl elimination may be occurring via this configuration. However, dissociation does not necessarily proceed through a specific intermediate since it has been shown [34] that highly unstable 1-$C_4H_8$ and methylcyclopropane ions are formed as important intermediates following ionization of cyclobutane. In view of the chemical evidence to the contrary it is very doubtful that dissociation occurs quantitatively via a 2-$C_4H_8^+$ structure in ethylene as assumed recently [42] in a quasi-equilibrium treatment (QET) of this system by Butrill. In fact, the accumulated evidence indicates that 2-$C_4H_8^+$ structures play a very minor role compared with 1-$C_4H_8^+$, $i$-$C_4H_8^+$, and $CH_3 - C_3H_5^+$. Consequently, the agreement between the experimental and calculated fragmentation pattern of $C_4H_8^+$* must be considered only as tentative since the QET treatment assumed an incorrect structure for the activated complex.

Finally, as indicated under Results, we observed some variation in the isotopic composition of the $C_3X_5^+$ products as the total pressure in the reaction chamber was increased. Under our conditions these changes cannot be ascribed to further reaction of ethyl ions produced by the initial reaction of ethylene ions with ethylene, as suggested by Tiernan and Futrell. The changes which are observed are apparently associated with exchange reactions involving $C_3X_5^+$ and $CH_2CD_2$ such as:

$$C_3H_3D_2^+ + C_2H_2D_2 \rightarrow C_3H_4D^+ + C_2D_3H, \text{ etc.} \qquad (15)$$

Based on recent measurements, the $(C_3H_5 - C_2H_4)^+$ collision complex has a lifetime $\geq 100$ microseconds, and this is certainly sufficient for hydrogen exchange to occur prior to dissociation.

## 5. Summary

The absolute rate coefficients for reaction of parent ions in ethylene and propylene have been found to decrease as the average internal energy content of the reactant ion is increased, and the distribution of products also shows considerable variation. In general, the variations observed in the product distribution are similar to those found elsewhere when the kinetic energy of the reactant ion is increased. We have also directly detected for the first time the formation of stable $C_6H_{12}^+$ dimeric ions in photoionized propylene, and have determined that these species react further with propylene via $H_2$ transfer. Finally, isotopic labeling experiments have confirmed that the $C_4H_8^+$ compound ion produced in the reaction of ethylene ions with ethylene has a structure in which all hydrogen atoms are equivalent.

## 6. References

[1a] For a review see: Futrell, J. H., and Tiernan, T. O., in Fundamental Processes in Radiation Chemistry, P. Ausloos, Ed. (Interscience Publishers, New York, Chapter 4, 1968).
[1b] Ion-Molecule Reactions, J. Franklin, Ed. (Plenum Press, 1970).
[2] Chupka, W. A., Russell, M. E., and Rafaey, K., J. Chem. Phys. **48**, 1518 (1968); Chupka, W. A., and Russell, M. E., ibid., **48**, 1527 (1968).
[3] Sieck, L. W., Hellner, L., and Gorden, R., Jr., Chem. Phys. Letters, To be published (1971).
[4] Gross, M. I., and Norbeck, J., J. Chem. Phys. **54**, 3651 (1971) and references cited therein.
[5] Henis, J. M. S., J. Chem. Phys. **52**, 282 (1970).
[6] Goode, G. C., O'Malley, R. M., Ferrer-Correia, A. J., Massey, R. I., Jennings, K. R., Futrell, J. H., and Llewellyn, P. M., Intern'l. J. Mass Spectrom. and Ion Phys. **5**, 393 (1970).
[7] Henis, J. M. S., J. Chem. Phys. **52**, 292 (1970).
[8] Strausz, O. P., Duholke, W. K., and Gunning, H. E., J. Am. Chem. Soc. **92**, 4128 (1970).
[9] Sieck, L. W., and Futrell, J. H., J. Chem. Phys. **45**, 560 (1966).
[10] Herod, A. A., and Harrison, A. G., Intern'l J. Mass Spectrom. and Ion Phys. **4**, 415 (1970).
[11] Aquilanti, V., Galli, A., Giardini-Guidoni, A., and Volpi, G. G., Trans. Faraday Soc. **64**, 124 (1968).
[12] Koyano, I., Omura, I., and Tanaka, I., J. Chem. Phys. **44**, 3850 (1966).

[13] Herod, A. A., and Harrison, A. G., J. Phys. Chem. **73**, 3189 (1969).
[14] Peers, A. MacKenzie, J. Phys. Chem. **73**, 4141 (1969).
[15] Abramson, F. P., and Futrell, J. H., J. Phys. Chem. **72**, 1994 (1968).
[16] Peers, A. MacKenzie, Intern'l J. Mass Spectrom. and Ion Phys. **5**, 483 (1970).
[17] Herod, A. A., Harrison, A. G., O'Malley, R. M., Ferrer-Correia, A. J., and Jennings, K. R., J. Phys. Chem. **74**, 2720 (1970).
[18] Abramson, F. P., and Futrell, J. H., J. Phys. Chem. **72**, 1826 (1968).
[19] Myher, J. J., and Harrison, A. G., Can. J. Chem. **46**, 101 (1968).
[20] Tiernan, T. O., and Futrell, J. H., J. Phys. Chem. **72**, 3080 (1968).
[21a] Kebarle, P., and Hogg, A. M., J. Chem. Phys. **42**, 668 (1965).
[21b] Kebarle, P., Haynes, R. M., and Searles, S., Advan. Chem. Sev. **58**, 210 (1966).
[22] Bowers, M. T., Elleman, D. D., and Beauchamp, J. L., J. Phys. Chem. **2**, 3599 (1968).
[23] Szabo, I., Ark. Fysik, **33**, 57 (1967).
[24] O'Malley, R. M., and Jennings, K. R., Intern'l J. Mass Spectrom. and Ion Phys. **2**, 441 (1969).
[25] Herman, Z., Lee, A., and Wolfgang, R., J. Chem. Phys. **51**, 452 (1969).
[26] Schissler, D. O., and Stevenson, D. P., J. Chem. Phys. **24**, 926 (1956).
[27] Field, F. H., Franklin, J. L., and Lampe, F. W., J. Am. Chem. Soc. **79**, 2419 (1957).
[28] Field, F. H., J. Am. Chem. Soc. **83**, 1523 (1961).
[29] Wexler, S., Lifshitz, A., and Quattrachi, A., Advan. Chem. Sev. **58**, 193 (1966).
[30] Heats of formation and ionization potentials are taken from Franklin, J. L., Dillard, J. G., Rosenstock, H. M., Herron, J. T., Draxl, K, and Field, F. H., Nat. Stand. Ref. Data Ser., Nat. Bur. Stand. (U.S.), 26, 289 pages (1969).
[31a] Sieck, L. W., Searles, S. K., and Ausloos, P., J. Am. Chem. Soc. **91**, 7627 (1969).
[31b] Searles, S. K., and Sieck, L. W., J. Am. Chem. Soc. **92**, 2937 (1970).
[32] Gorden, R., Doepker, R., and Ausloos, P., J. Chem. Phys. **44**, 3733 (1966).
[33] Sieck, L. W., and Ausloos, P., J. Chem. Phys., Submitted for publication.
[34a] Lias, S. G., and Ausloos, P., J. Res., Nat. Bur. Stand. (U.S.), **75A** (Phys. and Chem.) No. 5, 591–605 (1971).
[34b] Sieck, L. W., Lias, S., and Ausloos, P., NBS J. Res., Nat. Bur. Stand. (U.S.), **65A** (Phys. and Chem.), No. 3, 253 (May-June 1972).
[35] Wagner, C. D., Tetrahedron, **14**, 164 (1961).
[36] Harrison, A. G., private communication.
[37] Dewar, M. J. S., and Worley, S. D., J. Chem. Phys. **50**, 654 (1969).
[38] Gorden, R., Jr. and Ausloos, P., J. Res. Nat. Bur. Stand. (U.S.), **75A** (Phys. and Chem.), No. 3, 141–146 (1971).
[39a] Gill, P. S., Inel, Y., and Meisels, G. G., J. Chem. Phys. **54**, 2811 (1971).
[39b] Meisels, G. G., Advan. Chem. Sev. **58**, 243 (1966).
[39c] Meisels, G. G., J. Chem. Phys. **42**, 3239 (1965).
[40] Botter, R., Dibeler, V. H., Walker, J. A., and Rosenstock, H. M., J. Chem. Phys. **45**, 1298 (1966); Chupka, W. A., Berkowitz, J., and Rafaey, K. M., ibid., **50**, 1938 (1969).
[41] Tiernan, T. O., and Hills, L. P., reported at Nineteenth Annual Conf. on Mass Spectrometry and Allied Topics, Atlanta, Georgia, May 2–7 (1971).
[42] Butrill, S. E., J. Chem. Phys. **52**, 6174 (1971).

(Paper 76A3–720)

JOURNAL OF RESEARCH of the National Bureau of Standards—A. Physics and Chemistry
Vol. 76A, No. 3, May–June 1972

# Low Temperature Thermocouples: KP, "normal" silver, and copper versus Au-0.02 at% Fe and Au-0.07 at% Fe*

**Larry L. Sparks** and Robert L. Powell****

**Institute for Basic Standards, National Bureau of Standards, Boulder, Colorado 80302**

**(February 4, 1972)**

The Seebeck thermoelectric voltages of two dilute alloys of iron in gold, Au 0.02 at% Fe and Au-0.07 at% Fe, have been determined with respect to KP (a particular Ni-Cr alloy), "normal" silver, and copper in the temperature range from 4 to 280 K. The power series representation of these data, along with the calculated Seebeck coefficients and derivatives of the Seebeck coefficients, have been extrapolated to 0 K and are presented as a function of temperature. In addition to these reference data, seven different Au-0.07 at% Fe alloys were thermoelectrically intercompared in order to determine the variability in wires from different melts and from different manufacturers. The largest deviation found amounted to about 9 percent of the output of a KP versus Au-0.07 at% Fe thermocouple pair between 4 and 20 K. A more typical variation for this temperature range was 2 to 4 percent. Initial indications are that the reference data can be adjusted satisfactorily with data from spot calibrations on particular wires. The effect of heat treatment is illustrated by comparing our results to Rosenbaum's data for annealed and unannealed specimens of both Au-Fe alloys.

Key Words: Cryogenics; gold alloy; liquid helium; liquid hydrogen; liquid nitrogen; thermocouples.

## 1. Introduction

The increasing use of liquid hydrogen and liquid helium in the scientific and aerospace communities has created a demand for specialized thermometry below, say, 25 K. Ordinary thermocouple combinations are only marginally acceptable due to their low sensitivity in this range. Dilute alloys of noble metals and transition metals, however, do form thermoelements with relatively high temperature sensitivity below 25 K. Au-2.1 at% (atomic percent) Co is perhaps the best known of this type. Unfortunately, the Au-Co alloy forms a supersaturated solid solution; Co tends to migrate to the grain boundaries even at room temperature [1][1]. This migration changes the thermoelectric properties and reduces the worth of this material as a thermoelement. Another family of alloys of this type are alloys of Fe in Au. These alloys are metallurgically stable and exhibit extremely useful thermoelectric properties at very low temperatures. Work recently completed at the National Bureau of Standards in Boulder has resulted in precise calibrations and intercomparisons of two of these alloys, Au-0.02 at% Fe and Au-0.07 at% Fe. Our primary emphasis has been directed to the latter alloy. A differential thermocouple made with either of these Au-Fe alloys as the negative element and copper, "normal" silver (Ag-0.37 at% Au), or KP[2] as the positive element provides a usable sensitivity even below 4 K.

The fact that trace amounts of transition elements in noble metal solvents causes anomalous thermoelectric properties has been known for some time. Borelius [2, 3] and co-workers determined the thermoelectric sensitivity of many dilute alloys of copper, silver, gold, and platinum in 1932. The electrical resistivity and thermopower of these alloys are of interest because of the unusual electron scattering which must be present to cause the peculiar behavior. Much of the work done on dilute alloys has, therefore, been to understand the bulk transport properties involved. Development of the Au-Fe alloys for use in low temperature thermocouple thermometry didn't really begin until after 1960 when Berman [4] tested Au-0.02 at% Fe for possible use in their thermal conductivity apparatus. Since that time others, including ourselves, have been drawn into the field in search of better thermometers for use in thermal conductivity measurement systems.

Several necessary thermoelectric properties have been determined for the Au-Fe alloys, e.g., reproducibility after repeated thermal cycling [5], behavior in a

*This work was carried out at the National Bureau of Standards under the sponsorship of the National Aeronautics and Space Administration, Space Nuclear Propulsion Office (SNPO–C), Contract R–45.

**Cryogenic Properties of Solids, Cryogenics Division, National Bureau of Standards, Boulder, Colo. 80302.

[1] Figures in brackets indicate the literature references at the end of this paper.

[2] KP is the ASTM and ISA designation for a 90% Ni + 10% Cr alloy. Trade names for this material are: Chromel, Hoskins Manufacturing Co.; Tophel, Wilbur B. Driver Co.; T–1, Driver-Harris Co.; and Thermo Kanthal KP, Kanthal Corp. Use of trade names does not constitute an endorsement of any manufacturer's products.

magnetic field [6], and the effect of heat treatment [7, 8]. The number of investigations concerning these properties is small and the conclusions could, therefore, be representative of particular materials rather than a general material. The consensus is, however, that sufficient information is available to establish the Au-Fe alloys as the most promising thermoelement available for use at very low temperatures.

The intent of our work is to provide a precise, full range calibration for several practical thermocouple combinations involving Au-Fe alloys and to present comparison data from different manufacturers, different melts, and different spools. It is hoped that the tabular data presented in this paper can be used as reference data.

Discussion of the procedures needed to adjust the reference data to individual thermocouples must be delayed. Further analysis of our data may make such information available. The brief discussion of figure 5 in the text is an indication of what we hope the more detailed analysis will show.

## 2. Experimental Procedure

A detailed description of the items in this section appears in NBS Monograph 124 [9]. The contents of this section will, therefore, be general and brief.

The cryostat used in the experimental work consists basically of two working chambers. One chamber is filled with a cryogen which serves as the reference temperature for the thermocouples while the second chamber is controlled to some selected higher temperature. The thermal insulation surrounding the two working chambers consists of various radiation shields, high vacuum, and finally a liquid nitrogen shield. This arrangement allows the reference temperature to be established with liquid helium (approximately 4 K), liquid hydrogen (approximately 20 K), or liquid nitrogen (approximately 75 K). In the course of a calibration the temperature ranges spanned using these reference temperatures are 4 to 25 K, 20 to 90 K, and 75 to 290 K. Figure 1 shows schematically how the thermocouple wires are situated in the system.

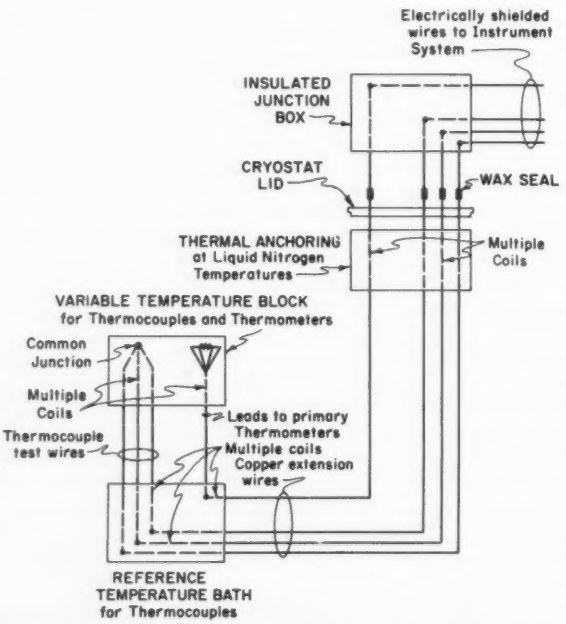


FIGURE 1. *Schematic of electrical and thermal situation of wires in the thermocouple calibration system.*

The temperature of the reference bath is determined with a platinum resistance thermometer (PRT) when either liquid hydrogen or liquid nitrogen are used as the reference cryogen. The vapor pressure of the liquid helium is used to determine the reference temperature when helium is used as the reference liquid. The variable temperature of the upper chamber is determined with a germanium resistance thermometer (GeRT) when the temperature is below 20 K and a PRT when the temperature is above 20 K. All PRT resistances are measured with a Mueller G2 bridge and all voltage readings are made on a potentiometer with a resolution of 0.01$\mu$V. All automatic temperature controllers are of in-house design. During the course of a one hour test the temperature difference between the variable and reference junctions of the thermocouples is held constant to within 5 mK.

## 3. Materials

The calibration system can accommodate up to 22 thermocouple test wires at one time. Two different sets of materials have been tested as part of the thermocouple thermometry program at NBS. The first set of materials contained only one Au-0.07 at% Fe wire and one Au-0.02 at% Fe wire. These two wires were thermoelectrically compared to KP, "normal" silver, and copper at a total of 68 different temperature gradients. The second set of wires to be tested contained seven different Au-0.07 at% Fe wires and one Au-0.02 at% Fe wire. In this calibration KP was compared to all of the Au-Fe specimens and the Au-0.07 at% Fe wires were intercompared. Table 1 contains additional information on the selection of samples used in both the first and second calibrations.

The KP wires used in the first and second calibrations were adjacent lengths from the same spool; dip tests indicate that there is no observable difference between adjacent lengths of wire from this particular spool. These two lengths will be referred to as the same wire for the remainder of the paper. The primary variability between the first and second calibrations involving KP must, therefore, be attributed to differences in the Au-0.07 at% Fe wires.

One of the seven wires in the second set of materials had completely different properties than the remaining six specimens. Spectrographic analysis indicated about 0.45 at% Fe rather than 0.07 at% Fe. Data obtained for this wire are not considered in the remainder of this paper or listed in table 1.

A micrograph was made for Au-0.07 at% $Fe_{47}$ used in the first calibration (subscripts indicate specimen

TABLE 1. *Specimens of* Au-0.07 *at%* Fe *and* Au-0.02 *at%* Fe *calibrated with the first and second sets of low temperature thermocouple materials*

| Alloy | Specimen number | Wire diameter (millimeters) | Comments | |
|---|---|---|---|---|
| Au-0.07 at% Fe ... | 5 | 0.152 | Supplier 1 | |
| | 6 | .152 | 1 | |
| | 7 | .152 | 1 | |
| | 47 | .152 | 1 | |
| | 10 | .127 | Supplier 2 | Bar 1 |
| | 11 | .127 | 2 | Bar 2 |
| | 8 | .254 | 2 | Bar 1 |
| Au-0.02 at% Fe ... | 45 | .127 | Supplier 2 | Bar 1 |
| | 12 | .127 | Supplier 2 | Bar 2 |

number as in table 1). Rather large grains were observed to be preferentially oriented along the axis of the wire. The maximum grain size encountered was approximately $300 \times 70$ $\mu$m.

As indicated in table 1, several different melts from two companies are represented. An important part in establishing the usefulness of Au-Fe alloys as thermocouple materials is the degree of uniformity among melts and among different producers. The results presented in the next section indicate the spread or nonuniformity found in the specimens available to us at the time of testing.

## 4. Results

The range of thermal voltages obtained by comparing a single KP wire to the seven Au-0.07 at% Fe wires listed in table 1 is shown in figure 2. The band in this figure is determined by plotting data for the combinations having the highest and lowest output of the KP versus Au-0.07 at% Fe pairs tested. Since the band width in this figure results from different Au-0.07 at% Fe wire versus the same KP wire, the observed spread in the data must be due to variation in the Au-0.07 at% Fe materials. Thermoelectric differences among the seven Au-0.07 at% Fe specimens are made more clear when the contribution of the KP element is eliminated as in figure 3. The data in this figure represent experimentally determined differences among the Au-0.07 at% Fe specimens except for the specimen 5 versus specimen 47 curve which is calculated.[3] The variations in the Au-0.07 at% Fe material are compared with the total output of the KP versus Au-0.07 at% Fe combination in table 2. Specimen 11 is used as the common Au-0.07 at% Fe wire in this table. The largest relative deviations are seen to be in the temperature range 4 K to 20 K; this is the same temperature range where the enhanced sensitivity is needed. Rosenbaum [7] compared different melts of Au-0.07 at% Fe from a single manufacturer and found voltage variations of 1.4 percent between 4.2 K and 77 K and 1.9 percent between 4.2 K and 273.2 K. These values appear reasonable when compared to the corresponding data for our wires given in table 2. It is interesting that wire 5 and

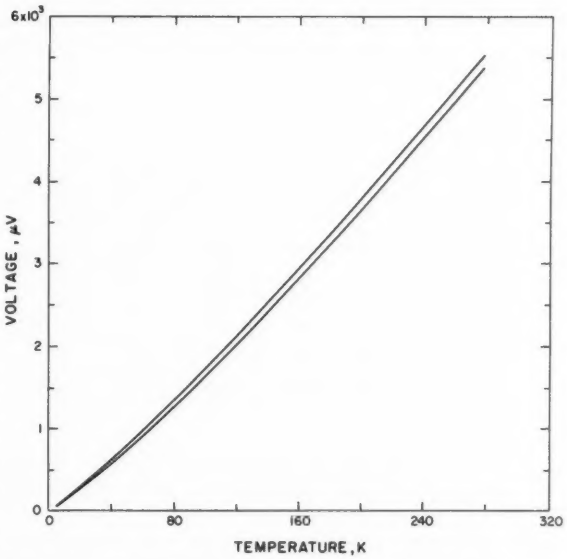


FIGURE 2. *Extremes of the thermoelectric voltage found in tests paring a single KP wire to seven different* Au-0.07 *at%* Fe *wires.*

wire 7, figure 3, are from the same company; within company variations are greater than intercompany variations for our limited selection of specimens. The general grouping in figure 3, however, indicates that the variation between wires 6 and 7 is more typical of the within company differences. The near identity of wires 10 and 11 is undoubtably fortuitous since wire 8 is from the same melt as wire 10.

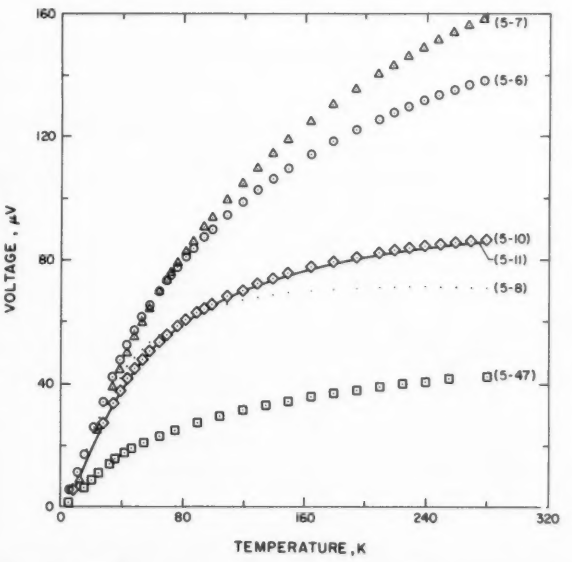


FIGURE 3. *Experimentally determined thermoelectric differences between* Au-0.07 *at%* Fe$_5$ *and the other six* Au-0.07 *at%* Fe *specimens.*

The numbers in parentheses represent the specimen numbers involved in the individual curves.

[3] Many experimental points have been omitted from the NBS curves throughout this paper in order to reduce the cluttered appearance of the point graphs. All experimental data were, however, used to determine the proper analytical representation and tables to be given later.



459-033 OL - 72 - 6

TABLE 2. *Voltage differences between* Au-0.07 *at%* $Fe_{11}$ *and the remaining* Au-0.07 *at%* Fe *specimens and percentage variation of the thermoelectric voltage of each KP versus* Au-0.07 *at%* Fe *pair from the thermoelectric voltage of KP versus* Au-0.07 *at%* $Fe_{11}$

| Au-0.07 at% Fe | Temperature Range | | | | | | | | | | | |
|---|---|---|---|---|---|---|---|---|---|---|---|---|
| | 4–20 K | | 4–75 K | | 4–280 K | | 20–75 K | | 20–280 K | | 75–280 K | |
| Specimen numbers | $\Delta E\mu V$ | $\Delta E/E \times 100$ (percent) | $\Delta E\mu V$ | $\Delta E/E \times 100$ (percent) | $\Delta E\mu V$ | $\Delta E/E \times 100$ (percent) | $\Delta E\mu V$ | $\Delta E/E \times 100$ (percent) | $\Delta E\mu V$ | $\Delta E/E \times 100$ (percent) | $\Delta E\mu V$ | $\Delta E/E \times 100$ (percent) |
| 5 vs 11 | 15.99 | 6.3 | 55.31 | 4.7 | 84.07 | 1.6 | 39.32 | 4.2 | 68.08 | 1.3 | 28.76 | 0.7 |
| 11 vs 6 | 4.00 | 1.6 | 16.89 | 1.4 | 49.53 | 0.9 | 13.79 | 1.5 | 46.43 | 0.9 | 32.64 | .8 |
| 11 vs 7 | 1.69 | 0.7 | 20.21 | 1.7 | 72.05 | 1.3 | 18.52 | 2.0 | 70.36 | 1.4 | 51.84 | 1.2 |
| 11 vs 10 | 0.07 | .0 | 0.10 | 0.0 | 0.11 | 0.0 | 0.03 | 0.0 | 0.04 | 0.0 | 0.01 | 0.0 |
| 8 vs 11 | 3.13 | 1.2 | .93 | .1 | 16.19 | .3 | 2.20 | .2 | 19.32 | .4 | 17.12 | .4 |
| 47 vs 11 | 8.18 | 3.2 | 31.28 | 2.6 | 43.00 | .8 | 23.10 | 2.5 | 34.82 | .7 | 11.72 | .3 |
| Average... | 5.51 | 2.2 | 20.79 | 1.8 | 44.16 | .8 | 16.16 | 1.7 | 39.84 | .8 | 23.68 | .6 |

Figure 4 contains the Seebeck coefficients for the KP versus Au-0.07 at% Fe thermocouple pairs tested. The close grouping of specimens 6, 7, 8, 10, and 11 is apparent here as well as the outlying characteristics of specimen 5. Table 3 details the temperatures and sensitivities at the low temperature inflections. Figure 5 plots Seebeck coefficients for three KP versus Au-0.07 at% Fe pairs. The lower line plot in this figure is for the single KP versus Au-0.07 at% $Fe_{47}$ from the first set of calibrations. The data for this KP versus Au-0.07 at% Fe combination has not been published, but it has been rather widely distributed. The data represented by the higher of the two line curves are for KP versus Au-0.07 at% $Fe_7$. The third curve, represented by rectangles, results when the data for KP versus Au-0.07 at% $Fe_{47}$ in this figure is adjusted by dip test data for a length of wire adjacent to specimen 7. The KP used in the dip tested thermocouple was from a different manufacturer than that used to determine KP versus Au-0.07 at% $Fe_{47}$. A detailed thermoelectric comparison had been made earlier for the two KP materials involved; there was no observable difference when the temperature was below 80 K and above 80 K there was a linear divergence to about 10$\mu$V when the temperature was 280 K. The lined data result from two separate and complete calibrations in the thermocouple calibration apparatus. There was approximately a three year time lapse between the calibrations. The rectangular data, on the other hand, resulted when information obtained from a series of dip tests was used to adjust the lower lined data.

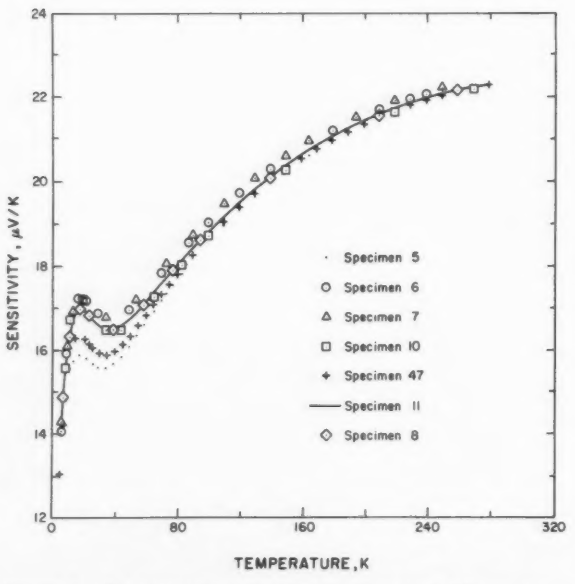


FIGURE 4. *Calculated Seebeck coefficients for a single KP wire versus seven specimens of* Au-0.07 *at%* Fe.

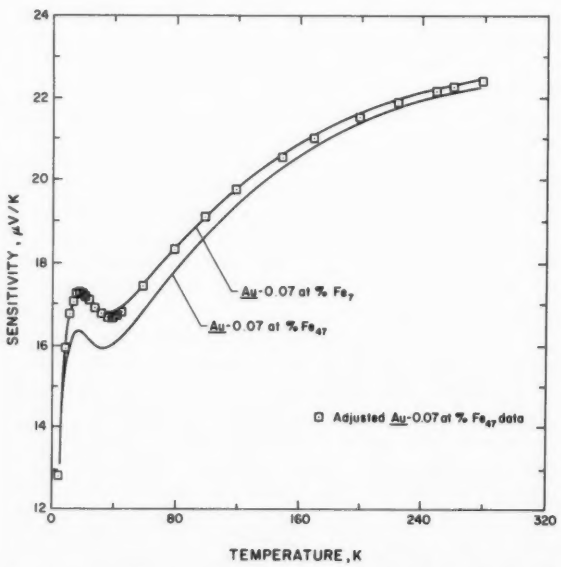


FIGURE 5. *Comparison of Seebeck coefficients for KP versus* Au-0.07 *at%* $Fe_{7,47}$ *and the Seebeck coefficient for KP versus* Au-0.07 *at%* $Fe_7$ *computed by applying dip test data to the KP versus* Au-0.07 *at%* $Fe_{47}$ *data.*

TABLE 3. *Temperatures and corresponding Seebeck coefficients for the low temperature inflection points in the KP versus* Au-0.07 *at%* Fe *data*

| Au-0.07 at% Fe Specimen number | Low temperature maximum | | Low temperature minimum | |
|---|---|---|---|---|
| | $T$(K) | $S(\mu V/K)$ | $T$(K) | $S(\mu V/K)$ |
| 5 | 17.8 | 15.84 | 32.3 | 15.53 |
| 6 | 18.1 | 17.23 | 37.1 | 16.71 |
| 7 | 18.8 | 17.21 | 36.5 | 16.79 |
| 8 | 17.3 | 17.14 | 38.6 | 16.43 |
| 10 | 18.1 | 16.99 | 37.3 | 16.45 |
| 11 | 18.0 | 17.00 | 37.3 | 16.45 |
| 47 | 17.2 | 16.36 | 34.2 | 15.91 |
| Average | 17.9 | 16.82 | 36.2 | 16.32 |
| Estimate of $\sigma$ | 0.54 | 0.53 | 2.2 | 0.45 |

Heat treatment of the Au-0.07 at% Fe material is critical as is shown in figure 6. The point curves by Rosenbaum [7] represent data from the same bar stock before and after annealing. The thermopower is enhanced by annealing as would be expected when physical defects are eliminated. The Seebeck coefficient for KP versus Au-0.07 at% $Fe_{11}$ is shown as a line in this figure. Rosenbaum's experimental data for KP versus Au-0.07 at% Fe extends down to about 1.3 K, while the lower limit for our experimental data is approximately 5 K. The Seebeck coefficients plotted in figure 7 represent data for KP versus specimens of Au-0.02 at% Fe used in the first and second calibrations and for Rosenbaum's [7] annealed and hard worked specimens. Specimen 12, used in the second calibration, was annealed by the supplier while specimen 45, used in the first calibration, was annealed in-house at 350 °C for 20 minutes in air. It appears that the in-house anneal may have been more effective than the producer anneal on our specimen 12. Rosenbaum's data for KP versus Au-0.02 at% Fe extends down to 0.437 K for the hard drawn specimen. Figures 8 and 9 are further comparisons of our results of those of Rosenbaum. In particular, copper versus Au-0.07 at% $Fe_{11}$ is compared to Rosenbaum's results [8] for copper versus annealed Au-0.07 at% Fe in figure 8 and copper

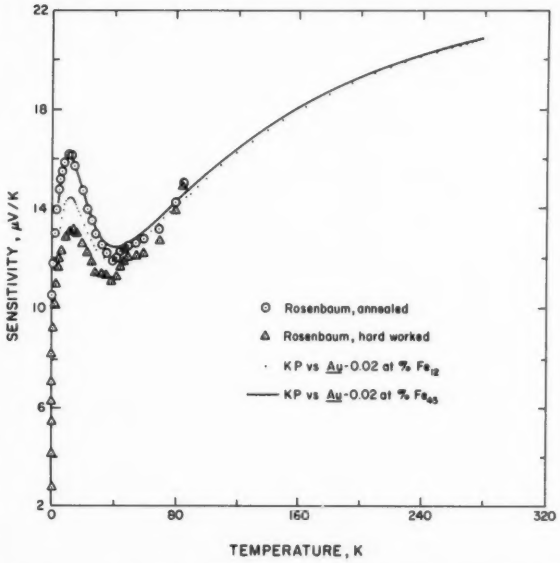


FIGURE 7. *Comparison of Seebeck coefficients for KP versus* Au-0.02 *at%* Fe *in the annealed and unannealed state.*

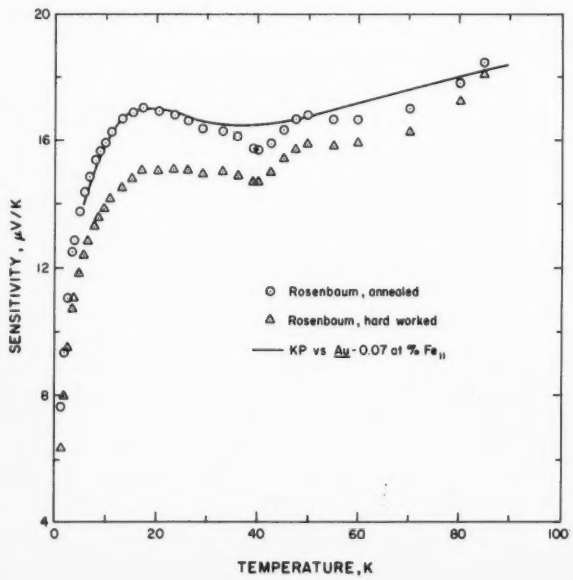


FIGURE 6. *Comparison of Seebeck coefficients for KP versus* Au-0.07 *at%* Fe *in the annealed and unannealed state.*

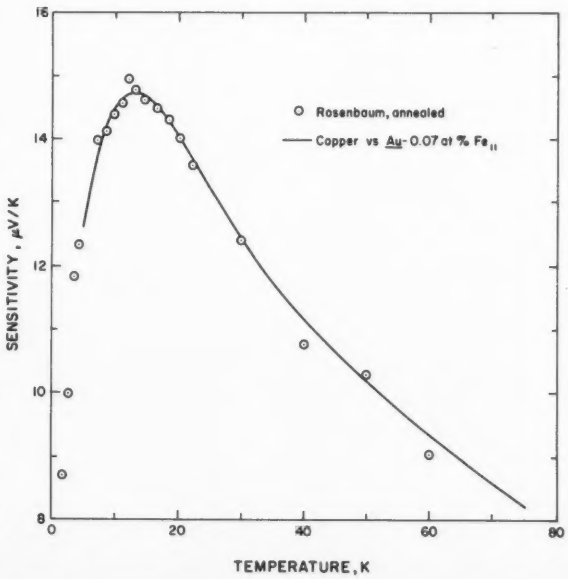


FIGURE 8. *Seebeck coefficients for copper versus* Au-0.07 *at%* Fe.

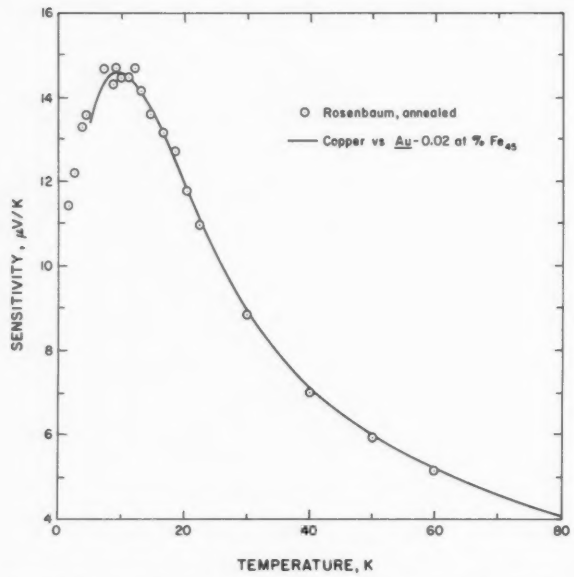


FIGURE 9. *Seebeck coefficients for copper versus* Au-0.02 *at%* Fe.

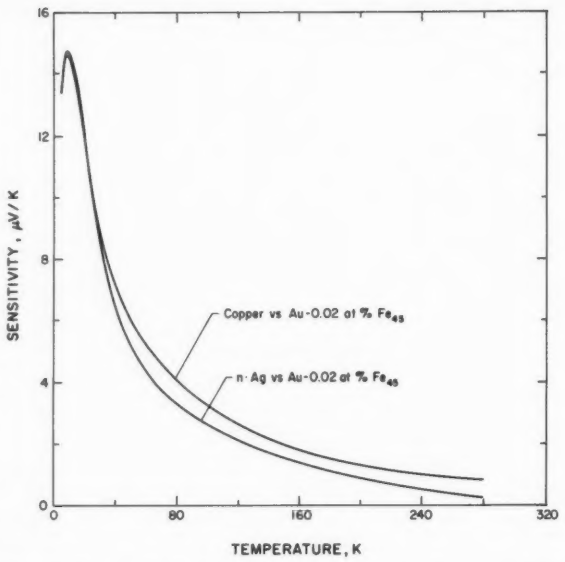


FIGURE 11. *Seebeck coefficients for copper and "normal" silver versus* Au-0.02 *at%* $Fe_{45}$.

versus Au-0.02 at% $Fe_{45}$ is compared to Rosenbaum's results for copper versus annealed Au-0.02 at% Fe in figure 9. Figures 10 and 11 show the Seebeck coefficients for copper and "normal" silver versus Au-0.07 at% $Fe_{11}$ and Au-0.02 at% $Fe_{45}$, respectively. The effect of KP in the thermoelectric circuit with the Au-Fe alloys is clear when the rapidly falling thermopowers in figure 10 are compared with the thermopowers shown in figure 4.

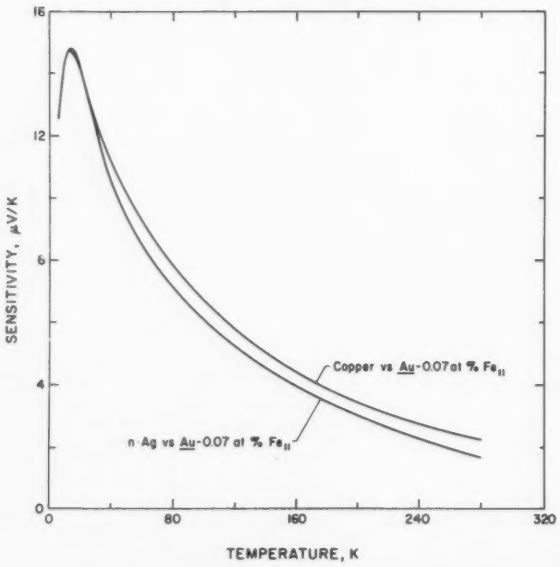


FIGURE 10. *Seebeck coefficients for copper and "normal" silver versus* Au-0.07 *at%* $Fe_{11}$.

A modified Gram-Schmidt approximation [10, 11] was used to represent the experimental data. Details of the fitting procedure are discussed elsewhere [9]. In order to facilitate computer programming of the data the original orthonormal polynomials and the associated orthonormal polynomial coefficients have been recombined to give simple power series coefficients. The relationship between temperature in degrees kelvin and the Seebeck voltage in microvolts for thermocouple types KP, copper, and "normal" silver versus Au-0.02 at% $Fe_{45}$ and Au-0.07 at% $Fe_{11}$ are represented by

$$E(T) = \sum_{n=1}^{L} B_n T^n.$$

The coefficients, $B_n$, for the above thermocouple combinations are listed in table 4. Tables 5 through 10 are tabular results of the power series representation for one degree intervals in temperature. The Seebeck coefficients and their derivatives are also given in these tables. The experimental basis for the data is $5 \leq T \leq 280$ K. Any extension of the power series representation for $T > 280$ K is an extrapolation and all of the uncertainties inherent in such extensions of experimental data must apply. Extension of the data to $T < 5$ K is more acceptable since the constraint $E = 0\ \mu V$ when $T = 0$ K was used in the original fit.

A detailed error analysis has been done for the thermocouple calibration system and is discussed in the previously mentioned monograph [9]. A similar analysis of the Au-Fe combinations result in the total uncertainties given in table 11. These uncertainties include random errors and estimates of systematic errors, but are exclusive of errors in the temperature

TABLE 4. *Power series coefficients for thermocouple types KP versus* Au-0.07 *at%* Fe, KP *versus* Au-0.02 *at%* Fe, *copper versus* Au-0.07 *at%* Fe, *copper versus* Au-0.02 *at%* Fe, *normal silver versus* Au-0.07 *at%* Fe, *and normal silver versus* Au-0.02 *at%* Fe.

| Power series coefficients | KP vs Au 7 Fe | KP vs Au 2 Fe | Cu vs Au 7 Fe | Cu vs Au 2 Fe | n. Ag vs Au 7 Fe | n. Ag vs Au 2 Fe |
|---|---|---|---|---|---|---|
| B(1) | 6.9864426367 | 7.2668579396 | 6.9819441789 | 7.2623594676 | 6.9616414011 | 7.2420566898 |
| B(2) | $9.0607276605 \times 10^{-1}$ | 1.0692244345 | $8.4001378651 \times 10^{-1}$ | 1.0031654569 | $8.1796982011 \times 10^{-1}$ | $9.8112149062 \times 10^{-1}$ |
| B(3) | $-4.3469694773 \times 10^{-2}$ | $-6.2220191022 \times 10^{-2}$ | $-4.5417070202 \times 10^{-2}$ | $-6.4167566583 \times 10^{-2}$ | $-4.1183301479 \times 10^{-2}$ | $-5.9933797876 \times 10^{-2}$ |
| B(4) | $1.2468246660 \times 10^{-3}$ | $1.9487031660 \times 10^{-3}$ | $1.3796048892 \times 10^{-3}$ | $2.0814833941 \times 10^{-3}$ | $1.1332864853 \times 10^{-3}$ | $1.8351649913 \times 10^{-3}$ |
| B(5) | $-2.3500537590 \times 10^{-5}$ | $-3.8863862277 \times 10^{-5}$ | $-2.7648679333 \times 10^{-5}$ | $-4.3012004132 \times 10^{-5}$ | $-2.0564116972 \times 10^{-5}$ | $-3.5927441812 \times 10^{-5}$ |
| B(6) | $3.0837610415 \times 10^{-7}$ | $5.3284892976 \times 10^{-7}$ | $3.8534874955 \times 10^{-7}$ | $6.0982157678 \times 10^{-7}$ | $2.6125849627 \times 10^{-7}$ | $4.8573132442 \times 10^{-7}$ |
| B(7) | $-2.9032251684 \times 10^{-9}$ | $-5.2094815173 \times 10^{-9}$ | $-3.8382718939 \times 10^{-9}$ | $-6.1445282582 \times 10^{-9}$ | $-2.3898974345 \times 10^{-9}$ | $-4.6961538119 \times 10^{-9}$ |
| B(8) | $1.9881512159 \times 10^{-11}$ | $3.6920742674 \times 10^{-11}$ | $2.7684122233 \times 10^{-11}$ | $4.4723352843 \times 10^{-11}$ | $1.5931957622 \times 10^{-11}$ | $3.2971188358 \times 10^{-11}$ |
| B(9) | $-9.9174829612 \times 10^{-14}$ | $-1.9020522841 \times 10^{-13}$ | $-1.4483161512 \times 10^{-13}$ | $-2.3586201427 \times 10^{-13}$ | $-7.7417132540 \times 10^{-14}$ | $-1.6844753253 \times 10^{-13}$ |
| B(10) | $3.5645229362 \times 10^{-16}$ | $7.0508285353 \times 10^{-16}$ | $5.4390389051 \times 10^{-16}$ | $8.9253445111 \times 10^{-16}$ | $2.7100280116 \times 10^{-16}$ | $6.1963336555 \times 10^{-16}$ |
| B(11) | $-8.9864698504 \times 10^{-19}$ | $-1.8317974022 \times 10^{-18}$ | $-1.4282076268 \times 10^{-18}$ | $-2.3613580435 \times 10^{-18}$ | $-6.6485927163 \times 10^{-19}$ | $-1.5980097000 \times 10^{-18}$ |
| B(12) | $1.5071673023 \times 10^{-21}$ | $3.1644035401 \times 10^{-21}$ | $2.4882871621 \times 10^{-21}$ | $4.1455233949 \times 10^{-21}$ | $1.0835762248 \times 10^{-21}$ | $2.7408124807 \times 10^{-21}$ |
| B(13) | $-1.5093916059 \times 10^{-24}$ | $-3.2636069898 \times 10^{-24}$ | $-2.5831198571 \times 10^{-24}$ | $-4.3373352305 \times 10^{-24}$ | $-1.0525122333 \times 10^{-24}$ | $-2.8067276336 \times 10^{-24}$ |
| B(14) | $6.8264293980 \times 10^{-28}$ | $1.5201593461 \times 10^{-27}$ | $1.2089129004 \times 10^{-27}$ | $2.0464292991 \times 10^{-27}$ | $4.6057748723 \times 10^{-28}$ | $1.2980938998 \times 10^{-27}$ |

TABLE 5. *Thermocouple KP versus* Au-0.07 *at%* $Fe_{11}$ *—thermoelectric voltage, Seebeck coefficient, and derivative of the Seebeck coefficient;* E = f(T)

| T K | E μV | S μV/K | dS/dT nV/K² | T K | E μV | S μV/K | dS/dT nV/K² | T K | E μV | S μV/K | dS/dT nV/K² |
|---|---|---|---|---|---|---|---|---|---|---|---|
| 0 | 0.00 | 0.000 | 0.0 | 60 | 962.74 | 17.139 | 43.4 | 120 | 2065.91 | 19.513 | 31.8 |
| 1 | 7.85 | 8.673 | 1565.8 | 61 | 979.90 | 17.183 | 43.6 | 121 | 2085.44 | 19.545 | 31.5 |
| 2 | 17.27 | 10.127 | 1346.7 | 62 | 997.11 | 17.226 | 43.7 | 122 | 2105.00 | 19.576 | 31.2 |
| 3 | 28.04 | 11.375 | 1152.4 | 63 | 1014.36 | 17.270 | 43.7 | 123 | 2124.59 | 19.607 | 30.9 |
| 4 | 39.96 | 12.439 | 980.4 | 64 | 1031.65 | 17.314 | 43.7 | 124 | 2144.21 | 19.638 | 30.6 |
| 5 | 52.86 | 13.342 | 828.8 | 65 | 1048.99 | 17.358 | 43.7 | 125 | 2163.87 | 19.668 | 30.3 |
| 6 | 66.59 | 14.103 | 695.4 | 66 | 1066.36 | 17.401 | 43.7 | 126 | 2183.55 | 19.698 | 30.0 |
| 7 | 81.03 | 14.739 | 578.6 | 67 | 1083.79 | 17.445 | 43.6 | 127 | 2203.26 | 19.728 | 29.7 |
| 8 | 96.04 | 15.265 | 476.7 | 68 | 1101.25 | 17.489 | 43.5 | 128 | 2223.00 | 19.758 | 29.4 |
| 9 | 111.52 | 15.697 | 388.1 | 69 | 1118.76 | 17.532 | 43.4 | 129 | 2242.78 | 19.787 | 29.2 |
| 10 | 127.40 | 16.045 | 311.5 | 70 | 1136.32 | 17.575 | 43.3 | 130 | 2262.58 | 19.816 | 28.9 |
| 11 | 143.59 | 16.323 | 245.6 | 71 | 1153.92 | 17.619 | 43.2 | 131 | 2282.41 | 19.845 | 28.7 |
| 12 | 160.03 | 16.540 | 189.2 | 72 | 1171.56 | 17.662 | 43.1 | 132 | 2302.27 | 19.873 | 28.4 |
| 13 | 176.65 | 16.704 | 141.4 | 73 | 1189.24 | 17.705 | 42.9 | 133 | 2322.16 | 19.902 | 28.2 |
| 14 | 193.42 | 16.825 | 101.0 | 74 | 1206.96 | 17.748 | 42.8 | 134 | 2342.07 | 19.930 | 28.0 |
| 15 | 210.29 | 16.909 | 67.3 | 75 | 1224.73 | 17.790 | 42.7 | 135 | 2362.02 | 19.958 | 27.7 |
| 16 | 227.23 | 16.962 | 39.5 | 76 | 1242.55 | 17.833 | 42.6 | 136 | 2381.99 | 19.985 | 27.5 |
| 17 | 244.21 | 16.989 | 16.8 | 77 | 1260.40 | 17.875 | 42.4 | 137 | 2401.99 | 20.013 | 27.3 |
| 18 | 261.20 | 16.997 | -1.4 | 78 | 1278.30 | 17.918 | 42.3 | 138 | 2422.01 | 20.040 | 27.1 |
| 19 | 278.19 | 16.988 | -15.7 | 79 | 1296.24 | 17.960 | 42.2 | 139 | 2442.07 | 20.067 | 26.9 |
| 20 | 295.17 | 16.966 | -26.6 | 80 | 1314.22 | 18.002 | 42.0 | 140 | 2462.15 | 20.094 | 26.7 |
| 21 | 312.12 | 16.935 | -34.6 | 81 | 1332.24 | 18.044 | 41.9 | 141 | 2482.25 | 20.120 | 26.5 |
| 22 | 329.04 | 16.898 | -40.1 | 82 | 1350.30 | 18.086 | 41.8 | 142 | 2502.39 | 20.147 | 26.3 |
| 23 | 345.92 | 16.856 | -43.5 | 83 | 1368.41 | 18.128 | 41.6 | 143 | 2522.55 | 20.173 | 26.1 |
| 24 | 362.75 | 16.811 | -45.1 | 84 | 1386.56 | 18.169 | 41.5 | 144 | 2542.73 | 20.199 | 26.0 |
| 25 | 379.54 | 16.766 | -45.3 | 85 | 1404.75 | 18.211 | 41.3 | 145 | 2562.94 | 20.225 | 25.8 |
| 26 | 396.28 | 16.721 | -44.2 | 86 | 1422.98 | 18.252 | 41.2 | 146 | 2583.18 | 20.250 | 25.6 |
| 27 | 412.98 | 16.678 | -42.1 | 87 | 1441.25 | 18.293 | 41.0 | 147 | 2603.45 | 20.276 | 25.4 |
| 28 | 429.64 | 16.637 | -39.2 | 88 | 1459.57 | 18.334 | 40.9 | 148 | 2623.73 | 20.301 | 25.3 |
| 29 | 446.26 | 16.600 | -35.7 | 89 | 1477.92 | 18.375 | 40.7 | 149 | 2644.05 | 20.327 | 25.1 |
| 30 | 462.84 | 16.566 | -31.8 | 90 | 1496.32 | 18.415 | 40.5 | 150 | 2664.39 | 20.352 | 24.9 |
| 31 | 479.39 | 16.536 | -27.5 | 91 | 1514.75 | 18.456 | 40.3 | 151 | 2684.75 | 20.376 | 24.7 |
| 32 | 495.92 | 16.511 | -23.0 | 92 | 1533.23 | 18.496 | 40.2 | 152 | 2705.14 | 20.401 | 24.6 |
| 33 | 512.42 | 16.490 | -18.4 | 93 | 1551.74 | 18.536 | 40.0 | 153 | 2725.55 | 20.426 | 24.4 |
| 34 | 528.90 | 16.474 | -13.8 | 94 | 1570.30 | 18.576 | 39.7 | 154 | 2745.99 | 20.450 | 24.2 |
| 35 | 545.37 | 16.463 | -9.2 | 95 | 1588.89 | 18.615 | 39.5 | 155 | 2766.45 | 20.474 | 24.1 |
| 36 | 561.83 | 16.456 | -4.7 | 96 | 1607.53 | 18.655 | 39.3 | 156 | 2786.94 | 20.498 | 23.9 |
| 37 | 578.28 | 16.453 | -0.4 | 97 | 1626.20 | 18.694 | 39.1 | 157 | 2807.45 | 20.522 | 23.7 |
| 38 | 594.73 | 16.455 | 3.8 | 98 | 1644.92 | 18.733 | 38.8 | 158 | 2827.98 | 20.545 | 23.5 |
| 39 | 611.19 | 16.461 | 7.8 | 99 | 1663.67 | 18.772 | 38.5 | 159 | 2848.54 | 20.569 | 23.4 |
| 40 | 627.66 | 16.471 | 11.6 | 100 | 1682.46 | 18.810 | 38.3 | 160 | 2869.12 | 20.592 | 23.2 |
| 41 | 644.13 | 16.484 | 15.2 | 101 | 1701.29 | 18.848 | 38.0 | 161 | 2889.72 | 20.615 | 23.0 |
| 42 | 660.63 | 16.501 | 18.5 | 102 | 1720.16 | 18.886 | 37.7 | 162 | 2910.35 | 20.638 | 22.8 |
| 43 | 677.14 | 16.521 | 21.5 | 103 | 1739.06 | 18.924 | 37.4 | 163 | 2931.00 | 20.661 | 22.6 |
| 44 | 693.67 | 16.544 | 24.3 | 104 | 1758.00 | 18.961 | 37.1 | 164 | 2951.67 | 20.683 | 22.5 |
| 45 | 710.22 | 16.569 | 26.9 | 105 | 1776.98 | 18.998 | 36.8 | 165 | 2972.37 | 20.706 | 22.3 |
| 46 | 726.81 | 16.597 | 29.3 | 106 | 1796.00 | 19.035 | 36.5 | 166 | 2993.08 | 20.728 | 22.1 |
| 47 | 743.42 | 16.628 | 31.4 | 107 | 1815.05 | 19.071 | 36.2 | 167 | 3013.82 | 20.750 | 21.9 |
| 48 | 760.06 | 16.660 | 33.3 | 108 | 1834.14 | 19.107 | 35.8 | 168 | 3034.58 | 20.772 | 21.7 |
| 49 | 776.74 | 16.694 | 35.0 | 109 | 1853.27 | 19.143 | 35.5 | 169 | 3055.37 | 20.793 | 21.5 |
| 50 | 793.45 | 16.730 | 36.5 | 110 | 1872.43 | 19.178 | 35.2 | 170 | 3076.17 | 20.815 | 21.3 |
| 51 | 810.20 | 16.767 | 37.8 | 111 | 1891.62 | 19.213 | 34.8 | 171 | 3096.99 | 20.836 | 21.1 |
| 52 | 826.99 | 16.806 | 38.9 | 112 | 1910.85 | 19.248 | 34.5 | 172 | 3117.84 | 20.857 | 21.0 |
| 53 | 843.81 | 16.845 | 39.9 | 113 | 1930.12 | 19.282 | 34.2 | 173 | 3138.71 | 20.878 | 20.8 |
| 54 | 860.68 | 16.885 | 40.7 | 114 | 1949.42 | 19.316 | 33.8 | 174 | 3159.60 | 20.899 | 20.6 |
| 55 | 877.58 | 16.926 | 41.4 | 115 | 1968.75 | 19.350 | 33.5 | 175 | 3180.51 | 20.919 | 20.4 |
| 56 | 894.53 | 16.968 | 42.0 | 116 | 1988.12 | 19.383 | 33.2 | 176 | 3201.44 | 20.939 | 20.2 |
| 57 | 911.52 | 17.010 | 42.5 | 117 | 2007.52 | 19.416 | 32.8 | 177 | 3222.38 | 20.960 | 20.1 |
| 58 | 928.55 | 17.053 | 42.9 | 118 | 2026.95 | 19.449 | 32.5 | 178 | 3243.35 | 20.980 | 19.9 |
| 59 | 945.63 | 17.096 | 43.2 | 119 | 2046.41 | 19.481 | 32.2 | 179 | 3264.34 | 20.999 | 19.7 |
| 60 | 962.74 | 17.139 | 43.4 | 120 | 2065.91 | 19.513 | 31.8 | 180 | 3285.35 | 21.019 | 19.6 |

TABLE 5. *Thermocouple KP versus* Au-0.07 *at%* $Fe_{11}$ *– thermoelectric voltage, Seebeck coefficient, and derivative of the Seebeck coefficient;* E = f(T) – Continued

| T K | E μV | S μV/K | dS/dT nV/K² | T K | E μV | S μV/K | dS/dT nV/K² | T K | E μV | S μV/K | dS/dT nV/K² |
|---|---|---|---|---|---|---|---|---|---|---|---|
| 180 | 3285.35 | 21.019 | 19.6 | 240 | 4576.81 | 21.930 | 9.5 | | | | |
| 181 | 3306.38 | 21.038 | 19.4 | 241 | 4598.74 | 21.940 | 9.4 | | | | |
| 182 | 3327.43 | 21.058 | 19.2 | 242 | 4620.69 | 21.949 | 9.3 | | | | |
| 183 | 3348.50 | 21.077 | 19.1 | 243 | 4642.64 | 21.958 | 9.3 | | | | |
| 184 | 3369.58 | 21.096 | 18.9 | 244 | 4664.61 | 21.968 | 9.2 | | | | |
| 185 | 3390.69 | 21.115 | 18.8 | 245 | 4686.58 | 21.977 | 9.2 | | | | |
| 186 | 3411.81 | 21.133 | 18.6 | 246 | 4708.56 | 21.986 | 9.3 | | | | |
| 187 | 3432.96 | 21.152 | 18.5 | 247 | 4730.55 | 21.995 | 9.3 | | | | |
| 188 | 3454.12 | 21.171 | 18.4 | 248 | 4752.55 | 22.005 | 9.4 | | | | |
| 189 | 3475.30 | 21.189 | 18.3 | 249 | 4774.56 | 22.014 | 9.5 | | | | |
| 190 | 3496.49 | 21.207 | 18.1 | 250 | 4796.58 | 22.024 | 9.6 | | | | |
| 191 | 3517.71 | 21.225 | 18.0 | 251 | 4818.61 | 22.034 | 9.8 | | | | |
| 192 | 3538.94 | 21.243 | 17.9 | 252 | 4840.64 | 22.043 | 10.0 | | | | |
| 193 | 3560.20 | 21.261 | 17.8 | 253 | 4862.69 | 22.053 | 10.2 | | | | |
| 194 | 3581.47 | 21.279 | 17.7 | 254 | 4884.75 | 22.064 | 10.3 | | | | |
| 195 | 3602.75 | 21.296 | 17.6 | 255 | 4906.82 | 22.074 | 10.6 | | | | |
| 196 | 3624.06 | 21.314 | 17.5 | 256 | 4928.90 | 22.085 | 10.8 | | | | |
| 197 | 3645.38 | 21.331 | 17.4 | 257 | 4950.99 | 22.096 | 11.0 | | | | |
| 198 | 3666.72 | 21.348 | 17.3 | 258 | 4973.09 | 22.107 | 11.1 | | | | |
| 199 | 3688.08 | 21.366 | 17.2 | 259 | 4995.20 | 22.118 | 11.3 | | | | |
| 200 | 3709.45 | 21.383 | 17.1 | 260 | 5017.33 | 22.129 | 11.5 | | | | |
| 201 | 3730.84 | 21.400 | 17.0 | 261 | 5039.46 | 22.141 | 11.6 | | | | |
| 202 | 3752.25 | 21.417 | 16.9 | 262 | 5061.61 | 22.152 | 11.6 | | | | |
| 203 | 3773.68 | 21.434 | 16.8 | 263 | 5083.77 | 22.164 | 11.7 | | | | |
| 204 | 3795.12 | 21.450 | 16.7 | 264 | 5105.94 | 22.176 | 11.6 | | | | |
| 205 | 3816.58 | 21.467 | 16.5 | 265 | 5128.12 | 22.187 | 11.5 | | | | |
| 206 | 3838.05 | 21.483 | 16.4 | 266 | 5150.31 | 22.199 | 11.3 | | | | |
| 207 | 3859.54 | 21.500 | 16.3 | 267 | 5172.52 | 22.210 | 11.1 | | | | |
| 208 | 3881.05 | 21.516 | 16.2 | 268 | 5194.73 | 22.221 | 10.7 | | | | |
| 209 | 3902.58 | 21.532 | 16.0 | 269 | 5216.96 | 22.231 | 10.3 | | | | |
| 210 | 3924.12 | 21.548 | 15.9 | 270 | 5239.19 | 22.241 | 9.7 | | | | |
| 211 | 3945.67 | 21.564 | 15.8 | 271 | 5261.44 | 22.251 | 9.0 | | | | |
| 212 | 3967.24 | 21.580 | 15.6 | 272 | 5283.70 | 22.259 | 8.2 | | | | |
| 213 | 3988.83 | 21.595 | 15.4 | 273 | 5305.96 | 22.267 | 7.3 | | | | |
| 214 | 4010.43 | 21.610 | 15.3 | 274 | 5328.23 | 22.274 | 6.3 | | | | |
| 215 | 4032.05 | 21.626 | 15.1 | 275 | 5350.51 | 22.280 | 5.2 | | | | |
| 216 | 4053.69 | 21.641 | 14.9 | 276 | 5372.79 | 22.284 | 4.0 | | | | |
| 217 | 4075.33 | 21.655 | 14.7 | 277 | 5395.08 | 22.288 | 2.7 | | | | |
| 218 | 4097.00 | 21.670 | 14.5 | 278 | 5417.36 | 22.290 | 1.3 | | | | |
| 219 | 4118.67 | 21.684 | 14.3 | 279 | 5439.65 | 22.290 | -0.1 | | | | |
| 220 | 4140.36 | 21.698 | 14.0 | 280 | 5461.94 | 22.289 | -1.4 | | | | |
| 221 | 4162.07 | 21.712 | 13.8 | | | | | | | | |
| 222 | 4183.79 | 21.726 | 13.6 | | | | | | | | |
| 223 | 4205.52 | 21.739 | 13.3 | | | | | | | | |
| 224 | 4227.27 | 21.753 | 13.1 | | | | | | | | |
| 225 | 4249.03 | 21.766 | 12.8 | | | | | | | | |
| 226 | 4270.80 | 21.778 | 12.5 | | | | | | | | |
| 227 | 4292.58 | 21.791 | 12.3 | | | | | | | | |
| 228 | 4314.38 | 21.803 | 12.0 | | | | | | | | |
| 229 | 4336.19 | 21.815 | 11.8 | | | | | | | | |
| 230 | 4358.01 | 21.826 | 11.5 | | | | | | | | |
| 231 | 4379.84 | 21.838 | 11.3 | | | | | | | | |
| 232 | 4401.68 | 21.849 | 11.0 | | | | | | | | |
| 233 | 4423.54 | 21.860 | 10.8 | | | | | | | | |
| 234 | 4445.40 | 21.870 | 10.5 | | | | | | | | |
| 235 | 4467.28 | 21.881 | 10.3 | | | | | | | | |
| 236 | 4489.17 | 21.891 | 10.1 | | | | | | | | |
| 237 | 4511.06 | 21.901 | 9.9 | | | | | | | | |
| 238 | 4532.97 | 21.911 | 9.8 | | | | | | | | |
| 239 | 4554.88 | 21.921 | 9.6 | | | | | | | | |
| 240 | 4576.81 | 21.930 | 9.5 | | | | | | | | |

TABLE 6. *Thermocouple KP versus* Au-0.02 *at%* $Fe_{45}$ *—thermoelectric voltage, Seebeck coefficient, and derivative of the Seebeck coefficient;* E = f(T)

| T K | E μV | S μV/K | dS/dT nV/K² | T K | E μV | S μV/K | dS/dT nV/K² | T K | E μV | S μV/K | dS/dT nV/K² |
|---|---|---|---|---|---|---|---|---|---|---|---|
| 0 | 0.00 | 0.000 | 0.0 | 60 | 808.49 | 13.053 | 55.5 | 120 | 1694.43 | 16.360 | 45.9 |
| 1 | 8.28 | 9.226 | 1787.8 | 61 | 821.57 | 13.109 | 56.1 | 121 | 1710.81 | 16.406 | 45.6 |
| 2 | 18.34 | 10.856 | 1479.4 | 62 | 834.71 | 13.166 | 56.6 | 122 | 1727.24 | 16.452 | 45.2 |
| 3 | 29.89 | 12.198 | 1209.2 | 63 | 847.90 | 13.222 | 57.1 | 123 | 1743.72 | 16.497 | 44.9 |
| 4 | 42.65 | 13.286 | 973.4 | 64 | 861.15 | 13.280 | 57.5 | 124 | 1760.24 | 16.541 | 44.6 |
| 5 | 56.39 | 14.155 | 768.6 | 65 | 874.46 | 13.337 | 57.8 | 125 | 1776.80 | 16.586 | 44.2 |
| 6 | 70.90 | 14.833 | 591.6 | 66 | 887.83 | 13.395 | 58.0 | 126 | 1793.41 | 16.630 | 43.9 |
| 7 | 86.00 | 15.346 | 439.4 | 67 | 901.25 | 13.453 | 58.2 | 127 | 1810.06 | 16.674 | 43.6 |
| 8 | 101.55 | 15.719 | 309.3 | 68 | 914.73 | 13.512 | 58.4 | 128 | 1826.75 | 16.717 | 43.4 |
| 9 | 117.40 | 15.972 | 199.1 | 69 | 928.27 | 13.570 | 58.5 | 129 | 1843.49 | 16.760 | 43.1 |
| 10 | 133.46 | 16.123 | 106.3 | 70 | 941.87 | 13.629 | 58.6 | 130 | 1860.27 | 16.803 | 42.8 |
| 11 | 149.62 | 16.189 | 29.1 | 71 | 955.53 | 13.687 | 58.6 | 131 | 1877.10 | 16.846 | 42.6 |
| 12 | 165.81 | 16.186 | -34.4 | 72 | 969.25 | 13.746 | 58.7 | 132 | 1893.97 | 16.888 | 42.4 |
| 13 | 181.97 | 16.125 | -85.9 | 73 | 983.02 | 13.805 | 58.7 | 133 | 1910.88 | 16.931 | 42.1 |
| 14 | 198.04 | 16.017 | -126.9 | 74 | 996.86 | 13.863 | 58.8 | 134 | 1927.83 | 16.973 | 41.9 |
| 15 | 213.99 | 15.874 | -158.7 | 75 | 1010.75 | 13.922 | 58.8 | 135 | 1944.82 | 17.015 | 41.7 |
| 16 | 229.78 | 15.703 | -182.5 | 76 | 1024.70 | 13.981 | 58.8 | 136 | 1961.86 | 17.056 | 41.5 |
| 17 | 245.39 | 15.511 | -199.5 | 77 | 1038.71 | 14.040 | 58.7 | 137 | 1978.93 | 17.098 | 41.3 |
| 18 | 260.80 | 15.306 | -210.6 | 78 | 1052.78 | 14.098 | 58.7 | 138 | 1996.05 | 17.139 | 41.1 |
| 19 | 276.00 | 15.091 | -216.7 | 79 | 1066.91 | 14.157 | 58.7 | 139 | 2013.21 | 17.180 | 40.9 |
| 20 | 290.98 | 14.874 | -218.6 | 80 | 1081.09 | 14.216 | 58.6 | 140 | 2030.41 | 17.221 | 40.8 |
| 21 | 305.75 | 14.656 | -216.9 | 81 | 1095.34 | 14.274 | 58.6 | 141 | 2047.65 | 17.261 | 40.6 |
| 22 | 320.29 | 14.441 | -212.4 | 82 | 1109.64 | 14.333 | 58.5 | 142 | 2064.93 | 17.302 | 40.4 |
| 23 | 334.63 | 14.231 | -205.5 | 83 | 1124.00 | 14.391 | 58.4 | 143 | 2082.26 | 17.342 | 40.2 |
| 24 | 348.76 | 14.030 | -196.7 | 84 | 1138.42 | 14.450 | 58.3 | 144 | 2099.62 | 17.382 | 40.0 |
| 25 | 362.69 | 13.839 | -186.5 | 85 | 1152.90 | 14.508 | 58.2 | 145 | 2117.02 | 17.422 | 39.9 |
| 26 | 376.44 | 13.658 | -175.2 | 86 | 1167.44 | 14.566 | 58.1 | 146 | 2134.46 | 17.462 | 39.7 |
| 27 | 390.01 | 13.488 | -163.1 | 87 | 1182.04 | 14.624 | 57.9 | 147 | 2151.94 | 17.502 | 39.5 |
| 28 | 403.42 | 13.332 | -150.5 | 88 | 1196.69 | 14.682 | 57.8 | 148 | 2169.47 | 17.541 | 39.3 |
| 29 | 416.68 | 13.188 | -137.6 | 89 | 1211.40 | 14.740 | 57.6 | 149 | 2187.03 | 17.580 | 39.1 |
| 30 | 429.80 | 13.057 | -124.6 | 90 | 1226.17 | 14.797 | 57.4 | 150 | 2204.63 | 17.619 | 38.9 |
| 31 | 442.80 | 12.938 | -111.7 | 91 | 1240.99 | 14.854 | 57.2 | 151 | 2222.26 | 17.658 | 38.7 |
| 32 | 455.68 | 12.833 | -99.0 | 92 | 1255.88 | 14.911 | 56.9 | 152 | 2239.94 | 17.696 | 38.5 |
| 33 | 468.47 | 12.740 | -86.7 | 93 | 1270.82 | 14.968 | 56.7 | 153 | 2257.66 | 17.735 | 38.2 |
| 34 | 481.17 | 12.659 | -74.8 | 94 | 1285.81 | 15.025 | 56.4 | 154 | 2275.41 | 17.773 | 38.0 |
| 35 | 493.79 | 12.590 | -63.4 | 95 | 1300.87 | 15.081 | 56.1 | 155 | 2293.20 | 17.811 | 37.8 |
| 36 | 506.35 | 12.533 | -52.5 | 96 | 1315.97 | 15.137 | 55.8 | 156 | 2311.03 | 17.848 | 37.5 |
| 37 | 518.86 | 12.485 | -42.2 | 97 | 1331.14 | 15.193 | 55.5 | 157 | 2328.90 | 17.886 | 37.3 |
| 38 | 531.33 | 12.448 | -32.5 | 98 | 1346.36 | 15.248 | 55.1 | 158 | 2346.80 | 17.923 | 37.0 |
| 39 | 543.76 | 12.420 | -23.4 | 99 | 1361.63 | 15.303 | 54.8 | 159 | 2364.75 | 17.960 | 36.7 |
| 40 | 556.17 | 12.401 | -15.0 | 100 | 1376.97 | 15.357 | 54.4 | 160 | 2382.72 | 17.996 | 36.5 |
| 41 | 568.56 | 12.390 | -7.1 | 101 | 1392.35 | 15.412 | 54.0 | 161 | 2400.74 | 18.033 | 36.2 |
| 42 | 580.95 | 12.386 | 0.1 | 102 | 1407.79 | 15.465 | 53.6 | 162 | 2418.79 | 18.069 | 35.9 |
| 43 | 593.34 | 12.390 | 6.7 | 103 | 1423.28 | 15.519 | 53.2 | 163 | 2436.88 | 18.105 | 35.6 |
| 44 | 605.73 | 12.400 | 12.8 | 104 | 1438.83 | 15.572 | 52.8 | 164 | 2455.00 | 18.140 | 35.3 |
| 45 | 618.14 | 12.415 | 18.3 | 105 | 1454.42 | 15.624 | 52.3 | 165 | 2473.16 | 18.175 | 35.0 |
| 46 | 630.56 | 12.436 | 23.4 | 106 | 1470.07 | 15.676 | 51.9 | 166 | 2491.35 | 18.210 | 34.7 |
| 47 | 643.01 | 12.462 | 27.9 | 107 | 1485.78 | 15.728 | 51.5 | 167 | 2509.58 | 18.245 | 34.4 |
| 48 | 655.49 | 12.492 | 31.9 | 108 | 1501.53 | 15.779 | 51.0 | 168 | 2527.84 | 18.279 | 34.1 |
| 49 | 668.00 | 12.526 | 35.6 | 109 | 1517.34 | 15.830 | 50.6 | 169 | 2546.13 | 18.313 | 33.8 |
| 50 | 680.54 | 12.563 | 38.8 | 110 | 1533.19 | 15.881 | 50.1 | 170 | 2564.46 | 18.346 | 33.5 |
| 51 | 693.12 | 12.603 | 41.7 | 111 | 1549.10 | 15.930 | 49.7 | 171 | 2582.83 | 18.380 | 33.2 |
| 52 | 705.75 | 12.646 | 44.2 | 112 | 1565.05 | 15.980 | 49.2 | 172 | 2601.22 | 18.413 | 32.9 |
| 53 | 718.42 | 12.691 | 46.4 | 113 | 1581.06 | 16.029 | 48.8 | 173 | 2619.65 | 18.445 | 32.6 |
| 54 | 731.13 | 12.739 | 48.3 | 114 | 1597.11 | 16.078 | 48.4 | 174 | 2638.11 | 18.478 | 32.3 |
| 55 | 743.90 | 12.788 | 50.0 | 115 | 1613.21 | 16.126 | 47.9 | 175 | 2656.61 | 18.510 | 32.0 |
| 56 | 756.71 | 12.839 | 51.5 | 116 | 1629.36 | 16.173 | 47.5 | 176 | 2675.13 | 18.542 | 31.7 |
| 57 | 769.57 | 12.891 | 52.7 | 117 | 1645.56 | 16.221 | 47.1 | 177 | 2693.69 | 18.573 | 31.4 |
| 58 | 782.49 | 12.944 | 53.8 | 118 | 1661.80 | 16.268 | 46.7 | 178 | 2712.28 | 18.605 | 31.1 |
| 59 | 795.46 | 12.998 | 54.7 | 119 | 1678.09 | 16.314 | 46.3 | 179 | 2730.90 | 18.636 | 30.8 |
| 60 | 808.49 | 13.053 | 55.5 | 120 | 1694.43 | 16.360 | 45.9 | 180 | 2749.55 | 18.666 | 30.6 |

TABLE 6. *Thermocouple KP versus* Au-0.02 *at%* $Fe_{45}$ *– thermoelectric voltage, Seebeck coefficient, and derivative of the Seebeck coefficient;* E = f(T) – Continued

| T K | E μV | S μV/K | dS/dT nV/K² | T K | E μV | S μV/K | dS/dT nV/K² | T K | E μV | S μV/K | dS/dT nV/K² |
|---|---|---|---|---|---|---|---|---|---|---|---|
| 180 | 2749.55 | 18.666 | 30.6 | 240 | 3918.02 | 20.167 | 19.1 | | | | |
| 181 | 2768.23 | 18.697 | 30.3 | 241 | 3938.19 | 20.186 | 19.0 | | | | |
| 182 | 2786.94 | 18.727 | 30.1 | 242 | 3958.39 | 20.205 | 19.0 | | | | |
| 183 | 2805.69 | 18.757 | 29.9 | 243 | 3978.60 | 20.224 | 19.0 | | | | |
| 184 | 2824.46 | 18.787 | 29.6 | 244 | 3998.84 | 20.243 | 19.0 | | | | |
| 185 | 2843.26 | 18.816 | 29.4 | 245 | 4019.09 | 20.262 | 18.9 | | | | |
| 186 | 2862.09 | 18.845 | 29.2 | 246 | 4039.36 | 20.281 | 19.0 | | | | |
| 187 | 2880.95 | 18.875 | 29.0 | 247 | 4059.65 | 20.299 | 19.0 | | | | |
| 188 | 2899.84 | 18.903 | 28.8 | 248 | 4079.96 | 20.318 | 19.0 | | | | |
| 189 | 2918.76 | 18.932 | 28.6 | 249 | 4100.29 | 20.337 | 18.9 | | | | |
| 190 | 2937.70 | 18.961 | 28.5 | 250 | 4120.63 | 20.356 | 18.9 | | | | |
| 191 | 2956.68 | 18.989 | 28.3 | 251 | 4141.00 | 20.375 | 18.9 | | | | |
| 192 | 2975.68 | 19.017 | 28.2 | 252 | 4161.38 | 20.394 | 18.8 | | | | |
| 193 | 2994.71 | 19.046 | 28.0 | 253 | 4181.79 | 20.413 | 18.7 | | | | |
| 194 | 3013.77 | 19.073 | 27.9 | 254 | 4202.21 | 20.431 | 18.5 | | | | |
| 195 | 3032.86 | 19.101 | 27.7 | 255 | 4222.65 | 20.450 | 18.3 | | | | |
| 196 | 3051.98 | 19.129 | 27.6 | 256 | 4243.11 | 20.468 | 18.1 | | | | |
| 197 | 3071.12 | 19.156 | 27.5 | 257 | 4263.59 | 20.486 | 17.7 | | | | |
| 198 | 3090.29 | 19.184 | 27.4 | 258 | 4284.08 | 20.503 | 17.4 | | | | |
| 199 | 3109.49 | 19.211 | 27.2 | 259 | 4304.59 | 20.521 | 16.9 | | | | |
| 200 | 3128.71 | 19.238 | 27.1 | 260 | 4325.12 | 20.537 | 16.4 | | | | |
| 201 | 3147.96 | 19.265 | 27.0 | 261 | 4345.67 | 20.553 | 15.9 | | | | |
| 202 | 3167.24 | 19.292 | 26.9 | 262 | 4366.23 | 20.569 | 15.2 | | | | |
| 203 | 3186.55 | 19.319 | 26.7 | 263 | 4386.80 | 20.584 | 14.6 | | | | |
| 204 | 3205.88 | 19.346 | 26.6 | 264 | 4407.40 | 20.598 | 13.9 | | | | |
| 205 | 3225.24 | 19.372 | 26.5 | 265 | 4428.00 | 20.612 | 13.2 | | | | |
| 206 | 3244.62 | 19.399 | 26.3 | 266 | 4448.62 | 20.625 | 12.6 | | | | |
| 207 | 3264.04 | 19.425 | 26.2 | 267 | 4469.25 | 20.637 | 12.0 | | | | |
| 208 | 3283.47 | 19.451 | 26.0 | 268 | 4489.89 | 20.649 | 11.5 | | | | |
| 209 | 3302.94 | 19.477 | 25.9 | 269 | 4510.55 | 20.660 | 11.2 | | | | |
| 210 | 3322.43 | 19.503 | 25.7 | 270 | 4531.21 | 20.671 | 11.1 | | | | |
| 211 | 3341.94 | 19.529 | 25.5 | 271 | 4551.89 | 20.682 | 11.4 | | | | |
| 212 | 3361.49 | 19.554 | 25.3 | 272 | 4572.58 | 20.694 | 12.0 | | | | |
| 213 | 3381.05 | 19.579 | 25.1 | 273 | 4593.28 | 20.706 | 13.2 | | | | |
| 214 | 3400.64 | 19.604 | 24.9 | 274 | 4613.99 | 20.721 | 15.1 | | | | |
| 215 | 3420.26 | 19.629 | 24.7 | 275 | 4634.72 | 20.737 | 17.8 | | | | |
| 216 | 3439.90 | 19.653 | 24.4 | 276 | 4655.47 | 20.757 | 21.5 | | | | |
| 217 | 3459.57 | 19.678 | 24.2 | 277 | 4676.23 | 20.780 | 26.5 | | | | |
| 218 | 3479.26 | 19.702 | 23.9 | 278 | 4697.03 | 20.810 | 33.0 | | | | |
| 219 | 3498.97 | 19.726 | 23.7 | 279 | 4717.86 | 20.847 | 41.2 | | | | |
| 220 | 3518.71 | 19.749 | 23.4 | 280 | 4738.72 | 20.893 | 51.5 | | | | |
| 221 | 3538.47 | 19.772 | 23.1 | | | | | | | | |
| 222 | 3558.25 | 19.795 | 22.9 | | | | | | | | |
| 223 | 3578.06 | 19.818 | 22.6 | | | | | | | | |
| 224 | 3597.89 | 19.841 | 22.3 | | | | | | | | |
| 225 | 3617.74 | 19.863 | 22.0 | | | | | | | | |
| 226 | 3637.62 | 19.885 | 21.7 | | | | | | | | |
| 227 | 3657.51 | 19.906 | 21.5 | | | | | | | | |
| 228 | 3677.43 | 19.928 | 21.2 | | | | | | | | |
| 229 | 3697.37 | 19.949 | 20.9 | | | | | | | | |
| 230 | 3717.32 | 19.969 | 20.7 | | | | | | | | |
| 231 | 3737.30 | 19.990 | 20.4 | | | | | | | | |
| 232 | 3757.30 | 20.010 | 20.2 | | | | | | | | |
| 233 | 3777.32 | 20.030 | 20.0 | | | | | | | | |
| 234 | 3797.37 | 20.050 | 19.8 | | | | | | | | |
| 235 | 3817.43 | 20.070 | 19.6 | | | | | | | | |
| 236 | 3837.51 | 20.090 | 19.5 | | | | | | | | |
| 237 | 3857.60 | 20.109 | 19.4 | | | | | | | | |
| 238 | 3877.72 | 20.128 | 19.2 | | | | | | | | |
| 239 | 3897.86 | 20.148 | 19.2 | | | | | | | | |
| 240 | 3918.02 | 20.167 | 19.1 | | | | | | | | |

TABLE 7. *Thermocouple copper versus* Au-0.07 *at%* $Fe_{11}$ *– thermoelectric voltage, Seebeck coefficient, and derivative of the Seebeck coefficient;* $E = f(T)$

| T K | E μV | S μV/K | dS/dT nV/K² | T K | E μV | S μV/K | dS/dT nV/K² | T K | E μV | S μV/K | dS/dT nV/K² |
|---|---|---|---|---|---|---|---|---|---|---|---|
| 0 | 0.00 | 0.000 | 0.0 | 60 | 719.52 | 9.331 | -81.7 | 120 | 1162.03 | 5.835 | -41.8 |
| 1 | 7.78 | 8.531 | 1423.5 | 61 | 728.81 | 9.250 | -80.9 | 121 | 1167.85 | 5.793 | -41.4 |
| 2 | 16.98 | 9.839 | 1197.0 | 62 | 738.02 | 9.169 | -80.1 | 122 | 1173.62 | 5.752 | -41.1 |
| 3 | 27.38 | 10.934 | 997.5 | 63 | 747.15 | 9.089 | -79.3 | 123 | 1179.35 | 5.711 | -40.7 |
| 4 | 38.79 | 11.842 | 822.3 | 64 | 756.20 | 9.010 | -78.5 | 124 | 1185.04 | 5.671 | -40.3 |
| 5 | 51.01 | 12.586 | 669.0 | 65 | 765.17 | 8.932 | -77.7 | 125 | 1190.69 | 5.630 | -40.0 |
| 6 | 63.91 | 13.187 | 535.4 | 66 | 774.07 | 8.855 | -76.9 | 126 | 1196.30 | 5.591 | -39.6 |
| 7 | 77.35 | 13.663 | 419.3 | 67 | 782.88 | 8.778 | -76.1 | 127 | 1201.87 | 5.551 | -39.2 |
| 8 | 91.20 | 14.030 | 318.9 | 68 | 791.62 | 8.703 | -75.2 | 128 | 1207.41 | 5.512 | -38.8 |
| 9 | 105.38 | 14.305 | 232.5 | 69 | 800.29 | 8.628 | -74.4 | 129 | 1212.90 | 5.474 | -38.5 |
| 10 | 119.78 | 14.500 | 158.5 | 70 | 808.88 | 8.554 | -73.5 | 130 | 1218.35 | 5.435 | -38.1 |
| 11 | 134.35 | 14.626 | 95.5 | 71 | 817.40 | 8.481 | -72.6 | 131 | 1223.77 | 5.397 | -37.7 |
| 12 | 149.02 | 14.694 | 42.3 | 72 | 825.84 | 8.409 | -71.7 | 132 | 1229.15 | 5.360 | -37.3 |
| 13 | 163.72 | 14.713 | -2.4 | 73 | 834.22 | 8.338 | -70.7 | 133 | 1234.49 | 5.323 | -36.9 |
| 14 | 178.43 | 14.692 | -39.5 | 74 | 842.52 | 8.267 | -69.8 | 134 | 1239.79 | 5.286 | -36.5 |
| 15 | 193.10 | 14.636 | -70.0 | 75 | 850.75 | 8.198 | -68.9 | 135 | 1245.06 | 5.250 | -36.1 |
| 16 | 207.69 | 14.553 | -94.8 | 76 | 858.92 | 8.130 | -67.9 | 136 | 1250.29 | 5.214 | -35.7 |
| 17 | 222.20 | 14.448 | -114.7 | 77 | 867.01 | 8.062 | -67.0 | 137 | 1255.49 | 5.178 | -35.3 |
| 18 | 236.58 | 14.326 | -130.2 | 78 | 875.04 | 7.996 | -66.0 | 138 | 1260.65 | 5.143 | -34.9 |
| 19 | 250.84 | 14.189 | -142.1 | 79 | 883.00 | 7.930 | -65.1 | 139 | 1265.78 | 5.109 | -34.6 |
| 20 | 264.96 | 14.042 | -150.8 | 80 | 890.90 | 7.866 | -64.2 | 140 | 1270.87 | 5.074 | -34.2 |
| 21 | 278.92 | 13.888 | -156.9 | 81 | 898.73 | 7.802 | -63.3 | 141 | 1275.92 | 5.040 | -33.8 |
| 22 | 292.73 | 13.729 | -160.8 | 82 | 906.51 | 7.739 | -62.3 | 142 | 1280.95 | 5.007 | -33.4 |
| 23 | 306.38 | 13.567 | -162.8 | 83 | 914.21 | 7.677 | -61.4 | 143 | 1285.94 | 4.973 | -33.1 |
| 24 | 319.87 | 13.404 | -163.2 | 84 | 921.86 | 7.616 | -60.6 | 144 | 1290.89 | 4.940 | -32.7 |
| 25 | 333.19 | 13.241 | -162.4 | 85 | 929.45 | 7.556 | -59.7 | 145 | 1295.82 | 4.908 | -32.4 |
| 26 | 346.35 | 13.080 | -160.7 | 86 | 936.97 | 7.497 | -58.9 | 146 | 1300.71 | 4.876 | -32.0 |
| 27 | 359.35 | 12.920 | -158.1 | 87 | 944.44 | 7.438 | -58.0 | 147 | 1305.57 | 4.844 | -31.7 |
| 28 | 372.19 | 12.764 | -155.0 | 88 | 951.85 | 7.381 | -57.2 | 148 | 1310.40 | 4.812 | -31.4 |
| 29 | 384.88 | 12.610 | -151.5 | 89 | 959.20 | 7.324 | -56.5 | 149 | 1315.20 | 4.781 | -31.1 |
| 30 | 397.41 | 12.461 | -147.6 | 90 | 966.50 | 7.268 | -55.7 | 150 | 1319.96 | 4.750 | -30.8 |
| 31 | 409.80 | 12.315 | -143.6 | 91 | 973.74 | 7.212 | -55.0 | 151 | 1324.70 | 4.720 | -30.5 |
| 32 | 422.04 | 12.173 | -139.5 | 92 | 980.92 | 7.158 | -54.3 | 152 | 1329.40 | 4.689 | -30.2 |
| 33 | 434.15 | 12.036 | -135.4 | 93 | 988.05 | 7.104 | -53.6 | 153 | 1334.07 | 4.659 | -29.9 |
| 34 | 446.12 | 11.903 | -131.4 | 94 | 995.13 | 7.051 | -52.9 | 154 | 1338.72 | 4.629 | -29.7 |
| 35 | 457.96 | 11.773 | -127.4 | 95 | 1002.15 | 6.998 | -52.3 | 155 | 1343.33 | 4.600 | -29.4 |
| 36 | 469.67 | 11.648 | -123.6 | 96 | 1009.13 | 6.946 | -51.7 | 156 | 1347.92 | 4.571 | -29.2 |
| 37 | 481.25 | 11.526 | -120.0 | 97 | 1016.05 | 6.894 | -51.1 | 157 | 1352.47 | 4.542 | -28.9 |
| 38 | 492.72 | 11.408 | -116.6 | 98 | 1022.92 | 6.844 | -50.6 | 158 | 1357.00 | 4.513 | -28.7 |
| 39 | 504.07 | 11.293 | -113.4 | 99 | 1029.73 | 6.793 | -50.0 | 159 | 1361.50 | 4.484 | -28.5 |
| 40 | 515.31 | 11.181 | -110.3 | 100 | 1036.50 | 6.744 | -49.5 | 160 | 1365.97 | 4.456 | -28.3 |
| 41 | 526.43 | 11.072 | -107.6 | 101 | 1043.22 | 6.694 | -49.0 | 161 | 1370.41 | 4.427 | -28.1 |
| 42 | 537.45 | 10.966 | -105.0 | 102 | 1049.89 | 6.645 | -48.6 | 162 | 1374.82 | 4.399 | -27.9 |
| 43 | 548.36 | 10.862 | -102.6 | 103 | 1056.51 | 6.597 | -48.1 | 163 | 1379.21 | 4.372 | -27.8 |
| 44 | 559.17 | 10.760 | -100.4 | 104 | 1063.09 | 6.549 | -47.7 | 164 | 1383.57 | 4.344 | -27.6 |
| 45 | 569.89 | 10.661 | -98.4 | 105 | 1069.61 | 6.502 | -47.3 | 165 | 1387.90 | 4.316 | -27.4 |
| 46 | 580.50 | 10.564 | -96.6 | 106 | 1076.09 | 6.455 | -46.8 | 166 | 1392.20 | 4.289 | -27.2 |
| 47 | 591.01 | 10.468 | -94.9 | 107 | 1082.52 | 6.408 | -46.5 | 167 | 1396.48 | 4.262 | -27.1 |
| 48 | 601.43 | 10.374 | -93.4 | 108 | 1088.90 | 6.362 | -46.1 | 168 | 1400.72 | 4.235 | -26.9 |
| 49 | 611.76 | 10.281 | -92.0 | 109 | 1095.24 | 6.316 | -45.7 | 169 | 1404.95 | 4.208 | -26.8 |
| 50 | 622.00 | 10.190 | -90.8 | 110 | 1101.54 | 6.270 | -45.3 | 170 | 1409.14 | 4.181 | -26.6 |
| 51 | 632.14 | 10.099 | -89.6 | 111 | 1107.78 | 6.225 | -45.0 | 171 | 1413.31 | 4.155 | -26.5 |
| 52 | 642.20 | 10.010 | -88.5 | 112 | 1113.99 | 6.180 | -44.6 | 172 | 1417.45 | 4.128 | -26.3 |
| 53 | 652.16 | 9.922 | -87.5 | 113 | 1120.15 | 6.136 | -44.2 | 173 | 1421.57 | 4.102 | -26.2 |
| 54 | 662.04 | 9.835 | -86.6 | 114 | 1126.26 | 6.092 | -43.9 | 174 | 1425.66 | 4.076 | -26.0 |
| 55 | 671.83 | 9.749 | -85.7 | 115 | 1132.33 | 6.048 | -43.5 | 175 | 1429.72 | 4.050 | -25.8 |
| 56 | 681.54 | 9.664 | -84.8 | 116 | 1138.36 | 6.005 | -43.2 | 176 | 1433.76 | 4.025 | -25.7 |
| 57 | 691.16 | 9.579 | -84.0 | 117 | 1144.34 | 5.962 | -42.9 | 177 | 1437.77 | 3.999 | -25.5 |
| 58 | 700.70 | 9.496 | -83.2 | 118 | 1150.28 | 5.919 | -42.5 | 178 | 1441.75 | 3.974 | -25.3 |
| 59 | 710.15 | 9.413 | -82.5 | 119 | 1156.18 | 5.877 | -42.2 | 179 | 1445.71 | 3.948 | -25.1 |
| 60 | 719.52 | 9.331 | -81.7 | 120 | 1162.03 | 5.835 | -41.8 | 180 | 1449.65 | 3.923 | -24.9 |

TABLE 7. *Thermocouple copper versus* Au-0.07 *at%* $Fe_{11}$ *– thermoelectric voltage, Seebeck coefficient, and derivative of the Seebeck coefficient;* E = f(T) – Continued

| T K | E μV | S μV/K | dS/dT nV/K² | T K | E μV | S μV/K | dS/dT nV/K² | T K | E μV | S μV/K | dS/dT nV/K² |
|---|---|---|---|---|---|---|---|---|---|---|---|
| 180 | 1449.65 | 3.923 | -24.9 | 240 | 1647.73 | 2.752 | -17.3 | | | | |
| 181 | 1453.56 | 3.898 | -24.7 | 241 | 1650.47 | 2.735 | -17.1 | | | | |
| 182 | 1457.45 | 3.874 | -24.5 | 242 | 1653.20 | 2.718 | -16.9 | | | | |
| 183 | 1461.31 | 3.849 | -24.3 | 243 | 1655.90 | 2.701 | -16.6 | | | | |
| 184 | 1465.15 | 3.825 | -24.1 | 244 | 1658.60 | 2.684 | -16.3 | | | | |
| 185 | 1468.96 | 3.801 | -23.9 | 245 | 1661.27 | 2.668 | -16.0 | | | | |
| 186 | 1472.75 | 3.777 | -23.6 | 246 | 1663.93 | 2.653 | -15.6 | | | | |
| 187 | 1476.51 | 3.754 | -23.4 | 247 | 1666.58 | 2.637 | -15.2 | | | | |
| 188 | 1480.26 | 3.731 | -23.2 | 248 | 1669.21 | 2.622 | -14.8 | | | | |
| 189 | 1483.98 | 3.708 | -22.9 | 249 | 1671.82 | 2.607 | -14.4 | | | | |
| 190 | 1487.67 | 3.685 | -22.7 | 250 | 1674.42 | 2.593 | -14.0 | | | | |
| 191 | 1491.35 | 3.662 | -22.4 | 251 | 1677.01 | 2.579 | -13.6 | | | | |
| 192 | 1495.00 | 3.640 | -22.1 | 252 | 1679.58 | 2.566 | -13.1 | | | | |
| 193 | 1498.63 | 3.618 | -21.9 | 253 | 1682.14 | 2.553 | -12.7 | | | | |
| 194 | 1502.23 | 3.596 | -21.6 | 254 | 1684.69 | 2.541 | -12.3 | | | | |
| 195 | 1505.82 | 3.575 | -21.3 | 255 | 1687.22 | 2.528 | -12.0 | | | | |
| 196 | 1509.38 | 3.554 | -21.1 | 256 | 1689.75 | 2.517 | -11.6 | | | | |
| 197 | 1512.93 | 3.533 | -20.8 | 257 | 1692.26 | 2.505 | -11.3 | | | | |
| 198 | 1516.45 | 3.512 | -20.5 | 258 | 1694.76 | 2.494 | -11.0 | | | | |
| 199 | 1519.95 | 3.492 | -20.3 | 259 | 1697.25 | 2.483 | -10.8 | | | | |
| 200 | 1523.43 | 3.472 | -20.0 | 260 | 1699.72 | 2.472 | -10.7 | | | | |
| 201 | 1526.89 | 3.452 | -19.7 | 261 | 1702.19 | 2.462 | -10.6 | | | | |
| 202 | 1530.33 | 3.432 | -19.5 | 262 | 1704.65 | 2.451 | -10.5 | | | | |
| 203 | 1533.76 | 3.413 | -19.3 | 263 | 1707.09 | 2.441 | -10.5 | | | | |
| 204 | 1537.16 | 3.394 | -19.0 | 264 | 1709.53 | 2.430 | -10.6 | | | | |
| 205 | 1540.54 | 3.375 | -18.8 | 265 | 1711.95 | 2.419 | -10.8 | | | | |
| 206 | 1543.91 | 3.356 | -18.6 | 266 | 1714.37 | 2.409 | -10.9 | | | | |
| 207 | 1547.26 | 3.337 | -18.4 | 267 | 1716.77 | 2.398 | -11.1 | | | | |
| 208 | 1550.58 | 3.319 | -18.3 | 268 | 1719.16 | 2.386 | -11.3 | | | | |
| 209 | 1553.89 | 3.301 | -18.1 | 269 | 1721.54 | 2.375 | -11.5 | | | | |
| 210 | 1557.19 | 3.283 | -18.0 | 270 | 1723.91 | 2.363 | -11.6 | | | | |
| 211 | 1560.46 | 3.265 | -17.8 | 271 | 1726.27 | 2.352 | -11.6 | | | | |
| 212 | 1563.72 | 3.247 | -17.7 | 272 | 1728.62 | 2.340 | -11.5 | | | | |
| 213 | 1566.95 | 3.229 | -17.6 | 273 | 1730.95 | 2.329 | -11.1 | | | | |
| 214 | 1570.17 | 3.212 | -17.6 | 274 | 1733.27 | 2.318 | -10.4 | | | | |
| 215 | 1573.38 | 3.194 | -17.5 | 275 | 1735.59 | 2.308 | -9.3 | | | | |
| 216 | 1576.56 | 3.177 | -17.5 | 276 | 1737.89 | 2.300 | -7.6 | | | | |
| 217 | 1579.73 | 3.159 | -17.4 | 277 | 1740.19 | 2.293 | -5.2 | | | | |
| 218 | 1582.88 | 3.142 | -17.4 | 278 | 1742.48 | 2.290 | -2.1 | | | | |
| 219 | 1586.01 | 3.125 | -17.4 | 279 | 1744.77 | 2.289 | 2.1 | | | | |
| 220 | 1589.13 | 3.107 | -17.5 | 280 | 1747.06 | 2.294 | 7.6 | | | | |
| 221 | 1592.23 | 3.090 | -17.5 | | | | | | | | |
| 222 | 1595.31 | 3.072 | -17.5 | | | | | | | | |
| 223 | 1598.37 | 3.055 | -17.6 | | | | | | | | |
| 224 | 1601.42 | 3.037 | -17.6 | | | | | | | | |
| 225 | 1604.45 | 3.019 | -17.7 | | | | | | | | |
| 226 | 1607.46 | 3.002 | -17.7 | | | | | | | | |
| 227 | 1610.45 | 2.984 | -17.8 | | | | | | | | |
| 228 | 1613.42 | 2.966 | -17.9 | | | | | | | | |
| 229 | 1616.38 | 2.948 | -17.9 | | | | | | | | |
| 230 | 1619.32 | 2.930 | -18.0 | | | | | | | | |
| 231 | 1622.24 | 2.912 | -18.0 | | | | | | | | |
| 232 | 1625.15 | 2.894 | -18.0 | | | | | | | | |
| 233 | 1628.03 | 2.876 | -18.0 | | | | | | | | |
| 234 | 1630.90 | 2.858 | -18.0 | | | | | | | | |
| 235 | 1633.75 | 2.840 | -17.9 | | | | | | | | |
| 236 | 1636.58 | 2.822 | -17.9 | | | | | | | | |
| 237 | 1639.39 | 2.805 | -17.8 | | | | | | | | |
| 238 | 1642.19 | 2.787 | -17.7 | | | | | | | | |
| 239 | 1644.97 | 2.769 | -17.5 | | | | | | | | |
| 240 | 1647.73 | 2.752 | -17.3 | | | | | | | | |

TABLE 8. *Thermocouple copper versus* Au-0.02 *at%* $Fe_{45}$ *– thermoelectric voltage, Seebeck coefficient, and derivative of the Seebeck coefficient;* E = f(T)

| T K | E μV | S μV/K | dS/dT nV/K² | T K | E μV | S μV/K | dS/dT nV/K² | T K | E μV | S μV/K | dS/dT nV/K² |
|---|---|---|---|---|---|---|---|---|---|---|---|
| 0 | 0.00 | 0.000 | 0.0 | 60 | 565.27 | 5.245 | -69.6 | 120 | 790.55 | 2.682 | -27.7 |
| 1 | 8.20 | 9.084 | 1645.5 | 61 | 570.48 | 5.176 | -68.4 | 121 | 793.22 | 2.655 | -27.4 |
| 2 | 18.06 | 10.568 | 1329.6 | 62 | 575.62 | 5.108 | -67.1 | 122 | 795.86 | 2.628 | -27.0 |
| 3 | 29.24 | 11.757 | 1054.3 | 63 | 580.70 | 5.042 | -66.0 | 123 | 798.48 | 2.601 | -26.7 |
| 4 | 41.48 | 12.689 | 815.3 | 64 | 585.70 | 4.976 | -64.8 | 124 | 801.07 | 2.574 | -26.4 |
| 5 | 54.55 | 13.399 | 608.9 | 65 | 590.65 | 4.912 | -63.7 | 125 | 803.63 | 2.548 | -26.0 |
| 6 | 68.22 | 13.916 | 431.5 | 66 | 595.53 | 4.849 | -62.6 | 126 | 806.16 | 2.522 | -25.7 |
| 7 | 82.32 | 14.270 | 280.0 | 67 | 600.35 | 4.787 | -61.5 | 127 | 808.67 | 2.497 | -25.3 |
| 8 | 96.71 | 14.484 | 151.5 | 68 | 605.10 | 4.726 | -60.4 | 128 | 811.15 | 2.471 | -24.9 |
| 9 | 111.25 | 14.580 | 43.4 | 69 | 609.80 | 4.666 | -59.3 | 129 | 813.61 | 2.447 | -24.5 |
| 10 | 125.84 | 14.577 | -46.7 | 70 | 614.43 | 4.607 | -58.2 | 130 | 816.05 | 2.422 | -24.1 |
| 11 | 140.38 | 14.492 | -121.0 | 71 | 619.01 | 4.550 | -57.1 | 131 | 818.46 | 2.398 | -23.7 |
| 12 | 154.80 | 14.340 | -181.4 | 72 | 623.53 | 4.493 | -56.0 | 132 | 820.85 | 2.375 | -23.3 |
| 13 | 169.04 | 14.133 | -229.7 | 73 | 628.00 | 4.438 | -54.9 | 133 | 823.21 | 2.352 | -22.9 |
| 14 | 183.05 | 13.884 | -267.4 | 74 | 632.41 | 4.383 | -53.9 | 134 | 825.55 | 2.329 | -22.5 |
| 15 | 196.80 | 13.601 | -296.0 | 75 | 636.77 | 4.330 | -52.8 | 135 | 827.87 | 2.307 | -22.1 |
| 16 | 210.25 | 13.294 | -316.8 | 76 | 641.07 | 4.278 | -51.7 | 136 | 830.16 | 2.285 | -21.7 |
| 17 | 223.38 | 12.970 | -331.0 | 77 | 645.32 | 4.226 | -50.7 | 137 | 832.44 | 2.263 | -21.3 |
| 18 | 236.18 | 12.634 | -339.4 | 78 | 649.52 | 4.176 | -49.6 | 138 | 834.69 | 2.242 | -20.9 |
| 19 | 248.65 | 12.293 | -343.1 | 79 | 653.67 | 4.127 | -48.6 | 139 | 836.92 | 2.222 | -20.5 |
| 20 | 260.77 | 11.950 | -342.8 | 80 | 657.78 | 4.079 | -47.6 | 140 | 839.13 | 2.201 | -20.1 |
| 21 | 272.55 | 11.608 | -339.2 | 81 | 661.83 | 4.032 | -46.6 | 141 | 841.32 | 2.181 | -19.7 |
| 22 | 283.99 | 11.272 | -333.0 | 82 | 665.84 | 3.986 | -45.6 | 142 | 843.50 | 2.162 | -19.3 |
| 23 | 295.09 | 10.943 | -324.7 | 83 | 669.81 | 3.941 | -44.6 | 143 | 845.65 | 2.143 | -19.0 |
| 24 | 305.88 | 10.623 | -314.8 | 84 | 673.72 | 3.897 | -43.7 | 144 | 847.78 | 2.124 | -18.6 |
| 25 | 316.34 | 10.314 | -303.7 | 85 | 677.60 | 3.853 | -42.8 | 145 | 849.90 | 2.105 | -18.3 |
| 26 | 326.51 | 10.016 | -291.7 | 86 | 681.43 | 3.811 | -42.0 | 146 | 851.99 | 2.087 | -18.0 |
| 27 | 336.38 | 9.731 | -279.1 | 87 | 685.22 | 3.769 | -41.1 | 147 | 854.07 | 2.069 | -17.6 |
| 28 | 345.97 | 9.458 | -266.3 | 88 | 688.97 | 3.729 | -40.3 | 148 | 856.13 | 2.052 | -17.3 |
| 29 | 355.30 | 9.198 | -253.3 | 89 | 692.68 | 3.689 | -39.6 | 149 | 858.17 | 2.035 | -17.1 |
| 30 | 364.37 | 8.951 | -240.4 | 90 | 696.35 | 3.650 | -38.9 | 150 | 860.20 | 2.018 | -16.8 |
| 31 | 373.21 | 8.717 | -227.8 | 91 | 699.98 | 3.611 | -38.2 | 151 | 862.21 | 2.001 | -16.5 |
| 32 | 381.81 | 8.495 | -215.5 | 92 | 703.57 | 3.573 | -37.5 | 152 | 864.20 | 1.985 | -16.3 |
| 33 | 390.20 | 8.286 | -203.7 | 93 | 707.13 | 3.536 | -36.9 | 153 | 866.18 | 1.969 | -16.1 |
| 34 | 398.39 | 8.088 | -192.3 | 94 | 710.64 | 3.499 | -36.3 | 154 | 868.14 | 1.953 | -15.9 |
| 35 | 406.38 | 7.901 | -181.6 | 95 | 714.12 | 3.463 | -35.7 | 155 | 870.08 | 1.937 | -15.7 |
| 36 | 414.19 | 7.725 | -171.4 | 96 | 717.57 | 3.428 | -35.2 | 156 | 872.01 | 1.921 | -15.5 |
| 37 | 421.83 | 7.558 | -161.8 | 97 | 720.98 | 3.393 | -34.7 | 157 | 873.93 | 1.906 | -15.4 |
| 38 | 429.31 | 7.401 | -152.9 | 98 | 724.36 | 3.359 | -34.3 | 158 | 875.82 | 1.890 | -15.3 |
| 39 | 436.64 | 7.252 | -144.6 | 99 | 727.70 | 3.324 | -33.8 | 159 | 877.71 | 1.875 | -15.1 |
| 40 | 443.82 | 7.111 | -136.9 | 100 | 731.01 | 3.291 | -33.4 | 160 | 879.57 | 1.860 | -15.0 |
| 41 | 450.86 | 6.978 | -129.8 | 101 | 734.28 | 3.258 | -33.0 | 161 | 881.43 | 1.845 | -14.9 |
| 42 | 457.78 | 6.851 | -123.3 | 102 | 737.52 | 3.225 | -32.7 | 162 | 883.26 | 1.830 | -14.9 |
| 43 | 464.57 | 6.731 | -117.4 | 103 | 740.73 | 3.192 | -32.4 | 163 | 885.09 | 1.815 | -14.8 |
| 44 | 471.24 | 6.616 | -111.9 | 104 | 743.91 | 3.160 | -32.0 | 164 | 886.90 | 1.801 | -14.7 |
| 45 | 477.80 | 6.507 | -107.0 | 105 | 747.05 | 3.128 | -31.7 | 165 | 888.69 | 1.786 | -14.7 |
| 46 | 484.25 | 6.402 | -102.5 | 106 | 750.16 | 3.097 | -31.4 | 166 | 890.47 | 1.771 | -14.6 |
| 47 | 490.61 | 6.302 | -98.4 | 107 | 753.24 | 3.065 | -31.2 | 167 | 892.23 | 1.757 | -14.6 |
| 48 | 496.86 | 6.205 | -94.8 | 108 | 756.29 | 3.034 | -30.9 | 168 | 893.98 | 1.742 | -14.5 |
| 49 | 503.02 | 6.112 | -91.4 | 109 | 759.31 | 3.003 | -30.6 | 169 | 895.71 | 1.728 | -14.5 |
| 50 | 509.09 | 6.022 | -88.4 | 110 | 762.30 | 2.973 | -30.4 | 170 | 897.44 | 1.713 | -14.5 |
| 51 | 515.06 | 5.935 | -86.7 | 111 | 765.26 | 2.943 | -30.1 | 171 | 899.14 | 1.699 | -14.4 |
| 52 | 520.96 | 5.851 | -83.2 | 112 | 768.19 | 2.913 | -29.9 | 172 | 900.83 | 1.684 | -14.4 |
| 53 | 526.77 | 5.769 | -81.0 | 113 | 771.08 | 2.883 | -29.6 | 173 | 902.51 | 1.670 | -14.4 |
| 54 | 532.49 | 5.689 | -79.0 | 114 | 773.95 | 2.854 | -29.4 | 174 | 904.17 | 1.655 | -14.3 |
| 55 | 538.14 | 5.611 | -77.1 | 115 | 776.79 | 2.824 | -29.1 | 175 | 905.82 | 1.641 | -14.3 |
| 56 | 543.72 | 5.534 | -75.4 | 116 | 779.60 | 2.795 | -28.8 | 176 | 907.45 | 1.627 | -14.2 |
| 57 | 549.21 | 5.460 | -73.8 | 117 | 782.38 | 2.767 | -28.6 | 177 | 909.07 | 1.613 | -14.2 |
| 58 | 554.64 | 5.387 | -72.3 | 118 | 785.13 | 2.738 | -28.3 | 178 | 910.68 | 1.599 | -14.1 |
| 59 | 559.99 | 5.315 | -70.9 | 119 | 787.86 | 2.710 | -28.0 | 179 | 912.27 | 1.585 | -14.0 |
| 60 | 565.27 | 5.245 | -69.6 | 120 | 790.55 | 2.682 | -27.7 | 180 | 913.85 | 1.571 | -13.9 |

TABLE 8. *Thermocouple copper versus* Au-0.02 *at%* $Fe_{45}$ *– thermoelectric voltage, Seebeck coefficient, and derivative of the Seebeck coefficient;* E = f(T) – Continued

| T K | E μV | S μV/K | dS/dT nV/K² | T K | E μV | S μV/K | dS/dT nV/K² | T K | E μV | S μV/K | dS/dT nV/K² |
|---|---|---|---|---|---|---|---|---|---|---|---|
| 180 | 913.85 | 1.571 | -13.9 | 240 | 988.94 | 0.988 | -7.7 | | | | |
| 181 | 915.41 | 1.557 | -13.8 | 241 | 989.92 | 0.981 | -7.5 | | | | |
| 182 | 916.96 | 1.543 | -13.7 | 242 | 990.90 | 0.973 | -7.2 | | | | |
| 183 | 918.50 | 1.529 | -13.5 | 243 | 991.87 | 0.966 | -6.9 | | | | |
| 184 | 920.02 | 1.516 | -13.4 | 244 | 992.83 | 0.960 | -6.6 | | | | |
| 185 | 921.53 | 1.503 | -13.3 | 245 | 993.79 | 0.953 | -6.3 | | | | |
| 186 | 923.03 | 1.489 | -13.1 | 246 | 994.74 | 0.947 | -5.9 | | | | |
| 187 | 924.51 | 1.476 | -12.9 | 247 | 995.68 | 0.941 | -5.6 | | | | |
| 188 | 925.98 | 1.464 | -12.7 | 248 | 996.62 | 0.936 | -5.3 | | | | |
| 189 | 927.44 | 1.451 | -12.5 | 249 | 997.55 | 0.931 | -5.0 | | | | |
| 190 | 928.88 | 1.439 | -12.3 | 250 | 998.48 | 0.926 | -4.7 | | | | |
| 191 | 930.31 | 1.426 | -12.1 | 251 | 999.40 | 0.921 | -4.5 | | | | |
| 192 | 931.73 | 1.414 | -11.9 | 252 | 1000.32 | 0.917 | -4.3 | | | | |
| 193 | 933.14 | 1.403 | -11.6 | 253 | 1001.24 | 0.912 | -4.2 | | | | |
| 194 | 934.54 | 1.391 | -11.4 | 254 | 1002.15 | 0.908 | -4.2 | | | | |
| 195 | 935.92 | 1.380 | -11.2 | 255 | 1003.05 | 0.904 | -4.2 | | | | |
| 196 | 937.30 | 1.369 | -10.9 | 256 | 1003.95 | 0.900 | -4.3 | | | | |
| 197 | 938.66 | 1.358 | -10.7 | 257 | 1004.85 | 0.895 | -4.5 | | | | |
| 198 | 940.01 | 1.347 | -10.4 | 258 | 1005.75 | 0.891 | -4.8 | | | | |
| 199 | 941.36 | 1.337 | -10.2 | 259 | 1006.63 | 0.886 | -5.2 | | | | |
| 200 | 942.69 | 1.327 | -9.9 | 260 | 1007.52 | 0.880 | -5.7 | | | | |
| 201 | 944.01 | 1.317 | -9.7 | 261 | 1008.39 | 0.874 | -6.3 | | | | |
| 202 | 945.32 | 1.308 | -9.5 | 262 | 1009.27 | 0.868 | -6.9 | | | | |
| 203 | 946.63 | 1.298 | -9.3 | 263 | 1010.13 | 0.860 | -7.6 | | | | |
| 204 | 947.92 | 1.289 | -9.1 | 264 | 1010.99 | 0.852 | -8.3 | | | | |
| 205 | 949.20 | 1.280 | -8.9 | 265 | 1011.83 | 0.844 | -9.0 | | | | |
| 206 | 950.48 | 1.271 | -8.7 | 266 | 1012.67 | 0.834 | -9.7 | | | | |
| 207 | 951.75 | 1.263 | -8.5 | 267 | 1013.50 | 0.824 | -10.2 | | | | |
| 208 | 953.01 | 1.254 | -8.4 | 268 | 1014.32 | 0.814 | -10.5 | | | | |
| 209 | 954.26 | 1.246 | -8.3 | 269 | 1015.13 | 0.803 | -10.6 | | | | |
| 210 | 955.50 | 1.238 | -8.2 | 270 | 1015.93 | 0.793 | -10.2 | | | | |
| 211 | 956.73 | 1.230 | -8.1 | 271 | 1016.72 | 0.783 | -9.3 | | | | |
| 212 | 957.96 | 1.222 | -8.0 | 272 | 1017.50 | 0.775 | -7.7 | | | | |
| 213 | 959.17 | 1.214 | -8.0 | 273 | 1018.27 | 0.768 | -5.2 | | | | |
| 214 | 960.38 | 1.206 | -7.9 | 274 | 1019.03 | 0.765 | -1.6 | | | | |
| 215 | 961.59 | 1.198 | -7.9 | 275 | 1019.80 | 0.765 | 3.4 | | | | |
| 216 | 962.78 | 1.190 | -7.9 | 276 | 1020.57 | 0.772 | 10.0 | | | | |
| 217 | 963.96 | 1.182 | -7.9 | 277 | 1021.34 | 0.786 | 18.6 | | | | |
| 218 | 965.14 | 1.174 | -8.0 | 278 | 1022.14 | 0.810 | 29.6 | | | | |
| 219 | 966.31 | 1.166 | -8.0 | 279 | 1022.97 | 0.846 | 43.4 | | | | |
| 220 | 967.47 | 1.158 | -8.1 | 280 | 1023.84 | 0.898 | 60.5 | | | | |
| 221 | 968.63 | 1.150 | -8.1 | | | | | | | | |
| 222 | 969.77 | 1.142 | -8.2 | | | | | | | | |
| 223 | 970.91 | 1.133 | -8.3 | | | | | | | | |
| 224 | 972.04 | 1.125 | -8.4 | | | | | | | | |
| 225 | 973.16 | 1.116 | -8.5 | | | | | | | | |
| 226 | 974.27 | 1.108 | -8.6 | | | | | | | | |
| 227 | 975.38 | 1.099 | -8.6 | | | | | | | | |
| 228 | 976.47 | 1.091 | -8.7 | | | | | | | | |
| 229 | 977.56 | 1.082 | -8.7 | | | | | | | | |
| 230 | 978.64 | 1.073 | -8.8 | | | | | | | | |
| 231 | 979.70 | 1.064 | -8.8 | | | | | | | | |
| 232 | 980.76 | 1.056 | -8.8 | | | | | | | | |
| 233 | 981.82 | 1.047 | -8.8 | | | | | | | | |
| 234 | 982.86 | 1.038 | -8.7 | | | | | | | | |
| 235 | 983.89 | 1.029 | -8.6 | | | | | | | | |
| 236 | 984.92 | 1.021 | -8.5 | | | | | | | | |
| 237 | 985.93 | 1.013 | -8.4 | | | | | | | | |
| 238 | 986.94 | 1.004 | -8.2 | | | | | | | | |
| 239 | 987.94 | 0.996 | -8.0 | | | | | | | | |
| 240 | 988.94 | 0.988 | -7.7 | | | | | | | | |

TABLE 9. *Thermocouple "normal" silver versus Au-0.07 at% $Fe_{11}$ – thermoelectric voltage, Seebeck coefficient, and derivative of the Seebeck coefficient; E = f(T)*

| T K | E μV | S μV/K | dS/dT nV/K² | T K | E μV | S μV/K | dS/dT nV/K² | T K | E μV | S μV/K | dS/dT nV/K² |
|---|---|---|---|---|---|---|---|---|---|---|---|
| 0 | 0.00 | 0.000 | 0.0 | 60 | 700.37 | 8.447 | -81.3 | 120 | 1099.00 | 5.267 | -37.0 |
| 1 | 7.74 | 8.478 | 1402.0 | 61 | 708.77 | 8.367 | -79.7 | 121 | 1104.25 | 5.230 | -36.8 |
| 2 | 16.88 | 9.774 | 1193.0 | 62 | 717.10 | 8.288 | -78.2 | 122 | 1109.46 | 5.194 | -36.5 |
| 3 | 27.22 | 10.872 | 1006.5 | 63 | 725.35 | 8.210 | -76.7 | 123 | 1114.63 | 5.157 | -36.2 |
| 4 | 38.57 | 11.794 | 840.7 | 64 | 733.52 | 8.134 | -75.3 | 124 | 1119.77 | 5.121 | -36.0 |
| 5 | 50.76 | 12.560 | 693.6 | 65 | 741.62 | 8.060 | -74.0 | 125 | 1124.88 | 5.085 | -35.7 |
| 6 | 63.64 | 13.187 | 563.5 | 66 | 749.64 | 7.986 | -72.7 | 126 | 1129.94 | 5.050 | -35.5 |
| 7 | 77.09 | 13.692 | 448.8 | 67 | 757.59 | 7.914 | -71.4 | 127 | 1134.98 | 5.014 | -35.3 |
| 8 | 90.99 | 14.089 | 348.0 | 68 | 765.47 | 7.843 | -70.2 | 128 | 1139.97 | 4.979 | -35.0 |
| 9 | 105.24 | 14.392 | 259.7 | 69 | 773.28 | 7.774 | -69.1 | 129 | 1144.93 | 4.944 | -34.8 |
| 10 | 119.75 | 14.612 | 182.8 | 70 | 781.02 | 7.705 | -67.9 | 130 | 1149.86 | 4.910 | -34.5 |
| 11 | 134.44 | 14.761 | 116.0 | 71 | 788.69 | 7.638 | -66.8 | 131 | 1154.75 | 4.875 | -34.3 |
| 12 | 149.25 | 14.847 | 58.4 | 72 | 796.29 | 7.572 | -65.8 | 132 | 1159.61 | 4.841 | -34.0 |
| 13 | 164.11 | 14.880 | 8.9 | 73 | 803.83 | 7.506 | -64.7 | 133 | 1164.44 | 4.807 | -33.8 |
| 14 | 178.99 | 14.868 | -33.3 | 74 | 811.31 | 7.442 | -63.7 | 134 | 1169.23 | 4.774 | -33.5 |
| 15 | 193.84 | 14.816 | -68.9 | 75 | 818.72 | 7.379 | -62.7 | 135 | 1173.98 | 4.740 | -33.3 |
| 16 | 208.61 | 14.732 | -98.8 | 76 | 826.06 | 7.317 | -61.7 | 136 | 1178.71 | 4.707 | -33.0 |
| 17 | 223.29 | 14.620 | -123.6 | 77 | 833.35 | 7.255 | -60.8 | 137 | 1183.40 | 4.674 | -32.8 |
| 18 | 237.85 | 14.486 | -143.9 | 78 | 840.57 | 7.195 | -59.8 | 138 | 1188.06 | 4.642 | -32.5 |
| 19 | 252.26 | 14.333 | -160.3 | 79 | 847.74 | 7.136 | -58.9 | 139 | 1192.68 | 4.609 | -32.3 |
| 20 | 266.51 | 14.166 | -173.1 | 80 | 854.85 | 7.077 | -58.0 | 140 | 1197.28 | 4.577 | -32.0 |
| 21 | 280.59 | 13.988 | -183.0 | 81 | 861.90 | 7.020 | -57.1 | 141 | 1201.84 | 4.545 | -31.7 |
| 22 | 294.48 | 13.801 | -190.2 | 82 | 868.89 | 6.963 | -56.3 | 142 | 1206.37 | 4.514 | -31.5 |
| 23 | 308.19 | 13.608 | -195.2 | 83 | 875.82 | 6.907 | -55.4 | 143 | 1210.86 | 4.482 | -31.2 |
| 24 | 321.70 | 13.412 | -198.2 | 84 | 882.70 | 6.852 | -54.6 | 144 | 1215.33 | 4.451 | -31.0 |
| 25 | 335.01 | 13.213 | -199.5 | 85 | 889.53 | 6.798 | -53.8 | 145 | 1219.77 | 4.420 | -30.7 |
| 26 | 348.12 | 13.013 | -199.5 | 86 | 896.30 | 6.745 | -53.0 | 146 | 1224.17 | 4.390 | -30.5 |
| 27 | 361.03 | 12.814 | -198.3 | 87 | 903.02 | 6.692 | -52.2 | 147 | 1228.55 | 4.359 | -30.3 |
| 28 | 373.75 | 12.617 | -196.1 | 88 | 909.68 | 6.640 | -51.5 | 148 | 1232.89 | 4.329 | -30.0 |
| 29 | 386.27 | 12.422 | -193.2 | 89 | 916.30 | 6.589 | -50.7 | 149 | 1237.20 | 4.299 | -29.8 |
| 30 | 398.60 | 12.231 | -189.6 | 90 | 922.86 | 6.539 | -50.0 | 150 | 1241.49 | 4.270 | -29.5 |
| 31 | 410.73 | 12.043 | -185.5 | 91 | 929.37 | 6.489 | -49.3 | 151 | 1245.74 | 4.240 | -29.3 |
| 32 | 422.68 | 11.860 | -181.0 | 92 | 935.84 | 6.440 | -48.7 | 152 | 1249.97 | 4.211 | -29.1 |
| 33 | 434.45 | 11.681 | -176.3 | 93 | 942.25 | 6.392 | -48.0 | 153 | 1254.17 | 4.182 | -28.8 |
| 34 | 446.05 | 11.507 | -171.4 | 94 | 948.62 | 6.344 | -47.4 | 154 | 1258.33 | 4.153 | -28.6 |
| 35 | 457.47 | 11.338 | -166.4 | 95 | 954.94 | 6.297 | -46.8 | 155 | 1262.47 | 4.125 | -28.4 |
| 36 | 468.72 | 11.174 | -161.3 | 96 | 961.22 | 6.250 | -46.2 | 156 | 1266.58 | 4.097 | -28.2 |
| 37 | 479.82 | 11.016 | -156.3 | 97 | 967.44 | 6.205 | -45.6 | 157 | 1270.67 | 4.068 | -28.0 |
| 38 | 490.76 | 10.862 | -151.3 | 98 | 973.63 | 6.159 | -45.1 | 158 | 1274.72 | 4.041 | -27.8 |
| 39 | 501.54 | 10.713 | -146.4 | 99 | 979.76 | 6.114 | -44.6 | 159 | 1278.75 | 4.013 | -27.6 |
| 40 | 512.19 | 10.569 | -141.6 | 100 | 985.85 | 6.070 | -44.1 | 160 | 1282.75 | 3.985 | -27.4 |
| 41 | 522.68 | 10.430 | -136.9 | 101 | 991.90 | 6.026 | -43.6 | 161 | 1286.72 | 3.958 | -27.2 |
| 42 | 533.05 | 10.295 | -132.5 | 102 | 997.91 | 5.983 | -43.1 | 162 | 1290.66 | 3.931 | -27.0 |
| 43 | 543.28 | 10.165 | -128.2 | 103 | 1003.87 | 5.940 | -42.6 | 163 | 1294.58 | 3.904 | -26.8 |
| 44 | 553.38 | 10.039 | -124.1 | 104 | 1009.79 | 5.898 | -42.2 | 164 | 1298.47 | 3.877 | -26.6 |
| 45 | 563.36 | 9.917 | -120.1 | 105 | 1015.66 | 5.856 | -41.8 | 165 | 1302.34 | 3.851 | -26.4 |
| 46 | 573.21 | 9.798 | -116.4 | 106 | 1021.50 | 5.814 | -41.4 | 166 | 1306.17 | 3.825 | -26.3 |
| 47 | 582.95 | 9.684 | -112.9 | 107 | 1027.29 | 5.773 | -41.0 | 167 | 1309.98 | 3.798 | -26.1 |
| 48 | 592.58 | 9.573 | -109.5 | 108 | 1033.04 | 5.732 | -40.6 | 168 | 1313.77 | 3.772 | -25.9 |
| 49 | 602.10 | 9.465 | -106.3 | 109 | 1038.76 | 5.692 | -40.3 | 169 | 1317.53 | 3.747 | -25.8 |
| 50 | 611.51 | 9.360 | -103.3 | 110 | 1044.43 | 5.651 | -39.9 | 170 | 1321.26 | 3.721 | -25.6 |
| 51 | 620.82 | 9.258 | -100.5 | 111 | 1050.06 | 5.612 | -39.6 | 171 | 1324.97 | 3.695 | -25.5 |
| 52 | 630.03 | 9.159 | -97.9 | 112 | 1055.65 | 5.572 | -39.3 | 172 | 1328.65 | 3.670 | -25.3 |
| 53 | 639.14 | 9.062 | -95.3 | 113 | 1061.20 | 5.533 | -39.0 | 173 | 1332.31 | 3.645 | -25.1 |
| 54 | 648.15 | 8.968 | -93.0 | 114 | 1066.72 | 5.494 | -38.7 | 174 | 1335.94 | 3.620 | -25.0 |
| 55 | 657.08 | 8.876 | -90.7 | 115 | 1072.19 | 5.456 | -38.4 | 175 | 1339.55 | 3.595 | -24.8 |
| 56 | 665.91 | 8.787 | -88.6 | 116 | 1077.63 | 5.418 | -38.1 | 176 | 1343.13 | 3.570 | -24.7 |
| 57 | 674.65 | 8.699 | -86.7 | 117 | 1083.03 | 5.380 | -37.8 | 177 | 1346.69 | 3.545 | -24.5 |
| 58 | 683.31 | 8.613 | -84.8 | 118 | 1088.39 | 5.342 | -37.5 | 178 | 1350.22 | 3.521 | -24.4 |
| 59 | 691.88 | 8.529 | -83.0 | 119 | 1093.71 | 5.304 | -37.3 | 179 | 1353.73 | 3.497 | -24.2 |
| 60 | 700.37 | 8.447 | -81.3 | 120 | 1099.00 | 5.267 | -37.0 | 180 | 1357.22 | 3.472 | -24.1 |

TABLE 9. *Thermocouple "normal" silver versus Au-0.07 at% $Fe_{11}$ – thermoelectric voltage, Seebeck coefficient, and derivative of the Seebeck coefficient; E = f(T)* – Continued

| T K | E μV | S μV/K | dS/dT nV/K² | T K | E μV | S μV/K | dS/dT nV/K² | T K | E μV | S μV/K | dS/dT nV/K² |
|---|---|---|---|---|---|---|---|---|---|---|---|
| 180 | 1357.22 | 3.472 | -24.1 | 240 | 1528.08 | 2.288 | -18.2 | | | | |
| 181 | 1360.68 | 3.448 | -23.9 | 241 | 1530.36 | 2.270 | -18.1 | | | | |
| 182 | 1364.11 | 3.425 | -23.8 | 242 | 1532.62 | 2.252 | -18.0 | | | | |
| 183 | 1367.53 | 3.401 | -23.6 | 243 | 1534.86 | 2.234 | -17.9 | | | | |
| 184 | 1370.92 | 3.377 | -23.4 | 244 | 1537.09 | 2.216 | -17.7 | | | | |
| 185 | 1374.28 | 3.354 | -23.3 | 245 | 1539.29 | 2.198 | -17.6 | | | | |
| 186 | 1377.62 | 3.331 | -23.1 | 246 | 1541.48 | 2.181 | -17.3 | | | | |
| 187 | 1380.94 | 3.308 | -22.9 | 247 | 1543.65 | 2.163 | -17.1 | | | | |
| 188 | 1384.24 | 3.285 | -22.8 | 248 | 1545.81 | 2.146 | -16.8 | | | | |
| 189 | 1387.51 | 3.262 | -22.6 | 249 | 1547.95 | 2.130 | -16.5 | | | | |
| 190 | 1390.76 | 3.240 | -22.4 | 250 | 1550.07 | 2.113 | -16.1 | | | | |
| 191 | 1393.99 | 3.217 | -22.2 | 251 | 1552.17 | 2.098 | -15.7 | | | | |
| 192 | 1397.20 | 3.195 | -22.0 | 252 | 1554.26 | 2.082 | -15.3 | | | | |
| 193 | 1400.38 | 3.173 | -21.9 | 253 | 1556.34 | 2.067 | -14.8 | | | | |
| 194 | 1403.54 | 3.152 | -21.7 | 254 | 1558.40 | 2.053 | -14.3 | | | | |
| 195 | 1406.69 | 3.130 | -21.5 | 255 | 1560.44 | 2.038 | -13.8 | | | | |
| 196 | 1409.80 | 3.109 | -21.3 | 256 | 1562.48 | 2.025 | -13.2 | | | | |
| 197 | 1412.90 | 3.087 | -21.1 | 257 | 1564.49 | 2.012 | -12.6 | | | | |
| 198 | 1415.98 | 3.067 | -20.9 | 258 | 1566.50 | 2.000 | -12.1 | | | | |
| 199 | 1419.04 | 3.046 | -20.7 | 259 | 1568.49 | 1.988 | -11.5 | | | | |
| 200 | 1422.07 | 3.025 | -20.5 | 260 | 1570.48 | 1.977 | -10.9 | | | | |
| 201 | 1425.09 | 3.005 | -20.3 | 261 | 1572.45 | 1.966 | -10.4 | | | | |
| 202 | 1428.08 | 2.985 | -20.1 | 262 | 1574.41 | 1.956 | -9.9 | | | | |
| 203 | 1431.06 | 2.965 | -19.9 | 263 | 1576.36 | 1.946 | -9.4 | | | | |
| 204 | 1434.01 | 2.945 | -19.7 | 264 | 1578.30 | 1.937 | -9.1 | | | | |
| 205 | 1436.94 | 2.925 | -19.6 | 265 | 1580.23 | 1.928 | -8.8 | | | | |
| 206 | 1439.86 | 2.906 | -19.4 | 266 | 1582.16 | 1.920 | -8.6 | | | | |
| 207 | 1442.76 | 2.886 | -19.2 | 267 | 1584.07 | 1.911 | -8.6 | | | | |
| 208 | 1445.63 | 2.867 | -19.0 | 268 | 1585.98 | 1.902 | -8.7 | | | | |
| 209 | 1448.49 | 2.848 | -18.9 | 269 | 1587.88 | 1.893 | -9.1 | | | | |
| 210 | 1451.33 | 2.829 | -18.7 | 270 | 1589.77 | 1.884 | -9.7 | | | | |
| 211 | 1454.15 | 2.811 | -18.6 | 271 | 1591.65 | 1.874 | -10.5 | | | | |
| 212 | 1456.95 | 2.792 | -18.5 | 272 | 1593.51 | 1.863 | -11.7 | | | | |
| 213 | 1459.73 | 2.774 | -18.3 | 273 | 1595.37 | 1.851 | -13.2 | | | | |
| 214 | 1462.50 | 2.755 | -18.2 | 274 | 1597.21 | 1.836 | -15.1 | | | | |
| 215 | 1465.24 | 2.737 | -18.1 | 275 | 1599.04 | 1.820 | -17.4 | | | | |
| 216 | 1467.97 | 2.719 | -18.0 | 276 | 1600.85 | 1.801 | -20.2 | | | | |
| 217 | 1470.68 | 2.701 | -18.0 | 277 | 1602.64 | 1.780 | -23.6 | | | | |
| 218 | 1473.38 | 2.683 | -17.9 | 278 | 1604.41 | 1.754 | -27.6 | | | | |
| 219 | 1476.05 | 2.665 | -17.9 | 279 | 1606.15 | 1.724 | -32.3 | | | | |
| 220 | 1478.71 | 2.648 | -17.8 | 280 | 1607.86 | 1.689 | -37.7 | | | | |
| 221 | 1481.34 | 2.630 | -17.8 | | | | | | | | |
| 222 | 1483.97 | 2.612 | -17.8 | | | | | | | | |
| 223 | 1486.57 | 2.594 | -17.8 | | | | | | | | |
| 224 | 1489.15 | 2.576 | -17.8 | | | | | | | | |
| 225 | 1491.72 | 2.559 | -17.8 | | | | | | | | |
| 226 | 1494.27 | 2.541 | -17.8 | | | | | | | | |
| 227 | 1496.80 | 2.523 | -17.8 | | | | | | | | |
| 228 | 1499.32 | 2.505 | -17.9 | | | | | | | | |
| 229 | 1501.81 | 2.487 | -17.9 | | | | | | | | |
| 230 | 1504.29 | 2.469 | -18.0 | | | | | | | | |
| 231 | 1506.75 | 2.451 | -18.0 | | | | | | | | |
| 232 | 1509.19 | 2.433 | -18.1 | | | | | | | | |
| 233 | 1511.62 | 2.415 | -18.1 | | | | | | | | |
| 234 | 1514.03 | 2.397 | -18.2 | | | | | | | | |
| 235 | 1516.41 | 2.379 | -18.2 | | | | | | | | |
| 236 | 1518.78 | 2.361 | -18.2 | | | | | | | | |
| 237 | 1521.13 | 2.342 | -18.2 | | | | | | | | |
| 238 | 1523.47 | 2.324 | -18.2 | | | | | | | | |
| 239 | 1525.78 | 2.306 | -18.2 | | | | | | | | |
| 240 | 1528.08 | 2.288 | -18.2 | | | | | | | | |

TABLE 10. *Thermocouple "normal" silver versus Au-0.02 at% $Fe_{45}$ — thermoelectric voltage, Seebeck coefficient, and derivative of the Seebeck coefficient; E = f(T)*

| T K | E μV | S μV/K | dS/dT nV/K² | T K | E μV | S μV/K | dS/dT nV/K² | T K | E μV | S μV/K | dS/dT nV/K² |
|---|---|---|---|---|---|---|---|---|---|---|---|
| 0 | 0.00 | 0.000 | 0.0 | 60 | 546.11 | 4.361 | -69.2 | 120 | 727.52 | 2.115 | -22.9 |
| 1 | 8.17 | 9.032 | 1624.0 | 61 | 550.44 | 4.293 | -67.2 | 121 | 729.62 | 2.092 | -22.7 |
| 2 | 17.96 | 10.503 | 1325.6 | 62 | 554.70 | 4.227 | -65.2 | 122 | 731.70 | 2.069 | -22.5 |
| 3 | 29.08 | 11.695 | 1063.4 | 63 | 558.89 | 4.163 | -63.3 | 123 | 733.76 | 2.047 | -22.3 |
| 4 | 41.27 | 12.641 | 833.7 | 64 | 563.02 | 4.100 | -61.6 | 124 | 735.80 | 2.025 | -22.0 |
| 5 | 54.29 | 13.372 | 633.5 | 65 | 567.09 | 4.039 | -59.9 | 125 | 737.81 | 2.003 | -21.8 |
| 6 | 67.95 | 13.917 | 459.6 | 66 | 571.10 | 3.980 | -58.4 | 126 | 739.80 | 1.981 | -21.6 |
| 7 | 82.07 | 14.299 | 309.5 | 67 | 575.05 | 3.923 | -56.9 | 127 | 741.77 | 1.960 | -21.3 |
| 8 | 96.50 | 14.543 | 180.6 | 68 | 578.95 | 3.867 | -55.4 | 128 | 743.72 | 1.939 | -21.1 |
| 9 | 111.11 | 14.667 | 70.7 | 69 | 582.79 | 3.812 | -54.0 | 129 | 745.65 | 1.918 | -20.8 |
| 10 | 125.80 | 14.690 | -22.4 | 70 | 586.57 | 3.758 | -52.7 | 130 | 747.56 | 1.897 | -20.6 |
| 11 | 140.46 | 14.627 | -100.5 | 71 | 590.30 | 3.706 | -51.4 | 131 | 749.44 | 1.876 | -20.3 |
| 12 | 155.03 | 14.493 | -165.3 | 72 | 593.98 | 3.656 | -50.1 | 132 | 751.31 | 1.856 | -20.1 |
| 13 | 169.43 | 14.300 | -218.4 | 73 | 597.61 | 3.606 | -48.9 | 133 | 753.16 | 1.836 | -19.8 |
| 14 | 183.61 | 14.060 | -261.2 | 74 | 601.20 | 3.558 | -47.8 | 134 | 754.98 | 1.817 | -19.5 |
| 15 | 197.54 | 13.781 | -294.9 | 75 | 604.73 | 3.511 | -46.6 | 135 | 756.79 | 1.797 | -19.3 |
| 16 | 211.17 | 13.473 | -320.8 | 76 | 608.22 | 3.465 | -45.5 | 136 | 758.58 | 1.778 | -19.0 |
| 17 | 224.48 | 13.142 | -339.9 | 77 | 611.66 | 3.420 | -44.4 | 137 | 760.35 | 1.759 | -18.7 |
| 18 | 237.45 | 12.795 | -353.1 | 78 | 615.06 | 3.376 | -43.4 | 138 | 762.10 | 1.741 | -18.5 |
| 19 | 250.06 | 12.437 | -361.2 | 79 | 618.41 | 3.333 | -42.4 | 139 | 763.83 | 1.722 | -18.2 |
| 20 | 262.32 | 12.074 | -365.1 | 80 | 621.72 | 3.291 | -41.4 | 140 | 765.54 | 1.704 | -17.9 |
| 21 | 274.21 | 11.708 | -365.3 | 81 | 624.99 | 3.250 | -40.4 | 141 | 767.24 | 1.686 | -17.7 |
| 22 | 285.73 | 11.344 | -362.5 | 82 | 628.22 | 3.210 | -39.5 | 142 | 768.91 | 1.669 | -17.4 |
| 23 | 296.90 | 10.984 | -357.1 | 83 | 631.41 | 3.171 | -38.6 | 143 | 770.57 | 1.652 | -17.2 |
| 24 | 307.70 | 10.630 | -349.8 | 84 | 634.57 | 3.133 | -37.7 | 144 | 772.22 | 1.635 | -16.9 |
| 25 | 318.16 | 10.285 | -340.8 | 85 | 637.68 | 3.095 | -36.9 | 145 | 773.84 | 1.618 | -16.7 |
| 26 | 328.28 | 9.949 | -330.5 | 86 | 640.76 | 3.059 | -36.1 | 146 | 775.45 | 1.601 | -16.4 |
| 27 | 338.06 | 9.624 | -319.3 | 87 | 643.80 | 3.023 | -35.3 | 147 | 777.05 | 1.585 | -16.2 |
| 28 | 347.53 | 9.311 | -307.4 | 88 | 646.80 | 2.988 | -34.6 | 148 | 778.62 | 1.569 | -16.0 |
| 29 | 356.69 | 9.010 | -295.0 | 89 | 649.77 | 2.954 | -33.9 | 149 | 780.18 | 1.553 | -15.8 |
| 30 | 365.55 | 8.721 | -282.4 | 90 | 652.71 | 2.921 | -33.2 | 150 | 781.73 | 1.537 | -15.6 |
| 31 | 374.14 | 8.445 | -269.7 | 91 | 655.62 | 2.888 | -32.5 | 151 | 783.26 | 1.522 | -15.4 |
| 32 | 382.45 | 8.182 | -257.0 | 92 | 658.49 | 2.856 | -31.9 | 152 | 784.77 | 1.507 | -15.2 |
| 33 | 390.50 | 7.931 | -244.6 | 93 | 661.33 | 2.824 | -31.3 | 153 | 786.27 | 1.491 | -15.0 |
| 34 | 398.31 | 7.692 | -232.4 | 94 | 664.14 | 2.793 | -30.7 | 154 | 787.75 | 1.476 | -14.9 |
| 35 | 405.89 | 7.466 | -220.5 | 95 | 666.91 | 2.762 | -30.2 | 155 | 789.22 | 1.462 | -14.7 |
| 36 | 413.25 | 7.251 | -209.1 | 96 | 669.66 | 2.733 | -29.7 | 156 | 790.68 | 1.447 | -14.6 |
| 37 | 420.40 | 7.048 | -198.1 | 97 | 672.38 | 2.703 | -29.2 | 157 | 792.12 | 1.433 | -14.4 |
| 38 | 427.35 | 6.855 | -187.6 | 98 | 675.07 | 2.674 | -28.8 | 158 | 793.54 | 1.418 | -14.3 |
| 39 | 434.11 | 6.672 | -177.6 | 99 | 677.73 | 2.646 | -28.3 | 159 | 794.95 | 1.404 | -14.2 |
| 40 | 440.70 | 6.499 | -168.2 | 100 | 680.36 | 2.617 | -27.9 | 160 | 796.35 | 1.390 | -14.1 |
| 41 | 447.11 | 6.336 | -159.2 | 101 | 682.96 | 2.590 | -27.6 | 161 | 797.73 | 1.376 | -14.0 |
| 42 | 453.37 | 6.181 | -150.8 | 102 | 685.54 | 2.562 | -27.2 | 162 | 799.10 | 1.362 | -13.9 |
| 43 | 459.48 | 6.034 | -143.0 | 103 | 688.09 | 2.535 | -26.9 | 163 | 800.46 | 1.348 | -13.8 |
| 44 | 465.44 | 5.895 | -135.6 | 104 | 690.61 | 2.508 | -26.6 | 164 | 801.80 | 1.334 | -13.8 |
| 45 | 471.27 | 5.763 | -128.7 | 105 | 693.10 | 2.482 | -26.3 | 165 | 803.13 | 1.320 | -13.7 |
| 46 | 476.97 | 5.637 | -122.3 | 106 | 695.57 | 2.456 | -26.0 | 166 | 804.44 | 1.307 | -13.7 |
| 47 | 482.55 | 5.518 | -116.4 | 107 | 698.02 | 2.430 | -25.7 | 167 | 805.74 | 1.293 | -13.6 |
| 48 | 488.01 | 5.404 | -110.9 | 108 | 700.43 | 2.404 | -25.5 | 168 | 807.03 | 1.279 | -13.6 |
| 49 | 493.36 | 5.296 | -105.7 | 109 | 702.82 | 2.379 | -25.2 | 169 | 808.30 | 1.266 | -13.5 |
| 50 | 498.60 | 5.193 | -101.0 | 110 | 705.19 | 2.354 | -25.0 | 170 | 809.56 | 1.252 | -13.5 |
| 51 | 503.74 | 5.094 | -96.6 | 111 | 707.53 | 2.329 | -24.8 | 171 | 810.80 | 1.239 | -13.4 |
| 52 | 508.79 | 4.999 | -92.6 | 112 | 709.85 | 2.305 | -24.5 | 172 | 812.04 | 1.226 | -13.4 |
| 53 | 513.74 | 4.909 | -88.8 | 113 | 712.14 | 2.280 | -24.3 | 173 | 813.25 | 1.212 | -13.4 |
| 54 | 518.61 | 4.822 | -85.4 | 114 | 714.41 | 2.256 | -24.1 | 174 | 814.46 | 1.199 | -13.3 |
| 55 | 523.39 | 4.738 | -82.2 | 115 | 716.65 | 2.232 | -23.9 | 175 | 815.65 | 1.186 | -13.3 |
| 56 | 528.09 | 4.657 | -79.2 | 116 | 718.87 | 2.208 | -23.7 | 176 | 816.83 | 1.172 | -13.2 |
| 57 | 532.70 | 4.579 | -76.4 | 117 | 721.07 | 2.184 | -23.5 | 177 | 818.00 | 1.159 | -13.2 |
| 58 | 537.25 | 4.504 | -73.9 | 118 | 723.24 | 2.161 | -23.3 | 178 | 819.15 | 1.146 | -13.2 |
| 59 | 541.71 | 4.432 | -71.5 | 119 | 725.39 | 2.138 | -23.1 | 179 | 820.29 | 1.133 | -13.1 |
| 60 | 546.11 | 4.361 | -69.2 | 120 | 727.52 | 2.115 | -22.9 | 180 | 821.41 | 1.120 | -13.0 |

TABLE 10. *Thermocouple "normal" silver versus Au-0.02 at% $Fe_{45}$ — thermoelectric voltage, Seebeck coefficient, and derivative of the Seebeck coefficient; E = f(T)* — Continued

| T K | E μV | S μV/K | dS/dT nV/K² | T K | E μV | S μV/K | dS/dT nV/K² | T K | E μV | S μV/K | dS/dT nV/K² |
|---|---|---|---|---|---|---|---|---|---|---|---|
| 180 | 821.41 | 1.120 | -13.0 | 240 | 869.29 | 0.524 | -8.6 | | | | |
| 181 | 822.53 | 1.107 | -13.0 | 241 | 869.81 | 0.516 | -8.5 | | | | |
| 182 | 823.63 | 1.094 | -12.9 | 242 | 870.32 | 0.507 | -8.4 | | | | |
| 183 | 824.71 | 1.081 | -12.8 | 243 | 870.82 | 0.499 | -8.2 | | | | |
| 184 | 825.79 | 1.068 | -12.7 | 244 | 871.32 | 0.491 | -8.0 | | | | |
| 185 | 826.85 | 1.055 | -12.6 | 245 | 871.80 | 0.483 | -7.9 | | | | |
| 186 | 827.90 | 1.043 | -12.5 | 246 | 872.28 | 0.475 | -7.7 | | | | |
| 187 | 828.94 | 1.030 | -12.4 | 247 | 872.75 | 0.468 | -7.5 | | | | |
| 188 | 829.96 | 1.018 | -12.3 | 248 | 873.22 | 0.460 | -7.3 | | | | |
| 189 | 830.97 | 1.006 | -12.2 | 249 | 873.68 | 0.453 | -7.1 | | | | |
| 190 | 831.97 | 0.994 | -12.1 | 250 | 874.12 | 0.446 | -6.9 | | | | |
| 191 | 832.96 | 0.982 | -11.9 | 251 | 874.57 | 0.439 | -6.6 | | | | |
| 192 | 833.94 | 0.970 | -11.8 | 252 | 875.00 | 0.433 | -6.5 | | | | |
| 193 | 834.90 | 0.958 | -11.6 | 253 | 875.43 | 0.426 | -6.3 | | | | |
| 194 | 835.85 | 0.946 | -11.5 | 254 | 875.86 | 0.420 | -6.1 | | | | |
| 195 | 836.79 | 0.935 | -11.3 | 255 | 876.27 | 0.414 | -6.0 | | | | |
| 196 | 837.72 | 0.924 | -11.1 | 256 | 876.68 | 0.408 | -5.9 | | | | |
| 197 | 838.64 | 0.913 | -11.0 | 257 | 877.09 | 0.402 | -5.9 | | | | |
| 198 | 839.55 | 0.902 | -10.8 | 258 | 877.49 | 0.396 | -5.8 | | | | |
| 199 | 840.44 | 0.891 | -10.6 | 259 | 877.88 | 0.391 | -5.9 | | | | |
| 200 | 841.33 | 0.881 | -10.4 | 260 | 878.27 | 0.385 | -6.0 | | | | |
| 201 | 842.20 | 0.870 | -10.3 | 261 | 878.65 | 0.379 | -6.1 | | | | |
| 202 | 843.07 | 0.860 | -10.1 | 262 | 879.03 | 0.372 | -6.3 | | | | |
| 203 | 843.93 | 0.850 | -9.9 | 263 | 879.40 | 0.366 | -6.5 | | | | |
| 204 | 844.77 | 0.840 | -9.8 | 264 | 879.76 | 0.359 | -6.8 | | | | |
| 205 | 845.61 | 0.831 | -9.6 | 265 | 880.12 | 0.353 | -7.1 | | | | |
| 206 | 846.43 | 0.821 | -9.5 | 266 | 880.46 | 0.345 | -7.4 | | | | |
| 207 | 847.25 | 0.812 | -9.3 | 267 | 880.81 | 0.338 | -7.7 | | | | |
| 208 | 848.05 | 0.802 | -9.2 | 268 | 881.14 | 0.330 | -7.9 | | | | |
| 209 | 848.85 | 0.793 | -9.1 | 269 | 881.47 | 0.322 | -8.1 | | | | |
| 210 | 849.64 | 0.784 | -8.9 | 270 | 881.78 | 0.314 | -8.2 | | | | |
| 211 | 850.42 | 0.775 | -8.8 | 271 | 882.09 | 0.305 | -8.2 | | | | |
| 212 | 851.19 | 0.767 | -8.7 | 272 | 882.39 | 0.297 | -7.9 | | | | |
| 213 | 851.95 | 0.758 | -8.7 | 273 | 882.69 | 0.290 | -7.3 | | | | |
| 214 | 852.71 | 0.749 | -8.6 | 274 | 882.97 | 0.283 | -6.3 | | | | |
| 215 | 853.45 | 0.741 | -8.5 | 275 | 883.25 | 0.277 | -4.8 | | | | |
| 216 | 854.19 | 0.732 | -8.5 | 276 | 883.53 | 0.274 | -2.7 | | | | |
| 217 | 854.92 | 0.724 | -8.5 | 277 | 883.80 | 0.272 | 0.2 | | | | |
| 218 | 855.64 | 0.715 | -8.4 | 278 | 884.08 | 0.274 | 4.0 | | | | |
| 219 | 856.35 | 0.707 | -8.4 | 279 | 884.35 | 0.281 | 9.0 | | | | |
| 220 | 857.05 | 0.698 | -8.4 | 280 | 884.64 | 0.293 | 15.3 | | | | |
| 221 | 857.74 | 0.690 | -8.5 | | | | | | | | |
| 222 | 858.43 | 0.681 | -8.5 | | | | | | | | |
| 223 | 859.11 | 0.673 | -8.5 | | | | | | | | |
| 224 | 859.78 | 0.664 | -8.5 | | | | | | | | |
| 225 | 860.44 | 0.656 | -8.6 | | | | | | | | |
| 226 | 861.09 | 0.647 | -8.6 | | | | | | | | |
| 227 | 861.73 | 0.639 | -8.7 | | | | | | | | |
| 228 | 862.36 | 0.630 | -8.7 | | | | | | | | |
| 229 | 862.99 | 0.621 | -8.8 | | | | | | | | |
| 230 | 863.61 | 0.612 | -8.8 | | | | | | | | |
| 231 | 864.22 | 0.604 | -8.8 | | | | | | | | |
| 232 | 864.81 | 0.595 | -8.9 | | | | | | | | |
| 233 | 865.40 | 0.586 | -8.9 | | | | | | | | |
| 234 | 865.99 | 0.577 | -8.9 | | | | | | | | |
| 235 | 866.56 | 0.568 | -8.9 | | | | | | | | |
| 236 | 867.12 | 0.559 | -8.9 | | | | | | | | |
| 237 | 867.68 | 0.550 | -8.8 | | | | | | | | |
| 238 | 868.22 | 0.542 | -8.8 | | | | | | | | |
| 239 | 868.76 | 0.533 | -8.7 | | | | | | | | |
| 240 | 869.29 | 0.524 | -8.6 | | | | | | | | |



459-033 OL - 72 - 7

scales used. Units for the thermocouple tables and functions are based on the "NBS as-maintained volt" [12]; the International Practical Temperature Scale, IPTS–68, [13, 14, 15] for temperature above 20 kelvin; and the NBS acoustical scale, P 2–20 (1965), [16, 17] for temperatures between 4 and 20 kelvin.

TABLE 11. *Total uncertainties in thermocouple calibrations*

| Thermocouple combination | Total uncertainty | | |
|---|---|---|---|
| | 4–20 K | 20–75 K | 75–280 K |
| KP vs Au-0.07 at% Fe | 9.8 mK | 11.3 mK | 31.9 mK |
| KP vs Au-0.02 at% Fe | 14.2 | 16.1 | 33.1 |
| Cu vs Au-0.07 at% Fe | 17.1 | 20.1 | 54.7 |
| Cu vs Au-0.02 at% Fe | 14.4 | 22.8 | 81.4 |
| n.Ag vs Au-0.07 at% Fe | 16.2 | 19.9 | 59.1 |
| n.Ag vs Au-0.02 at% Fe | 14.3 | 23.5 | 84.8 |

## 5. Discussion

It is apparent from figure 4 that the Au-0.07 at% $Fe_{47}$ alloy, used in the first calibration, has a lower Seebeck coefficient than all but one of the specimens tested in the second calibration. A possible reason for the lower thermopower is suggested by comparison with Rosenbaum's data in figure 6. The Seebeck coefficient for specimen 47 falls below that of Rosenbaum's annealed sample results by 4.7 percent at 20 K. This is in the right direction and appears to be of a reasonable magnitude to be caused by underannealing or annealing at a high temperature in the presence of oxygen. Oxygen combines with iron which, in effect, removes the iron from the transport processes which are responsible for the high thermopower of the dilute alloys [18]. Regardless of the reason for the lower sensitivity the fact remains that specimen 47 should not be chosen to represent the alloy in light of the information from the specimens used in the second calibration. The data shown in figures 3 and 4 indicate that the specimens 8, 10, or 11 would have the general properties desired and have a sensitivity near the average of the materials tested. The choice among these three wires is rather arbitrary and perhaps unimportant since, in general, published tables must be adjusted to the particular thermocouple wires being used. The important consideration is that the published data can be adjusted to fit any particular working thermocouple of this type.

The "normal" silver and copper versus Au-0.07 at% $Fe_{11}$ data presented in this paper were calculated since neither "normal" silver nor copper were included in the second calibration with Au-0.07 at% $Fe_{11}$. The following relationships were used to arrive at "normal" silver and copper versus Au-0.07 at% $Fe_{11}$:

$$E(\text{Cu vs Au } 7\,\text{Fe}_{47}) - E(\text{KP vs Au } 7\,\text{Fe}_{47}) + E(\text{KP vs Au } 7\,\text{Fe}_{11}) = E(\text{Cu vs Au } 7\,\text{Fe}_{11})$$

$$E(\text{n. Ag vs Au } 7\,\text{Fe}_{47}) - E(\text{KP vs Au } 7\,\text{Fe}_{47}) + E(\text{KP vs Au } 7\,\text{Fe}_{11}) = E(\text{n. Ag vs Au } 7\,\text{Fe}_{11})$$

The actual combination was accomplished by combining the power series coefficients, e.g.,

$$E(\text{Cu vs Au } 7\,\text{Fe}_{47}) = A_1 + A_2T + A_3T^2 + \ldots \equiv E_A$$

$$+$$

$$E(\text{KP vs Au } 7\,\text{Fe}_{11}) = B_1 + B_2T + B_3T^2 + \ldots \equiv E_B$$

$$-$$

$$E(\text{KP vs Au } 7\,\text{Fe}_{47}) = C_1 + C_2T + C_3T^2 + \ldots \equiv E_C$$

$$E(\text{Cu vs Au } 7\,\text{Fe}_{11}) = (A_1 + B_1 - C_1) + (A_2 + B_2 - C_2)T + (A_3 + B_3 - C_3)T^2 + \ldots$$

The uncertainty in the calculated tables will be the combination of uncertainties, e.g.,

$$\sigma_{\text{Cu vs Au } 7\,\text{Fe}_{11}} = [\sigma^2(E_A) + \sigma^2(E_B) + \sigma^2(E_C)]^{1/2}.$$

The selection of the Au-0.02 at% Fe specimen to be reported in detail is not as difficult as was the Au-0.07 at% Fe, primarily because we have only two specimens to consider. Figures 7 and 9 indicate that our Au-0.02 at% $Fe_{45}$ is probably nearer to the optimum anneal than is the later specimen 12. Specimen 45 was used in the first calibration and was compared directly to both copper and "normal" silver. This eliminates the need to combine coefficients and increase the uncertainty as was the case for Au-0.07 at% Fe.

Mr. W. J. Hall was largely responsible for the computer programs used to fit the experimental data. Mr. Ed Zysk of Engelhard Industries and the late Dr. Bert Brenner of Sigmund Cohn Corporation were extremely cooperative in producing and supplying the Au-Fe test wire.

## 6. References

[1] Powell, R. L., Caywood, L. P., and Bunch, M. D., Low-Temperature Thermocouples, Chapter in Temperature, Its Measurement and Control in Science and Industry **3**, Part 2, 65–77 (Reinhold Publishing Corp., New York, N.Y., 1962).

[2] Borelius, G., Keesom, W. H., Johansson, C. H., and Linde, J. O., Measurement of the thermoelectric force per degree of some

alloys down to the temperature of liquid hydrogen, and calculation of the Thomson-effect, Proc. Kon. Akad. Amsterdam **33,** 17, 23–36 (1930).
[3] Borelius, G., Keesom, W. H., Johansson, C. H., and Linde, J. O., Measurements on thermoelectric forces down to temperatures obtainable with liquid or solid hydrogen, Proc. Kon. Akad. Amsterdam **35,** 15, 22–33 (1932).
[4] Berman, R., and Huntley, D. J., Dilute gold-iron alloys as thermocouple material for low temperature heat conductivity measurements, Cryogenics **3,** 70–76 (June 1963).
[5] Finnemore, D. K., Ostenson, J. E., and Stromberg, T. F., Secondary thermometer for the 4 to 20 K range, Rev. Sci. Instrum. **36,** No. 9, 1369–1370 (Sept. 1965).
[6] Berman, R., Brock, J. C. F., and Huntley, D. J., Properties of gold + 0.03 percent (at.) iron thermoelements between 1 and 300 K and behavior in a magnetic field, Cryogenics **4,** 223–239 (August 1964).
[7] Rosenbaum, R. L., Some properties of gold-iron thermocouple wire, Rev. Sci. Instrum. **39,** No. 6, 890–899 (1968).
[8] Rosenbaum, R. L., Some low temperature thermometry observations, Rev. Sci. Instrum. **40,** No. 4, 577–583 (April 1969).
[9] Sparks, L. L., Powell, R. L., and Hall, W. J., Reference Tables for Low Temperature Thermocouples, Nat. Bur Stand. (U.S.), Monogr. 124, to be published.
[10] Björck, A., Solving linear least squares problems by Gram-Schmidt orthogonalization, Bit, Nordisk Tidsprift for Informationsbehandling, **7,** 1–21 (1967).
[11] Powell, R. L., Hall, W. J., and Hust, J. G., The fitting of resistance thermometer data by orthogonal functions, Fifth Symposium on Temperature, Washington, D.C., June 21–24, 1971.
[12] Reference Base of the Volt to be Changed, Nat. Bur. Stand. (U.S.), Tech. News Bull. **52,** 204–206 (Sept. 1968).
[13] International Practical Temperature Scale of 1968, Adopted by the Comité International des Poids et Mesures, Metrologia **5,** No. 2, 35–44 (April 1969).
[14] Bedford, R. E., Durieuz, M., Muijlwijk, R., and Barber, C. R., Relationships between the International Practical Temperature Scale of 1968 and the NBS–55, NPL–61, PRMI–54, and PSU–54 temperature scales in the range from 13.81 to 90.188 K, Metrologia **5,** No. 2, 47–49 (April 1969).
[15] Bedford, R. E., Kirby, C. G. M., Notes on the application of the International Practical Temperature Scale of 1968, Metrologia **5,** No. 3, 83–87 (July 1969).
[16] Rogers, J. S., Tainish, R. J., Anderson, M. S., and Swenson, C. A., Comparison between gas thermometer, acoustic, and platinum resistance temperature scales between 2 and 20 K, Metrologia **4,** No. 2, 47–58 (April 1969).
[17] Plumb, H. H., and Cataland, G., Acoustical thermometer and the National Bureau of Standards Provisional Temperature Scale 2–20 (1965), Metrologia, **2,** No. 4, 127–139 (1966).
[18] Anderson, H. H., and Nielsen, M., Thermo-electricity in gold at low temperatures, Physics Lett. **6,** No. 1, 17–18 (Aug. 15, 1963).

(Paper 76A3–721)

JOURNAL OF RESEARCH of the National Bureau of Standards—A. Physics and Chemistry
Vol. 76A, No. 3, May–June 1972

# Infrared Spectra of Cerium (Ce I and Ce II) Between 0.8 and 2.4 μm

**J. Verges,* C. H. Corliss, and W. C. Martin**

**Institute for Basic Standards, National Bureau of Standards, Washington, D.C. 20234**

**(December 28, 1971)**

The cerium spectrum emitted by an electrodeless lamp has been observed with a SISAM spectrometer in the region from 0.82 to 2.42 μm. Of the 2076 lines observed, about 1100 lines have been classified as transitions in the energy level system of Ce I and 400 lines in Ce II. The average deviation between the observed wave numbers and those calculated from the two energy levels is ±0.023 cm$^{-1}$.

Key words: Cerium spectra; Ce I and II; infrared spectra; spectra; wavelengths.

## 1. Introduction

The analysis of Ce I was begun about ten years ago at the National Bureau of Standards by Martin [1963] and has been carried forward to an advanced state, *v.* Martin [1971]. The analysis of Ce II on the other hand has been carried on intermittently over the past forty years by Albertson and Harrison [1937]; Harrison, Albertson, and Hosford [1941]; Racah [1955]; Goldschmidt [1968], and Corliss [1971].

In both of these spectra observations of the infrared are of great interest because of the existence of low lying levels of both parities. The observations reported here were important in confirming the low even levels of Ce I and they contain hundreds of transitions of Ce II. The present infrared list is published separately, since it is based on data obtained with a single instrument that covers a range mostly inaccessible by photographic techniques. Cerium spectra photographed at NBS have considerably more lines than the present list in the region of overlap, 0.8–1.0 μm. The complete NBS wavelength lists and analyses for Ce I and Ce II are, however, not yet ready for publication.

## 2. Observations

The measurements were made at the Laboratoire Aimé Cotton with the low resolution SISAM spectrometer and methods previously described by Verges [1969]. The instrument used has a resolution of 0.2 cm$^{-1}$ and lines were observed in air from 0.82 to 2.42 μm. The light source was an electrodeless lamp of the type described by Corliss, Bozman, and Westfall [1953]. It contained about a milligram of cerium iodide and was excited in a microwave cavity at 2450 MHz with a maximum power of about 50 W. No experimental separation of Ce I and Ce II was made.

A channel spectrum from a Fabry-Perot interferometer furnished a scale of wave numbers on the records of the cerium spectrum and the absolute values were referred to interferometric values of argon lines at 5901.373 cm$^{-1}$ and 12096.588 cm$^{-1}$. The faintest lines in each region are assigned an intensity 1 and stronger lines are assigned ordinal numbers in a geometric progression of ratio 2, i.e., $N = \log_2 2I$. The numbers range from 1 to 7, representing an intensity span from 1 to 64. Numbers in widely separated regions of the spectrum are not necessarily comparable.

## 3. Results and Classification of Infrared Lines

The wavelengths in air, wave numbers in vacuum and intensities of 2076 infrared cerium lines are listed in table 1. For classified lines the numerical values of the lower and upper energy levels with their $J$ values are given, the decimal parts being omitted. The levels are taken from the most recent NBS lists (unpublished).

The line list was searched for all possible transitions in Ce II with $\Delta J = \pm 1, 0$ by using all known levels below 22 300 cm$^{-1}$ and a tolerance of ±0.075 cm$^{-1}$. Levels above a certain energy in each spectrum were not used, so as to reduce the number of mere chance coincidences of observed wave numbers with calculated level differences. Nearly all the 400 lines thus classified fell within ±0.05 cm$^{-1}$ of the calculated values. The wave numbers of the Ce I levels are somewhat more precisely known, and the list was searched with a tolerance of ±0.05 cm$^{-1}$ by using all levels below 22 065 cm$^{-1}$. In this case nearly all of the 1100 classified lines fell within ±0.04 cm$^{-1}$ of the calculated values. The difference between the observed and calculated wave numbers is given in the last column of table 1 in units of 0.001 cm$^{-1}$. Its average value is ±0.023 cm$^{-1}$.

*Laboratoire Aimé Cotton, C.N.R.S. II, (91) Orsay, France.

TABLE 1. *Observed infrared cerium lines*

| Wavelength Å | Wavenumber ($cm^{-1}$) | Intensity | Spectrum | Classification | O−C (.001 $cm^{-1}$) | Wavelength Å | Wavenumber ($cm^{-1}$) | Intensity | Spectrum | Classification | O−C (.001 $cm^{-1}$) |
|---|---|---|---|---|---|---|---|---|---|---|---|
| 8215.42 | 12168.887 | 1 | | | | 8783.00 | 11382.505 | 2 | I | $4173^{\circ}_{4}$ $15555_{3}$ | 7 |
| 8220.68 | 12161.101 | 3 | I | $3210^{\circ}_{5}$ $15371_{4}$ | 37 | 8793.77 | 11368.565 | 2 | | | |
| 8223.61 | 12156.768 | 2 | I | $4746^{\circ}_{6}$ $16903_{5}$ | 15 | 8798.96 | 11361.859 | 2 | I | $0^{\circ}_{4}$ $11361_{4}$ | −35 |
| 8239.45 | 12133.397 | 3 | I | $6809^{\circ}_{8}$ $18942_{7}$ | 47 | 8808.21 | 11349.928 | 1 | I | $5572^{\circ}_{4}$ $16921_{3}$ | 22 |
| 8245.20 | 12124.935 | 3 | I | $1388^{\circ}_{3}$ $13513_{4}$ | 2 | 8808.89 | 11349.051 | 2 | I | $5519^{\circ}_{3}$ $16868_{2}$ | 33 |
| 8251.36 | 12115.884 | 3 | | | | 8810.85 | 11346.527 | 5 | I | $2437^{\circ}_{4}$ $13784_{5}$ | 5 |
| 8252.52 | 12114.181 | 3 | | | | 8813.92 | 11342.575 | 2 | I | $3196^{\circ}_{4}$ $14539_{3}$ | −29 |
| 8261.11 | 12101.584 | 2 | I | $2437^{\circ}_{4}$ $14539_{3}$ | 1 | 8842.62 | 11305.761 | 1 | I | $6856^{\circ}_{4}$ $18162_{4}$ | 9 |
| 8300.72 | 12043.837 | 2 | I | $5572^{\circ}_{4}$ $17615_{4}$ | 18 | 8845.16 | 11302.514 | 2 | I | $5571^{\circ}_{6}$ $16873_{1}$ | −29 |
| 8310.27 | 12029.997 | 2 | I | $3210^{\circ}_{5}$ $15240_{4}$ | −38 | 8853.36 | 11292.046 | 1 | I | $8055^{\circ}_{6}$ $19347_{6}$ | 30 |
| 8336.96 | 11991.484 | 1 | I | $9333^{\circ}_{6}$ $21324_{6}$ | −29 | 8860.18 | 11283.354 | 3 | I | $4417^{\circ}_{5}$ $15700_{4}$ | −5 |
| 8396.38 | 11906.622 | 3 | I | $5802^{\circ}_{7}$ $17708_{7}$ | 23 | 8870.84 | 11269.795 | 1 | I | $4746^{\circ}_{6}$ $16016_{5}$ | 13 |
| 8401.93 | 11898.757 | 1 | I | $7174^{\circ}_{4}$ $19072_{3}$ | 16 | 8871.11 | 11269.452 | 2 | I | $9830^{\circ}_{6}$ $21100_{6}$ | −4 |
| 8440.88 | 11843.851 | 2 | I | $4173^{\circ}_{4}$ $16017_{3}$ | −12 | 8875.30 | 11264.132 | 2 | I | $5802^{\circ}_{7}$ $17066_{6}$ | −5 |
| 8460.04 | 11817.028 | 1 | I | $4199^{\circ}_{5}$ $16016_{5}$ | −13 | 8891.21 | 11243.976 | 3 | II | $1873^{\circ}_{3\frac{1}{2}}$ $13117_{4\frac{1}{2}}$ | −8 |
| 8467.35 | 11806.826 | 2 | I | $4160^{\circ}_{3}$ $15967_{2}$ | 22 | 8904.68 | 11226.967 | 1 | I | $3312^{\circ}_{4}$ $14539_{3}$ | −4 |
| 8482.73 | 11785.419 | 2 | | | | 8909.79 | 11220.528 | 2 | I | $7841^{\circ}_{5}$ $19062_{5}$ | −14 |
| 8495.85 | 11767.219 | 5 | I | $2369^{\circ}_{3}$ $14136_{3}$ | −34 | 8910.74 | 11219.332 | 2 | | | |
| 8504.95 | 11754.629 | 2 | I | $5637^{\circ}_{1}$ $17391_{1}$ | 3 | 8927.57 | 11198.182 | 5 | I | $4173^{\circ}_{4}$ $15371_{4}$ | 29 |
| 8511.34 | 11745.804 | 2 | II | $2879^{\circ}_{5\frac{1}{2}}$ $14625_{5\frac{1}{2}}$ | −13 | 8942.42 | 11179.586 | 2 | I | $8055^{\circ}_{6}$ $19235_{6}$ | 14 |
| 8523.38 | 11729.212 | 4 | I | $2369^{\circ}_{3}$ $14098_{2}$ | −24 | 8964.10 | 11152.548 | 2 | I | $7467^{\circ}_{5}$ $18619_{5}$ | 23 |
| 8539.14 | 11707.565 | 1 | II | $1410^{\circ}_{4\frac{1}{2}}$ $13117_{4\frac{1}{2}}$ | −55 | 8970.27 | 11144.877 | 4 | | | |
| 8543.44 | 11701.672 | 1 | I | $6303^{\circ}_{2}$ $18005_{3}$ | 4 | 8971.13 | 11143.808 | 3 | | | |
| 8560.93 | 11677.766 | 1 | | | | 8984.06 | 11127.770 | 1 | | | |
| 8564.57 | 11672.803 | 4 | I | $2208^{\circ}_{5}$ $13881_{5}$ | 16 | 8989.42 | 11121.135 | 1 | I | $5572^{\circ}_{4}$ $16693_{4}$ | 57 |
| 8566.65 | 11669.968 | 1 | I | $4173^{\circ}_{4}$ $15843_{4}$ | 13 | | | | I | $8991^{\circ}_{5}$ $20112_{4}$ | −18 |
| 8567.46 | 11668.865 | 4 | I | $3976^{\circ}_{6}$ $15644_{6}$ | 26 | 8992.29 | 11117.586 | 5 | I | $4160^{\circ}_{3}$ $15277_{3}$ | 17 |
| 8582.21 | 11648.810 | 1 | I | $3100^{\circ}_{4}$ $14748_{4}$ | 16 | 9001.98 | 11105.618 | 3 | I | $4455^{\circ}_{6}$ $15561_{5}$ | 29 |
| 8612.62 | 11607.680 | 5 | I | $3764^{\circ}_{5}$ $15371_{4}$ | 41 | 9016.72 | 11087.464 | 2 | | | |
| 8615.93 | 11603.221 | 2 | I | $1388^{\circ}_{3}$ $12992_{2}$ | 47 | 9024.69 | 11077.672 | 3 | II | $4203^{\circ}_{6\frac{1}{2}}$ $15281_{6\frac{1}{2}}$ | 0 |
| 8619.36 | 11598.603 | 2 | | | | 9025.87 | 11076.224 | 5 | I | $2437^{\circ}_{4}$ $13513_{4}$ | −21 |
| 8629.30 | 11585.243 | 2 | I | $3976^{\circ}_{6}$ $15561_{5}$ | 1 | 9031.11 | 11069.797 | 1 | | | |
| 8631.39 | 11582.438 | 1 | I | $6303^{\circ}_{2}$ $17886_{2}$ | 43 | 9032.43 | 11068.179 | 3 | I | $6234^{\circ}_{3}$ $17302_{3}$ | 29 |
| 8636.55 | 11575.518 | 3 | I | $2208^{\circ}_{5}$ $13784_{5}$ | 24 | 9033.23 | 11067.199 | 2 | | | |
| 8639.35 | 11571.766 | 1 | I | $8055^{\circ}_{6}$ $19627_{6}$ | 17 | 9041.08 | 11057.590 | 1 | I | $8603^{\circ}_{6}$ $19661_{5}$ | 45 |
| 8647.65 | 11560.660 | 5 | I | $4455^{\circ}_{6}$ $16016_{5}$ | 7 | 9043.41 | 11054.741 | 2 | II | $8927^{\circ}_{5\frac{1}{2}}$ $19982_{4\frac{1}{2}}$ | 53 |
| 8653.86 | 11552.364 | 2 | I | $3196^{\circ}_{4}$ $14748_{4}$ | 26 | 9050.13 | 11046.533 | 2 | | | |
| 8659.72 | 11544.546 | 2 | | | | 9056.03 | 11039.336 | 1 | I | $8587^{\circ}_{7}$ $19627_{6}$ | 34 |
| 8664.34 | 11538.391 | 4 | I | $3210^{\circ}_{5}$ $14748_{4}$ | 29 | | | | I | $9135^{\circ}_{3}$ $20174_{4}$ | −21 |
| 8668.24 | 11533.199 | 1 | | | | 9056.30 | 11039.007 | 1 | I | $6856^{\circ}_{4}$ $17895_{5}$ | 27 |
| 8672.52 | 11527.507 | 3 | I | $4417^{\circ}_{5}$ $15945_{4}$ | 15 | 9058.33 | 11036.533 | 2 | | | |
| 8677.53 | 11520.852 | 2 | I | $5315^{\circ}_{7}$ $16836_{6}$ | 8 | 9058.60 | 11036.204 | 3 | I | $3100^{\circ}_{4}$ $14136_{3}$ | 33 |
| 8691.00 | 11502.996 | 2 | I | $4746^{\circ}_{6}$ $16249_{6}$ | 22 | | | | I | $3703^{\circ}_{3\frac{1}{2}}$ $14739_{2\frac{1}{2}}$ | 34 |
| 8692.04 | 11501.620 | 2 | I | $4199^{\circ}_{5}$ $15700_{4}$ | 9 | 9060.71 | 11033.634 | 2 | II | $4201^{\circ}_{1\frac{1}{2}}$ $15235_{1\frac{1}{2}}$ | −38 |
| 8702.38 | 11487.954 | 2 | II | $3793^{\circ}_{6\frac{1}{2}}$ $15281_{6\frac{1}{2}}$ | −24 | | | | II | $5118^{\circ}_{2\frac{1}{2}}$ $16152_{3\frac{1}{2}}$ | 53 |
| 8704.24 | 11485.499 | 3 | I | $6809^{\circ}_{8}$ $18294_{7}$ | −17 | 9062.09 | 11031.954 | 2 | | | |
| 8706.65 | 11482.320 | 2 | | | | 9063.93 | 11029.714 | 2 | | | |
| 8709.47 | 11478.602 | 2 | I | $6663^{\circ}_{5}$ $18141_{4}$ | −19 | 9065.00 | 11028.412 | 1 | | | |
| 8714.68 | 11471.740 | 1 | I | $5637^{\circ}_{1}$ $17108_{2}$ | 6 | 9068.09 | 11024.654 | 1 | | | |
| 8716.66 | 11469.134 | 1 | II | $987^{\circ}_{4\frac{1}{2}}$ $12456_{3\frac{1}{2}}$ | −9 | 9071.06 | 11021.045 | 2 | | | |
| 8725.69 | 11457.265 | 1 | I | $5210^{\circ}_{2}$ $16668_{3}$ | −18 | 9075.12 | 11016.114 | 3 | I | $5572^{\circ}_{4}$ $16588_{4}$ | −13 |
| 8735.93 | 11443.835 | 2 | I | $2437^{\circ}_{4}$ $13881_{5}$ | 20 | 9076.16 | 11014.852 | 4 | | | |
| 8748.30 | 11427.654 | 1 | I | $4160^{\circ}_{3}$ $15587_{2}$ | 10 | 9076.53 | 11014.403 | 2 | II | $5118^{\circ}_{2\frac{1}{2}}$ $16133_{2\frac{1}{2}}$ | −11 |
| 8749.16 | 11426.530 | 1 | II | $6549^{\circ}_{2\frac{1}{2}}$ $17976_{2\frac{1}{2}}$ | 28 | 9086.24 | 11002.632 | 2 | | | |
| 8751.04 | 11424.076 | 1 | I | $4455^{\circ}_{6}$ $15879_{5}$ | 54 | 9086.96 | 11001.761 | 3 | | | |
| | | | I | $9996^{\circ}_{3}$ $21420_{2}$ | −48 | 9092.97 | 10994.489 | 1 | | | |
| 8756.26 | 11417.265 | 3 | I | $6475^{\circ}_{4}$ $17892_{4}$ | −8 | 9094.26 | 10992.929 | 5 | | | |
| 8767.19 | 11403.032 | 2 | I | $3196^{\circ}_{4}$ $14599_{4}$ | 41 | 9100.99 | 10984.800 | 4 | | | |
| 8771.90 | 11396.909 | 2 | I | $9333^{\circ}_{6}$ $20730_{5}$ | −3 | 9105.33 | 10979.565 | 1 | | | |
| 8772.13 | 11396.610 | 4 | II | $2879^{\circ}_{5\frac{1}{2}}$ $14276_{5\frac{1}{2}}$ | −4 | 9106.25 | 10978.455 | 2 | | | |
| 8772.77 | 11395.779 | 2 | I | $4160^{\circ}_{3}$ $15555_{3}$ | 70 | 9106.98 | 10977.575 | 2 | I | $7715^{\circ}_{5}$ $18692_{4}$ | 18 |
| | | | II | $4737^{\circ}_{2\frac{1}{2}}$ $16133_{2\frac{1}{2}}$ | −68 | 9108.00 | 10976.346 | 2 | | | |
| 8778.85 | 11387.886 | 2 | I | $4173^{\circ}_{4}$ $15561_{5}$ | 34 | 9115.72 | 10967.050 | 1 | | | |
| 8782.18 | 11383.568 | 5 | I | $5315^{\circ}_{7}$ $16699_{6}$ | −12 | 9118.30 | 10963.947 | 3 | II | $2563^{\circ}_{5\frac{1}{2}}$ $13527_{4\frac{1}{2}}$ | −56 |

TABLE 1. *Observed infrared cerium lines*—Continued

| Wavelength Å | Wavenumber ($cm^{-1}$) | Intensity | Spectrum | Classification | O−C (.001 $cm^{-1}$) |
|---|---|---|---|---|---|
| 9127.68 | 10952.680 | 3 | I | $6663^{\circ}_{5}$ $17615_{4}$ | 13 |
| 9128.07 | 10952.212 | 5 | I | $2437^{\circ}_{4}$ $13389_{3}$ | 14 |
| 9131.41 | 10948.206 | 3 | I | $8509^{\circ}_{4}$ $19457_{3}$ | 22 |
| 9133.23 | 10946.025 | 5 | I | $7715^{\circ}_{5}$ $18661_{5}$ | −27 |
| | | | II | $2581^{\circ}_{4\,1/2}$ $13527_{4\,1/2}$ | 48 |
| 9138.49 | 10939.724 | 6 | I | $3196^{\circ}_{4}$ $14136_{3}$ | 9 |
| 9139.30 | 10938.755 | 2 | I | $5409^{\circ}_{2}$ $16347_{2}$ | 13 |
| 9141.65 | 10935.943 | 5 | I | $3710^{\circ}_{1}$ $14646_{2}$ | 11 |
| 9143.40 | 10933.850 | 6 | | | |
| 9151.02 | 10924.745 | 2 | I | $3710^{\circ}_{1}$ $14635_{1}$ | 15 |
| 9152.06 | 10923.504 | 3 | I | $7696^{\circ}_{6}$ $18619_{5}$ | 29 |
| 9153.31 | 10922.012 | 2 | | | |
| 9169.13 | 10903.168 | 3 | I | $4160^{\circ}_{3}$ $15063_{3}$ | 0 |
| 9172.18 | 10899.542 | 3 | I | $6809^{\circ}_{8}$ $17708_{7}$ | −36 |
| | | | I | $9830^{\circ}_{6}$ $20730_{5}$ | 15 |
| 9172.93 | 10898.651 | 2 | | | |
| 9173.13 | 10898.413 | 2 | | | |
| 9173.96 | 10897.427 | 2 | | | |
| 9175.46 | 10895.646 | 1 | I | $8400^{\circ}_{5}$ $19296_{4}$ | 23 |
| 9180.23 | 10889.984 | 1 | I | $4173^{\circ}_{4}$ $15063_{3}$ | 27 |
| 9181.19 | 10888.846 | 2 | | | |
| 9182.78 | 10886.960 | 3 | I | $8055^{\circ}_{6}$ $18942_{7}$ | 8 |
| | | | I | $10774^{\circ}_{3}$ $21661_{3}$ | 28 |
| 9185.22 | 10884.068 | 6 | | | |
| 9197.08 | 10870.033 | 1 | | | |
| 9201.32 | 10865.024 | 2 | I | $5519^{\circ}_{3}$ $16384_{3}$ | 34 |
| 9205.95 | 10859.560 | 1 | | | |
| 9210.73 | 10853.924 | 4 | I | $9135^{\circ}_{3}$ $19988_{3}$ | 37 |
| 9219.10 | 10844.070 | 2 | I | $8400^{\circ}_{5}$ $19244_{4}$ | 13 |
| | | | I | $9947^{\circ}_{2}$ $20791_{1}$ | 17 |
| 9226.31 | 10835.596 | 5 | I | $3764^{\circ}_{5}$ $14599_{4}$ | 6 |
| 9227.02 | 10834.762 | 5 | | | |
| 9227.38 | 10834.339 | 1 | I | $8400^{\circ}_{5}$ $19235_{6}$ | −28 |
| 9227.56 | 10834.128 | 1 | | | |
| 9233.38 | 10827.299 | 3 | I | $7467^{\circ}_{5}$ $18294_{6}$ | 8 |
| 9237.03 | 10823.020 | 3 | I | $4417^{\circ}_{5}$ $15240_{4}$ | 19 |
| 9238.26 | 10821.579 | 1 | I | $4766^{\circ}_{2}$ $15587_{2}$ | −24 |
| 9241.40 | 10817.902 | 1 | | | |
| 9242.36 | 10816.779 | 1 | | | |
| 9244.08 | 10814.766 | 2 | I | $4746^{\circ}_{6}$ $15561_{5}$ | 47 |
| 9245.86 | 10812.684 | 5 | I | $5572^{\circ}_{4}$ $16384_{3}$ | 17 |
| 9254.49 | 10802.601 | 2 | I | $3100^{\circ}_{4}$ $13902_{3}$ | −7 |
| | | | I | $8270^{\circ}_{3}$ $19072_{3}$ | −47 |
| 9254.74 | 10802.309 | 1 | | | |
| 9258.46 | 10797.969 | 2 | I | $5210^{\circ}_{2}$ $16008_{3}$ | 44 |
| 9258.80 | 10797.573 | 3 | II | $4165^{\circ}_{4\,1/2}$ $14963^{\circ}_{5\,1/2}$ | 11 |
| 9264.20 | 10791.279 | 3 | I | $5409^{\circ}_{2}$ $16200_{3}$ | 22 |
| 9285.36 | 10766.687 | 1 | | | |
| 9291.42 | 10759.665 | 5 | | | |
| 9294.37 | 10756.250 | 2 | | | |
| 9297.81 | 10752.270 | 1 | I | $2208^{\circ}_{5}$ $12960_{6}$ | −22 |
| 9317.79 | 10729.214 | 3 | I | $3210^{\circ}_{5}$ $13939_{6}$ | 5 |
| 9319.67 | 10727.050 | 3 | | | |
| 9320.33 | 10726.291 | 1 | | | |
| 9321.19 | 10725.301 | 3 | | | |
| 9321.96 | 10724.415 | 1 | | | |
| 9330.50 | 10714.599 | 1 | I | $6337^{\circ}_{3}$ $17051_{3}$ | 18 |
| 9337 (6 | 10706.154 | 5 | I | $3196^{\circ}_{4}$ $13902_{3}$ | 1 |
| 9343.39 | 10699.818 | 1 | | | |
| 9355.03 | 10686.504 | 1 | | | |
| 9355.73 | 10685.705 | 2 | | | |
| 9356.10 | 10685.282 | 2 | | | |
| 9357.60 | 10683.569 | 2 | II | $3703^{\circ}_{3\,1/2}$ $14387_{4\,1/2}$ | 50 |
| 9358.03 | 10683.078 | 1 | | | |
| 9360.48 | 10680.282 | 1 | II | $7713^{\circ}_{4\,1/2}$ $18393_{3\,1/2}$ | 35 |
| 9362.96 | 10677.453 | 1 | | | |
| 9364.88 | 10675.264 | 2 | | | |
| 9368.61 | 10671.014 | 5 | | | |
| 9374.17 | 10664.685 | 2 | I | $7933^{\circ}_{5}$ $18598_{6}$ | −17 |
| 9377.64 | 10660.739 | 5 | I | $3974^{\circ}_{0}$ $14635_{1}$ | 0 |
| 9378.13 | 10660.182 | 2 | I | $7348^{\circ}_{4}$ $18008_{5}$ | 39 |
| 9380.60 | 10657.375 | 3 | I | $7348^{\circ}_{4}$ $18005_{3}$ | 22 |
| | | | I | $8101^{\circ}_{2}$ $18758_{3}$ | 49 |
| 9383.36 | 10654.240 | 4 | | | |
| 9386.40 | 10650.789 | 4 | | | |
| 9387.37 | 10649.689 | 2 | I | $4746^{\circ}_{6}$ $15396_{6}$ | 30 |
| | | | I | $9119^{\circ}_{0}$ $19768_{1}$ | −48 |
| 9398.79 | 10636.749 | 2 | II | $2581^{\circ}_{4\,1/2}$ $13217_{3\,1/2}$ | 16 |
| 9400.78 | 10634.497 | 2 | I | $6234^{\circ}_{3}$ $16869_{4}$ | 36 |
| 9401.22 | 10634.000 | 4 | I | $6234^{\circ}_{3}$ $16868_{2}$ | 22 |
| 9404.29 | 10630.528 | 3 | | | |
| 9408.74 | 10625.500 | 4 | I | $4020^{\circ}_{1}$ $14646_{2}$ | 10 |
| 9410.90 | 10623.062 | 4 | I | $2369^{\circ}_{3}$ $12992_{2}$ | 15 |
| 9418.61 | 10614.366 | 3 | I | $4020^{\circ}_{1}$ $14635_{1}$ | 76 |
| | | | I | $9947^{\circ}_{2}$ $20562_{1}$ | 29 |
| 9431.70 | 10599.634 | 2 | I | $5409^{\circ}_{2}$ $16008_{3}$ | 40 |
| 9441.40 | 10588.744 | 3 | | | |
| 9446.61 | 10582.905 | 1 | | | |
| 9446.86 | 10582.625 | 1 | | | |
| 9450.13 | 10578.963 | 1 | | | |
| 9452.93 | 10575.829 | 1 | | | |
| 9453.18 | 10575.549 | 1 | | | |
| 9454.89 | 10573.637 | 1 | | | |
| 9464.89 | 10562.465 | 1 | | | |
| 9465.68 | 10561.584 | 1 | | | |
| 9466.01 | 10561.216 | 2 | ' | $4266^{\circ}_{3\,1/2}$ $14827_{3\,1/2}$ | −15 |
| 9469.66 | 10557.145 | 3 | | | |
| 9474.25 | 10552.030 | 3 | I | $5097^{\circ}_{1}$ $15649_{0}$ | 33 |
| 9478.16 | 10547.677 | 1 | | | |
| 9480.51 | 10545.063 | 1 | | | |
| 9484.08 | 10541.093 | 5 | | | |
| 9486.51 | 10538.393 | 2 | | | |
| 9490.85 | 10533.574 | 5 | I | $6856^{\circ}_{4}$ $17390_{4}$ | 19 |
| 9492.00 | 10532.298 | 2 | | | |
| 9503.03 | 10520.073 | 1 | | | |
| 9505.77 | 10517.041 | 1 | | | |
| 9513.94 | 10508.010 | 2 | | | |
| 9522.35 | 10498.729 | 2 | I | $7696^{\circ}_{6}$ $18194_{5}$ | 49 |
| 9533.07 | 10486.923 | 2 | | | |
| 9533.59 | 10486.351 | 3 | I | $10243^{\circ}_{4}$ $20730_{5}$ | −3 |
| 9535.09 | 10484.702 | 3 | I | $7169^{\circ}_{3}$ $17654_{3}$ | 35 |
| 9536.91 | 10482.701 | 1 | I | $8762^{\circ}_{4}$ $19244_{4}$ | 40 |
| | | | II | $3793^{\circ}_{6\,1/2}$ $14276_{5\,1/2}$ | 30 |
| 9539.83 | 10479.492 | 3 | | | |
| 9541.71 | 10477.428 | 1 | | | |
| 9542.39 | 10476.681 | 1 | II | $5675^{\circ}_{4\,1/2}$ $16152_{3\,1/2}$ | 53 |
| 9545.35 | 10473.432 | 1 | II | $4266^{\circ}_{3\,1/2}$ $14739_{2\,1/2}$ | 61 |
| 9549.71 | 10468.650 | 1 | | | |
| 9558.57 | 10458.947 | 1 | I | $6856^{\circ}_{4}$ $17315_{4}$ | 68 |
| | | | I | $8603^{\circ}_{6}$ $19062_{5}$ | −19 |
| 9559.08 | 10458.389 | 1 | I | $6234^{\circ}_{3}$ $16693_{4}$ | 29 |
| 9569.07 | 10447.471 | 3 | I | $5802^{\circ}_{7}$ $16249_{6}$ | −21 |
| 9578.11 | 10437.610 | 2 | I | $7348^{\circ}_{4}$ $17785_{3}$ | −27 |
| 9578.84 | 10436.815 | 2 | | | |
| 9581.91 | 10433.471 | 1 | | | |
| 9583.07 | 10432.208 | 2 | I | $7933^{\circ}_{5}$ $18365_{5}$ | 41 |
| 9589.36 | 10425.365 | 3 | I | $5519^{\circ}_{3}$ $15945_{4}$ | 5 |
| 9591.09 | 10423.484 | 1 | | | |

TABLE 1. *Observed infrared cerium lines*—Continued

| Wavelength Å | Wavenumber ($cm^{-1}$) | Intensity | Spectrum | Classification | O−C (.001 $cm^{-1}$) |
|---|---|---|---|---|---|
| 9591.93 | 10422.572 | 1 | I | $8270^{\circ}_{3}$ $18692_{4}$ | 28 |
| 9592.90 | 10421.518 | 2 | II | $4203^{\circ}_{6\frac{1}{2}}$ $14625_{5\frac{1}{2}}$ | —49 |
| 9600.05 | 10413.756 | 2 | I | $3100^{\circ}_{4}$ $13513_{4}$ | 32 |
| | | | I | $9787^{\circ}_{3}$ $20200_{2}$ | 12 |
| 9615.43 | 10397.099 | 2 | I | $5210^{\circ}_{2}$ $15607_{2}$ | 24 |
| 9617.92 | 10394.407 | 2 | I | $3210^{\circ}_{5}$ $13605_{6}$ | —9 |
| | | | I | $10774^{\circ}_{3}$ $21168_{2}$ | 25 |
| 9618.60 | 10393.673 | 2 | I | $6475^{\circ}_{4}$ $16869_{4}$ | —39 |
| 9620.44 | 10391.685 | 1 | II | $3995^{\circ}_{3\frac{1}{2}}$ $14387_{4\frac{1}{2}}$ | 30 |
| 9622.88 | 10389.050 | 2 | | | |
| 9637.70 | 10373.074 | 1 | I | $5572^{\circ}_{4}$ $15945_{4}$ | 38 |
| 9642.31 | 10368.115 | 1 | I | $7853^{\circ}_{1}$ $18221_{1}$ | 42 |
| 9651.19 | 10358.575 | 4 | I | $6809^{\circ}_{8}$ $17167_{7}$ | 23 |
| 9655.93 | 10353.491 | 2 | | | |
| 9656.39 | 10352.997 | 2 | I | $10723^{\circ}_{4}$ $21076_{4}$ | 32 |
| 9659.86 | 10349.278 | 3 | | | |
| 9668.92 | 10339.581 | 1 | I | $4455^{\circ}_{6}$ $14795_{5}$ | 47 |
| 9669.45 | 10339.014 | 2 | | | |
| 9676.76 | 10331.204 | 1 | | | |
| 9678.67 | 10329.165 | 3 | I | $5315^{\circ}_{7}$ $15644_{6}$ | 25 |
| 9683.75 | 10323.747 | 1 | I | $5519^{\circ}_{3}$ $15843_{4}$ | 49 |
| 9686.92 | 10320.368 | 2 | I | $7841^{\circ}_{5}$ $18162_{4}$ | 12 |
| | | | I | $10586^{\circ}_{4}$ $20907_{4}$ | 24 |
| 9689.76 | 10317.343 | 2 | | | |
| 9694.47 | 10312.331 | 3 | II | $3363^{\circ}_{2\frac{1}{2}}$ $13675_{2\frac{1}{2}}$ | 31 |
| | | | II | $7259^{\circ}_{3\frac{1}{2}}$ $17571_{4\frac{1}{2}}$ | 6 |
| 9696.41 | 10310.267 | 1 | | | |
| 9696.90 | 10309.746 | 2 | | | |
| 9701.99 | 10304.338 | 3 | II | $3745^{\circ}_{1\frac{1}{2}}$ $14049_{1\frac{1}{2}}$ | 54 |
| 9705.69 | 10300.410 | 2 | I | $3764^{\circ}_{5}$ $14064_{4}$ | 36 |
| | | | I | $8762^{\circ}_{4}$ $19062_{5}$ | 38 |
| 9712.88 | 10292.785 | 1 | | | |
| 9722.41 | 10282.695 | 2 | II | $9198^{\circ}_{3\frac{1}{2}}$ $19481_{4\frac{1}{2}}$ | —23 |
| 9725.54 | 10279.386 | 3 | | | |
| 9739.28 | 10264.884 | 2 | | | |
| 9739.67 | 10264.473 | 3 | | | |
| 9741.26 | 10262.798 | 2 | | | |
| 9742.59 | 10261.397 | 1 | | | |
| 9744.67 | 10259.207 | 5 | I | $2208^{\circ}_{5}$ $12467_{5}$ | 37 |
| 9759.41 | 10243.712 | 2 | | | |
| 9763.74 | 10239.169 | 3 | I | $8055^{\circ}_{6}$ $18294_{7}$ | 50 |
| 9768.22 | 10234.473 | 2 | | | |
| 9769.91 | 10232.703 | 2 | | | |
| 9772.01 | 10230.504 | 2 | I | $6303^{\circ}_{2}$ $16534_{2}$ | 37 |
| 9773.60 | 10228.839 | 1 | I | $7933^{\circ}_{5}$ $18162_{4}$ | 66 |
| | | | I | $11271^{\circ}_{4}$ $21499_{3}$ | 12 |
| 9774.09 | 10228.327 | 1 | | | |
| 9774.54 | 10227.856 | 2 | | | |
| 9779.05 | 10223.139 | 1 | II | $4910^{\circ}_{5\frac{1}{2}}$ $15134_{4\frac{1}{2}}$ | 41 |
| 9780.75 | 10221.362 | 2 | | | |
| 9781.72 | 10220.348 | 1 | I | $7169^{\circ}_{3}$ $17390_{4}$ | —14 |
| 9783.38 | 10218.614 | 4 | | | |
| 9785.96 | 10215.920 | 2 | I | $7174^{\circ}_{4}$ $17390_{4}$ | —37 |
| 9788.98 | 10212.768 | 2 | | | |
| 9792.27 | 10209.337 | 2 | | | |
| 9798.57 | 10202.773 | 1 | | | |
| 9799.56 | 10201.742 | 1 | | | |
| 9801.82 | 10199.390 | 2 | | | |
| 9802.39 | 10198.797 | 3 | II | $8280^{\circ}_{2\frac{1}{2}}$ $18479_{1\frac{1}{2}}$ | —27 |
| 9805.90 | 10195.146 | 4 | I | $6856^{\circ}_{4}$ $17051_{3}$ | 63 |
| | | | I | $9135^{\circ}_{3}$ $19330_{2}$ | 30 |
| 9806.95 | 10194.055 | 2 | | | |
| 9808.27 | 10192.683 | 3 | I | $6475^{\circ}_{4}$ $16668_{3}$ | 33 |
| 9817.00 | 10183.619 | 1 | I | $8509^{\circ}_{4}$ $18692_{4}$ | 35 |
| | | | I | $10723^{\circ}_{4}$ $20907_{4}$ | 15 |
| | | | II | $5675^{\circ}_{4\frac{1}{2}}$ $15859_{4\frac{1}{2}}$ | 20 |
| 9819.47 | 10181.057 | 2 | | | |
| 9822.55 | 10177.865 | 1 | | | |
| 9824.51 | 10175.834 | 1 | I | $3764^{\circ}_{5}$ $13939_{6}$ | 49 |
| 9826.80 | 10173.463 | 2 | I | $6663^{\circ}_{5}$ $16836_{6}$ | 42 |
| 9830.52 | 10169.613 | 1 | I | $7174^{\circ}_{4}$ $17343_{5}$ | 35 |
| | | | I | $10612^{\circ}_{2}$ $20782_{3}$ | —29 |
| 9842.74 | 10156.987 | 2 | I | $7841^{\circ}_{5}$ $17998_{4}$ | —31 |
| 9846.24 | 10153.377 | 4 | I | $4455^{\circ}_{6}$ $14609_{7}$ | 45 |
| 9849.51 | 10150.006 | 3 | | | |
| 9850.70 | 10148.780 | 2 | I | $7467^{\circ}_{5}$ $17615_{4}$ | 47 |
| 9852.62 | 10146.802 | 3 | I | $5409^{\circ}_{2}$ $15555_{3}$ | 46 |
| 9857.94 | 10141.326 | 2 | I | $7174^{\circ}_{4}$ $17315_{4}$ | 44 |
| | | | I | $9425^{\circ}_{2}$ $19566_{1}$ | —5 |
| 9859.81 | 10139.403 | 2 | I | $8055^{\circ}_{6}$ $18194_{5}$ | 39 |
| 9865.04 | 10134.027 | 2 | II | $7341^{\circ}_{5\frac{1}{2}}$ $17475^{\circ}_{4\frac{1}{2}}$ | —12 |
| 9869.98 | 10128.955 | 3 | | | |
| 9877.48 | 10121.264 | 1 | I | $5637^{\circ}_{1}$ $15758_{2}$ | 40 |
| 9881.17 | 10117.485 | 2 | I | $3764^{\circ}_{5}$ $13881_{5}$ | 49 |
| 9883.28 | 10115.325 | 1 | | | |
| 9885.13 | 10113.432 | 2 | | | |
| 9893.53 | 10104.845 | 1 | I | $5904^{\circ}_{2}$ $16008_{3}$ | 20 |
| 9894.37 | 10103.987 | 2 | | | |
| 9897.48 | 10100.812 | 1 | I | $8101^{\circ}_{2}$ $18201_{1}$ | 29 |
| 9906.53 | 10091.585 | 1 | I | $8101^{\circ}_{2}$ $18192_{3}$ | 6 |
| 9907.78 | 10090.312 | 1 | I | $7348^{\circ}_{4}$ $17438_{4}$ | 45 |
| | | | II | $4737^{\circ}_{2\frac{1}{2}}$ $14827_{3\frac{1}{2}}$ | 61 |
| 9909.81 | 10088.245 | 1 | I | $5519^{\circ}_{3}$ $15607_{2}$ | 15 |
| 9912.01 | 10086.006 | 2 | I | $6856^{\circ}_{4}$ $16942_{4}$ | 39 |
| 9914.30 | 10083.676 | 3 | I | $5674^{\circ}_{1}$ $15758_{2}$ | 47 |
| 9915.45 | 10082.506 | 1 | I | $1279^{\circ}_{4}$ $11361_{4}$ | 36 |
| 9916.49 | 10081.449 | 1 | I | $9462^{\circ}_{5}$ $19544_{4}$ | 49 |
| 9917.22 | 10080.707 | 2 | | | |
| 9920.20 | 10077.679 | 1 | | | |
| 9921.54 | 10076.318 | 2 | | | |
| 9922.90 | 10074.937 | 4 | | | |
| 9924.34 | 10073.475 | 2 | II | $3363^{\circ}_{2\frac{1}{2}}$ $13436_{2\frac{1}{2}}$ | 60 |
| 9926.70 | 10071.080 | 2 | I | $8991^{\circ}_{5}$ $19062_{5}$ | 33 |
| 9930.65 | 10067.074 | 2 | | | |
| 9932.20 | 10065.503 | 1 | | | |
| 9934.01 | 10063.669 | 2 | | | |
| 9939.79 | 10057.817 | 4 | | | |
| 9943.92 | 10053.640 | 2 | | | |
| 9944.80 | 10052.750 | 2 | | | |
| 9955.88 | 10041.562 | 1 | | | |
| 9958.83 | 10038.588 | 1 | I | $11626^{\circ}_{1}$ $21664_{0}$ | —39 |
| 9961.08 | 10036.320 | 4 | | | |
| 9963.64 | 10033.742 | 2 | | | |
| 9967.10 | 10030.259 | 4 | | | |
| 9984.69 | 10012.588 | 2 | I | $5637^{\circ}_{1}$ $15649_{0}$ | 47 |
| 9986.93 | 10010.343 | 5 | | | |
| 9993.16 | 10004.102 | 4 | II | $5513^{\circ}_{5\frac{1}{2}}$ $15517^{\circ}_{6\frac{1}{2}}$ | 43 |
| 9994.25 | 10003.011 | 1 | I | $11337^{\circ}_{3}$ $21340_{3}$ | 6 |
| | | | II | $5819^{\circ}_{4\frac{1}{2}}$ $15822_{3\frac{1}{2}}$ | 65 |
| 9998.96 | 9998.299 | 2 | | | |
| 10002.20 | 9995.060 | 2 | | | |
| 10002.48 | 9994.780 | 2 | | | |
| 10005.09 | 9992.173 | 2 | | | |
| 10007.89 | 9989.377 | 1 | | | |
| 10011.46 | 9985.815 | 1 | II | $4266^{\circ}_{3\frac{1}{2}}$ $14252_{3\frac{1}{2}}$ | 34 |
| 10013.27 | 9984.010 | 1 | | | |

TABLE 1. *Observed infrared cerium lines*—Continued

| Wavelength Å | Wavenumber ($cm^{-1}$) | Intensity | Spectrum | Classification | O−C (.001 $cm^{-1}$) |
|---|---|---|---|---|---|
| 10016.60 | 9980.691 | 1 | I | $9947^{\circ}_{2}$ $19928_{3}$ | 45 |
| 10021.24 | 9976.070 | 1 | I | $4160^{\circ}_{3}$ $14136_{3}$ | 31 |
| 10022.33 | 9974.985 | 1 | I | $5674^{\circ}_{1}$ $15649_{0}$ | 40 |
| 10031.59 | 9965.777 | 1 | I | $8101^{\circ}_{2}$ $18066_{1}$ | 33 |
| 10033.61 | 9963.771 | 2 | I | $8088^{\circ}_{2}$ $18052_{2}$ | —6 |
| 10056.41 | 9941.181 | 2 | | | |
| 10058.82 | 9938.799 | 4 | | | |
| 10064.36 | 9933.328 | 2 | II | $3593^{\circ}_{4\frac{1}{2}}$ $13527_{4\frac{1}{2}}$ | —34 |
| 10070.45 | 9927.321 | 2 | | | |
| 10072.75 | 9925.055 | 2 | | | |
| 10074.57 | 9923.262 | 1 | | | |
| 10078.27 | 9919.618 | 2 | | | |
| 10088.78 | 9909.285 | 1 | | | |
| 10091.03 | 9907.075 | 2 | II | $6638^{\circ}_{4\frac{1}{2}}$ $16545_{5\frac{1}{2}}$ | 70 |
| 10096.07 | 9902.130 | 2 | I | $9903^{\circ}_{1}$ $19805_{2}$ | —37 |
| 10096.20 | 9902.002 | 2 | I | $8509^{\circ}_{4}$ $18411_{4}$ | 41 |
| 10097.50 | 9900.727 | 3 | | | |
| 10102.78 | 9895.553 | 1 | I | $7890^{\circ}_{4}$ $17785_{3}$ | 45 |
| 10103.18 | 9895.161 | 1 | II | $4844^{\circ}_{1\frac{1}{2}}$ $14739_{2\frac{1}{2}}$ | 45 |
| 10105.04 | 9893.340 | 2 | I | $10249^{\circ}_{0}$ $20142_{1}$ | 0 |
| 10107.65 | 9890.785 | 1 | | | |
| 10112.97 | 9885.582 | 1 | | | |
| 10114.56 | 9884.028 | 1 | I | $9996^{\circ}_{3}$ $19880_{2}$ | —31 |
| 10116.61 | 9882.025 | 1 | | | |
| 10118.45 | 9880.228 | 1 | | | |
| 10136.59 | 9862.547 | 1 | | | |
| 10137.00 | 9862.148 | 1 | | | |
| 10137.16 | 9861.992 | 3 | | | |
| 10142.07 | 9857.218 | 1 | II | $5964^{\circ}_{3\frac{1}{2}}$ $15822_{3\frac{1}{2}}$ | 53 |
| 10142.80 | 9856.509 | 1 | I | $8509^{\circ}_{4}$ $18365_{5}$ | —6 |
| 10144.88 | 9854.488 | 5 | I | $5904^{\circ}_{2}$ $15758_{2}$ | 36 |
| 10150.28 | 9849.245 | 2 | I | $8762^{\circ}_{4}$ $18611_{3}$ | —14 |
| 10151.29 | 9848.265 | 3 | I | $7467^{\circ}_{5}$ $17315_{4}$ | —12 |
| 10151.61 | 9847.955 | 5 | I | $5904^{\circ}_{2}$ $15751_{1}$ | 12 |
| 10155.76 | 9843.930 | 1 | I | $10586^{\circ}_{4}$ $20430_{3}$ | 45 |
| 10156.91 | 9842.816 | 4 | I | $5802^{\circ}_{7}$ $15644_{6}$ | —18 |
| 10158.79 | 9840.994 | 1 | I | $3764^{\circ}_{5}$ $13605_{6}$ | 2 |
| 10159.87 | 9839.948 | 1 | | | |
| 10160.77 | 9839.077 | 1 | | | |
| 10163.32 | 9836.608 | 3 | I | $6856^{\circ}_{4}$ $16693_{4}$ | 15 |
| | | | I | $7853^{\circ}_{1}$ $17689_{2}$ | —19 |
| 10164.81 | 9835.166 | 1 | | | |
| 10165.50 | 9834.499 | 2 | I | $8307^{\circ}_{3}$ $18141_{4}$ | —39 |
| 10168.49 | 9831.607 | 1 | I | $6836^{\circ}_{2}$ $16668_{3}$ | 45 |
| 10169.83 | 9830.311 | 2 | II | $7341^{\circ}_{5\frac{1}{2}}$ $17171^{\circ}_{5\frac{1}{2}}$ | 69 |
| 10174.53 | 9825.770 | 3 | I | $10604^{\circ}_{3}$ $20430_{3}$ | 2 |
| | | | II | $5455^{\circ}_{7\frac{1}{2}}$ $15281_{6\frac{1}{2}}$ | 6 |
| 10175.65 | 9824.689 | 1 | I | $10673^{\circ}_{6}$ $20498_{5}$ | 21 |
| 10177.57 | 9822.836 | 3 | I | $11796^{\circ}_{4}$ $21619_{4}$ | —28 |
| 10184.37 | 9816.277 | 1 | | | |
| 10185.44 | 9815.246 | 3 | II | $2641^{\circ}_{3\frac{1}{2}}$ $12456_{3\frac{1}{2}}$ | 57 |
| 10189.00 | 9811.816 | 2 | I | $3312^{\circ}_{4}$ $13124_{5}$ | 46 |
| 10192.89 | 9808.072 | 2 | I | $3976^{\circ}_{6}$ $13784_{5}$ | 25 |
| 10193.87 | 9807.129 | 1 | I | $7841^{\circ}_{5}$ $17649_{6}$ | 48 |
| 10196.86 | 9804.253 | 1 | | | |
| 10201.65 | 9799.650 | 3 | | | |
| 10202.00 | 9799.314 | 3 | | | |
| 10203.26 | 9798.103 | 3 | | | |
| 10203.62 | 9797.758 | 2 | | | |
| 10204.69 | 9796.730 | 2 | | | |
| 10205.06 | 9796.375 | 3 | | | |
| 10207.31 | 9794.216 | 1 | I | $10318^{\circ}_{3}$ $20112_{4}$ | 49 |
| 10209.23 | 9792.374 | 1 | II | $4459^{\circ}_{3\frac{1}{2}}$ $14252_{3\frac{1}{2}}$ | 72 |
| 10215.51 | 9786.354 | 1 | | | |
| 10216.69 | 9785.224 | 3 | I | $8101^{\circ}_{2}$ $17886_{2}$ | 32 |
| 10219.41 | 9782.619 | 3 | | | |
| 10228.19 | 9774.222 | 1 | | | |
| 10228.43 | 9773.993 | 1 | I | $6234^{\circ}_{3}$ $16008_{3}$ | —45 |
| 10231.42 | 9771.136 | 1 | I | $8430^{\circ}_{1}$ $18201_{1}$ | 12 |
| 10234.38 | 9768.310 | 3 | | | |
| 10235.52 | 9767.222 | 1 | I | $12297^{\circ}_{5}$ $22064_{6}$ | 37 |
| 10237.93 | 9764.923 | 2 | | | |
| 10240.78 | 9762.205 | 1 | I | $8603^{\circ}_{6}$ $18365_{5}$ | 12 |
| 10241.43 | 9761.586 | 2 | I | $8400^{\circ}_{5}$ $18162_{4}$ | 5 |
| 10245.08 | 9758.108 | 4 | I | $5519^{\circ}_{3}$ $15277_{3}$ | 7 |
| 10245.44 | 9757.765 | 2 | II | $9723^{\circ}_{4\frac{1}{2}}$ $19481_{4\frac{1}{2}}$ | 58 |
| 10246.39 | 9756.861 | 1 | I | $9787^{\circ}_{3}$ $19544_{4}$ | —23 |
| 10250.16 | 9753.272 | 1 | II | $4523^{\circ}_{4\frac{1}{2}}$ $14276_{5\frac{1}{2}}$ | 1 |
| 10251.29 | 9752.197 | 3 | I | $7169^{\circ}_{3}$ $16921_{3}$ | —31 |
| 10252.14 | 9751.388 | 3 | I | $11061^{\circ}_{7}$ $20812_{7}$ | 18 |
| 10253.71 | 9749.895 | 3 | I | $3764^{\circ}_{5}$ $13513_{4}$ | 28 |
| | | | I | $8902^{\circ}_{3}$ $18652_{3}$ | —40 |
| 10255.54 | 9748.155 | 2 | II | $3508^{\circ}_{01/2}$ $13256_{1\frac{1}{2}}$ | —60 |
| 10255.85 | 9747.861 | 3 | I | $7174^{\circ}_{4}$ $16921_{3}$ | 37 |
| 10258.80 | 9745.058 | 5 | I | $2369^{\circ}_{3}$ $12114_{4}$ | 11 |
| 10261.76 | 9742.247 | 3 | I | $5006^{\circ}_{3}$ $14748_{4}$ | 21 |
| 10265.22 | 9738.963 | 4 | | | |
| 10271.21 | 9733.284 | 4 | I | $10586^{\circ}_{4}$ $20320_{4}$ | 16 |
| | | | II | $3703^{\circ}_{3\frac{1}{2}}$ $13436_{2\frac{1}{2}}$ | 38 |
| 10279.10 | 9725.813 | 2 | | | |
| 10279.39 | 9725.538 | 4 | | | |
| 10289.71 | 9715.784 | 2 | I | $8351^{\circ}_{0}$ $18066_{1}$ | 20 |
| 10290.45 | 9715.085 | 2 | II | $2382^{\circ}_{4\frac{1}{2}}$ $12097_{3\frac{1}{2}}$ | 56 |
| 10290.96 | 9714.604 | 2 | II | $4910^{\circ}_{5\frac{1}{2}}$ $14625_{5\frac{1}{2}}$ | 57 |
| 10297.05 | 9708.858 | 2 | II | $5118^{\circ}_{2\frac{1}{2}}$ $14827_{3\frac{1}{2}}$ | 40 |
| 10298.77 | 9707.237 | 1 | II | $10274^{\circ}_{3\frac{1}{2}}$ $19982_{4\frac{1}{2}}$ | 16 |
| 10299.36 | 9706.681 | 2 | I | $8587^{\circ}_{7}$ $18294_{7}$ | 9 |
| 10302.85 | 9703.393 | 1 | I | $7348^{\circ}_{4}$ $17051_{3}$ | 50 |
| 10304.97 | 9701.397 | 1 | | | |
| 10308.74 | 9697.849 | 3 | I | $6836^{\circ}_{2}$ $16534_{2}$ | 26 |
| 10309.61 | 9697.030 | 1 | I | $8088^{\circ}_{2}$ $17785_{3}$ | 5 |
| 10311.65 | 9695.112 | 3 | I | $7174^{\circ}_{4}$ $16869_{4}$ | 15 |
| 10315.64 | 9691.362 | 1 | II | $3745^{\circ}_{1\frac{1}{2}}$ $13436_{2\frac{1}{2}}$ | —5 |
| 10318.36 | 9688.807 | 3 | I | $7841^{\circ}_{5}$ $17530_{5}$ | 1 |
| | | | I | $9947^{\circ}_{2}$ $19636_{3}$ | —6 |
| 10321.79 | 9685.587 | 2 | | | |
| 10323.56 | 9683.927 | 3 | I | $5904^{\circ}_{2}$ $15587_{2}$ | 6 |
| 10325.30 | 9682.295 | 3 | I | $7933^{\circ}_{5}$ $17615_{4}$ | —39 |
| 10327.42 | 9680.307 | 2 | I | $6337^{\circ}_{3}$ $16017_{3}$ | 10 |
| | | | II | $3995^{\circ}_{3\frac{1}{2}}$ $13675_{2\frac{1}{2}}$ | 41 |
| 10331.51 | 9676.475 | 6 | I | $2437^{\circ}_{4}$ $12114_{4}$ | —10 |
| 10333.25 | 9674.846 | 3 | I | $7715^{\circ}_{5}$ $17390_{4}$ | —31 |
| 10333.80 | 9674.331 | 5 | I | $8055^{\circ}_{6}$ $17729_{5}$ | —17 |
| 10336.10 | 9672.178 | 2 | I | $10673^{\circ}_{6}$ $20346_{6}$ | 4 |
| 10336.48 | 9671.823 | 5 | | | |
| 10338.74 | 9669.708 | 2 | | | |
| 10339.98 | 9668.549 | 5 | I | $5572^{\circ}_{4}$ $15240_{4}$ | 4 |
| 10356.50 | 9653.126 | 1 | I | $8509^{\circ}_{4}$ $18162_{4}$ | 24 |
| 10357.32 | 9652.362 | 1 | II | $5924^{\circ}_{1\frac{1}{2}}$ $15576_{1\frac{1}{2}}$ | 6 |
| 10357.75 | 9651.961 | 3 | I | $5904^{\circ}_{2}$ $15555_{3}$ | —24 |
| | | | I | $11517^{\circ}_{1}$ $21168_{2}$ | 18 |
| 10360.91 | 9649.017 | 1 | I | $8762^{\circ}_{4}$ $18411_{4}$ | —26 |
| 10374.57 | 9636.313 | 2 | | | |
| 10378.55 | 9632.617 | 1 | I | $8509^{\circ}_{4}$ $18141_{4}$ | —21 |
| 10381.45 | 9629.927 | 2 | | | |
| 10382.61 | 9628.851 | 3 | I | $3976^{\circ}_{6}$ $13605_{6}$ | —44 |

TABLE 1. *Observed infrared cerium lines*—Continued

| Wavelength Å | Wavenumber ($cm^{-1}$) | Intensity | Spectrum | Classification | O−C (.001 $cm^{-1}$) |
|---|---|---|---|---|---|
| 10387.12 | 9624.670 | 5 | II | $5969^{\circ}_{5\frac{1}{2}}$ $15593_{6\frac{1}{2}}$ | 32 |
| 10396.33 | 9616.144 | 2 | I | $8270^{\circ}_{3}$ $17886_{2}$ | 14 |
| 10396.87 | 9615.644 | 1 | II | $6517^{\circ}_{2\frac{1}{2}}$ $16133_{2\frac{1}{2}}$ | 42 |
| 10402.24 | 9610.680 | 3 | I | $4173^{\circ}_{4}$ $13784_{5}$ | 23 |
| 10403.14 | 9609.849 | 1 | | | |
| 10403.56 | 9609.461 | 1 | | | |
| 10404.32 | 9608.759 | 1 | II | $5118^{\circ}_{2\frac{1}{2}}$ $14727_{1\frac{1}{2}}$ | 27 |
| 10405.09 | 9608.048 | 3 | I | $6337^{\circ}_{3}$ $15945_{4}$ | −1 |
| 10405.40 | 9607.762 | 3 | I | $8400^{\circ}_{5}$ $18008_{5}$ | 50 |
| 10410.93 | 9602.658 | 1 | I | $11796^{\circ}_{4}$ $21399_{3}$ | 11 |
| 10411.30 | 9602.317 | 1 | I | $10673^{\circ}_{6}$ $20276_{5}$ | 44 |
| 10412.86 | 9600.878 | 3 | I | $8088^{\circ}_{2}$ $17689_{2}$ | 44 |
| 10413.54 | 9600.251 | 3 | I | $7715^{\circ}_{5}$ $17315_{4}$ | 50 |
| | | | II | $11340^{\circ}_{3\frac{1}{2}}$ $20940_{3\frac{1}{2}}$ | 8 |
| 10423.12 | 9591.428 | 2 | | | |
| 10428.73 | 9586.268 | 2 | I | $11578^{\circ}_{1}$ $21165_{1}$ | −39 |
| 10437.06 | 9578.617 | 1 | I | $6621^{\circ}_{3}$ $16200_{3}$ | 16 |
| 10439.85 | 9576.057 | 1 | | | |
| 10442.27 | 9573.838 | 1 | | | |
| 10455.70 | 9561.541 | 1 | | | |
| 10456.86 | 9560.480 | 3 | | | |
| 10458.78 | 9558.725 | 3 | | | |
| 10462.79 | 9555.062 | 1 | I | $7348^{\circ}_{4}$ $16903_{5}$ | −18 |
| 10465.90 | 9552.222 | 2 | | | |
| 10466.42 | 9551.748 | 1 | I | $8762^{\circ}_{4}$ $18313_{3}$ | 13 |
| 10470.44 | 9548.081 | 2 | I | $6836^{\circ}_{2}$ $16384_{3}$ | −31 |
| 10471.13 | 9547.451 | 2 | I | $9996^{\circ}_{3}$ $19544_{4}$ | −6 |
| 10477.24 | 9541.884 | 3 | | | |
| 10486.68 | 9533.294 | 3 | I | $6475^{\circ}_{4}$ $16008_{3}$ | 3 |
| 10488.96 | 9531.222 | 1 | I | $6234^{\circ}_{3}$ $15766_{3}$ | −33 |
| 10492.26 | 9528.224 | 1 | I | $6856^{\circ}_{4}$ $16384_{3}$ | 42 |
| 10496.95 | 9523.967 | 2 | | | |
| 10497.29 | 9523.658 | 2 | I | $6234^{\circ}_{3}$ $15758_{2}$ | −7 |
| 10498.94 | 9522.162 | 2 | I | $4417^{\circ}_{5}$ $13939_{6}$ | −12 |
| | | | I | $10318^{\circ}_{3}$ $19840_{4}$ | −30 |
| 10499.96 | 9521.237 | 1 | | | |
| 10504.22 | 9517.375 | 1 | | | |
| 10505.26 | 9516.433 | 1 | I | $9830^{\circ}_{6}$ $19347_{5}$ | −22 |
| 10505.82 | 9515.926 | 1 | II | $10454^{\circ}_{1\frac{1}{2}}$ $19970_{2\frac{1}{2}}$ | 23 |
| 10511.11 | 9511.137 | 2 | | | |
| 10513.34 | 9509.119 | 3 | I | $9787^{\circ}_{3}$ $19296_{4}$ | −13 |
| 10515.91 | 9506.795 | 2 | I | $8695^{\circ}_{1}$ $18201_{1}$ | 27 |
| | | | I | $9903^{\circ}_{1}$ $19409_{2}$ | 20 |
| 10517.04 | 9505.774 | 1 | I | $9200^{\circ}_{2}$ $18706_{2}$ | −20 |
| 10521.46 | 9501.781 | 1 | I | $7841^{\circ}_{5}$ $17343_{5}$ | 2 |
| 10524.29 | 9499.226 | 2 | I | $8509^{\circ}_{4}$ $18008_{5}$ | −6 |
| 10525.15 | 9498.449 | 3 | I | $7169^{\circ}_{3}$ $16668_{3}$ | 11 |
| 10529.20 | 9494.796 | 1 | I | $8400^{\circ}_{5}$ $17895_{5}$ | −12 |
| 10530.70 | 9493.444 | 1 | | | |
| 10532.32 | 9491.983 | 2 | | | |
| 10534.51 | 9490.010 | 2 | | | |
| 10543.27 | 9482.125 | 1 | I | $6856^{\circ}_{4}$ $16338_{4}$ | −19 |
| 10545.29 | 9480.309 | 3 | I | $9462^{\circ}_{5}$ $18943_{5}$ | 1 |
| 10550.93 | 9475.241 | 3 | I | $8055^{\circ}_{6}$ $17530_{5}$ | 6 |
| 10556.03 | 9470.663 | 1 | | | |
| 10557.15 | 9469.659 | 2 | | | |
| 10563.59 | 9463.886 | 3 | | | |
| 10565.55 | 9462.130 | 1 | | | |
| 10566.59 | 9461.199 | 1 | I | $6337^{\circ}_{3}$ $15798_{3}$ | 34 |
| 10568.93 | 9459.104 | 3 | I | $10879^{\circ}_{5}$ $20338_{5}$ | 4 |
| 10569.78 | 9458.343 | 2 | I | $9947^{\circ}_{2}$ $19406_{3}$ | 8 |
| | | | II | $5675^{\circ}_{4\frac{1}{2}}$ $15134_{4\frac{1}{2}}$ | 49 |
| 10571.74 | 9456.590 | 2 | I | $7933^{\circ}_{5}$ $17390_{4}$ | 34 |
| 10572.91 | 9455.543 | 1 | I | $8430^{\circ}_{1}$ $17886_{2}$ | 10 |
| 10575.64 | 9453.102 | 3 | I | $4455^{\circ}_{6}$ $13908_{7}$ | 32 |
| 10580.09 | 9449.126 | 1 | I | $9709^{\circ}_{2}$ $19158_{2}$ | 4 |
| 10587.02 | 9442.941 | 2 | | | |
| 10598.45 | 9432.757 | 2 | I | $8762^{\circ}_{4}$ $18194_{5}$ | −6 |
| 10600.59 | 9430.853 | 4 | I | $3764^{\circ}_{5}$ $13194_{4}$ | 12 |
| 10604.02 | 9427.803 | 1 | I | $5315^{\circ}_{7}$ $14743_{6}$ | −19 |
| 10606.36 | 9425.723 | 2 | I | $4455^{\circ}_{6}$ $13881_{5}$ | 35 |
| 10608.14 | 9424.141 | 1 | I | $8603^{\circ}_{6}$ $18027_{7}$ | 3 |
| 10613.00 | 9419.826 | 3 | I | $8366^{\circ}_{2}$ $17785_{3}$ | −12 |
| 10614.60 | 9418.406 | 2 | I | $7169^{\circ}_{3}$ $16588_{4}$ | −44 |
| 10615.36 | 9417.731 | 3 | | | |
| 10619.43 | 9414.122 | 6 | | | |
| 10629.02 | 9405.628 | 4 | I | $4199^{\circ}_{5}$ $13605_{6}$ | −4 |
| 10630.93 | 9403.938 | 1 | | | |
| 10632.99 | 9402.116 | 3 | I | $7467^{\circ}_{5}$ $16869_{4}$ | 23 |
| 10646.48 | 9390.203 | 2 | I | $11357^{\circ}_{5}$ $20747_{4}$ | 2 |
| | | | II | $5437^{\circ}_{3\frac{1}{2}}$ $14827_{3\frac{1}{2}}$ | −4 |
| 10647.73 | 9389.101 | 1 | I | $10723^{\circ}_{4}$ $20112_{4}$ | 8 |
| 10648.71 | 9388.237 | 5 | I | $6663^{\circ}_{5}$ $16051_{4}$ | −14 |
| 10650.14 | 9386.976 | 3 | I | $6621^{\circ}_{3}$ $16008_{3}$ | 37 |
| 10653.90 | 9383.663 | 3 | I | $11578^{\circ}_{1}$ $20962_{2}$ | 6 |
| 10655.32 | 9382.413 | 3 | I | $8307^{\circ}_{3}$ $17689_{2}$ | −24 |
| | | | I | $9947^{\circ}_{2}$ $19330_{2}$ | 20 |
| 10655.94 | 9381.867 | 2 | I | $7933^{\circ}_{5}$ $17315_{4}$ | −12 |
| 10658.38 | 9379.719 | 3 | I | $8762^{\circ}_{4}$ $18141_{4}$ | −2 |
| 10659.03 | 9379.147 | 5 | I | $0^{\circ}_{4}$ $9379_{4}$ | 0 |
| 10665.82 | 9373.176 | 3 | I | $6234^{\circ}_{3}$ $15607_{2}$ | −12 |
| | | | I | $9947^{\circ}_{2}$ $19321_{2}$ | −20 |
| 10667.69 | 9371.533 | 3 | I | $8603^{\circ}_{6}$ $17975_{6}$ | 4 |
| 10669.42 | 9370.013 | 1 | I | $4766^{\circ}_{2}$ $14136_{3}$ | 15 |
| | | | I | $7696^{\circ}_{6}$ $17066_{6}$ | −22 |
| 10670.03 | 9369.478 | 5 | I | $7467^{\circ}_{5}$ $16836_{6}$ | −8 |
| 10670.57 | 9369.004 | 4 | I | $12454^{\circ}_{2}$ $21823_{1}$ | −25 |
| 10671.86 | 9367.871 | 3 | I | $6475^{\circ}_{4}$ $15843_{4}$ | −37 |
| 10673.40 | 9366.520 | 3 | I | $4417^{\circ}_{5}$ $13784_{5}$ | −12 |
| 10674.80 | 9365.291 | 1 | II | $4910^{\circ}_{5\frac{1}{2}}$ $14276_{5\frac{1}{2}}$ | −52 |
| 10680.79 | 9360.039 | 5 | I | $3764^{\circ}_{5}$ $13124_{5}$ | 37 |
| 10688.17 | 9353.576 | 2 | I | $4160^{\circ}_{3}$ $13513_{4}$ | −15 |
| 10688.70 | 9353.112 | 1 | I | $6234^{\circ}_{3}$ $15587_{2}$ | −22 |
| 10696.46 | 9346.327 | 4 | II | $5616^{\circ}_{4\frac{1}{2}}$ $14963_{5\frac{1}{2}}$ | −44 |
| 10697.25 | 9345.637 | 1 | I | $8270^{\circ}_{3}$ $17615_{4}$ | −6 |
| 10700.23 | 9343.034 | 2 | I | $11810^{\circ}_{4}$ $21153_{5}$ | 3 |
| 10703.25 | 9340.398 | 2 | I | $4173^{\circ}_{4}$ $13513_{4}$ | 17 |
| 10711.69 | 9333.038 | 1 | | | |
| 10717.07 | 9328.353 | 1 | I | $5210^{\circ}_{2}$ $14539_{3}$ | 47 |
| | | | I | $4455^{\circ}_{6}$ $13784_{5}$ | −41 |
| 10718.13 | 9327.430 | 2 | | | |
| 10725.29 | 9321.203 | 2 | I | $6234^{\circ}_{3}$ $15555_{3}$ | 4 |
| 10726.84 | 9319.857 | 1 | I | $7348^{\circ}_{4}$ $16668_{3}$ | −33 |
| 10728.76 | 9318.189 | 1 | I | $10318^{\circ}_{3}$ $19636_{3}$ | −8 |
| 10731.82 | 9315.532 | 1 | I | $11030^{\circ}_{6}$ $20346_{6}$ | −18 |
| 10732.53 | 9314.916 | 2 | II | $5819^{\circ}_{4\frac{1}{2}}$ $15134_{4\frac{1}{2}}$ | −21 |
| 10735.25 | 9312.555 | 1 | II | $5969^{\circ}_{5\frac{1}{2}}$ $15281_{6\frac{1}{2}}$ | −49 |
| 10736.33 | 9311.619 | 2 | I | $11301^{\circ}_{2}$ $20613_{3}$ | −15 |
| | | | II | $7233^{\circ}_{5\frac{1}{2}}$ $16545_{5\frac{1}{2}}$ | −18 |
| 10743.32 | 9305.560 | 2 | I | $7841^{\circ}_{5}$ $17147_{4}$ | −22 |
| 10750.03 | 9299.752 | 5 | I | $9996^{\circ}_{3}$ $19296_{4}$ | 46 |
| 10757.54 | 9293.260 | 2 | I | $5315^{\circ}_{7}$ $14609_{7}$ | −24 |
| 10757.84 | 9293.000 | 2 | II | $1410^{\circ}_{4\frac{1}{2}}$ $10703_{3\frac{1}{2}}$ | −7 |
| 10758.35 | 9292.560 | 3 | I | $9135^{\circ}_{3}$ $18427_{3}$ | 47 |
| 10760.63 | 9290.591 | 4 | | | |
| 10763.37 | 9288.226 | 5 | I | $8055^{\circ}_{6}$ $17343_{5}$ | 18 |
| 10771.01 | 9281.638 | 3 | I | $3710^{\circ}_{1}$ $12992_{2}$ | 36 |
| 10771.73 | 9281.017 | 1 | I | $9425^{\circ}_{2}$ $18706_{2}$ | 44 |

TABLE 1. *Observed infrared cerium lines*—Continued

| Wavelength Å | Wavenumber ($cm^{-1}$) | Intensity | Spectrum | Classification | O−C (.001 $cm^{-1}$) |
|---|---|---|---|---|---|
| 10774.64 | 9278.511 | 1 | | | |
| 10777.43 | 9276.109 | 3 | I | $9135^{\circ}_{3}$ $18411_{4}$ | 38 |
| 10778.11 | 9275.523 | 1 | | | |
| 10779.82 | 9274.052 | 2 | | | |
| 10781.46 | 9272.641 | 1 | | | |
| 10783.38 | 9270.990 | 3 | | | |
| 10786.44 | 9268.360 | 1 | | | |
| 10788.36 | 9266.711 | 3 | I | $3100^{\circ}_{4}$ $12366_{5}$ | 28 |
| 10795.20 | 9260.839 | 1 | II | $4266_{3^1/_2}$ $13527_{4^1/_2}$ | −2 |
| 10797.47 | 9258.892 | 1 | I | $8430^{\circ}_{1}$ $17689_{2}$ | −8 |
| 10802.00 | 9255.010 | 1 | I | $9923^{\circ}_{1}$ $19158_{2}$ | −2 |
| 10803.38 | 9253.827 | 1 | I | $10586_{4}$ $19840_{4}$ | −31 |
| | | | II | $7746_{2^1/_2}$ $17000_{3^1/_2}$ | −7 |
| 10808.05 | 9249.829 | 1 | I | $11850_{5}$ $21100_{6}$ | 16 |
| 10809.93 | 9248.220 | 1 | | | |
| 10814.61 | 9244.218 | 2 | I | $6836^{\circ}_{2}$ $16080_{2}$ | −35 |
| 10819.48 | 9240.057 | 1 | | | |
| 10822.83 | 9237.197 | 4 | I | $5409^{\circ}_{2}$ $14646_{2}$ | −11 |
| 10823.24 | 9236.847 | 4 | I | $8762^{\circ}_{4}$ $17998_{4}$ | 0 |
| 10824.76 | 9235.550 | 3 | | | |
| 10826.27 | 9234.262 | 2 | | | |
| 10827.56 | 9233.162 | 3 | I | $7841^{\circ}_{5}$ $17075_{5}$ | 10 |
| 10831.18 | 9230.076 | 4 | I | $9462^{\circ}_{5}$ $18692_{4}$ | −11 |
| | | | I | $12351^{\circ}_{4}$ $21581_{5}$ | −11 |
| 10832.21 | 9229.198 | 4 | I | $5519^{\circ}_{3}$ $14748_{4}$ | 4 |
| 10834.43 | 9227.307 | 5 | I | $7715^{\circ}_{5}$ $16942_{4}$ | 17 |
| 10835.95 | 9226.013 | 6 | I | $5409^{\circ}_{2}$ $14635_{1}$ | 6 |
| | | | I | $7467^{\circ}_{5}$ $16693_{4}$ | 21 |
| 10839.29 | 9223.170 | 1 | I | $5572^{\circ}_{4}$ $14795_{5}$ | −45 |
| 10840.48 | 9222.158 | 2 | | | |
| 10842.23 | 9220.669 | 1 | I | $8509^{\circ}_{4}$ $17729_{5}$ | 3 |
| 10844.25 | 9218.951 | 4 | I | $6337^{\circ}_{3}$ $15555^{\circ}_{3}$ | 21 |
| 10847.10 | 9216.529 | 2 | I | $6663^{\circ}_{5}$ $15879_{5}$ | −22 |
| 10849.63 | 9214.380 | 1 | I | $10774^{\circ}_{3}$ $19988^{\circ}_{3}$ | 0 |
| 10854.11 | 9210.577 | 3 | I | $7174^{\circ}_{4}$ $16384_{3}$ | −7 |
| 10858.13 | 9207.167 | 5 | I | $7696^{\circ}_{6}$ $16903_{5}$ | −2 |
| 10862.57 | 9203.404 | 1 | I | $8991^{\circ}_{5}$ $18194_{5}$ | −34 |
| 10870.20 | 9196.943 | 6 | I | $3764^{\circ}_{5}$ $12960_{6}$ | 2 |
| | | | II | $8278_{5^1/_2}$ $17475^{\circ}_{4^1/_2}$ | −33 |
| 10874.69 | 9193.146 | 3 | I | $4746_{6}$ $13939_{6}$ | −19 |
| 10876.97 | 9191.219 | 1 | I | $8695^{\circ}_{1}$ $17886_{2}$ | 41 |
| | | | II | $5942_{3^1/_2}$ $15134_{4^1/_2}$ | −32 |
| 10879.40 | 9189.166 | 1 | | | |
| 10881.54 | 9187.359 | 3 | I | $4417^{\circ}_{5}$ $13605_{6}$ | −22 |
| 10884.70 | 9184.692 | 1 | I | $7890^{\circ}_{4}$ $17075_{5}$ | 14 |
| | | | I | $11545^{\circ}_{4}$ $20730_{5}$ | −44 |
| 10886.10 | 9183.511 | 1 | | | |
| 10887.81 | 9182.068 | 5 | | | |
| 10889.46 | 9180.677 | 1 | II | $7011_{4^1/_2}$ $16192^{\circ}_{4^1/_2}$ | 18 |
| 10891.71 | 9178.781 | 2 | I | $9135^{\circ}_{3}$ $18313_{3}$ | 19 |
| 10893.98 | 9176.868 | 3 | I | $5572^{\circ}_{4}$ $14748_{4}$ | −2 |
| 10894.61 | 9176.337 | 2 | I | $6621^{\circ}_{3}$ $15798_{3}$ | 3 |
| 10900.08 | 9171.732 | 1 | | | |
| 10901.94 | 9170.167 | 5 | | | |
| 10903.67 | 9168.712 | 2 | II | $8402^{\circ}_{3^1/_2}$ $17571_{4^1/_2}$ | −18 |
| 10904.16 | 9168.300 | 5 | I | $8270^{\circ}_{3}$ $17438_{4}$ | −16 |
| 10907.29 | 9165.669 | 1 | I | $11626^{\circ}_{1}$ $20791_{1}$ | −12 |
| 10907.94 | 9165.123 | 1 | II | $5969_{5^1/_2}$ $15134_{4^1/_2}$ | 73 |
| 10908.79 | 9164.409 | 4 | II | $4511^{\circ}_{2^1/_2}$ $13675_{2^1/_2}$ | −61 |
| 10909.69 | 9163.653 | 2 | | | |
| 10911.47 | 9162.158 | 5 | I | $4746^{\circ}_{6}$ $13908_{7}$ | −40 |
| 10912.61 | 9161.201 | 1 | I | $7890^{\circ}_{4}$ $17051_{3}$ | −11 |
| 10914.23 | 9159.841 | 6 | I | $6856^{\circ}_{4}$ $16016_{5}$ | −8 |
| 10917.18 | 9157.366 | 2 | | | |
| 10917.65 | 9156.972 | 2 | I | $9462^{\circ}_{5}$ $18619_{5}$ | −7 |
| 10918.49 | 9156.268 | 1 | I | $3210^{\circ}_{5}$ $12366_{5}$ | 17 |
| 10919.31 | 9155.580 | 2 | I | $3312^{\circ}_{4}$ $12467_{5}$ | −6 |
| 10923.31 | 9152.227 | 3 | I | $6856^{\circ}_{4}$ $16008_{3}$ | −44 |
| 10926.83 | 9149.279 | 5 | I | $4455^{\circ}_{6}$ $13605_{6}$ | 35 |
| 10929.68 | 9146.893 | 3 | I | $8270^{\circ}_{3}$ $17417_{2}$ | −7 |
| 10931.07 | 9145.730 | 1 | | | |
| 10931.72 | 9145.186 | 2 | I | $8509^{\circ}_{4}$ $17654_{3}$ | −22 |
| 10934.19 | 9143.120 | 5 | I | $6238^{\circ}_{5}$ $15382_{6}$ | 27 |
| 10937.41 | 9140.429 | 3 | I | $4762^{\circ}_{4}$ $13903^{\circ}_{3}$ | 2 |
| | | | I | $7696^{\circ}_{6}$ $16836_{6}$ | −7 |
| 10941.68 | 9136.862 | 2 | I | $6234^{\circ}_{3}$ $15371_{4}$ | 7 |
| 10942.63 | 9136.068 | 2 | I | $11131^{\circ}_{3}$ $20267_{3}$ | −6 |
| 10944.16 | 9134.791 | 2 | I | $4746^{\circ}_{6}$ $13881^{\circ}_{5}$ | −25 |
| 10948.40 | 9131.254 | 2 | I | $8307^{\circ}_{3}$ $17438_{4}$ | −2 |
| 10949.33 | 9130.478 | 3 | I | $6836^{\circ}_{2}$ $15967_{2}$ | 19 |
| 10950.50 | 9129.502 | 1 | I | $11578^{\circ}_{1}$ $20708_{2}$ | −27 |
| 10951.05 | 9129.044 | 2 | I | $10901^{\circ}_{2}$ $20030_{3}$ | 36 |
| 10952.37 | 9127.944 | 2 | I | $12454^{\circ}_{2}$ $21582_{3}$ | 29 |
| 10956.79 | 9124.261 | 2 | I | $10586_{4}$ $19711_{3}$ | 26 |
| 10958.88 | 9122.521 | 1 | II | $3995^{\circ}_{3^1/_2}$ $13117_{4^1/_2}$ | 61 |
| 10960.62 | 9121.073 | 1 | I | $7467^{\circ}_{5}$ $16588_{4}$ | 31 |
| 10960.92 | 9120.823 | 2 | | | |
| 10972.14 | 9111.497 | 2 | | | |
| 10983.91 | 9101.733 | 1 | | | |
| 10994.10 | 9093.297 | 3 | I | $10586_{4}$ $19680_{4}$ | −8 |
| | | | II | $3363^{\circ}_{2^1/_2}$ $12456^{\circ}_{3^1/_2}$ | −29 |
| | | | II | $7059^{\circ}_{4^1/_2}$ $16152^{\circ}_{3^1/_2}$ | −16 |
| 11001.11 | 9087.503 | 2 | | | |
| 11001.92 | 9086.834 | 2 | II | $5010^{\circ}_{2^1/_2}$ $14097^{\circ}_{3^1/_2}$ | −7 |
| 11009.61 | 9080.487 | 3 | I | $6475^{\circ}_{4}$ $15555^{\circ}_{3}$ | 35 |
| 11010.39 | 9079.843 | 1 | I | $5519^{\circ}_{3}$ $14599_{4}$ | −3 |
| 11011.28 | 9079.110 | 3 | I | $6621^{\circ}_{3}$ $15700_{4}$ | 24 |
| 11011.83 | 9078.656 | 1 | | | |
| 11014.91 | 9076.118 | 2 | II | $2382^{\circ}_{4^1/_2}$ $11458_{5^1/_2}$ | 0 |
| 11023.25 | 9069.251 | 1 | I | $11131^{\circ}_{3}$ $20200_{2}$ | −2 |
| 11025.11 | 9067.721 | 1 | | | |
| 11027.19 | 9066.010 | 2 | I | $10774^{\circ}_{3}$ $19840_{4}$ | −15 |
| 11029.58 | 9064.046 | 1 | I | $5571^{\circ}_{6}$ $14635_{1}$ | −40 |
| 11033.20 | 9061.072 | 5 | I | $8587^{\circ}_{7}$ $17649_{6}$ | 9 |
| 11035.19 | 9059.438 | 3 | I | $10901^{\circ}_{2}$ $19961_{1}$ | −1 |
| 11040.33 | 9055.220 | 1 | II | $6521^{\circ}_{1^1/_2}$ $15576^{\circ}_{1^1/_2}$ | −7 |
| 11040.82 | 9054.818 | 1 | II | $4201^{\circ}_{1^1/_2}$ $13256^{\circ}_{1^1/_2}$ | 17 |
| 11042.27 | 9053.629 | 2 | II | $0^{\circ}_{3^1/_2}$ $9053^{\circ}_{3^1/_2}$ | −6 |
| 11043.56 | 9052.572 | 1 | I | $10243^{\circ}_{4}$ $19296_{4}$ | 0 |
| 11044.12 | 9052.113 | 1 | I | $7890^{\circ}_{4}$ $16942_{4}$ | 16 |
| 11045.44 | 9051.031 | 2 | I | $8366^{\circ}_{2}$ $17417_{2}$ | −20 |
| 11047.37 | 9049.450 | 1 | I | $7174^{\circ}_{4}$ $16223_{5}$ | −36 |
| 11052.28 | 9045.429 | 1 | I | $11578^{\circ}_{1}$ $20624_{2}$ | 5 |
| | | | I | $12454^{\circ}_{2}$ $21499_{3}$ | 1 |
| 11061.66 | 9037.759 | 4 | I | $6663^{\circ}_{5}$ $15700_{4}$ | 7 |
| 11065.54 | 9034.590 | 5 | I | $4160^{\circ}_{3}$ $13194_{4}$ | 24 |
| | | | I | $6337^{\circ}_{3}$ $15371_{4}$ | 4 |
| 11067.81 | 9032.737 | 1 | I | $8270^{\circ}_{3}$ $17302_{3}$ | 43 |
| | | | I | $11030^{\circ}_{6}$ $20063_{6}$ | 27 |
| 11069.22 | 9031.587 | 2 | I | $7890^{\circ}_{4}$ $16921_{3}$ | 36 |
| 11070.36 | 9030.657 | 2 | I | $10774^{\circ}_{3}$ $19805_{2}$ | −27 |
| | | | I | $12425^{\circ}_{4}$ $21456_{5}$ | 27 |
| 11075.58 | 9026.400 | 1 | | | |
| 11078.66 | 9023.891 | 1 | | | |
| 11080.15 | 9022.677 | 3 | II | $7522^{\circ}_{5^1/_2}$ $16545_{5^1/_2}$ | 36 |
| 11081.74 | 9021.383 | 1 | I | $4173^{\circ}_{4}$ $13194_{4}$ | 28 |
| 11082.73 | 9020.577 | 3 | I | $7853^{\circ}_{1}$ $16873_{1}$ | −3 |
| 11083.46 | 9019.983 | 1 | | | |

TABLE 1. *Observed infrared cerium lines*—Continued

| Wavelength Å | Wavenumber ($cm^{-1}$) | Intensity | Spectrum | Classification | O−C (.001 $cm^{-1}$) |
|---|---|---|---|---|---|
| 11084.10 | 9019.462 | 1 | I | $5519^{\circ}_{3}$ $14539_{3}$ | 1 |
| 11090.85 | 9013.973 | 4 | I | $3100^{\circ}_{4}$ $12114_{4}$ | 9 |
| 11102.95 | 9004.149 | 1 | II | $4523^{\circ}_{4\frac{1}{2}}$ $13527_{4\frac{1}{2}}$ | −56 |
| 11104.16 | 9003.168 | 2 | I | $7696^{\circ}_{6}$ $16699_{6}$ | −5 |
| 11105.11 | 9002.398 | 2 | I | $8509^{\circ}_{4}$ $17511_{3}$ | 11 |
| 11105.85 | 9001.798 | 3 | II | $4266^{\circ}_{3\frac{1}{2}}$ $13268_{2\frac{1}{2}}$ | −16 |
| 11106.64 | 9001.158 | 1 | I | $9830^{\circ}_{6}$ $18831_{5}$ | −15 |
| 11110.50 | 8998.031 | 2 | I | $5637^{\circ}_{1}$ $14635_{1}$ | 21 |
| 11114.85 | 8994.509 | 1 | I | $8695^{\circ}_{1}$ $17689_{2}$ | −36 |
| 11127.51 | 8984.276 | 1 | | | |
| 11131.59 | 8980.983 | 3 | II | $9723^{\circ}_{4\frac{1}{2}}$ $18704_{5\frac{1}{2}}$ | 5 |
| 11137.04 | 8976.588 | 1 | I | $10243^{\circ}_{4}$ $19220_{4}$ | 8 |
| 11143.23 | 8971.602 | 2 | I | $5674^{\circ}_{1}$ $14646_{2}$ | −13 |
| 11156.63 | 8960.826 | 2 | I | $10879^{\circ}_{5}$ $19840_{4}$ | −11 |
| 11157.16 | 8960.400 | 5 | I | $5674^{\circ}_{1}$ $14635_{1}$ | −13 |
| 11168.12 | 8951.607 | 5 | II | $4266^{\circ}_{3\frac{1}{2}}$ $13217_{3\frac{1}{2}}$ | 9 |
| 11169.49 | 8950.509 | 2 | I | $4173^{\circ}_{4}$ $13124_{5}$ | −6 |
| 11170.45 | 8949.740 | 2 | II | $5675^{\circ}_{4\frac{1}{2}}$ $14625_{5\frac{1}{2}}$ | −2 |
| 11172.07 | 8948.442 | 1 | I | $9462^{\circ}_{5}$ $18411_{4}$ | −22 |
| 11174.42 | 8946.560 | 2 | II | $1873^{\circ}_{3\frac{1}{2}}$ $10820_{2\frac{1}{2}}$ | 14 |
| 11184.68 | 8938.353 | 1 | II | $4737^{\circ}_{2\frac{1}{2}}$ $13675_{2\frac{1}{2}}$ | 3 |
| 11192.70 | 8931.949 | 3 | | | |
| 11195.92 | 8929.380 | 2 | I | $6836^{\circ}_{2}$ $15766_{3}$ | −39 |
| | | | I | $8509^{\circ}_{4}$ $17438_{4}$ | 23 |
| 11198.64 | 8927.211 | 2 | I | $8603^{\circ}_{6}$ $17530_{5}$ | −18 |
| 11200.89 | 8925.418 | 2 | I | $5210^{\circ}_{2}$ $14136_{3}$ | 2 |
| 11208.51 | 8919.350 | 1 | | | |
| 11210.85 | 8917.488 | 4 | I | $3196^{\circ}_{4}$ $12114_{4}$ | −19 |
| 11229.47 | 8902.702 | 2 | | | |
| 11235.33 | 8898.058 | 1 | | | |
| 11241.53 | 8893.151 | 1 | II | $8278_{5\frac{1}{2}}$ $17171^{\circ}_{5\frac{1}{2}}$ | −28 |
| 11244.00 | 8891.197 | 1 | | | |
| 11245.26 | 8890.201 | 4 | I | $7696^{\circ}_{6}$ $16586_{5}$ | −11 |
| | | | I | $12793^{\circ}_{5}$ $21683_{5}$ | −16 |
| 11252.11 | 8884.789 | 2 | II | $5942^{\circ}_{3\frac{1}{2}}$ $14827_{3\frac{1}{2}}$ | −33 |
| 11253.44 | 8883.739 | 1 | II | $12057^{\circ}_{2\frac{1}{2}}$ $20940_{3\frac{1}{2}}$ | 17 |
| 11258.48 | 8879.762 | 3 | II | $2879^{\circ}_{5\frac{1}{2}}$ $11759_{5\frac{1}{2}}$ | −3 |
| 11285.67 | 8858.368 | 3 | I | $4746^{\circ}_{6}$ $13605_{6}$ | −4 |
| 11294.27 | 8851.623 | 2 | II | $8448_{2\frac{1}{2}}$ $17300^{\circ}_{3\frac{1}{2}}$ | −50 |
| 11294.76 | 8851.239 | 2 | I | $7841^{\circ}_{5}$ $16693_{4}$ | 42 |
| 11299.34 | 8847.652 | 2 | I | $7169^{\circ}_{3}$ $16017_{3}$ | 45 |
| 11322.63 | 8829.453 | 1 | | | |
| 11329.76 | 8823.896 | 2 | II | $4203^{\circ}_{6\frac{1}{2}}$ $13027_{6\frac{1}{2}}$ | 75 |
| 11351.50 | 8806.997 | 3 | I | $9379^{\circ}_{4}$ $18186^{\circ}_{3}$ | −14 |
| | | | I | $5802^{\circ}_{7}$ $14609_{7}$ | 17 |
| 11352.17 | 8806.477 | 2 | I | $11030^{\circ}_{6}$ $19836_{7}$ | 11 |
| 11356.22 | 8803.336 | 2 | I | $9903^{\circ}_{1}$ $18706_{2}$ | −43 |
| | | | II | $5924^{\circ}_{1\frac{1}{2}}$ $14727_{1\frac{1}{2}}$ | 5 |
| 11358.05 | 8801.918 | 2 | I | $3312^{\circ}_{4}$ $12114_{4}$ | 43 |
| 11358.84 | 8801.306 | 1 | I | $10604^{\circ}_{3}$ $19406_{3}$ | 38 |
| 11360.15 | 8800.291 | 1 | I | $10879^{\circ}_{5}$ $19680_{4}$ | 6 |
| | | | II | $7059^{\circ}_{4\frac{1}{2}}$ $15859_{4\frac{1}{2}}$ | 6 |
| 11364.00 | 8797.310 | 3 | I | $7169^{\circ}_{3}$ $15967_{2}$ | −25 |
| 11366.12 | 8795.669 | 1 | I | $9425^{\circ}_{2}$ $18221_{1}$ | 6 |
| 11368.60 | 8793.750 | 3 | I | $8509^{\circ}_{4}$ $17302_{3}$ | 16 |
| 11374.52 | 8789.173 | 3 | | | |
| 11383.31 | 8782.386 | 1 | | | |
| 11384.94 | 8781.129 | 2 | I | $8055^{\circ}_{6}$ $16836_{6}$ | 8 |
| 11388.10 | 8778.692 | 1 | I | $12297^{\circ}_{5}$ $21076_{4}$ | −3 |
| 11393.09 | 8774.847 | 2 | II | $5964^{\circ}_{3\frac{1}{2}}$ $14739_{2\frac{1}{2}}$ | −19 |
| 11400.00 | 8769.529 | 1 | I | $10774^{\circ}_{3}$ $19544_{4}$ | 29 |
| 11401.21 | 8768.598 | 1 | I | $8762^{\circ}_{4}$ $17530_{5}$ | −36 |
| | | | II | $8531_{3\frac{1}{2}}$ $17300^{\circ}_{3\frac{1}{2}}$ | −23 |
| 11402.48 | 8767.621 | 1 | I | $8101^{\circ}_{2}$ $16868_{2}$ | 38 |
| | | | I | $9830^{\circ}_{6}$ $18598_{6}$ | −31 |
| 11403.00 | 8767.221 | 1 | I | $9425^{\circ}_{2}$ $18192_{3}$ | −15 |
| | | | II | $8804^{\circ}_{4\frac{1}{2}}$ $17571_{4\frac{1}{2}}$ | 52 |
| 11414.86 | 8758.112 | 3 | II | $4459^{\circ}_{3\frac{1}{2}}$ $13217_{3\frac{1}{2}}$ | −5 |
| 11416.58 | 8756.793 | 1 | I | $4762^{\circ}_{4}$ $13519^{\circ}_{5}$ | 34 |
| 11418.24 | 8755.520 | 1 | I | $11357^{\circ}_{5}$ $20112_{4}$ | −48 |
| 11419.74 | 8754.370 | 2 | | | |
| 11423.76 | 8751.289 | 3 | I | $6836^{\circ}_{2}$ $15587_{2}$ | −9 |
| | | | I | $9135^{\circ}_{3}$ $17886_{2}$ | 9 |
| 11426.14 | 8749.466 | 1 | I | $8762^{\circ}_{4}$ $17511_{3}$ | −3 |
| | | | I | $12873^{\circ}_{2}$ $21623_{2}$ | 47 |
| 11427.85 | 8748.157 | 1 | I | $13315^{\circ}_{4}$ $22063_{4}$ | 17 |
| 11428.76 | 8747.461 | 1 | I | $10879^{\circ}_{5}$ $19627_{6}$ | −20 |
| 11429.60 | 8746.818 | 1 | I | $8400^{\circ}_{5}$ $17147_{4}$ | 10 |
| 11431.48 | 8745.379 | 1 | II | $4511^{\circ}_{2\frac{1}{2}}$ $13256_{1\frac{1}{2}}$ | −64 |
| 11432.76 | 8744.400 | 4 | | | |
| 11435.32 | 8742.442 | 3 | I | $5904^{\circ}_{2}$ $14646_{2}$ | 4 |
| 11454.95 | 8727.461 | 2 | I | $13219^{\circ}_{6}$ $21946_{5}$ | 1 |
| 11455.46 | 8727.072 | 5 | I | $5409^{\circ}_{2}$ $14136_{3}$ | −13 |
| 11460.37 | 8723.333 | 1 | | | |
| 11465.15 | 8719.696 | 4 | I | $8400^{\circ}_{5}$ $17120_{5}$ | 25 |
| 11467.54 | 8717.879 | 1 | I | $11271^{\circ}_{4}$ $19988_{3}$ | −18 |
| | | | II | $6517^{\circ}_{2\frac{1}{2}}$ $15235_{1\frac{1}{2}}$ | −70 |
| 11479.39 | 8708.880 | 1 | I | $11131^{\circ}_{3}$ $19840_{4}$ | −40 |
| 11480.00 | 8708.417 | 1 | I | $6663^{\circ}_{5}$ $15371_{4}$ | −3 |
| | | | II | $7746^{\circ}_{2\frac{1}{2}}$ $16454_{2\frac{1}{2}}$ | 59 |
| 11482.62 | 8706.430 | 1 | I | $4417^{\circ}_{5}$ $13124_{5}$ | 38 |
| 11486.02 | 8703.853 | 5 | I | $3764^{\circ}_{5}$ $12467_{5}$ | 34 |
| 11491.75 | 8699.513 | 2 | II | $4737^{\circ}_{2\frac{1}{2}}$ $13436_{2\frac{1}{2}}$ | 47 |
| 11499.96 | 8693.302 | 1 | I | $7853^{\circ}_{1}$ $16546_{0}$ | 3 |
| 11501.91 | 8691.828 | 1 | I | $5210^{\circ}_{2}$ $13902_{3}$ | −25 |
| 11502.41 | 8691.451 | 2 | I | $10604^{\circ}_{3}$ $19296_{4}$ | −12 |
| 11502.85 | 8691.118 | 1 | | | |
| 11505.56 | 8689.071 | 1 | I | $5409^{\circ}_{2}$ $14098_{2}$ | 2 |
| 11508.99 | 8686.481 | 1 | | | |
| 11512.52 | 8683.818 | 1 | I | $13139^{\circ}_{2}$ $21823_{1}$ | −29 |
| 11514.03 | 8682.679 | 1 | I | $10723^{\circ}_{4}$ $19406_{3}$ | 34 |
| 11515.81 | 8681.337 | 1 | I | $6238^{\circ}_{5}$ $14920^{\circ}_{4}$ | 9 |
| | | | I | $7853^{\circ}_{1}$ $16534_{2}$ | 5 |
| 11518.82 | 8679.069 | 2 | | | |
| 11522.15 | 8676.560 | 1 | | | |
| 11525.02 | 8674.400 | 1 | I | $8400^{\circ}_{5}$ $17075_{5}$ | 23 |
| 11526.03 | 8673.639 | 1 | | | |
| 11526.61 | 8673.203 | 1 | I | $10673^{\circ}_{6}$ $19347_{5}$ | −13 |
| 11527.88 | 8672.248 | 1 | I | $8270^{\circ}_{3}$ $16942_{4}$ | −28 |
| 11533.16 | 8668.277 | 3 | I | $4455^{\circ}_{6}$ $13124_{5}$ | 23 |
| 11538.43 | 8664.318 | 1 | I | $10879^{\circ}_{5}$ $19544_{4}$ | 6 |
| 11538.63 | 8664.168 | 1 | I | $12359^{\circ}_{1}$ $21023_{2}$ | 24 |
| 11543.85 | 8660.250 | 1 | II | $5437^{\circ}_{3\frac{1}{2}}$ $14097_{3\frac{1}{2}}$ | −40 |
| 11546.73 | 8658.090 | 1 | I | $13219^{\circ}_{6}$ $21877_{6}$ | −10 |
| | | | II | $4459^{\circ}_{3\frac{1}{2}}$ $13117_{4\frac{1}{2}}$ | 44 |
| 11557.98 | 8649.663 | 1 | I | $13297^{\circ}_{5}$ $21946_{5}$ | 26 |
| 11568.43 | 8641.849 | 1 | I | $9333^{\circ}_{6}$ $17975_{6}$ | 12 |
| 11571.00 | 8639.930 | 1 | I | $9947^{\circ}_{2}$ $18587_{2}$ | 3 |
| | | | I | $10604^{\circ}_{3}$ $19244_{4}$ | 32 |
| | | | I | $11874^{\circ}_{3}$ $20513_{2}$ | −19 |
| 11574.78 | 8637.108 | 1 | I | $8509^{\circ}_{4}$ $17146_{3}$ | 10 |
| 11578.59 | 8634.266 | 1 | I | $11796^{\circ}_{4}$ $20430_{3}$ | −24 |
| 11579.56 | 8633.543 | 1 | I | $10586^{\circ}_{4}$ $19220_{4}$ | −44 |
| 11582.15 | 8631.612 | 1 | | | |
| 11586.36 | 8628.476 | 1 | I | $7169^{\circ}_{3}$ $15798_{3}$ | 1 |
| 11587.24 | 8627.821 | 1 | I | $10243^{\circ}_{4}$ $18871_{4}$ | −4 |
| 11589.75 | 8625.952 | 3 | | | |

TABLE 1. *Observed infrared cerium lines*—Continued

| Wavelength Å | Wavenumber ($cm^{-1}$) | Intensity | Spectrum | Classification | O−C (.001 $cm^{-1}$) |
|---|---|---|---|---|---|
| 11590.01 | 8625.759 | 5 | II | $7233^{\circ}_{5\,1/2}\ 15859_{4\,1/2}$ | 25 |
| 11591.08 | 8624.963 | 2 | II | $5651^{\circ}_{5\,1/2}\ 14276_{5\,1/2}$ | 22 |
| 11593.05 | 8623.497 | 1 | I | $4766^{\circ}_{2}\ 13389_{3}$ | −6 |
| | | | I | $7715^{\circ}_{5}\ 16338_{4}$ | 29 |
| 11599.40 | 8618.776 | 1 | I | $6621^{\circ}_{3}\ 15240_{4}$ | 49 |
| | | | I | $11061^{\circ}_{7}\ 19680_{6}$ | −15 |
| 11601.27 | 8617.387 | 1 | I | $11650^{\circ}_{2}\ 20267_{3}$ | −30 |
| 11602.76 | 8616.280 | 2 | II | $4910^{\circ}_{5\,1/2}\ 13527_{4\,1/2}$ | 1 |
| 11604.89 | 8614.699 | 3 | I | $8307^{\circ}_{3}\ 16921_{3}$ | 28 |
| | | | I | $9996^{\circ}_{3}\ 18611_{3}$ | −39 |
| 11612.17 | 8609.298 | 1 | I | $8902^{\circ}_{3}\ 17511_{3}$ | 8 |
| | | | I | $12297^{\circ}_{5}\ 20907_{4}$ | −36 |
| 11615.38 | 8606.919 | 1 | | | |
| 11617.31 | 8605.489 | 1 | | | |
| 11624.32 | 8600.299 | 4 | II | $7259^{\circ}_{3\,1/2}\ 15859_{4\,1/2}$ | 12 |
| 11628.39 | 8597.289 | 1 | II | $8402^{\circ}_{3\,1/2}\ 17000_{3\,1/2}$ | −64 |
| 11629.07 | 8596.786 | 1 | I | $7348^{\circ}_{4}\ 15945_{4}$ | −25 |
| | | | I | $11030^{\circ}_{6}\ 19627_{6}$ | −18 |
| 11631.62 | 8594.902 | 3 | II | $4523^{\circ}_{4\,1/2}\ 13117_{4\,3/2}$ | 12 |
| 11634.17 | 8593.018 | 1 | I | $5315^{\circ}_{7}\ 13908_{7}$ | −4 |
| 11635.32 | 8592.169 | 1 | II | $4844^{\circ}_{1\,1/2}\ 13436_{2\,1/2}$ | −22 |
| 11635.79 | 8591.822 | 2 | I | $11650^{\circ}_{2}\ 20242_{3}$ | 3 |
| 11641.06 | 8587.932 | 4 | I | $6475^{\circ}_{4}\ 15063_{3}$ | 20 |
| 11643.35 | 8586.243 | 4 | I | $13139^{\circ}_{2}\ 21725_{1}$ | 46 |
| | | | II | $4165_{4\,1/2}\ 12751^{\circ}_{5\,1/2}$ | −11 |
| 11652.26 | 8579.677 | 3 | I | $8587^{\circ}_{7}\ 17167_{7}$ | −30 |
| 11652.81 | 8579.272 | 1 | I | $8088^{\circ}_{2}\ 16668_{3}$ | −5 |
| | | | I | $11131^{\circ}_{3}\ 19711_{3}$ | −25 |
| 11653.63 | 8578.669 | 1 | II | $2879^{\circ}_{5\,1/2}\ 11458_{5\,1/2}$ | −4 |
| 11655.37 | 8577.388 | 3 | I | $6663^{\circ}_{5}\ 15240_{4}$ | −4 |
| 11658.60 | 8575.012 | 5 | II | $2879^{\circ}_{5\,1/2}\ 11454_{6\,1/2}$ | 3 |
| 11665.84 | 8569.690 | 1 | | | |
| 11666.60 | 8569.132 | 1 | | | |
| 11668.10 | 8568.030 | 4 | II | $5819^{\circ}_{4\,1/2}\ 14387_{4\,1/2}$ | 32 |
| 11673.37 | 8564.162 | 2 | I | $8603^{\circ}_{6}\ 17167_{7}$ | 12 |
| 11677.15 | 8561.390 | 1 | | | |
| 11683.63 | 8556.641 | 1 | I | $11874^{\circ}_{3}\ 20430_{3}$ | 0 |
| 11687.18 | 8554.042 | 2 | | | |
| 11688.13 | 8553.347 | 3 | I | $7696^{\circ}_{6}\ 16249_{6}$ | −43 |
| | | | I | $8762^{\circ}_{4}\ 17315_{4}$ | 35 |
| 11688.80 | 8552.857 | 1 | I | $4762_{4}\ 13315^{\circ}_{4}$ | 7 |
| 11700.03 | 8544.648 | 2 | I | $5519^{\circ}_{3}\ 14064_{4}$ | 17 |
| 11705.22 | 8540.859 | 1 | I | $8762^{\circ}_{4}\ 17302_{3}$ | 42 |
| 11711.86 | 8536.017 | 3 | II | $5716^{\circ}_{3\,1/2}\ 14252_{3\,1/2}$ | 60 |
| 11713.12 | 8535.098 | 1 | I | $9830^{\circ}_{6}\ 18365_{5}$ | −18 |
| 11718.01 | 8531.537 | 2 | | | |
| 11723.63 | 8527.447 | 3 | I | $7696^{\circ}_{6}\ 16223_{5}$ | 14 |
| 11728.18 | 8524.139 | 1 | I | $10723^{\circ}_{4}\ 19247_{3}$ | 24 |
| 11731.37 | 8521.821 | 1 | I | $13139^{\circ}_{2}\ 21661_{3}$ | −47 |
| 11734.79 | 8519.337 | 3 | I | $9135^{\circ}_{3}\ 17654_{3}$ | 18 |
| | | | II | $4737^{\circ}_{2\,1/2}\ 13256_{1\,1/2}$ | 13 |
| 11741.13 | 8514.737 | 1 | I | $10243^{\circ}_{4}\ 18758_{3}$ | 4 |
| | | | II | $7061^{\circ}_{0\,1/2}\ 15576_{1\,1/2}$ | 12 |
| 11741.90 | 8514.179 | 1 | I | $6234^{\circ}_{3}\ 14748_{4}$ | 26 |
| 11744.42 | 8512.352 | 2 | I | $9462^{\circ}_{5}\ 17975_{6}$ | −2 |
| 11746.37 | 8510.939 | 3 | II | $8789^{\circ}_{2\,1/2}\ 17300_{3\,1/2}$ | 1 |
| 11753.27 | 8505.942 | 1 | I | $13219^{\circ}_{6}\ 21725_{5}$ | −16 |
| 11757.66 | 8502.766 | 2 | I | $11337^{\circ}_{3}\ 19840_{4}$ | −5 |
| | | | II | $4201^{\circ}_{1\,1/2}\ 12704_{1\,1/2}$ | 38 |
| 11767.26 | 8495.829 | 4 | II | $6638^{\circ}_{4\,1/2}\ 15134_{4\,1/2}$ | 34 |
| 11770.40 | 8493.563 | 3 | I | $5409^{\circ}_{2}\ 13902_{3}$ | 39 |
| 11772.11 | 8492.329 | 1 | I | $5572^{\circ}_{4}\ 14064_{4}$ | 21 |
| 11781.64 | 8485.460 | 1 | | | |
| 11784.81 | 8483.177 | 2 | I | $6856^{\circ}_{4}\ 15339_{5}$ | 19 |
| 11788.14 | 8480.781 | 2 | I | $9135^{\circ}_{3}\ 17615_{4}$ | −12 |
| 11791.59 | 8478.300 | 2 | I | $8587^{\circ}_{7}\ 17066_{6}$ | 27 |
| 11792.02 | 8477.991 | 1 | I | $7467^{\circ}_{5}\ 15945_{4}$ | 40 |
| 11799.34 | 8472.731 | 1 | | | |
| 11802.87 | 8470.197 | 1 | I | $10774^{\circ}_{3}\ 19244_{4}$ | 15 |
| 11805.93 | 8468.002 | 1 | I | $10604^{\circ}_{3}\ 19072_{3}$ | −6 |
| 11806.25 | 8467.772 | 2 | I | $10879^{\circ}_{5}\ 19347_{6}$ | 23 |
| 11811.69 | 8463.872 | 2 | I | $9830^{\circ}_{6}\ 18294_{6}$ | 29 |
| 11815.34 | 8461.258 | 4 | II | $3995^{\circ}_{3\,1/2}\ 12456_{3\,1/2}$ | −34 |
| 11820.98 | 8457.221 | 5 | II | $5819^{\circ}_{4\,1/2}\ 14276_{5\,1/2}$ | 37 |
| 11825.78 | 8453.788 | 1 | | | |
| 11833.00 | 8448.630 | 6 | II | $0^{\circ}_{3\,1/2}\ 8448_{2\,1/2}$ | −11 |
| 11839.08 | 8444.291 | 1 | II | $5942^{\circ}_{3\,1/2}\ 14387_{4\,1/2}$ | −20 |
| 11843.63 | 8441.047 | 5 | I | $8695^{\circ}_{1}\ 17136_{1}$ | 34 |
| | | | I | $12720^{\circ}_{4}\ 21161_{4}$ | −29 |
| 11844.80 | 8440.213 | 1 | II | $1873^{\circ}_{3\,1/2}\ 10314_{4\,1/2}$ | −20 |
| 11848.12 | 8437.848 | 1 | | | |
| 11848.36 | 8437.677 | 1 | II | $6389^{\circ}_{4\,1/2}\ 14827_{3\,1/2}$ | −3 |
| 11851.32 | 8435.570 | 3 | I | $13629^{\circ}_{5}\ 22064_{6}$ | −37 |
| 11851.98 | 8435.100 | 1 | | | |
| 11854.66 | 8433.193 | 2 | | | |
| 11855.14 | 8432.852 | 2 | I | $9462^{\circ}_{5}\ 17895_{5}$ | 18 |
| | | | I | $12359^{\circ}_{1}\ 20791_{1}$ | −13 |
| | | | I | $12793^{\circ}_{5}\ 21226_{5}$ | −4 |
| 11858.00 | 8430.818 | 4 | | | |
| 11861.84 | 8428.088 | 2 | I | $10586^{\circ}_{4}\ 19014_{4}$ | −2 |
| | | | I | $13297^{\circ}_{5}\ 21725_{5}$ | −47 |
| 11862.94 | 8427.307 | 1 | | | |
| 11864.75 | 8426.021 | 2 | II | $5010^{\circ}_{2\,1/2}\ 13436_{2\,1/2}$ | 47 |
| 11868.26 | 8423.529 | 1 | II | $4844^{\circ}_{1\,1/2}\ 13268_{2\,1/2}$ | −30 |
| 11869.19 | 8422.869 | 3 | I | $8270^{\circ}_{3}\ 16693_{4}$ | −33 |
| 11870.49 | 8421.947 | 3 | II | $5675^{\circ}_{4\,1/2}\ 14097_{3\,1/2}$ | 0 |
| 11871.25 | 8421.408 | 2 | II | $9053_{3\,1/2}\ 17475^{\circ}_{4\,1/2}$ | −4 |
| 11876.04 | 8418.011 | 1 | | | |
| 11878.02 | 8416.608 | 1 | I | $10879^{\circ}_{5}\ 19296_{4}$ | 48 |
| 11884.95 | 8411.700 | 1 | I | $6234^{\circ}_{3}\ 14646_{2}$ | 47 |
| 11892.63 | 8406.268 | 5 | II | $7746^{\circ}_{2\,1/2}\ 16152_{3\,1/2}$ | 65 |
| 11903.94 | 8398.281 | 1 | I | $10673^{\circ}_{6}\ 19072_{6}$ | 25 |
| 11904.33 | 8398.006 | 2 | | | |
| 11908.83 | 8394.833 | 1 | | | |
| 11910.41 | 8393.719 | 3 | II | $3703^{\circ}_{3\,1/2}\ 12097_{3\,1/2}$ | 44 |
| 11921.62 | 8385.827 | 1 | I | $8307^{\circ}_{3}\ 16693_{4}$ | −15 |
| 11922.21 | 8385.412 | 1 | I | $8762^{\circ}_{4}\ 17147_{4}$ | 0 |
| 11924.10 | 8384.082 | 2 | I | $6856^{\circ}_{4}\ 15240_{4}$ | 23 |
| 11924.90 | 8383.520 | 1 | I | $10774^{\circ}_{3}\ 19158_{2}$ | −9 |
| 11927.13 | 8381.953 | 4 | II | $4322^{\circ}_{2\,1/2}\ 12704_{1\,1/2}$ | 39 |
| 11927.73 | 8381.531 | 5 | II | $5716^{\circ}_{3\,1/2}\ 14097_{3\,1/2}$ | 41 |
| 11931.58 | 8378.826 | 1 | I | $12351^{\circ}_{4}\ 20730_{5}$ | 11 |
| 11933.65 | 8377.373 | 1 | I | $4746^{\circ}_{6}\ 13124_{5}$ | −9 |
| 11938.39 | 8374.047 | 1 | II | $2641^{\circ}_{3\,1/2}\ 11015_{3\,1/2}$ | 26 |
| | | | II | $7202^{\circ}_{2\,1/2}\ 15576_{1\,1/2}$ | 13 |
| 11941.07 | 8372.167 | 1 | I | $7780_{6}\ 16152^{\circ}_{6}$ | −24 |
| 11943.12 | 8370.730 | 1 | I | $7696^{\circ}_{6}\ 16066_{6}$ | 0 |
| 11946.67 | 8368.243 | 4 | II | $6913^{\circ}_{6\,1/2}\ 15281_{6\,1/2}$ | 27 |
| 11951.60 | 8364.791 | 3 | I | $6234^{\circ}_{3}\ 14599_{4}$ | −14 |
| 11953.22 | 8363.657 | 1 | I | $11517^{\circ}_{1}\ 19880_{2}$ | −5 |
| 11955.55 | 8362.027 | 2 | I | $13219^{\circ}_{6}\ 21581_{5}$ | 9 |
| 11957.21 | 8360.867 | 1 | I | $8307^{\circ}_{3}\ 16668_{3}$ | −13 |
| 11960.94 | 8358.259 | 2 | I | $8762^{\circ}_{4}\ 17120_{5}$ | −16 |
| 11978.52 | 8345.993 | 1 | I | $13315^{\circ}_{4}\ 21661_{3}$ | 24 |
| 11983.49 | 8342.531 | 1 | | | |
| 11987.23 | 8339.928 | 1 | | | |
| 11989.05 | 8338.662 | 1 | I | $12366_{5}\ 20705^{\circ}_{6}$ | −38 |
| | | | I | $11650^{\circ}_{2}\ 19988_{3}$ | 43 |

TABLE 1. *Observed infrared cerium lines*—Continued

| Wavelength Å | Wavenumber ($cm^{-1}$) | Intensity | Spectrum | Classification | O−C (.001 $cm^{-1}$) |
|---|---|---|---|---|---|
| 11992.46 | 8336.291 | 3 | I | $7715_5$ $16051_4$ | 49 |
| 11999.73 | 8331.241 | 1 | I | $6303_2$ $14635_1$ | —17 |
| 12002.41 | 8329.380 | 5 | | | |
| 12010.11 | 8324.040 | 1 | | | |
| 12014.34 | 8321.110 | 3 | II | $2382^{\circ}_{41/2}$ $10703_{41/2}$ | 44 |
| 12015.60 | 8320.237 | 5 | I | $7696^{\circ}_6$ $16016_5$ | 38 |
| 12017.98 | 8318.589 | 1 | | | |
| 12022.52 | 8315.448 | 1 | II | $1410^{\circ}_{41/2}$ $9725_{31/2}$ | 13 |
| 12030.37 | 8310.022 | 2 | I | $7890^{\circ}_4$ $16200_3$ | —41 |
| | | | II | $6517^{\circ}_{21/2}$ $14827_{31/2}$ | 17 |
| 12031.29 | 8309.387 | 3 | I | $6337^{\circ}_3$ $14646_2$ | 3 |
| | | | I | $5572^{\circ}_4$ $13881_5$ | 17 |
| | | | II | $5942^{\circ}_{31/2}$ $14252_{31/2}$ | 14 |
| 12038.44 | 8304.451 | 1 | I | $6234^{\circ}_3$ $14539_3$ | 31 |
| 12040.39 | 8303.106 | 3 | | | |
| 12045.20 | 8299.791 | 1 | | | |
| 12047.16 | 8298.440 | 1 | I | $8991^{\circ}_5$ $17289_6$ | 13 |
| 12048.22 | 8297.710 | 3 | II | $7278^{\circ}_{11/2}$ $15576_{11/2}$ | 66 |
| 12055.95 | 8292.390 | 1 | I | $8400^{\circ}_5$ $16693_4$ | —31 |
| 12060.12 | 8289.523 | 1 | I | $8762^{\circ}_4$ $17051_3$ | 7 |
| 12060.59 | 8289.200 | 1 | I | $5315^{\circ}_7$ $13605_6$ | 3 |
| 12061.86 | 8288.327 | 2 | II | $2581^{\circ}_{41/2}$ $10869_{41/2}$ | 43 |
| 12075.97 | 8278.643 | 2 | II | $5819^{\circ}_{41/2}$ $14097_{31/2}$ | 51 |
| | | | II | $8175^{\circ}_{21/2}$ $16454_{21/2}$ | —33 |
| 12083.54 | 8273.456 | 3 | | | |
| 12090.70 | 8268.557 | 1 | I | $9462^{\circ}_5$ $17731_4$ | 34 |
| 12097.54 | 8263.882 | 5 | II | $2382^{\circ}_{41/2}$ $10646_{51/2}$ | 51 |
| 12100.63 | 8261.772 | 3 | I | $3100^{\circ}_4$ $11361_4$ | 28 |
| 12104.59 | 8259.069 | 1 | I | $8088^{\circ}_2$ $16347_2$ | 3 |
| 12105.73 | 8258.291 | 1 | | | |
| 12107.14 | 8257.329 | 2 | II | $5010^{\circ}_{21/2}$ $13268_{21/2}$ | —12 |
| 12110.53 | 8255.018 | 1 | I | $9135^{\circ}_3$ $17390_4$ | 3 |
| 12114.31 | 8252.442 | 2 | | | |
| 12116.87 | 8250.698 | 4 | II | $7278^{\circ}_{11/2}$ $15529_{21/2}$ | 31 |
| 12119.81 | 8248.697 | 3 | I | $8587^{\circ}_7$ $16836_6$ | 23 |
| 12135.11 | 8238.297 | 2 | II | $5437^{\circ}_{31/2}$ $13675_{21/2}$ | —10 |
| 12139.08 | 8235.603 | 2 | II | $6389^{\circ}_{41/2}$ $14625_{51/2}$ | 44 |
| 12141.71 | 8233.819 | 1 | I | $7467^{\circ}_5$ $15700_4$ | 1 |
| 12142.65 | 8233.181 | 1 | | | |
| 12144.51 | 8231.921 | 1 | | | |
| 12146.62 | 8230.491 | 1 | | | |
| 12148.94 | 8228.919 | 1 | I | $9425^{\circ}_2$ $17654_3$ | 30 |
| 12149.94 | 8228.242 | 1 | | | |
| 12152.01 | 8226.840 | 1 | I | $6836^{\circ}_2$ $15063_3$ | 16 |
| 12154.73 | 8224.999 | 2 | I | $7841^{\circ}_5$ $16066_6$ | 14 |
| 12161.38 | 8220.501 | 1 | | | |
| 12164.30 | 8218.528 | 1 | | | |
| 12167.41 | 8216.427 | 2 | I | $9200^{\circ}_2$ $17417_2$ | —15 |
| 12170.46 | 8214.368 | 1 | I | $4746^{\circ}_6$ $12960_6$ | 45 |
| 12172.55 | 8212.958 | 1 | I | $11850^{\circ}_5$ $20063_6$ | 30 |
| 12179.75 | 8208.103 | 5 | II | $11742^{\circ}_{51/2}$ $19950_{61/2}$ | —5 |
| 12181.57 | 8206.877 | 1 | I | $6856^{\circ}_4$ $15063_3$ | —15 |
| 12183.05 | 8205.880 | 3 | I | $12425^{\circ}_4$ $20631_5$ | —25 |
| | | | I | $13519^{\circ}_5$ $21725_5$ | 9 |
| 12184.77 | 8204.721 | 2 | I | $13315^{\circ}_4$ $21520_4$ | 2 |
| 12188.93 | 8201.921 | 1 | I | $7169^{\circ}_3$ $15371_4$ | 25 |
| 12191.34 | 8200.300 | 3 | II | $4165^{\circ}_{41/2}$ $12365^{\circ}_{41/2}$ | 42 |
| 12198.09 | 8195.762 | 1 | II | $8804^{\circ}_{41/2}$ $17000_{31/2}$ | —30 |
| 12201.64 | 8193.377 | 3 | I | $4173^{\circ}_4$ $12366_5$ | 38 |
| | | | II | $4511^{\circ}_{21/2}$ $12704_{11/2}$ | 7 |
| 12204.93 | 8191.169 | 1 | I | $13605^{\circ}_6$ $21796^{\circ}_6$ | 0 |
| | | | I | $9200^{\circ}_2$ $17391_1$ | 17 |
| 12206.69 | 8189.988 | 1 | | | |
| 12213.01 | 8185.750 | 3 | II | $2634^{\circ}_{21/2}$ $10820_{21/2}$ | —65 |
| 12216.22 | 8183.599 | 5 | I | $7696^{\circ}_6$ $15879_5$ | 31 |
| 12221.00 | 8180.398 | 2 | I | $8762^{\circ}_4$ $16942_4$ | —1 |
| 12223.22 | 8178.912 | 2 | I | $5210^{\circ}_2$ $13389_3$ | —8 |
| | | | II | $2641^{\circ}_{31/2}$ $10820_{21/2}$ | —4 |
| 12224.37 | 8178.143 | 2 | I | $13089^{\circ}_3$ $21267_4$ | 38 |
| | | | II | $12762^{\circ}_{41/2}$ $20940_{31/2}$ | —60 |
| 12226.39 | 8176.792 | 6 | II | $7341^{\circ}_{51/2}$ $15517^{\circ}_{61/2}$ | 30 |
| 12228.16 | 8175.608 | 2 | | | |
| 12228.98 | 8175.060 | 1 | | | |
| 12229.92 | 8174.431 | 1 | I | $7841^{\circ}_5$ $16016_5$ | —22 |
| 12230.95 | 8173.743 | 3 | II | $7061^{\circ}_{01/2}$ $15235_{11/2}$ | 11 |
| 12233.92 | 8171.759 | 1 | I | $10586^{\circ}_4$ $18758_3$ | 18 |
| 12235.18 | 8170.917 | 1 | I | $10901^{\circ}_2$ $19072_3$ | —9 |
| 12238.65 | 8168.601 | 1 | | | |
| 12239.37 | 8168.120 | 3 | I | $8055^{\circ}_6$ $16223_5$ | 3 |
| 12243.19 | 8165.571 | 2 | I | $7174^{\circ}_4$ $15339_5$ | 10 |
| | | | II | $3593^{\circ}_{41/2}$ $11759_{51/2}$ | —7 |
| 12243.66 | 8165.258 | 1 | I | $3196^{\circ}_4$ $11361_4$ | —29 |
| 12245.17 | 8164.251 | 2 | I | $13519^{\circ}_5$ $21683_5$ | 6 |
| 12248.04 | 8162.338 | 2 | | | |
| 12251.79 | 8159.840 | 1 | I | $8762^{\circ}_4$ $16921_3$ | —13 |
| 12257.48 | 8156.052 | 2 | I | $8991^{\circ}_5$ $17147_4$ | —34 |
| 12261.81 | 8153.172 | 1 | I | $9462^{\circ}_5$ $17615_4$ | —15 |
| 12267.52 | 8149.377 | 1 | I | $8902^{\circ}_3$ $17051_3$ | 41 |
| | | | II | $5118^{\circ}_{21/2}$ $13268_{21/2}$ | —23 |
| 12273.13 | 8145.652 | 1 | I | $10612^{\circ}_2$ $18758_3$ | 6 |
| | | | II | $5513^{\circ}_{31/2}$ $13659^{\circ}_{41/2}$ | 30 |
| 12279.71 | 8141.287 | 1 | I | $8762^{\circ}_4$ $16903_5$ | 33 |
| 12281.52 | 8140.087 | 1 | II | $2563^{\circ}_{51/2}$ $10703_{41/2}$ | 12 |
| 12284.81 | 8137.907 | 1 | II | $5118^{\circ}_{21/2}$ $13256_{11/2}$ | 16 |
| 12286.38 | 8136.867 | 2 | I | $7780^{\circ}_6$ $15917_7$ | —7 |
| | | | I | $13283^{\circ}_3$ $21420_2$ | —15 |
| 12290.64 | 8134.047 | 6 | II | $4322^{\circ}_{21/2}$ $12456_{31/2}$ | 6 |
| 12293.60 | 8132.089 | 4 | I | $6663^{\circ}_5$ $14795_5$ | 25 |
| | | | I | $11796^{\circ}_4$ $19928_3$ | —11 |
| 12294.93 | 8131.209 | 6 | II | $0^{\circ}_{31/2}$ $8131_{41/2}$ | 0 |
| 12297.39 | 8129.582 | 2 | | | |
| 12302.86 | 8125.968 | 1 | I | $7890^{\circ}_4$ $16016_5$ | —11 |
| 12305.76 | 8124.053 | 2 | I | $6475^{\circ}_4$ $14599_4$ | —4 |
| 12308.79 | 8122.053 | 2 | II | $2581^{\circ}_{41/2}$ $10703_{41/2}$ | 5 |
| 12312.78 | 8119.421 | 2 | | | |
| 12315.16 | 8117.852 | 1 | | | |
| 12316.77 | 8116.791 | 2 | II | $4910^{\circ}_{51/2}$ $13027_{61/2}$ | —8 |
| 12324.96 | 8111.397 | 5 | I | $8587^{\circ}_7$ $16699_6$ | —13 |
| 12335.30 | 8104.598 | 1 | I | $11301^{\circ}_2$ $19406_3$ | —21 |
| 12336.77 | 8103.632 | 1 | I | $8430^{\circ}_1$ $16534_2$ | 27 |
| 12342.73 | 8099.719 | 5 | I | $1279^{\circ}_4$ $9379_4$ | —4 |
| 12357.76 | 8089.868 | 6 | II | $5437^{\circ}_{31/2}$ $13527_{41/2}$ | 50 |
| 12367.20 | 8083.693 | 1 | I | $8991^{\circ}_5$ $17075_5$ | 37 |
| 12368.46 | 8082.869 | 2 | I | $7933^{\circ}_5$ $16016_5$ | 18 |
| | | | II | $2563^{\circ}_{51/2}$ $10646_{51/2}$ | 29 |
| 12372.22 | 8080.413 | 1 | I | $6663^{\circ}_5$ $14743_6$ | 13 |
| 12375.41 | 8078.330 | 2 | I | $11517^{\circ}_1$ $19595_2$ | 14 |
| 12376.74 | 8077.462 | 2 | I | $8307^{\circ}_3$ $16384_3$ | 30 |
| 12379.10 | 8075.922 | 4 | II | $7746^{\circ}_{21/2}$ $15822_{31/2}$ | 45 |
| 12380.64 | 8074.917 | 1 | II | $7059^{\circ}_{41/2}$ $15134_{41/2}$ | —62 |
| 12386.59 | 8071.039 | 3 | II | $7522^{\circ}_{51/2}$ $15593_{61/2}$ | 19 |
| 12394.28 | 8066.031 | 2 | II | $987^{\circ}_{41/2}$ $9053_{31/2}$ | 7 |
| 12397.88 | 8063.689 | 3 | I | $6475^{\circ}_4$ $14539_3$ | 17 |
| 12401.85 | 8061.107 | 3 | I | $9709^{\circ}_2$ $17770_2$ | 15 |
| 12402.71 | 8060.549 | 2 | | | |
| 12403.66 | 8059.931 | 2 | | | |
| 12404.99 | 8059.067 | 1 | | | |
| 12412.58 | 8054.139 | 2 | II | $7522^{\circ}_{01/2}$ $15576_{11/2}$ | 38 |

TABLE 1. *Observed infrared cerium lines*—Continued

| Wavelength Å | Wavenumber ($cm^{-1}$) | Intensity | Spectrum | Classification | O−C (.001 $cm^{-1}$) |
|---|---|---|---|---|---|
| 12413.26 | 8053.698 | 1 | | | |
| 12419.44 | 8049.690 | 4 | I | $3312^{\circ}_{4}$ $11361_{4}$ | 35 |
| 12422.03 | 8048.012 | 5 | II | $7233^{\circ}_{5\,1/2}$ $15281_{6\,1/2}$ | 29 |
| 12433.33 | 8040.698 | 2 | I | $8307^{\circ}_{3}$ $16347_{2}$ | 29 |
| | | | I | $12359^{\circ}_{1}$ $20399_{1}$ | −17 |
| 12433.82 | 8040.381 | 1 | | | |
| 12435.14 | 8039.527 | 1 | I | $13622_{2}$ $21661_{3}$ | 11 |
| 12437.75 | 8037.840 | 1 | I | $7841^{\circ}_{5}$ $15879_{5}$ | 17 |
| 12446.62 | 8032.112 | 1 | | | |
| 12447.69 | 8031.422 | 2 | I | $8307^{\circ}_{3}$ $16338_{4}$ | 27 |
| 12460.20 | 8023.358 | 1 | I | $7348^{\circ}_{4}$ $15371_{4}$ | 10 |
| 12467.52 | 8018.647 | 1 | I | $8366^{\circ}_{2}$ $16384_{3}$ | 4 |
| 12486.05 | 8006.747 | 6 | I | $228^{\circ}_{2}$ $8235_{2}$ | −8 |
| 12498.46 | 7998.797 | 2 | I | $5904_{2}$ $13902_{3}$ | 43 |
| 12501.43 | 7996.897 | 1 | II | $4459^{\circ}_{3\,1/2}$ $12456_{3\,1/2}$ | 18 |
| 12502.27 | 7996.360 | 2 | | | |
| 12505.60 | 7994.230 | 2 | | | |
| 12509.11 | 7991.987 | 1 | I | $8088^{\circ}_{2}$ $16080_{2}$ | 17 |
| 12511.38 | 7990.537 | 2 | I | $11357^{\circ}_{5}$ $19347_{6}$ | 31 |
| 12513.21 | 7989.369 | 1 | I | $7890^{\circ}_{4}$ $15879_{5}$ | 20 |
| 12514.68 | 7988.430 | 3 | | | |
| 12516.31 | 7987.390 | 3 | | | |
| 12523.27 | 7982.951 | 2 | | | |
| 12525.01 | 7981.842 | 1 | I | $8366^{\circ}_{2}$ $16347_{2}$ | −37 |
| 12526.87 | 7980.657 | 3 | | | |
| 12528.36 | 7979.707 | 1 | I | $8101^{\circ}_{2}$ $16080_{2}$ | 13 |
| 12533.27 | 7976.581 | 3 | I | $11271^{\circ}_{4}$ $19247_{3}$ | 42 |
| | | | II | $8175^{\circ}_{2\,1/2}$ $16152_{3\,1/2}$ | 59 |
| 12534.29 | 7975.932 | 3 | | | |
| 12537.55 | 7973.858 | 1 | I | $9135^{\circ}_{3}$ $17108_{2}$ | −9 |
| 12538.44 | 7973.292 | 1 | I | $9947^{\circ}_{2}$ $17921_{3}$ | 27 |
| 12547.98 | 7967.230 | 1 | II | $4737^{\circ}_{2\,1/2}$ $12704_{1\,1/2}$ | −20 |
| 12548.31 | 7967.021 | 2 | | | |
| 12550.20 | 7965.821 | 1 | II | $3793^{\circ}_{6\,1/2}$ $11759_{5\,1/2}$ | 0 |
| 12573.18 | 7951.262 | 1 | II | $7011^{\circ}_{4\,1/2}$ $14963^{\circ}_{5\,1/2}$ | −37 |
| 12575.86 | 7949.568 | 1 | | | |
| 12577.11 | 7948.777 | 3 | I | $7696^{\circ}_{6}$ $15644_{6}$ | 45 |
| 12578.89 | 7947.653 | 1 | I | $6238^{\circ}_{5}$ $14186^{\circ}_{6}$ | 20 |
| 12582.22 | 7945.549 | 4 | II | $4511^{\circ}_{2\,1/2}$ $12456_{3\,1/2}$ | 51 |
| 12584.63 | 7944.028 | 1 | I | $9787^{\circ}_{3}$ $17731_{4}$ | 20 |
| 12589.35 | 7941.049 | 2 | I | $12720^{\circ}_{4}$ $20661_{3}$ | 35 |
| 12593.96 | 7938.142 | 1 | | | |
| 12595.19 | 7937.367 | 1 | | | |
| 12595.60 | 7937.109 | 1 | | | |
| 12598.09 | 7935.540 | 1 | I | $9200^{\circ}_{2}$ $17136_{1}$ | 33 |
| 12600.27 | 7934.167 | 1 | | | |
| 12603.79 | 7931.951 | 2 | II | $2382^{\circ}_{4\,1/2}$ $10314_{4\,1/2}$ | 23 |
| 12608.27 | 7929.133 | 1 | I | $7467^{\circ}_{5}$ $15396_{6}$ | 7 |
| | | | I | $13297^{\circ}_{5}$ $21226_{5}$ | −15 |
| 12608.85 | 7928.768 | 1 | I | $10723^{\circ}_{4}$ $18652_{3}$ | 38 |
| | | | II | $13012^{\circ}_{2\,1/2}$ $20940_{3\,1/2}$ | 31 |
| 12609.29 | 7928.491 | 3 | I | $8088^{\circ}_{2}$ $16017_{3}$ | 46 |
| 12611.01 | 7927.410 | 2 | I | $9462^{\circ}_{5}$ $17390_{4}$ | 1 |
| 12625.06 | 7918.588 | 1 | | | |
| 12627.34 | 7917.158 | 1 | I | $8430^{\circ}_{1}$ $16347_{2}$ | 26 |
| 12628.31 | 7916.550 | 1 | I | $9135^{\circ}_{3}$ $17051_{3}$ | 7 |
| 12635.56 | 7912.008 | 3 | I | $11030^{\circ}_{6}$ $18942_{7}$ | 0 |
| | | | I | $11545^{\circ}_{4}$ $19457_{3}$ | 13 |
| 12640.14 | 7909.141 | 5 | II | $987^{\circ}_{4\,1/2}$ $8896_{5\,1/2}$ | 16 |
| 12641.56 | 7908.253 | 3 | I | $9200^{\circ}_{2}$ $17108_{2}$ | −6 |
| | | | I | $13089^{\circ}_{3}$ $20998_{4}$ | 35 |
| 12642.56 | 7907.627 | 3 | I | $8101^{\circ}_{2}$ $16008_{3}$ | −16 |
| 12644.15 | 7906.633 | 3 | II | $1410^{\circ}_{4\,1/2}$ $9316_{3\,1/2}$ | 31 |
| 12654.05 | 7900.447 | 2 | II | $7233^{\circ}_{5\,1/2}$ $15134_{4\,1/2}$ | 18 |
| 12658.77 | 7897.501 | 4 | I | $7780_{6}$ $15677^{\circ}_{7}$ | 39 |
| 12665.84 | 7893.093 | 1 | I | $12720^{\circ}_{4}$ $20613_{3}$ | 36 |
| 12667.03 | 7892.351 | 1 | I | $6856^{\circ}_{4}$ $14748_{4}$ | −34 |
| | | | I | $7348^{\circ}_{4}$ $15249_{4}$ | 31 |
| 12676.64 | 7886.368 | 4 | II | $6389^{\circ}_{4\,1/2}$ $14276_{5\,1/2}$ | 12 |
| 12685.32 | 7880.972 | 3 | I | $11061^{\circ}_{7}$ $18942_{7}$ | 45 |
| 12690.48 | 7877.767 | 3 | I | $8991^{\circ}_{5}$ $16869_{4}$ | −34 |
| 12696.00 | 7874.342 | 2 | I | $10318^{\circ}_{3}$ $18192_{3}$ | 14 |
| 12698.87 | 7872.563 | 1 | I | $7467^{\circ}_{5}$ $15339_{5}$ | 5 |
| 12710.79 | 7865.180 | 1 | I | $7696^{\circ}_{6}$ $15561^{\circ}_{5}$ | 44 |
| 12713.65 | 7863.411 | 1 | | | |
| 12715.61 | 7862.199 | 1 | I | $13924^{\circ}_{3}$ $21786_{2}$ | 4 |
| | | | II | $6389^{\circ}_{4\,1/2}$ $14252_{3\,1/2}$ | −31 |
| 12719.18 | 7859.992 | 2 | II | $4844^{\circ}_{1\,1/2}$ $12704_{1\,1/2}$ | 15 |
| 12724.78 | 7856.533 | 3 | I | $10901^{\circ}_{2}$ $18758_{3}$ | −8 |
| | | | I | $13297^{\circ}_{5}$ $21153_{5}$ | 42 |
| 12732.47 | 7851.788 | 4 | II | $1873^{\circ}_{3\,1/2}$ $9725_{3\,1/2}$ | −10 |
| 12734.09 | 7850.789 | 3 | | | |
| 12742.53 | 7845.589 | 2 | I | $13315^{\circ}_{4}$ $21161_{4}$ | −34 |
| | | | I | $13815^{\circ}_{4}$ $21661_{3}$ | 48 |
| 12743.18 | 7845.189 | 3 | I | $8991^{\circ}_{5}$ $16836_{6}$ | −6 |
| 12747.94 | 7842.259 | 2 | | | |
| 12766.60 | 7830.797 | 5 | II | $5437^{\circ}_{3\,1/2}$ $13268_{2\,1/2}$ | 6 |
| 12777.23 | 7824.282 | 2 | I | $8055^{\circ}_{6}$ $15879_{5}$ | 30 |
| | | | I | $8762^{\circ}_{4}$ $16586_{5}$ | −14 |
| 12779.42 | 7822.941 | 1 | I | $8400^{\circ}_{5}$ $16223_{5}$ | 28 |
| | | | I | $13139^{\circ}_{2}$ $20962_{2}$ | 1 |
| 12783.74 | 7820.298 | 1 | I | $11337^{\circ}_{3}$ $19158_{2}$ | 22 |
| 12792.73 | 7814.802 | 1 | I | $12297^{\circ}_{5}$ $20112_{4}$ | −21 |
| 12795.30 | 7813.232 | 2 | | | |
| 12795.58 | 7813.061 | 2 | | | |
| 12798.83 | 7811.077 | 6 | II | $5716^{\circ}_{3\,1/2}$ $13527_{4\,1/2}$ | 60 |
| 12804.76 | 7807.460 | 3 | I | $9135^{\circ}_{3}$ $16942_{4}$ | 33 |
| 12808.34 | 7805.278 | 1 | I | $13519^{\circ}_{5}$ $21324_{6}$ | 19 |
| 12809.52 | 7804.559 | 1 | I | $10901^{\circ}_{2}$ $18706_{2}$ | 28 |
| 12812.28 | 7802.878 | 1 | I | $5802^{\circ}_{7}$ $13605_{6}$ | −13 |
| | | | I | $13297^{\circ}_{5}$ $21100_{6}$ | 25 |
| 12817.11 | 7799.937 | 1 | I | $6809^{\circ}_{8}$ $14609_{7}$ | −22 |
| 12819.75 | 7798.331 | 2 | I | $12948^{\circ}_{5}$ $20747_{4}$ | −4 |
| 12826.91 | 7793.978 | 2 | | | |
| 12828.57 | 7792.969 | 2 | | | |
| 12831.12 | 7791.421 | 2 | I | $11271^{\circ}_{4}$ $19062_{5}$ | 11 |
| 12838.03 | 7787.227 | 3 | I | $9333^{\circ}_{6}$ $17120_{5}$ | 47 |
| 12839.18 | 7786.529 | 3 | II | $987^{\circ}_{4\,1/2}$ $8774_{4\,1/2}$ | 74 |
| 12844.01 | 7783.601 | 3 | II | $4165^{\circ}_{4\,1/2}$ $11949^{\circ}_{3\,1/2}$ | −42 |
| 12844.28 | 7783.438 | 3 | II | $7746^{\circ}_{2\,1/2}$ $15529_{2\,1/2}$ | 36 |
| 12847.23 | 7781.650 | 3 | | | |
| 12849.08 | 7780.530 | 2 | II | $5437^{\circ}_{3\,1/2}$ $13217_{3\,1/2}$ | −43 |
| 12850.83 | 7779.470 | 3 | II | $10924^{\circ}_{4\,1/2}$ $18704_{5\,1/2}$ | 31 |
| 12858.90 | 7774.588 | 1 | II | $4322^{\circ}_{2\,1/2}$ $12097_{3\,1/2}$ | 30 |
| 12878.06 | 7763.021 | 1 | I | $6238^{\circ}_{5}$ $14001^{\circ}_{6}$ | −4 |
| 12878.88 | 7762.527 | 1 | | | |
| 12884.75 | 7758.990 | 6 | II | $7522^{\circ}_{5\,1/2}$ $15281_{6\,1/2}$ | 4 |
| 12891.11 | 7755.163 | 1 | I | $10243^{\circ}_{4}$ $17998_{4}$ | −30 |
| 12894.01 | 7753.418 | 2 | I | $13622^{\circ}_{2}$ $21375_{2}$ | −35 |
| 12895.21 | 7752.697 | 3 | I | $13572^{\circ}_{7}$ $21324_{6}$ | −24 |
| 12897.02 | 7751.609 | 2 | | | |
| 12899.21 | 7750.293 | 1 | I | $10901^{\circ}_{2}$ $18652_{3}$ | 22 |
| 12900.16 | 7749.722 | 3 | II | $8402^{\circ}_{3\,1/2}$ $16152_{3\,1/2}$ | 0 |
| 12901.63 | 7748.839 | 2 | II | $6638^{\circ}_{4\,1/2}$ $14387_{4\,1/2}$ | −16 |
| 12903.49 | 7747.722 | 1 | I | $11796^{\circ}_{4}$ $19544_{4}$ | −15 |
| 12907.21 | 7745.489 | 1 | | | |
| 12911.38 | 7742.987 | 1 | I | $13572^{\circ}_{7}$ $21314_{7}$ | 6 |
| 12914.70 | 7740.997 | 1 | II | $8804^{\circ}_{4\,1/2}$ $16545_{5\,1/2}$ | −38 |

TABLE 1. *Observed infrared cerium lines*—Continued

| Wavelength Å | Wavenumber ($cm^{-1}$) | Intensity | Spectrum | Classification | O−C (.001 $cm^{-1}$) | Wavelength Å | Wavenumber ($cm^{-1}$) | Intensity | Spectrum | Classification | O−C (.001 $cm^{-1}$) |
|---|---|---|---|---|---|---|---|---|---|---|---|
| 12918.78 | 7738.552 | 2 | I | $8270^{\circ}_{3}$ $16008_{3}$ | −29 | 13172.72 | 7589.371 | 3 | I | $8055^{\circ}_{6}$ $15644_{6}$ | −45 |
| 12925.45 | 7734.559 | 2 | I | $9996^{\circ}_{3}$ $17731_{4}$ | −21 | 13181.32 | 7584.419 | 3 | II | $5942^{\circ}_{3\frac{1}{2}}$ $13527_{4\frac{1}{2}}$ | −13 |
| | | | II | $6517^{\circ}_{2\frac{1}{2}}$ $14252_{3\frac{1}{2}}$ | 4 | 13185.25 | 7582.159 | 1 | | | |
| 12926.18 | 7734.122 | 1 | I | $9135^{\circ}_{3}$ $16869_{4}$ | −31 | 13190.41 | 7579.193 | 1 | I | $7169^{\circ}_{3}$ $14748_{4}$ | 0 |
| 12928.12 | 7732.961 | 1 | II | $2581^{\circ}_{4\frac{1}{2}}$ $10314_{4\frac{1}{2}}$ | 52 | | | | I | $11578^{\circ}_{1}$ $19158_{2}$ | 9 |
| | | | II | $5942^{\circ}_{3\frac{1}{2}}$ $13675_{2\frac{1}{2}}$ | 39 | 13194.82 | 7576.659 | 3 | II | $4165^{\circ}_{4\frac{1}{2}}$ $11742^{\circ}_{5\frac{1}{2}}$ | −39 |
| 12932.24 | 7730.408 | 1 | II | $8402^{\circ}_{3\frac{1}{2}}$ $16133_{2\frac{1}{2}}$ | −57 | 13200.93 | 7573.153 | 1 | I | $8270^{\circ}_{3}$ $15843_{4}$ | −46 |
| 12937.73 | 7727.218 | 3 | | | | | | | I | $12022^{\circ}_{2}$ $19595_{2}$ | −7 |
| 12941.76 | 7724.811 | 1 | I | $14338^{\circ}_{5}$ $22063_{4}$ | −24 | 13203.25 | 7571.822 | 1 | | | |
| 12944.16 | 7723.379 | 1 | I | $14001^{\circ}_{6}$ $21725_{5}$ | −8 | 13210.42 | 7567.712 | 1 | | | |
| 12944.95 | 7722.908 | 1 | | | | 13212.73 | 7566.389 | 4 | II | $7059^{\circ}_{4\frac{1}{2}}$ $14625_{5\frac{1}{2}}$ | −39 |
| 12946.05 | 7722.251 | 2 | II | $0^{\circ}_{3\frac{1}{2}}$ $7722_{2\frac{1}{2}}$ | −33 | 13219.82 | 7562.331 | 2 | II | $5964^{\circ}_{3\frac{1}{2}}$ $13527_{4\frac{1}{2}}$ | −6 |
| 12950.90 | 7719.360 | 6 | I | $7841^{\circ}_{5}$ $15561_{5}$ | −30 | 13233.02 | 7554.788 | 1 | | | |
| | | | II | $4737^{\circ}_{2\frac{1}{2}}$ $12456_{3\frac{1}{2}}$ | −17 | 13237.13 | 7552.442 | 1 | | | |
| 12956.49 | 7716.029 | 3 | I | $1663^{\circ}_{3}$ $9379_{4}$ | 1 | 13238.01 | 7551.940 | 1 | I | $5572^{\circ}_{4}$ $13124_{5}$ | 4 |
| 12958.12 | 7715.059 | 1 | I | $11357^{\circ}_{5}$ $19072_{6}$ | −7 | | | | II | $5716^{\circ}_{3\frac{1}{2}}$ $13268_{2\frac{1}{2}}$ | −49 |
| 12959.19 | 7714.422 | 1 | I | $8509^{\circ}_{4}$ $16223_{5}$ | −11 | 13249.50 | 7545.391 | 1 | I | $12793^{\circ}_{5}$ $20338_{5}$ | 2 |
| 12963.06 | 7712.118 | 2 | I | $11650^{\circ}_{2}$ $19362_{1}$ | −4 | 13251.36 | 7544.332 | 3 | I | $8400^{\circ}_{5}$ $15945_{4}$ | −48 |
| | | | II | $6913^{\circ}_{6\frac{1}{2}}$ $14625_{5\frac{1}{2}}$ | 8 | 13253.37 | 7543.188 | 5 | I | $1663^{\circ}_{3}$ $9206_{3}$ | 3 |
| 12964.30 | 7711.381 | 2 | I | $7933^{\circ}_{5}$ $15644_{6}$ | −3 | 13255.21 | 7542.141 | 4 | I | $10243^{\circ}_{4}$ $17785_{3}$ | −15 |
| 12966.50 | 7710.072 | 1 | I | $8307^{\circ}_{3}$ $16017_{3}$ | 23 | 13257.13 | 7541.048 | 2 | II | $8280^{\circ}_{2\frac{1}{2}}$ $15822_{3\frac{1}{2}}$ | −69 |
| | | | II | $12260^{\circ}_{3\frac{1}{2}}$ $19970_{2\frac{1}{2}}$ | −19 | 13258.94 | 7540.019 | 2 | I | $13519^{\circ}_{5}$ $21059_{5}$ | −23 |
| 12967.72 | 7709.347 | 1 | I | $8088^{\circ}_{2}$ $15798_{3}$ | 33 | | | | I | $14273^{\circ}_{3}$ $21813_{3}$ | −14 |
| 12968.46 | 7708.907 | 1 | | | | 13261.14 | 7538.768 | 2 | I | $14186^{\circ}_{6}$ $21725_{5}$ | −12 |
| 12969.82 | 7708.099 | 2 | I | $9709^{\circ}_{2}$ $17417_{2}$ | −38 | 13266.63 | 7535.648 | 1 | II | $10035^{\circ}_{5\frac{1}{2}}$ $17571_{4\frac{1}{2}}$ | −41 |
| | | | II | $5819^{\circ}_{4\frac{1}{2}}$ $13527_{4\frac{1}{2}}$ | −19 | 13269.52 | 7534.007 | 2 | II | $11949^{\circ}_{3\frac{1}{2}}$ $19483_{2\frac{1}{2}}$ | −22 |
| 12970.46 | 7707.718 | 4 | II | $6389^{\circ}_{4\frac{1}{2}}$ $14097_{3\frac{1}{2}}$ | −45 | 13272.86 | 7532.111 | 3 | I | $11874^{\circ}_{3}$ $19406_{3}$ | −29 |
| 12981.05 | 7701.430 | 3 | II | $10274^{\circ}_{3\frac{1}{2}}$ $17976_{2\frac{1}{2}}$ | −10 | | | | II | $6517^{\circ}_{2\frac{1}{2}}$ $14049_{1\frac{1}{2}}$ | −24 |
| 12982.06 | 7700.831 | 2 | I | $13297^{\circ}_{5}$ $20998_{4}$ | 27 | 13276.12 | 7530.262 | 1 | | | |
| 12983.38 | 7700.048 | 3 | I | $7696^{\circ}_{6}$ $15396_{6}$ | −27 | 13277.22 | 7529.638 | 2 | | | |
| 12995.93 | 7692.613 | 2 | | | | 13279.47 | 7528.362 | 2 | II | $6521^{\circ}_{1\frac{1}{2}}$ $14049_{1\frac{1}{2}}$ | −58 |
| 12997.24 | 7691.837 | 1 | I | $10673^{\circ}_{6}$ $18365_{5}$ | −40 | 13280.06 | 7528.028 | 3 | I | $13572^{\circ}_{7}$ $21100_{6}$ | −22 |
| 12998.87 | 7690.873 | 2 | | | | 13284.79 | 7525.347 | 3 | I | $7715^{\circ}_{5}$ $15240_{4}$ | −35 |
| 13005.13 | 7687.171 | 1 | I | $10318^{\circ}_{3}$ $18005_{3}$ | −42 | 13300.80 | 7516.289 | 6 | II | $3793^{\circ}_{6\frac{1}{2}}$ $11309_{7\frac{1}{2}}$ | −53 |
| 13007.35 | 7685.859 | 2 | I | $8902^{\circ}_{3}$ $16588_{4}$ | −36 | 13306.46 | 7513.092 | 1 | I | $9830^{\circ}_{6}$ $17343_{5}$ | −33 |
| | | | I | $13044^{\circ}_{4}$ $20730_{5}$ | 18 | 13307.49 | 7512.511 | 1 | I | $12600^{\circ}_{3}$ $20112_{4}$ | −6 |
| 13011.48 | 7683.419 | 1 | I | $9425^{\circ}_{2}$ $17108_{2}$ | −18 | | | | I | $13450^{\circ}_{3}$ $20962_{2}$ | 47 |
| 13016.48 | 7680.468 | 5 | II | $5437^{\circ}_{3\frac{1}{2}}$ $13117_{4\frac{1}{2}}$ | −33 | 13317.03 | 7507.129 | 3 | | | |
| 13022.21 | 7677.088 | 2 | I | $8088^{\circ}_{2}$ $15766_{3}$ | −47 | 13327.06 | 7501.479 | 2 | | | |
| 13025.99 | 7674.860 | 2 | I | $8270^{\circ}_{3}$ $15945_{4}$ | −1 | 13331.45 | 7499.009 | 2 | I | $8088^{\circ}_{2}$ $15587_{2}$ | −5 |
| 13029.22 | 7672.958 | 2 | I | $9200^{\circ}_{2}$ $16873_{1}$ | −34 | 13334.44 | 7497.327 | 1 | I | $11850^{\circ}_{5}$ $19347_{6}$ | 37 |
| | | | I | $12988^{\circ}_{4}$ $20661_{3}$ | −30 | 13338.67 | 7494.950 | 4 | II | $2563^{\circ}_{5\frac{1}{2}}$ $10058_{6\frac{1}{2}}$ | −59 |
| 13041.57 | 7665.692 | 3 | II | $7061^{\circ}_{6\frac{1}{2}}$ $14727_{1\frac{1}{2}}$ | −8 | 13349.89 | 7488.650 | 1 | | | |
| 13043.29 | 7664.681 | 3 | II | $3793^{\circ}_{6\frac{1}{2}}$ $11458_{5\frac{1}{2}}$ | −48 | 13350.76 | 7488.162 | 1 | I | $8270^{\circ}_{3}$ $15758_{2}$ | −46 |
| 13044.60 | 7663.911 | 1 | | | | 13353.94 | 7486.379 | 6 | II | $1410^{\circ}_{4\frac{1}{2}}$ $8896_{5\frac{1}{2}}$ | −55 |
| 13047.36 | 7662.290 | 1 | | | | 13354.99 | 7485.791 | 3 | I | $5904^{\circ}_{2}$ $13389_{3}$ | −29 |
| 13049.51 | 7661.028 | 3 | I | $11796^{\circ}_{4}$ $19457_{3}$ | 2 | 13360.88 | 7482.491 | 5 | | | |
| | | | II | $3793^{\circ}_{6\frac{1}{2}}$ $11454_{6\frac{1}{2}}$ | −36 | 13363.20 | 7481.192 | 1 | I | $7890^{\circ}_{4}$ $15371_{4}$ | −25 |
| 13051.72 | 7659.730 | 2 | I | $8307^{\circ}_{3}$ $15967_{2}$ | −47 | 13365.76 | 7479.759 | 2 | | | |
| 13057.41 | 7656.392 | 2 | I | $7715^{\circ}_{5}$ $15371_{4}$ | −18 | 13367.12 | 7478.998 | 3 | I | $8587^{\circ}_{7}$ $16066_{6}$ | 31 |
| | | | I | $13569^{\circ}_{4}$ $21226_{5}$ | −8 | 13371.37 | 7476.621 | 2 | | | |
| 13063.64 | 7652.741 | 1 | I | $8695^{\circ}_{1}$ $16347_{2}$ | −35 | 13374.70 | 7474.759 | 1 | I | $11357^{\circ}_{5}$ $18831_{5}$ | 13 |
| 13065.33 | 7651.751 | 1 | I | $10243^{\circ}_{4}$ $17895_{5}$ | −7 | 13379.85 | 7471.882 | 3 | II | $5964^{\circ}_{3\frac{1}{2}}$ $13436_{2\frac{1}{2}}$ | −60 |
| 13067.09 | 7650.721 | 1 | I | $8101^{\circ}_{2}$ $15751_{1}$ | −40 | 13387.79 | 7467.451 | 2 | I | $9200^{\circ}_{2}$ $16668_{3}$ | −31 |
| | | | I | $8400^{\circ}_{5}$ $16051_{4}$ | −26 | | | | I | $10318^{\circ}_{3}$ $17785_{3}$ | −47 |
| 13079.71 | 7643.339 | 3 | II | $1410^{\circ}_{4\frac{1}{2}}$ $9053_{3\frac{1}{2}}$ | 5 | | | | I | $14186^{\circ}_{6}$ $21654_{7}$ | −41 |
| 13080.77 | 7642.719 | 2 | I | $8366^{\circ}_{2}$ $16008_{3}$ | −13 | 13391.95 | 7465.131 | 1 | | | |
| 13088.87 | 7637.990 | 6 | II | $6638^{\circ}_{4\frac{1}{2}}$ $14276_{5\frac{1}{2}}$ | −51 | 13395.15 | 7463.348 | 2 | I | $13283^{\circ}_{3}$ $20747_{4}$ | 0 |
| 13101.27 | 7630.761 | 3 | | | | 13396.44 | 7462.629 | 1 | | | |
| 13109.40 | 7626.028 | 1 | | | | 13402.31 | 7459.360 | 2 | | | |
| 13116.23 | 7622.057 | 3 | II | $7341^{\circ}_{5\frac{1}{2}}$ $14963^{\circ}_{5\frac{1}{2}}$ | −48 | 13403.53 | 7458.681 | 2 | | | |
| 13118.74 | 7620.599 | 3 | I | $10673^{\circ}_{6}$ $18294_{6}$ | −4 | 13406.52 | 7457.018 | 1 | I | $11301^{\circ}_{2}$ $18758_{3}$ | 42 |
| 13123.66 | 7617.742 | 1 | II | $8927^{\circ}_{5\frac{1}{2}}$ $16545_{5\frac{1}{2}}$ | −16 | | | | I | $13450^{\circ}_{3}$ $20907_{4}$ | 46 |
| 13125.83 | 7616.483 | 1 | | | | | | | II | $3363^{\circ}_{2\frac{1}{2}}$ $10820_{2\frac{1}{2}}$ | −36 |

TABLE 1. *Observed infrared cerium lines*—Continued

| Wavelength Å | Wavenumber ($cm^{-1}$) | Intensity | Spectrum | Classification | O−C (.001 $cm^{-1}$) |
|---|---|---|---|---|---|
| 13421.80 | 7448.528 | 2 | | | |
| 13424.66 | 7446.942 | 1 | I | $7348^{\circ}_{4}$ $14795_{5}$ | −48 |
| 13426.72 | 7445.799 | 1 | | | |
| 13431.91 | 7442.922 | 2 | II | $1873^{\circ}_{3\frac{1}{2}}$ $9316_{3\frac{1}{2}}$ | −43 |
| 13433.43 | 7442.080 | 2 | | | |
| 13436.05 | 7440.629 | 1 | I | $9462^{\circ}_{5}$ $16903_{5}$ | −45 |
| 13437.64 | 7439.748 | 1 | | | |
| 13440.28 | 7438.287 | 1 | | | |
| 13447.22 | 7434.448 | 6 | II | $2879^{\circ}_{5\frac{1}{2}}$ $10314_{4\frac{1}{2}}$ | −34 |
| 13454.06 | 7430.669 | 3 | | | |
| 13457.34 | 7428.857 | 2 | I | $14027^{\circ}_{4}$ $21456_{5}$ | 47 |
| 13460.54 | 7427.091 | 1 | I | $13194^{\circ}_{4}$ $20621^{\circ}_{4}$ | 14 |
| 13462.45 | 7426.038 | 2 | II | $12057^{\circ}_{2\frac{1}{2}}$ $19483_{2\frac{1}{2}}$ | −63 |
| 13464.57 | 7424.868 | 1 | | | |
| 13468.67 | 7422.608 | 3 | | | |
| 13470.54 | 7421.578 | 3 | II | $5283^{\circ}_{0\frac{1}{2}}$ $12704_{1\frac{1}{2}}$ | −16 |
| 13471.84 | 7420.862 | 2 | | | |
| 13474.49 | 7419.402 | 3 | II | $8402^{\circ}_{3\frac{1}{2}}$ $15822_{3\frac{1}{2}}$ | 6 |
| 13478.22 | 7417.349 | 1 | I | $14531^{\circ}_{4}$ $21948_{3}$ | 4 |
| 13487.22 | 7412.399 | 1 | I | $13219^{\circ}_{6}$ $20631_{5}$ | −15 |
| 13488.11 | 7411.910 | 1 | I | $10901^{\circ}_{2}$ $18313_{3}$ | 20 |
| 13499.02 | 7405.920 | 1 | I | $6475^{\circ}_{4}$ $13881_{5}$ | 16 |
| 13506.77 | 7401.670 | 4 | II | $5716^{\circ}_{3\frac{1}{2}}$ $13117_{4\frac{1}{2}}$ | −30 |
| 13508.61 | 7400.662 | 2 | I | $7348^{\circ}_{4}$ $14748_{4}$ | 16 |
| | | | II | $8175^{\circ}_{2\frac{1}{2}}$ $15576_{1\frac{1}{2}}$ | −34 |
| 13509.89 | 7399.961 | 1 | I | $8366^{\circ}_{2}$ $15766_{3}$ | 11 |
| | | | I | $9709^{\circ}_{2}$ $17108_{2}$ | 6 |
| 13512.16 | 7398.718 | 1 | | | |
| 13515.15 | 7397.081 | 1 | I | $12948^{\circ}_{5}$ $20346_{6}$ | −38 |
| 13518.30 | 7395.357 | 1 | | | |
| 13524.73 | 7391.842 | 1 | II | $7233^{\circ}_{5\frac{1}{2}}$ $14625_{5\frac{1}{2}}$ | −35 |
| 13547.66 | 7379.331 | 1 | | | |
| 13553.08 | 7376.379 | 1 | II | $5651^{\circ}_{5\frac{1}{2}}$ $13027_{6\frac{1}{2}}$ | −17 |
| 13565.86 | 7369.430 | 1 | I | $7169^{\circ}_{3}$ $14539_{3}$ | −30 |
| 13569.93 | 7367.220 | 1 | I | $10774^{\circ}_{3}$ $18141_{4}$ | −22 |
| 13572.01 | 7366.091 | 1 | | | |
| 13583.48 | 7359.871 | 1 | II | $4737^{\circ}_{2\frac{1}{2}}$ $12097_{3\frac{1}{2}}$ | −23 |
| | | | II | $8169^{\circ}_{1\frac{1}{2}}$ $15529_{2\frac{1}{2}}$ | −21 |
| 13585.01 | 7359.042 | 1 | I | $9787^{\circ}_{3}$ $17146_{3}$ | −45 |
| 13594.93 | 7353.672 | 2 | II | $8175^{\circ}_{2\frac{1}{2}}$ $15529_{2\frac{1}{2}}$ | −48 |
| 13618.96 | 7340.697 | 2 | | | |
| 13622.17 | 7338.967 | 1 | I | $12297^{\circ}_{2}$ $19636_{3}$ | −39 |
| 13624.15 | 7337.901 | 3 | II | $5118^{\circ}_{2\frac{1}{2}}$ $12456_{3\frac{1}{2}}$ | −43 |
| 13628.09 | 7335.779 | 1 | I | $11357^{\circ}_{5}$ $18692_{4}$ | 22 |
| 13636.08 | 7331.481 | 1 | | | |
| 13636.70 | 7331.148 | 1 | | | |
| 13637.70 | 7330.610 | 2 | I | $13301^{\circ}_{6}$ $20631_{5}$ | −46 |
| 13655.49 | 7321.060 | 1 | I | $8430^{\circ}_{1}$ $15751_{1}$ | −42 |
| 13662.60 | 7317.250 | 3 | I | $5674^{\circ}_{1}$ $12992_{2}$ | −35 |
| 13672.47 | 7311.968 | 2 | II | $3703^{\circ}_{3\frac{1}{2}}$ $11015_{3\frac{1}{2}}$ | −21 |
| 13697.01 | 7298.868 | 2 | I | $12022^{\circ}_{2}$ $19321_{2}$ | 48 |
| | | | II | $5819^{\circ}_{4\frac{1}{2}}$ $13117_{4\frac{1}{2}}$ | 65 |
| 13712.83 | 7290.447 | 4 | II | $987^{\circ}_{4\frac{1}{2}}$ $8278_{5\frac{1}{2}}$ | −12 |
| 13781.01 | 7254.379 | 4 | II | $4203^{\circ}_{6\frac{1}{2}}$ $11458_{5\frac{1}{2}}$ | −44 |
| 13808.91 | 7239.722 | 2 | II | $8278_{5\frac{1}{2}}$ $15517^{\circ}_{6\frac{1}{2}}$ | 23 |
| 13812.10 | 7238.050 | 2 | II | $5513_{5\frac{1}{2}}$ $12751^{\circ}_{5\frac{1}{2}}$ | −45 |
| 13814.83 | 7236.619 | 1 | I | $13924^{\circ}_{3}$ $21161_{4}$ | −3 |
| 13852.00 | 7217.201 | 2 | II | $7059^{\circ}_{4\frac{1}{2}}$ $14276_{5\frac{1}{2}}$ | −24 |
| 13870.09 | 7207.788 | 1 | I | $6856^{\circ}_{4}$ $14064_{4}$ | −34 |
| 13924.35 | 7179.701 | 2 | II | $1873^{\circ}_{3\frac{1}{2}}$ $9053_{3\frac{1}{2}}$ | 3 |
| 13926.58 | 7178.551 | 3 | I | $8902^{\circ}_{3}$ $16080_{2}$ | −24 |
| | | | II | $2879^{\circ}_{5\frac{1}{2}}$ $10058_{6\frac{1}{2}}$ | −4 |
| 13966.43 | 7158.069 | 1 | II | $6517^{\circ}_{2\frac{1}{2}}$ $13675_{2\frac{1}{2}}$ | −35 |
| 13975.51 | 7153.418 | 4 | II | $7233^{\circ}_{5\frac{1}{2}}$ $14387_{4\frac{1}{2}}$ | −70 |
| 13984.32 | 7148.912 | 1 | II | $5969^{\circ}_{5\frac{1}{2}}$ $13117_{4\frac{1}{2}}$ | −3 |
| 13994.84 | 7143.538 | 4 | I | $12366^{\circ}_{5}$ $19510^{\circ}_{4}$ | 40 |
| | | | II | $987^{\circ}_{4\frac{1}{2}}$ $8131_{4\frac{1}{2}}$ | −59 |
| 14001.70 | 7140.038 | 1 | I | $11271^{\circ}_{4}$ $18411_{4}$ | −43 |
| 14007.17 | 7137.249 | 2 | II | $6389^{\circ}_{4\frac{1}{2}}$ $13527_{4\frac{1}{2}}$ | −41 |
| 14011.45 | 7135.069 | 2 | II | $5616_{4\frac{1}{2}}$ $12751^{\circ}_{5\frac{1}{2}}$ | 4 |
| 14018.78 | 7131.339 | 1 | | | |
| 14027.57 | 7126.870 | 2 | II | $8402^{\circ}_{3\frac{1}{2}}$ $15529_{2\frac{1}{2}}$ | −50 |
| 14029.72 | 7125.778 | 1 | I | $14273^{\circ}_{3}$ $21399_{3}$ | −22 |
| | | | II | $6549^{\circ}_{2\frac{1}{2}}$ $13675_{2\frac{1}{2}}$ | −37 |
| 14067.76 | 7106.509 | 2 | I | $8902^{\circ}_{3}$ $16008_{3}$ | −15 |
| 14068.35 | 7106.211 | 4 | | | |
| 14074.99 | 7102.859 | 3 | II | $7522^{\circ}_{5\frac{1}{2}}$ $14625_{5\frac{1}{2}}$ | −22 |
| 14098.41 | 7091.060 | 1 | II | $2634^{\circ}_{2\frac{1}{2}}$ $9725_{3\frac{1}{2}}$ | −8 |
| 14098.77 | 7090.879 | 1 | | | |
| 14104.36 | 7088.068 | 2 | I | $5904^{\circ}_{2}$ $12992_{2}$ | −40 |
| 14117.52 | 7081.461 | 1 | II | $7746^{\circ}_{2\frac{1}{2}}$ $14827_{3\frac{1}{2}}$ | 21 |
| 14120.41 | 7080.012 | 3 | I | $7715^{\circ}_{5}$ $14795_{5}$ | −41 |
| | | | I | $12600^{\circ}_{3}$ $19680_{4}$ | 21 |
| 14134.73 | 7072.839 | 2 | | | |
| 14148.39 | 7066.010 | 1 | I | $11545^{\circ}_{4}$ $18611_{3}$ | 22 |
| 14151.74 | 7064.338 | 4 | I | $8307^{\circ}_{3}$ $15371_{4}$ | 0 |
| 14166.58 | 7056.937 | 4 | I | $8587^{\circ}_{7}$ $15644_{6}$ | −32 |
| 14176.18 | 7052.159 | 5 | I | $8509^{\circ}_{4}$ $15561_{5}$ | 22 |
| | | | II | $3593^{\circ}_{4\frac{1}{2}}$ $10646_{5\frac{1}{2}}$ | −39 |
| 14195.30 | 7042.660 | 2 | I | $14116^{\circ}_{4}$ $21158_{3}$ | 44 |
| | | | II | $7233^{\circ}_{5\frac{1}{2}}$ $14276_{5\frac{1}{2}}$ | −14 |
| 14197.32 | 7041.658 | 2 | I | $13297^{\circ}_{5}$ $20338_{5}$ | −22 |
| | | | I | $15021^{\circ}_{7}$ $22063_{7}$ | −46 |
| 14197.80 | 7041.420 | 2 | I | $8603^{\circ}_{6}$ $15644_{6}$ | 8 |
| 14204.09 | 7038.302 | 2 | I | $6475^{\circ}_{4}$ $13513_{4}$ | −32 |
| 14257.86 | 7011.758 | 7 | II | $0^{\circ}_{3\frac{1}{2}}$ $7011_{4\frac{1}{2}}$ | −56 |
| 14272.21 | 7004.708 | 1 | I | $11545^{\circ}_{4}$ $18550_{4}$ | 5 |
| 14280.14 | 7000.819 | 2 | I | $12988^{\circ}_{4}$ $19988_{3}$ | −26 |
| 14283.79 | 6999.030 | 3 | | | |
| 14288.51 | 6996.718 | 1 | | | |
| 14296.00 | 6993.052 | 1 | II | $7259^{\circ}_{3\frac{1}{2}}$ $14252_{3\frac{1}{2}}$ | −50 |
| 14318.10 | 6982.258 | 1 | | | |
| 14321.95 | 6980.381 | 1 | | | |
| 14327.00 | 6977.921 | 1 | | | |
| 14342.54 | 6970.360 | 2 | I | $8270^{\circ}_{3}$ $15240_{4}$ | −9 |
| 14377.07 | 6953.619 | 1 | I | $8991^{\circ}_{5}$ $15945_{4}$ | −40 |
| 14380.65 | 6951.888 | 1 | | | |
| 14386.11 | 6949.250 | 2 | I | $12992_{2}$ $19941^{\circ}_{2}$ | −16 |
| | | | II | $7878^{\circ}_{3\frac{1}{2}}$ $14827_{3\frac{1}{2}}$ | −49 |
| 14407.65 | 6938.860 | 1 | I | $8762^{\circ}_{4}$ $15700_{4}$ | 8 |
| 14410.93 | 6937.281 | 1 | I | $11301^{\circ}_{2}$ $18238_{2}$ | −2 |
| | | | I | $12297^{\circ}_{5}$ $19235_{6}$ | −35 |
| 14411.56 | 6936.978 | 1 | | | |
| 14415.09 | 6935.279 | 2 | II | $4523^{\circ}_{4\frac{1}{2}}$ $11458_{5\frac{1}{2}}$ | −50 |
| 14416.48 | 6934.610 | 3 | II | $2382^{\circ}_{4\frac{1}{2}}$ $9316_{3\frac{1}{2}}$ | −49 |
| 14422.28 | 6931.822 | 1 | II | $8927^{\circ}_{5\frac{1}{2}}$ $15859_{4\frac{1}{2}}$ | −32 |
| 14424.36 | 6930.822 | 2 | | | |
| 14429.32 | 6928.440 | 2 | | | |
| 14438.30 | 6924.130 | 1 | | | |
| 14444.56 | 6921.130 | 2 | I | $12425^{\circ}_{4}$ $19347_{5}$ | −35 |
| 14454.42 | 6916.408 | 2 | I | $9135^{\circ}_{3}$ $16051_{4}$ | 29 |
| | | | I | $9333^{\circ}_{6}$ $16249_{6}$ | 29 |
| 14462.80 | 6912.401 | 1 | II | $7713^{\circ}_{4\frac{1}{2}}$ $14625_{5\frac{1}{2}}$ | −13 |
| 14469.08 | 6909.401 | 1 | I | $11626^{\circ}_{1}$ $18535_{1}$ | 19 |
| | | | II | $7818^{\circ}_{1\frac{1}{2}}$ $14727_{1\frac{1}{2}}$ | 10 |
| 14474.09 | 6907.009 | 1 | I | $7841^{\circ}_{5}$ $14748_{4}$ | 19 |
| 14485.33 | 6901.650 | 1 | I | $7841^{\circ}_{5}$ $14743_{6}$ | −20 |
| 14488.50 | 6900.140 | 2 | II | $1873^{\circ}_{3\frac{1}{2}}$ $8774_{4\frac{1}{2}}$ | 11 |



459-033 OL - 72 - 8

TABLE 1. *Observed infrared cerium lines*—Continued

| Wavelength Å | Wavenumber ($cm^{-1}$) | Intensity | Spectrum | Classification | O−C (.001 $cm^{-1}$) |
|---|---|---|---|---|---|
| 14512.08 | 6888.928 | 1 | II | $6638^{*}_{4\frac{1}{2}}$ $13527_{4\frac{1}{2}}$ | −48 |
| 14546.60 | 6872.580 | 1 | I | $9996^{*}_{3}$ $16869_{4}$ | −25 |
| 14556.94 | 6867.698 | 6 | II | $1410_{4\frac{1}{2}}$ $8278^{*}_{5\frac{1}{2}}$ | −71 |
| 14575.70 | 6858.859 | 1 | I | $12707^{*}_{2}$ $19566_{1}$ | −25 |
| | | | I | $13315^{*}_{4}$ $20174_{4}$ | −29 |
| 14589.40 | 6852.418 | 2 | II | $3793_{6\frac{1}{2}}$ $10646_{5\frac{1}{2}}$ | −23 |
| 14633.11 | 6831.950 | 1 | I | $9135^{*}_{3}$ $15967^{*}_{2}$ | −37 |
| | | | II | $8131_{4\frac{1}{2}}$ $14963^{*}_{5\frac{1}{2}}$ | 45 |
| 14641.62 | 6827.979 | 3 | II | $6389_{4\frac{1}{2}}$ $13217_{3\frac{1}{2}}$ | −67 |
| 14642.78 | 6827.438 | 2 | I | $2378^{*}_{2}$ $9206^{*}_{3}$ | −39 |
| 14650.35 | 6823.910 | 1 | | | |
| 14651.70 | 6823.281 | 1 | I | $11796^{*}_{4}$ $18619^{*}_{5}$ | −36 |
| 14654.65 | 6821.908 | 1 | I | $12960_{6}$ $19782^{*}_{5}$ | −26 |
| 14654.65 | 6821.908 | 1 | II | $9723_{4\frac{1}{2}}$ $16545_{5\frac{1}{2}}$ | −19 |
| 14661.44 | 6818.749 | 1 | I | $11874^{*}_{3}$ $18692^{*}_{4}$ | −27 |
| 14668.75 | 6815.351 | 1 | I | $7933^{*}_{5}$ $14748^{*}_{4}$ | −35 |
| | | | I | $13297^{*}_{5}$ $20112^{*}_{4}$ | −41 |
| 14679.91 | 6810.169 | 1 | | | |
| 14680.43 | 6809.928 | 2 | I | $15255^{*}_{5}$ $22064_{6}$ | 2 |
| 14711.30 | 6795.638 | 1 | | | |
| 14717.88 | 6792.600 | 1 | | | |
| 14727.88 | 6787.988 | 1 | I | $7348^{*}_{4}$ $14136^{*}_{3}$ | −34 |
| 14730.24 | 6786.901 | 2 | I | $9462^{*}_{5}$ $16249_{6}$ | 5 |
| 14740.65 | 6782.108 | 2 | I | $7853^{*}_{1}$ $14635^{*}_{1}$ | −15 |
| 14770.00 | 6768.631 | 2 | I | $2437^{*}_{4}$ $9206^{*}_{3}$ | −44 |
| | | | I | $8509^{*}_{4}$ $15277^{*}_{3}$ | −11 |
| 14784.22 | 6762.120 | 1 | | | |
| 14790.45 | 6759.272 | 2 | II | $4165_{4\frac{1}{2}}$ $10924^{*}_{4\frac{1}{2}}$ | −51 |
| 14796.56 | 6756.481 | 1 | | | |
| 14812.85 | 6749.051 | 3 | II | $5616_{4\frac{1}{2}}$ $12365^{*}_{4\frac{1}{2}}$ | −16 |
| 14831.64 | 6740.500 | 2 | I | $13881^{*}_{5}$ $20621^{*}_{4}$ | 18 |
| | | | II | $5716_{3\frac{1}{2}}$ $12456_{3\frac{1}{2}}$ | −33 |
| 14843.05 | 6735.319 | 1 | I | $15077^{*}_{4}$ $21813^{*}_{3}$ | 48 |
| | | | II | $6521^{*}_{1\frac{1}{2}}$ $13256_{1\frac{1}{2}}$ | −43 |
| 14845.23 | 6734.330 | 2 | I | $9333^{*}_{6}$ $16067^{*}_{7}$ | −34 |
| 14865.87 | 6724.980 | 1 | II | $10274_{3\frac{1}{2}}$ $17000_{3\frac{1}{2}}$ | −68 |
| | | | II | $15565_{2\frac{1}{2}}$ $22290_{1\frac{1}{2}}$ | 73 |
| 14874.98 | 6720.861 | 5 | II | $1410_{4\frac{1}{2}}$ $8131_{4\frac{1}{2}}$ | −46 |
| 14900.17 | 6709.499 | 1 | I | $8991^{*}_{5}$ $15700^{*}_{4}$ | −27 |
| | | | I | $13629^{*}_{5}$ $20338^{*}_{5}$ | −35 |
| 14932.64 | 6694.910 | 3 | | | |
| 14944.45 | 6689.619 | 4 | | | |
| 14960.93 | 6682.250 | 1 | II | $2634^{*}_{2\frac{1}{2}}$ $9316_{3\frac{1}{2}}$ | 14 |
| 14979.45 | 6673.988 | 1 | II | $7713_{4\frac{1}{2}}$ $14387^{*}_{4\frac{1}{2}}$ | −37 |
| 14988.63 | 6669.901 | 1 | I | $10673_{6}$ $17343^{*}_{5}$ | 14 |
| 14991.80 | 6668.491 | 1 | I | $13194_{4}$ $19863^{*}_{5}$ | 32 |
| 14993.42 | 6667.770 | 1 | I | $11337^{*}_{3}$ $18005^{*}_{3}$ | −22 |
| 15013.44 | 6658.879 | 2 | I | $13124^{*}_{5}$ $19782^{*}_{5}$ | 4 |
| | | | I | $14417^{*}_{4}$ $21076^{*}_{4}$ | 14 |
| 15020.02 | 6655.962 | 1 | I | $14186_{6}$ $20842_{6}$ | 25 |
| 15039.21 | 6647.469 | 2 | II | $7011_{4\frac{1}{2}}$ $13659^{*}_{4\frac{1}{2}}$ | −49 |
| 15051.73 | 6641.939 | 1 | I | $11357^{*}_{5}$ $17998^{*}_{4}$ | 1 |
| | | | I | $14417^{*}_{4}$ $21059^{*}_{5}$ | 31 |
| 15073.15 | 6632.501 | 1 | I | $14609_{7}$ $21241^{*}_{7}$ | −20 |
| 15166.54 | 6591.660 | 1 | I | $12351^{*}_{4}$ $18943^{*}_{5}$ | −32 |
| 15176.23 | 6587.451 | 2 | I | $11061^{*}_{7}$ $17649_{6}$ | −33 |
| 15182.27 | 6584.831 | 1 | I | $11301^{*}_{2}$ $17886^{*}_{2}$ | −10 |
| 15194.85 | 6579.379 | 1 | | | |
| 15199.08 | 6577.548 | 3 | I | $8762^{*}_{4}$ $15339^{*}_{5}$ | −43 |
| 15202.15 | 6576.220 | 1 | I | $12720^{*}_{4}$ $19296^{*}_{4}$ | −17 |
| 15204.69 | 6575.121 | 1 | I | $4762^{*}_{4}$ $11337^{*}_{3}$ | −19 |
| 15205.69 | 6574.689 | 3 | II | $1873^{*}_{3\frac{1}{2}}$ $8448_{2\frac{1}{2}}$ | −14 |
| 15210.94 | 6572.419 | 2 | | | |
| 15217.84 | 6569.439 | 4 | I | $12960_{6}$ $19530^{*}_{5}$ | 10 |
| 15219.18 | 6568.861 | 2 | | | |
| 15220.78 | 6568.171 | 1 | | | |
| 15226.11 | 6565.871 | 1 | I | $9135^{*}_{3}$ $15700^{*}_{4}$ | −7 |
| 15228.57 | 6564.811 | 1 | I | $15382^{*}_{6}$ $21946^{*}_{5}$ | −9 |
| 15230.66 | 6563.910 | 1 | II | $8175^{*}_{2\frac{1}{2}}$ $14739_{2\frac{1}{2}}$ | 12 |
| 15233.45 | 6562.708 | 1 | I | $12114^{*}_{4}$ $18676^{*}_{4}$ | −2 |
| 15253.46 | 6554.098 | 2 | II | $4266^{*}_{3\frac{1}{2}}$ $10820_{2\frac{1}{2}}$ | 12 |
| 15254.67 | 6553.579 | 1 | I | $8055^{*}_{6}$ $14609^{*}_{7}$ | 17 |
| | | | I | $11874^{*}_{3}$ $18427^{*}_{3}$ | −16 |
| | | | I | $12793^{*}_{5}$ $19347^{*}_{5}$ | 19 |
| 15259.42 | 6551.539 | 1 | I | $13389^{*}_{3}$ $19941^{*}_{2}$ | −15 |
| 15269.49 | 6547.218 | 2 | | | |
| 15271.52 | 6546.348 | 2 | I | $8088^{*}_{2}$ $14635^{*}_{1}$ | 17 |
| 15277.65 | 6543.721 | 5 | I | $13519^{*}_{5}$ $20063_{6}$ | 18 |
| | | | II | $4910_{5\frac{1}{2}}$ $11454_{6\frac{1}{2}}$ | −16 |
| 15280.76 | 6542.389 | 2 | I | $11650^{*}_{2}$ $18192^{*}_{3}$ | −9 |
| 15283.02 | 6541.422 | 2 | I | $10604^{*}_{3}$ $17146^{*}_{3}$ | 3 |
| 15328.91 | 6521.839 | 2 | | | |
| 15337.96 | 6517.991 | 2 | I | $15063^{*}_{5}$ $21581^{*}_{5}$ | −24 |
| 15340.03 | 6517.111 | 2 | I | $12425^{*}_{4}$ $18943^{*}_{5}$ | −3 |
| 15346.27 | 6514.461 | 3 | II | $2382^{*}_{4\frac{1}{2}}$ $8896_{5\frac{1}{2}}$ | −31 |
| 15357.94 | 6509.511 | 3 | II | $10035^{*}_{5\frac{1}{2}}$ $16545_{5\frac{1}{2}}$ | −44 |
| 15385.72 | 6497.758 | 2 | II | $4322^{*}_{2\frac{1}{2}}$ $10820_{2\frac{1}{2}}$ | −10 |
| 15395.33 | 6493.702 | 2 | | | |
| 15402.81 | 6490.548 | 1 | I | $13301^{*}_{6}$ $19791^{*}_{5}$ | −44 |
| 15409.83 | 6487.591 | 1 | | | |
| 15429.50 | 6479.321 | 4 | | | |
| 15431.15 | 6478.628 | 2 | | | |
| 15435.22 | 6476.920 | 2 | | | |
| 15437.17 | 6476.102 | 2 | | | |
| 15444.26 | 6473.129 | 3 | II | $7202^{*}_{2\frac{1}{2}}$ $13675_{2\frac{1}{2}}$ | −66 |
| 15460.59 | 6466.291 | 1 | II | $13515^{*}_{3\frac{1}{2}}$ $19982_{4\frac{1}{2}}$ | −52 |
| 15477.01 | 6459.431 | 2 | II | $11015_{3\frac{1}{2}}$ $17475_{4\frac{1}{2}}$ | −29 |
| 15498.92 | 6450.300 | 1 | I | $8088^{*}_{2}$ $14539^{*}_{3}$ | 0 |
| 15507.86 | 6446.581 | 1 | I | $10673^{*}_{6}$ $17120^{*}_{5}$ | 26 |
| | | | II | $8280^{*}_{2\frac{1}{2}}$ $14727_{1\frac{1}{2}}$ | −13 |
| 15508.90 | 6446.149 | 2 | | | |
| 15518.60 | 6442.120 | 1 | II | $4203^{*}_{6\frac{1}{2}}$ $10646_{5\frac{1}{2}}$ | −15 |
| 15519.71 | 6441.659 | 2 | I | $8307^{*}_{3}$ $14748^{*}_{4}$ | 23 |
| | | | I | $13219^{*}_{6}$ $19661^{*}_{5}$ | −27 |
| 15528.77 | 6437.901 | 2 | I | $7780^{*}_{6}$ $14218^{*}_{6}$ | 20 |
| 15531.18 | 6436.902 | 2 | I | $9947^{*}_{2}$ $16384^{*}_{3}$ | −16 |
| | | | II | $4266^{*}_{3\frac{1}{2}}$ $10703_{4\frac{1}{2}}$ | −10 |
| 15533.79 | 6435.820 | 2 | I | $7348^{*}_{4}$ $13784^{*}_{5}$ | −31 |
| 15548.60 | 6429.690 | 2 | I | $13194_{4}$ $19624^{*}_{3}$ | −8 |
| | | | I | $13451^{*}_{1}$ $19880^{*}_{2}$ | 0 |
| 15563.05 | 6423.720 | 2 | | | |
| 15586.00 | 6414.262 | 2 | I | $7467^{*}_{5}$ $13881^{*}_{5}$ | −21 |
| 15588.46 | 6413.249 | 1 | I | $9787^{*}_{3}$ $16200^{*}_{3}$ | −23 |
| 15591.38 | 6412.048 | 2 | II | $2641^{*}_{3\frac{1}{2}}$ $9053_{3\frac{1}{2}}$ | −20 |
| 15596.22 | 6410.058 | 1 | I | $10879^{*}_{5}$ $17289^{*}_{6}$ | −26 |
| 15605.22 | 6406.362 | 2 | I | $7780^{*}_{6}$ $14186^{*}_{6}$ | −2 |
| | | | I | $13124^{*}_{5}$ $19530^{*}_{5}$ | −7 |
| 15608.98 | 6404.818 | 2 | I | $8991^{*}_{5}$ $15396_{6}$ | −16 |
| 15610.95 | 6404.010 | 1 | | | |
| 15640.75 | 6391.809 | 2 | II | $2382^{*}_{4\frac{1}{2}}$ $8774_{4\frac{1}{2}}$ | −13 |
| 15642.46 | 6391.110 | 5 | | | |
| 15654.17 | 6386.329 | 4 | I | $13124^{*}_{5}$ $19510^{*}_{4}$ | 7 |
| 15667.93 | 6380.721 | 1 | I | $9462^{*}_{5}$ $15843^{*}_{4}$ | −22 |
| | | | I | $13214^{*}_{1}$ $19595^{*}_{2}$ | 38 |
| 15674.81 | 6377.920 | 2 | | | |
| 15676.75 | 6377.131 | 2 | I | $13605_{6}$ $19982^{*}_{6}$ | −6 |

TABLE 1. *Observed infrared cerium lines*—Continued

| Wavelength Å | Wavenumber ($cm^{-1}$) | Intensity | Spectrum | Classification | O−C (.001 $cm^{-1}$) |
|---|---|---|---|---|---|
| 15679.01 | 6376.211 | 1 | I | $8270^{*}_{3}$ $14646_{2}$ | 15 |
| 15680.61 | 6375.561 | 1 | I | $8902^{*}_{3}$ $15277_{3}$ | 15 |
| | | | I | $14531^{*}_{4}$ $20907_{4}$ | —24 |
| 15684.82 | 6373.850 | 2 | I | $14218^{*}_{6}$ $20591_{6}$ | —3 |
| | | | II | $7878^{*}_{3\frac{1}{2}}$ $14252_{3\frac{1}{2}}$ | 0 |
| 15702.53 | 6366.661 | 1 | | | |
| 15705.76 | 6365.351 | 3 | I | $12366^{*}_{5}$ $18732^{*}_{5}$ | —18 |
| 15709.47 | 6363.848 | 1 | I | $13297^{*}_{5}$ $19661_{5}$ | —15 |
| 15713.32 | 6362.289 | 1 | II | $3363^{*}_{2\frac{1}{2}}$ $9725_{3\frac{1}{2}}$ | —18 |
| 15717.64 | 6360.540 | 2 | II | $4459^{*}_{3\frac{1}{2}}$ $10820_{2\frac{1}{2}}$ | —66 |
| 15740.46 | 6351.319 | 1 | I | $9996^{*}_{3}$ $16347_{2}$ | —11 |
| 15756.71 | 6344.769 | 1 | I | $11271^{*}_{4}$ $17615_{4}$ | —35 |
| 15758.37 | 6344.101 | 2 | I | $7169^{*}_{3}$ $13513_{4}$ | —22 |
| | | | I | $14001^{*}_{6}$ $20346_{6}$ | 40 |
| 15761.40 | 6342.881 | 2 | I | $8400^{*}_{5}$ $14743_{6}$ | —14 |
| 15777.92 | 6336.240 | 2 | II | $12057^{*}_{2\frac{1}{2}}$ $18393_{3\frac{1}{2}}$ | 26 |
| 15784.75 | 6333.498 | 7 | II | $2563^{*}_{3\frac{1}{2}}$ $8896_{5\frac{1}{2}}$ | —3 |
| 15811.56 | 6322.759 | 3 | I | $12467^{*}_{5}$ $18790^{*}_{5}$ | —18 |
| 15821.72 | 6318.699 | 2 | II | $3995^{*}_{3\frac{1}{2}}$ $10314_{4\frac{1}{2}}$ | —9 |
| 15822.82 | 6318.260 | 2 | II | $7341_{5\frac{1}{2}}$ $13659^{*}_{4\frac{1}{2}}$ | —64 |
| 15829.83 | 6315.462 | 6 | I | $13194_{4}$ $19510^{*}_{4}$ | —20 |
| | | | II | $2581^{*}_{4\frac{1}{2}}$ $8896_{5\frac{1}{2}}$ | —12 |
| 15832.14 | 6314.540 | 5 | | | |
| 15843.48 | 6310.021 | 3 | I | $12366^{*}_{5}$ $18676^{*}_{4}$ | 29 |
| 15845.59 | 6309.180 | 1 | II | $4511^{*}_{2\frac{1}{2}}$ $10820_{2\frac{1}{2}}$ | —45 |
| 15881.92 | 6294.748 | 1 | I | $12720^{*}_{4}$ $19014_{4}$ | 0 |
| 15885.37 | 6293.381 | 1 | | | |
| 15888.23 | 6292.248 | 2 | I | $8307^{*}_{3}$ $14599_{4}$ | —40 |
| 15903.87 | 6286.060 | 1 | I | $8509^{*}_{4}$ $14795_{5}$ | —20 |
| 15904.81 | 6285.689 | 1 | | | |
| 15911.41 | 6283.081 | 1 | | | |
| 15918.36 | 6280.338 | 4 | I | $8366^{*}_{2}$ $14646_{2}$ | —8 |
| 15921.80 | 6278.981 | 3 | I | $3100^{*}_{4}$ $9379_{4}$ | —15 |
| 15943.72 | 6270.349 | 1 | I | $13409^{*}_{3}$ $19680_{4}$ | 3 |
| 15944.94 | 6269.869 | 2 | | | |
| 15947.25 | 6268.961 | 1 | I | $13513_{4}$ $19782^{*}_{5}$ | —48 |
| | | | I | $8270^{*}_{3}$ $14539_{3}$ | —1 |
| | | | I | $12793^{*}_{5}$ $19062_{5}$ | —32 |
| 15948.93 | 6268.300 | 2 | | | |
| 15950.36 | 6267.738 | 2 | I | $10879^{*}_{5}$ $17147_{4}$ | —6 |
| 15958.40 | 6264.581 | 6 | II | $3793^{*}_{6\frac{1}{2}}$ $10058_{6\frac{1}{2}}$ | —30 |
| 15977.12 | 6257.241 | 6 | II | $1873^{*}_{3\frac{1}{2}}$ $8131_{4\frac{1}{2}}$ | —30 |
| 15997.81 | 6249.148 | 1 | I | $8991^{*}_{5}$ $15240_{4}$ | —19 |
| 16030.18 | 6236.529 | 2 | I | $9135^{*}_{3}$ $15371_{4}$ | —18 |
| 16033.29 | 6235.319 | 1 | | | |
| 16034.83 | 6234.721 | 2 | I | $13389_{3}$ $19624^{*}_{3}$ | 0 |
| 16041.99 | 6231.938 | 1 | I | $8307^{*}_{3}$ $14539_{3}$ | 35 |
| 16048.27 | 6229.499 | 1 | I | $10673_{6}$ $16903_{5}$ | —33 |
| 16050.77 | 6228.529 | 2 | I | $13315^{*}_{4}$ $19544_{4}$ | —7 |
| | | | II | $5513_{5\frac{1}{2}}$ $11742^{*}_{5\frac{1}{2}}$ | —10 |
| 16101.15 | 6209.040 | 2 | I | $12467^{*}_{5}$ $18676^{*}_{4}$ | 41 |
| 16113.11 | 6204.431 | 1 | I | $8430^{*}_{1}$ $14635_{1}$ | 34 |
| 16114.57 | 6203.869 | 2 | I | $9996^{*}_{3}$ $16200_{3}$ | 23 |
| | | | I | $14116^{*}_{4}$ $20320_{4}$ | 44 |
| | | | I | $14310^{*}_{2}$ $20513_{2}$ | —20 |
| 16120.75 | 6201.491 | 1 | I | $9053_{3}$ $15255^{*}_{5}$ | 87 |
| | | | II | $10798_{2\frac{1}{2}}$ $17000_{3\frac{1}{2}}$ | 27 |
| 16124.97 | 6199.868 | 1 | I | $15677^{*}_{7}$ $21877_{6}$ | 42 |
| 16127.64 | 6198.842 | 1 | I | $8400^{*}_{5}$ $14599_{4}$ | —25 |
| 16130.64 | 6197.689 | 1 | | | |
| 16140.06 | 6194.072 | 3 | | | |
| 16143.32 | 6192.821 | 3 | II | $2581^{*}_{4\frac{1}{2}}$ $8774_{4\frac{1}{2}}$ | 16 |
| 16147.83 | 6191.091 | 1 | | | |
| 16150.18 | 6190.190 | 2 | | | |
| 16161.88 | 6185.709 | 1 | | | |
| 16167.05 | 6183.731 | 2 | I | $11131^{*}_{3}$ $17315_{4}$ | 3 |
| | | | I | $11517_{1}$ $17700_{0}$ | —22 |
| | | | II | $11387^{*}_{3\frac{1}{2}}$ $17571_{4\frac{1}{2}}$ | 67 |
| 16176.08 | 6180.279 | 1 | II | $4523^{*}_{4\frac{1}{2}}$ $10703_{4\frac{1}{2}}$ | 2 |
| 16193.27 | 6173.718 | 1 | I | $11337^{*}_{3}$ $17511_{3}$ | —18 |
| | | | I | $11357^{*}_{5}$ $17530_{5}$ | —6 |
| 16195.99 | 6172.681 | 1 | I | $11517^{*}_{1}$ $17689_{2}$ | —21 |
| | | | I | $12707^{*}_{2}$ $18880_{2}$ | —4 |
| 16213.04 | 6166.190 | 1 | I | $7715^{*}_{5}$ $13881_{5}$ | —17 |
| 16214.70 | 6165.559 | 2 | I | $7348^{*}_{4}$ $13513_{4}$ | —16 |
| 16226.33 | 6161.140 | 2 | I | $8902^{*}_{3}$ $15063_{3}$ | —5 |
| 16233.02 | 6158.601 | 4 | | | |
| 16250.65 | 6151.919 | 2 | | | |
| 16251.76 | 6151.499 | 2 | I | $12720^{*}_{4}$ $18871_{4}$ | 8 |
| 16257.10 | 6149.478 | 2 | I | $12793^{*}_{5}$ $18943_{5}$ | —30 |
| | | | II | $2382^{*}_{4\frac{1}{2}}$ $8531_{3\frac{1}{2}}$ | 29 |
| 16261.41 | 6147.849 | 1 | I | $13214^{*}_{1}$ $19362_{1}$ | 36 |
| | | | I | $15917^{*}_{7}$ $22064_{6}$ | —39 |
| | | | II | $2641_{3\frac{1}{2}}$ $8789_{2\frac{1}{2}}$ | 38 |
| 16274.93 | 6142.741 | 1 | I | $9135^{*}_{3}$ $15277_{3}$ | —11 |
| 16302.32 | 6132.421 | 1 | II | $5964_{3\frac{1}{2}}$ $12097_{3\frac{1}{2}}$ | 49 |
| 16307.48 | 6130.480 | 2 | I | $9425^{*}_{2}$ $15555_{3}$ | 18 |
| 16313.79 | 6128.109 | 1 | I | $13219^{*}_{6}$ $19347_{6}$ | —43 |
| 16320.71 | 6125.511 | 2 | II | $5616_{4\frac{1}{2}}$ $11742^{*}_{5\frac{1}{2}}$ | 2 |
| 16325.83 | 6123.590 | 1 | | | |
| 16327.32 | 6123.031 | 4 | II | $4523^{*}_{4\frac{1}{2}}$ $10646_{5\frac{1}{2}}$ | —10 |
| 16350.45 | 6114.369 | 1 | II | $6913_{6\frac{1}{2}}$ $13027_{6\frac{1}{2}}$ | 5 |
| 16360.40 | 6110.651 | 2 | I | $13513_{4}$ $19624^{*}_{3}$ | —21 |
| 16368.46 | 6107.642 | 3 | I | $12114_{4}$ $18221_{5}$ | —25 |
| 16376.48 | 6104.651 | 7 | II | $987^{*}_{4\frac{1}{2}}$ $7092_{5\frac{1}{2}}$ | —8 |
| 16392.62 | 6098.640 | 1 | I | $9462^{*}_{5}$ $15561_{5}$ | 0 |
| 16403.32 | 6094.662 | 1 | I | $10774^{*}_{3}$ $16869_{4}$ | 14 |
| 16415.37 | 6090.188 | 2 | | | |
| 16420.68 | 6088.219 | 1 | I | $10604^{*}_{3}$ $16693_{4}$ | —43 |
| 16424.91 | 6086.651 | 1 | | | |
| 16429.82 | 6084.832 | 1 | I | $11810^{*}_{4}$ $17895_{5}$ | —34 |
| 16432.88 | 6083.699 | 2 | II | $5675^{*}_{4\frac{1}{2}}$ $11759_{5\frac{1}{2}}$ | 8 |
| 16438.74 | 6081.530 | 1 | I | $11357^{*}_{5}$ $17438_{4}$ | 0 |
| 16445.23 | 6079.130 | 2 | I | $13784^{*}_{5}$ $19863^{*}_{5}$ | —26 |
| 16456.11 | 6075.111 | 1 | II | $10924^{*}_{4\frac{1}{2}}$ $17000_{3\frac{1}{2}}$ | —35 |
| 16458.06 | 6074.391 | 1 | I | $12988^{*}_{4}$ $19062_{5}$ | 33 |
| 16459.99 | 6073.679 | 1 | | | |
| 16460.96 | 6073.321 | 1 | I | $13908_{7}$ $19982^{*}_{6}$ | 9 |
| 16463.86 | 6072.251 | 1 | | | |
| 16464.35 | 6072.070 | 1 | I | $12114_{4}$ $18186^{*}_{3}$ | 25 |
| 16478.46 | 6066.871 | 1 | I | $3312^{*}_{4}$ $9379_{4}$ | —36 |
| | | | II | $6389^{*}_{4\frac{1}{2}}$ $12456_{3\frac{1}{2}}$ | 63 |
| 16486.18 | 6064.030 | 1 | | | |
| 16495.78 | 6060.501 | 1 | | | |
| 16500.30 | 6058.841 | 1 | I | $6238_{5}$ $12297^{*}_{5}$ | —5 |
| | | | II | $7059^{*}_{4\frac{1}{2}}$ $13117_{4\frac{1}{2}}$ | —3 |
| 16507.41 | 6056.231 | 2 | I | $9787^{*}_{3}$ $15843_{4}$ | 2 |
| 16509.89 | 6055.321 | 1 | I | $10612^{*}_{2}$ $16668_{3}$ | —1 |
| 16530.48 | 6047.779 | 1 | II | $4266_{3\frac{1}{2}}$ $10314_{4\frac{1}{2}}$ | 4 |
| 16531.41 | 6047.439 | 2 | I | $8088^{*}_{2}$ $14136_{3}$ | 29 |
| 16537.20 | 6045.321 | 1 | I | $11850^{*}_{5}$ $17895_{5}$ | 34 |
| 16545.28 | 6042.369 | 3 | I | $13939_{6}$ $19982^{*}_{6}$ | 24 |
| 16551.80 | 6039.989 | 1 | | | |
| 16553.14 | 6039.500 | 2 | I | $7841^{*}_{5}$ $13881_{5}$ | 11 |
| 16595.18 | 6024.200 | 7 | II | $987^{*}_{4\frac{1}{2}}$ $7011_{4\frac{1}{2}}$ | —2 |
| 16614.87 | 6017.061 | 3 | II | $2879^{*}_{5\frac{1}{2}}$ $8896_{5\frac{1}{2}}$ | 13 |

TABLE 1. *Observed infrared cerium lines*—Continued

| Wavelength Å | Wavenumber ($cm^{-1}$) | Intensity | Spectrum | Classification | O−C (.001 $cm^{-1}$) | Wavelength Å | Wavenumber ($cm^{-1}$) | Intensity | Spectrum | Classification | O−C (.001 $cm^{-1}$) |
|---|---|---|---|---|---|---|---|---|---|---|---|
| 16622.17 | 6014.419 | 1 | I | $12351^{\circ}_{4}$ $18365_{5}$ | 14 | 17076.97 | 5854.241 | 4 | II | $4203^{\circ}_{6\frac{1}{2}}$ $10058_{6\frac{1}{2}}$ | —64 |
| 16636.05 | 6009.401 | 2 | I | $8088^{\circ}_{2}$ $14098_{2}$ | 8 | | | | II | $4459^{\circ}_{3\frac{1}{2}}$ $10314_{4\frac{1}{2}}$ | —53 |
| 16665.73 | 5998.699 | 1 | I | $13784_{5}$ $19782^{\circ}_{5}$ | —34 | 17077.47 | 5854.069 | 5 | II | $5455^{\circ}_{7\frac{1}{2}}$ $11309_{7\frac{1}{2}}$ | —59 |
| | | | I | $15101^{\circ}_{6}$ $21100_{6}$ | 5 | 17080.74 | 5852.949 | 3 | II | $2595^{\circ}_{1\frac{1}{2}}$ $8448_{2\frac{1}{2}}$ | —52 |
| 16671.37 | 5996.669 | 1 | I | $12297^{\circ}_{5}$ $18294_{6}$ | 0 | 17094.20 | 5848.340 | 1 | II | $1873^{\circ}_{3\frac{1}{2}}$ $7722_{2\frac{1}{2}}$ | —6 |
| 16672.15 | 5996.389 | 2 | I | $13409^{\circ}_{3}$ $19406_{3}$ | —35 | 17098.03 | 5847.030 | 1 | I | $9709^{\circ}_{2}$ $15555_{3}$ | 50 |
| | | | I | $14116^{\circ}_{4}$ $20112_{4}$ | 0 | 17099.40 | 5846.561 | 2 | I | $7348^{\circ}_{4}$ $13194_{4}$ | 12 |
| 16683.53 | 5992.298 | 1 | I | $6475^{\circ}_{4}$ $12467_{5}$ | 11 | 17103.03 | 5845.321 | 2 | I | $15396_{6}$ $21241^{\circ}_{7}$ | —2 |
| 16698.71 | 5986.851 | 1 | I | $8762^{\circ}_{4}$ $14748_{4}$ | 32 | | | | II | $10314_{4\frac{1}{2}}$ $16159^{\circ}_{3\frac{1}{2}}$ | —56 |
| | | | I | $14920^{\circ}_{4}$ $20907_{4}$ | —2 | 17106.63 | 5844.090 | 4 | I | $12297^{\circ}_{5}$ $18141_{4}$ | 24 |
| 16705.41 | 5984.450 | 1 | II | $8402^{\circ}_{3\frac{1}{2}}$ $14387_{4\frac{1}{2}}$ | 2 | 17109.38 | 5843.151 | 4 | I | $13219^{\circ}_{6}$ $19062_{5}$ | 42 |
| 16708.57 | 5983.318 | 1 | I | $10604^{\circ}_{3}$ $16588_{4}$ | 5 | 17122.51 | 5838.670 | 1 | | | |
| 16712.64 | 5981.861 | 2 | I | $13881_{5}$ $19863^{\circ}_{5}$ | —2 | 17125.01 | 5837.818 | 1 | | | |
| 16714.63 | 5981.149 | 1 | I | $14338^{\circ}_{5}$ $20320_{4}$ | —18 | 17133.34 | 5834.980 | 1 | I | $14001^{\circ}_{6}$ $19836_{7}$ | 4 |
| 16715.52 | 5980.830 | 1 | I | $13315^{\circ}_{4}$ $19296_{4}$ | 45 | 17139.13 | 5833.009 | 2 | | | |
| 16718.23 | 5979.861 | 4 | I | $10243^{\circ}_{4}$ $16223_{5}$ | —1 | 17148.09 | 5829.961 | 1 | I | $12720^{\circ}_{4}$ $18550_{4}$ | —24 |
| 16722.51 | 5978.330 | 7 | II | $3793^{\circ}_{6\frac{1}{2}}$ $9771_{7\frac{1}{2}}$ | 13 | 17150.98 | 5828.978 | 2 | I | $8307^{\circ}_{3}$ $14136_{3}$ | —34 |
| 16729.42 | 5975.861 | 2 | II | $4844^{\circ}_{1\frac{1}{2}}$ $10820_{2\frac{1}{2}}$ | 29 | 17165.55 | 5824.031 | 2 | I | $4762_{4}$ $10586^{\circ}_{4}$ | —22 |
| 16742.25 | 5971.282 | 2 | I | $9787^{\circ}_{3}$ $15758_{2}$ | 44 | 17168.32 | 5823.091 | 2 | II | $14097_{3\frac{1}{2}}$ $19920^{\circ}_{3\frac{1}{2}}$ | —12 |
| | | | I | $15255^{\circ}_{5}$ $21226_{5}$ | —38 | 17175.23 | 5820.748 | 3 | I | $9787^{\circ}_{3}$ $15607_{2}$ | —12 |
| | | | II | $8280^{\circ}_{2\frac{1}{2}}$ $14252_{3\frac{1}{2}}$ | 51 | | | | I | $15021^{\circ}_{7}$ $20842_{6}$ | 13 |
| 16744.55 | 5970.461 | 1 | I | $9996^{\circ}_{3}$ $15967_{2}$ | 22 | 17187.16 | 5816.708 | 3 | I | $12467_{5}$ $18284^{\circ}_{5}$ | —47 |
| 16768.57 | 5961.909 | 2 | I | $14743_{6}$ $20705^{\circ}_{6}$ | 0 | | | | II | $8280^{\circ}_{2\frac{1}{2}}$ $14097_{3\frac{1}{2}}$ | —55 |
| 16783.21 | 5956.709 | 3 | I | $10243^{\circ}_{4}$ $16200_{3}$ | —3 | 17189.11 | 5816.048 | 2 | | | |
| 16792.26 | 5953.498 | 3 | II | $3363^{\circ}_{2\frac{1}{2}}$ $9316_{3\frac{1}{2}}$ | 23 | 17194.10 | 5814.360 | 3 | I | $9830^{\circ}_{6}$ $15644_{6}$ | 25 |
| 16808.09 | 5947.891 | 1 | I | $7933^{\circ}_{5}$ $13881_{5}$ | 5 | 17196.23 | 5813.640 | 3 | | | |
| 16808.91 | 5947.601 | 2 | I | $13297^{\circ}_{5}$ $19244_{4}$ | 26 | 17196.38 | 5813.589 | 1 | I | $10774^{\circ}_{3}$ $16588_{4}$ | —7 |
| 16829.29 | 5940.399 | 1 | II | $5819^{\circ}_{4\frac{1}{2}}$ $11759_{5\frac{1}{2}}$ | 64 | 17203.98 | 5811.021 | 1 | I | $12351^{\circ}_{4}$ $18162_{4}$ | 30 |
| 16832.86 | 5939.139 | 2 | II | $6517^{\circ}_{2\frac{1}{2}}$ $12456_{3\frac{1}{2}}$ | 7 | 17208.43 | 5809.519 | 1 | | | |
| 16844.85 | 5934.911 | 1 | I | $11796^{\circ}_{4}$ $17731_{4}$ | 50 | 17211.66 | 5808.428 | 2 | I | $11337^{\circ}_{3}$ $17146_{3}$ | —20 |
| 16848.69 | 5933.559 | 2 | I | $9462^{\circ}_{5}$ $15396_{6}$ | —21 | 17213.91 | 5807.669 | 2 | I | $10243^{\circ}_{4}$ $16051_{4}$ | —28 |
| 16850.65 | 5932.869 | 1 | I | $11357^{\circ}_{5}$ $17289_{6}$ | 27 | 17215.89 | 5807.001 | 2 | II | $5651^{\circ}_{5\frac{1}{2}}$ $11458_{5\frac{1}{2}}$ | 1 |
| 16856.78 | 5930.711 | 2 | II | $1410^{\circ}_{4\frac{1}{2}}$ $7341_{5\frac{1}{2}}$ | 4 | 17223.01 | 5804.601 | 3 | I | $6663^{\circ}_{5}$ $12467_{5}$ | 0 |
| 16863.07 | 5928.499 | 5 | | | | 17226.60 | 5803.391 | 4 | II | $5651^{\circ}_{5\frac{1}{2}}$ $11454_{6\frac{1}{2}}$ | 56 |
| 16871.89 | 5925.400 | 5 | I | $13605_{6}$ $19530^{\circ}_{5}$ | 20 | 17230.52 | 5802.071 | 2 | | | |
| 16884.23 | 5921.069 | 1 | | | | 17254.10 | 5794.141 | 1 | I | $8270^{\circ}_{3}$ $14064_{4}$ | 8 |
| 16891.39 | 5918.559 | 1 | I | $10774^{\circ}_{3}$ $16693_{4}$ | 12 | | | | II | $7233^{\circ}_{5\frac{1}{2}}$ $13027_{6\frac{1}{2}}$ | 10 |
| 16893.76 | 5917.729 | 1 | I | $12366_{5}$ $18284^{\circ}_{5}$ | —19 | 17265.25 | 5790.399 | 3 | II | $5969^{\circ}_{5\frac{1}{2}}$ $11759_{5\frac{1}{2}}$ | —48 |
| 16897.55 | 5916.402 | 1 | I | $15879_{5}$ $21796^{\circ}_{6}$ | 10 | 17288.45 | 5782.629 | 3 | II | $5675^{\circ}_{4\frac{1}{2}}$ $11458_{5\frac{1}{2}}$ | 30 |
| 16905.16 | 5913.738 | 1 | I | $9787^{\circ}_{3}$ $15700_{4}$ | —19 | 17306.76 | 5776.511 | 1 | | | |
| 16908.56 | 5912.549 | 1 | I | $10673^{\circ}_{6}$ $16586_{5}$ | —26 | 17309.58 | 5775.570 | 1 | I | $13572^{\circ}_{7}$ $19347_{6}$ | 42 |
| | | | I | $16152^{\circ}_{6}$ $22064_{6}$ | —22 | 17322.39 | 5771.299 | 5 | I | $12960_{6}$ $18732^{\circ}_{5}$ | 45 |
| 16917.60 | 5909.390 | 1 | | | | 17328.09 | 5769.401 | 1 | I | $9996^{\circ}_{3}$ $15766_{3}$ | 0 |
| 16922.01 | 5907.850 | 1 | | | | 17329.47 | 5768.941 | 2 | | | |
| 16940.07 | 5901.551 | 2 | | | | 17340.41 | 5765.302 | 2 | I | $13297^{\circ}_{5}$ $19062_{5}$ | 16 |
| 16945.76 | 5899.570 | 1 | I | $12720^{\circ}_{4}$ $18619_{5}$ | 0 | 17364.15 | 5757.419 | 2 | | | |
| 16956.54 | 5895.819 | 2 | II | $2382^{\circ}_{4\frac{1}{2}}$ $8278_{5\frac{1}{2}}$ | —8 | 17365.29 | 5757.041 | 1 | I | $8307^{\circ}_{3}$ $14064_{4}$ | —31 |
| 16958.72 | 5895.061 | 1 | I | $13815^{\circ}_{4}$ $19711_{3}$ | 49 | 17386.07 | 5750.161 | 2 | | | |
| 16962.61 | 5893.709 | 3 | I | $7890^{\circ}_{4}$ $13784_{5}$ | —12 | 17387.71 | 5749.618 | 3 | | | |
| 16969.60 | 5891.282 | 2 | I | $6475^{\circ}_{4}$ $12366_{5}$ | —11 | 17399.11 | 5745.851 | 1 | II | $9771_{7\frac{1}{2}}$ $15517^{\circ}_{6\frac{1}{2}}$ | 30 |
| | | | I | $12720^{\circ}_{4}$ $18611_{3}$ | 11 | 17404.20 | 5744.171 | 2 | I | $8902^{\circ}_{3}$ $14646_{2}$ | 32 |
| 16972.63 | 5890.230 | 3 | | | | 17426.29 | 5736.889 | 2 | | | |
| 16989.71 | 5884.308 | 2 | I | $8055^{\circ}_{6}$ $13939_{6}$ | 41 | 17444.99 | 5730.740 | 2 | I | $9830^{\circ}_{6}$ $15561_{5}$ | 2 |
| | | | II | $7233^{\circ}_{5\frac{1}{2}}$ $13117_{4\frac{1}{2}}$ | 14 | 17446.66 | 5730.191 | 1 | | | |
| 16999.33 | 5880.978 | 1 | I | $11850^{\circ}_{5}$ $17731_{4}$ | 2 | 17482.21 | 5718.539 | 1 | I | $14064_{4}$ $19782^{\circ}_{5}$ | 36 |
| 17005.25 | 5878.931 | 2 | I | $13194_{4}$ $19073^{\circ}_{5}$ | 40 | 17493.56 | 5714.828 | 2 | II | $2563^{\circ}_{5\frac{1}{2}}$ $8278_{5\frac{1}{2}}$ | —8 |
| | | | I | $9709^{\circ}_{2}$ $15587_{2}$ | 16 | 17496.65 | 5713.819 | 2 | I | $11337^{\circ}_{3}$ $17051_{3}$ | 36 |
| 17015.33 | 5875.448 | 1 | | | | | | | I | $12600^{\circ}_{3}$ $18313_{3}$ | 45 |
| 17044.80 | 5865.290 | 1 | | | | 17508.54 | 5709.939 | 7 | II | $5455^{\circ}_{7\frac{1}{2}}$ $11165_{8\frac{1}{2}}$ | —3 |
| 17047.10 | 5864.498 | 3 | I | $12297^{\circ}_{5}$ $18162_{4}$ | —31 | 17519.09 | 5706.500 | 6 | | | |
| 17058.88 | 5860.449 | 7 | II | $2563^{\circ}_{5\frac{1}{2}}$ $8423_{6\frac{1}{2}}$ | 0 | 17524.13 | 5704.859 | 2 | I | $9903^{\circ}_{1}$ $15607_{2}$ | 0 |
| 17062.14 | 5859.329 | 2 | I | $12454^{\circ}_{2}$ $18313_{3}$ | —45 | 17548.86 | 5696.820 | 6 | II | $2581^{\circ}_{4\frac{1}{2}}$ $8278_{5\frac{1}{2}}$ | 10 |
| 17063.24 | 5858.951 | 2 | | | | 17567.18 | 5690.879 | 3 | | | |
| 17069.63 | 5856.758 | 2 | I | $2378^{\circ}_{2}$ $8235_{2}$ | —19 | 17594.72 | 5681.971 | 6 | II | $1410^{\circ}_{4\frac{1}{2}}$ $7092_{5\frac{1}{2}}$ | 1 |

TABLE 1. *Observed infrared cerium lines*—Continued

| Wavelength Å | Wavenumber ($cm^{-1}$) | Intensity | Spectrum | Classification | O−C (.001 $cm^{-1}$) |
|---|---|---|---|---|---|
| 17613.67 | 5675.858 | 6 | I | $12366_5$ $18042^{\circ}_4$ | 18 |
| 17623.07 | 5672.831 | 4 | | | |
| 17625.84 | 5671.939 | 3 | I | $7841^{\circ}_5$ $13513_4$ | 19 |
| 17642.48 | 5666.590 | 3 | I | $13124_5$ $18790^{\circ}_5$ | —4 |
| 17653.38 | 5663.091 | 3 | I | $13572^{\circ}_7$ $19235_6$ | 7 |
| 17664.58 | 5659.500 | 2 | II | $7092_{5\frac{1}{2}}$ $12751^{\circ}_{5\frac{1}{2}}$ | —35 |
| 17671.98 | 5657.130 | 1 | I | $12351^{\circ}_4$ $18008_5$ | 9 |
| | | | I | $14186^{\circ}_6$ $19843_5$ | —6 |
| 17675.61 | 5655.969 | 2 | II | $10798^{\circ}_{2\frac{1}{2}}$ $16454_{2\frac{1}{2}}$ | —17 |
| 17685.30 | 5652.870 | 1 | | | |
| 17695.38 | 5649.650 | 2 | | | |
| 17696.22 | 5649.381 | 3 | I | $12948^{\circ}_5$ $18598_6$ | 21 |
| 17697.54 | 5648.960 | 1 | I | $13881_5$ $19530^{\circ}_5$ | 24 |
| | | | II | $7878^{\circ}_{3\frac{1}{2}}$ $13527_{4\frac{1}{2}}$ | 50 |
| 17703.24 | 5647.141 | 2 | | | |
| 17708.01 | 5645.620 | 2 | I | $12720^{\circ}_4$ $18365_5$ | 10 |
| 17716.92 | 5642.781 | 1 | II | $7061^{\circ}_{10\frac{1}{2}}$ $12704_{11\frac{1}{2}}$ | —5 |
| 17730.06 | 5638.599 | 4 | I | $6475^{\circ}_4$ $12114_4$ | 24 |
| 17732.13 | 5637.941 | 2 | I | $9425^{\circ}_2$ $15063_3$ | 18 |
| 17735.31 | 5636.930 | 3 | I | $8902^{\circ}_3$ $14539_3$ | 24 |
| 17738.17 | 5636.021 | 3 | I | $10243^{\circ}_4$ $15879_5$ | 23 |
| 17760.52 | 5628.928 | 1 | I | $13881_5$ $19510^{\circ}_4$ | 41 |
| 17766.10 | 5627.160 | 1 | I | $8509^{\circ}_3$ $14136_3$ | 48 |
| 17777.76 | 5623.470 | 1 | I | $7890^{\circ}_4$ $13513_4$ | 24 |
| | | | I | $12297^{\circ}_2$ $17921_3$ | 12 |
| 17787.25 | 5620.470 | 1 | I | $11301^{\circ}_2$ $16921_3$ | 27 |
| 17799.00 | 5616.759 | 1 | II | $0^{\circ}_{3\frac{1}{2}}$ $5616_{4\frac{1}{2}}$ | 16 |
| 17801.79 | 5615.879 | 1 | | | |
| 17808.19 | 5613.861 | 3 | I | $9135^{\circ}_3$ $14748_4$ | 15 |
| 17816.38 | 5611.280 | 1 | I | $6238^{\circ}_5$ $11850^{\circ}_5$ | —37 |
| | | | I | $6856^{\circ}_4$ $12467_5$ | 12 |
| 17817.65 | 5610.880 | 1 | | | |
| 17820.99 | 5609.828 | 1 | | | |
| 17827.98 | 5607.629 | 1 | | | |
| 17833.89 | 5605.771 | 1 | I | $13629^{\circ}_5$ $19235_6$ | 31 |
| 17835.71 | 5605.199 | 1 | I | $14186^{\circ}_6$ $19791_5$ | 26 |
| 17845.58 | 5602.098 | 1 | I | $11545^{\circ}_4$ $17147_4$ | —41 |
| 17847.42 | 5601.521 | 4 | II | $1410^{\circ}_{4\frac{1}{2}}$ $7011_{4\frac{1}{2}}$ | 8 |
| 17853.29 | 5599.679 | 2 | I | $10243^{\circ}_4$ $15843_4$ | 10 |
| 17865.89 | 5595.730 | 3 | I | $13194_4$ $18790^{\circ}_5$ | —25 |
| 17867.97 | 5595.079 | 1 | I | $12297^{\circ}_5$ $17892_4$ | 46 |
| 17872.21 | 5593.751 | 1 | I | $11796^{\circ}_4$ $17390_4$ | 4 |
| | | | I | $12720^{\circ}_4$ $18313_3$ | 5 |
| 17882.19 | 5590.629 | 2 | I | $13939_6$ $19530^{\circ}_5$ | 42 |
| 17906.92 | 5582.909 | 1 | II | $8804^{\circ}_{4\frac{1}{2}}$ $14387_{4\frac{1}{2}}$ | 22 |
| 17917.19 | 5579.709 | 1 | I | $12425^{\circ}_4$ $18005_3$ | —44 |
| | | | II | $6517^{\circ}_{2\frac{1}{2}}$ $12097_{3\frac{1}{2}}$ | 60 |
| 17918.02 | 5579.450 | 1 | I | $11810^{\circ}_4$ $17390_4$ | 8 |
| 17924.51 | 5577.430 | 1 | I | $13409^{\circ}_3$ $18987_2$ | 12 |
| 17943.43 | 5571.549 | 2 | I | $2208^{\circ}_5$ $7780_6$ | 4 |
| 17954.74 | 5568.039 | 6 | II | $4203^{\circ}_{6\frac{1}{2}}$ $9771_{7\frac{1}{2}}$ | 28 |
| 17965.93 | 5564.571 | 1 | I | $11874^{\circ}_3$ $17438_4$ | 21 |
| 17988.14 | 5557.701 | 3 | | | |
| 18003.89 | 5552.839 | 1 | I | $13124_5$ $18676^{\circ}_4$ | 23 |
| 18013.26 | 5549.950 | 5 | II | $2581^{\circ}_{4\frac{1}{2}}$ $8131_{4\frac{1}{2}}$ | 2 |
| 18021.70 | 5547.351 | 1 | I | $11796^{\circ}_4$ $17343_5$ | —15 |
| | | | II | $6549^{\circ}_{2\frac{1}{2}}$ $12097_{3\frac{1}{2}}$ | —8 |
| 18024.43 | 5546.511 | 1 | | | |
| 18026.16 | 5545.979 | 2 | | | |
| 18033.34 | 5543.770 | 1 | | | |
| 18040.83 | 5541.469 | 1 | I | $12351^{\circ}_4$ $17892_4$ | —24 |
| | | | II | $9198^{\circ}_{3\frac{1}{2}}$ $14739_{2\frac{1}{2}}$ | 28 |
| 18046.04 | 5539.869 | 1 | I | $11850^{\circ}_5$ $17390_4$ | 7 |
| 18053.01 | 5537.730 | 1 | | | |
| 18063.19 | 5534.609 | 1 | I | $13297^{\circ}_5$ $18831_5$ | 39 |
| 18068.15 | 5533.090 | 1 | I | $11810^{\circ}_4$ $17343_5$ | 28 |
| 18080.73 | 5529.240 | 1 | | | |
| 18092.22 | 5525.729 | 2 | | | |
| 18094.51 | 5525.029 | 2 | I | $10318^{\circ}_3$ $15843_4$ | 18 |
| 18101.95 | 5522.759 | 2 | | | |
| 18144.72 | 5509.740 | 1 | | | |
| 18159.65 | 5505.211 | 3 | | | |
| 18160.02 | 5505.098 | 3 | II | $7522^{\circ}_{3\frac{1}{2}}$ $13027_{6\frac{1}{2}}$ | —36 |
| 18176.33 | 5500.159 | 2 | I | $10723^{\circ}_4$ $16223_5$ | 28 |
| 18207.84 | 5490.640 | 2 | I | $9787^{\circ}_3$ $15277_3$ | 8 |
| 18211.22 | 5489.621 | 6 | II | $2641^{\circ}_{3\frac{1}{2}}$ $8131_{4\frac{1}{2}}$ | —21 |
| 18224.01 | 5485.768 | 2 | | | |
| 18236.47 | 5482.020 | 2 | I | $13194_4$ $18676^{\circ}_4$ | 43 |
| 18244.39 | 5479.641 | 3 | I | $7715^{\circ}_5$ $13194_4$ | 28 |
| | | | I | $11357^{\circ}_5$ $16836_6$ | 30 |
| | | | I | $15333^{\circ}_8$ $20812_7$ | 18 |
| 18269.50 | 5472.109 | 1 | II | $8804^{\circ}_{4\frac{1}{2}}$ $14276_{5\frac{1}{2}}$ | 36 |
| 18276.88 | 5469.900 | 2 | | | |
| 18286.71 | 5466.959 | 3 | I | $12425^{\circ}_4$ $17892_4$ | 43 |
| 18289.79 | 5466.039 | 3 | I | $14064_4$ $19530^{\circ}_5$ | 41 |
| 18294.81 | 5464.539 | 2 | I | $9135^{\circ}_3$ $14599_4$ | 40 |
| 18357.22 | 5445.961 | 1 | I | $10901^{\circ}_2$ $16347_2$ | —45 |
| | | | I | $14064_4$ $19510^{\circ}_4$ | 11 |
| 18385.48 | 5437.590 | 1 | | | |
| 18424.85 | 5425.971 | 1 | II | $3363^{\circ}_{2\frac{1}{2}}$ $8789_{2\frac{1}{2}}$ | 22 |
| 18435.83 | 5422.739 | 1 | | | |
| 18452.57 | 5417.820 | 1 | | | |
| 18494.59 | 5405.510 | 1 | | | |
| 18507.53 | 5401.731 | 2 | | | |
| 18510.79 | 5400.780 | 2 | | | |
| 18556.04 | 5387.610 | 1 | I | $9379_4$ $14766^{\circ}_5$ | 31 |
| 18577.80 | 5381.299 | 3 | I | $15240_4$ $20621^{\circ}_4$ | —7 |
| | | | II | $8278_{5\frac{1}{2}}$ $13659^{\circ}_{4\frac{1}{2}}$ | 37 |
| 18578.66 | 5381.050 | 1 | | | |
| 18587.30 | 5378.549 | 1 | I | $12351^{\circ}_4$ $17729_5$ | —5 |
| 18597.91 | 5375.480 | 1 | II | $15565^{\circ}_{2\frac{1}{2}}$ $20940_{3\frac{1}{2}}$ | 64 |
| 18606.15 | 5373.100 | 5 | I | $14609_7$ $19982^{\circ}_6$ | 50 |
| | | | I | $13214^{\circ}_4$ $18587_2$ | 28 |
| | | | I | $13569^{\circ}_4$ $18943_5$ | 47 |
| 18628.44 | 5366.671 | 1 | I | $11301^{\circ}_2$ $16668_3$ | 18 |
| 18631.60 | 5365.760 | 1 | | | |
| 18634.31 | 5364.980 | 1 | I | $12873^{\circ}_2$ $18238_2$ | 9 |
| 18638.93 | 5363.650 | 2 | | | |
| 18642.34 | 5362.669 | 1 | | | |
| 18658.66 | 5357.979 | 1 | I | $11545^{\circ}_4$ $16903_5$ | —2 |
| 18671.20 | 5354.380 | 2 | | | |
| 18675.84 | 5353.050 | 3 | | | |
| 18680.06 | 5351.840 | 2 | I | $8587^{\circ}_7$ $13939_6$ | 21 |
| | | | I | $13622^{\circ}_2$ $18973_1$ | —14 |
| 18682.09 | 5351.259 | 2 | I | $12297^{\circ}_5$ $17649_6$ | 4 |
| 18686.35 | 5350.039 | 1 | II | $3703^{\circ}_{3\frac{1}{2}}$ $9053_{3\frac{1}{2}}$ | 1 |
| 18689.39 | 5349.169 | 1 | I | $10409^{\circ}_1$ $15758_2$ | —15 |
| 18700.15 | 5346.091 | 2 | | | |
| 18707.22 | 5344.070 | 2 | I | $15277_3$ $20621^{\circ}_4$ | —3 |
| 18707.89 | 5343.879 | 2 | I | $10879^{\circ}_5$ $16223_5$ | 29 |
| 18708.69 | 5343.651 | 1 | | | |
| 18736.50 | 5335.719 | 2 | | | |
| 18737.30 | 5335.491 | 3 | | | |
| 18763.75 | 5327.970 | 1 | I | $10723^{\circ}_4$ $16051_4$ | 4 |
| 18779.05 | 5323.629 | 5 | I | $12960_6$ $18284^{\circ}_5$ | —3 |
| 18786.85 | 5321.419 | 1 | I | $13044^{\circ}_4$ $18365_5$ | —11 |
| | | | I | $13089^{\circ}_3$ $18411_4$ | 47 |
| | | | II | $3995^{\circ}_{3\frac{1}{2}}$ $9316_{3\frac{1}{2}}$ | —21 |

TABLE 1. *Observed infrared cerium lines*—Continued

| Wavelength Å | Wavenumber ($cm^{-1}$) | Intensity | Spectrum | Classification | O−C (.001 $cm^{-1}$) |
|---|---|---|---|---|---|
| 18802.01 | 5317.128 | 1 | I | $11271^{*}_{4}$ $16588_{4}$ | 14 |
| 18811.42 | 5314.469 | 2 | II | $2140^{*}_{0\,1/2}$ $7454_{1\,1/2}$ | 7 |
| 18822.25 | 5311.411 | 2 | | | |
| 18828.14 | 5309.749 | 2 | I | $11810^{*}_{4}$ $17120_{5}$ | 19 |
| 18833.85 | 5308.139 | 2 | II | $5616^{*}_{4\,1/2}$ $10924^{*}_{4\,1/2}$ | 5 |
| 18852.49 | 5302.891 | 3 | II | $3593^{*}_{4\,1/2}$ $8896_{5\,1/2}$ | 30 |
| 18854.56 | 5302.309 | 2 | | | |
| 18899.22 | 5289.779 | 1 | I | $11578^{*}_{4}$ $16868_{2}$ | −39 |
| | | | II | $7722^{*}_{2\,1/2}$ $13012^{*}_{2\,1/2}$ | −45 |
| 18909.05 | 5287.029 | 2 | I | $13389^{*}_{3}$ $18676_{4}$ | 30 |
| 18911.23 | 5286.420 | 1 | | | |
| 18941.61 | 5277.941 | 1 | I | $8603^{*}_{6}$ $13881_{5}$ | 28 |
| 18945.42 | 5276.880 | 2 | I | $10774^{*}_{3}$ $16051_{4}$ | 7 |
| 18947.65 | 5276.259 | 2 | I | $9787^{*}_{3}$ $15063_{3}$ | 27 |
| 18969.51 | 5270.178 | 1 | I | $11850^{*}_{5}$ $17120_{5}$ | 28 |
| 18971.77 | 5269.551 | 1 | I | $13044^{*}_{4}$ $18313_{3}$ | −15 |
| 18977.61 | 5267.929 | 2 | | | |
| 18980.24 | 5267.199 | 2 | II | $8169^{*}_{1\,1/2}$ $13436^{*}_{2\,1/2}$ | 53 |
| 18985.68 | 5265.690 | 1 | | | |
| 18997.26 | 5262.480 | 1 | I | $14417^{*}_{4}$ $19680_{4}$ | 14 |
| 19035.89 | 5251.801 | 1 | | | |
| 19057.88 | 5245.741 | 1 | I | $7715^{*}_{5}$ $12960_{6}$ | 27 |
| 19067.34 | 5243.138 | 1 | | | |
| 19079.23 | 5239.871 | 1 | | | |
| 19083.86 | 5238.600 | 2 | I | $10604^{*}_{3}$ $15843_{4}$ | 40 |
| 19095.71 | 5235.349 | 1 | | | |
| 19100.89 | 5233.929 | 1 | I | $4762^{*}_{4}$ $9996^{*}_{3}$ | 0 |
| 19103.77 | 5233.140 | 1 | I | $14001^{*}_{6}$ $19235_{6}$ | 2 |
| 19108.70 | 5231.790 | 2 | | | |
| 19116.37 | 5229.691 | 3 | | | |
| 19152.12 | 5219.929 | 1 | I | $14027^{*}_{4}$ $19247_{3}$ | 20 |
| 19161.22 | 5217.450 | 1 | | | |
| 19172.06 | 5214.500 | 3 | I | $8235^{*}_{2}$ $13450^{*}_{3}$ | −38 |
| | | | II | $4511^{*}_{2\,1/2}$ $9725_{3\,1/2}$ | 21 |
| 19189.43 | 5209.780 | 2 | I | $16586^{*}_{5}$ $21796_{6}$ | 33 |
| 19209.30 | 5204.391 | 1 | | | |
| 19219.35 | 5201.669 | 1 | I | $13409^{*}_{3}$ $18611_{3}$ | 15 |
| 19230.18 | 5198.740 | 1 | I | $10409^{*}_{1}$ $15607_{2}$ | 32 |
| 19247.40 | 5194.089 | 2 | I | $12992^{*}_{2}$ $18186^{*}_{3}$ | 44 |
| 19247.88 | 5193.959 | 2 | | | |
| 19262.64 | 5189.979 | 3 | I | $12425^{*}_{4}$ $17615_{4}$ | −15 |
| 19277.87 | 5185.879 | 1 | I | $12600^{*}_{3}$ $17785^{*}_{3}$ | 29 |
| 19279.58 | 5185.419 | 2 | | | |
| 19288.47 | 5183.029 | 3 | I | $15917^{*}_{7}$ $21100_{6}$ | 41 |
| 19304.37 | 5178.760 | 1 | | | |
| 19319.85 | 5174.611 | 1 | | | |
| 19321.94 | 5174.051 | 2 | I | $16067^{*}_{7}$ $21241^{*}_{7}$ | 28 |
| 19330.80 | 5171.680 | 1 | I | $10879^{*}_{5}$ $16051_{4}$ | −4 |
| 19343.44 | 5168.300 | 2 | II | $3363^{*}_{2\,1/2}$ $8531_{3\,1/2}$ | 35 |
| 19355.99 | 5164.949 | 1 | | | |
| 19372.38 | 5160.579 | 1 | I | $13124^{*}_{5}$ $18284^{*}_{5}$ | 6 |
| 19373.43 | 5160.300 | 2 | I | $12351^{*}_{4}$ $17511^{*}_{3}$ | 24 |
| 19422.25 | 5147.329 | 6 | II | $4910^{*}_{5\,1/2}$ $10058_{6\,1/2}$ | 44 |
| 19457.89 | 5137.901 | 4 | II | $1873^{*}_{3\,1/2}$ $7011_{4\,1/2}$ | 24 |
| 19464.86 | 5136.061 | 2 | | | |
| 19467.82 | 5135.280 | 1 | I | $15677^{*}_{7}$ $20812_{7}$ | 23 |
| 19498.35 | 5127.239 | 4 | I | $13605^{*}_{6}$ $18732^{*}_{5}$ | 35 |
| | | | I | $13283^{*}_{3}$ $18411_{4}$ | −41 |
| 19521.15 | 5121.251 | 5 | II | $6638^{*}_{4\,1/2}$ $11759_{5\,1/2}$ | 58 |
| 19527.52 | 5119.580 | 2 | I | $8270^{*}_{3}$ $13389^{*}_{3}$ | 2 |
| 19529.58 | 5119.040 | 1 | I | $7841^{*}_{5}$ $12960_{6}$ | 45 |
| 19551.93 | 5113.189 | 5 | I | $8400^{*}_{5}$ $13513_{4}$ | 44 |
| 19562.25 | 5110.491 | 1 | | | |
| 19565.24 | 5109.710 | 1 | | | |
| 19583.68 | 5104.899 | 1 | I | $12425^{*}_{4}$ $17530_{5}$ | 36 |
| 19586.36 | 5104.200 | 1 | II | $5716^{*}_{3\,1/2}$ $10820_{2\,1/2}$ | −61 |
| 19590.51 | 5103.119 | 3 | II | $3793^{*}_{6\,1/2}$ $8896_{5\,1/2}$ | 15 |
| 19605.53 | 5099.210 | 1 | | | |
| 19616.42 | 5096.379 | 2 | | | |
| 19617.45 | 5096.111 | 2 | I | $10604^{*}_{3}$ $15700_{4}$ | 22 |
| | | | I | $14310^{*}_{2}$ $19406_{3}$ | 30 |
| 19617.96 | 5095.979 | 2 | I | $10243^{*}_{4}$ $15339_{5}$ | 41 |
| 19631.94 | 5092.350 | 2 | I | $12297^{*}_{5}$ $17390_{4}$ | 17 |
| | | | II | $8175^{*}_{2\,1/2}$ $13268_{2\,1/2}$ | 8 |
| 19641.97 | 5089.749 | 2 | I | $13194^{*}_{4}$ $18284^{*}_{5}$ | 15 |
| 19642.93 | 5089.501 | 3 | | | |
| 19650.11 | 5087.641 | 2 | II | $2634^{*}_{2\,1/2}$ $7722_{2\,1/2}$ | 24 |
| 19652.51 | 5087.020 | 2 | II | $8169^{*}_{1\,1/2}$ $13256_{1\,1/2}$ | 16 |
| 19657.53 | 5085.721 | 1 | I | $12425^{*}_{4}$ $17511^{*}_{3}$ | 23 |
| | | | II | $3703^{*}_{3\,1/2}$ $8789_{2\,1/2}$ | −58 |
| 19658.96 | 5085.351 | 2 | I | $14539^{*}_{3}$ $19624^{*}_{3}$ | 15 |
| 19663.95 | 5084.060 | 2 | | | |
| 19669.79 | 5082.551 | 2 | I | $8307^{*}_{3}$ $13389^{*}_{3}$ | 33 |
| 19671.81 | 5082.029 | 1 | | | |
| 19676.37 | 5080.851 | 1 | II | $8175^{*}_{2\,1/2}$ $13256_{1\,1/2}$ | 19 |
| 19695.56 | 5075.901 | 1 | | | |
| 19707.25 | 5072.890 | 1 | I | $11796^{*}_{4}$ $16869_{4}$ | 4 |
| | | | I | $8991^{*}_{5}$ $14064_{4}$ | −40 |
| 19716.31 | 5070.559 | 2 | | | |
| 19722.96 | 5068.849 | 1 | I | $10774^{*}_{3}$ $15843_{4}$ | 5 |
| 19724.55 | 5068.440 | 3 | I | $8055^{*}_{6}$ $13124^{*}_{5}$ | −43 |
| | | | II | $6389^{*}_{4\,1/2}$ $11458_{5\,1/2}$ | 25 |
| 19726.19 | 5068.019 | 2 | I | $14795^{*}_{5}$ $19863^{*}_{5}$ | 1 |
| 19730.78 | 5066.840 | 1 | I | $9996^{*}_{3}$ $15063^{*}_{3}$ | 35 |
| | | | II | $11387^{*}_{3\,1/2}$ $16454_{2\,1/2}$ | 30 |
| 19755.11 | 5060.600 | 1 | I | $15561^{*}_{5}$ $20621^{*}_{4}$ | 20 |
| | | | I | $15644_{6}$ $20705_{6}$ | 8 |
| 19762.80 | 5058.631 | 1 | I | $11810^{*}_{4}$ $16869_{4}$ | 50 |
| 19784.24 | 5053.149 | 1 | I | $11850^{*}_{5}$ $16903^{*}_{5}$ | 21 |
| 19794.42 | 5050.550 | 4 | II | $4266^{*}_{3\,1/2}$ $9316_{3\,1/2}$ | 43 |
| 19799.87 | 5049.160 | 2 | | | |
| 19810.62 | 5046.420 | 2 | I | $11301^{*}_{2}$ $16347_{2}$ | −20 |
| 19815.53 | 5045.169 | 1 | I | $14027^{*}_{4}$ $19072^{*}_{3}$ | −10 |
| 19820.52 | 5043.899 | 1 | II | $3745^{*}_{1\,1/2}$ $8789_{2\,1/2}$ | −2 |
| 19824.88 | 5042.790 | 1 | I | $11545^{*}_{4}$ $16588_{4}$ | −13 |
| 19838.73 | 5039.269 | 2 | I | $14743_{6}$ $19782^{*}_{5}$ | 11 |
| 19858.79 | 5034.179 | 2 | II | $8402^{*}_{3\,1/2}$ $13436_{2\,1/2}$ | 5 |
| 19864.35 | 5032.770 | 1 | I | $4173^{*}_{4}$ $9206^{*}_{3}$ | −40 |
| | | | II | $4165^{*}_{4\,1/2}$ $9198^{*}_{3\,1/2}$ | −3 |
| 19866.72 | 5032.170 | 1 | I | $6238^{*}_{3}$ $11271^{*}_{4}$ | 16 |
| 19877.66 | 5029.400 | 1 | I | $11517^{*}_{1}$ $16546_{0}$ | 26 |
| | | | I | $12022^{*}_{2}$ $17051^{*}_{3}$ | −42 |
| 19887.35 | 5026.950 | 2 | I | $13194^{*}_{4}$ $18221^{*}_{5}$ | 16 |
| 19890.16 | 5026.239 | 2 | I | $13572^{*}_{7}$ $18598_{6}$ | −7 |
| 19895.42 | 5024.911 | 2 | I | $14599^{*}_{4}$ $19624^{*}_{3}$ | −38 |
| 19900.49 | 5023.630 | 1 | I | $10774^{*}_{3}$ $15798^{*}_{3}$ | 9 |
| 19906.91 | 5022.010 | 1 | I | $8762^{*}_{4}$ $13784^{*}_{5}$ | −14 |
| 19941.58 | 5013.279 | 1 | I | $7780_{6}$ $12793^{*}_{5}$ | −22 |
| 19950.17 | 5011.121 | 1 | I | $12720^{*}_{4}$ $17731^{*}_{4}$ | 8 |
| 19954.23 | 5010.101 | 1 | I | $11337^{*}_{3}$ $16347_{2}$ | −17 |
| 19973.01 | 5005.390 | 1 | I | $11061^{*}_{7}$ $16066_{6}$ | 1 |
| 19975.92 | 5004.661 | 2 | I | $8509^{*}_{4}$ $13513_{4}$ | −4 |
| 20007.31 | 4996.809 | 1 | I | $10243^{*}_{4}$ $15240^{*}_{4}$ | −29 |
| 20026.62 | 4991.991 | 2 | I | $16249_{6}$ $21241^{*}_{7}$ | −17 |
| 20028.91 | 4991.420 | 1 | I | $10774^{*}_{3}$ $15766^{*}_{3}$ | −22 |
| 20041.24 | 4988.349 | 3 | II | $4737^{*}_{2\,1/2}$ $9725_{3\,1/2}$ | −9 |
| 20046.18 | 4987.120 | 5 | I | $14027^{*}_{4}$ $19014_{4}$ | −24 |
| | | | II | $5716^{*}_{3\,1/2}$ $10703_{4\,1/2}$ | 32 |

TABLE 1. *Observed infrared cerium lines*—Continued

| Wavelength Å | Wavenumber ($cm^{-1}$) | Intensity | Spectrum | Classification | O−C (.001 $cm^{-1}$) | Wavelength Å | Wavenumber ($cm^{-1}$) | Intensity | Spectrum | Classification | O−C (.001 $cm^{-1}$) |
|---|---|---|---|---|---|---|---|---|---|---|---|
| 20062.96 | 4982.949 | 1 | | | | 20854.19 | 4793.891 | 1 | II | $3995^{\circ}_{3\frac{1}{2}}$ $8789_{2\frac{1}{2}}$ | −23 |
| 20077.14 | 4979.430 | 1 | | | | | | | II | $4523^{\circ}_{4\frac{1}{2}}$ $9316_{3\frac{1}{2}}$ | 20 |
| 20085.04 | 4977.471 | 2 | I | $10723^{\circ}_{4}$ $15700_{4}$ | 5 | 20859.42 | 4792.689 | 1 | I | $8991^{\circ}_{5}$ $13784_{5}$ | −10 |
| | | | I | $13450^{\circ}_{3}$ $18427_{3}$ | 3 | 20876.62 | 4788.740 | 1 | | | |
| 20091.66 | 4975.831 | 1 | | | | 20933.10 | 4775.820 | 1 | | | |
| 20093.08 | 4975.479 | 1 | I | $13219^{\circ}_{6}$ $18194_{5}$ | −21 | 20950.91 | 4771.760 | 1 | I | $12366_{5}$ $17138_{6}$ | 7 |
| 20136.95 | 4964.640 | 1 | I | $9830^{\circ}_{6}$ $14795_{5}$ | −41 | 20962.55 | 4769.110 | 1 | I | $12351^{\circ}_{4}$ $17120_{5}$ | 28 |
| 20140.85 | 4963.679 | 2 | I | $10879^{\circ}_{5}$ $15843_{4}$ | 23 | 20976.98 | 4765.830 | 1 | I | $7348^{\circ}_{4}$ $12114_{4}$ | 14 |
| 20157.82 | 4959.500 | 5 | I | $1279^{\circ}_{4}$ $6238_{5}$ | −9 | 20979.88 | 4765.171 | 1 | I | $10879^{\circ}_{5}$ $15644_{6}$ | 21 |
| 20204.34 | 4948.081 | 2 | I | $13784_{5}$ $18732^{\circ}_{5}$ | 28 | 20990.50 | 4762.760 | 5 | I | $0^{\circ}_{4}$ $4762_{4}$ | 42 |
| 20235.63 | 4940.430 | 1 | | | | 21000.33 | 4760.530 | 1 | II | $5942^{\circ}_{3\frac{1}{2}}$ $10703_{4\frac{1}{2}}$ | 26 |
| 20248.09 | 4937.390 | 3 | I | $9709^{\circ}_{2}$ $14646_{2}$ | −42 | 21003.69 | 4759.769 | 1 | I | $14920^{\circ}_{4}$ $19680_{4}$ | −46 |
| | | | I | $12454^{\circ}_{2}$ $17391_{1}$ | 17 | | | | II | $2581^{\circ}_{4\frac{1}{2}}$ $7341_{5\frac{1}{2}}$ | 22 |
| | | | II | $7011_{4\frac{1}{2}}$ $11949^{\circ}_{3\frac{1}{2}}$ | 8 | 21027.85 | 4754.300 | 1 | | | |
| 20252.31 | 4936.361 | 1 | I | $12793^{\circ}_{5}$ $17729_{5}$ | −9 | 21037.98 | 4752.011 | 1 | I | $9787^{\circ}_{3}$ $14539_{3}$ | 19 |
| 20269.68 | 4932.131 | 2 | | | | 21056.99 | 4747.721 | 1 | | | |
| 20280.83 | 4929.419 | 1 | I | $11271^{\circ}_{4}$ $16200_{3}$ | 14 | 21068.98 | 4745.019 | 1 | I | $10318^{\circ}_{3}$ $15063_{3}$ | 5 |
| | | | I | $14417^{\circ}_{4}$ $19347_{5}$ | −32 | | | | II | $3703^{\circ}_{3\frac{1}{2}}$ $8448_{2\frac{1}{2}}$ | −24 |
| 20283.99 | 4928.651 | 1 | | | | 21091.29 | 4740.000 | 2 | I | $6621^{\circ}_{3}$ $11361_{4}$ | −2 |
| 20289.26 | 4927.371 | 1 | | | | 21103.58 | 4737.239 | 2 | I | $12793^{\circ}_{5}$ $17530_{5}$ | −17 |
| 20292.15 | 4926.669 | 2 | II | $5942^{\circ}_{3\frac{1}{2}}$ $10869_{4\frac{1}{2}}$ | −70 | 21172.63 | 4721.790 | 1 | I | $11626^{\circ}_{1}$ $16347_{2}$ | 5 |
| 20293.51 | 4926.339 | 2 | I | $10774^{\circ}_{3}$ $15700_{4}$ | −33 | | | | I | $13283^{\circ}_{3}$ $18005_{3}$ | 27 |
| | | | I | $17138^{\circ}_{6}$ $22064_{6}$ | −39 | 21199.34 | 4715.841 | 2 | I | $11301^{\circ}_{2}$ $16017_{3}$ | 20 |
| 20325.11 | 4918.680 | 3 | I | $13124_{5}$ $18042^{\circ}_{4}$ | 16 | 21203.57 | 4714.900 | 2 | II | $5010^{\circ}_{2\frac{1}{2}}$ $9725_{3\frac{1}{2}}$ | 33 |
| 20357.85 | 4910.769 | 2 | I | $14599_{4}$ $19510^{\circ}_{4}$ | 35 | 21221.98 | 4710.810 | 1 | I | $9425^{\circ}_{2}$ $14136_{3}$ | 17 |
| 20366.23 | 4908.749 | 1 | | | | 21225.31 | 4710.071 | 2 | II | $2382^{\circ}_{4\frac{1}{2}}$ $7092_{5\frac{1}{2}}$ | 43 |
| 20368.26 | 4908.260 | 1 | I | $11626^{\circ}_{1}$ $16534_{2}$ | 2 | 21234.96 | 4707.930 | 1 | I | $13513_{4}$ $18221^{\circ}_{5}$ | 22 |
| 20383.13 | 4904.679 | 2 | I | $12988^{\circ}_{4}$ $17892_{4}$ | 5 | 21268.98 | 4700.400 | 3 | II | $7059^{\circ}_{4\frac{1}{2}}$ $11759_{5\frac{1}{2}}$ | 23 |
| | | | II | $5964^{\circ}_{3\frac{1}{2}}$ $10869_{4\frac{1}{2}}$ | 34 | 21269.98 | 4700.179 | 1 | I | $12948^{\circ}_{5}$ $17649_{6}$ | 44 |
| 20388.61 | 4903.361 | 1 | | | | 21303.52 | 4692.779 | 1 | II | $4203^{\circ}_{6\frac{1}{2}}$ $8896_{5\frac{1}{2}}$ | −18 |
| 20417.97 | 4896.310 | 1 | II | $5924^{\circ}_{4\frac{1}{2}}$ $10820_{5\frac{1}{2}}$ | 37 | 21334.52 | 4685.960 | 1 | I | $10901^{\circ}_{2}$ $15587_{2}$ | 4 |
| 20454.61 | 4887.539 | 1 | I | $8307^{\circ}_{3}$ $13194_{4}$ | 0 | 21363.56 | 4679.590 | 1 | I | $13605^{\circ}_{6}$ $18284_{5}$ | 7 |
| | | | I | $10673^{\circ}_{6}$ $15561_{5}$ | 40 | 21417.29 | 4667.851 | 2 | I | $14064_{4}$ $18732^{\circ}_{5}$ | 29 |
| 20479.20 | 4881.671 | 1 | | | | 21435.94 | 4663.789 | 1 | I | $14310^{\circ}_{2}$ $18973_{1}$ | −10 |
| 20499.78 | 4876.770 | 3 | I | $13044^{\circ}_{4}$ $17921_{3}$ | −22 | | | | II | $9723^{\circ}_{4\frac{1}{2}}$ $14387_{4\frac{1}{2}}$ | 11 |
| | | | I | $13815^{\circ}_{4}$ $18692_{4}$ | −26 | 21440.35 | 4662.830 | 1 | II | $5651^{\circ}_{5\frac{1}{2}}$ $10314_{4\frac{1}{2}}$ | 21 |
| | | | II | $5437_{3\frac{1}{2}}$ $10314_{4\frac{1}{2}}$ | 19 | 21486.20 | 4652.880 | 3 | I | $13389_{3}$ $18042^{\circ}_{4}$ | 33 |
| 20512.31 | 4873.791 | 2 | | | | 21521.22 | 4645.309 | 1 | | | |
| 20515.47 | 4873.040 | 1 | | | | 21553.09 | 4638.440 | 2 | II | $5675^{\circ}_{4\frac{1}{2}}$ $10314_{4\frac{1}{2}}$ | 32 |
| 20548.83 | 4865.129 | 2 | I | $13297^{\circ}_{5}$ $18162_{4}$ | 30 | 21592.15 | 4630.049 | 2 | II | $3793^{\circ}_{6\frac{1}{2}}$ $8423_{6\frac{1}{2}}$ | −2 |
| 20553.18 | 4864.099 | 1 | I | $10901^{\circ}_{2}$ $15766_{3}$ | 22 | 21594.43 | 4629.560 | 2 | II | $2382^{\circ}_{4\frac{1}{2}}$ $7011_{4\frac{1}{2}}$ | −10 |
| 20560.74 | 4862.311 | 1 | | | | 21596.30 | 4629.159 | 2 | II | $987^{\circ}_{4\frac{1}{2}}$ $5616_{4\frac{1}{2}}$ | 28 |
| 20609.62 | 4850.779 | 1 | I | $13881^{\circ}_{5}$ $18732^{\circ}_{5}$ | 19 | 21621.99 | 4623.659 | 1 | I | $12366_{5}$ $16990^{\circ}_{6}$ | 12 |
| | | | I | $13939_{6}$ $18790^{\circ}_{5}$ | −32 | | | | I | $12720^{\circ}_{4}$ $17343_{5}$ | 40 |
| 20615.18 | 4849.471 | 1 | | | | 21663.50 | 4614.800 | 1 | I | $8509^{\circ}_{4}$ $13124_{5}$ | 0 |
| 20619.35 | 4848.490 | 1 | I | $12454^{\circ}_{2}$ $17302_{3}$ | 33 | 21674.49 | 4612.460 | 1 | I | $14064_{4}$ $18676^{\circ}_{4}$ | 16 |
| | | | I | $13044_{4}$ $17892_{4}$ | −29 | 21700.46 | 4606.940 | 1 | II | $5118^{\circ}_{2\frac{1}{2}}$ $9725_{3\frac{1}{2}}$ | 14 |
| 20622.20 | 4847.820 | 1 | I | $13194_{4}$ $18042^{\circ}_{4}$ | −4 | 21706.40 | 4605.679 | 1 | II | $9053_{3\frac{1}{2}}$ $13659^{\circ}_{4\frac{1}{2}}$ | −18 |
| 20629.09 | 4846.201 | 3 | I | $13519^{\circ}_{5}$ $18365_{5}$ | −46 | 21721.91 | 4602.391 | 1 | II | $5455^{\circ}_{5\frac{1}{2}}$ $10058_{6\frac{1}{2}}$ | −6 |
| 20635.57 | 4844.679 | 1 | I | $13297_{5}$ $18141_{4}$ | 43 | 21742.70 | 4597.990 | 1 | II | $5716^{\circ}_{3\frac{1}{2}}$ $10314_{4\frac{1}{2}}$ | 40 |
| 20642.08 | 4843.151 | 2 | | | | 21781.54 | 4589.791 | 1 | II | $10035^{\circ}_{5\frac{1}{2}}$ $14625_{5\frac{1}{2}}$ | −4 |
| 20690.57 | 4831.801 | 1 | | | | 21789.76 | 4588.059 | 1 | I | $11357^{\circ}_{5}$ $15945_{4}$ | −15 |
| 20698.93 | 4829.849 | 1 | I | $14001^{\circ}_{6}$ $18831_{5}$ | 27 | 21811.91 | 4583.400 | 3 | I | $11061^{\circ}_{7}$ $15644_{6}$ | 8 |
| 20706.52 | 4828.079 | 2 | II | $3703^{\circ}_{3\frac{1}{2}}$ $8531_{3\frac{1}{2}}$ | −16 | 21830.20 | 4579.560 | 1 | II | $4737^{\circ}_{2\frac{1}{2}}$ $9316_{3\frac{1}{2}}$ | 34 |
| 20711.19 | 4826.990 | 1 | II | $5819^{\circ}_{4\frac{1}{2}}$ $10646_{5\frac{1}{2}}$ | 35 | 21864.43 | 4572.391 | 1 | I | $11271^{\circ}_{4}$ $15843_{4}$ | 30 |
| 20716.43 | 4825.769 | 1 | I | $15879_{5}$ $20705^{\circ}_{6}$ | 12 | 21877.64 | 4569.630 | 2 | I | $3210^{\circ}_{5}$ $7780_{6}$ | 11 |
| 20740.75 | 4820.111 | 4 | II | $6638^{\circ}_{4\frac{1}{2}}$ $11458_{5\frac{1}{2}}$ | 10 | 21980.48 | 4548.250 | 2 | I | $9333^{\circ}_{6}$ $13881_{5}$ | 28 |
| 20742.60 | 4819.681 | 2 | I | $10243_{4}$ $15063_{3}$ | 9 | 21996.05 | 4545.030 | 1 | I | $14116^{\circ}_{4}$ $18661_{5}$ | −43 |
| 20745.01 | 4819.121 | 1 | I | $11874^{\circ}_{3}$ $16693_{4}$ | −14 | | | | II | $6913^{\circ}_{6\frac{1}{2}}$ $11458_{5\frac{1}{2}}$ | 63 |
| 20753.80 | 4817.080 | 2 | I | $12600^{\circ}_{3}$ $17417_{2}$ | 17 | 22033.43 | 4537.320 | 2 | II | $3593^{\circ}_{4\frac{1}{2}}$ $8131_{4\frac{1}{2}}$ | −13 |
| 20769.80 | 4813.369 | 1 | I | $10774^{\circ}_{3}$ $15587_{2}$ | 47 | 22073.61 | 4529.060 | 1 | II | $2563^{\circ}_{5\frac{1}{2}}$ $7092_{5\frac{1}{2}}$ | 24 |
| | | | I | $11131^{\circ}_{3}$ $15945_{4}$ | −31 | 22087.95 | 4526.120 | 1 | I | $13089^{\circ}_{3}$ $17615_{4}$ | 25 |
| 20814.51 | 4803.030 | 1 | I | $13089^{\circ}_{3}$ $17892_{4}$ | 14 | | | | II | $987^{\circ}_{4\frac{1}{2}}$ $5513_{5\frac{1}{2}}$ | 20 |
| | | | II | $11742_{5\frac{1}{2}}$ $16545_{5\frac{1}{2}}$ | 15 | 22092.83 | 4525.120 | 2 | I | $3710^{\circ}_{1}$ $8235_{2}$ | 28 |

TABLE 1. *Observed infrared cerium lines*—Continued

| Wavelength Å | Wavenumber ($cm^{-1}$) | Intensity | Spectrum | Classification | O−C (.001 $cm^{-1}$) | Wavelength Å | Wavenumber ($cm^{-1}$) | Intensity | Spectrum | Classification | O−C (.001 $cm^{-1}$) |
|---|---|---|---|---|---|---|---|---|---|---|---|
| 22104.70 | 4522.690 | 2 | I | $12467_5$ $16990^*_6$ | 36 | 22790.27 | 4386.640 | 1 | I | $15396_6$ $19782^*_5$ | 41 |
| 22131.91 | 4517.130 | 1 | I | $10723^*_4$ $15240_4$ | 23 | 22846.10 | 4375.920 | 1 | I | $10901^*_2$ $15277_3$ | 39 |
| 22185.05 | 4506.310 | 1 | I | $17289_6$ $21796^*_6$ | 18 | | | | II | $7011_{4½}$ $11387^*_{3½}$ | −1 |
| 22240.43 | 4495.089 | 1 | II | $5819^*_{4½}$ $10314_{4½}$ | 37 | 22857.28 | 4373.780 | 2 | | | |
| 22277.65 | 4487.579 | 1 | | | | 22864.13 | 4372.470 | 2 | I | $5006^*_3$ $9379_4$ | 41 |
| 22293.19 | 4484.451 | 1 | II | $3793^*_{5½}$ $8278_{5½}$ | 12 | 22869.62 | 4371.420 | 2 | II | $5942^*_{3½}$ $10314_{4½}$ | 54 |
| 22331.64 | 4476.730 | 1 | I | $10586^*_4$ $15063_3$ | 50 | 22909.71 | 4363.770 | 1 | I | $14001^*_6$ $18365_5$ | 6 |
| 22346.56 | 4473.741 | 1 | II | $8278_{5½}$ $12751^*_{5½}$ | 5 | 23146.60 | 4319.110 | 2 | I | $13451^*_1$ $17770_2$ | 22 |
| 22356.91 | 4471.670 | 1 | II | $11387^*_{3½}$ $15859_{4½}$ | 44 | 23216.64 | 4306.080 | 2 | II | $5010^*_{2½}$ $9316_{3½}$ | 46 |
| 22404.16 | 4462.239 | 1 | II | $9053_{3½}$ $13515^*_{3½}$ | 23 | 23339.24 | 4283.461 | 1 | | | |
| 22408.57 | 4461.361 | 1 | II | $2879^*_{5½}$ $7341_{5½}$ | 41 | 23541.05 | 4246.740 | 2 | II | $4201^*_{1½}$ $8448_{2½}$ | 0 |
| 22460.88 | 4450.971 | 2 | I | $9333^*_6$ $13784_5$ | 42 | 23620.25 | 4232.500 | 1 | I | $15277_3$ $19510^*_4$ | 20 |
| 22481.24 | 4446.940 | 1 | | | | 23640.92 | 4228.800 | 1 | | | |
| 22500.01 | 4443.230 | 1 | I | $14218^*_6$ $18661_5$ | 24 | 23663.36 | 4224.790 | 2 | II | $7233^*_{5½}$ $11458_{5½}$ | 56 |
| 22516.38 | 4439.999 | 2 | I | $4766^*_2$ $9206_3$ | 18 | 23766.36 | 4206.480 | 1 | II | $1410^*_{4½}$ $5616_{4½}$ | 39 |
| 22586.53 | 4426.210 | 1 | I | $12720^*_4$ $17146_3$ | 17 | 23853.80 | 4191.060 | 1 | | | |
| 22685.24 | 4406.950 | 1 | II | $5651^*_{5½}$ $10058_{6½}$ | 68 | 23855.45 | 4190.771 | 1 | I | $9379_4$ $13569^*_4$ | −40 |
| 22714.41 | 4401.290 | 2 | II | $7341_{5½}$ $11742^*_{5½}$ | 47 | 23999.65 | 4165.591 | 2 | II | $0^*_{3½}$ $4165_{4½}$ | 38 |
| 22724.58 | 4399.321 | 2 | I | $11850^*_5$ $16249_6$ | −27 | 24172.58 | 4135.790 | 1 | II | $3995^*_{3½}$ $8131_{4½}$ | 43 |
| | | | II | $7059^*_{4½}$ $11458_{5½}$ | 36 | 24230.41 | 4125.919 | 1 | II | $4322^*_{2½}$ $8448_{2½}$ | −7 |
| 22738.54 | 4396.620 | 2 | II | $6913^*_{6½}$ $11309_{7½}$ | 40 | | | | | | |

We thank Jack L. Tech for help with the Univac 1108 computer programs and Ruth L. Peterson for help with punched cards.

## 4. References

Albertson, W. E., and Harrison, G. R. (1937), Phys. Rev. **52**, 1209.
Corliss, C. H. (1971), unpublished.
Corliss, C. H., Bozman, W. R., and Westfall, F. O. (1953), J. Opt. Soc. Am. **43**, 398.
Goldschmidt, Z. B. (1968), Ph.D. Thesis, Hebrew Univ. of Jerusalem.
Harrison, G. R., Albertson, W. E., and Hosford, N. F. (1941), J. Opt. Soc. Am. **31**, 439.
Martin, W. C. (1963), J. Opt. Soc. Am. **53**, 1047.
Martin, W. C. (1971), Phys. Rev. **A3**, 1810.
Racah, G. (1955), Bull. Res. Council Israel, **5A**, 78.
Verges, J. (1969), Spectrochimica Acta **24B**, 177.

(Paper 76A3−722)

JOURNAL OF RESEARCH of the National Bureau of Standards—A. Physics and Chemistry
Vol. 76A, No. 3, May–June 1972

# Publications of the National Bureau of Standards*

## Selected Abstracts

Ambler, E., **Measurement standards, physical constants, and science teaching,** *Sci. Teacher* **38,** *No. 8, 63–71 (Nov. 1971).*

Key words: Measurement standards; physical constants; science teaching.

Man's intuitive ability to perceive and recognize such concepts as temperature and distance is well-developed even before his formal education begins. The inherited internal measurement, or sensory, systems are extremely sensitive and lead to a direct awareness and comprehension of the physical world in ways we do not yet completely understand. Man's need to measure and quantify more formally and less intuitively goes back as far as recorded history itself.

Barnes, I. L., Sappenfield, K. M., Shields, W. R., **The mass spectrometric analysis of subpicogram quantities of lead** *(Proc. Int. Conf. Mass Spectroscopy, Kyoto, Japan, 1970), Chapter in Recent Developments in Mass Spectroscopy, K. Ogata and T. Hayakawa, Ed., pp. 682–687 (University of Tokyo Press, Tokyo, Japan, 1970).*

Key words: Lead; mass spectrometer; microsample.

An analytical method has been developed which gives stable measurable ion beams from samples containing $10^{-8}$ to $10^{-14}$ grams of lead.
Using a two stage twelve inch radius mass spectrometer equipped with an ion multiplier and electronics for fast pulse counting, a series of chemical microstandards loaded with known quantities of NBS standard lead samples (as small as $10^{-14}$ grams of lead) were analyzed. These analyses showed that accuracy and precision of better than 0.5 percent (95% L. E. for a single analyses) could be obtained and that usually, the accuracy and precision were limited only by random counting statistics.
A series of quantitative analyses were done with two microgram or smaller samples taken from a single wafer of a silicate glass of known composition by the method of isotopic dilution. The required "spiking" of the sample was done utilizing an NBS Microstandard Ion Exchange Bead loaded with lead of known weight and composition.
The results obtained show severe cross-sectional variations of lead in the sample and demonstrate the importance of careful handling of samples for trace element analysis.
The use of the technique for the direct analyses of small crystals and/or particles is described. In this use only minimal chemical treatment is necessary thus eliminating most, if not all, of the usual sources of contamination and all chemical treatment may be performed directly on the mass spectrometer filament.

Bederson, B., Kieffer, L. J., **Total electron-atom collision cross sections at low energies—A critical review,** *Rev. Mod. Phys.* **43,** *No. 4, 601–641 (Oct. 1971).*

Key words: Critical review; cross-section measurement electron-atom collisions; total cross-section data.

The techniques for making total electron atom (molecule) cross section measurements are critically reviewed. Defects in the various techniques are pointed out. Three techniques are singled out as meeting minimum criteria of reliability. These techniques are extensively discussed and comparisons made between cross section data obtained from them. In particular a careful comparison is made of the data for helium. This atom is considered because there are many measurements and a large number of calculations. At low energies only elastic scattering takes place and theory and experiment can be directly compared. The agreement between theory and experiment is about 10% and this is the best case.

Bennett, L. H., Carter, G. C., **Enhanced lever rule for high-precision phase diagram determination,** *Met. Trans.* **2,** *3079–3081 (Nov. 1971).*

Key words: Alloys; high-precision; lever rule; nuclear magnetic resonance; phase diagrams.

A description is given of the conditions under which high-precision phase boundary determinations result from the application of the lever rule. This high precision results from a multiplication factor to the lever rule ratio, which is present only for experiments sampling one elemental site at a time. The multiplication factor is larger for smaller solubility limits. Precision of tenths of a percent can be readily attained under the indicated conditions. An example involving the $^{115}In$ nuclear magnetic resonance for the determination of the solubility of $AuIn_2$ in $AuAl_2$ is presented.

Blaine, R. L., Arni, H. T., **Interrelations between cement and concrete properties, Part 5,** *Nat. Bur. Stand. (U.S.), Bldg. Sci. Ser. 35, 129 pages (Nov. 1971) $1.25, SD Catalog No. C13.29/2:35.*

Key words: Absorption; autogenous healing; durability factor; dynamic modulus of elesticity; saturation coefficient.

The concretes described in earlier parts of this series were subjected to laboratory freezing and thawing tests, and measurements were made of the weight loss, dynamic modulus, durability factor, and number of cycles required to reach 40 percent reduction in dynamic modulus. Companion specimens were subjected to drying and subsequent soaking in the laboratory and to dynamic modulus tests at various ages and moisture conditions. The effect on these properties of a large number of variables connected with chemical and physical properties of the cements and with properties of the concretes was studied by multivariable regression techniques. Air content of the concretes and degree of saturation generally had the greatest effect on the measurements. In general, minor constituents and trace elements did not show significant relationships with the measured properties, but there was evidence that some of the variables, such as alkali content, water cement ratio, slump, and possibly setting time might have influenced durability through an effect on the air-void system. Specimens stored in the fog room after the freezing-and-thawing tests generally regained most or all of their original dynamic modulus. There were significant differences between cements with respect to regain of dynamic modulus (autogenous healing), with the non-air-entrained cements gaining more than the air-entraining cements, on the average.

Blandford, J. M., Baker, H. A., **Sewing threads for the apparel industry,** *Apparel Research Foundation, Inc., Washington, D.C., pp. 1–153 (May 15, 1971).*

Key words: Apparel industry; industry, apparel; performance, sewing thread; properties, sewing thread; quality control, sewing threads; sewing threads; testing programs, sewing threads; tests, sewing thread; thread properties; threads, sewing.

The objectives, development, and achievements of the National Bureau of Standards (NBS) Sewing Thread Project, carried out in

collaboration with The Apparel Research Foundation, Inc. (ARF) are discussed.
The results of two questionnaire surveys conducted among thread and apparel companies are summarized, as are the opinions expressed by thread and apparel manufacturers on industry-wide adoption of a uniform thread-sizing system.
Included are tabulations, graphs, and a statistical analysis of NBS tests of threads representative of those currently used by the apparel industry: soft and mercerized cotton; core and spun polyester; and nylon.
Testing programs for evaluating 1) the quality of threads purchased by the apparel manufacturer, and 2) the performance of threads in the apparel product, are discussed in detail. The following information is tabulated: testing procedures and evaluation materials employed: and sources of supply and approximate prices of the equipment and evaluation materials. Supplementing the test are reprints of the 21 referenced test methods.

Blandford, J. M., Bensing, P. L., **Testing programs for the apparel industry. Evaluation of material and components—Parts I and II,** *Part I, 35 pages (2nd ed. May 15, 1971); Part II, 249 pages (May 15, 1971).*

Key words: Apparel industry: equipment, textile testing; industry, apparel: performance, apparel materials; properties, apparel; quality control, apparel industry; testing programs, apparel industry; test methods, textile; textile testing, apparel materials.

This publication presents the details of minimum, intermediate, and advanced textile testing programs for evaluating the appearance and performance of materials and components used by the apparel industries. Tabulations give testing equipment, properties its use may determine, testing procedures and evaluation materials employed, and sources of supply and approximate prices of the equipment and evaluation materials.
Included are: 1) sections on the significance of a textile testing program, conditioning for testing textiles, performance requirements for textile fabrics (American National Standard L22), evaluation of fabric defects, and the availability of short laboratory training courses for apparel company employees; 2) bibliography; 3) reprints of the sixty-eight referenced test methods.

Bardy, R. F., Jr., **Enolization of hexodiulose acetals. Synthesis of derivatives of D-psicose by reduction of a hex-3-enulopyranose,** *Carbohydrate Res.* **20,** *170–175 (Nov. 1971).*

Key words: Cyclic acetals; hex-3-enulopyranose; hexodiulose; hexulose; psicose; stereospecific reduction; tagatose.

1,2:4,5-Di-*O*-isopropylidene-β-D-*erythro*-2,3-hexodiulo-2,6-pyranose is converted by an acetic anhydride-triethylamine reagent into a crystalline 3,4-enediol acetate, namely, 3-*O*-acetyl-1,2:4,5-di-*O*-isopropylidene-β-D-*glycero*-hex-3-enulopyranose (2). Reduction of diacetal **2** with hydrogen over a palladium catalyst is stereospecific, and affords only 3-*O*-acetyl-1,2:4,5-di-*O*-isopropylidene-β-D-psicopyranose.

Brandenberger, H., Hadron, F., Halford, D., Shoaf, J. H., **High quality quartz crystal oscillators: Frequency domain and time domain stability,** *Proc. 25th Frequency Control Annual Symp. Atlantic City, N.J., April 26–28, 1971, pp. 226–234 (Electronic Industries Association, Washington, D.C., April 1971).*

Key words: Allan variance; flicker of phase noise; frequency stability; oscillator noise models; phase noise spectral density; quartz crystal oscillator; time domain stability.

We measured the frequency stability of a pair of commercial 5-MHz quartz crystal oscillators which incorporate improved electronic design for enhanced short-term stability. The spectral density (frequency domain) of the phase noise, per oscillator, measured by each of our two laboratories, is

$$S_{\delta\phi} = + (10^{-11.8}\ \text{radians}^2\ \text{Hz}^2)\ \frac{1}{f^3} + (10^{-12.5}\ \text{radians}^2)\ \frac{1}{f} + (10^{-14.4}\ \text{radians}^2\ \text{Hz}^{-1})f^0,$$

over the range of about $10^{-2}$ Hz to $10^{+3}$ Hz.

Brauer, G. M., **A review of recent studies of *In Vitro* reactivity of surfaces of calcified tissues,** *(Proc. Int. Symp. Calcified Tissues, Dental and Surgical Materials and Tissue Material Interactions, University of Nijmegen, Nijmegen, The Netherlands, 1970), Dent. Tissues Mater. pp. 193–231 (1971).*

Key words: Adhesion to tooth surfaces; adsorption on calcified tissues; bone; calcified tissues; dentin; enamel; modification of tooth surfaces; reactivity of calcified tissues.

Studies of the reactivity and modification of the surfaces of calcified tissues offer an attractive approach for obtaining useful information to reduce dental caries and improve adhesion between tooth structure and restoratives. Investigation of the interaction of gases on such surfaces provides considerable insight into the structural details of surfaces of hard tissues. Effectiveness of potential conditioning agents can be demonstrated from alterations of the surface properties of teeth or bone as indicated by changes in: critical surface tension, oil-wettability, adsorption isotherms and adhesionability. Measurement and evaluation of heats of immersion and heats of reaction are useful for observing modifications and determining those groups that bond to tooth structure in aqueous environments. Application of dilute polyfunctional acids removes debris, etches enamel and increases surface wettability. Etching creates an increased surface area and opens pores into which resin can flow. Excellent adhesion is obtained after hardening because of mechanical interlocking of resin at the enamel-resin interphase. Long side chains have been grafted to collagenous surfaces (collagen powder or film, bone). Grafting monomers containing additional functional groups that are potential reactive centers for further modification is feasible. Surfaces with the desired degree of hydrophil-lipophil balance to suit specific applications can be prepared.

Breden, L. H., Editor, **World index of plastics standards,** *Nat. Bur. Stand. (U.S.), Spec. Publ. 352, 458 pages (Dec. 1971) $5.50, SD Catalog No. C13.10:352.*

Key words: Index of plastics standards; plastics standards, world index; standards, plastics.

This computer-produced Index contains the printed titles of more than 9,000 national and international standards on plastics and related materials which were in effect as of December 31, 1970. These standards are published by technical societies, trade associations, government agencies and military organizations. The title of each standard can be found under all the significant key words which it contains. These key words are arranged alphabetically down the center of each page together with their surrounding context. The date of publication or last revision, the standard number, and an acronym designating the standard-issuing organization appear as part of each entry. A list of these acronyms and the names and addresses of the organizatons which they represent are found at the beginning of the World Index.

Brown, D. W., Lowry, R. E., Wall, L. O., **Radiation-induced polymerization at high pressure of 2,3,3,3-tetrafluoropropene in bulk and with tetrafluoroethylene,** *J. Polymer Sci: Part A-1,* **9,** *1999–2007 (1971).*

Key words: High pressure; polymerization; radiation; tetrafluoroethylene; tetrafluoropropene.

The radiation-induced polymerization of 2,3,3,3-tetrafluoropropene was studied as a function of temperature (22–100 °C) and pressure (autogenous to $10^4$ atm). Rates have varied 100 fold for the same reaction conditions probably because of trace impurities. The most rapidly polymerizing material has a rate of 4.5%/hr at 6000 atm, 22 °C, and 1500rad/hr. The activation enthalpy and volume are 4kcal/mole and 13cc/mole, respectively. Rates are proportional to the square root of the radiation intensity. Decrees of polymerization varied between $2 \times 10^3$ and $2 \times 10^6$. In copolymerization with tetrafluoroethylene the reactivity ratios at 22 °C and 5000 atm are 0.37 (the ratio for addition to the tetrafluoroethylene-ended radical) and 5.4 (the ratio for addition to the tetrafluoropropene-ended radical). Comparison of ratios for the copolymerization of other

fluorine-containing monomers with tetrafluoroethylene shows that they generally disfavor incorporation of the latter.

Brown, W. E., **Physicochemical aspects of decay and decalcification,** (*Proc. Int. Symp. Calcified Tissues, Dental and Surgical Materials and Tissue Material Interactions, University of Nijmegen, Nijmegen, The Netherlands, 1970*), *Dent. Tissues Mater. pp. 69–97 (1971).*

Key words: Calcium phosphate; caries; caries mechanism; enamel; hydroxyapatite.

Standard thermodynamic concepts (chemical components, chemical potentials and phase diagrams) were used to evaluate equilibrium and steady-state models for the caries mechanism. The chemical potential of the acid responsible for dissolution is a variable that ranks in importance with pH and needs to be given far greater consideration. Another variable of great value is $U(\pm)$ which is a measure of excess base over acid in the solution, and is defined by $U(\pm)\Sigma_j c_j z_j = -\Sigma_i c_i z_i$, where $i$ is summed over the ions present in the system $Ca(OH)_2 - H_3PO_4 - H_2O$ and $j$ is summed over the ions foreign to this system.
Variability in the solubility of tooth mineral is a major factor in causing the extended form of the caries lesion. A possibly very important factor in determining the speed with which the lesion develops is the relative rate of transport of calcium ions relative to that of the phosphate ions. An unequivocal interpretation of the Donnan-membrane effect, described by von Barthold, is not possible because even though the pH within the tooth may be tooth mineral, solubility.

Bullis, W. M., Editor, **Methods of measurement for semiconductor materials, process control, and devices,** *Quarterly Report—April to June 30, 1971, Nat. Bur. Stand. (U.S.), Tech. Note 702, 45 pages (Dec. 1971) 50 cents, SD Catalog No. C13.46:702.*

Key words: Alpha-particle detectors; aluminum wire; base transit time; carrier lifetime; die attachment; electrical properties; epitaxial silicon; gamma-ray detectors; germanium; gold-doped silicon; methods of measurement; microelectronics; microwave devices; nuclear radiation detectors; probe techniques (a–c); resistivity; semiconductor devices; semiconductor materials; semiconductor process control; silicon; thermal resistance; thermographic measurements; ultrasonic bonder; wire bonds.

This quarterly progress report, twelfth of a series, describes NBS activities directed toward the development of methods of measurement for semiconductor materials, process control, and devices. Significant accomplishments during this reporting period include a demonstration of the high sensitivity of the infrared response technique by the identification of gold in a germanium diode doped to a level of $10^{11}$ gold atoms per cubic centimeter, verification that transient thermal response is significantly more sensitive to the presence of voids in die attachment than steady-state thermal resistance, and development of a simplified circuit for screening transistors for susceptibility to hot-spot formation by the current-gain technique. Work is continuing on measurement of resistivity of semiconductor crystals; study of gold-doped silicon; specification of germanium for gamma-ray detectors; evaluation of wire bonds and die attachment; measurement of thermal properties of semiconductor devices, transit time and related carrier transport properties in junction devices, and electrical properties of microwave devices; and characterization of silicon nuclear radiation detectors. Supplementary data concerning staff, standards committee activities, technical services, and publications are included as appendixes.

Burdick, M. D., **A test for the cleanability of surface finishes,** *Porcelain Enamel Inst. Bull.* **T-28,** *pp. 1–17 (1971).*

Key words: Cleanability; cleanability index; fluorescence; porcelain enamel; standard reference surface.

A detailed procedure is given to permit a numerical evaluation of the cleanability of surfaces. The method employes a fluorescent, water soluble soiling agent, a mechanized procedure for its application and partial removal, the water extraction of the retained soil and the calculation of a cleanability index through the use of a standard reference surface.

Clifton, J. R., **The infrared spectra of supposed α and β forms of calcium sulphate hemihydrate,** *Nature (London), Phys. Sci.* **232,** *No. 32, 125–126 (August 9, 1971).*

*Key words:* $-CaS04.11/2H_2O$; $CaS04 \cdot 1/2H_2O$; gypsum; infrared spectra; lattice water.

The infrared absorption spectra of supposed and forms of calcium sulfate hemihydrate were measured from 580 to 4000 $cm^{-1}$, using doped potassium bromide pellets and mineral oil mulls.

It was impossible to differentiate between the two supposed forms of calcium sulfate hemihydrate because their infrared spectra were closely similar. The spectra of the supposed forms dispersed in potassium bromide consisted of 13 absorptions and the maximum difference in position between analogous bands of the two spectra was 5 $cm^{-1}$, while 8 absorptions had identical frequencies. Both supposed forms gave the same spectral features when made into mineral mulls.
Because of the high frequencies of 1 ($H_2O$), 3528 $cm^{-1}$, and 3 ($H_2O$), 3604 $cm^{-1}$, for calcium sulfate hemihydrate, it has been proposed that the water molecules are only interstitially held in the hemihydrate.

Cooper, M. J., **Generalized scaling and the parametric equation of state in the critical region,** *Chapter in Critical Phenomena in Alloys, Magnets, and Superconductors, pp. 77–87 (McGraw-Hill Book Co., Inc., New York, N.Y., 1971).*

Key Words: Critical phenomena; equation of state; parametric equation of state; scaling laws.

A description of the critical region is developed using a local parametric characterization of the thermodynamic potential surface. The physical consequences of the formalism are presented and its predictions compared with some of the experimental data. Results indicate an extended description of the thermodynamic properties over a much enlarged region about the critical point.

Coriell, S. R., Hardy, S. C., Sekerka, R. F., **A non-linear analysis of experiments on the morphological stability of ice cylinders freezing from aqueous solutions,** *J. Crystal Growth* **11,** *53–67 (May 1971).*

Key words: Cylinders; ice; morphology; non-linear; stability; surface tension.

A non-linear theory of morphological stability of a solid circular cylinder growing in a supercooled melt is developed and applied to recent experiments on the growth of ice cylinders in distilled water and in aqueous solution. The cylinders develop Φ perturbations in the circular shape and $z$ perturbations parallel to the axes of the cylinders. The theory successfully predicts the dependence of the $z$ perturbation growth rate on the amplitude of the Φ perturbation. The non-linearity arises because the Φ perturbations have grown to a substantial size before the $z$ perturbations are measured. From an analysis of the $z$ perturbation growth rates, a value of 25 $mJ/m^2$ is obtained for the ice-water surface tension; the corresponding value obtained from a less-satisfactory linear analysis was 22 $mJ/m^2$.

Corliss, E. L. R., **Estimate of the inherent channel capacity of the ear,** *J. Acoust. Soc. Am.,* **50,** *No. 2, 671–677 (1971).*

Key words: Articulation function of ear; "bit" capacity of ear; channel capacity of ear; distinctive features of ear and hearing; intelligibility vs word lengths as block codes; speech; speech intelligibility as channel capacity; word ity lengths as block codes.

The growth of intelligibility of speech stimuli as a function of level above threshold can be computed from the "circuit parameters" of the hearing mechanism by applying Shannon's concepts of channel capacity, equivocation and "bits". The calculation starts from the "least count" of the ear, derived from data on the hearing process for a model resembling a frequency-selective circuit (Corliss, 1967).

By considering the rate at which phonemes are produced in speak- and the number of "distinctive features" characterizing the phonemes, intelligibility functions can be predicted that agree fairly closely with random-word and random-syllable intelligibility data obtained experimentally. This agreement shows that the listener need recognize no more than a single distinctive feature of each phoneme to display the recognition functions that have been observed. The duration of correlated utterance may be considered the "code length" that has the effect of lowering the channel capacity required for polysyllabic utterances as opposed to monosyllables (Shannon, 1957). Evidently, contextual effects are not prominent in the intelligibility of random-word lists; the hearing process involved is primarily recognition of groups of sounds; meaning is secondary. The results also lead to the inference that a direct relation may exist between channel capacity and loudness perception in broadband speech transmission, and suggest that loudness functions for impaired ears might be correlated with intelligibility functions.

Corliss, Edith L. R., **Facts about hearing and hearing aids,** *Nat. Bur. Stand. (U.S.) Consumer Info. Series 4, 31 pages (Nov. 1971), 60 cents, Stock Number 0303-0920.*

Key words: Audition; communications; hearing; hearing aids; selection of hearing aids; speech communication.

A consumers information publication containing information on hearing aids including selection, use, and maintenance.

Coxon, B., **Studies of $^{15}$N-labeled amino sugars. The synthesis and mass spectrometry of derivatives of 6-amino-6-deoxy-D-glucose-6-$^{15}$N,** *Carbohydrate Res.* **19,** *197-210 (1971).*

Key words: Derivatives of 6-amino-6-deoxy-D-glucose-6-$^{15}$N; differential scanning calorimetry; derivative; infra-red isotopic shift; mass spectrometry; nucleophilic substitution.

Derivatives of 6-amino-6-deoxy-D-glucose-6-$^{15}$N have been synthesized in high yield and high chemical and isotopic purity by reaction of the 6-*O*-*p*-tolylsulfonyl or 6-deoxy-6-iodo derivative of 1,2:3,5-di-*O*-isopropylidene-α-D-glucofuranose with potassium phthalimide-$^{15}$N. The infrared and mass spectra of some of these derivatives are discussed. Comparisons of the mass spectra of the $^{14}$N- and $^{15}$N-labeled derivatives afforded confirmation of the pathways of fragmentation.

Coxon, B., Johnson, L. F., **The N.M.R. spectroscopy of derivatives of 6-amino-6-deoxy-D-glucose-6-$^{15}$N. $^{13}$C Fourier-transform and internuclear, double- and triple-resonance studies,** *Carbohydrate Res.* **20,** *105-122 (Nov. 1971).*

Key words: 6-Amino-6-deoxy-D-glucose-6-$^{15}$N derivatives; $^{13}$C Fourier and continuous wave n.m.r. spectroscopy; $^{19}$F n.m.r. spectroscopy; internuclear double resonance; internuclear triple resonance; nitrogen-$^{15}$coupling-constants; nuclear Overhauser effects; p.m.r. spectroscopy.

A series of $^{15}$N-labeled 6-amino-6-deoxy-1,2:3,5-di-*O*-isopropyl-idene-α-D-glucofuranose derivatives and their $^{14}$N analogs has been studied by continuous-wave proton, $^{13}$C, $^{19}$F magnetic resonance spectroscopy, and by $^{13}$C Fourier-transform techniques. Characteristic chemical shifts and the magnitudes of $^{1}$H—$^{1}$H, $^{1}$H—$^{15}$N, $^{1}$H—$^{19}$F, $^{13}$C—$^{15}$N, and $^{15}$N—$^{19}$F coupling-constants are reported and discussed. The $^{1}$H—$^{15}$N and $^{13}$C—$^{15}$N coupling-constants over one bond have been used to assess the hybridization of the $^{15}$N atom in three of the derivatives. Heteronuclear, internuclear, double-resonance (indor) and triple-resonance ("intripler") experiments have been performed in which $^{15}$NH proton transitions were monitored while the $^{15}$N or $^{19}$F frequencies were swept or maintained on resonance. Replicas of the computed theoretical $^{15}$N spectrum were recorded indirectly, and are discussed in relation to nuclear Overhauser effects.

Coxon, B., Schaffer, R., **Characterization and quantitative analysis of D-glucose for use in clinical analysis,** *Anal. Chem.* **43,** *No. 12, 1565-1570 (Oct. 1971).*

Key words: α-D-glucose; anomerization; β-D-glucose; calorimetry; clinical analysis; differential scanning calorimetry; equilibration; gas chromatography; polarimetry; proton magnetic.

The results from analysis of α-D-glucose and β-D-glucose by a variety of spectroscopic, chromatographic, and polarimetric techniques are presented and discussed. The apparent values of purity obtained for α-D-glucose by differential scanning calorimetry are discussed in relation to the content of β anomer as determined by gas chromatography and proton magnetic resonance spectroscopy. It is shown that, during melting, both α-D-glucose and β-D-glucose anomerize rapidly to give an equilibrated mixture of these anomers.

Danos, M., **One physicist's view of special functions** *(Proc. SIAM National Meeting, Washington, D.C., June 10-12, 1969), Chapter in Studies in Applied Mathematics* **6,** *pp. 18-29 (1970).*

Key words: Analytical continuation; electron scattering; potential scattering; re coupling coefficients; Regge poles; special functions.

The need for presently unavailable information is illustrated with three examples taken from physics problems of present interest. They involve both the evaluation of integrals over special functions and the analytic continuation in one or several variables of diverse quantities which can be defined by differential or difference equations. Of particular interest would be the solution of the Schrodinger equation for the scattering of a particle in a Yukawa potential.

Davis, J. E., **The dry and wet bulb psychrometer** *(Proc. ASHRAE Symp. Humidity Measurement, Columbus, Ohio, Feb. 5-8, 1968), Chapter in ASHRAE (Amer. Soc. Heat Refrig. Air-Cond. Eng.) Bull. Humidity Measurement pp. 6-17 (May 1970).*

Key words: Aspirating psychrometers; errors in psychrometric measurements; psychrometric formulas; thermocouple psychrometers; thermodynamic wet; wet-bulb psychrometers.

A paper describing the state of the art of dry and wet bulb psychrometry is presented. Mathematical relationships applicable to a sling psychrometer (or a dry and wet bulb thermometer in a test duct) are given. Short discussions of the universal psychrometric formula and three equations for use with the sling psychrometer are presented. Two of these equations consider effects which cause the reading of the wet-bulb to deviate from the true thermodynamic wet bulb temperature, but they have limitations which are described. The aspirating psychrometer is discussed and the performance of a simple thermocouple psychrometer devised at the National Bureau of Standards is described. Accuracy, precision, and laboratory fabrication techniques are also discussed. Results of tests at NBS using techniques published by earlier investigators at temperatures at 32 °F (0 °C) or below are given. Reference is made to instruments developed which measure true thermodynamic wet bulb temperature, but in their present stage of development are too large to be used in a test duct.

deWit, R., **Relation between dislocations and disclinations,** *J. Appl. Phys.* **42,** *No. 9, 3304-3308 (Aug. 1971).*

Key words: Burgers vector; crystal; disclination; dislocation; distant parallelism; hexagonal; wedge.

The theory of disclinations contains the equation $\partial_i \alpha_{ij} + e_{jmn}\theta_{mn} = 0$, where $\alpha$ and $\theta$ are the dislocation and disclination density tensors, respectively. This expression is interpreted to mean that dislocations can end on twist disclinations. A concrete example in a hexagonal crystal is discussed to illustrate this concept. It contains a 60° wedge disclination normal to the basal plane. By basic geometrical construction it is shown how a dislocation can be made to end on a jog in the wedge disclination. This jog is a small segment of twist disclination. Several ramifications of this concept are that disclinations can act as sources and sinks of dislocations, that dislocations change their Burgers vectors as they glide around disclinations, that a dislocation which crosses a disclination remains connected to it by a dislocation, that dislocations encircling a disclination must have a node, and that the local Burgers vector is not conserved on following a dislocation around a disclination.

Dibeler, V. H., **Photoionization studies and thermodynamic properties of some halogen molecules,** *(Proc. Intern. Conf. on*

*Mass Spectroscopy, Kyoto, Japan, Sept. 6–13, 1969), Chapter in Recent Development in Mass Spectroscopy, K. Ogata and T. Hayakawa, Ed., pp. 781–790 (University of Tokyo Press, Tokyo, Japan, 1970).*

Key words: Chlorine monofluoride; dissociative ionization; fluorine; heats of formation; hot bands; hydrogen fluoride; ion pairs; mass spectrometry; molecular ionization; photoionization; vacuum ultraviolet.

Mass spectra and ion yield curves for molecular and dissociative ionization processes are measured for fluorine, hydrogen fluoride, chlorine, and chlorine monofluoride by means of a combined vacuum uv monochromator and mass spectrometer. Ionization and dissociation energies and heats of formation of the molecules are obtained and compared with values derived from thermochemical and spectroscopic studies.

Dibeler, V. H., Walker, J. A., McCulloh, K. E., **Dissociation energy of fluorine,** *J. Chem. Phys. Letters to Editor* **50,** *No. 10, 4592–4593 (May 15, 1969).*

Key words: Dissociation energy; fluorine; mass spectrometry; photoionization; vacuum ultraviolet.

Photoionization and mass analysis are used to determine the dissociation energy and estimated uncertainty $D_0^\circ(F_2) = 1.34 \pm 0.03$ eV. The molecular ionization energy is also determined to be $15.69 \pm 0.01$ eV. Both $F^+$ and $F^-$ ions are obtained by the ion-pair process.

Dibeler, V. H., Walker, J. A., McCulloh, K. E., **Photoionization study of the dissociation energy of fluorine and the heat of formation of hydrogen fluoride,** *J. Chem. Phys.* **51,** *No. 10, 4230–4235 (Nov. 15, 1969).*

Key words: Bond dissociation energies; fluorine; heats of formation; hydrogen fluoride; ionization thresholds; mass spectra; photoionization; vacuum uv.

Mass spectra and photoionization yield curves are obtained for the molecular and atomic ions of fluorine and hydrogen fluoride. The atomic ions of both molecules are formed by ion-pair and by dissociative ionization processes. The $F_2^+$ curve has a weak onset at 15.58 eV, ascribed to a hot band, followed by an abrupt, intense onset at 15.69 eV, are observed. The onset of the dissociative ionization process occurs at 18.76 eV, from which we calculate $D_0^\circ(F_2) = 1.34 \pm 0.03$ eV (30.9 kcal $mol^{-1}$). The only observed ion-pair process is spin forbidden, producing $F^+(^3P) + F^-(^1S)$, for which the thermodynamic threshold is not reached. The $HF^+$ curve has a slightly tailing onset at 15.92 eV. No $F^+$ ion is observed. The dissociative ionization process yielding $H^+$ occurs at 19.34 eV, permitting the calculation of $D_0^\circ(HF) = 5.47$ eV. and $\Delta Hf_0^\circ(HF) = -2.83 \pm 0.03$ eV ($-65.3$ kcal $mol^{-1}$). Identical ion-pair curves have a threshold at 15.87 eV resulting in $EA(F) = 3.47$ eV. The indicated uncertainties are estimated limits of error.

Dibeler, V. H., Walker, J. A., McCulloh, K. E., **Threshold for molecular photoionization of bromine,** *J. Chem. Phys.* **53,** *No. 12, 4715–4716 (Dec. 15, 1970).*

Key words: Bromine; hot-bands; mass spectrometry; molecular ionization; photoionization.

This brief communication reports on a photoionization measurement of the threshold for molecular ionization of bromine. Ionization of vibrationally-excited molecules is resolved from the 0,0 transition and a value of $I(Br_2) = 10.52 \pm 0.01$ eV is obtained.

Dibeler, V. H., Walker, J. A., McCulloh, K. E., Rosenstock, H. M., **Effect of hot bands on the ionization threshold of some diatomic halogen molecules,** *Intern. J. Mass Spectrom. Ion Phys.* **7,** *209–219 (1971).*

Key words: Halogen molecules; hot bands; ionization threshold; mass spectrometry; monochromator; vacuum ultraviolet.

Photon-yield curves are obtained for the molecular ions of the homonuclear diatomic halogens and for iodine monochloride and iodine monobromide. Excepting iodine, ionization thresholds of ground-state and vibrationally-excited molecules are separately identified by measurements made at several ion-source temperatures. The adiabatic ionization energies (in eV) are: $I(F_2) = 15.69$, $I(Cl_2) = 11.48$, $I(Br_2) = 10.52$, $I(ICl) = 10.07$, and $I(Br) = 9.79$. A preferred value of $I(I_2) = 9.37$ eV is proposed.

DiMarzio, E. A., Rubin, R. J., **Absorption of a chain polymer between two plates,** *J. Chem. Phys.* **55,** *No. 9, 4318–4336 (Nov. 1, 1971).*

Key words: Adhesion; adsorption random walk model; grand canonical ensemble formalism; polymer.

A lattice model of adsorption of an isolated chain polymer between two plates is investigated using a matrix formalism and a grand canonical ensemble (GCE) formalism. The matrix formalism is particularly convenient for calculating the polymer segment density as a function of the distance from one of the plates for different fixed plate separations. The GCE formalism can be used to calculate the fraction of loops (sequences of polymer segments whose ends are in contact with one plate and whose intermediate segments lie between the two plates), bridges (sequences of polymer segments whose ends are in contact with different plates and whose intermediate segments lie between the two plates), and trains (sequences of polymer segments which are wholly in contact with one plate or the other). All of the foregoing quantities have been calculated in the limit of infinite molecular weight as a function of the distance of separation between the plates and the energy of adsorption of a polymer segment on a plate. The self-excluded volume of the polymer chain is ignored. In addition the average sizes of loops, bridges, and trains, and the effective force of attraction between the plates is calculated.

Distefano, G., Dibeler, V. H., **Photoionization study of the dimethyl compounds of zinc, cadmium, and mercury,** *Intern. J. Mass Spectrom. Ion Phys.* **4,** *59–68 (1970).*

Key words: Heats of formation; ionization thresholds; mass spectrometry; metal alkyls; photoionization.

Photoionization yield curves from onset to 600 Å and ionization threshold values have been obtained for the ions $M(CH_3)_2^+$, $CH_3M^+$ of the dimethyl compounds of zinc, cadmium, and mercury, and the $CH_3^+$ from dimethyl mercury. Bond dissociation energies and heats of formation of the ions are also reported.

Douglas, C. A., **A survey of the use of flashing lights in aviation,** *Proc. Intern. Symp. on Perception and Application of Flashing Lights, London, England, April 1971, pp. 251–270 (Adam Hilger Ltd., London, England, April 1971).*

Key words: Aerodrome lighting; aircraft lighting; anti-collision lights; beacons; effective intensity; flashing lights.

Flashing lights have been used as beacons since the first days of night flying. They are also used as identification lights in approach and runway light systems. They have been used for many years to mark obstructions and other hazards by night and are now being introduced as daytime markers. Flashing lights have been used since the 1940's to supplement the navigation lights on aircraft. Photometric performance of these lights is usually specified in terms of steady state intensity and minimum flash duration or in terms of the candela seconds in the flash. Use of the integral form of the Blondel-Rey relation was introduced in the 1950's and use of this relation is increasing.

Driscoll, R. L., Olsen, P. T., **Compensation of earth's field variations by field controlled rubidium oscillator,** *Rev. Sci. Instr.* **42,** *No. 10, 1427–1431 (Oct. 1971).*

Key words: Absorption cell; earth's magnetic field; Helmholtz coil; magnetometer; optical pumping; resonance line; rubidium oscillator; solenoid.

The east-west variations of the earth's magnetic field over the working volume of the NBS precision solenoid are being canceled out by a closed loop system featuring a field controlled rubidium oscillator. The rubidium oscillator and solenoid are sufficiently sepa-

rated in distance and do not affect each other's operation. Each system is enclosed in three-dimensional Helmholtz coils. Vertical and north-south components of earth's field are canceled. An east-west bias field is provided for rubidium oscillator operation at 10 kHz. The output of a phase sensitive detector locked to the 10-kHz frequency standard provides current for the electrically series connected east-west Helmholtz coils at both locations. The magnitude of this current is proportional to the phase difference of oscillator and reference. The full range of compensation is 100 nT. The rate of compensation is limited by a time constant of 0.002 sec, an adequate rate for most disturbances. To the extent that the two separated components of the closed loop system can be oriented directionally the same at any given time, the earth's field east-west variation is compensated exactly.

Durst, R. A., **Ion-selective electrodes in science, medicine, and technology,** *Am. Sci.* **59,** *No. 3, 353–361 (May–June 1971).*

Key words: Electrodes; ion-selective electrode review; ion-selective electrodes, membrane electrodes; potentiometry.

The state of the art of the newer, non-glass types of ion-selective electrodes is reviewed. This brief survey includes discussions of the characteristics of the solid-state, liquid ion-exchange, and heterogeneous membrane electrodes. Applications of these sensors to a wide variety of scientific disciplines is presented, including biomedical research and industrial monitoring and control systems.

Eisele, J. W., **Technical Standards Coordinator, Flame-resistant paper and paperboard,** *Nat. Bur. Stand. (U.S.), Prod. Stand. 46–71, 10 pages (Oct. 1971), 10 cents, SD Catalog No. C13.20/2:26–71.*

Key words: Flame-resistant, paper and paperboard; paper, paperboard, flame-resistant; paperboard, paper, flame-resistant.

This Voluntary Product Standard covers requirements and test methods for flame-resistant paper and paperboard which are 0.060 inch or less thick. Definitions are provided, and a method for identifying products conforming to the standard is given. Two classifications of flame-resistant paper and paperboard are covered: Type I, which is flame-resistant only before water leaching and Type II, which is flame-resistant both before and after water leaching.

Ekstrom, M. P., McCaa, W. D., Jr., Nahman, N. S., **The measured time and frequency response of a miniature superconducting coaxial line,** *IEEE Trans. Nucl. Sci.* **NS–18,** *No. 5, 18–25 (Oct. 1971).*

Key words: Attenuation measurement; picosecond; rise-time measurement; superconducting; transmission lines; two fluid theory.

A miniature superconducting 52 ohm coaxial transmission line 278 meters long, having a lead outer conductor (0.129 cm id), a teflon dielectric, and a niobium center conductor (0.038 cm), has been measured in both the time and frequency domains. The observed system step response (10%–90%) times were 1.5 $\mu$s at room temperature, 375 ns at 77K, and 225 ps at 4.2K. The system step response data for 4.2K was processed by a numerical system identification routine to determine the step response of the miniature superconducting line; the processed data gave a 220 ps risetime. Although the observed step responses at 4.2K were smooth transitions, the observed swept frequency (0.1 GHz – 12 GHz) attenuation at 4.2K was a quasi-periodic function of frequency, which indicated that the nonuniformity of the superconducting line was significant. For example, near 5 GHz and at 4.2K, the attenuation minimum was 1.1 dB while about 0.5 MHz away the attenuation was 5 dB. By making normal conductivity measurements of the Nb conductor and incorporating the results into the two fluid model, the uniform line attenuation for 5 and 10 GHz was calculated with the classical and anomalous limits. The lowest observed attenuation values in the vicinity of 5 and 10 GHz fell between the computed classical and anomalous limit attenuation values

Fatiadi, A. J. **(*p*-Bromophenyl)osotriazoles from inositols,** *Carbohydrate Res.* **20,** *179–184 (Nov. 1971).*

Key words: Infrared; inositol; osotriazole; parabromophenyl; preparation; spectra; study.

(*p*-Bromophenyl)osotriazoles from inositols (D, L and DL). (+) *proto*-quercitol and their derivatives have been prepared and characterized. The i.r. spectra of D, L and DL forms revealed some differences.

Fickett, F. R., **Martensite transformation detection in cryogenic steels (magnetometer development),** *Nat. Bur. Stand. (U.S.), Tech. Note 613, 31 pages (Dec. 1971) 40 cents, SD Catalog No. C13.46:613.*

Key words: Fatigue monitor; low temperature; magnetometer; martensite; nondestructive.

This report presents design criteria for a magnetometer device developed to determine the martensite concentration in 304 stainless steel. Specifically, the device is designed to monitor the cold tank of an airborne liquid oxygen container which is subject to periodic stress pulses. The amount of martensite is relatable to the plastic strain and thus provides a mechanism for the prediction of impending failure. The magnetometer, developed after a critical review of the constraints, is an excitation coil-Hall effect system. The system is very versatile in design and is easily adapted to particular problems. It is relatively insensitive to thermal and mechanical shock and easily capable of detecting martensite at the 1% level.

Forthofer, R. J., **Developing standards technology for automotive braking systems,** *Proc. 1969 18th Annual Meeting Standards Engineers Society, Washington, D.C., Sept. 15–17, 1969, pp. 27–42 (Sept. 1969).*

Key words: Automotive; brake; brake fluid; brake lining; standards; testing.

The Office of Vehicle Systems Research (OVSR) of the National Bureau of Standards (NBS), U.S. Department of Commerce, is concerned with the research, development, testing and evaluation necessary to provide the technical basis for recommended safety performance standards of motor vehicle systems issued by the National Highway Safety Bureau in the Department of Transportation.
This paper discusses briefly the history of the Government's interest in automotive braking safety standards. Problems associated with the collection of research data for the performance of brake systems, brake linings, and brake fluid in more detail. The author comments on the direction that research is expected to take in the 1970's.

Franklin, A. D., **Theory of linear dielectrics,** *Proc. Conf. Electronic Phenomena in Ceramics, University of Florida, Gainesville, Fla., Nov. 10–14, 1969, Chapt. 17, 451–489 (1971).*

Key words: ceramics; dielectric constant; electronic polarization; interfacial polarization; lattice polarization; orientation polarization; theory.

A cursory review is given of the theory of the linear response of a dielectric to an impressed electric field, including the electronic, lattice, dipole orientation, and linear interfacial polarizations. Most emphasis is given to the crystalline ionic, insulating models appropriate for the more ionic ceramics. Modifications to the theory for semiconducting and vitreous materials are briefly touched upon.

Freeman, D. H., Enagonio, D. P., **Interactive gel networks for organic separations,** *Nature (London), Phys. Sci.* **230,** *135–136 (April 1971).*

Key words: Chromatography; interactive gel networks; liquid chromatography; organic separations.

Conventional organic networks, such as crosslinked polyvinylpyridine, can be used or modified so that chemical interactions of various specific types are obtained. They show excellent resolution and high capacity. The chromatographic properties are related to complexative interactions whose understanding in liquid media is independently established.

Geist, J., **Note on the quality of freezing point blackbodies,** *Appl. Opt.* **10,** *No. 9, 2188–2190 (Sept. 1971).*

Key words: Apparent emissivity; freezing point blackbodies; quality.

For freezing point blackbodies a quantity which satisfies the intuitive ideas suggested by the word quality, and which is the solution to a Fredholm integral equation of the second kind, can be defined. The integral equation provides significant physical insight into the interaction of the reflectance and thermal resistance of the wall material in reducing the quality of freezing point blackbodies. In the case where the walls of the cavity reflect diffusely, the integral equation for the quality of a freezing point blackbody reduces to an equation of the same form as the integral equation for the apparent emissivity if an isothermal cavity of the same geometry. Thus the previously published results for the apparent emissivity of cavities with diffusely reflecting walls can be modified to yield the quality of freezing point blackbodies with diffusely reflecting walls.

Haar, L., Shenker, S. H., **Equation of state for dense gases,** *J. Chem. Phys.* **55,** *No. 10, 4951–4958 (Nov. 15, 1971).*

Key words: Argon; compressibility factor; dense fluids; equation of state; molecular dynamics; molecular interactions; nitrogen; pair potentials; temperature perturbation theory.

A simple quantitative equation of state of the van der Waals type is proposed for dense fluids. The equation yields compressibility factors with a precision comparable to those from the more complicated temperature perturbation theory when tested against "computer experiments", including isotherms as low as 0.8 liquid-vapor critical temperature. The equation is capable of predicting compressibility factors for real gases as illustrated by calculations for argon and nitrogen at pressures up to 10 000 atm. The derivation of the equation is based on a rearrangement of the terms in the Ursell-Mayer density expansion of the configuration integral. The equation contains two temperature-dependent parameters, to be determined from the dilute gas second virial coefficients. A principal feature of our approach is that it does not require explicit knowledge of the details of the pair interaction.

Hall, J. L., Barger, R. L., Bender, P. L., Boyne, H. S., Faller, J. E., Ward, J., **Precision long path interferometry and the velocity of light,** A. Smolinski, and S. Hahn, Ed. *(Proc. URSI Conf. Laser Measurements, Warsaw, Poland, Sept. 24–26, 1968), Electron Technol.* **2,** *No. 2/3, 53–66 (Panstwowe Wydawnictwo Naukowe Polish Scientific Publ., Warsaw, Poland, 1969).*

Key words: Interferometry; laser; optical heterodyne; velocity of light.

We report on several aspects of the JILA/NASA/NBS velocity of light experiment. We discuss first the theory of the experiment and illustrate numerically that signal-to-noise ratio is not of primary concern. Considerable thought has gone into planning the experiment to be free as possible from systematic error and these considerations will be briefly reviewed. We discuss a promising pair of laser transitions in pure neon and report two technological developments related to them. We will give a few illustrations of the kind of geophysical information that can be obtained from long-baseline interferometry of the type developed in this work. Finally we briefly report a useful laser transfer standard and a new wavelength reference based on laser saturation of a methane absorption line. A reproducibility of 3 parts in $10^{11}$ has already been demonstrated by optical heterodyne techniques in preliminary experiments.

Hammond, H. K., III, Mason, H. L., Editors, **Precision measurement and calibration. Selected NBS papers on radiometry and photometry,** *Nat. Bur. Stand. (U.S.), Spec. Publ. 300,* **V. 7,** *685 pages (Nov. 1971) $7.00, SD Catalog No. C13.10:300/v.7.*

Key words: Emissivity; flashing light; flux measurement; irradiance; material properties; photometry; projectors; radiance; radiometry; reflectometry.

This volume is one of an extended series which brings together some of the previously published papers, monographs, abstracts and bibliographies by NBS authors dealing with the precision measurement of specific physical quantities and the calibration of the related metrology equipment. The contents have been selected as being useful to the standards laboratories of the United States in tracing to NBS standards the accuracies of measurement needed for research work, factory production, or field evaluation.
Volume 7 contains reprints of more than 60 items on radiometry and photometry published between 1957 and 1970. The material has been placed in groups according to the following subjects: general radiometry, emissivity standards, emissivity measurements and techniques, material properties, irradiance standards, radiometric measurement techniques, radiance standards, flux measurement, reflectometry, general photometry, projectors, flashing lights, and chronological bibliography of publications by NBS staff.

Hermach, F. L., **Testing hospital electric equipment for safe performance,** *Proc. National Research Council Workshop on Electric Hazards in Hospitals, Washington, D.C., April 4–5, 1968, pp. 175–177 (National Academy of Sciences, Washington, D.C., 1970).*

Key words: Electric equipment; hospitals; safety; testing.

The importance of testing hospital electric equipment to determine the extent of the conformance with accepted performance standards is emphasized. The need for test sets to make measurements of leakage currents from electric equipment to ground is paramount. Standardizing bodies can help by outlining performance requirements for such test sets.

Herron, J. T., **Mass spectrometric studies of atomic and free radical reactions,** *Advan. Mass Spectrometry* **5,** *453–461 (1971).*

Key words: Atomic; chemical kinetics; free radicals; mass spectrometry; mechanism; review.

The application of mass spectrometry to the study of the kinetics and mechanisms of atomic and free radical reactions in the gas phase is reviewed.

Hogben, D., Peavy, S. T., Varner, R. N., **OMNITAB II—User's reference manual,** *Nat. Bur. Stand. (U.S.), Tech. Note 552, 264 pages (Oct. 1971) $2, Stock Number 0303–0918.*

Key words: Automatic printing; bessel functions; data analysis; data manipulation; easy and effective programming in English; list of instructions; matrix operations; numerical analysis; OMNITAB II user oriented computing system; self-teaching; statistical analysis.

OMNITAB II, a highly user-oriented system for a large computer, is designed to make computing easy, accurate and effective, particularly for persons who are not programmers. It is a general-purpose program, which can be learned quickly, for both simple and complex numerical, statistical and data analysis. OMNITAB executes instructions written in the form of simple English sentences. Problem-solving is further enhanced by the natural structure of the system and its many features. OMNITAB has been used successfully in government, industry and universities across the country and in several centers abroad. The system has been implemented on large computers of at least seven different manufacturers.
The original version of OMNITAB has been completely rewritten to make it as machine independent as possible and to implement many improvements. This manual describes Version 5.0. Details are presented so that the user can easily find the specific information needed in any particular instance. PART A is a simple, compact introduction to OMNITAB for people who have had no experience using a large computer. PART B describes the general and special features of the OMNITAB system. PART C gives explanations, with short examples, for the use of specific instructions. PART D is a complete list of the instructions which are in the system.

Hudson, P. A., Saulsbery, L. F., **An adjustable-slot-length UHF coaxial coupler with decade bandwidth,** *IEEE Trans. Micro. Theory Tech.* **MTT-19,** *No. 9, 781–783 (Sept. 1971).*

Key words: Attenuator; directional coupler, coaxial; power measurement, rf.

A coaxial directional coupler has been developed which allows adjustment of the length of the coupling slot to $\lambda/4$ or $3\lambda/4$ throughout the frequency range 0.3 to 8.5 GHz. Coupling is flat to within 0.05 dB from 0.3 to 3 GHz ($\lambda/4$ mode) and 0.1 dB from 0.9 to 8.5 GHz ($3\lambda/4$ mode). The coupler has 50 dB coupling, 30 to 40 dB directivity and was designed primarily for high power measurement (1–1000 W) using a low-power meter on the sidearm. The VSWR for the two modes of operation is 1.02 to 1.05. Five octave bandwidth type couplers would be required to cover this same frequency range.

Hudson, R. P., Mangum, B. W., **Effects of applied magnetic fields on cooperative Jahn-Teller transition temperatures of $DyAsO_4$ and $DyVO_4$,** *Physics Letters* **36A,** *No. 3, 157–158 (Aug. 30, 1971).*

Key words: Jahn-Teller effect; magnetic susceptibility.

We have measured the effects of applied magnetic fields on the cooperative Jahn-Teller transition temperatures of $DyAsO_4$ and $DyVO_4$. We find that even relatively weak fields produce a very pronounced increase in the transition temperature of $DyAsO_4$.

Hussmann, E. K., McLaughlin, W. L., **Dye films and gels for megarad dosimetry,** *Proc. United Kingdom Panel on Gamma and Electron Irradiation, The National Physical Laboratory, Teddington, England, July 1970, pp. 35–60 (April 1971).*

Key words: Dosimetry; dyes; films; gels; pulsed beams.

The liquid, gel, and thin-film radiochromic dye system developed by McLaughlin and Chalkley for dosimetry have been shown to be useful for measuring large doses from electron and x and gamma irradiations. The thin films are particularly suited to imaging and measuring radiation field profiles and dose distributions in various materials, even across interfaces of media with different stopping powers and absorption coefficients.

Hust, J. G., Sparks, L. L., **Standard reference materials: Thermal conductivity of electrolytic iron, SRM 734, from 4 to 300 K,** *Nat. Bur. Stand. (U.S.), Spec. Publ. 260–31, 19 pages (Nov. 1971) 35 cents, SD Catalog No. C13.10:260–31.*

Key words: Cryogenics; electrical resistivity; electrolytic iron; Lorenz ratio; Seeback effect; thermal conductivity; transport properties.

Thermal conductivity data are reported for a specimen of electrolytic iron, SRM 734, for temperatures from 4 to 300 K. Variability of this iron was studied by means of electrical residual resistivity ratio measurements on 63 specimens. This study showed that with a 2-hour anneal at 1000 °C one can obtain a thermal conductivity Standard Reference Material that has variability of less than 1% in thermal conductivity.

Johannesen, R. B., Duerst, R. W., **Nuclear magnetic resonance studies of inorganic fluorides VI. Magnetic nonequivalence in *bis*(perfluorovinyl) mercury,** *J. Magn. Resonance* **5,** *No. 3, 355–366 (Dec. 1971).*

Key words: Double resonance; fluorine, INDOR; mercury; nuclear magnetic resonance.

Fluorine magnetic resonance and $^{19}F$ $\{^{199}Hg\}$ resonance spectra of *bis*(perfluorovinyl)mercury and methyl(perfluorovinyl)mercury have been observed. Proton resonance and $^1H$ $^{199}Hg$ spectra of methyl(perfluorovinyl)mercury and dimethylmercury have also been observed. The magnitudes and signs of all possible F—F, F—Hg and H—Hg coupling constants in these three compounds have been determined. The spectrum of *bis*(perfluorovinyl)mercury calculated from the determined parameters is in excellent agreement with observation and the presence of long-range F—F coupling constants in this molecule, none of which are zero, verifies an earlier suggestion as to the reason for the complexity of the spectrum. The fluorine chemical shifts and F—F coupling constants within a perfluorovinyl group are within the previously reported range for these parameters. The mercury chemical shifts determined by INDOR spectroscopy are as follows: dimethylmercury 0 (reference), methyl (perfluorovinyl)mercury $+482\pm3$ ppm, *bis*(perfluorovinyl)mercury $+957\pm3$ ppm.

Julienne, P. S., Krauss, M., Donn, B., **Formation of OH through inverse predissociation,** *Astrophys. J.* **170,** *65–70 (Nov. 15, 1971).*

Key words: Interstellar clouds: interstellar molecule formation; inverse predissociation; non-adiatatic mixing; OH radiative association rate; predissociation widths.

OH formation can occur by inverse predissociation from continuum levels to the $v=1$, $k=1$ levels of the $A^2\Sigma^+$ state. A rate constant of $1\text{–}3\times10^{-20}$ $cm^3s^{-1}$ is calculated for temperatures greater than 20 K. Predicted OH densities are consistent with observations in dense, heavily obscured clouds but appear to be somewhat low for HI clouds.

Julienne, P. S., Neumann, D., Krauss, M., **Calculation of the temperature dependence for absorption in $CO_2$ in the 1750–1200 Å region,** *J. Atmospheric Sci.* **28,** *No. 6, 833–837 (Sept. 1971).*

Key words: Ab initio potential curve; carbon dioxide; Quasi-linear molecule; Renner splitting; temperature dependent absorption coefficient; transition moment.

The absorption cross section of the diffuse absorption bands of $CO_2$ in the region 1750–1200 Å is of prime importance for understanding $CO_2$ photolysis, especially as a constituent of a planetary atmosphere. The upper state of the absorption is a $^1B_2$ state correlating with a $^1\Delta_u$ state in the linear geometry. Although the cross section for this vibronically allowed electric-dipole absorption will be temperature-dependent, there are no experimental studies of this temperature dependence, and room temperature values have been used in discussions of the atmospheres of Mars and Venus despite the widely disparate temperature distributions of their atmospheres.
We have calculated the temperature dependence of the integrated absorption coefficient for the 1750–1200 Å region. The electronic energies and transition moments were calculated ab initio as a function of the bending angle of the molecule; in this way the Renner type splitting of the degenerate $^1\Delta_u$ state into $^1B_2$ and $^1A_2$ energy curves is obtained. The integrated absorption cross section is proportional to the square of the transition moment averaged over the ground state vibrational wave functions. At room temperature the average of the transition moment squared over a Boltzmann distribution is $2.9\times10^{-3}$ $(ea_0)^2$, which corresponds roughly to an oscillator strength of $6\times10^{-4}$. Although halving the temperature produces only about 10% decrease in absorption, there is a dramatic increase by 75% when the temperature is doubled. The temperature dependence of individual lines, particularly in the wings of the overall distribution, is likely to be even more sensitive.

Kaldor, A., **Absorption spectrum of borazine in the vacuum ultraviolet,** *J. Chem. Phys.* **55,** *No. 9, 4641–4643 (Nov. 1, 1971).*

Key words: Borazine; gas phase; matrix isolation; photochemistry; vacuum ultraviolet; vibronic structure.

The absorption spectrum of both vapor-phase and matrix-isolated borazine has been investigated in the 2000–1500 Å region. Three electronic transitions have been observed. The strongest absorption, with a maximum at 1650 Å, is assigned to the allowed $^1E'-{}^1A_1'$ transition. Two weaker absorptions, with forbidden transitions $^1A_2'-{}^1A_1'$, and $^1A_1'-{}^1A_1'$, respectively. The $^1A_2'-{}^1A_1'$ transition is made vibronically allowed by one quantum change in the $\nu_{16}$ and $\nu_{17}e'$ vibrations. The vibration making allowed the $^1A_1'-{}^1A_1'$ transition could not be determined.

Kao, R., Perrone, N., Capps, W., **Large-deflection solution of the coaxial-ring-circular-glass-plate flexure problem,** *J. Am. Ceramic Soc.* **54,** *No. 11, 566–571 (Nov. 1971).*

Key words: Coaxial ring; flexure; glass; nonlinear elastic theory; strength.

Nonlinear deflections and radial surface stresses in thin elastic circular plates laterally deformed into symmetrical concave shapes are analyzed. The deformations are induced by loading each plate

with a small center ring while the plate is resting on a ring of nearly the same diameter as the plate. The rings and plate are coaxial, i.e., concentric. Center deflections up to 3 and 4.5 times the plate thickness were predicted for ring-diameter ratios of 0.5 and 0.2, respectively. The predicted deflection profiles at various loads agreed quite well with those which were determined experimentally on a chemically strengthened glass plate. This analysis provides a new criterion for using the coaxial-ring loading method for flexural strength testing of brittle materials.

Kaufman, V., Sugar, J., **One-electron spectrum of doubly ionized lutetium (Lu III) and nuclear magnetic dipole moment of** $^{175}$Lu, *J. Opt. Soc. Am.* **61,** *No. 12, 1693–1698 (Dec. 1971).*

Key words: Lutetium; spectra; wavelengths.

Thirteen new terms of the $4f^{14}(^1S_0)nl$ doublet system of $Lu^{2+}$ have been found, comprising the $ns$ series ($7 \leq n \leq 10$), the $nf$ series ($5 \leq n \leq 9$), and the $5g$, $6d$, $7d$, and $7p$ terms. Previously, only the $5d$, $6s$, and $6p$ terms were known. The $ns$ series was used to derive an ionization energy of $169049 \pm 10$ cm$^{-1}$. From the completely resolved hyperfine structure (hfs) of $6s\ ^2S_{1/2}$, the value $a(6s) = 0.436 \pm 0.002$ cm$^{-1}$ was obtained for the hyperfine splitting factor. With these data, the nuclear magnetic dipole moment $\mu_I$ was found to be $2.204 \pm 0.010 \mu_N$, where the stated uncertainty includes only the experimental uncertainty for $a(6s)$.

King, D. A., Madey, T. E., Yates, J. T., Jr., **Interaction of oxygen with polycrystalline tungsten II. Corrosive oxidation,** *J. Chem. Phys.* **55,** *No. 7, 3247–3253 (Oct. 1, 1971).*

Key words: Adsorption; chemisorption; corrosion; flash desorption; oxidation; oxygen; tungsten; tungsten oxides.

The kinetics of formation of a corrosive oxide layer of apparently unlimited thickness during the interaction of oxygen with a polycrystalline tungsten filament at temperatures between 500 and 1000 K has been investigated by line-of-sight flash desorption mass spectrometry. The major desorption product from this multilayer oxide film is $WO_2$, which desorbs over the temperature range 1000–1300 K. The rate of formation of the oxide film was shown to be directly proportional to the oxygen gas phase pressure at pressures $\lesssim 10^{-4}$ torr. A study of the temperature dependence of the oxidation rate revealed that the formation of the $WO_2$-producing oxide layer proceeds through two distinct steps; these occur subsequent to the first three stages in the interaction of oxygen with W characterized in paper I. In the final state of oxidation, the rate is shown to be independent of the thickness of the oxide film. The results are in qualitative accord with the theoretical model of Mott. Desorption of the oxide film is a zero order process, with a desorption activation energy of 420 kJ mol$^{-1}$.

Koonce, C. S., Mangum, B. W., Thornton, D. D., **Low Temperature properties of $DyPO_4$ in a magnetic field,** *Proc. 12th Intern. Conf. on Low Temperature Physics, Kyoto, Japan, Sept. 4–10, 1970, pp. 705–707 (Keigaku Publishing Co., Japan, March 1971).*

Key words: Antiferromagnet; $DyPO_4$; heat capacity; Ising model; magnetization; susceptibility.

The magnetization and the peaks in the heat capacity at constant applied field of $DyPO_4$, a material for which the Ising model is particularly appropriate have been measured, and compared with a Bethe-Peierls approximation including dipolar interactions.

Kranbuehl, D. E., **Atomic, molecular, and ionic interactions,** *Dig. Lit. Dielectrics* **33,** *No. 2, 84–118 (1969).*

Key words: Dielectric; ionic; polarizability; relaxation.

A review of those papers in the 1969 literature on dielectrics which make a significant contribution toward understanding the fundamental dielectric properties of atoms, molecules and ions.

Kranbuehl, D. E., Verdier, P. H., **Stochastic molecular model studies of the relaxation of vector end-to-end length in polymer chains,** *Am. Chem. Soc. Polymer Preprints* **12,** *No. 2, 625–628 (1971).*

Key words: End-to-end length; excluded volume; Monte Carlo; polymer chain dynamics; relaxation.

The effects of excluded volume interactions upon the dynamical behavior of random-coil polymer chains are studied by obtaining autocorrelation functions for the vector end-to-end length of lattice model chains of 9, 15, 33, and 63 beads by a Monte Carlo simulation technique. The configuration of the polymer chain, N−1 units long, is represented by a string of N connected points on a 3-dimensional cubic lattice. Excluded volume is accounted for by not allowing two beads to occupy the same lattice site. It is found that the relaxation of vector end-to-end length for a lattice chain with excluded volume varies substantially from that of a lattice chain without excluded volume. Relaxation of the vector end-to-end length requires from four to seven times as long as relaxation of its square, contrary to the predictions of simple models without excluded volume effects. This behavior suggest that the ratio of the relaxation time of vector end-to-end length to that of its square is a measure of the presence or absence of excluded volume effects.

Kuriyama, M., Alexandropoulos, N. G., **On the relationship between X-ray inelastic scattering and absorption spectra,** *J. Phys. Soc. Japan* **31,** *No. 2, 561–562 (August 1971).*

Key words: Compton scattering; plasmon scattering; relation between spectra; Raman scattering; X-ray absorption; X-ray inelastic scattering.

A general formula which connects X-ray inelastic scattering spectra to absorption spectra has been derived for polycrystals from first principles. This derivation ensures the Mizuno-Ohmura relation for X-ray Raman scattering to be valid generally not only for Raman scattering but for plasmon and Compton scattering.

Lee, J. N., Moos, H. W., Mangum, B. W., **Magnetic properties of $TbPO_4$, a canted antiferromagnet,** *Solid State Commun.* **9,** *No. 13, 1139–1141 (1971).*

Key words: Antiferromagnetism; canted antiferromagnet; Jahn-Teller distortion; low temperature; magnetic susceptibility; optical spectroscopy; $TbPO_4$.

The magnetic properties of $TbPO_4$ at low temperatures have been investigated by high resolution optical spectroscopy, magnetic susceptibility, magnetization, and heat capacity measurements. $TbPO_4$ orders antiferromagnetically into a canted spin structure with zero net moment at 2.17 K. Metamagnetic behavior is observed. A magnetically induced lattice distortion mechanism is probably responsible for the detailed behavior.

Lee, T. G., **Interlaboratory evaluation of smoke density chamber,** *Nat. Bur. Stand. (U.S.), Tech. Note 708, 80 pages (Dec. 1971) 75 cents, SD Catalog No. C13.46:708.*

Key words: Building materials; fire tests; interlaboratory tests; optical density; round robin; smoke; smoke density chamber; statistical analysis.

Results are reported of an interlaboratory (round-robin) evaluation of the smoke density chamber method for measuring the smoke generated by solid materials in fire. A statistical analysis of the results from 10 material-condition combinations and 18 laboratories is presented. For the materials tested, the median coefficient of variation of reproducibility was 7.2% under non-flaming exposure conditions and 13% under flaming exposure conditions. A discussion of errors and recommendations for improved procedures based on user experience is given. A tentative test method description is included as an appendix.

Little, J. L., Standards Coordinator, **Hollerith punched card code,** *Nat. Bur. Stand. (U.S.), Fed. Info. Process. Stand. Publ. (FIPS Pub.) 14, 4 pages (1971) 10 cents, SD Catalog No. C13.52:14.*

Key words: American Standard Code for Information Interchange; ASCII; card punch; card reader; data communications; data inter-



459-033 OL - 72 - 9

change; data processing; electric accounting machine; EAM cards; Federal Information Processing Standard; Hollerith punched card code; Hollerith punched cards; information interchange; information processing; punched cards.

This publication provides a standard set of 128 hole patterns which represent the 128 characters of the Federal Standard Code for Information Interchange (ASCII) FIPS 1, in 12-row, 80 column, rectangular hole, "Hollerith" punched cards, or the subsets of ASCII as specified in FIPS 15. Subsets of the Standard Code for Information Interchange. It adopts one-half of the 256 hole patterns given in the American National Standard X3.26–1969, Hollerith Punched Card Code.

McBee, C. L., Kruger, J., **Optical changes in oxide films on iron prior to breakdown,** *Nature Phys. Sci.* **230,** *No. 17, 194–195 (April 26, 1971).*

Key words: Chloride; ellipsometry; passive film; spectroscopy.

Evidence for optical changes in the passive film on iron prior to complete breakdown by chloride is presented. The technique of ellipsometric-spectroscopy is used to locate a wavelength affected by the chloride addition. The recovery of the passive film by removal of the chloride ion is also reported.

McDowell, H., Brown, W. E., Sutter, J. R., **Solubility study of calcium hydrogen phosphate. Ion-pair formation,** *Inorg. Chem.* **10,** *1638–1643 (Aug. 1971).*

Key words: Calcium-phosphate ion pairs; solubility of anhydrous dicalcium phosphate; solubility of calcium monohydrogen phosphate; solubility of dibasic calcium phosphate.

The solubility of $CaHPO_4$ has been determined in the ternary system, $Ca(OH)_2$—$H_3PO_4$—$H_2O$, at 5, 15, 25 and 37 °C. The same results are obtained when equilibrium is approached from super- and under-saturation. Solubility product constant, $K_{sp}=(Ca^{2+})(HPO_4^{2-})$, varies with pH unless formation of ion pairs $CaHPO_4^\circ$ and $CaH_2PO_4^+$ is taken into account. Solubility product constants and standard errors for $CaHPO_4$ are $1.97\pm0.03\times10^{-7}$, $1.64\pm0.01\times10^{-7}$, $1.25\pm0.01\times10^{-7}$ and $0.94\pm0.01\times10^{-7}$ at 5, 15, 25 and 37 °C, respectively. Association constants and standard errors are $243\pm32$, $187\pm24$, $377\pm37$ and $355\pm62$ for $CaHPO_4^\circ$ and $5.2\pm0.7$, $9.6\pm0.6$, $9.6\pm0.7$ and $8.1\pm0.6$ for $CaH_2PO_4^+$ at the same respective temperatures. Thermodynamic functions for the dissolution reaction for $CaHPO_4$ and the association reactions for $CaHPO_4^\circ$ and $CaH_2PO_4^+$ are also presented.

Manning, J. R., **Correlation factors for diffusion in nondilute alloys,** *Phys. Rev.* **B. 4,** *No. 4, 1111–1121 (Aug. 15, 1971).*

Key words: Alloys; atom jump frequencies; binary alloys; correlation factor; diffusion; multicomponent alloys; random alloy model; and vacancies.

Correlation factors for diffusion in binary and multicomponent alloys are calculated for a random-alloy model with diffusion by a vacancy mechanism. This model, which should apply best for nondilute alloys, assumes that atoms and vacancies are randonly distributed and that suitable average values can be used to represent the actual atom and vacancy jump frequencies in the crystal. In alloys, both atoms and vacancies follow correlated walks. Also, the atom correlation factors are influenced by the nonrandom motion of the vacancies. Thus, in order to treat correlation effects in concentrated alloys properly, one must consider not only the correlation factors $f_i$ for diffusion of atoms but also the correlation factor $f_v$ for diffusion of vacancies. In specific calculations, one also must find the partial correlation factors $f_v^i$ for diffusion of vacancies by exchange with atoms of the particular species $i$. Analytic expressions for all of these correlation factors are calculated. These equations can be expressed directly in terms of the measurable tracer-diffusion-coefficient ratios $D_i^*/D_k^*$ with no unknown jump frequencies appearing. The calculations also yield a forbidden region in the plot of diffusion-coefficient ratio as a function of alloy composition, with correlation factors going to zero at the boundary of this region. Specific applications to binary alloys are discussed.

Marsden, C. P., **Tabulation of data on semiconductor amplifiers and oscillators at microwave frequencies,** *Nat. Bur. Stand. (U.S.), Tech. Note 597, 48 pages (Dec. 1971) 50 cents, SD Catalog No. C13.46:597.*

Key words: Amplifiers; basic characteristics; microwave; oscillators; semiconductor; solid state.

This tabulation includes some of the basic characteristics of semiconductor microwave devices, specifically amplifiers and oscillators of foreign and domestic origin.

Martin, W. C., **Energy differences between two spectroscopic systems in neutral, singly ionized and doubly ionized lanthanide atoms,** *J. Opt. Soc. Am.* **61,** *No. 12, 1682–1686 (Dec. 1971).*

Key words: Lanthanides; spectra.

Energy differences of the type $4f^{N-1}5d-4f^N$ (doubly ionized atoms), $4f^{N-1}5d6s-4f^N6s$ (singly ionized atoms) and $4f^{N-1}5d6s^2-4f^N6s^2$ (neutral atoms) are important for the interpretation of rare-earth spectra. Here N=1 for La, . . . 14 for Yb, and each configuration is represented by its lowest level in these system differences (SD). Nineteen of these differences are now known exactly from analyses of the spectra. Five additional SD values are approximately fixed by a combination of observation and calculation. Regularities deduced from these known values allow predictions for the remaining 18 SD values. The estimated probable error for most of the predictions is either 1000 or 1500 $cm^{-1}$.

Marzetta, L., **A high-performance phase-sensitive detector,** *IEEE Trans. Instr. Meas.* **IM-20,** *No. 4, 296–301 (Nov. 1971).*

Key words: Operational amplifier; op amp; operational rectifier; phase-sensitive detector; signal extraction ratio.

A phase-sensitive detector is described that enables the retrieval of signals submerged 90 dB (voltage) below the noise level. Operation over four decades of signal amplitude (a full scale linearity error of 0.01%) is possible for a frequency range of 0 to 150 Hz. Design features are offered allowing an experimenter to construct the device from inexpensive components and be assured a predictable performance.

Masters, L. W., Lutz, G. J., **Determination of thallium by photon activation analysis,** *Anal. Chim. Acta* **56,** *365–370 (1971).*

Key words: Activation analysis; bremsstrahlung; determination; glass; photon activation analysis; thallium.

The determination of trace amounts of thallium by the thermal neutron reaction $^{203}Tl\ (n,\gamma)\ ^{204}Tl$ is complicated because $^{204}Tl$ is a pure beta-emitter, requiring a lengthy and rigorous separation. In addition the half-life of $^{204}Tl$ is too long to permit decay measurements. A photon activation analysis method has been developed for this determination. Bremsstrahlung from a beam of 35-MeV electrons induces the photonuclear reaction $^{203}Tl\ (\gamma, n)\ ^{202}Tl$. The detection limit is of the order of tens of nanograms. It was determined that there are no interfering photonuclear reactions from lead.

Menis, O., Schultz, J. I., Editors, **Analytical Coordination Chemistry Section: Summary of Activities July 1970 to June 1971,** *Nat. Bur. Stand. (U.S.), Tech. Note 584, 175 pages (Dec. 1971) $1.50, SD Catalog No. C13.46:584*

Key words: Aluminum in steel; bilirubin; DTA standards; fluorescence filters Tl(I), Ce(III), Pb(II); glass filters (SRM 930); mercury in botanical; quantum efficiencies.

Progress in research in spectrophotometry, spectrofluorometry, flame emission, atomic absorption, thermal analysis and related photometric measurements led to the construction of a high accuracy spectrophotometer, certification of glass filters, establishment of a more accurate value for molar absorptivity of the acid dichromate system, and the evaluation of spectrally neutral filters of interest for automation in clinical studies. The linearity of the single beam

spectrophotometer was calibrated by the light addition technique. Glass filters were calibrated at 4 wavelengths with an uncertainty of 0.5 percent. Data for the dichromate system in perchloric acid led to new values for the dimerization equilibrium constant.
Studies were made of new fluorescence filters incorporating Ti(I), Ce(III), Pb(II) and rare earths in a variety of glass matrices. Quantum efficiencies of Tl in KCl and Eu in a silicate matrix were determined.
Developments in instrumentation led to increased sensitivity and improved precision and accuracy by flame spectroscopy. Mg, Ca, K and Na were determined with the multichannel spectrometer. A newly designed optical system and an ultrasonic spraying system provided increased signal and efficiency. The repetitive optical scan of flame emission overcame matrix and flame background problems for the determination of aluminum in steel. Certification was made on eight new materials in cooperation with the International Confederation on Thermal Analysis.

Mighell, A. D., Santoro, A., Donnay, J. D. H., **Reduced cells, Chapter in International Tables for X-ray Crystallography,** Norman F. Henry, and Kathleen Lonsdale, Ed., **II,** *530–535 (The Kynoch Press, Birmingham, England, 1969).*

Key words: Bravais lattice; identification; reduced cells; transformation matrix.

Tables and text are given that make it possible to determine the reduced cell for any lattice. Finally, a detailed table is presented which establishes the relationship of each of the 44 reduced cell types to one of the Bravais lattice.

Milligan, D. E., Jacox, M. E., **Matrix-isolation study of the interaction of electrons and alkali metal atoms with various nitrogen oxides. Infrared spectra of the species $NO^-$, $NO_2^-$ and $N_2O_2^-$,** *J. Chem. Phys.* **55,** *No. 7, 3404–3418 (Oct. 1, 1971).*

Key words: Alkali metal reactions; charge transfer; electron attachment; infrared spectrum; matrix isolation; $NO^-$; $NO_2^-$; $N_2O_2^-$; O-reactions.
The infrared spectra which result when samples of $NO_2$ are codeposited with the various alkali metals in an argon matrix at 4 or at 14 K are consistent with the occurrence of strong charge-transfer interaction. In addition to isolated $NO_2^-$, previously identified in this system, ion pairs of general formula $M_x^+NO_2^-$ are stabilized. When NO is substituted for $NO_2$, the infrared spectrum of the initial deposit shows an absorption between 1350 and 1375 $cm^{-1}$ which can be assigned to the $NO^-$ stretching fundamental of $M_x^+NO^-$ ion pairs, in good agreement with the vibrational spacing recently reported for ground-state $NO^-$ in the gas phase. Weak charge-transfer interaction occurs between alkali-metal atoms and $N_2O$ in an argon matrix environment. Results of the present experiments can be explained by postulating that the upper, predominantly ionic state of the charge-transfer complex decomposes producing $O^-$ which may diffuse through the matrix. A new absorption which appears at 1205 $cm^{-1}$ has tentatively been assigned to $\nu_4(b_1)$ of a planar $O_2N=N^-$ anion. In studies of the interaction of sodium atoms with Ar:NO:$N_2O$ mixtures mercury-arc irradiation of the sample leads to the appearance not only of the $N_2O_2^-$ absorption, but also of absorptions due to isolated $NO_2^-$ and to $Na_x^+NO_2^-$.

Moore, G. A., **Design of a practical scanner unit for precision analysis of micrographs,** *Pattern Recognition* **3,** *91–122 (Oct. 1971).*

Key words: Analysis of microstructures; automatic scanning (of micrographs); precision scanning (of micrographs); quantitative microscopy.

A precision mechanical scanner has been constructed for the purpose of preparing digital transcriptions of micrographs for computer analysis, and of performing elementary analysis without resort to a computer. Design criteria include convenience of operation and precision sufficient to correctly record all of the real information in one micrographic field.
Performance data are included. An analysis is given of the precision which may be expected in estimating area and volume percentage of a phase under various conditions. The attained precision is at least an order of magnitude greater than is normally obtained by manual methods.

Nagasawa, T., Kobayashi, K., **Paracrystalline structure of polymer-crystal lattice distortion induced by electron irradiation,** *J. Appl. Phys.* **41,** *No. 11, 4276–4284 (Oct. 1970).*

Key words: Crystal; defects; irradiation; polyethylene; unit cell.

The melting temperature of polyethylene crystals decreases and the lattice constants (both a and b) and lattice distortion increase, but the macroscopic volume of the specimen does not change with electron irradiation. From these results a model of a deformed lattice structure with point defects produced by irradiation is proposed. Calculations indicate that the anisotropy of a polymer crystal (difference between the elastic modulus along the molecular axis and perpendicular to the axis) increases the range of the distortion in a crystal caused by a defect. The presence of lattice distortion in electron irradiated polymer single crystals produces observable features in the Moiré patterns obtained from the crystals.

Negas, T., Roth, R. S., **Phase equilibria and structural relations in the system $BaMnO_{3-x}$,** *J. Solid State Chem.* **3,** *323–339 (1971).*

Key words: Four-layer $SrMnO_3$; perovskites; phase equilibria; strontium manganates; tetravalent manganese; trivalent manganese.

The system $BaMnO_{3-x}$ ($0 \leq x < 0.5$) in air was investigated by gravimetric, quenching, single-crystal and powder-x-ray diffraction studies. Below 1150 °C hexagonal, two-layer $BaMnO_3$ ($a=5.699$ Å, $c=4.817$ Å) is stable. Above 1150 °C a series of anion deficient $BaMnO_{3-x}$ phase exists. With increasing temperature, these include a rhombohedral 15-layer form ($a=5.681$ Å, $c=35.377$ Å; hexagonal indexing) and hexagonal 8-layer ($a=5.699$ Å, $c=18.767$ Å), 6-layer ($a=5.683$ Å, $c=14.096$ Å), 10-layer ($a=5.680$ Å, $c=23.373$ Å) and 4-layer ($a=5.672$ Å, $c=9.319$ Å) forms. The 6-layer modification is not of the hexagonal $BaTiO_3$-type. A simple orderly structural sequence involving a progressive increase of cubic-type layer stacking with increasing temperature characterizes the phases prepared. Influence of anion stoichiometry on phase formation is considered.

Newman, M., **Units in cyclotomic number fields,** *J. Reine Angew. Math.* **250,** *1–11 (1971).*

Key words: Cyclotomic units; diophantine equations; roots of unity.

Conditions for a unit in a cyclotomic number field to be a power of another unit in that field are derived, and the results applied to show that equations such a $1+\zeta=\alpha^r$, $\zeta$ a primitive nth root of unity, $n$ odd and $>3$, have only the trivial solution $r=1$, $\alpha=1+\zeta$.

Parker, V. B., Wagman, D. D., Evans, W. H., **Selected values of chemical thermodynamic properties—Tables for the alkaline earth elements (Elements 92 through 97 in the standard order of arrangement),** *Nat. Bur. Stand. (U.S.), Tech. Note 270–6, 119 pages (Nov. 1971) $1.25, SD Catalog No. C13.46:270–6.*

Key words: Barium compounds; beryllium compounds; calcium compounds; enthalpy; entropy; Gibbs energy of formation; magnesium compounds; radium compounds; strontium compounds.

Contains tables of values for the standard heats and Gibbs (free) energies of formation, entropies and enthalpies at 298.15 K and heats of formation at 0 K for compounds of beryllium, magnesium, calcium, strontium, barium, and radium (elements 92–97 in the Standard Order of Arrangement). These tables are a continuation of the comprehensive revision of NBS Circular 500.

Persson, K-B, Johnson, E. G., Jr., **The errors in plasma measurements by the microwave cavity techniques,** *Nat. Bur. Stand. (U.S.), Tech. Note 607, 64 pages (Oct. 1971) 65 cents, SD Catalog No. C13.46:607.*

Key words: Collision frequency; helium negative glow discharge; microwave cavity; plasma density.

This report presents the results of a theoretical and experimental

study of the microwave cavity techniques used in measuring electron density and collision frequency in transient plasmas. Sources of errors are discussed and certain calibration procedures are recommended to minimize the error. In particular, the abnormal negative glow discharge in helium is presented as an inexpensive reference plasma for calibration purposes.

Phucas, C. B., Technical Standards Coordinator, **Package quantities of cubed, sized, crushed and block ice,** *Nat. Bur. Stand. (U.S.), Prod. Stand. 48–71, 10 pages (Nov. 1971) 15 cents, SD Catalog No. C13.20/2:48–71.*

Key words: Block ice, package quantities of; crushed ice, package quantities of; cubed ice, package quantities of; ice, package quantities of; package quantities of ice; sized ice, package quantities of.

This Voluntary Product Standard covers the net weights of the package quantities recommended for cubed, sized, crushed, and block ice. Definitions of terms and methods for identifying products packaged in accordance with this Standard are included.

Plitt, K. F., Utech, H. P., **Flammability of turnout coats tested,** *Fire Eng.* **124,** *No. 10, 60 (Nov. 1971).*

Key words: Bunker coats; fabric flammability; firefighter clothing; fireman; flame resistance; turnout coats.

Flame resistance tests (vertical burn method) were conducted on four commercially purchased firefighters' turnout coats. Each coat had three fabric layers: outer shell, inter lining, and inner lining. The results show that 2 of 3 fabric layers in each coat produced a char length of 12 inches.

Post, M. A., **Copolymer determination in surface filler,** *Paint Varnish Prod.* **61,** *No. 9, 31–38 (Sept. 1971).*

Key words: Absorbance ratio method; infrared spectroscopy; resins; styrene-butadiene; surface fillers; vinyl toluene-acrylate; vinyl toluene-butadiene.

Styrene-butadiene, vinyl toluene-butadiene and vinyl toluene-acrylate copolymers in surface fillers are quantitatively determined by two methods. In one, a dual extraction method, which should be useful in acceptance testing of solvent type fillers, the resin is determined as the difference between the total benzene and n-pentane extractables. The second method, a combination of single extraction and infrared analysis, involves determination of the total benzene extractables and the resin content therein. The latter is determined by measuring the 3.3 $\mu$m/3.5 $\mu$m absorbance ratio of cast films from the benzene extract, using the baseline method, and reading the weight percent resin from the appropriate standard curve. This method depends on a constant ratio of styrene to butadiene, vinyl toluene to butadiene or vinyl toluene to acrylate. Its use is restricted to resins of a particular monomer ratio for which a standard curve has been made. These methods were developed and confirmed using commercially prepared fillers of known resin content.

Powell, F. J., Robinson, H. E., **The effect of moisture on the heat transfer performance of insulated flat-roof constructions,** *Nat. Bur. Stand. (U.S.), Bldg. Sci. Ser. 37, 81 pages (Oct. 1971) 75 cents, SD Catalog No. C13.29/2:37.*

Key words: Flat roofs; heat transfer; moisture transfer; thermal insulation.

A solution to the problem of unwanted moisture in the thermal insulation of flat roofs was found during a recently completed laboratory investigation of the effects of moisture on heat transfer through these constructions. The objective of the research was to ascertain how much the insulating performance of conventional constructions, having insulation over concrete decks, was affected by moisture. This is presented as Part I. Also, the objective was to investigate properties of materials, their arrangement and dimensions which would yield a construction having an adequate degree of self-drying ability, combined with low winter moisture regain rate. This is presented as Part II. The results show that the best insulating and moisture performance was obtained by utilizing the heat of the summer sun on the roof to vaporize and transfer to the room beneath any free moisture contained within the construction. Roof specimens made from moderately vapor-permeable materials without conventional vapor barriers were, in winter, able to accommodate the small quantity of slowly accumulated condensation without dripping or severe loss of insulating value. During the nine-year investigation, the performance characteristics of 73 insulated roof deck specimens were obtained and two new methods of measurement were developed. Criteria for the design of self-drying insulated flat roofs were developed and limits of the parameters containing the main variables that affect performance were suggested. This paper presents complete results of the research which was sponsored jointly by the National Bureau of Standards, the Army, the Navy, and the Air Force.

Prince, E., **Refinement of the crystal structure of apophyllite II. Determination of the hydrogen positions by neutron diffraction,** *Am. Mineralogist* **56,** *1243–1251 (July-August 1971).*

Key words: Apophyllite; fluoro silicate; hydrated minerals; hydrogen bonds; mineral structure; neutron diffraction.

The crystal structure of apophyllite, a mineral with the ideal formula $KCa_4(Si_4O_{10})_2F \cdot 8H_2O$, has been refined using three-dimensional neutron diffraction data. 671 independent reflections were observed on a 4-circle diffractometer. Of these 516 had observable intensities. A least-squares refinement, with anisotropic temperature factors, led to an $R$ index of 0.046. However, a difference Fourier synthesis revealed a region of negative scattering density in the vicinity of the fluorine atom. Accordingly a further refinement was carried out assuming a model in which $\frac{1}{8}$ of the water molecules are replaced by $OH^-$ ions, with the remaining proton bonded to fluorine to form an HF molecule. This model refined quickly to an $R$ value of 0.037. The water molecules and $OH^-$ ions are hydrogen bonded to the silicate framework. A preliminary mass spectrometric analysis of the gases evolved when apophyllite is heated revealed that the higher temperature specific-heat anomaly is due to the evolution of hydrogen fluoride. This suggests that the structural formula is $KCa_4(Si_4O_{10})F_{1-x}(HF)_x \cdot [(H_2O)_{8-x}]$ with $x \approx 1$.

Rosenstock, H. M., **Harmonic oscillator Franck-Condon factors for the ionization of $N_2O$,** *Intern. J. Mass Spectrom. Ion Phys.* **7,** *33–39 (1971).*

Key words: Franck-Condon Factors; ionization; $N_2O$; theoretical.

Harmonic oscillator Franck-Condon factors have been calculated for the ionization of $N_2O$. The Franck-Condon factors are quite sensitive to the form of the valence force field for the ion. The results are in fair agreement with experimental values obtained by photoelectron spectroscopy.

Saylor, C. P., **Refractive index,** *Chapter in The Characterization of Chemical Purity of Organic Compounds,* L. A. K. Staveley, Ed., *pp. 67–79 (July 1971).*

Key words: Crystals; liquids; purity; refractive index.

Usually measurement of refractive index on liquids has limited usefulness in the evaluation of purity. The tendency of materials and their contaminants to have similar values is demonstrated. The methods of refractive index measurement are described and evaluated. The dissimilar conditions that occur with solid substances are pointed out. Instances of application of refractive index measurement to solids are appraised.

Schafft, H. A., **Wire-bond electrical connections: Testing, fabrication and degradation—A bibliography 1957–1971,** *Nat. Bur. Stand. (U.S.), Tech. Note 593, 58 pages (Jan. 1972) 60 cents, SD Catalog No. C13.46:593.*

Key words: Bibliography; degradation (wire-bond); discrete devices; electrical interconnection; fabrication (wire-bond); failure (wire-bond); hybrid circuits; integrated circuits; microelectronics; reliability; testing; (wire-bond); wire-bond.

More than 245 papers relevant to wire-bond type electrical inter-

connections used in microelectronic and low-power discrete and hybrid devices are listed together with key words. The bibliographic search concentrated on compiling papers which appeared in the period from 1965 to 1970, inclusive. The selection of papers was generally limited to those that were pertinent to wire-bonds where the wire diameter is less than about 50$\mu$m (2 mils) and where the wire is bonded by either thermocompressive or ultrasonic means. Two indexes are provided: (1) an Author Index and (2) a Key Word Index. The latter includes a tabulation of the literature citations.

Scheer, M. D., Klein, R., McKinley, J. D., **Surface lifetimes of alkali metals on molybdenum,** *J. Chem. Phys.* **55,** *No. 7, 3577–3584 (Oct. 1, 1971).*

Key words: Alkali metals; desorption energies; polycrystalline molybdenum; surface ionization; surface lifetimes.

The surface lifetimes ($\bar{\tau}$) of all the alkali metals on a polycrystalline molybdenum surface in the temperature region 900–1350 K were measured. The temperature dependence followed an Arrhenius expression of the form $\bar{\tau}^{\circ} \exp(\bar{I}/kT)$. Desorption energies ($\bar{I}$) were found to be 3.14, 2.60, 2.53, 2.31, and 2.10 eV for Li, Na, K, Rb, and Cs. The corresponding pre-exponential factors ($\tau^{\circ}$) were $3 \times 10^{-16}$, $3 \times 10^{-15}$, $2 \times 10^{-14}$, $1 \times 10^{-13}$, and $3 \times 10^{-13}$ s. From these data, ion and neutral desorption energies were calculated using a model employing a partial surface charge for the adsorbed particle and the Schottky relation. The validity of the Schottky relation for an adsorbed alkali was supported by analysis of recently available theory of partial charges. An explanation of the variation of the pre-exponential factors is presented on the basis of relative mobility of the adsorbed species. A pre-exponential factor was calculated using a partition function for an adsorbate with mixed localized and nonlocalized character. The extremes of completely localized and completely non-localized adsorption led to pre-exponentials that spanned the experimental values.

Schwartz, R. B., Heaton, H. T., II, Schrack, R. A., **High-accuracy total-cross-section measurements with the NBS Linac,** *(Proc. Symp. Neutron Standards and Flux Normalization, Argonne National Laboratory, Argonne, Ill., Oct. 21–23, 1970), AEC Symp. (Aug. 1971).*

Key words: Cross section; MeV; neutron; time-of-flight.

A high-accuracy fast-neutron time-of-flight spectrometer used for neutron energies between 0.5 and 20 MeV is described. The neutrons are produced by a 2-ns-wide electron-beam pulse from the National Bureau of Standards Linac. The resolution, with a 40-m flight path, is approximately 0.1 ns/m, and the accuracy of the measurements is estimated to be 1%.

Schwartz, R. B., Schrack, R. A., Heaton, H. T., II. **A search for structure in the n–p total cross section,** *Proc. Neutron Standards and Flux Normalization Symp. Argonne National Laboratory, Argonne, Ill., Oct. 21–23, 1970. Sponsored by the European American Nuclear Data Committee, AEC Symposium Series* **23,** *pp. 57–62 (Aug. 1971).*

Key words: Cross section; hydrogen; neutron; $n$–$p$; scattering; time-of-flight.

High-precision measurements of the $n$–$p$ total cross section below 30 MeV show no evidence of any structure. A careful measurement of the differential scattering cross section also shows no evidence of any anisotropy.

Sher, A. H., Croll, W. K., Thurber, W. R., **Determination of oxygen in germanium below 20 parts per billion by measurements of lithium mobility and precipitation,** *Anal. Chem.* **43,** *No. 13, 1831–1834 (Nov. 1971).*

Key words: Germanium; infrared absorption; lithium mobility; lithium precipitation; oxygen.

The range of sensitivity and the expected degree of precision for the analysis of oxygen concentration in germanium by measurements of lithium-ion drift mobility and lithium precipitation have been determined. The relative sample standard deviations have been found to be $\pm 10\%$ and $\pm 15\%$, respectively, in the range of oxygen concentration from 20 ppb (atomic) to 0.2 ppb (atomic). However, the lithium precipitation method alone cannot be used unambiguously in the determination of oxygen concentration in germanium. The sole previously-published value for the dissociation constant of the $LiO^+$ complex in germanium at 295 K has been confirmed. A newly-observed feature in the lithium precipitation curve is shown to give semiquantitative information about oxygen concentration.

Sher, A. H., Thurber, W. R., **Minority carrier and lithium-ion drift mobilities and oxygen concentration in $p$-type germanium,** *J. Appl. Phys.* **42,** *No. 11, 4508–4509 (Oct. 1971).*

Key words: Electron mobility; germanium; lithium mobility; oxygen concentration.

No correlations have been experimentally observed between electron drift mobility and lithium drift mobility nor between electron drift mobility and oxygen concentration in $p$-type germanium single crystals, as had been previously suggested.

Shirk, J. S., **Laser excited fluorescence of $CCl_2$,** *J. Chem. Phys.* **55,** *No. 7, 3608–3609 (Oct. 1, 1971).*

Key words: Fluorescence; force field; matrix.

Laser-excited fluorescence of $CCl_2$ trapped in a low temperature matrix was observed in the 6000–8500 Å region. A normal coordinate analysis was carried out, using a Urey-Bradley force field, to determine the molecular force constants.

Simpson, J. A., **Use of a microscope as a noncontacting microdisplacement measurement device,** *Rev. Sci. Instr.* **42,** *No. 9, 1378–1380 (Sept. 1971).*

Key words: Dimensional metrology; displacement measurement; microscope; noncontact sensing; optical surface probe; surface detection.

It is shown that a common research microscope with vertical illuminator can be easily converted to a noncontacting measuring device of sub-microinch resolution.

Smith, S. J., **Molecular negative ion structure,** *Comments At. Mol. Phys.* **2,** *No. 6, 175–180 (Feb.–March 1971).*

Key words: Elastic scattering; electron affinity; high resolution internuclear distance; molecular negative ions; photodetachment.

This paper is a commentary on the reasons for limited progress in obtaining mechanical constants for molecular negative ions. It points out that two experimental technologies, one a sophistication of the photodetachment technique which incorporates energy analysis of detached electrons, the other a refinement of electron-neutral molecule scattering measurements with high energy resolution, now are yielding complementary data on molecular negative ion constants. In principle, these methods are widely applicable.

Swanson, H. E., McMurdie, H. F., Morris, M. C., Evans, E. H., Paretzkin, B., DeGroot, J. H., Carmel, S. J., **Standard x-ray diffraction powder patterns,** *Nat. Bur. Stand. (U.S.), Monogr. 25-Section 9, 128 pages (Dec. 1971) $1.25, SD Catalog No. C13.44:25/Sec. 9.*

Key words: Crystal structure; integrated intensities; lattice constants; peak intensities; powder patterns; reference intensities; standard; x-ray diffraction.

Standard x-ray diffraction patterns are presented for 63 substances. Forty of these patterns represent experimental data and 23 are calculated. The experimental x-ray powder diffraction patterns were obtained with an x-ray diffractometer. All d-values were assigned Miller indices determined by comparison with computer interplanar spacings consistent with space group extinctions. The densities and lattice constants were calculated, and the re-

fractive indices were measured whenever possible. The calculated x-ray powder diffraction patterns were computed from published crystal structure data. Both peak height and integrated intensities are reported for the calculated patterns.

Swartzendruber, L. J., Bennett, L. H., **Use of ultrasonics in laboratory development tests of cupro-nickel alloys for desalination,** *Desalination 9, 387–389 (June 1971).*

Key words: Alloys; corrosion; cupro-nickel; high velocity; sea water; ultrasonics.

Ultrasonic agitation of the salt water bath is suggested as a simple laboratory corrosion test method for evaluating the relative performance of alloys intended for use at moderate or high sea water velocities.

Thomas, D. B., **Some studies on the reproducibility of tungsten-rhenium type thermocouples,** *Proc. 26th Intern. Instrument Society of America Conf. and Exhibit on Advances in Instrumentation, Chicago, Ill., Oct 4–7, 1971,* **26,** *Part II, Paper 71–611 (Oct. 1971).*

Key words: Anneal; beryllium-oxide; calibrations; electromotive force; thermal-cycling; thermocouple; tungsten-rhenium.

Representative samples of commercially available tungsten-rhenium type thermocouples were obtained from American manufacturers and calibrated in an argon atmosphere up to 2100 °C. After the initial calibrations were performed, the thermocouples were subjected to thermal-cycling between 1000 °C and 2100 °C and were also annealed for periods up to 420 hours at 2300 °C in argon. A comparison is made between the emfs of the thermocouples before and after the thermal-cycling and annealing periods. In general, the tungsten versus tungsten-26% rhenium thermocouples indicated the largest changes in emf after the thermal-cycling and annealing periods while the tungsten-3% rhenium versus tungsten-25% rhenium thermocouples indicated the least change in emf. Some of the thermocouples were calibrated with and without beryllium-oxide insulation in argon, helium, and vacuum and a comparison is made between the thermocouple emfs under these conditions.

Tsai, D. H., MacDonald, R. A., **Molecular dynamical studies of the phase transformation of iron under pressure** (*Proc. Symp. Mechanisms of the Phase Transitions, University of South Carolina, Columbia, S.C., Feb. 1, 1971*), *Trans. Am. Crystallogr. Assoc.* **7,** *107–129 (Feb. 1, 1971).*

Key words: Iron; lattice structure; molecular dynamics; *P–V–T* data; phase diagram; transition mechanism.

We have applied molecular dynamics to the study of the transformation of iron from the $\alpha$(bcc) phase to the $\epsilon$(hcp) phase under hydrostatic pressure. The atomic interaction energy in both phases was represented by a two-body, central force potential fitted (1) to the elastic properties of the $\alpha$ phase at zero pressure and zero absolute temperature, and (2) to an assumed transition pressure of 130 kb at zero absolute temperature, with a volume decrease of 0.2 $cm^3$/mol upon transition from the $\alpha$ to the $\epsilon$ phase. The classical equations of motion of the lattice points were solved by numerical computation, and the equation of state and specific heat data were obtained from the appropriate time-averages of the dynamical solutions. From these quantities, the Gibbs free energies of the two phases were calculated and a phase diagram for the $\alpha$ to $\epsilon$ transition was constructed. We found that the phase diagram thus obtained was in satisfactory agreement with experimental results. By observing the details of the lattice point motion given by the dynamical solutions, it was possible to follow the process of phase transformation when it occurred in the model. We describe here a martensitic type of buckling mechanism which was observed to transform the $\alpha$ phase to the $\epsilon$ phase.

Tsang, W., Wasik, S. P., **The application of the isotope dilution GLC technique to air pollution analysis,** *J. Chromatog. Sci.* **9,** *567–569 (Sept. 1971).*

Key words: Air pollution; benzene; benzene-$d_6$; gas analysis; gas chromatography; isotope dilution; isotope effect.

It is shown that the isotope dilution technique provides a simple means of accurately determining air pollutant concentrations under adverse conditions. This is demonstrated in various simulated situations with a sample of approximately 20 ppm benzene in argon.

Wagner, H. L., Hoeve, C. A. J., **Effect of molecular weight on the refractive increment of polyethylene and *n*-alkanes,** *J. Polymer Sci. Part A-2,* **9,** *1763–1776 (1971).*

Key words: Differential refractive index; differential refractometer; Lorenz-Lorenz; molecular weight; *n*-Alkanes; polyethylene; polystyrene.

As in the case with other polymers previously reported, the values of the refractive index increment $dn/dc$ of polyethylene and the *n*-alkanes change with molecular weight. Most of the variation may be understood by examination of the role of density in the Lorenz-Lorenz mixing equation for specific refractivity, $R_{12} = p_1R_1 + p_2R_2$ used to calculate $dn/dc$. It may also be shown that as the absolute refractive index difference between solute and solvent becomes smaller, $dn/dc$ becomes more sensitive to density change of the solute.

Weir, C. E., **Concerning the maximum melting point,** *Jap. J. Appl. Phys.* **10,** *No. 6, 714–716 (June 1971).*

Key words: High pressure; melting point.

The theory of Kawai and Inokuti of the behavior of the melting point of solids as a function of pressure is discussed. The general theory is not considered applicable to the vast majority of materials known to date.

---


Argentar, H., Determination of the dégree of polymerization of a polymeric amine from NMR data using a "least-squares" approach, J. Polymer Sci. **9,** Part B, 657–659 (1971).

Casella, R. C., The reversal symmetry and its breaking in physics, Phys. Teacher **8,** No. 3, 114–123 (March 1970).

Devereux, C. W., II, Technical Standards Coordinator, Body measurements for the sizing of boys' apparel, Nat, Bur. Stand. (U.S.), Prod. Stand. 36–70, 24 pages (Dec. 1971) 35 cents, SD Catalog No. C13.20/2:36–70.

Douglas, T. B., Summary of recent thermodynamic measurements by calorimetric, transpiration, mass spectrometric microwave, and infrared techniques, Proc. Conf. Interagency Chemical Rocket Propulsion Group, Thermochemistry Working Group, Huntington Beach, Calif., March 25–27, 1968, 6th Meeting Bulletin 173, I, 93–104, (Chemical Propulsion Information Agency, The Johns Hopkins University, Applied Physics Laboratory, Silver Spring, Md., August 1968).

Flynn, T. M., Smith, C. N., Trends in cryogenic fluid production in the United States, (Proc. Int. Institute of Refrigeration, Tokyo, Japan, 1970), Int. Inst. Refrig. Bull. Suppl. Commission I, pp. 241–247 (Annex 1970–2).

Franklin, A. D., Bennett, H. S., Editors, ARPA–NBS program of research on high temperature materials and laser materials, Reporting Period–January 1 to June 30, 1971, Nat. Bur. Stand. (U.S.), Tech. Note 703, 39 pages (Dec. 1971) 50 cents, SD Catalog No. C13.46:703.

Freeman, D. H., Zielinski, W. L., Jr., Editors, Separation and Purification Section: Summary of Activities–July 1970 to June 1971, Nat. Bur. Stand. (U.S.), Tech. Note 589, 64 pages (Oct. 1971) 60 cents, SD Catalog No. C13.46:589.

Mason, H. L., Pounds, atoms, papers, and laws, Instrument Society of America Silver Jubilee International Conference and Exhibit, 1–5 (1970).

Moore, R. T., Determination of performance of digital data communication systems, (Proc. IEEE, ICC 71 CIC Intern. Conf. Communications, Montreal, Canada, June 14–16, 1971), IEEE, ICC 71 CIC Conf. Record VII. Session 12A, VIII, 12–1—12–3 (1971).

Powell, F. J., Research needs in thermal insulation, (Proc. Symp. Thermal Insulation, Columbus, Ohio, Feb. 5–8, 1968), ASHRAE (Amer. Soc. Heat Refrig. Air-Cond. Eng.) Bull. Thermal Insulation, pp. 14–17 (1971).

Rasberry, S. D., Applications of x-ray analysis, 20th annual Denver

x-ray conference, Denver, 11–13, August 1971, Appl. Opt. 10, No. 12, 2795 (Dec. 1971).

Rubin, S., Oettinger, F. F., Thermal hysteresis and its possible effect in restricting the hot-spot-free operating range of some power transistors, IEEE Trans. Electron Devices **ED–18**, No. 6, 393–394 (June 1971).

Schade, P. A., Signal decoder eliminates jitter, Electron. Design **19**, No. 24, 1 (Nov. 25, 1971).

Wexler, A., Book review on "modern hygrometry" by A. Pande, Bull. Am. Meteorol. Soc. **52**, No. 9, 897–898 (September 1971).

**Publications for which a price is indicated are available by purchase from the Superintendent of Documents, U.S. Government Printing Office, Washington, D.C. 20402 (foreign postage, one-fourth additional). The NBS non-periodical series are also available from the National Technical Information Service (NTIS), Springfield, Va. 22151, which was formerly the Clearinghouse. Reprints from outside journals and the NBS Journal of Research may often be obtained directly from the authors.*



U. S. GOVERNMENT PRINTING OFFICE : 1972 OL - 459-033

UNITED STATES
GOVERNMENT PRINTING OFFICE
PUBLIC DOCUMENTS DEPARTMENT
WASHINGTON, D.C. 20402

OFFICIAL BUSINESS
PENALTY FOR PRIVATE USE, $300

U.S. DEPARTMENT OF COMMERCE
POSTAGE AND FEES PAID

U.S.MAIL

JOURNAL OF RESEARCH of the National Bureau of Standards
A. Physics and Chemistry

Vol. 76A, No. 3 May–June 1972

# Contents

Page

**Thermodynamics of standard cells of the saturated cadmium sulfate type. Walter J. Hamer.** 185

**An improved state equation in the vicinity of the critical point. Olav B. Verbeke.** 207

**Dilute solution theory of polymer crystal growth: fractionation effects. Isaac C. Sanchez and Edmund A. DiMarzio.** 213

**The formation of curved polymer crystals: poly(4-methylpentene-1). F. Khoury and J. D. Barnes.** 225

**Photoionization of propylene, cyclopropane, and ethylene. The effect of internal energy on the bimolecular reactions of $C_2H_4^+$ and $C_3H_6^+$. L. W. Sieck and P. Ausloos.** 253

**Low temperature thermocouples: KP, "normal" silver, and copper versus Au-0.02 at% Fe and Au-0.07 at% Fe. Larry L. Sparks and Robert L. Powell.** 263

**Infrared spectra of cerium (Ce I and Ce II) between 0.8 and 2.4 μm. J. Verges, C. H. Corliss, and W. C. Martin.** 285

**Publications of the National Bureau of Standards.** 305

Library of Congress Catalog Card Number: 62–37059

For sale by the Superintendent of Documents, U.S. Government Printing Office, Washington, D.C. 20402. (Order by SD Catalog No. C 13.22/sec.A:76/3). Single copy price varies. This issue $1.75 Subscription price: $9.50 a year; $2.25 additional for foreign mailing.

UNITED STATES GOVERNMENT PRINTING OFFICE, WASHINGTON : 1972